Discovery of novel inhibitors of mycobacterial β-sliding clamp

Dissertation

zur Erlangung des Grades
des Doktors der Naturwissenschaften
der Naturwissenschaftlich-Technischen Fakultät
der Universität des Saarlandes

vorgelegt von

Dipl.-Chemiker Uladzislau Hapko

Saarbrücken
2023

Tag des Kolloquiums:	November 14th 2023
Dekan:	Prof. Dr. Ludger Santen
Berichterstatter:	Prof. Dr. Anna K. H. Hirsch
	Prof. Dr. Rolf Müller
Akad. Mitglied:	Dr. Angelika Ulrich
Vorsitz:	Prof. Dr. Uli Kazmaier

Die vorliegende Arbeit wurde von September 2018 bis März 2022 unter Anleitung von Frau Prof. Dr. Anna K. H. Hirsch in der Fachrichtung Pharmazeutische und Medizinische Chemie der Naturwissenschaftlich-Technischen Fakultät der Universität des Saarlandes, sowie am Helmholtz-Institut für Pharmazeutische Forschung Saarland (HIPS) in der Abteilung Wirkstoffdesign und Optimierung (DDOP) angefertigt.

To my friends and family

Acknowledgements

First and foremost, I am deeply grateful to Prof. Dr. Anna K. H. Hirsch, whose unwavering trust in me began our collaboration back in the summer of 2016. It was then, as a summer internship student, that she believed in my potential and opened the door to a world of possibilities. Her guidance and mentorship during that time set the foundation for what would become an extraordinary journey. As my PhD advisor, she continued to be an unwavering source of support and inspiration throughout my thesis, guiding me with wisdom and dedication.

Prof. Dr. Anna K. H. Hirsch's belief in my potential has been transformative, shaping not only my academic pursuits but also my character. Her mentorship instilled in me a passion for knowledge, a thirst for discovery, and the confidence to pursue my dreams. I am forever grateful for your guidance, and I cherish the experiences and cherished moments of our collaboration. Thank you, Anna, for being the driving force behind my growth as a researcher and for believing in me every step of the way.

I would also like to thank my second supervisor Prof. Dr. Rolf Müller and the thesis committee member Dr. Angelika Ulrich for providing strategic perspective during our committee meetings.

Next, I would like to say thank you to the members of our small DnaN team: the inspirator and perpetuator of the project Dr. Walid M. Elgaher, the analytically savvy Federica Mancini and, finally, our new doctoral student Ahmed Amin.

Collaboration is the heartbeat of progress, where unity nurtures the seeds of success. A special thanks goes to Dr. Sari Rasheed for being a committed and reliable collaborator, providing results from biophysical and microbiological studies of all the compounds I made. There would be no medicinal chemistry possible in our shared DnaN project but for your help, Sari.

I would also like to thank my external collaborators:

- Dr. Peer Lukat for performing structural biology studies of DnaN proteins and demonstrating creativity in solving concomitant problems.
- Dr. Norbert Reiling for conducting tests of my compounds against pathogenic strains of *Mycobacterium tuberculosis* and always being available and helpful for any related discussions.

Many thanks to Dr. Andreas Kany for his significant contribution to the first chapter of the present thesis by performing ADME/Tox profiling of compounds outside of the Institute and the country.

Special thanks to Dr. Zivota Selakovic for painstakingly reading and correcting the fragment episode of the thesis, accomplishing this incredibly fast.

I would personally like to thank Dr. Serena della Volpe and Dr. Sandra Johannsen for igniting my interest for NMR-based fragment screening methods and providing thorough and high-quality hands-on training in STD-NMR.

I would like to gratefully mention my office mates Henni Ropponen, Ben Zoller and Dominik Kolling for making fascinating interlocutors and great company.

Among others, I would also like to bring up two amazing students whom I had the lucky chance to mentor in the lab and beyond and to whom I am truly grateful: Muniba Bhatti and Nikita Shikut.

I extend my heartfelt thanks to the DDOP members from other projects: Dr. Christian Schütz, your inspiring discussions of chemistry, fueled by shared passion, have been a true source of motivation; Dr. Jelena Konstantinovic, whose collected demeanor and unwavering support have brightened even the toughest days; Dr. Alexander Kiefer, whose goal-oriented and ambitious spirit has infected me with the same drive to excel. A particular thanks goes to Christina Kosch, who is hands down the most straight-to-the point person I know, and for that, I am truly grateful.

And all other former and present DDOP/AVID members whom I was lucky to work side-by-side with: Dr. Ravi Jumde, Dr. Eleonora Diamanti, Dr. Mostafa Hamed, Dr. Ahmed Merabet, Dr. Gwenaëlle Jézéquel, Tizian Ramspoth, Samira Speicher, Daan Willocx, Tony Lacour, Konrad Wagner, Yingwen Wu, Dr. Alaa Alhayek, Atanaz Shams and of course my former partition III mates Ioulia Exapichedou and Dr. Virgyl Camberlein. Together, you've enriched my journey, and I am grateful for each of your contributions and camaraderie.

I would also like to thank all CBCH group members, but in particular Marta Czekanska for her uplifting positivity and friendship throughout; Joscha Meiers for his goal-oriented mindset, unwavering support, and memorable musical collaboration during our Christmas party back in the day; Dr. Eva Zahorska, Dirk Hauck, Mario Fares and Zeyue Zhang for being a wonderful company. Thank you all for being an essential part of my stay at HIPS and making this experience more fulfilling.

Thanks to all the members of the NAPANTI consortium (of which I was also a part), and a special thanks to Prof. Dr. Philipp Klahn for providing an inspiring example of the kind of chemist one should strive to become.

I would also like to express my appreciation to Prof. Dr. Martin Empting, whose lectures in Chemical Biology sparked my vivid interest in the subject. Your ability to blend science and didactics has left and enduring impact that inspired me to take a different look at drug discovery and pursue gaining more knowledge in its biology-related aspect.

Gratitude flows to Prof. Dr. Jesko Köhnke, who opened the door to the captivating world of structural biology and biochemistry, igniting a flame of interest that burns brighter with each passing day.

Behind every scientific breakthrough, there's a well-coordinated team making the gears of progress turn seamlessly as one. Grateful recognition goes to Bahareh Kadkhodazadeh, Annette Herkströter, Julia Mohr, Christian Zeuner, Frank Jakob, Mark Caspari and Michael Roth for their invaluable contributions in making this possible.

Finally, with the deepest gratitude, I extend my heartfelt appreciation to Olga Metelkina, not only as a wonderful spouse but also as an unwavering pillar of support in every aspect of my life. Your constant presence and encouragement have been a guiding light, brightening my journey through every challenge and triumph. Your belief in me has been a source of strength, motivating me to reach for the stars. Thank you for being my rock and my inspiration, and for making every moment of this incredible journey more meaningful. I am truly blessed to have you by my side.

Curriculum Vitae

Uladzislau Hapko
born on 8th March 1995 in Luninets, Belarus

Education

2018–2023	PhD studies in the group of Prof. Dr. Anna K.H. Hirsch Helmholtz Institute for Pharmaceutical Research Saarland (HIPS)
2012–2018	Diploma (with distinct), specialization Organic Chemistry Lomonosov Moscow State University
2012	Graduation from Luninets Lyceum

Research Experience

2022	Research internship at the Medicinal Chemistry department of Merck KGaA (Darmstadt, Germany)
2018	Diploma thesis in the group of Prof. Dr. Majouga Lomonosov Moscow State University “New theranostic agents for targeted delivery into hepatic cells”
2017	Research internship at the Drug discovery department of Biocad (Saint-Petersburg, Russia)
2016	Research internship at the group of Prof. Dr. Anna K.H. Hirsch Groningen University, the Netherlands
2016–2018	Research student at the Laboratory of tissue-specific ligands Lomonosov Moscow State University
2014	Research student at the Laboratory chromatography Lomonosov Moscow State University
2013	Research student at the Laboratory of semiconductor materials Lomonosov Moscow State University

Publications

Uladzislau Hapko, Sari Rasheed, Walid A. M. Elgaher, Rolf Müller, Anna K. H. Hirsch, *Targeting the bacterial β-sliding clamp (DnaN): A promising strategy for novel antibiotics*, Annual Reports on Medicinal Chemistry Vol. 61: Natural Products, manuscript submitted on 1st August 2023.

Contribution: writing the chemistry/drug discovery part of the manuscript.

Uladzislau Hapko, Sari Rasheed, Walid Elgaher, Jennifer Herrmann, Peer Lukat, Norbert Reiling, Wulf Blankenfeldt, Rolf Müller, Anna K. H. Hirsch, *Structure–activity relationships exploration and optimization of a new class of bacterial β-sliding clamp inhibitors highly active against Gram-positive and mycobacterial pathogens*, manuscript in preparation.

Contribution: synthesis of the virtual screening hit, design and synthesis of derivatives for SAR exploration.

Uladzislau Hapko, Sari Rasheed, Walid Elgaher, Jennifer Herrmann, Rolf Müller, Anna K. H. Hirsch, *Fragment-based discovery of novel mycobacterial β-sliding clamp inhibitors*, manuscript in preparation

Contribution: synthesis of fragment molecules, SAR establishment and their further elaboration; writing the manuscript.

Ramon van der Vlag, Hao Guo, **Uladzislau Hapko**, Nikolaos Eleftheriadis, Leticia Monjas, Frank J. Dekker, Anna K.H. Hirsch, *A combinatorial approach for the discovery of drug-like inhibitors of 15-lipoxygenase-1*, European Journal of Medicinal Chemistry 2019, 174, 45-55.

Contribution: synthesis of small-molecule 15-LOX inhibitors

S.Y. Maklakova, F.A. Kucherov, R.A. Petrov, **V. V. Gopko** G. A. Shipulin, T. S. Zatsepin, E. K. Beloglazkina, N. V. Zyk, A. G. Majouga V. E. Koteliansky, *A new approach to the synthesis of ligands of asialoglycoprotein receptor for targeted delivery of oligonucleotides to hepatocytes.* Russ Chem Bull 2015 *64, 1655–1662*

Contribution: synthesis of precursors triantennary ASGPr ligands for further conjugation to siRNA.

Summary

The development of total antibiotic resistance is becoming a looming threat for world healthcare, thereby underlining the need for the development of novel antibiotics with unprecedented modes of action. A promising target in this respect is the bacterial β-sliding clamp (DnaN), which has recently been identified and proven to be crucial for bacterial replication and resistance development.

For this thesis, we established SAR around the structure of a highly promising virtual screening hit **H1**, that demonstrated significant binding to DnaN and antibacterial activity. Derivatives of **H1**, synthesized in the course of SAR establishment efforts, demonstrated improved inhibitory activity against Mycobacteria and Gram-positive bacteria, but failed to impact efflux-competent Gram-negative pathogens. Using a combination of biophysical methods, we elucidated the details of **H1**'s interaction with the β-clamp.

As a second approach, a fragment-based screening campaign led to the discovery of hits that were synthetically optimized and grown to achieve improved DnaN binding and enhanced antibacterial activity.

Overall, the results of the work summarized in the present thesis feature the identification of two new classes of small-molecule inhibitors of *M. tuberculosis* β-sliding clamp. The most promising representatives of both classes demonstrated appreciable target engagement *in vitro* and concomitant antibacterial activity, which paves the way for their further optimization and development.

Zusammenfassung

Die Entwicklung einer vollständigen Antibiotikaresistenz stellt eine bedrohliche Gefahr für die weltweite Gesundheitsversorgung dar und unterstreicht somit die Notwendigkeit der Entwicklung neuartiger Antibiotika mit beispiellosen Wirkungsweisen. Ein vielversprechendes Ziel in diesem Zusammenhang ist die bakterielle β-klammer (DnaN), die kürzlich identifiziert wurde und sich als entscheidend für die bakterielle Replikation und die Entwicklung von Resistenz erwiesen hat.

In dieser Dissertation haben wir eine Struktur-Wirkungs-Beziehung (SAR) um das vielversprechende virtuelle Screening-Hit **H1** etabliert, das eine signifikante Bindung an DnaN und antibakterielle Aktivität zeigte. Abkömmlinge von **H1**, die im Zuge der SAR-Bemühungen synthetisiert wurden, zeigten eine verbesserte Hemmaktivität gegen Mykobakterien und grampositive Bakterien, hatten jedoch keinen Einfluss auf Gram-negative Krankheitserreger mit Efflux-Kompetenz. Mit einer Kombination von biophysikalischen Methoden haben wir die Details der Wechselwirkung von **H1** mit der β-Klammer aufgeklärt.

Als zweiter Ansatz führte eine fragmentbasierte Screening-Kampagne zur Entdeckung von Treffern, die synthetisch optimiert und weiterentwickelt wurden, um eine verbesserte Bindung an DnaN und eine verstärkte antibakterielle Aktivität zu erreichen.

Insgesamt umfasst die Arbeit, die in dieser Dissertation zusammengefasst ist, die Identifizierung von zwei neuen Klassen von kleinen Molekülinhibitoren der *M. tuberculosis* β-klammer. Die vielversprechendsten Vertreter beider Klassen zeigten eine signifikante Bindung an das Zielprotein in vitro und gleichzeitig antibakterielle Aktivität, was den Weg für weitere Optimierung und Entwicklung ebnet.

List of abbreviations

%inh	percentage of inhibition
3D	three-dimensional
A. baumannii	*Acinetobacter baumannii*
A. baylyi	*Acinetobacter baylyi*
ADMET	Absorption, distribution, metabolism, excretion and toxicity
Ala	L-alanine
Arg	L-arginine
ATP	adenosine triphosphate
B. subtilis	*Bacillus subtilis*
CGM	cyclohexylgriselymycin
CHI	chromatographic hydrophobicity index
clogP	*in silico* computed logP
CL_{int}	intrinsic clearance
Cryo-EM	cryoelectronic microscopy
CYP	cytochrome P450
Da	Dalton
DCM	dichloromehtane
DHFR	dihydrofolate reductase
DIPEA	diisopropyl ethylamine
DMF	dimethyl formamide
DMSO	dimethyl sulfoxide
DNA	deoxyribonucleic acid
DNA-pol	DNA polymerase
ds	double-stranded (DNA or RNA)
DSF	differential scanning fluorimetry
E. coli	*Escherichia coli*
E. faecalis	*Enterococcus faecalis*
e.g.	*exempli gratia*
ESI	electrospray ionization
ESKAPE	a collective acronym including *Enterococcus faecium, Staphylococcusaureus, Klebsiella pneumonia, Acinetobacter baumannii, Pseudomonas aeruginosa and Enterobacter species*
et al.	*et alii*
EtOAc	ethyl acetate
FP-assay	fluorescence polarization assay
Gly	L-glycine
GM	griselimycine
H-bond	hydrogen bond
HBTU	2-(1H-Benzotriazol-1-yl)-1,1,3,3-tetramethyluronium- hexafluorophosphate
H. pylori	*Helicobacter pylori*

HPLC	high-performance liquid chromatography
HSA	human serum albumin
HepG2	hepatocellular carcinoma cell line
His	L-histidine
HMBC	heteronuclear multiple bond correlation
HRMS	high resolution mass-spectrometry
HTS	high-throughput screening
Hz	Hertz
IC_{50}	half maximal inhibitory concentration
Ile	L-isoleucine
IMP	inosine monophosphate
IMPDH	inosine monophosphate dehydrogenase
ITC	isothermal titration calorimetry
kb	kilobase, i.e thousand of bases or base pairs
K_d	dissociation constant
K_i	inhibition constant
K. pneumoniae	*Klebsiella pneumonia*
LC-MS	liquid chromatography – mass-spectrometry
LE	ligand efficiency
Leu	L-leucine
LLE	ligand lipophilicity efficiency
logP	logarithm of the octanol-water partition coefficient (determined experimentally)
M. abscessus	*Mycobacterium abscessus*
MDCK	Madin Darby Canine Kidney
Met	L-methionine
MGM	methylgriselimycin
MIC	minimal inhibitory concentration
M. leprae	*Mycobacterium leprae*
MS	mass-spectrometry
MST	microscale thermophoresis
M. tb	*Mycobacterium tuberculosis*
MtDHFR	*Mycobacterium tuberculosis* dihydrofolate reductase
M. thermoresistibile	*Mycobacterium thermoresistibile*
M. tuberculosis	*Mycobacterium tuberculosis*
NMR	nuclear magnetic resonance
NSAID	non-steroidal anti-inflammatory drug
P. aeruginosa	*Pseudomonas aeruginosa*
PBS	phosphate-buffered saline
PCNA	proliferating cell nuclear antigen
PCR	polymerase chain reaction
PDB	protein data bank

Phe	L-phenylalanine
PPAT	phosphopantetheine adenylyl transferase
PPI	protein-protein interaction
ppm	parts per million
Pro	L-proline
QAC	quaternary ammonium salt
RNA	ribonucleic acid
Ro3	rule of three
R. typhi	*Rickettsia typhi*
RU	resonance units (SPR)
SAICAR	phosphoribosylaminoimidazolesuccinocarboxamide
SAR	Structure-actvity relationship
S. aureus	*Staphylococcus aureus*
S. epidermidis	*Staphylococcus epidermidis*
S. pneumoniae	*Streptococcus pneumoniae*
S. pyogenes	*Streptococcus pyogenes*
Ser	L-serine
SICLOPPS	split-intein circular ligation of peptides and proteins
SPR	surface plasmon resonance
ss	single-stranded (DNA or RNA)
SSB	single-strand binding protein
STD-NMR	saturation transfer difference NMR
T3P	propanephosphonic acid anhydride
TBAF	tetrabutylammonium fluoride
TBDMS	*tert*-butyl dimethylsilyl
TFA	trifluoroacetic acid
Thr	L-threonine
tRNA	transfer RNA
TSA	thermal shift assay
Tyr	L-tyrosine
UDP	uridine diphosphate
UV	ultraviolet
Val	L-valine
Water-LOGSY	Water-Ligand Observed via Gradient SpectroscopY

Table of contents

1 Introduction

The emergence of antibiotic resistant, highly virulent and pathogenic bacterial strains is becoming a looming threat for global healthcare, potentially capable of bringing the era highly efficacious antibiotics to its end. This is primarily associated with non-commensurate usage of broad-spectrum antibiotics, which lead to the development and spreading of resistance genes across communities making antibiotics less efficient.

Antibiotic resistance-associated changes of bacterial genome are linked to increasing of active molecules' efflux or their incapacitation, which can succeed either by modification of active molecules by dedicated enzymes or by decreasing their target affinity by introducing mutations in targets' structures.

The systematic risk assessment taking into account growing multidrug resistance and virulence has resulted in grouping most important pathogens into the "ESKAPE" set, which includes *Enterococcus faecium, Staphylococcus aureus, Klebsiella pneumoniae, Acinetobacter baumannii, Pseudomonas aeruginosa*, and various *Enterobacter* species.[1] These pathogens are responsible for most of hospital-acquired infections and are known to be able to "escape" the biocidal action of antimicrobial agents.[1] So far certain strains of ESKAPE pathogens are known to have developed resistance mechanisms against almost all classes of routinely used antibiotics and last-resort ones alike.[1] World Health Organization has recently included ESKAPE pathogens along with multidrug resistant *Mycobacterium tuberculosis* into the priority list of bacteria against which new antibiotics are urgently needed.[2]

Nevertheless, potential antibiotic crisis can be further aggravated by steady waning of global antibiotic development pipeline.[3] Moreover, most of newly approved molecules are further derivatives belonging to well-known antibiotics classes, which are intrinsically amenable to being developed resistance against by modification of an already known mechanism. Only a handful of molecules currently in development can be identified as truly innovative ones exploiting novel antibacterial action mechanisms.[4]

Therefore, the intensification of effort aimed at discovery of innovative antibiotics is absolutely necessary to significantly impede the development of resistance in dangerous, highly virulent bacterial species.

The present work features our contribution to discovery and early-stage development of antimicrobial molecules that act by engaging a previously validated target called β-sliding clamp. Although this target has yet not been exploited by clinically used antibiotics, it has a number of advantages favoring the minimization of risks of resistance development.

1.1 Bacterial replication machinery

The process of DNA replication is crucial for all living organisms as it precedes cell division and proliferation. Inhibition or impairment of this process in bacterial cells has been shown to be essential for highly efficient classes of antibiotics such as the fluoroquinolones (topoisomerase inhibitors), which renders this approach attractive for antibiotic discovery.[5]

The central function in the bacterial replisome is carried out by the Polymerase III holoenzyme complex responsible for the synthesis of deoxyribonucleotide chains. The holoenzyme III consists of three sets of subunits having structural and synthetic functions (**Figure 1**).

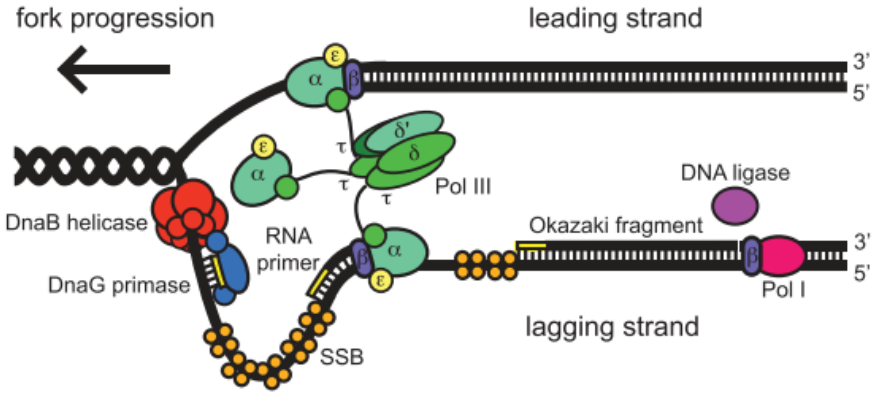

Figure 1. Schematic representation of leading and lagging strand synthesis at a replication fork in *Escherichia coli* (adapted from Robinson *et al*).[6]

One DNA polymerase III enzymatic complex subunit set is engaged into the uninterrupted elongation of the leading strand, while two other sets are responsible for the synthesis of ~2 kb Okazaki fragments, which eventually become a lagging strand of nascent DNA.[7]

1.1.1 Role of the β-sliding clamp in DNA replication and repair.

The *E. coli* DNA polymerase III is known to perform template DNA synthesis with the speed of **350–500 nucleotides/sec** only in a complex with the accessory protein called β-sliding clamp, while in the absence of the sliding clamp, the DNA polymerase III incorporates deoxy nucleotides at a rate of **10 nucleotides/sec** with a processivity of 10–20 base-pairs.[8] The β-sliding clamp protein is known to interact with different types of DNA-polymerases and ligases.[9]

This protein encircles and slides the along newly synthesized double-stranded DNA (**Figure 2, A**). β-clamp is engaged into DNA synthesis at the ds-ss DNA interface and is known to act as a tether for DNA-polymerase III, assuring its firm attachment to the template strand by involving the polymerase in a tight protein-protein interaction.[7]

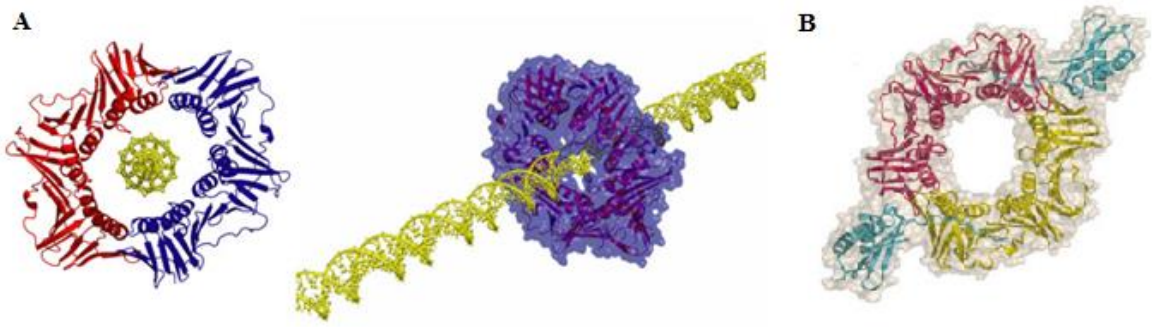

Figure 2. A) *Streptococcus pyogenes* DnaN surrounding ds-DNA (adapted from Argiriadi *et al.*)[10]; **B)** The structure of ternary complex between two units of DNA-Pol-IV and *E. coli* DnaN(adapted from Bunting *et al.*)[11]

The binding between DnaN and its partnering polymerases takes place at the C-terminus of the polymerase by coordination of the relatively short characteristic peptide sequence (linear motif) at the binding sites of the clamp protein (see **Figure 2, B**).

1.1.2 Structure of the bacterial β-sliding clamp.

The sliding clamp is a head-to-tail homodimeric donut-shaped protein that exists in two principal states: closed and opened.

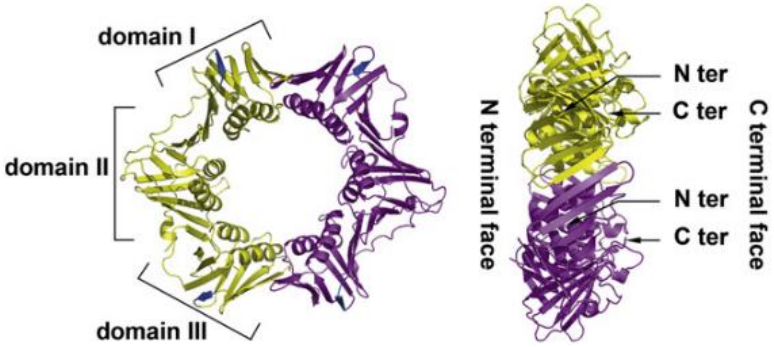

Figure 3. The structure of *M. tuberculosis* sliding clamp (reproduced from Gui *et al.*)[12]

The loading of the clamp onto DNA is associated with ATP-dependent opening-closure of β at the interface between the two protomers with the help of a subcomplex of DNA-polymerase holoenzyme III subunits γ called clamp loader protein complex.[13]

Each protomer of DnaN includes a mainly hydrophobic binding interface, located between domains two and three that bind characteristic linear motifs found in prokaryotic DNA polymerases.[14] The sequence of β-sliding clamp is highly conserved throughout bacterial species.

Owing to the importance of its function, proteins analogous to prokaryotic sliding clamp are found in archaea, eukaryotes (proliferating cell nuclear antigen, PCNA)[15] and certain viruses (e.g., gp45 in phage T4)[16]. However, in spite of topological similarity, PCNA and β-clamp were found to be only remotely similar, while the similarity between clamps found in bacteria and phages was not detected.[17]

1.2 The binding site of bacterial β-sliding clamp.

The polymerase peptide binding interface consists of a deep hydrophobic pocket (*subsite I*) located between domains two and three of the β monomer and connected by a groove to a more shallow *subsite II* located within the domain three (see **Figure 3** and **Figure 4**).[18]

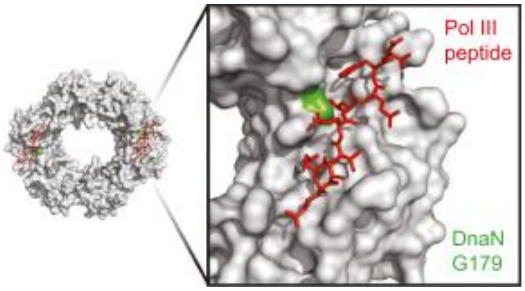

Figure 4 The surface presentation of the DNA-pol III linear peptide binding site of a β-sliding clamp(reproduced from Aakre *et al*).[19]

The two subsites are separated by the side chain of the Met-362 residue, that, in the absence of ligands, blocks the passageway between the *subsite I* and *II*.[18] Upon "anchoring" of hydrophobic portion of linear peptides to *subsite I*, the side chains of Met-362 and Ser-346 undergo simultaneous rotation, thereby opening the way for the ligand to the other subsite in the process called sequential binding (**Figure 5a**,**b**).[20]

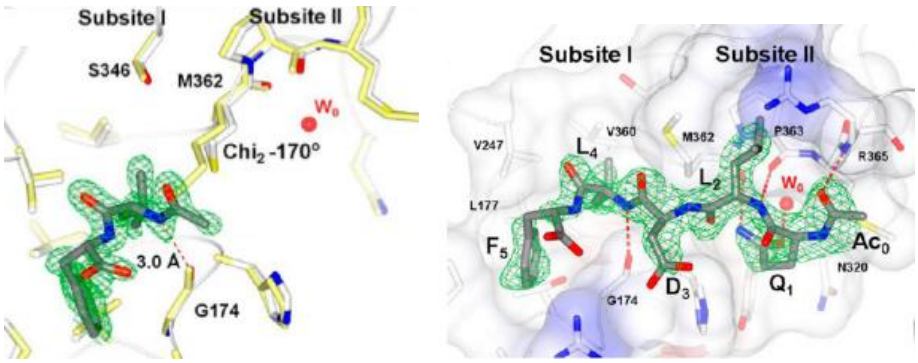

Figure 5. The structure of the **a)** *N*-acetylated terminal dipeptide L_4F_5 and **b)** pentapeptide $Ac_0Q_1L_2D_3L_4F_5$ bound to *E. coli* β-clamp (PDB: 4K3L and 3Q4J, respectively; reproduced from Yin *et al*).[20]

However, in spite of high similarity of linear peptide binding interfaces in sliding clamps of different bacterial species, it was demonstrated that model peptides (e.g., **P_1**) binding to sliding clamps of Gram-negative and Gram-positive bacteria have significantly different thermodynamic signatures, which is associated with mutations or differential placements of single amino acid residues adjacent to *subsites I* and *II* and to decreased (mycobacterial β) to no binding (*S. aureus* and *B. subtilis* clamp) of linear motif-mimicking peptides optimized for *E. coli* DnaN.[21] Additionally, the aforementioned Met-362 gating side-chain and adjacent Ser-346 were found to be replaced by Leu and Pro, respectively in Gram-positive bacteria, while mycobacterial DnaN represented a transition state with only Ser-346 replaced with Pro.[21]

The painstaking analysis of thermodynamics and kinetics of model peptide binding to *E. coli* and *B. subtilis* sliding clamps together with extensive structural studies of *E. coli* clamps bearing various mutations revealed the strategic function of Ser-346 for *subsite I* binding dynamics and confirmed that of the methionine residue for induction of binding to *subsite II*.[22]

The discovery of highly active competitive binders of bacterial β-sliding clamp can result in indirect inhibition of the DNA polymerases by making them less processive. This, in turn, impairs the whole DNA replication process resulting in bacterial growth inhibition and eventually in a bactericidal effect. The sliding clamp is also indispensable for the action of error-prone DNA polymerases involved in various DNA repair processes after induction of the SOS response; therefore DnaN inhibitors could potentially contribute to the mitigation of SOS response and delay the development of antibiotic resistance associated with various genetic mutations.[23] Thus, the multiple essential functions of DnaN in bacterial cells combined with significant structural divergence from PCNA make it a highly attractive target for antibacterial drug discovery.

1.3 Known ligands of bacterial sliding clamp

Linear peptides. Peptides constitute the most extensively investigated class of known DnaN binders since model peptides were actively employed as tool ligands for biochemical and structural studies of the replication process. These studies revealed the minimal consensus linear peptide sequence in DNA polymerases responsible for binding with DnaN to be $Q_1L_2[S/D]_3L_4F_5$, where the third position can be occupied by either serine or aspartic acid (**Figure 6**).[24],[25]

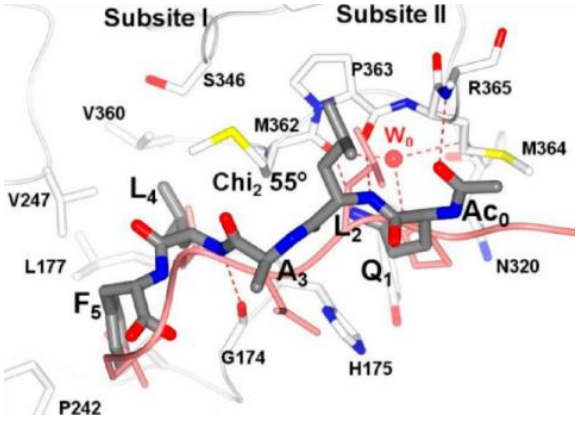

Figure 6. Binding of the acetylated model peptide (gray) and DNA-pol III linear motif (pink) to *E. coli* DnaN (reproduced from Yin *et al.*)[20]

The affinity of various decapeptides derived from natural β-clamp-binding proteins was assessed using SPR and an *in vitro* DNA replication assay in the work by Wijffels *et al.*[26] The majority of oligopeptides included the aforementioned consensus sequence with slight modifications together with different flanking sequences. This allowed for the ranking of peptides, that showed a wide range of affinity to DnaN (K_d by SPR from 0.38 to > 10 μM) and DNA replication inhibition (IC_{50} from 0.6±0.2 to >500 μM).

Bacteriophage genomics enabled the discovery of three polypeptides of non-disclosed structure, which showed the ability to bind *E. coli* DnaN.[27]

The structure-based attempts to discover high-affinity peptide binders of the *E. coli* β-clamp were undertaken by Wolff *et al*.[18] Starting from a known polymerase-derived linear motif **P1** (RQLVLGL, IC_{50} = 8 μM), reducing it to the more effective binder pentapeptide **P5** (QLDLF, K_d 12 μM), by acetylating the *N*-terminal glutamine residue **P6** (AcQLDLF, K_d 1 μM), replacing phenylalanine with β-cyclohexyl-alanine and adding extra chlorine atoms **P14** (Ac-QChaDLdiClF; "Cha" – L-cyclohexyl alanine, "diClF" – L-3,4-dichlorophenylalanine) the authors managed to improve the K_d of the peptide-DnaN complex by two orders of magnitude achieving the value of 77 nM. The optimized ligands were also investigated by isothermal titration calorimetry (ITC), which made it possible to estimate their thermodynamic binding profiles. In the follow-up paper by the same authors, the SAR establishment around the structure of a generic clamp-binding peptide was used to generate a 3D-pharmacophore for a ligand-based query,[28] which in the end gave rise to a small-molecule *E. coli* DnaN ligand, which will be discussed below.

Recently, dual-function peptides targeting *E. coli* DnaN and ribosome were designed, synthesized and tested by Andre *et al*.[29] The dual-function peptides combined sequences of previously described $\mathbf{P_7}$[18] (sliding clamp binding) and two different proline-reach antimicrobial peptides (PrAMP's) **Onc112** and unglycosylated pyrrhocoricin (**Py**). **Onc112** and **Py** are also known to interact with the peptide-exit channel of the bacterial ribosome.

Table 1. Summary of performance of oligopeptides from work by Andre *et al*.[29]

Name	**Sequence**	**K_d (SPR), μM**	***E. coli* MIC, μM**
$\mathbf{P_7}$	Ac-QXDLF-OH	194±58	>357
Onc112-P_7	VDKPPYLPRPRPPRrIYNrNGPRQXDLF-OH	200±0.1	0.15–0.29
Py-P_7	VDKGSYLPRPTPPRPIYNRNGPRQXDLF-OH	120±20	1.2–2.4

The combined peptides demonstrated high activity against *E. coli*, which was not essentially different to that of the peptides' **Onc112** and **Py** alone. This observation was explained by significant prevalence of ribosomes in bacterial cells compared to DnaN.

More recently, highly affine modified peptide binders were disclosed in the paper of Monsarrat *et al*.[30] As a result of extensive crystallography and structure-based optimization of previously discovered modified peptide **1.3.1**, which already showed good affinity to *E. coli* sliding clamp (K_d 194 nM), comprehensive SAR around the structure of **1.3.1** was established. These

efforts culminated in the discovery of **1.3.2** and **1.3.3**, that possessed low-nanomolar DnaN binding affinity (**Figure 7**) and were potent inhibitors of DnaN-dependent *in vitro* replication (IC_{50} of **46** and **51** are 0.35 and 0.15 μM, respectively).

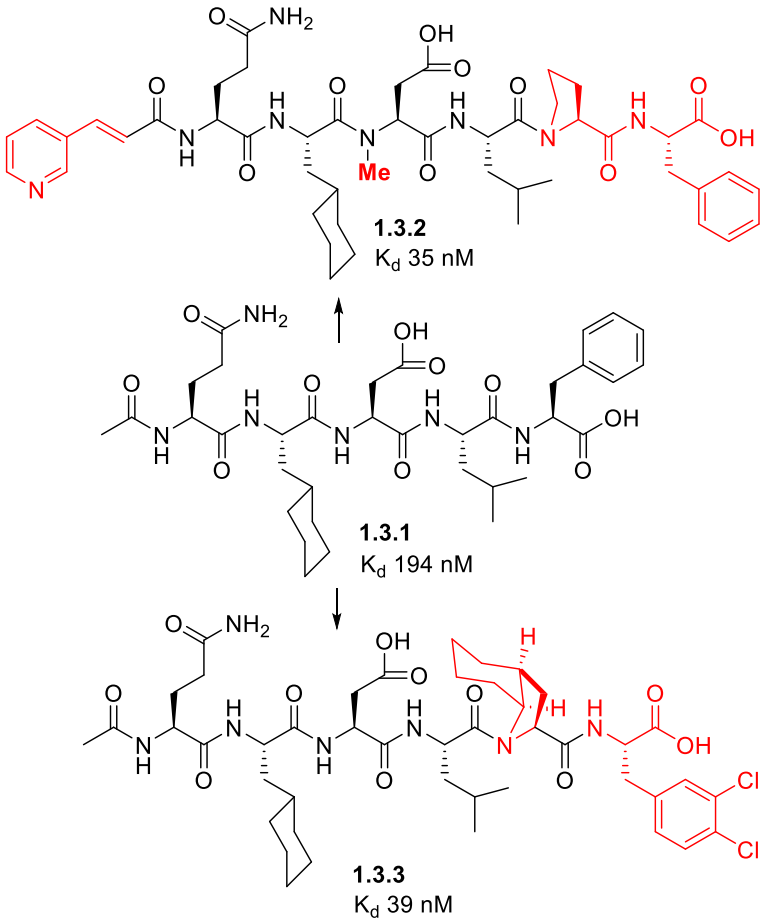

Figure 7. Structures of optimized *E. coli* DnaN binding peptides reported by Monsarrat *et al.*[30]

Nevertheless, in spite of excellent target affinity compounds **1.3.2** and **1.3.3** showed marginal activity (128 μg/mL) even against an efflux-deficient *E. coli* strain.

Addressing the problem of limited permeability of the bacterial cell wall towards polypeptides, Nedal *et al.*[31] synthesized peptides containing eukaryotic sliding clamp PCNA consensus sequences APIM (these were originally developed as potential anticancer drugs) [32], complemented by positively charged cell-penetrating polyarginine motifs (**Table 2**).

Table 2. Activity of polypeptides in the work [31]

Name of the peptide	**Sequence**	**K_d (MST)**	**MIC (μM):**		
			MRSE	***E. coli* BL21**	***E. coli* MG1655**
RWLVK	Ac-MD-**RWLVK**-WKKKRKI-RRRRRRRRRR	35	3	5	11
RWLVK*	Ac-MD-**RWLVK**-GILQWRKI-RRRRRRRRRR	--	3	3	4
RFSLK	Ac-MD-**RFSLK**-WKKKRKI-	--	3	4	7.5

	RRRRRRRRRRR				
RFSLK*	Ac-MD-**RFSLK**-GILQWRKI-RRRRRRRRRR	19	3	4	6.5
RALVK	Ac-MD-**RALVK**-WKKKRKI-RRRRRRRRRR	769	3	5	9
RWLK	Ac-MD-**RWLK**-WKKKRKI-RRRRRRRRRR	n/a	4	6	12
R11	RRRRRRRRRRR	n/a	12	11	14.5

MRSE – Methicillin-resistant *S. epidermidis*, PCNA-binding motif is highlighted in **bold,** "--" **–** "not determined" n/a – "not applicable.

In spite of the differences between prokaryotic (DnaN) and eukaryotic (PCNA) sliding clamps, the chimeric peptides including APIM sequences shown considerable affinity to the bacterial sliding clamp. The peptides were found to strongly inhibit bacterial DNA replication (complete inhibition achieved at 6 μM for the **RWLVK*** sequence) and showed growth inhibition of various *E. coli* strains and methicillin-resistant *S. epidermidis* in standard MIC tests (**Table 2**) as well as in the murine skin wound infection model, where the most active peptides were shown to have significantly reduced the bacterial load with no toxicity towards skin.[31]

The synthesized peptides were proved to bind the *subsites I* and *II* of the bacterial sliding clamp using site-directed mutagenesis of amino acid residues lining the protein-protein interaction interface of *E. coli* DnaN. These mutations were previously shown to be responsible for the impairment of naturally occurring clamp-binding motifs.[33]

Additionally, the inhibition of DnaN interaction with bacterial polymerases by the synthesized polypeptides was proven to considerably reduce the frequency of spontaneous mutations in *E. coli*, which renders the described peptides potentially promising means for mitigating the risks of antibiotic resistance development.[31]

A recent follow-up paper Raeder *et al.*[34] reported the discovery of significant synergy of action of the previously discovered polypeptide **RWLVK** (sequence: Ac-MD-**RWLVK**-WKKKRKI-R11/R10)[31] and antibiotic gentamicin against various strains of *S. epidermidis* both *in vitro* and in *in vivo* bone graft infection model. Moreover, the antibacterial peptide was shown to inhibit the growth and eradicate the *S. epidermidis* biofilm, which makes it a potentially promising agent for the combination treatment of prostethic joint infections.[34]

A more recent follow-up work by Nepal *et al.*[35] features more detailed investigation of the antibacterial peptide **RWLVK*** (sequence: Ac-MD-**RWLVK**-GILQWRKI-R11, called **betatide** by the authors). This peptide demonstrated its broad spectrum and reasonably high activity (MIC values 8-16 μg/mL) against a wide panel of pathogenic bacteria (including multidrug resistant ESKAPE pathogens and clinical isolates). **Betatide** also showed the ability to eradicate MRSE

infection in an *in vitro* wound assay, with no significant impact on epithelialization even in relatively high dosages.

Additionally, according to an intracellular infection experiments, the peptide of interest was shown to enter the eukaryotic cells infected by *S. aureus* and exert bactericidal effect.

Finally, as a result of a resistance development assay, *E. coli* and *S. aureus* showed lowered capacity to develop resistance against **betatide**, which is in accordance with its ability to considerably lower the frequency mutations supported the reported by Raeder *et al.*[34]

Cyclic peptides. In comparison to their linear counterparts, cyclic peptides are known to have increased proteolytic stability and are therefore more likely to exert antibacterial effects.

The split-intein circular ligation of peptides and proteins (SICLOPPS) technology[36] employed by Kjelstrup *et al.*[37] enabled the discovery of three cyclic octapeptide hits that demonstrated modest antibacterial effect on *S. aureus*. It was, however, subsequently established that it was the inhibition β-clamp's subunits dimerization that was probably responsible for compounds' antibacterial action.

Table 3. Activity of discovered cyclic peptides in the work [37]

Cyclic peptide	Sequence	MIC values *S. aureus*	
		µg/ml	µM
III-5	CR**VFLCGC**	50	57
III-6	CR**SQGLFK**	50	54
III-7	CR**GHVWVD**	20*	21*

* - tested against *Staphylococcus epidermidis;* binding subsequence in **bold**

The cyclic depsipeptide natural product griselimycin (**GM**) was discovered in the 1970's by isolation from *Streptomyces.*[38]

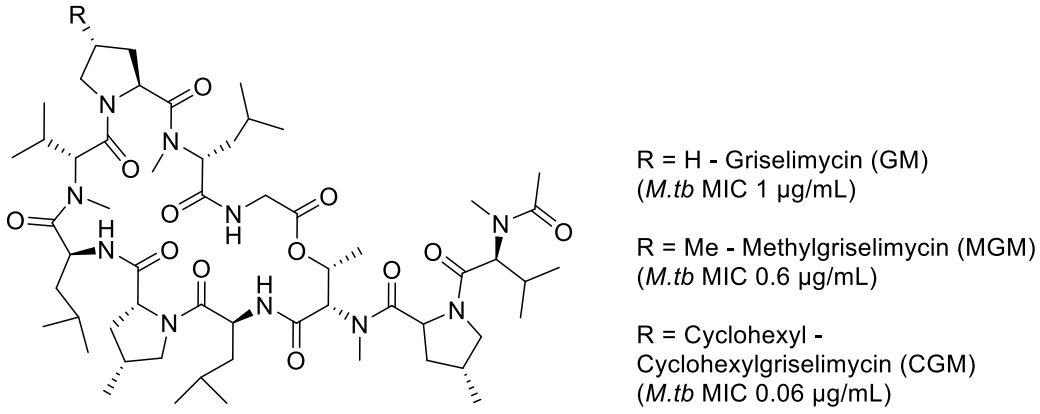

Figure 8. The structure of substituted griselimycins and their MICs against *Mycobacterium tuberculosis*.

The mechanism of action of **GM**s was studied in detail by Kling *et al*. and was found to be DnaN binding and the inhibition of protein-protein interaction between the β-sliding clamp and DNA-polymerases.[23] The co-crystal structure of **GM** with *M. tuberculosis* DnaN revealed the antibiotic molecule bound to the peptide-binding interface of the bacterial β-sliding clamp: the

subsite I was occupied by the macrocyclic part, while the linear appendage of GM was accomodated by *subsite II* (**Figure 9**).

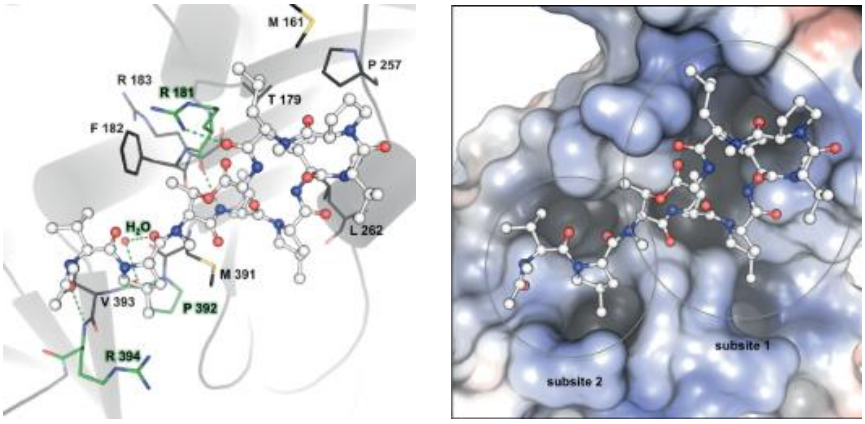

Figure 9. The co-crystal structure of griselimycin and *Mycobacterium tuberculosis* β-sliding clamp (PDB: 5AGU; reproduced from Kling *et al*).[23]

GM showed the highest affinity to sliding clamps of *M. smegmatis* and *M. tuberculosis* (SPR K_d 8.3×10^{-11} and 1.0×10^{-10} M, respectively), while the affinity in the case of *E. coli* sliding clamp turned out to be considerably lower (K_d 6.5×10^{-7} M). These findings were consistent with the strain-specific activity of **GM**s. The high activity of **GM**s against *M. tuberculosis* and the unfavorable ADME profile inspired optimizations effort to yield methyl- and cyclohexyl-griselimycins (**MGM** and **CGM**), which demonstrated greater metabolic stability and a more favorable pharmacokinetic profile compared to their natural predecessor.[23] The optimized derivatives showed promising *in vitro* and *in vivo* activity, yet a high efficient dose (> 100 mg/kg) in the acute model. Additionally, the cyclic peptide **GM**s proved highly active against resistant *M. tuberculosis* strains and demonstrated low frequency of resistance (5×10^{-10}), which was accompanied with extremely high fitness costs.[23]

Overall, linear peptides showed good sliding clamp affinity and *in vitro* DNA replication inhibition, but mostly lacked antibacterial activity, which could be associated with low permeability or intrinsic metabolic lability of peptides. Simultaneously, the cyclic peptide **GM** and its derivatives of comparable potency demonstrated significantly better antibacterial activity, possibly due to higher metabolic stability. Nevertheless, in view of the strain-limited activity of **GM**, further optimization of the cyclic peptides' permeability and target affinity remains to be undertaken.

Small molecules. Protein-protein interactions are generally considered difficult to inhibit with small molecules. Studies indicated so called "hot spot" regions within the interaction interface to contribute the major part of the binding energy, and therefore, these seem to be the most promising regions to be addressed by small-molecule inhibitors.[39] In the bacterial β-sliding clamp, *subsite I* was previously identified as such a "hot spot" initiating sequential linear motif binding.[20] Simultaneously, the proximity of *subsite II* suggests that fragment-based approaches

are suited to identify DnaN inhibitors. Additionally, small molecules are more likely to penetrate the bacterial cell wall as well as to have intrinsically higher metabolic stability. Therefore, finding potent and efficient DnaN binders among them could potentially solve the problem of limited strain susceptibility.

Various approaches had been employed to discover small-molecule binders of β-sliding clamp. The first small-molecule DnaN binder **RU7** was discovered as a result of high-throughput screening (HTS) effort by Georgescu *et al*.[40]

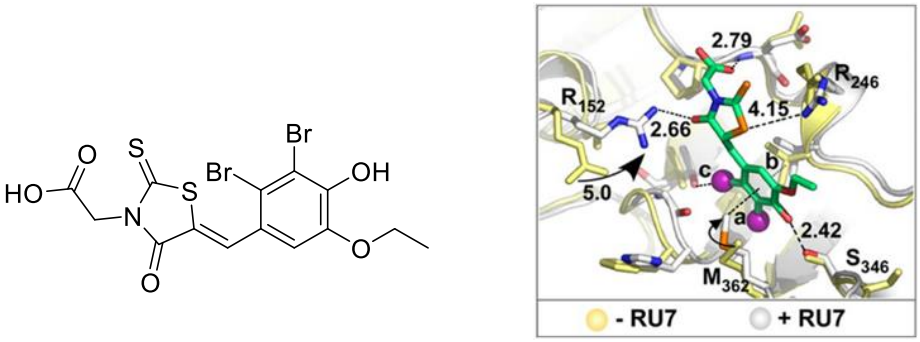

Figure 10. **A)** The structure of **RU7** – the first discovered small-molecule DnaN binder. **B)** The co-crystal structure of **RU7** with *E. coli* β-sliding clamp (PDB: 3DIG) illustrating the conformational changes in the structure of DnaN upon ligand binding (adapted from Georgescu *et al*.[40]).

RU7 was discovered as a tool compound able to selectively inhibit the protein-protein interaction between *E. coli* sliding clamp and different types of bacterial DNA-polymerases (I, III and IV) thereby discriminating among them. According to the fluorescence polarization assay, the apparent K_d of **RU7** was 2.7 ± 0.4 μM and the same compound showed the K_i of 10 μM in the relevant *in vitro* DNA replication inhibition assay.

The compound **RU7** was demonstrated to selectively disrupt the interaction between the β-sliding clamp and DNA-Pol III. Its co-crystal structure with *E. coli* DnaN was solved and revealed that **RU7** binds to *subsite I* of the interface and formed hydrophobic and polar contacts within the interface. The antibacterial activity of **RU7** was, however, not reported.

The ligand-based virtual screening afforded the discovery of another small molecule, which was demonstrated to bind DnaN.[28]

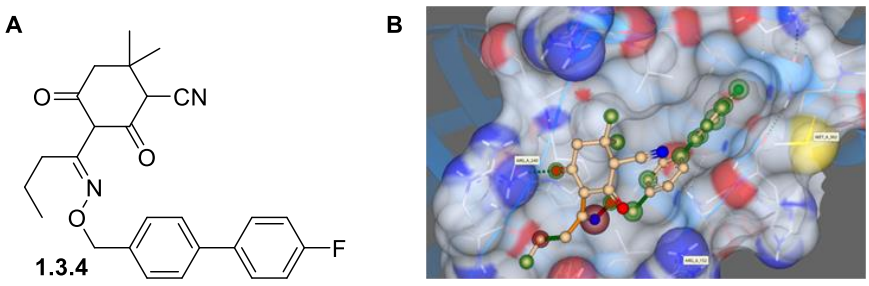

Figure 11. **A)** The structure of compound **1.3.4**, small-molecule DnaN *E. coli* β.clamp binder reported by Wijffels *et al*.[28] **B)** The co-crystal structure compound **4** with *E. coli* β-sliding clamp (PDB: 3QSB).

The solved co-crystal structure of compound **1.3.4** and *E. coli* sliding clamp showed that the small molecule was bound in *subsite I*, making mainly hydrophobic contacts with the protein with the 4-fluorobiphenyl portion of the molecule (**Figure 11, B**).

The antibacterial activity of **1.3.4** was not reported in the respective work. However, the compound **1.3.4** was named a promising starting point for structure-based binding optimization and drug discovery.[28]

First small-molecule DnaN inhibitors active against bacteria were discovered by Yin *et al*.[41] The authors pursued an X-ray crystallography fragment screening campaign and solved five crystal structures of *E. coli* β-sliding clamp with fragment-sized molecules bound in *subsite I* (**Figure 12, A**).

The discovered fragments **1-4** had shown very weak DnaN binding (FP-assay) and no DNA replication inhibition. In order to further develop the inhibitors, the authors considered the co-crystal structure of the only active fragment **5**. As a result of a similarity search in the ZINC database, docking of selected structures into the *subsite I* of *E. coli* DnaN and structure-based optimization a set of substituted tetrahydrocarbazoles were found to be optimal binders (**Figure 12, B**).

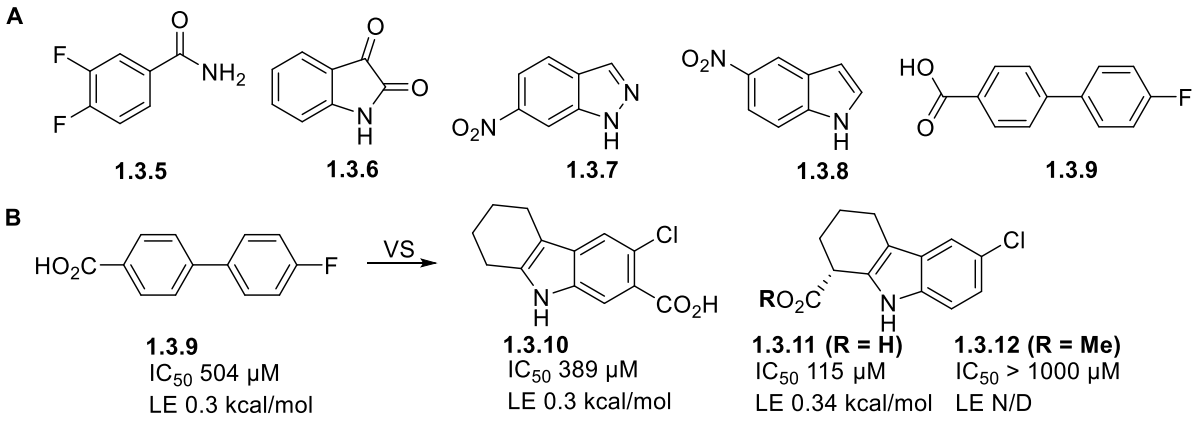

Figure 12. **A**) Fragments found to bind the *subsite I* of *E. coli* DnaN by Yin *et al*.[41]; **B)** Structures and activities of lead compounds **1.3.10**-**12** presented by Yin *et al*.[41]

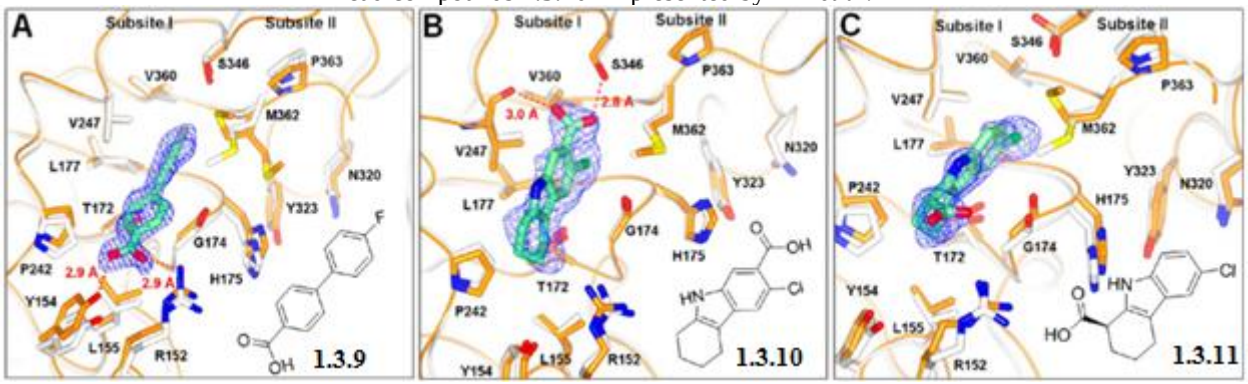

Figure 13. X-ray co-crystal structures of compounds **1.3.9(A)**, **1.3.10(B)** and **1.3.11(C)** with the *E. coli* DnaN (PDB codes: 4N98, 4N99 and 4N9A respectively). Adapted from Yin *et al*.[41]

The discovered sliding clamp ligands were proven to fully occupy the *subsite I* of *E. coli* DnaN (**Figure 13a–c**.) and showed antibacterial activity (MICs up to 115 μM) that correlated with the molecules' target affinities.

The β-sliding clamp protein was also found to be an off-target for certain common non-steroidal anti-inflammatory drugs (NSAIDs), which could be the cause of their slight antibacterial activity.[42] Out of twenty NSAID molecules tested for binding to *E. coli* DnaN by Yin *et al.* five were found active in the corresponding fluorescence polarization assay (see **Figure 14**).

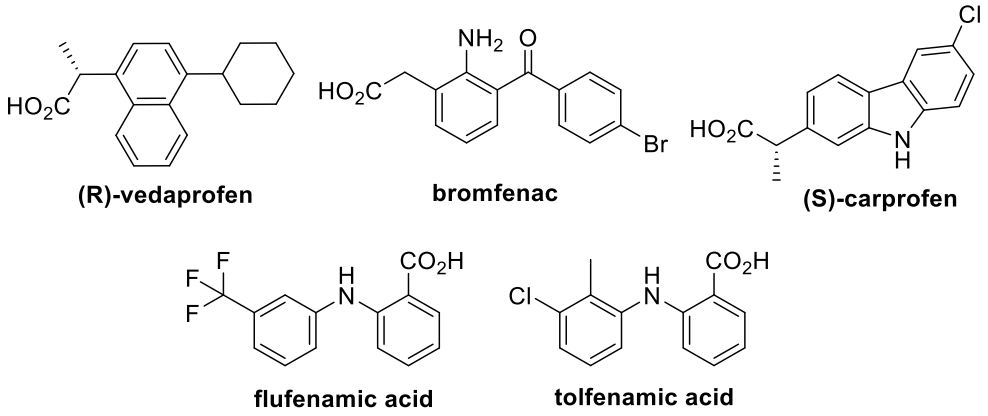

Figure 14. Structures of NSAID binders of *E. coli* sliding clamp found in the work by Yin *et al.*[42]

Flufenamic and **tolfenamic acids** demonstrated only marginal binding to sliding clamp, while **vedaprofen**, **bromfenac** and **carprofen** demonstrated mid-micromolar IC_{50} values and detectable *in vitro* DNA replication inhibition. These molecules also showed quite moderate antibacterial activity: best MIC values against *S. aureus* and *Bacillus subtilis* achieved 156 μM for **vedaprofen**, while **carprofen** turned out to be most efficient (yet objectively poorly active) against Gram-negative bacteria with MICs of 2500 and 1250 μM for *E. coli* and *Acinetobacter baylyi*, respectively.[42]

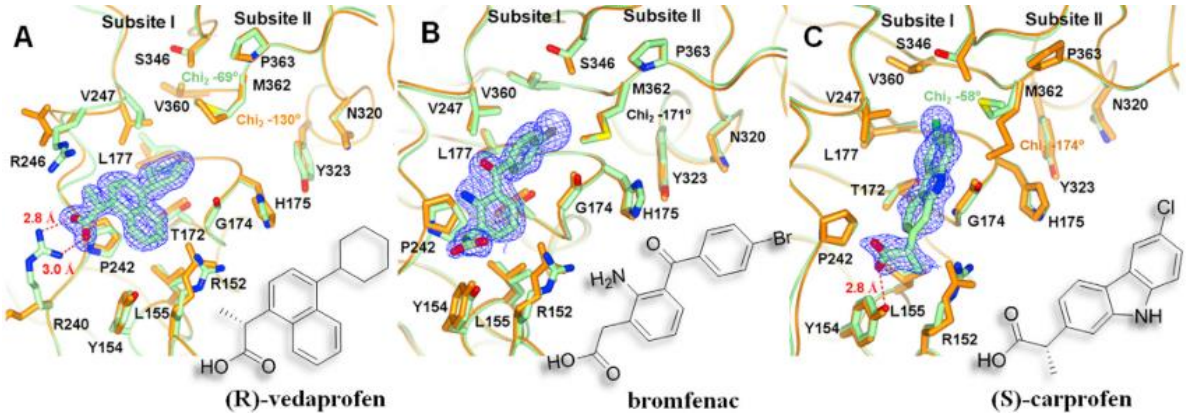

Figure 15. Co-crystal structures of NSAID binders occupying the *subsite I* of *E. coli* DnaN (adapted from Yin *et al.*).[42]

Furthermore, the co-crystal structures of vedaprofen, bromfenac and carprofen and *E. coli* sliding clamp (PBD codes 4MJP, 4MJP and 4MJR respectively) revealed all molecules to occupy the *subsite I* within the clamp's binding site (**Figure 15a-c**).[42]

The follow-up work by the same authors[43] capitalized on the previously described tetrahydrocarbazole scaffold[41] and was focused on extending inhibitors into the *subsite II* of the peptide binding interface of the β-sliding clamp. As a result of structure-based growing and optimization, enlarged ligands made by the extension from carbazole nitrogen were discovered.

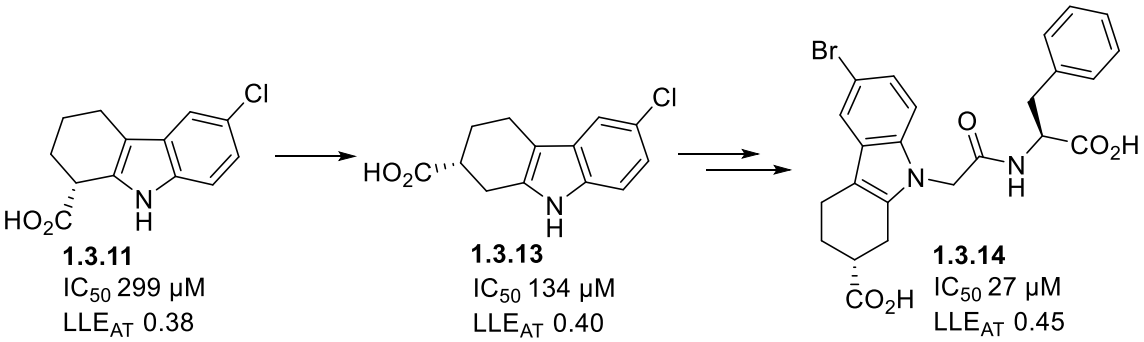

Figure 16. Fragment growing to target DnaN subsite II performed in the follow-up work by Yin *et al*.[43]

According to crystallographic studies, binding of grown inhibitors such as **1.3.14** to *E. coli* DnaN caused the conformational changes and opening of a new area within the peptide binding interface called *subsite III*, which could be of interest for further inhibitor development (**Figure 17**). Simultaneously, the *subsite II*, targeting of which had originally inspired the growing attempts, stayed empty, which marked the failure of the growing strategy pursued by Yin *et al*.

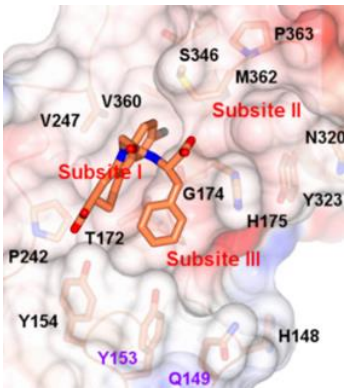

Figure 17. The position of **1.3.14** in the binding site of *E. coli* DnaN (PDB: 4PNW; adapted from Yin *et al*.).[43]

Nevertheless, in spite of high affinity and effective binding of **1.3.14** and its derivatives to DnaN and the analogues' excellent performance in sliding clamp-dependent DNA replication inhibition tests, the grown fragments showed no antimicrobial effect probably owing to the presence of two carboxyls that make the molecule negatively charged at physiological conditions.

Recently, another anti-inflammatory drug was reported to bind the β-clamp of *Helicobacter pylori*. Diflunisal (**Figure 18, A**) was found by virtual screening and its co-crystal structure with *H. pylori* DnaN confirmed the molecule's occupation of *subsite I* (**Figure 18, B**) analogous to compound **4** from work by Wijffels *et al*.[28]

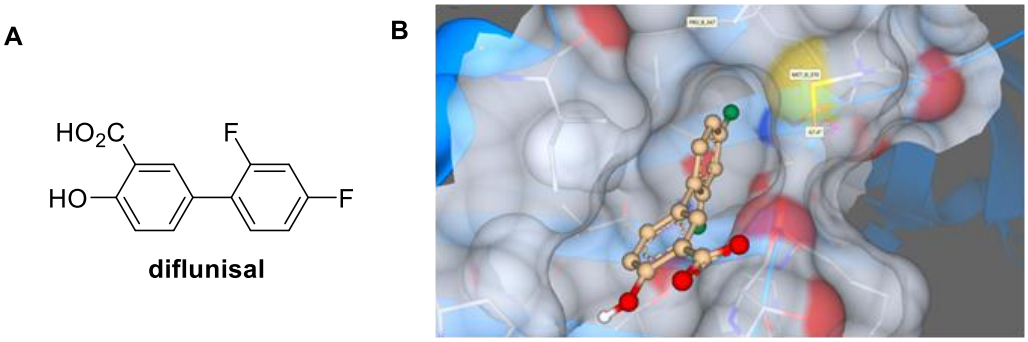

Figure 18. A) Structure of diflunisal; **B)** Binding mode of diflunisal in the co-crystal structure with *Helicobacter pylori* sliding clamp (PDB: 5G48).[44]

Diflunisal was shown to be a good DnaN binder in SPR competition measurements as well as active against *H. pylori* with a MIC value of 85 μM.

Finally, the application of protein-templated Ugi reaction in the context of kinetic target-guided synthesis (KTGS) by Mancini *et al*. enabled the discovery and validation of small peptide-like DnaN ligands,[45] which were proven to be binders of the *subsite I* of *M.tuberculosis* protein (**Figure 19**).

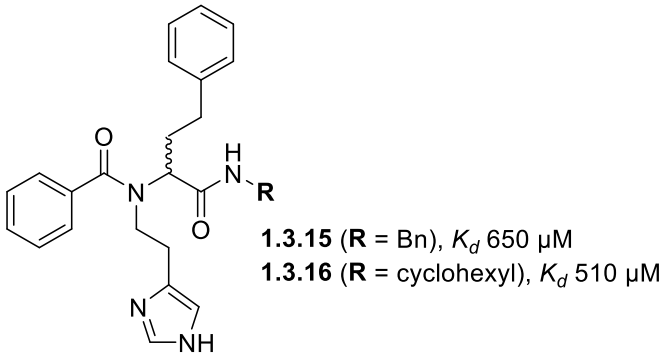

Figure 19. Peptide-like *Mycobacterium tuberculosis* β-clamp binders discovered by KTGS in the work by Mancini *et al*.[45]

In spite of clear binding to DnaN the compounds had only shown marginal activities against some gram-positive and negative bacterial strains (*Micrococcus luteus* and TolC-defficient *E. coli* MICs 128 μM), which can be attributed to difficulties with compounds' transport and proteolytic instability.

To sum up, significant efforts were undertaken to discover small-molecule DnaN inhibitors, some of which showed modest activity against pathogenic bacteria. However, the problem of overcoming the cellular barriers and efflux that are salient in Gram-negative strains still seems to be unsolved as no small molecules showing high activity against wild-type *E. coli* and other pathogens have been discovered hitherto. It is however noteworthy, that nearly all molecules were screened and optimized relying on structural information from the *E. coli* β-clamp. Taking into account considerable difference in thermodynamics of ligand binding of Gram-positive and Gram-negative sliding clamps,[21] DnaN proteins of *M. tuberculosis* and other pathogenic Gram-

positive bacteria remain virtually unaddressed with small molecules, which presents the opportunity to tackle the problem of extensively resistant pathogenic bacterial strains by targeting DnaN for drug discovery.

1.4 A short primer on the principles of fragment-based lead discovery

Fragments are small molecules used to obtain starting points for ligand discovery and optimization into high-affinity binders of biologically relevant targets.[46] The major advantages of fragments include: 1) their relatively small size, which allows for a reduction of their possible diversity and therefore more effective scouting of analogues' chemical space upon optimization; 2) the higher quality of protein–fragment hit interactions, which makes hit elaboration more straightforward.[47]

Construction of fragment libraries

Due to the high concentration used in initial screening, fragments are preferably highly soluble molecules. To meet aforementioned criteria a "rule of 3" was proposed for streamlining the design of fragment libraries: number of H-bond donors <3, number of H-bond acceptors <3, the number of rotatable bonds ≤ 3, MW not greater than 300 Da and logP not greater than 3.[48],[49] The overarching principles of design of fragments library are summarized in a comprehensive and detailed review by G. Keserü.[50] Diverse fragment libraries are commercially available: ranging from broad libraries covering a significant part of fragment space and ending up with dedicated screening libraries designed specifically for kinases or protein-protein interactions.

Methods of fragment screening.

Owing to their relatively small size, only rarely do fragments demonstrate tight binding to the target of interest. Therefore, due to their higher intrinsic sensitivity, biophysical methods are mostly used for early fragment screening and further affinity optimization.

Biophysical methods

Surface Plasmon Resonance (SPR)[51] can be used for a diverse range of targets, including GPCR's.[52] SPR is one of the most popular biophysical methods used in fragment campaigns. The target (ligand) is immobilized covalently on a gold chip, and the fragment (analyte) is flowing in the solution. The binding of analytes to the modified surface of the chip is detected optically. Major advantages of this method include the very low amount of required protein, that is immobilized and used for multiple runs, the high sensitivity and throughput of the technique.[53]

Thermal shift assay (differential scanning fluorimetry or DSF)[54] relies on the increase of thermodynamic stability of the receptor–ligand complex upon binding, which can result in the

proportional increase of the protein unfolding temperature.[55] One major advantage of DSF is that it does not require sophisticated machinery: equipment for PCR is sufficient for experiments. One of the salient disadvantages – increased false-positives and high sensitivity of the method to the type of protein used and conditions of the experiment.[53]

Microscale thermophoresis (MST) is based on the registration of change in the relative thermophoretic motility of target protein once it forms a complex with a ligand.[56] The assay is performed in capillaries and requires fluorescent labeling of either protein (most frequent case) or ligand or an intrinsically fluorescent binding partner. Due to the requirement of relatively low protein quantity and possibility of automation,[57] this method can be adapted for high-throughput experimentation. However, due to the high sensitivity of thermophoresis to aggregation in solution, which could be a common reaction of a protein of interest to high concentration of fragment ligands, hits discovered using this relatively new method in screening require additional thorough validation.

NMR-based methods can be divided into two categories: protein- and ligand-observed methods.

Protein-observed methods. These methods are based on observing the change of NMR signals associated with protein of interest, which occur upon binding of a ligand. Most frequently used experiments are ^{1}H-^{15}N (basis of the "SAR by NMR" approach featured in the seminal work by Stephen Fesik)[58] and ^{19}F experiments.[59] These experiments, in spite of providing structural insights into ligand-protein binding, require either isotopic (^{15}N) labeling or incorporation of certain amino acid analogues (such as ^{19}F-triptophan) into the target structure, which could be impractical in cases of large molecular mass or underrepresentation of suitable amino acids in the structure of interest. Apart from that, the aforementioned techniques typically require relatively large amounts of protein per experiment.[53]

Ligand-observed methods. Most widely used for fragment screening experiments include STD-NMR[60] and water-LOGSY[61], which rely on the transfer of magnetization to ligands from protein or water molecules, respectively. These experiments have made it into routine fragment-based screening procedures and can also be used to reconstitute the binding mode of the ligand of interest, which could be extremely helpful in the absence of structural information.[61],[62] The ^{19}F chemical shift perturbation relies on the observation of small changes of chemical shift of fluorine nuclei within ligands tested for binding.[59] The data derived from ligand-observed methods are much simpler to interpret and these experiments typically do not require large quantities of protein of interest.

Many other NMR-based ligand-observed methods can be used to guide fragment elaboration in the absence of structural data, which is showcased in a recent review.[63]

The most-used **MS-based** fragment screening method is *native mass spectrometry*, which is based on the observation of mass peaks corresponding to weakly bonded ligand–protein complex, which is the case in fragment-based screening. Even though native MS remains an exotic method, its utility was demonstrated for fragment screening on RNA[64] and various protein targets.[65],[66] A major advantage of this method is high throughput and phenomenally low amounts of target required for screening.

In the **Isothermal titration calorimetry (ITC)** experiment, the heat of complex formation between ligand and receptor is measured, which in the end allows for determination of enthalpic and entropic contributions to the binding free energy.[67] This method can serve as an ultimate validation of hits and leads; however, it requires certain minimal level of ligand binding affinity, which is limited by method sensitivity.[67] Additionally, the reliable thermodynamic profiling of the ligand usually requires a fairly high amount of the protein of interest (up to several milligrams for one titration).[68]

X-ray crystallography screening provides structural information and hit validation in one step. Previously obtained crystals of the target protein can be soaked with high concentration fragment mixtures or, in case the ligand binding is connected to substantial rearrangement of the protein, co-crystal structures of individual fragments are solved. Apart from the apparent pros, the cons of the methodology include its relatively low throughput, which follows from the necessity to obtain the crystals of the target which is not always possible for certain classes of proteins. Nevertheless, X-ray crystallography is known to be capable of delivering extremely weak binders when used as primary screening method,[69] which provides significantly more starting points, that could be missed by other biophysical screening methods, for further elaboration.

Cryo-EM-based screening. Due to fast-paced advances of the emerging Cryo-EM method in terms of usability and resolution, this method has all chances to succeed X-ray crystallography as it does not require crystallization of the protein macromolecule, which can significantly reduces the time needed for structure solving.[70] Furthermore, due to the peculiarities of sample preparation, the target structure can be obtained in multiple orientations and states, which is precluded in the “traditional” X-ray-based structural biology approach. Nevertheless, the main bottle neck of the progress in the field is the development of computational approaches to processing and interpreting data arrays collected during cryo-EM experiments.

Simultaneously, all biophysical methods are known to be prone to producing false-positive and negative fragment hits, which calls for the cross-validation of fragment screening results by an orthogonal method as recommended in widely accepted screening protocols.[71] Practically, each biophysical method of fragment screening is known to lead to occasionally significantly

different sets of hits. The overlap between the sets of hits originating from several mutually orthogonal methods embodies, as a rule, the most reliable validated hit set.

Biochemical methods of fragment screening capitalize on the function of the target of interest. A robust biochemical assay can be especially helpful not only for functional validation of hits coming from biophysical screening, but also due to its scalability and automatization, which is indispensable for screening of analogues during the optimization campaigns. Additional advantages include relatively low protein amount required and low frequency of artifacts. Nevertheless, a significant drawback of biochemical method lies in their relatively high activity detection thresholds, which can result in impossibility to detect or validate weak fragment binders.

The combination of biophysical and biochemical screening approaches can enable discovery of allosteric modulators of enzymes and receptors.

Whole-cell fragment screening. This approach was used to discover and optimize potent antibacterial compounds demonstrating activity against *S. aureus*[72] and various strains of *M. tuberculosis.*[73] This methodology, in contrast to target-based methods, allows selecting for the chemotypes already possessing whole-cell activity, which can abolish or significantly facilitate optimization steps ensuring the penetration through the bacterial cell envelope right from the start. However, owing to relatively weak target affinities fragments do not necessarily display detectable whole-cell activity. The whole-cell screening approach therefore implies selecting for highly active fragments possessing good bacterial cell wall penetration.

In silico fragment screening – computational methods.

Generally, owing to the small size and intrinsically low affinity of fragments, docking is known to be not particularly efficient for finding reliable binding poses of fragments.[74] Nevertheless, given the high-quality target structural data, *in silico* methods can be instrumental in finding hot spots for fragment binding and guiding fragment-to-lead optimization.[75],[76]

Methods of fragment hit elaboration.

Fragment's potency optimization. As fragment hits act as anchors for subsequent derivatization, they can be optimized by modification of their structural elements in a manner similar to that in conventional medicinal chemistry. The most straightforward way would rely on the structural data, while the "blind" optimization is also possible using parallel synthesis and NMR.[77]

Fragment growing implies progressive addition of groups to the original fragment hit structure and, as a consequence, extending it to establish new polar and hydrophobic interactions within the target's binding site. Structural information can be extremely useful for efficient and successful fragment growing.[46]

Fragment linking implies connection of hits' molecules occupying different and non-conjunctive portions of target's binding site. This strategy thus capitalizes on the concept of su-

peradditivity, which postulates the affinity of the linked inhibitor to be greater than the affinity derived from simple addition of binding energy of fragments to be linked.[78] Owing to relatively low occurrence of simultaneous occupation of a binding site by multiple fragments, linking is used quite rarely in comparison to other hit elaboration approaches. Recent comprehensive summary of linking strategies with their successful application in drug discovery is provided in recent reviews.[79],[63]

Fragment merging signifies making an improved binder by unifying the structures of fragments, which bind to overlapping subsites within a binding site or interface of the target. This strategy was suggested to produce more efficient leads since no restrictions imposed by linker design were needed.[46]

Efficiency metrics. In order to assess the efficiency of ligand binding and hit elaboration steps, several concepts based on normalization of binding by size were proposed. One of them is ligand efficiency $LE = -\ln(K_d)/N$, where K_d is the apparent dissociation constant, N – non-hydrogen atom count.[80] On the basis of ligand efficiency and presumption of ligand's ionization insignificance, the ligand lipophilicity efficiency index expressed as $LLE = -\log(K_d) - clogP$ can be used as an alternative to LE as LLE normalizes binding affinity by either calculated logP or logD, which allows to keep track of the ligand's lipophilicity during development.[81] Finally, antibacterial ligand efficiency metrics, as a variation of LE, is based on MIC values obtained in whole-cell screening and calculated as $LE_{ab} = -\ln(MIC[\mathrm{mg/ml}])/N$.[82] Generally, higher ligand efficiency implies greater potential for further development: a typical cut-off value above which the lead is considered worth further development is 0.3. Although the concept of ligand efficiency has been used as a rule of thumb in multiple drug discovery programs,[83] its meaning in terms of physical chemistry has been the subject for debate. A critical review and in-depth analysis of aforementioned concepts has been provided by Peter Kenny.[83]

1.5 Recent advances of Fragment-based approach to antibacterial drug discovery

Several reviews summarizing successful applications of fragment-based approaches to the discovery of antibacterials have been published: recently, reviews devoted to mycobacterial targets and targets relevant to combating *P. aeruginosa* were published by Togre *et al.*[84] and Arif *et al.*,[85] respectively. Simultaneously, a general review featuring the fragment-based discovery of new antibacterials and not concentrated on any particular type of bacteria was last published in 2018.[86] Therefore, here we are providing a short overview of published results from frag-

ment-based drug discovery programs aimed at discovering antibacterial compounds and addressing various types of targets since the start of 2018.

- *Protein-protein interactions in bacteria*. Due to the intrinsic challenge of tackling PPIs with fragments and challenges related to antibacterial drug discovery the number of reports that describe fragment-based targeting PPIs in this context is low. Apart from previously discussed fragment-based discovery of inhibitors of the PPI between the β-clamp and various DNA-polymerases (which is also the subject of this work), only one more PPI was addressed using fragment-based design so far. This is the interaction between bacterial RNA-primase DnaG and the single-strand binding protein (SSB). The work by Oakley *et al*.[87] disclosed a handful of fragments, that were shown to bind DnaG by protein- and ligand observed NMR techniques. The humble SAR by catalogue effort capitalizing on compound **1.5.1** allowed for the discovery of slightly improved binders **1.5.2** and **1.5.3** (**Figure 20**), that provide starting points for further elaboration.

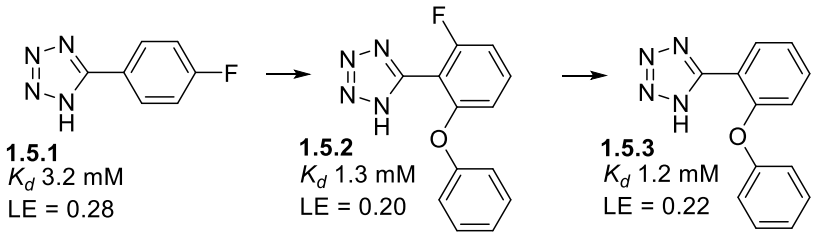

Figure 20. Graphical summary of fragment optimization undertaken in the work by Oakley *et al*.[87]

A recent review by Barnard *et al*. summarizes the progress in discovery of PPI inhibitors to fight bacteria.[88]

- *Bacterial protein synthesis machinery (RNA translation).*

Although the antibiotic discovery had successfully addressed RNA translation machinery (ca. 60% of approved antibiotics have different regions of the bacterial ribosome as their main target),[89] the record on fragment-based efforts to discover novel translation inhibitors is relatively scarce.

The work by Akabayov *et al*.[90] described the discovery of *in vitro* inhibitors of bacterial protein synthesis targeting ribosomal peptidyl transferase center using fragment-based approach. A fragment library was screened using NMR (T_2-relaxation measurement), the most prominent hit **1.5.4** were used for subsequent structure-based virtual screening using ZINC database, which yielded thiazoles **1.5.5** and **1.5.6** showing low micromolar activity *in vitro* (**Fig**. **21**).

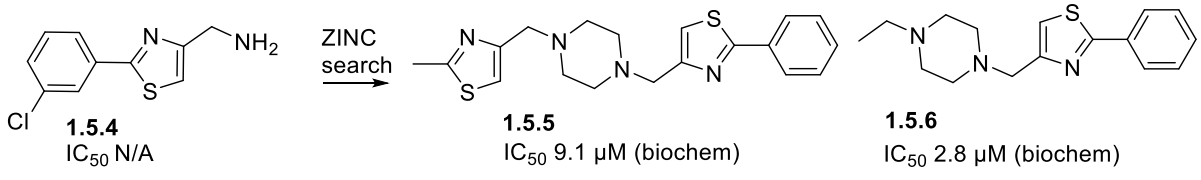

Figure 21. Hit optimization efforts from the work by Akabayov *et al.*[90]

The *in vitro* activity of discovered inhibitors presumably did not translate into any activity in cell-based assays as no antibacterial activity was reported.

Bacterial metabolic enzymes.

As a rule, the majority of metabolic enzymes are known to have well-defined, compact binding sites, which makes fragment binding better detectable and increases the chances for successful co-crystallization, which is crucial for fragment elaboration.

Fragment-based discovery of phosphopantetheine adenylyl transferase (PPAT) inhibitors without[91] and with moderate antibacterial activity[92] was described in two consecutive papers from Novartis. By employing fragment screening using DSF and highly sensitive biochemical assay, a number of unique scaffolds capable of binding to the pantetheine site of *E. coli* PPAT were discovered. The cross-validation using ligand-observed NMR combined with limited expansion of the cross-validated sublibrary yielded 125 hits, of which 39 furnished high-quality X-ray structural data.[91]

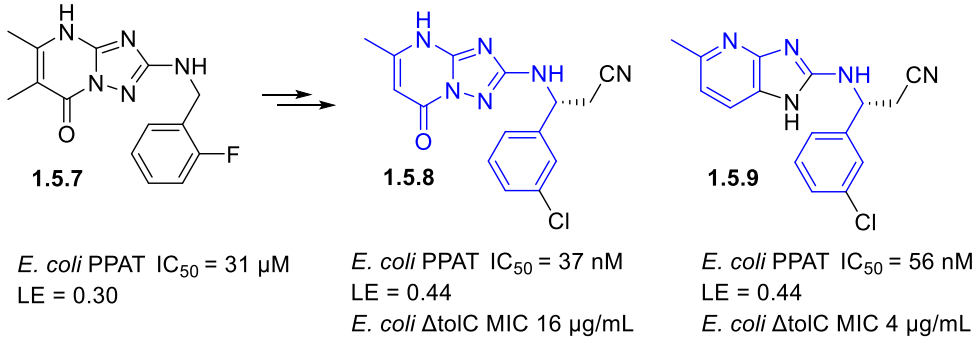

Figure 22 Schematic representation of optimization of initial fragment **6.**[91]

Further structure-based optimization of **1.5.7** (**Figure 22),** which was chosen on the basis of initial potency and binding efficiency, yielded compound **1.5.8** with a nanomolar activity on target and modest cellular potency against an efflux-deficient *E. coli* strain**.** The scaffold-hopping suggested by another crystallized fragment from screening gave **1.5.9**, which while having comparable target inhibition showed 4-fold increase in potency against the same *E. coli* strain.

Subsequent extensive elaboration of triazolopyrimidine **1.5.8** aimed at conferring cellular activity against wild-type *E. coli* led to the grown derivative **1.5.10**, which demonstrated excellent on-target activity together with weak yet measurable potency against wild-type *E. coli* (MIC 32 μg/mL ≈ 64 μM, **Figure 23**).[92] Simultaneously, the 4-azabenzimidazolic lead **1.5.9** was optimized into a less compact yet more efficient compound **1.5.11**, that showed comparable activity to **1.5.10** against wild-type *E. coli*.

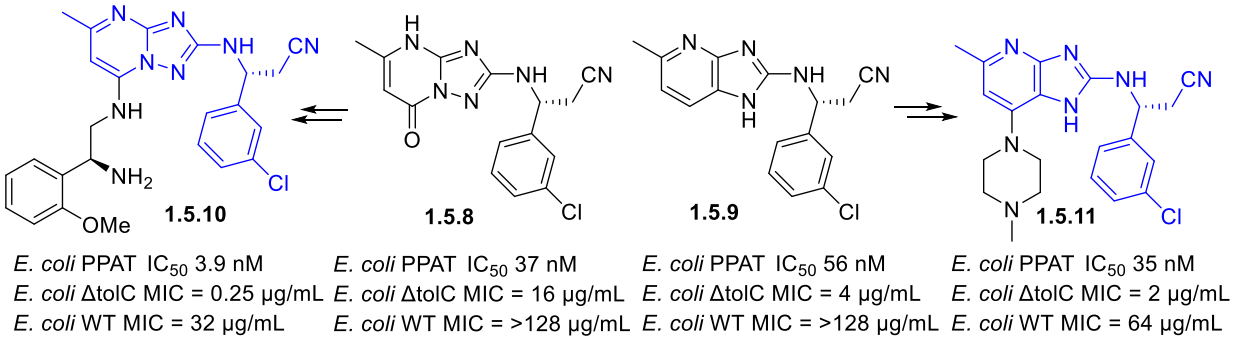

Figure 23. Summary of elaboration of fragments **3** and **4** undertaken by Moreau *et al.*[92]

Interestingly**,** analogues based on 4-azabenzimidazole scaffold were demonstrated to be more permeable through the inner membrane of *E. coli* using MS-based metabolomics assay and various *E. coli* knockout strains.[92] Unfortunately, the possibilities for further optimization of either lead structure were exhausted and therefore sufficient level of potency against *E. coli* could not be obtained, which precluded further development of the aforementioned leads.

The fragment-based effort to target *M. tuberculosis* inosine monophosphate dehydrogenase (IMPDH) was described in the paper by Trapero *et al.*[93] Authors employed a biochemical assay and screened a 960-membered fragment library against a highly identical l target protein from *M. thermoresistibile*, which yielded 18 hits (2% hit rate). The subsequent structure-based fragment growing and linking of the sole hit **1.5.12** validated by crystallography gave a family of inhibitors with enhanced potency, from which compound **1.5.13** shows marked 1300-fold biochemical potency improvement.

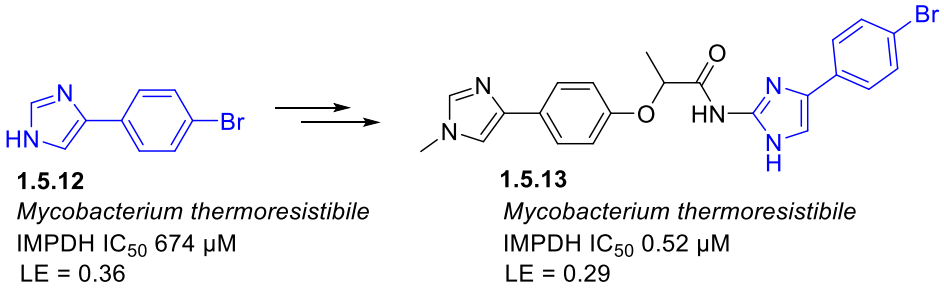

Figure 24. Schematic representation of fragment elaboration conducted in work by Trapero *et al.*[93]

Submicromolar on-target potency of elaborated fragments was, however, not translated into any antimycobacterial activity.

A fragment-based effort to identify efficient inhibitors of *M. abscessus* tRNA (m^1G37) methyltransferase TrmD was undertaken by Coyne *et al.*[94]

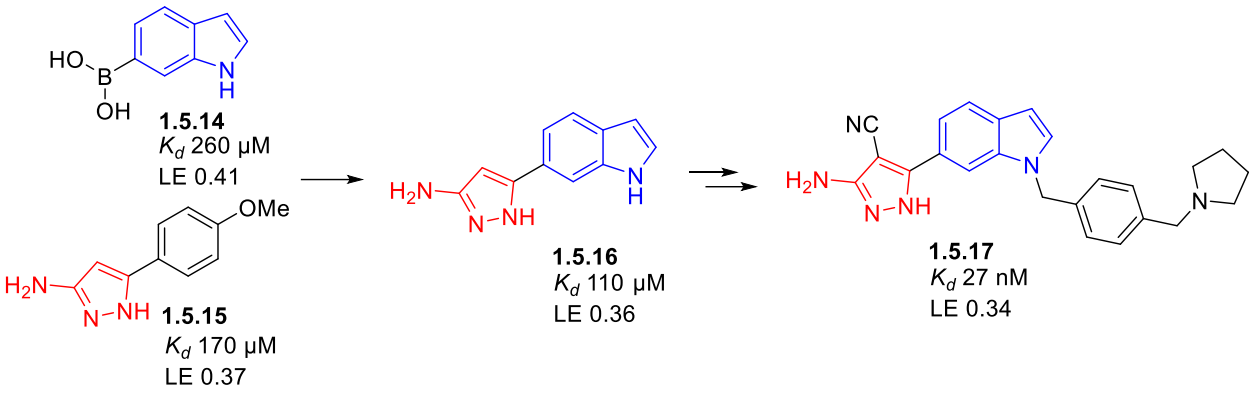

Figure 25. Merging and optimization of fragment TrmD inhibitors from work by Coyne *et al.*[94]

The internal library consisting of 960 fragments was screened using DSF as a primary method yielding 53 hits, 27 of which were validated by X-ray crystallography (2.8% hit rate). The two most efficient fragment binders **1.5.14** and **1.5.15** were elaborated by structure-guided merging (**1.5.16**) and growing into a nanomolar inhibitor **1.5.17** (**Figure 25**), which exhibited considerable antimycobacterial activity (MIC *Mycobacterium abscessus* 50 μM, *M. tuberculosis* 2.3–100 μM) at various growing conditions as well as against *M. abscessus* and *M. leprae* in a human macrophage infection model. The observed data demonstrated the potential utility of the optimized series against Mycobacteria and provided multiple starting points for further attempts of anitubercular drug discovery and development.

Novel bacterial dihydrofolate reductase inhibitors were discovered using fragment-based approach in the work by Ribeiro *et al.*[95] The DSF screen of 1250 members of fragment library, followed by the validation using STD-NMR yielded 21 hits (1.7% hit rate), which were additionally profiled using ITC. Of the validated hits, compound **1.5.18** was found to be binding in the *M. tuberculosis* DHFR pocket, distinguishing it from the human counterpart and by performing SAR by catalogue, low micromolar inhibitors (IC_{50} up to 17 μM for **1.5.19**) were identified (**Figure 26**).

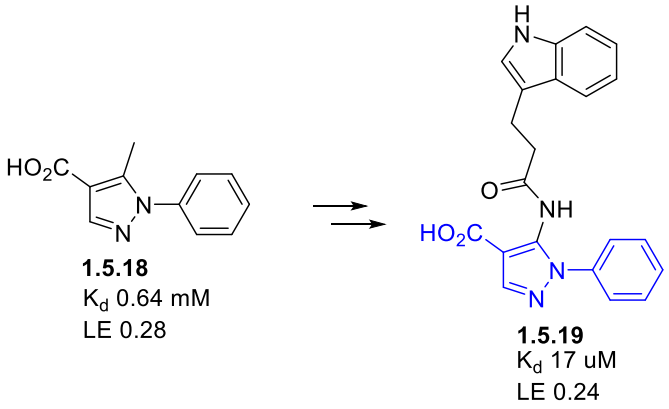

Figure 26. Schematic elaboration of fragment hit **1.5.18** featured in work by Ribeiro *et al.* [95]

For the elaborated fragments, no antibacterial activity had unfortunately been reported. Nevertheless, this work was the first fragment-based campaign approaching MtDHFR ever reported and to identify novel highly efficient binding scaffolds with development potential.[95]

The work describing the discovery of inhibitors of *P. aeruginosa* zinc metalloenzyme UDP-3-*O*-acyl-B-acetylglucosamine deacetylase LpxC catalyzing the first step in the biosynthesis of Lipid A, was published by Hubbard *et al*.[96] The library consisting of 1152 fragments was screened using ligand-observed NMR, yielding 252 primary hits, of which 28 were validated using NMR-based competition experiments and FP-assay (2.4% hit rate). Supported by modeling and X-ray crystallography, a glycine-based fragment **1.5.20** was elaborated into the lead **1.5.21** that showed low-nanomolar activity in a functional assay and retained high ligand efficiency. Its outstanding *in vitro* performance did not, however, translate into antibacterial activity (**Fig. 27, a**).

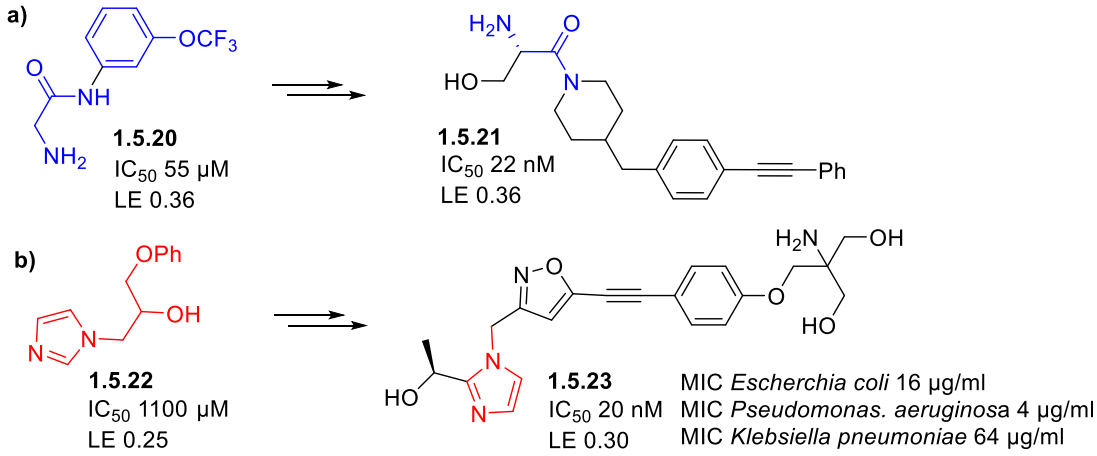

Figure 27. Schematic representation of **a)** Optimization and growing of fragment **6**; **b)** Optimization and growing of fragment **9** from work by Hubbard *et al*.[96]

The development of the imidazole fragment hit **1.5.22** proved more efficient: the lead structure **1.5.23** showed considerable activity against various Gram-negative pathogens (Fig. **27, b**) with minimal HSA influence. Thus, the advanced lead **1.5.23** was submitted for advanced *in vivo* efficacy studies.[96]

The work disclosing the inhibitors of mycobacterial mycocyclosin synthase CYP121A1 elaborated from fragment starting points was published by Blundell *et al*.[97] After approbation of the new approach to fragment screening (X-ray crystallography combined with phenotypic screening) on a focused moderately sized screening set of 36 fragment-like compounds, several of them showed good activity against wild-type *M. tuberculosis*. The hit **1.5.24** was elaborated based on its distinct binding mode, which is essential for the selectivity over other CYP proteins.

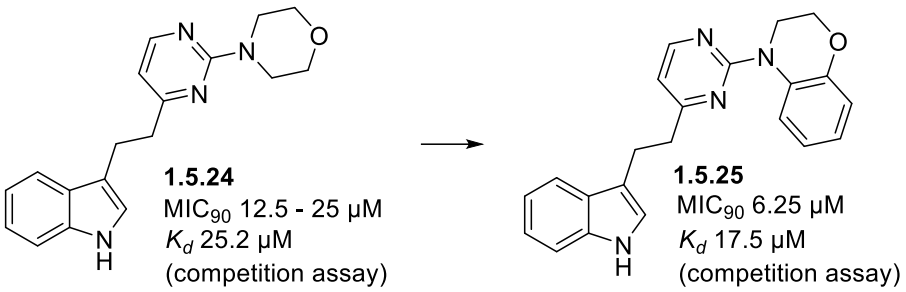

Figure 28. Optimization of mycocyclosin synthase inhibitors undertaken in the work by Blundell *et al.*[97]

The optimized compound **1.5.25** showed improved whole-cell activity against *M. tuberculosis* and presented good opportunities for further development.

Recently, the fragment-based approach was applied to discover novel inhibitors of Uridine Diphosphate-*N*-acetylenolpyruvylglucosamine Reductase (MurB), an enzyme catalyzing a critical step in the bacterial peptidoglycan biosynthesis from *P. aeruginosa*.[98] The initial hits were discovered by screening a dedicated 960-member fragment library using DSF, that gave nine molecules (0.9% hit rate), of which only the arylpyrazole derivative **1.5.26** gave an X-ray crystal structure. (**Figure 29**)

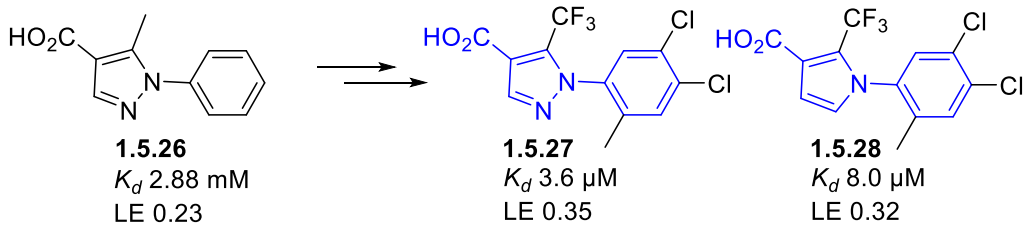

Figure 29. Optimization of MurB inhibitors from *Pseudomonas aeruginosa* undertaken in the work by Blundell *et al.*[98]

As a result of iterative establishment of SAR, compounds **1.5.27** and **1.5.28** were obtained as optimized leads that could potentially be starting points for further development into antibacterial candidates.

More recently, the team of Tom Blundell presented their work discovering selective inhibitors of mycobacterial SAICAR synthase (PurC), a crucial metabolic enzyme catalyzing a step in the biosynthesis of inosine monophosphate (IMP) – an intermediate in the *de novo* purine biosynthesis pathway known to be vital for bacterial growth.[99]

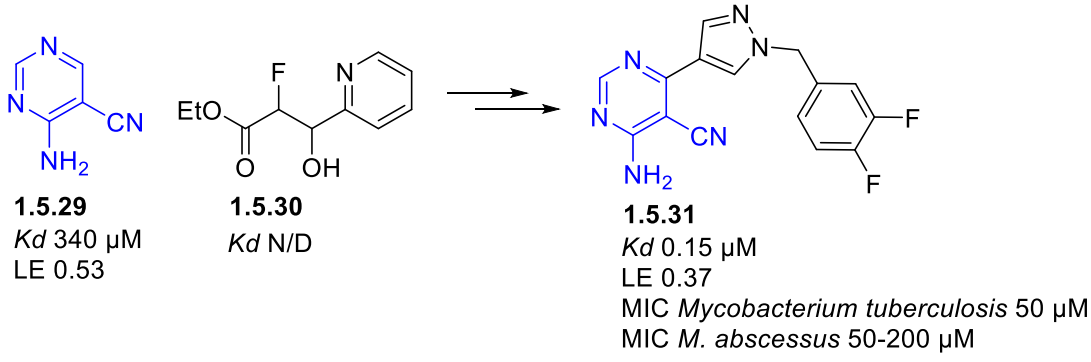

Figure 30. Elaboration of PurC inhibitors from work by Blundell *et al*.[99]

The authors used the combination X-ray crystallography and DSF for primary fragment screening and found two most potent hits occupying slightly different binging pockets in the enzyme (compounds **1.5.29** and **1.5.30** in **Figure 30**). Structure-based optimization and merging of the fragments eventually gave rise to compound **1.5.31,** which showed good biochemical potency yet proved insufficiently active against *M. abscessus* and *M. tuberculosis* (**Figure 30**).

Overall, a plethora of validated antibacterial targets were addressed with fragments, which yielded highly potent and efficient lead inhibitors. However, the majority of discovered molecules failed to demonstrate broad-spectrum antibacterial properties showing either not detectable or strain-limited activity. These results therefore highlight challenges associated with development of fragment-derived leads into potent antibiotics, which can be attributed to the low membrane permeability and/or adaptive efflux mechanisms inherent to Gram-negative and Mycobacteria. However, lead molecules discovered as a result of certain fragment-based programs provide ample room for further optimization of physicochemical properties, that can in the end lead to antibacterial activity.[92],[96]

1.6 Imidazolium salts as antibacterials

Quaternary ammonium salts (QAC's) are known for their biocidal properties since the fifth decade of the 20th century with benzalkonium chloride being the first commercial example of such an agent. A plethora of comprehensive reviews covered the diversity of chemical structures and biological activity of different kinds of QAC's in general, the most recent and comprehensive being the review by Vereshchagin *et al*.[100]

The major mechanism of antibacterial action of this class of agents is believed to involve electrostatic interactions with negatively charged bacterial cell wall components, which impairs the integrity of bacterial cell membranes.[101] Another possible mechanism – complexation and aggregation with intracellular component of bacteria. QAC's were long believed to not cause the development of resistance in bacteria; however, the first plausible evidence of such resistance/adaptation was obtained[102],[103] and involves the development and overexpression of speci-fic efflux transporters presented on bacterial cell membranes.

1.6.1 Plain imidazolium small-molecule salts as antibacterials.

Plain alkylmidazolium salts are known to be ionic liquids. One of the first imidazolium salts were synthesized and assessed as antibacterials by Pernak *et al*.[104] In this work, the antibacterial and antifungal effects of a library comprised of various 1-alkyl-3-alkylthiomethylimidazolium chlorides was found to linearly correlate with the compounds' hy-

drophobicity index and critical micelle concentration. The follow-up communication by the same authors[105] disclosed the structures of previously mentioned imidazolium salts (**Figure 31**).

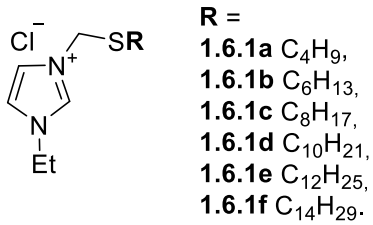

Figure 31. The common structure of imidazolium antiseptics featured in the work by Pernak *et al*.[105]

The imidazolium salt **1.6.1d** (**R** = *n*-$C_{10}H_{21}$) showed the peak performance against a representative panel of microorganisms with MIC values of 8, 10 and 8 μM in cases of *S. aureus*, *K. pneumoniae* and the fungus *Serratia marcescens*, respectively.

Another class of imidazolium ionic liquids as antibacterials was presented in the work by Demberelnyamba *et al.* (**Figure 32**).[106]

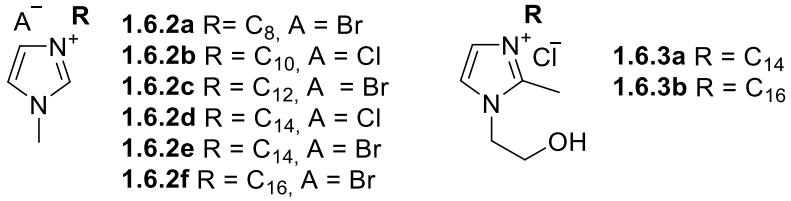

Figure 32. Two classes of imidazolium biocidal molecules from the work by Demberelnyamba *et al*.[106]

Compounds **1.6.2d–f** were found to perform best against bacteria and fungi alike, which indicated the optimal length of the alkyl substituent to be 14–16 carbon atoms. **1.6.2d** and **1.6.2e** showed no difference in MIC values against virtually all bacterial strains tested (corresponding MIC values varied between 4 and 8 μM against various *Staphylococci*, *B. subtilis* and *E. coli*), which had also demonstrated the independence of performance on the nature of the anion.

The class of 3-alkylated 1-hydroxyethyl-2-methyl imidazolium salts, in spite of carrying optimal-length 3-alkyl chains, was proven to be 2–8 times less efficient against the same bacterial strains.

Alkylated imidazolium salts with a biodegradable linker (**Figure 33**) were described by Morrissey *et al*.[107]

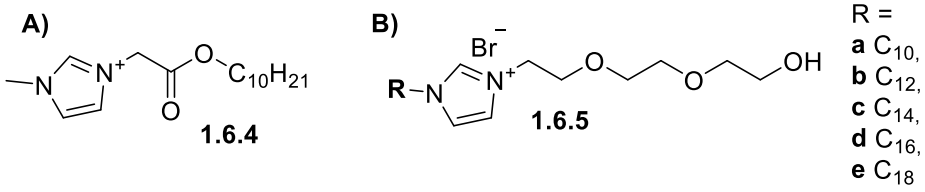

Figure 33. **A)** Imidazolium biocide with a degradable linker described in the work by Morrisey *et al*.[107]; **B)** Imidazolium biocide equipped with a triethyleneglycol moiety described by Huang *et al*.[108]

Compound **1.6.4** was the only one found to modestly inhibit bacterial growth (*S. aureus* and *E. coli*_MIC ≈700 μM) from the library with linear ester's alkyl length ranging from C_4 to C_{10}.

Imidazolium salts functionalized by triethylene glycol were described by Huang *et al*.[108] These compounds were studied for liquid-crystal properties and were also found to be bacteriostatic and bactericidal at various concentrations. Among the studied derivatives ones carrying tetradecyl and hexadecyl alkyl groups (**1.6.5c, d**) were found to perform best against Gram-positive (MIC up to 1 μM against *S. aureus*) and Gram-negative bacteria (MIC as low as 8 μM against *E. coli* and 89 μM against *P. aeruginosa*, respectively). The corresponding bactericidal concentrations were found to be 5–10 times higher.

The analysis of antibacterial performance of different instances of 1,3-dialkyl substituted imidazolium salts indicated the optimal length of the hydrophobic alkyl tail to be 12–16 carbon atoms. Imidazole-based ionic liquids equipped with alkyl substituents of appropriate lengths show relatively high activity against Gram-negative and positive bacteria.

1.6.2 Amide linker-containing imidazolium salts

Following the trend of developing more environmentally benign and biodegradable QAC's,[109] 1-Methylimidazolium salts with appended peptide motifs were described by Coleman and coworkers (**Figure 34, A**).[110] A library of compounds carrying various alkyl substituents at designated positions was synthesized and tested against a diverse set of pathogenic bacteria and fungi. A single dipeptide containing certain amino acids (Phe, R = Bn; Leu, R^1 = iPr; R^2 = Et) was found conducive to antibacterial activity mainly against *S. aureus* (MIC 500 μM) and, surprisingly, against methicillin-resistant *S. aureus* (MIC 125 μM), while other derivatives demonstrated only marginal activity against other bacteria (MIC ≥ 2000 μM). Nevertheless, no speculation on this phenomenon as well as on possible action mechanism of peptide-containing ionic liquids was made by authors of the study.

Another example of antibacterial imidazolium salts containing amino acid residues was described by Valls *et al*[111]. A set of corresponding monotopic and ditopic quaternary imidazolium salts (**Figure 34, B**) was synthesized and tested against *E. coli* and *B. subtilis*.

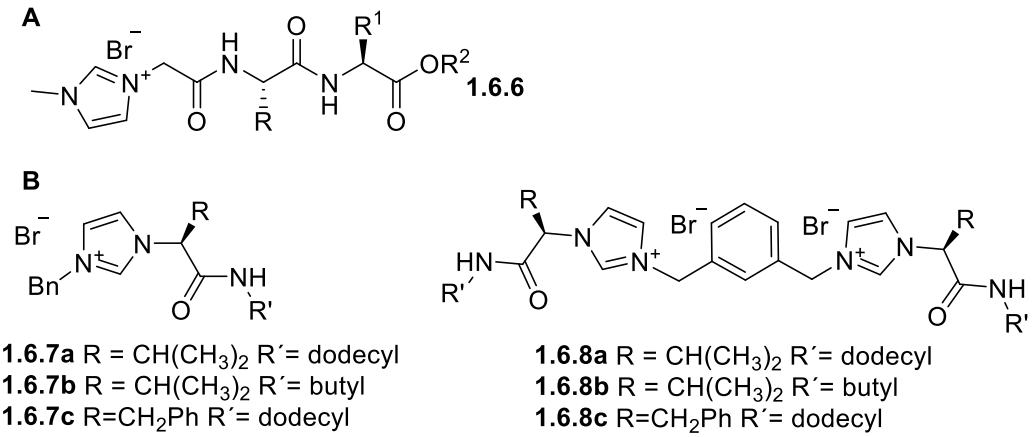

Figure 34. **A)** Imidazolium biocide with an appended tripeptide motif described by Coleman *et al.*[110]; **B)** Mono- and diimidazolium-based biocides containing peptide motifs from the work by Valls *et al.*[111]

More lipophilic monotopic salts **1.6.7a** and **1.6.7.c** were found to be more active against *B. subtilis* (MIC ≈8 μM for both compounds) and expectably much less active against *E. coli* (MIC ≈256 and ≈64 μM, respectively). The analogously substituted ditopic salts **1.6.8a** and **1.6.8c** showed in general 2-4 times weaker activity, which is in accordance with their lower membrane permeability due to higher molecular charge.

Overall, the efficiency of imidazolium salts equipped with peptide-like substituents as antibacterials is considerably lower compared to 1,3-dialkylimidazolic salts probably owing to decreased hydrophobicity caused by peptide bonds.

1.6.3 Imidazolium salts with fused cycles as antimicrobials

Antibacterial and antifungal action of imidazole-containing fused ring systems was first described by Demchenko *et al.*[112]

Alkylated benzimidazolium salts are active against certain bacterial species. The work of Pernak[113] describes the following quaternized benzimidazoles and their antibacterial and antifungal activities (**Figure 35**).

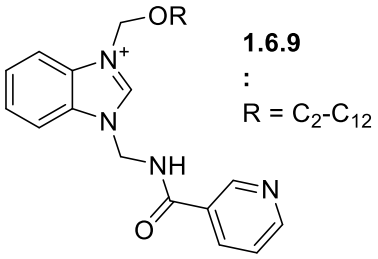

Figure 35. Common structure of benzimidazolium antibacterials discovered by Pernak *et al.*[113]

Among the alkylated benzimidazolic analogues compounds **2h–j** were demonstrated to have the highest activity against Gram-positive (*S. aureus* MIC 280–130 μM, *Enterococcus faecalis* MIC 70–34 μM) and some Gram-negative bacteria (*E. coli* and *K. pneumoniae* MICs 1100–530 μM), rendering *n*-C_9-C_{11} substituting chains on such a scaffold optimal.

Arylated imidazolium quaternary salts with antibacterial and antifungal properties were described in a work by Demchenko.[114] The compounds contained an *N*-arylated imidazolium moiety fused with an aza-cycloheptane ring (**Figure 36**).

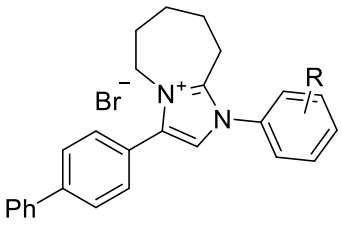

1.6.10a R = H;
1.6.10b R = 4-CH_3;
1.6.10c R = 4-C_2H_5;
1.6.10d R = 2-OCH_3.

Figure 36. General structure of *N*-arylated compounds containing imidazolium and aliphatic fused rings in the work by Demchenko *et al.*[114]

The described compounds showed activity only against *S. aureus* (MIC 4-32 μg/mL) combined with relatively high cytotoxicity (HEK293 IC_{50} 2 μg/mL), which in all cases exceeded the antimicrobial activity.

5H-pyrrolo[1,2-a]imidazole quaternary salts

The similar *N*-alkylated imidazolium salts were synthesized and found to demonstrate antibacterial activity in another work by Demchenko *et al.*[115] The simplest representative of the series 1-benzyl-4-phenyl-pyrroloimidazolinium chloride **1.6.11** (**Figure 37, A**) proved inactive against bacteria, which supported the hypothesis, that antibacterial activity is not endowed solely by the presence of the positively charged fused imidazole ring in the structure.

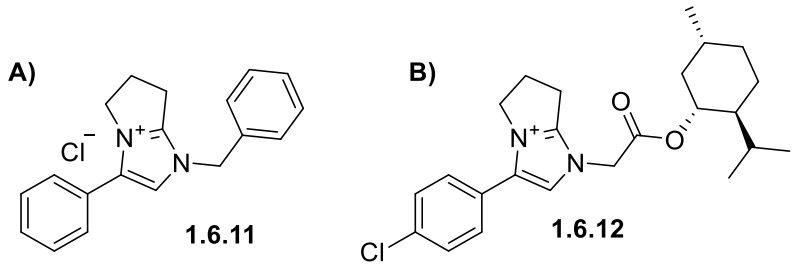

Figure 37. **A)** Fused 1-benzyl-4-arylimidazolium salt **1.6.11**; **B)** An alkylated pyrroloimidazolium salt with an acetate linker **1.6.12** (both from the work by Demchenko *et al.*).[115]

The acylated levomenthol derivative **1.6.12** demonstrated only limited activity against *S. aureus* and fungus *Cryptococcus neoformans* with MIC 17.7 and 70.9 μM, respectively. Along with that, this compound showed relatively high cytotoxicity with an IC_{50} value in HEK-293 cells of about 8 μM.

Appending the acylamide linker to the imidazolic core had been found to significantly improve antibacterial and cytotoxic profile of the fused imidazolic scaffold. The antibacterial SAR of a small library of analogues (**Figure 38**) was explored by changing substituents on the phenyl ring adjacent to the imidazole moiety.

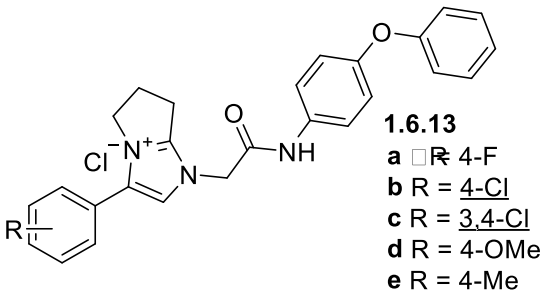

Figure38. Acetamide library showing distinct SAR from work by Demchenko *et al.*[115]

Overall, this type of imidazolium salts turned out to be active against Gram-positive and Gram-negative strains alike. The best activities were achieved for *para*-Cl (**1.6.13b**) and 3,4-diCl (**1.6.13c**) derivatives, that demonstrated MIC values as low as 8 μM against *S. aureus*, but were moderately active against *E. coli* and *K. pneumoniae* with MIC values of 31 and 15.5 μM, respectively. At the same time the cytotoxicity of **1.6.13b** and **1.6.13c** was considerably lower than the reported MIC values.

5H-imidazo[1,2-a]azepines quaternary salts

In addition to pyrazolinoimidazoles **1.6.11-13**, a library of analogues with an enlarged aliphatic part of the imidazole-containing fused ring system was disclosed.[115] The simplest benzylated azepine derivative **1.6.14** (**Figure 39**) showed no activity similarly to compound **4.**

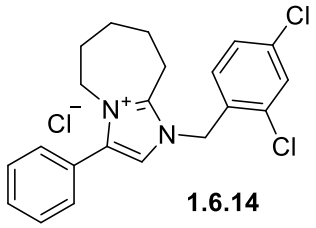

Figure 39. Azepinoimidazolic salt **1.6.14** described by Demchenko *et al.*[115]

By direct analogy to compound **1.6.12**, acylated menthol **1.6.16** (**Figure 40**) only showed activity against *S. aureus* (MIC 17 μM), which was accompanied by high cytotoxicity with IC_{50} (HEK-293) of 3 μM.

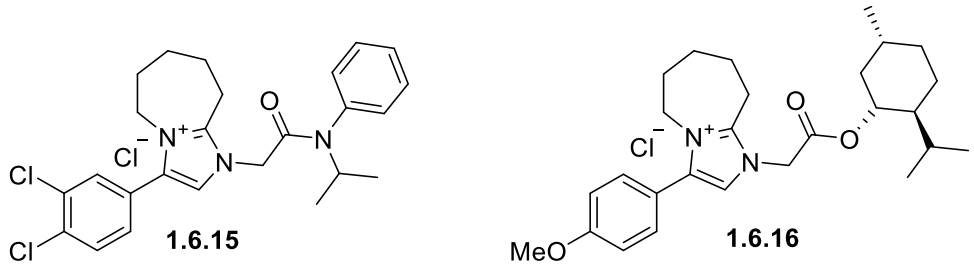

Figure 40. Azepinoimidazolic salts equipped with acetamide (11) and acetate (12) linkers.[115]

The acetamide **1.6.15** showed only marginal antibacterial activity against *S. aureus* with an MIC value of 74 μM rendering the 3,4-diCl substitution pattern on the 4-phenyl ring not favorable for activity. Simultaneously, for alkylated series showed on **Figure 41** antibacterial SAR was established.

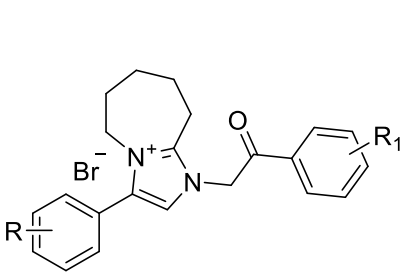

1.6.17
a R = H, R_1 = 2-$OCHF_2$;
b R = H, R_1 = 4-i-Pr;
c R = H, R_1 = 4-OPh;
d R = 4-F, R_1 = 4-cyclohexane;
e R = 4-Cl, R_1 = 4-cyclohexane;
f R = 3,4-Cl_2, R_1 = 4-Br;
g R = H, R_1 = 4-Me;
h R = 3,4-Cl_2, R_1 = 4-OMe.

Figure 41. N-alkylated azepinoimidazolic salts with various substitutions from work [115].

Among these molecules, relationship between the anti-staphylococcal activity and the character of substitution was established suggesting the derivatives **1.6.17d** and **1.6.17e** equipped with cyclohexyl and halogens to be the optimal with (*S. aureus* MIC values of 8 and 4 μM respectively). However, in spite of comparable antibacterial activities of **1.6.17d** and **1.6.17e** to their counterparts **1.6.17b** and **1.6.17c,** the toxicity of azepine derivatives was considerably higher reaching the level of 10 μM.

Despite good activity against Gram-positive bacteria, both classes of fused imidazolium compounds showed very low activity against such Gram-negative strains such as *E. coli*, *K. pneumoniae* and *A. baumannii* and the absence of activity against *P. aeruginosa*. This supports the strong dependence of the antibacterial effect on the permeability of compounds through the bacterial cell wall or efflux rate, which are typically impaired or upregulated in Gram-negative species. Structurally related compounds are also known to have certain antifungal activity.[112],[115]

All research items featuring the antibacterial activity of imidazolium salts were found either focused on preparation of fused ring structures or non-systematic description of their apparent antibacterial activity. It is also worth noting that fused imidazolium salts featured in this review were not discovered and optimized in the context of target-based discovery.

The scaffolds including imidazolium-based fused ring systems are relatively new and not largely represented in literature. Nevertheless, certain combinations of pyrrolinoimidazolic system with acetamide linker were recently shown to possess significant activity against *S. aureus* and *E. coli* and exhibit some antibacterial SAR when combined with fairly hydrophobic aromatic amines.[115] The possible mechanism of action of this class of compounds however remains unkown.

Simultaneously, the inclusion of the imidazolium salt motif into otherwise non-penetrating inhibitors of relevant antibacterial targets was shown to enhance the penetration and retention of compounds in bacteria and significantly increase compound's cell activity.[116] Therefore, the discovery of DnaN ligands that include imidazolium motif seems an appealing approach to enhancing the antibacterial activity of potent target binders. Additionally, owing to ancillary action

mechanism common to all QACs, this can potentiate the overall antibiotic action of thereby modified candidate molecules and potentially mitigate the risk of resistance development.

2 Aim of the Thesis

Emergence of multi- and extensively antibiotic resistant strains of common pathogenic bacteria (ESKAPE pathogens, Mycobacteria) as an outcome of persistent use of antibiotics has become new reality for global healthcare system posing an existential threat of losing effective means for bacterial infection control. In view of this, the necessity of intensification of research efforts aiming at discovering novel antibiotic molecules with unprecedented action mechanisms becomes urgent. Among the most attractive mechanisms are those exploiting bacterial targets, which do not have immediate analogues in eukaryotic cells, since this allows to greatly reduce the risk of toxicity. The bacterial β-sliding clamp (DnaN) can be considered a promising target to address in this context as its orthologue in eukaryotic cells shares miniscule similarity to its prokaryotic counterpart.

Recently, at the Helmholtz Institute for Pharmaceutical Research Saarland (HIPS) molecular basis of the mechanism of action of the natural product griselimycin (**GM**) was established and pharmaceutical properties of **GM** were extensively studied.[23] Furthermore, this research effort generated high-quality structural data for *M. tuberculosis* DnaN that could be employed for modeling support of drug discovery efforts as the mycobacterial β-sliding clamp has not hitherto been targeted by small molecule inhibitors.

More recently, the in-house structure-based virtual screening was carried out on the Princeton compound library using pharmacophore constrains derived from the co-crystal structure of **CGM** and *M. tuberculosis* DnaN (PDB: 5AGU). As a result, among a handful of promising VS hits the imidazolium compound **WAM-N17** demonstrated binding to its target combined with good activity against various Mycobacteria and certain ESKAPE pathogens.

Lately, the fragment-sized binders of *M. tuberculosis* DnaN were found by in-house screening of the commercial Maybridge Ro3 library. Particular fragment hits showed appreciable DnaN binding together with antimycobacterial activity, which rendered them attractive starting points for further elaboration.

In view of aforementioned developments, the present thesis has the following objectives:

1. Chemical space exploration based on the structure of a previously discovered fragment class and optimization of its β-clamp binding and antibacterial activity.
2. Development of a robust synthetic route for SAR establishment around the scaffold of compound **WAM-N17** and its multiparameter optimization.

References

[1] L. B. Rice, *J. Infect. Dis.* **2008**, *197*, 1079–1081.

[2] E. Tacconelli, E. Carrara, A. Savoldi, S. Harbarth, M. Mendelson, D. L. Monnet, C. Pulcini, G. Kahlmeter, J. Kluytmans, Y. Carmeli, M. Ouellette, K. Outterson, J. Patel, M. Cavaleri, E. M. Cox, C. R. Houchens, M. L. Grayson, P. Hansen, N. Singh, U. Theuretzbacher, N. Magrini, A. O. Aboderin, S. S. Al-Abri, N. Awang Jalil, N. Benzonana, S. Bhattacharya, A. J. Brink, F. R. Burkert, O. Cars, G. Cornaglia, O. J. Dyar, A. W. Friedrich, A. C. Gales, S. Gandra, C. G. Giske, D. A. Goff, H. Goossens, T. Gottlieb, M. Guzman Blanco, W. Hryniewicz, D. Kattula, T. Jinks, S. S. Kanj, L. Kerr, M. P. Kieny, Y. S. Kim, R. S. Kozlov, J. Labarca, R. Laxminarayan, K. Leder, L. Leibovici, G. Levy-Hara, J. Littman, S. Malhotra-Kumar, V. Manchanda, L. Moja, B. Ndoye, A. Pan, D. L. Paterson, M. Paul, H. Qiu, P. Ramon-Pardo, J. Rodríguez-Baño, M. Sanguinetti, S. Sengupta, M. Sharland, M. Si-Mehand, L. L. Silver, W. Song, M. Steinbakk, J. Thomsen, G. E. Thwaites, J. W. van der Meer, N. Van Kinh, S. Vega, M. V. Villegas, A. Wechsler-Fördös, H. F. L. Wertheim, E. Wesangula, N. Woodford, F. O. Yilmaz, A. Zorzet, *Lancet Infect. Dis.* **2018**, *18*, 318–327.

[3] M. O. A. Sommer, C. Munck, R. V. Toft-Kehler, D. I. Andersson, *Nat. Rev. Microbiol. 2017 1511* **2017**, *15*, 689–696.

[4] M. Terreni, M. Taccani, M. Pregnolato, *Molecules* **2021**, *26*, DOI 10.3390/molecules26092671.

[5] M. A. Kohanski, D. J. Dwyer, J. J. Collins, *Nat. Rev. Microbiol. 2010 86* **2010**, *8*, 423–435.

[6] A. Robinson, R. J. Causer, N. E. Dixon, *Curr. Drug Targets* **2012**, *13*, 352–372.

[7] A. J. Oakley, *Protein Sci.* **2019**, *28*, 990–1004.

[8] N. A. Tanner, G. Tolun, J. J. Loparo, S. Jergic, J. D. Griffith, N. E. Dixon, A. M. Van Oijen, *EMBO J.* **2011**, *30*, 1830–1840.

[9] J. B. Vivona, Z. Kelman, *FEBS Lett.* **2003**, *546*, 167–172.

[10] M. A. Argiriadi, E. R. Goedken, I. Bruck, M. O'Donnell, J. Kuriyan, *BMC Struct. Biol.* **2006**, *6*, 1–6.

[11] K. A. Bunting, S. M. Roe, L. H. Pearl, *EMBO J.* **2003**, *22*, 5883–5892.

[12] W. J. Gui, S. Q. Lin, Y. Y. Chen, X. E. Zhang, L. J. Bi, T. Jiang, *Biochem. Biophys. Res. Commun.* **2011**, *405*, 272–277.

[13] D. Jeruzalmi, M. O'Donnell, J. Kuriyan, *Cell* **2001**, *106*, 429–441.

[14] X. P. Kong, R. Onrust, M. O'Donnell, J. Kuriyan, *Cell* **1992**, *69*, 425–437.

[15] Z. Kelman, *Oncogene* **1997**, *14*, 629–640.

[16] I. Moarefi, D. Jeruzalmi, J. Turner, M. O'Donnell, J. Kuriyan, *J. Mol. Biol.* **2000**, *296*,

1215–1223.

[17] S. Acharya, A. Dahal, H. K. Bhattarai, *PLoS One* **2021**, *16*, 1–17.

[18] P. Wolff, V. Oliéric, J. P. Briand, O. Chaloin, A. Dejaegere, P. Dumas, E. Ennifar, G. Guichard, J. Wagner, D. Y. Burnouf, *J. Med. Chem.* **2011**, *54*, 4627–4637.

[19] C. D. Aakre, T. N. Phung, D. Huang, M. T. Laub, *Mol. Cell* **2013**, *52*, 617–628.

[20] Z. Yin, M. J. Kelso, J. L. Beck, A. J. Oakley, *J. Med. Chem.* **2013**, *56*, 8665–8673.

[21] P. Wolff, I. Amal, V. Oliéric, O. Chaloin, G. Gygli, E. Ennifar, B. Lorber, G. Guichard, J. Wagner, A. Dejaegere, D. Y. Burnouf, *J. Med. Chem.* **2014**, *57*, 7565–7576.

[22] C. André, I. Martiel, P. Wolff, M. Landolfo, B. Lorber, C. Silva Da Veiga, A. Dejaegere, P. Dumas, G. Guichard, V. Oliéric, J. Wagner, D. Y. Burnouf, *ACS Infect. Dis.* **2019**, *5*, 1022–1034.

[23] A. Kling, P. Lukat, D. V. Almeida, A. Bauer, E. Fontaine, S. Sordello, N. Zaburannyi, J. Herrmann, S. C. Wenzel, C. König, N. C. Ammerman, M. B. Barrio, K. Borchers, F. Bordon-Pallier, M. Brönstrup, G. Courtemanche, M. Gerlitz, M. Geslin, P. Hammann, D. W. Heinz, H. Hoffmann, S. Klieber, M. Kohlmann, M. Kurz, C. Lair, H. Matter, E. Nuermberger, S. Tyagi, L. Fraisse, J. H. Grosset, S. Lagrange, R. Müller, *Science (80-.).* **2015**, *348*.

[24] B. P. Dalrymple, K. Kongsuwan, G. Wijffels, N. E. Dixon, P. A. Jennings, *Proc. Natl. Acad. Sci. U. S. A.* **2001**, *98*, 11627–11632.

[25] N. Lenne-Samuel, J. Wagner, H. Etienne, R. P. P. Fuchs, *EMBO Rep.* **2002**, *3*, 45–49.

[26] G. Wijffels, B. P. Dalrymple, P. Prosselkov, K. Kongsuwan, V. C. Epa, P. E. Lilley, S. Jergic, J. Buchardt, S. E. Brown, P. F. Alewood, P. A. Jennings, N. E. Dixon, *Biochemistry* **2004**, *43*, 5661–5671.

[27] J. Liu, M. Dehbi, G. Moeck, F. Arhin, P. Banda, D. Bergeron, M. Callejo, V. Ferretti, N. Ha, T. Kwan, J. McCarty, R. Srikumar, D. Williams, J. J. Wu, P. Gros, J. Pelletier, M. DuBow, *Nat. Biotechnol.* **2004**, *22*, 185–191.

[28] G. Wijffels, W. M. Johnson, A. J. Oakley, K. Turner, V. C. Epa, S. J. Briscoe, M. Polley, A. J. Liepa, A. Hofmann, J. Buchardt, C. Christensen, P. Prosselkov, B. P. Dalrymple, P. F. Alewood, P. A. Jennings, N. E. Dixon, D. A. Winkler, *J. Med. Chem.* **2011**, *54*, 4831–4838.

[29] C. André, F. Veillard, P. Wolff, A. M. Lobstein, G. Compain, C. Monsarrat, J. M. Reichhart, C. Noûs, D. Y. Burnouf, G. Guichard, J. E. Wagner, *RSC Chem. Biol.* **2020**, *1*, 137–147.

[30] C. Monsarrat, G. Compain, C. André, S. Engilberge, I. Martiel, V. Oliéric, P. Wolff, K. Brillet, M. Landolfo, C. Silva Da Veiga, J. Me Wagner, G. Guichard, D. Y. Burnouf, *J.*

Med. Chem. **2021**, acs.jmedchem.1c00918.

[31] A. Nedal, S. B. Ræder, B. Dalhus, E. Helgesen, R. J. Forstrøm, K. Lindland, B. K. Sumabe, J. H. Martinsen, B. B. Kragelund, K. Skarstad, M. Bjørås, M. Otterlei, *Nucleic Acids Res.* **2020**, *48*, 5540–5554.

[32] C. K. Søgaard, A. Blindheim, L. M. Røst, V. Petrović, A. Nepal, S. Bachke, N.-B. Liabakk, O. A. Gederaas, T. Viset, C.-J. Arum, P. Bruheim, M. Otterlei, C. Krogh Søgaard, A. Blindheim, L. M. Røst, V. Petrović, A. Nepal, S. Bachke, N.-B. Liabakk, O. A. Gederaas, T. Viset, C.-J. Arum, P. Bruheim, M. Otterlei, *Oncotarget* **2018**, *9*, 32448–32465.

[33] A. A. Patoli, J. A. Winter, K. A. Bunting, *BMC Struct. Biol.* **2013**, *13*, 1–13.

[34] S. B. Raeder, E. T. Sandbakken, A. Nepal, K. Løseth, K. Bergh, E. Witsø, M. Otterlei, *Front. Microbiol.* **2021**, *12*, 565.

[35] A. Nepal, S. B. Ræder, C. K. Søgaard, M. S. Haugan, M. Otterlei, *Front. Microbiol.* **2021**, *12*, 3515.

[36] C. P. Scott, E. Abel-Santos, M. Wall, D. C. Wahnon, S. J. Benkovic, *Proc. Natl. Acad. Sci. U. S. A.* **1999**, *96*, 13638–13643.

[37] S. Kjelstrup, P. M. P. Hansen, L. E. Thomsen, P. R. Hansen, A. Løbner-Olesen, *PLoS One* **2013**, *8*, e72273.

[38] B. Terlain, J. P. Thomas, *Bull. Soc. Chim. Fr.* **1971**, *6*, 2349–56.

[39] L. Silvian, I. Enyedy, G. Kumaravel, *Drug Discov. Today Technol.* **2013**, *10*, e509–e515.

[40] R. E. Georgescu, O. Yurieva, S. S. Kim, J. Kuriyan, X. P. Kong, M. O'Donnell, *Proc. Natl. Acad. Sci. U. S. A.* **2008**, *105*, 11116–11121.

[41] Z. Yin, L. R. Whittell, Y. Wang, S. Jergic, M. Liu, E. J. Harry, N. E. Dixon, J. L. Beck, M. J. Kelso, A. J. Oakley, *J. Med. Chem.* **2014**, *57*, 2799–2806.

[42] Z. Yin, Y. Wang, L. R. Whittell, S. Jergic, M. Liu, E. Harry, N. E. Dixon, M. J. Kelso, J. L. Beck, A. J. Oakley, *Chem. Biol.* **2014**, *21*, 481–487.

[43] Z. Yin, L. R. Whittell, Y. Wang, S. Jergic, C. Ma, P. J. Lewis, N. E. Dixon, J. L. Beck, M. J. Kelso, A. J. Oakley, *J. Med. Chem.* **2015**, *58*, 4693–4702.

[44] P. Pandey, V. Verma, G. Gautam, N. Kumari, S. K. Dhar, S. Gourinath, *FEBS Lett.* **2017**, *591*, 2311–2322.

[45] F. Mancini, M. Y. Unver, W. A. M. Elgaher, V. R. Jumde, A. Alhayek, P. Lukat, J. Herrmann, M. D. Witte, M. Köck, W. Blankenfeldt, R. Müller, A. K. H. Hirsch, *Chem. – A Eur. J.* **2020**, chem.202002250.

[46] D. E. Scott, A. G. Coyne, S. A. Hudson, C. Abell, *Biochemistry* **2012**, *51*, 4990–5003.

[47] F. Giordanetto, C. Jin, L. Willmore, M. Feher, D. E. Shaw, *J. Med. Chem.* **2019**, *62*,

3381–3394.

[48] M. Congreve, R. Carr, C. Murray, H. Jhoti, *Drug Discov. Today* **2003**, *8*, 876–877.

[49] H. Jhoti, G. Williams, D. C. Rees, C. W. Murray, *Nat. Rev. Drug Discov. 2013 128* **2013**, *12*, 644–644.

[50] G. M. Keseru, D. A. Erlanson, G. G. Ferenczy, M. M. Hann, C. W. Murray, S. D. Pickett, *J. Med. Chem.* **2016**, *59*, 8189–8206.

[51] H.-D. Junker, H. Aalen, T. Neumann, H.-D. Junker, K. Schmidt, R. Sekul, *Curr. Top. Med. Chem.* **2007**, *7*, 1630–1642.

[52] C. A. Shepherd, A. L. Hopkins, I. Navratilova, *Prog. Biophys. Mol. Biol.* **2014**, *116*, 113–123.

[53] R. E. Hubbard, J. B. Murray, *Experiences in Fragment-Based Lead Discovery*, Elsevier Inc., **2011**.

[54] F. H. Niesen, H. Berglund, M. Vedadi, *Nat. Protoc. 2007 29* **2007**, *2*, 2212–2221.

[55] G. Senisterra, I. Chau, M. Vedadi, *Assay Drug Dev. Technol.* **2012**, *10*, 128–136.

[56] S. A. I. Seidel, C. J. Wienken, S. Geissler, M. Jerabek-Willemsen, S. Duhr, A. Reiter, D. Trauner, D. Braun, P. Baaske, *Angew. Chemie Int. Ed.* **2012**, *51*, 10656–10659.

[57] P. Linke, K. Amaning, M. Maschberger, F. Vallee, V. Steier, P. Baaske, S. Duhr, D. Breitsprecher, A. Rak, *J. Biomol. Screen.* **2016**, *21*, 414–421.

[58] S. B. Shuker, P. J. Hajduk, R. P. Meadows, S. W. Fesik, *Science (80-.).* **1996**, *274*, 1531–1534.

[59] C. R. Buchholz, W. C. K. Pomerantz, *RSC Chem. Biol.* **2021**, *2*, 1312–1330.

[60] M. Mayer, B. Meyer, *Angew. Chemie - Int. Ed.* **1999**, *38*, 1784–1788.

[61] C. Raingeval, O. Cala, B. Brion, M. Le Borgne, R. E. Hubbard, I. Krimm, *J. Enzyme Inhib. Med. Chem.* **2019**, *34*, 1218–1225.

[62] M. Mayer, B. Meyer, *J. Am. Chem. Soc.* **2001**, *123*, 6108–6117.

[63] A. Bancet, C. Raingeval, T. Lomberget, M. Le Borgne, J. F. Guichou, I. Krimm, *J. Med. Chem.* **2020**, *63*, 11420–11435.

[64] E. E. Swayze, E. A. Jefferson, K. A. Sannes-Lowery, L. B. Blyn, L. M. Risen, S. Arakawa, S. A. Osgood, S. A. Hofstadler, R. H. Griffey, *J. Med. Chem.* **2002**, *45*, 3816–3819.

[65] F. Riccardi Sirtori, D. Caronni, M. Colombo, C. Dalvit, M. Paolucci, L. Regazzoni, C. Visco, G. Fogliatto, *Eur. J. Pharm. Sci.* **2015**, *76*, 83–94.

[66] H. Vu, L. Pedro, T. Mak, B. McCormick, J. Rowley, M. Liu, A. Di Capua, B. Williams-Noonan, N. B. Pham, R. Pouwer, B. Nguyen, K. T. Andrews, T. Skinner-Adams, J. Kim, W. G. J. Hol, R. Hui, G. J. Crowther, W. C. Van Voorhis, R. J. Quinn, *ACS Infect. Dis.*

2018, *4*, 431–444.

[67] W. H. J. Ward, G. A. Holdgate, *Prog. Med. Chem.* **2001**, *38*, 309–376.

[68] C. M. Johnson, *Methods Mol. Biol.* **2021**, *2263*, 135–159.

[69] J. Schiebel, N. Radeva, S. G. Krimmer, X. Wang, M. Stieler, F. R. Ehrmann, K. Fu, A. Metz, F. U. Huschmann, M. S. Weiss, U. Mueller, A. Heine, G. Klebe, *ACS Chem. Biol.* **2016**, *11*, 1693–1701.

[70] J. P. Renaud, A. Chari, C. Ciferri, W. T. Liu, H. W. Rémigy, H. Stark, C. Wiesmann, *Nat. Rev. Drug Discov.* **2018**, *17*, 471–492.

[71] E. H. Mashalidis, P. Śledå, S. Lang, C. Abell, *Nat. Protoc. 2013 811* **2013**, *8*, 2309–2324.

[72] D. J. Haydon, N. R. Stokes, R. Ure, G. Galbraith, J. M. Bennett, D. R. Brown, P. J. Baker, V. V. Barynin, D. W. Rice, S. E. Sedelnikova, J. R. Heal, J. M. Sheridan, S. T. Aiwale, P. K. Chauhan, A. Srivastava, A. Taneja, I. Collins, J. Errington, L. G. Czaplewski, *Science (80-.).* **2008**, *321*, 1673–1675.

[73] K. Andries, P. Verhasselt, J. Guillemont, H. W. H. Göhlmann, J. M. Neefs, H. Winkler, J. Van Gestel, P. Timmerman, M. Zhu, E. Lee, P. Williams, D. De Chaffoy, E. Huitric, S. Hoffner, E. Cambau, C. Truffot-Pernot, N. Lounis, V. Jarlier, *Science (80-.).* **2005**, *307*, 223–227.

[74] M. L. Verdonk, I. Giangreco, R. J. Hall, O. Korb, P. N. Mortenson, C. W. Murray, *J. Med. Chem.* **2011**, *54*, 5422–5431.

[75] L. R. de Souza Neto, J. T. Moreira-Filho, B. J. Neves, R. L. B. R. Maidana, A. C. R. Guimarães, N. Furnham, C. H. Andrade, F. P. Silva, *Front. Chem.* **2020**, *8*, 93.

[76] M. Bissaro, M. Sturlese, S. Moro, *Drug Discov. Today* **2020**, *25*, 1693–1701.

[77] P. J. Hajduk, J. Dinges, J. M. Schkeryantz, D. Janowick, M. Kaminski, M. Tufano, D. J. Augeri, A. Petros, V. Nienaber, P. Zhong, R. Hammond, M. Coen, B. Beutel, L. Katz, S. W. Fesik, *J. Med. Chem.* **1999**, *42*, 3852–3859.

[78] W. P. Jencks, *Proc. Natl. Acad. Sci.* **1981**, *78*, 4046–4050.

[79] E. V. Bedwell, W. J. McCarthy, A. G. Coyne, C. Abell, *Chem. Biol. Drug Des.* **2022**, *100*, 469–486.

[80] A. L. Hopkins, C. R. Groom, A. Alex, *Drug Discov. Today* **2004**, *9*, 430–431.

[81] P. D. Leeson, B. Springthorpe, *Nat. Rev. Drug Discov. 2007 611* **2007**, *6*, 881–890.

[82] L. G. Czaplewski, I. Collins, E. A. Boyd, D. Brown, S. P. East, M. Gardiner, R. Fletcher, D. J. Haydon, V. Henstock, P. Ingram, C. Jones, C. Noula, L. Kennison, C. Rockley, V. Rose, H. B. Thomaides-Brears, R. Ure, M. Whittaker, N. R. Stokes, *Bioorg. Med. Chem. Lett.* **2009**, *19*, 524–527.

[83] P. W. Kenny, *J. Cheminform.* **2019**, *11*, 1–18.

[84] N. S. Togre, A. M. Vargas, G. Bhargavi, M. K. Mallakuntla, S. Tiwari, *Int. J. Mol. Sci.* **2022**, *23*, DOI 10.3390/ijms231810669.

[85] S. M. Arif, R. A. Floto, T. L. Blundell, *Front. Mol. Biosci.* **2022**, *9*, 248.

[86] B. Lamoree, R. E. Hubbard, *SLAS Discov.* **2018**, *23*, 495–510.

[87] Z. Chilingaryan, S. J. Headey, A. T. Y. Lo, Z. Q. Xu, G. Otting, N. E. Dixon, M. J. Scanlon, A. J. Oakley, *Antibiot. 2018, Vol. 7, Page 14* **2018**, *7*, 14.

[88] R. Kahan, D. J. Worm, G. V. De Castro, S. Ng, A. Barnard, *RSC Chem. Biol.* **2021**, *2*, 387–409.

[89] J. Lin, D. Zhou, T. A. Steitz, Y. S. Polikanov, M. G. Gagnon, *https://doi.org/10.1146/annurev-biochem-062917-011942* **2018**, *87*, 451–478.

[90] B. Tam, D. Sherf, S. Cohen, S. A. Eisdorfer, M. Perez, A. Soffer, D. Vilenchik, S. R. Akabayov, G. Wagner, B. Akabayov, *Chem. Sci.* **2019**, *10*, 8764–8767.

[91] R. J. Moreau, C. K. Skepper, B. A. Appleton, A. Blechschmidt, C. J. Balibar, B. M. Benton, J. E. Drumm, B. Y. Feng, M. Geng, C. Li, M. K. Lindvall, A. Lingel, Y. Lu, M. Mamo, W. Mergo, V. Polyakov, T. M. Smith, K. Takeoka, K. Uehara, L. Wang, J. R. Wei, A. H. Weiss, L. Xie, W. Xu, Q. Zhang, J. De Vicente, *J. Med. Chem.* **2018**, *61*, 3309–3324.

[92] C. K. Skepper, R. J. Moreau, B. A. Appleton, B. M. Benton, J. E. Drumm, B. Y. Feng, M. Geng, C. Hu, C. Li, A. Lingel, Y. Lu, M. Mamo, W. Mergo, M. Mostafavi, C. M. Rath, M. Steffek, K. T. Takeoka, K. Uehara, L. Wang, J. R. Wei, L. Xie, W. Xu, Q. Zhang, J. De Vicente, *J. Med. Chem.* **2018**, *61*, 3325–3349.

[93] A. Trapero, A. Pacitto, V. Singh, M. Sabbah, A. G. Coyne, V. Mizrahi, T. L. Blundell, D. B. Ascher, C. Abell, *J. Med. Chem.* **2018**, *61*, 2806–2822.

[94] A. J. Whitehouse, S. E. Thomas, K. P. Brown, A. Fanourakis, D. S. H. Chan, M. D. J. Libardo, V. Mendes, H. I. M. Boshoff, R. A. Floto, C. Abell, T. L. Blundell, A. G. Coyne, *J. Med. Chem.* **2019**, *62*, 7210–7232.

[95] J. A. Ribeiro, A. Hammer, G. A. Libreros-Zúñiga, S. M. Chavez-Pacheco, P. Tyrakis, G. S. De Oliveira, T. Kirkman, J. El Bakali, S. A. Rocco, M. L. Sforça, R. Parise-Filho, A. G. Coyne, T. L. Blundell, C. Abell, M. V. B. Dias, *ACS Infect. Dis.* **2020**, *6*, 2192–2201.

[96] Y. Yamada, H. Takashima, D. L. Walmsley, F. Ushiyama, Y. Matsuda, H. Kanazawa, T. Yamaguchi-Sasaki, N. Tanaka-Yamamoto, J. Yamagishi, R. Kurimoto-Tsuruta, Y. Ogata, N. Ohtake, H. Angove, L. Baker, R. Harris, A. Macias, A. Robertson, A. Surgenor, H. Watanabe, K. Nakano, M. Mima, K. Iwamoto, A. Okada, I. Takata, K. Hitaka, A. Tanaka, K. Fujita, H. Sugiyama, R. E. Hubbard, *J. Med. Chem.* **2020**, *63*, 14805–14820.

[97] M. Frederickson, I. R. Selvam, D. Evangelopoulos, K. J. McLean, M. M. Katariya, R. B.

Tunnicliffe, B. Campbell, M. E. Kavanagh, S. Charoensutthivarakul, R. T. Blankley, C. W. Levy, L. P. S. de Carvalho, D. Leys, A. W. Munro, A. G. Coyne, C. Abell, *Eur. J. Med. Chem.* **2022**, *230*, 114105.

[98] M. Acebrón-Garciá-De-Eulate, J. Mayol-Llinàs, M. T. O. Holland, S. Y. Kim, K. P. Brown, C. Marchetti, J. Hess, O. Di Pietro, V. Mendes, C. Abell, R. A. Floto, A. G. Coyne, T. L. Blundell, *J. Med. Chem.* **2022**, *65*, 2149–2173.

[99] S. Charoensutthivarakul, S. E. Thomas, A. Curran, K. P. Brown, J. M. Belardinelli, A. J. Whitehouse, M. Acebrón-García-de-Eulate, J. Sangan, S. G. Gramani, M. Jackson, V. Mendes, R. A. Floto, T. L. Blundell, A. G. Coyne, C. Abell, *ACS Infect. Dis.* **2022**, *8*, 296–309.

[100] A. N. Vereshchagin, N. A. Frolov, K. S. Egorova, M. M. Seitkalieva, V. P. Ananikov, *Int. J. Mol. Sci. 2021, Vol. 22, Page 6793* **2021**, *22*, 6793.

[101] X. Z. Li, H. Nikaido, *Drugs* **2004**, *64*, 159–204.

[102] J. M. Tennent, B. R. Lyon, M. Midgley, I. G. Jones, A. S. Purewal, R. A. Skurray, *J. Gen. Microbiol.* **1989**, *135*, 1–10.

[103] Y. Joon Chung, M. H. Saier, *J. Bacteriol.* **2002**, *184*, 2543–2545.

[104] B. M. B. Pernak, J., Skrypczak A., *Chem. Pharm. Bull.* **1995**, *43*, 2019–2020.

[105] J. Pernak, A. Skrzypczak, *Eur. J. Med. Chem.* **1996**, *31*, 901–903.

[106] D. Demberelnyamba, K. S. Kim, S. Choi, S. Y. Park, H. Lee, C. J. Kim, I. D. Yoo, *Bioorganic Med. Chem.* **2004**, *12*, 853–857.

[107] S. Morrissey, B. Pegot, D. Coleman, M. T. Garcia, D. Ferguson, B. Quilty, N. Gathergood, *Green Chem.* **2009**, *11*, 475–483.

[108] R. T. W. Huang, K. C. Peng, H. N. Shih, G. H. Lin, T. F. Chang, S. J. Hsu, T. S. T. Hsu, I. J. B. Lin, *Soft Matter* **2011**, *7*, 8392–8400.

[109] T. Thorsteinsson, M. Má, K. G. Kristinsson, M. A. Hjá, H. Hilmarsson, T. Loftsson, *J. Med. Chem.* **2003**, *46*, 4173–4181.

[110] D. Coleman, M. Špulák, M. T. Garcia, N. Gathergood, *Green Chem.* **2012**, *14*, 1350–1356.

[111] A. Valls, J. J. Andreu, E. Falomir, S. V. Luis, E. Atrián-Blasco, S. G. Mitchell, B. Altava, *Pharmaceuticals* **2020**, *13*, 1–17.

[112] and F. S. B. A. M. Demchenko, V. G. Sinchenko, N. G. Prodanchuk, V. A. Kovtunenko, V. K. Patratii, A. K. Tyltin, *Pharm. Chem. J.* **1987**, *21*, 789–791.

[113] J. Pernak, J. Rogoza, I. Mirska, *Eur. J. Med. Chem.* **2001**, *36*, 313–320.

[114] S. Demchenko, R. Lesyk, J. Zuegg, A. G. Elliott, Y. Fedchenkova, Z. Suvorova, A. Demchenko, *Eur. J. Med. Chem.* **2020**, *201*, 112477.

[115] S. Demchenko, R. Lesyk, O. Yadlovskyi, J. Zuegg, A. G. Elliott, I. Drapak, Y. Fedchenkova, Z. Suvorova, A. Demchenko, *Mol. 2021, Vol. 26, Page 4253* **2021**, *26*, 4253.

[116] S. J. Perlmutter, E. J. Geddes, B. S. Drown, S. E. Motika, M. R. Lee, P. J. Hergenrother, *ACS Infect. Dis.* **2020**, *7*, 162–173.

3 Structure–activity relationships exploration and optimization of a new class of bacterial β-sliding clamp inhibitors highly active against Gram-positive and mycobacterial pathogens

Uladzislau Hapko[1,2], Sari Rasheed[2], Walid Elgaher[1,2], Jennifer Herrmann[2], Peer Lukat[4], Norbert Reiling[3], Wulf Blankenfeldt[4], Rolf Müller[1,2], Anna K. H. Hirsch[1,2]

[1]Department of Pharmacy, Saarland University, Unversitätscampus C2.3, 66123 Saarbrücken, Germany
[2]Helmholtz Institute for Pharmaceutical Research Saarland, Unversitätscampus E8.1, 66123 Saarbrücken, Germany
[3]Forschungszentrum Borstel, Parkallee 1, 23845 Sülfeld, Germany
[4]Helmholtz Centre for Infection Research, Inhoffenstraße 7, 38124 Braunschweig, Germany

Abstract

Based on the structure of a recently discovered novel β-sliding clamp ligand, we report systematic structure-activity relationship exploration efforts around the discovered scaffold. DnaN binding of analogues was estimated by SPR and their functional activity was determined using an *E. coli* replisome assay. Optimized derivatives demonstrated high activity against Gram-positive and mycobacterial strains (MIC_{95} up to 2 and 8 μM, respectively), while activity against wild-type Gram-negative strains was observed at higher concentrations (64–128 μM). To guide further optimization, *in vitro* ADMET parameters of the most promising derivatives were determined.

3.1 Introduction

The emergence of multi- and extensively drug-resistant bacterial pathogens is becoming a serious threat for the global healthcare system, necessitating the discovery of new classes of antibiotics with novel modes of action.

The bacterial β-sliding clamp (DnaN) is a part of the Polymerase III holoenzyme, the multi-protein complex responsible for DNA replication in prokaryotes. DnaN serves as a processivity factor for DNA-polymerase III, assuring its firm attachment to DNA at the replication fork.[1] The β-sliding clamp is a homodimeric protein of circular shape capable of encircling double-stranded DNA.[2]

The possibility to inhibit the interaction between the β-sliding clamp and its binding partners DNA-polymerases renders the former a promising target for antibacterial drug discovery. DnaN is essential for cell viability and has a highly conserved structure in bacteria,[3] which is distinct from its homotrimeric counterpart found in eukaryotes called proliferating cell nuclear antigen (PCNA). Moreover, the rate of resistance development for the natural DnaN inhibitors (griselimycins) was shown to be low, accompanied by a high fitness cost.[4]

Therefore, DnaN has been the target in a number of hit discovery and optimization projects making use of various methods: high-throughput screening,[5] fragment-based drug discovery,[6][7] structure-based drug design[8],[9],[10],[11] and kinetic target-guided synthesis (KTGS).[12] However, the ligands discovered as a result of the aforementioned attempts either demonstrated no or only modest bacterial growth inhibitory activities or only proved to be highly active against particular strains.[8]

Here, we report the discovery of a novel class of bacterial DnaN–DNA-polymerase interaction inhibitor and feature a systematic structure-activity relationship (SAR) exploration and optimization around the discovered scaffold.

3.2 Results and discussion

3.2.1 Antibacterial properties and cytotoxicity screening

The original virtual screening hit **H1** had been extensively evaluated for its ability to bind the *Mycobacterium smegmatis* DnaN protein (Surface Plasmon Resonance (SPR), microscale thermophoresis (MST), and STD NMR spectroscopy), to disrupt the bacterial DNA replication (*in vitro* bacterial replisome assay) as well as for the ability to inhibit bacterial growth using a panel of various model microorganisms: *Mycobacterium smegmatis* MC^2155, *M. smegmatis* $MC^2155\ GM^R$ (DnaN-overexpressing mutant strain, resistant to griselimycin), *Streptococcus pneumoniae DSM20566, Staphylococcus aureus Newman, Escherichia coli ΔacrB, Pseudomonas aeruginosa PA14, Enterococcus faecium 20477,* and *Mycobacterium tuberculosis* H37Rv. Here, we rely on the same set of assays to assess the analogues' performance in the course of our optimization efforts.

H1 binds the *M. smegmatis* β-sliding clamp and is capable of inhibiting the *in vitro* replication with an IC_{50} value of 150 ± 30 μM**.** The initial hit also exerts a strong antibacterial effect in representative Gram-positive, Gram-negative and mycobacterial strains (MIC_{95} 8, 8, and 4 μM, respectively). The growth-inhibiting effect on the griselimycin-resistant *M. smegmatis* was expectedly weaker, which can be interpreted as an indirect evidence of the mechanism of action of this compound class. Along with that, the compound **H1** showed low cytotoxicity on the HepG2 cell line (IC_{50} 37 μM).

Even though a co-crystal structure of **H1** in complex with DnaN was not available at the beginning of this work, the structure of **H1** provided a good starting point for further step-by-step ligand-based SAR exploration and optimization, which is the focus of the present work.

3.2.2 SAR studies of the hit H1

To explore the qualitative SAR around the structure of **H1**, we hypothetically dissected it into several principal modules (see **Figure1**).

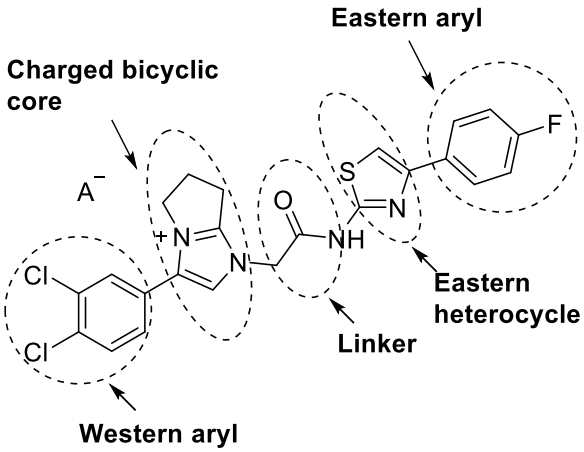

Figure 1. Different parts of **H1** addressed in the course of SAR establishment**.**

In the following SAR exploration, we addressed every module separately to establish its contribution to the sliding clamp binding and antibacterial activity.

3.2.2.1 Eastern phenyl

We addressed this part of the molecule first in the course of our SAR exploration. The replacements of the *para*-fluorine atom were inspired by the Topliss decision tree[13] and bioisosterism-driven phenyl ring substitutions (see Scheme **1** in the **SI**).

First, the original fluorine atom in the ring was removed to give **H2**, which was accompanied by a dramatic drop in activity in the replisome assay. However, the analogue **H2** had largely retained its antibacterial activity (see **Table 1**). The installation of the *–Cl* in *para*-position resulted in the 1.5-fold increase of biochemical potency, 2-fold increase of inhibitory activity on *M. smegmatis* and *M. tuberculosis* species. These gains were, however accompanied by an increase in cytotoxicity.

In parallel, we addressed other branches of the Topliss tree by synthesizing *para*-methoxy and methyl derivatives **H4** and **H5.** While activities against various strains of the **H4** and **H5** remained essentially similar to those of **H3**, both analogues demonstrated lower cytotoxicity and had slightly lower biochemical potencies compared to **H3**. The potency of **H5** in the replisome assay was slightly higher than that of **H4** (IC_{50} values were 130 and 160 μM respectively), which could be also a cause of a more pronounced ability of **H5** to inhibit the growth of *M. tuberculosis*.

The deviation from the expected outcome of the Topliss decision tree was observed during the optimization process: while the introduction of chlorine was supposed to improve the compound's activity (observed fact), the introduction of the methoxy-group (**H3**) would only be considered only if the drop in activity resulting from the introduction of chlorine had been observed. To prevent potential drawbacks and ensure all potential derivatives were considered, we chose to explore all branches of the Topliss tree.

Table 1. Results of introduction of electron-donating groups at the *para*-position of Eastern phenyl ring

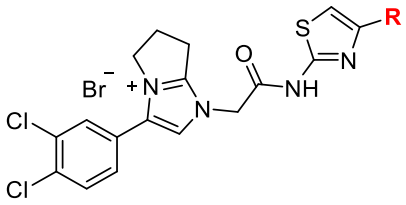

Name	R	SPR (*RU*)		Repl. Assay IC_{50} (*μM*)	MIC$_{95}$ (*μM*)					*MTb growth inh @16 μM, %*	*HepG2 IC_{50} (μM)*
		250 μM	1 mM		*M. smegmatis*	*M. smegmatis* GM^R	*S. pneumoniae*	*S. aureus*	*E. coli ΔacrB*		
H1	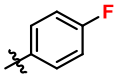	**26**	**	**150±30**	**4**	**16**	**16**	**8**	**8**	**43±30**	**37**
H2		**44**	**N/D**	**250±40**	**4**	**8**	**16**	**16**	**8**	**50±18**	**37**
H3	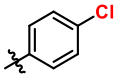	**	**	**100±20**	**2**	**8**	**4**	**4**	**8**	**80±14**	**12.3**
H4	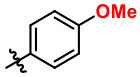	**56**	**N/D**	**160±30**	**2**	**8**	**16**	**8**	**8**	**80±10**	**37**
H5	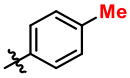	**	**	**130±30**	**2**	**8**	**8**	**4**	**8**	**90±1**	**37**
H6	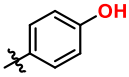	**38**	**N/D**	**260±50**	**8**	**16**	**16**	**16**	**8**	**96±1**	**>37**
H7	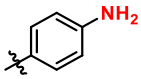	**N/D**	**N/D**	**60±10**	**8**	**16**	**64**	**16**	**4**	**0**	**>37**
H8	**-H**	**3**	**24**	**320±60**	**2**	**>128**	**>128**	**>128**	**>128**	**20±6**	**>37**

* - misbehavior on the SPR chip; ** - precipitation; N/D- no data.

Thus, in order to probe for possible effects associated with hydrogen bonding, we synthesized derivatives **H6** and **H7** bearing hydroxyl and amino moieties, respectively. In spite of differences in biochemical potencies of **H6** and **H7**, both derivatives demonstrated similarly diminished activity against the *M. smegmatis* and *S. pneumoniae* strains compared to **H1**. Simultaneously, the ability of the less biochemically potent analogue **H6** to inhibit the growth of *M. tuberculosis* turned out to be as high as 96% at 16 μM, while **H7** showed no inhibitory activity at all. This absence of correlation between biochemical potency and antitubercular properties could be attributed to the ionizability of the amino group in **H7** and difficulties of penetration through the cellular membrane of *M. tuberculosis* of highly charged molecular species.

The deletion of the whole Eastern phenyl ring had a detrimental effect on the overall performance: not only did the compound **H8** completely lose its binding to DnaN, but also its antibacterial activity. These observations, therefore, indicate the critical importance of this part of

the molecule and make a strong case for the target-associated antibacterial activity of the chemotype of interest.

As a complement to the modifications described above, we investigated the effect of the permutation of the fluorine substituent within the Eastern phenyl ring. The *ortho*- and *meta*- analogues **H10** and **H11**, respectively revealed the sensitivity of the replication inhibition towards the substitution of the *ortho*-position in the Eastern phenyl ring: the corresponding positional isomer **H10** demonstrated a significantly higher IC_{50} value in the biochemical assay (see **Table 2**). Simultaneously, the substitution of the *meta*-position with fluorine in **H11** did not affect the biochemical potency, while the effect of insertion of a larger chlorine in the same position in **H12** was comparable to that in **H10**. This rendered the *meta*-position moderately sensitive to the larger substituents with respect to the inhibition of replication.

Table 2. Results of modifications at *meta*- and *ortho*- positions of the Eastern phenyl ring.

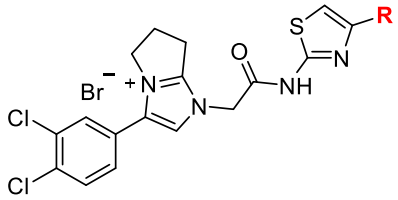

Name	R	SPR (*RU*)		Repl. assay IC_{50} (*μM*)	MIC$_{95}$ (*μM*)					*MTb* growth inh @16 μM, %	HepG2 IC_{50}. (*μM*)
		250 μM	1 mM		*M. smegmatis*	*M. smegmatis* GM^R	*S. pneumoniae*	*S. aureus*	*E. coli ΔacrB*		
H1	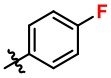	**26**	**	**150 ± 30**	**4**	**16**	**16**	**8**	**8**	**43±30**	**37**
H10		**165**	**	**220 ± 40**	**4**	**8**	**8**	**4**	**4**	**85±3**	**12.3**
H11	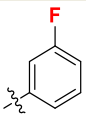	**165**	**	**150 ± 30**	**4**	**8**	**4**	**8**	**16**	**80±5**	**37**
H12	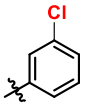	**	**	**250 ± 40**	**4**	**32**	**8**	**8**	**16**	**95±5**	**>37**

* - misbehavior on the SPR chip. ** - precipitation

The permutation of fluorine led to only modest improvement of growth inhibition of the GM-resistant *M. smegmatis* and *S. pneumoniae* strains (**Table 2**). The effect on the growth of *M. tuberculosis* was nevertheless more pronounced: both regioisomers demonstrated an almost two-fold increase of growth inhibition at 16 μM. Moreover, the enlargement of the substituent in **H12** ultimately resulted in 95% inhibition of *M. tuberculosis* growth. The absence of correlation between the biochemical potencies of **H11** and **H12** and their activity against *M. tuberculosis* could

be ascribed to a higher penetration ability of **H12** through the bacterial cell wall due to the compound's larger lipophilicity (cLogP of **H11** and **H12** are 1.42 and 1.99, respectively).

Regarding the toxicity of positional isomers, the *ortho*-fluoro pattern in **H10** accounted for significantly higher HepG2 cytotoxicity (IC_{50} 12.3 μM compared to ≥37 μM of **H1** and **H11**), making the *meta*-substitution of the ring more advantageous with regard to this parameter.

The introduction of strong π-electron-acceptor groups in *para*-position was found to be generally detrimental for either DnaN binding or antibacterial activity (see **H15-H19** in **Table 3**). Although the considerable enlargement of the substituent in **H13** led to a slight improvement of biochemical IC_{50}, which had no influence on the growth of most bacterial strains, the activity against *M. tuberculosis* was abolished despite the concomitant increase in lipophilicity.

Table 3. Results of introduction of electron-withdrawing groups in *para*-position of the Eastern phenyl ring.

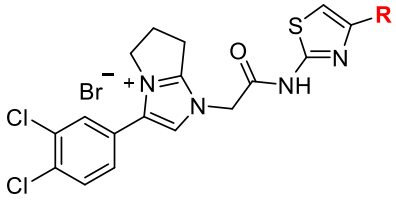

Name	R	SPR (*RU*)		Repl. assay IC_{50} (*μM*)	MIC_{95} (*μM*)					*MTb growth inh @16 μM, %*	HepG2 IC_{50} (*μM*)
		250 μM	1 mM		*M. smegmatis*	*M. smegmatis GMR*	*S. pneumoniae*	*S. aureus*	*E. coli ΔacrB*		
H1		**26**	**	**150 ± 30**	**4**	**16**	**16**	**8**	**8**	**43±30**	**37**
H13	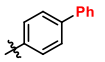	*	*	**120 ± 20**	**4**	**32**	**8**	**8**	**32**	**0**	**37**
H14	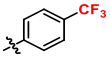	*	*	**110 ± 20**	**4**	**8**	**8**	**4**	**8**	**64±6**	**12.3**
H15	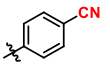	**21**	**N/D**	**140 ± 20**	**8**	**32**	**16**	**16**	**16**	**49±17**	**12.3**
H16	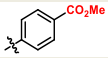	**	**	**N/D**	**8**	**16**	**8**	**8**	**8**	**12±3**	**37**
H17	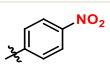	**	**	**90± 15**	**8**	**16**	**8**	**8**	**8**	**42±31**	**>37**
H18		**41**	**N/D**	**270 ± 50**	**32**	**64**	128	**32**	128	**75±12**	**>37**
H19	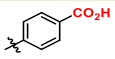	**	**	**>400**	128	128	>128	>128	128	**20±5**	**>37**

* - misbehavior on the SPR chip. ** - precipitation; N/D- no data.

The further modest improvement of replication inhibition was associated with the introduction of the 4-trifluoromethyl substituent in **H14,** which also led to a slight improvement of activity against *M. tuberculosis*.

The highest biochemical activity of the series was demonstrated by the *para*-nitro derivative **H17** with an IC_{50} of 90 μM. This improvement was not, however, corroborated by any significant gain in antibacterial activity, which stayed on the level of **H1** in all strains tested**.** Remarkably, the 4-pyridyl derivative **H18** showed quite an opposite trend in the case of *M. tuberculosis*: while the 2-fold decrease in biochemical potency was reflected in MIC_{95} values across the panel of microorganisms (**Table 3**), **H18** inhibited the growth of *M. tuberculosis* by 75% at 16 μM, which rendered this compound the most active against *M. tuberculosis* in the subseries. This had also exemplified the disconnect between the molecule's ability to inhibit the *in vitro* DNA replication or growth of Gram-positive and -negative strains and its ability to inhibit the growth of *M. tuberculosis*, which can be attributed to subtle differences in the binding sites of DnaN in different bacteria.

While the introduction of methoxycarbonyl (**H16**) and nitro (**H17)** moieties resulted in a substantial activity drop, the presence of a free carboxyl group at the same position in **H19** led to a complete loss of both replication inhibitory and antibacterial activities. A possible explanation for this observation could be the compensation of the permanent positive charge of the molecule due to the deprotonation of the carboxyl moiety at physiological pH (the pH of broth is 7.3). This might therefore be considered an additional indirect evidence of the essential role of the permanent positive charge for the target engagement and in the transport through the bacterial cell wall.[14],[15]

Overall, the Eastern phenyl part of the molecule was shown to be crucial for both DNA replication inhibition and antibacterial activity. The fluorine scan of the positions of the Eastern phenyl revealed negative sensitivities of the *ortho*- position and, to a lesser extent, *meta*- positions of the ring. In the case of *para*-position the most balanced derivatives were found to be those bearing non-ionizable, electron-donating groups (compounds **H4** and **H5**).

Western phenyl

To estimate contributions of the chlorines to DnaN binding and antibacterial activity, the first round of modifications of the Western phenyl ring involved the stepwise removal of the chlorine atoms. As a result, while removal of either or both chlorine atoms was associated with a commensurate negative effect on DNA replication inhibition, the *meta*-Cl was shown to be more important for DnaN binding and antibacterial activity (**Table 4**).

Table 4. Results of the Western phenyl ring modifications.

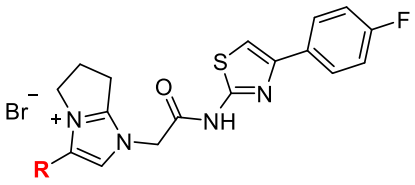

Name	R	SPR (*RU*)		Repl. assay IC_{50} (*μM*)	MIC$_{95}$ (*μM*)					*MTb growth inh @16 μM, %*	HepG2 IC_{50} (*μM*)
		250 μM	1 mM		*M. smegmatis*	*M. smegmatis GM^R*	*S. pneumoniae*	*S. aureus*	*E. coli ΔacrB*		
H1	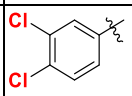	26	**	150 ± 30	4	16	16	8	8	43±30	>37
H21	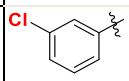	40	**	270 ± 50	4	16	32	16	16	54±6	>37
H22	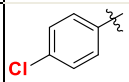	22	**	290 ± 50	8	8	32	32	32	40±8	>37
H23		24	52	250 ± 40	16	16	128	64	64	0	>37

** - precipitation

Nevertheless, compared to **H22**, the analogue deprived of both chlorines **H23** showed significantly higher MIC values against all bacterial strains and complete absence of activity against *M. tuberculosis*, which renders the presence of both chlorines important for antibacterial activity and crucial for antitubercular activity of the chemotype.

The cytotoxicity on HepG2 cells, however, remained unaffected (HepG2 IC_{50} >37 μM) during all modifications.

Charged fused cycle core.

According to the docked pose of the hit **H1** into the subsite I of *M. tuberculosis* β-sliding clamp (**Figure 2**), the Western part of **H1** was predicted to bind within the hydrophobic cavity lined by side chains of the following residues (Chain B): Ala-179, Thr-181, Arg-185 Leu-186, Phe-261, Leu-264, Leu-394, Met-396 called *subsite I*.

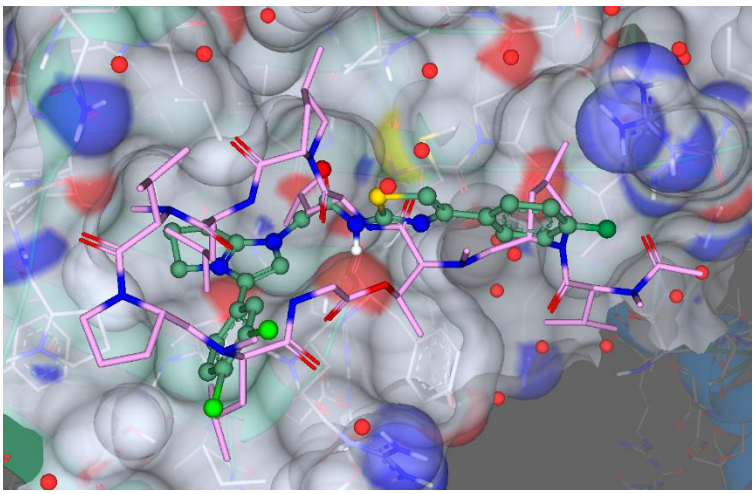

Figure 2. The docked pose of **H1** (green) superimposed onto a co-crystal structure of *M. tuberculosis* sliding clamp with griselimycin (PDB: 5AGU). The griselimycin molecule is depicted in magenta.

As it was presumed in our working hypothesis, modeling did not suggest any obvious role of the charge on the ring in the interaction with DnaN. The aliphatic part of the pyrrolinoimidazolic ring is, however, suggested to be pointing into a hydrophobic subpocket within the *subsite I*, which prompts the design of derivatives to probe the importance of the aliphatic part for binding to DnaN.

We therefore synthesized the following derivatives for SAR investigation:

- The enlarged ring analogue **H31** is supposed to help investigate the importance of the size of the aliphatic part of the bicyclic system.
- The 1,4-triazole **H32** probes the importance of both presence of the aliphatic part and the permanent charge of this part of **H1**.
- **H33** elucidated the role of the positive charge for DnaN binding and antibacterial activity alike.

The results are summarized in **Table 5**.

Remarkably, the aforementioned modifications had almost no significant influence on the *in vitro* replication inhibition: the IC_{50} values of synthesized analogues remained close to that of **H1** within the experimental error. However, the behavior of synthesized analogues in biophysical and cell-based tests varied dramatically.

Table 5. Results of the charged fragment modifications

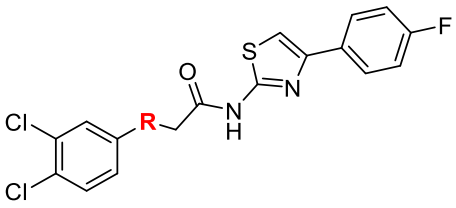

Name	R	SPR (*RU*)		Repl. assay IC_{50} (*μM*)	MIC_{95} (*μM*)					*MTb growth inh @16 μM, %*	HepG2 IC_{50} (*μM*)
		250 μM	1 mM		*M. smegmatis*	*M. smegmatis GM*^{R}	*S. pneumoniae*	*S. aureus*	*E. coli ΔacrB*		
H1	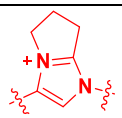	26	**	150 ± 30	4	16	16	8	8	43±30	37
H31	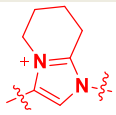	111	**	170 ± 30	4	8	8	8	8	Agg	>37
H32	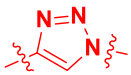	0	0	120 ± 20	>128	>128	>128	>128	>128	0	>37
H33	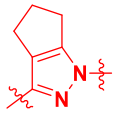	0	0	140 ± 20	>128	>128	>128	>128	>128	Agg	>37

** - precipitation. *Agg* – forms aggregates (DLS measurements).

The enlargement of the aliphatic ring by adding one methylene in compound **H31** resulted in a slightly higher activity across the panel of microorganisms. **H31** also demonstrated a stronger response in SPR, which could imply higher affinity for DnaN and therefore favor the accommodation of larger cycles by the *subsite I* of the sliding clamp. However, this modification led to an expected increase in lipophilicity, which negatively affected the compound's aqueous solubility. The compound **H31** was found to form aggregates at 16 μM, which precluded it from being tested against *M. tuberculosis*.

The 1,4-triazole **H32** showed neither DnaN binding, nor antibacterial activity, which supports the assumption of the crucial role played by the aliphatic part together with the charge of the bicyclic fragment in binding of **H1** to the sliding clamp.

Along with that, the pyrazole **H33** failed to demonstrate any binding to DnaN and antibacterial activity, which renders the positive charge on the fused bicyclic fragment of the molecule a crucial feature for the antibacterial effect of the compound class.

Overall, although the biochemical potency of all analogues stayed the same, the uncharged analogues **H32** and **H33** showed no binding by SPR and no antibacterial activity. This discrep-

ancy could be explained by the tendency of both derivatives to form aggregates, which presumably influenced the biochemical assay.

Eastern heterocycle

One of the obvious first modifications of the original 4-aryl-2-aminothiazole was swapping the positions of sulfur and nitrogen within the five-membered ring to form the isomeric 5-aryl-2-aminothiazole **H41**. Compound **H41** showed better binding to DnaN by SPR, however, it demonstrated no ability to inhibit DNA replication *in vitro*. The thiazole isomer also showed antibacterial activity profile similar to that of original hit **H1**.

The oxazole analogue **H42** had surprisingly demonstrated a dramatic decrease of both DnaN binding, biochemical potency and antibacterial activity compared to **H1,** being active only marginally against Gram-positive strains in the panel. The changes observed render the substitution of sulfur with oxygen non-favorable in this position.

Table 6. Performance of molecules with modified Eastern heterocycle

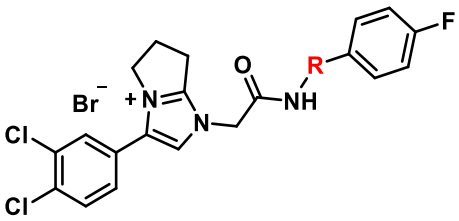

Name	R	SPR (*RU*)		Repl. assay IC_{50} (*μM*)	MIC_{95} (*μM*)					*MTb growth inh @16 μM, %*	HepG2 IC_{50} (*μM*)
		250 μM	1 mM		*M. smegmatis*	*M. smegmatis GM^R*	*S. pneumoniae*	*S. aureus*	*E. coli ΔacrB*		
H1	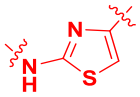	26	**	150 ± 30	4	16	16	8	8	43±30	37
H41	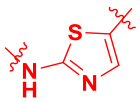	125	290	> 400	4	>128	16	16	32	42±35	>37
H42	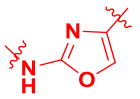	0	0	290 ± 50	128	128	64	64	>128	N/D	>37
H43	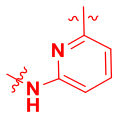	51	*	180 ± 30	4	8	16	8	8	90±8	37
H44	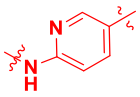	184	N/D	130 ± 20	4	16	16	4	8	69±7	>37
H45		39	72	290 ± 50	16	128	>128	64	8-16	20±20	>37
H46	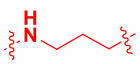	N/D	61	280 ± 50	16	32	>64	32	32	0	>37

* - misbehavior on the SPR chip; ** - precipitation; N/D- no data.

To evaluate the effect of replacement of the five-membered heterocycle by its close six-membered analogues, we synthesized the isomeric pyridine derivatives **H43** and **H44**. Both analogues were shown to bind DnaN by SPR and to inhibit DNA replication *in vitro*. Nevertheless, the *para*-substituted analogue **H44** demonstrated higher SPR response as well as more pronounced biochemical potency compared to its isomer. This difference in target engagement was not, however, reflected in antibacterial activities: MIC_{95} values determined for both isomers were identical for most strains, while the activity against *M. tuberculosis* was found to be considerably higher in the case of **H43** (see **Table 6**).

Finally, in order to investigate the importance of the aromaticity of this portion in **H1,** we synthesized the analogues **H45** and **H46** in which the thiazole ring was replaced with spacers designed to keep the distance between the amide nitrogen and 4-fluorophenyl ring approximately equal to that in **H1** (ca 4.5 Å)**.** In **H45,** the spacer retains partial rigidity, while in **H46** it was made flexible to probe the impact of the rigid connection of the two parts of the molecule. As a result, either of exchanges mentioned led to similar drops in sliding clamp binding, biochemical potency and MIC_{95} values relative to those of **H1**. While the alkyne-containing **H45** still has marginal activity against *M. tuberculosis*, its more flexible counterpart **H46** lost the ability to inhibit the growth of *M. tuberculosis.*

All in all, the aromaticity, polarity as well as the substitution pattern of the five-membered ring in this part of the molecules was found to be essential. Replacement of the original thiazole with isomeric pyridines is possible, in some cases improves the binding to DnaN and overall antibacterial properties of the chemotype. Moreover, the observations underscore the importance of a rigid connection between the linker and Eastern phenyl parts of the molecule.

Combining beneficial prior modifications.

Based on data obtained and assuming mutual independence and additivity of the effects associated with modifications of parts of the scaffold, we synthesized several derivatives combining modifications demonstrated to be beneficial. In all cases, we decided to keep only the 3-Cl-substituent in the Western part and attempted to achieve maximal improvement of DnaN binding, *in vitro* replication inhibition and antibacterial activity by combining favorable ring arrangements involving the Eastern phenyl and the heterocycle. Keeping the o*rtho*-fluorine was supposed to improve DnaN binding and bestow good activity across the entire panel of microorganisms, while *para*-OH and -OMe – excellent activity against *M. tuberculosis*. and improved biochemical potency respectively. The multiparameter performance of the resulting compounds **H51** – **H55** is summarized in **Table 7**.

Table 7. Performance of the chimeric molecules

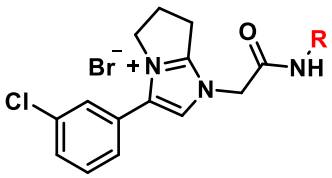

Name	R	SPR (*RU*)		Repl. assay IC_{50} (*μM*)	MIC$_{95}$ (*μM*)					*MTb growth inh @16 μM, %*	HepG2 IC_{50} (*μM*)
		250 μM	1 mM		*M. smegmatis*	*M. smegmatis GM^R*	*S. pneumoniae*	*S. aureus*	*E. coli ΔacrB*		
H1		**26**	**	**150 ± 30**	**4**	**16**	**16**	**8**	**8**	**43±30**	**37**
H51	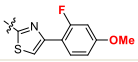	**98**	**324**	**> 400**	**4**	**64**	**8**	**16**	**16**	**30±50**	**>37**
H52	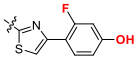	**62**	**148**	**290 ± 50**	**8**	**64**	**64**	**32**	**32**	**62±13**	**>37**
H53	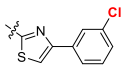	**N/D**	**N/D**	**180 ± 30**	**4**	**32**	**16**	**16**	**16**	**97±1**	**>37**
H54	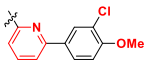	**39**	**N/D**	**N/D**	**4**	**8**	**16**	**8**	**8**	**77±8**	**>37**

** - precipitation; N/D- no data.

Not unexpectedly, derivatives **H51** and **H52** showed no additivity of the effects of the substituents equipping Eastern and Western parts of the molecules: despite improved SPR binding, compounds **H51** and **H52** failed to show any significant improvements in DNA replication inhibition or antibacterial activity compared to their progenitors **H4**, **H6**, **H10** and **H21.**

The thiazole **H53** was designed as a less lipophilic version of **H12** with a focus on activity against *M. tuberculosis*. As a result, **H53** was found to have significantly higher biochemical potency (IC_{50} 180 μM) compared to both its progenitors **H12** and **H21** and preserved antibacterial activity.

Finally, **H54** has largely retained properties of the pyridine **H43** only showing a slight diminution of activity against *M. tuberculosis*.

Notably, **H51**, **H52** and **H53** in this series of optimized analogues demonstrated significantly larger difference in antibacterial activity against a wild-type *M. smegmatis* and the respective griselimycin-resistant strain. Thus, the antibacterial activity at least in part comes from inhibition of DnaN.

3.2.3 Investigation into the possible binding mode by modeling supported by crystallography and STD-NMR

Evaluation of H1 binding by epitope mapping STD-NMR

In our attempts to shed light on possible binding mode of the initial hit **H1**, we turned to STD-NMR, the ligand-observed method widely used for biophysical screening. The degree of ligand's proton saturation in the difference spectrum is proportional to the strength of its contact

to the protein, which allows to infer the binding epitope of the ligand.[16] To obtain further confirmation of the binding of **H1** to the *M. tuberculosis* DnaN, we performed STD-NMR measurements at single concentration of 100 μM**.** The analysis of the difference spectrum revealed that all aromatic proton groups within the molecule took part in binding, albeit to a different extent (**Figure 3**).

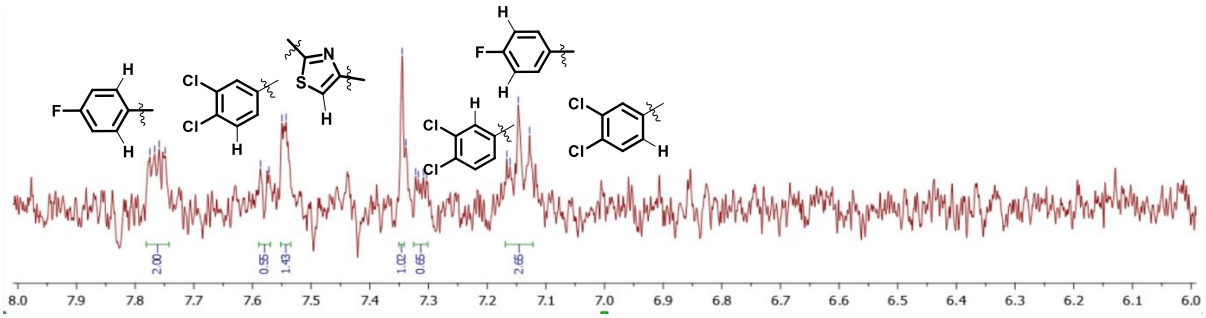

Figure 3 A section of the difference spectrum of compound **H1** with assignments

Integration of aromatic proton signals found in the difference spectrum of the molecule **H1** revealed higher intensities belonging to protons 3, 4, 6 and 7 (**Figure 4**), which implies a tighter contact with the protein than other protons (1, 2 and 5).

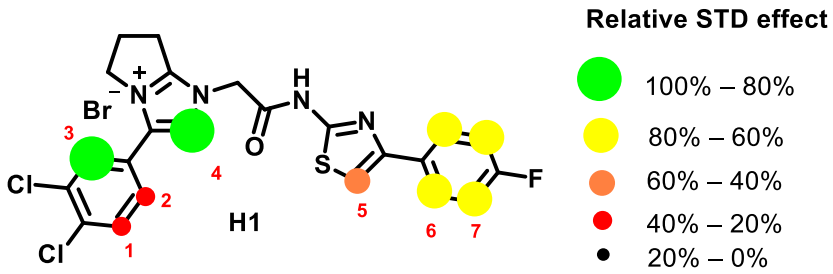

Figure 4. Summary of relative saturation difference effects observed within **H1**

The previously mentioned docking pose of **H1** (**Figure 2**) is in partial accordance with STD-NMR data: the protons of the Western phenyl and imidazole are predicted to form contacts with DnaN. Nevertheless, the protons of the Eastern phenyl and thiazole are predicted to be relatively distant from the protein surface as this portion of **H1** points in the direction of *subsite II*. This discrepancy may be a consequence of the dynamic effects and induced fit on binding of **H1** to the β-sliding clamp.

The soaked structure of Rickettsia Typhi DnaN and H1: binding model refinement

The X-ray crystallographic structure of the β-sliding clamp protein from *Rickettsia typhi* was determined in the presence of the compound **H1** using soaking. Soaking experiments with crystals of *Mycobacterium tuberculosis* and *Mycobacterium smegmatis* DnaN proved unsuccessful due to the presence of crystal contacts, which blocked ligand-access to the *subsite I* of these proteins. However, *R. typhi* DnaN was found to be the only protein of this type that can crystal-

lize in the *apo*-form without forming such contacts, allowing for the successful determination of its structure in complex with **H1** after soaking.

Detailed analysis of the electron density maps revealed the binding mode of **H1** within a narrow and hydrophobic *subsite I* cavity, formed by backbones of Gly-174, His-175, Arg-176, Val-375, Ile-376, Met-377 and side chains of Leu-177, Tyr-248, Phe-251, Val-375 and Met-377. The 4-chlorine is estimated by the HYDE scoring function[17] to contribute –5.5 kJ/mol of binding free energy. The 3-chlorine contributes –8.3 kJ/mol. Both atoms are predicted to be involved in hydrophobic interactions with side chains lining the cavity. Furthermore, the 3-chlorine is also positioned properly to exhibit halogen bonding with the backbone carbonyl oxygen of Arg-176 (3.0 Å, $\Theta_1 = 145^o$ $\Theta_2 = 79^o$, $\Psi = -87^o$).[18]

The Western phenyl ring is mainly held in the cavity by π–π staggered stacking with the side chain of Phe-251 (<d> = 3.9 Å) and a hydrophobic interaction with Met-377 (<d> = 3.8 Å). The pyrrolinoimidazolic part of **H1** is also suggested to be involved in π–π stacking: partially with Phe-251 (parallel displaced arrangement, <d> = 3.8 Å) and Tyr-248 (T-shaped arrangement, <d> = 4.3 Å).

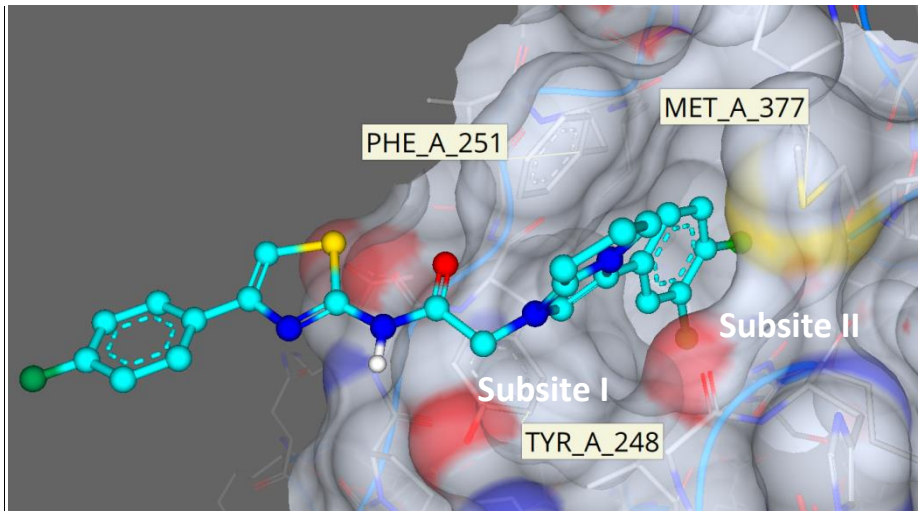

Figure 5. **H1** soaked into the crystals of *Ricketsia typhi* β-sliding clamp.

It is important to note that the soaking was performed on the static *apo*-form of the protein from a different organism, which ruled out the concomitant dynamic effects known to happen during the sequential binding of ligands to DnaN.[19] This implies the binding of the ligand with the hydrophobic cavity within *subsite I*, that triggers the further accommodation of the ligand by the protein in the direction of *subsite II* and the formation of it. Therefore, in the light of the new data, we sought to integrate the newly obtained structural insights from soaking experiments with STD-NMR epitope mapping data and find the plausible docking poses of **H1,** which will be fully supported by experimental data. In order to take into account the possible dynamic effects on ligand binding, we used the "opened" DnaN protein from *M. tuberculosis* co-crystallized with

griselimycin (PDB code: 5AGU). We implemented constrained docking in SeeSAR by introducing a hydrophobic pharmacophore restrain located within *subsite I* such that re-docking of **H1** into the *subsite I* of *M. tuberculosis* DnaN (PDB code: 5AGU) prioritized the solutions with hydrophobic portions of **H1** buried in the hydrophobic cavity of the *subsite I.*

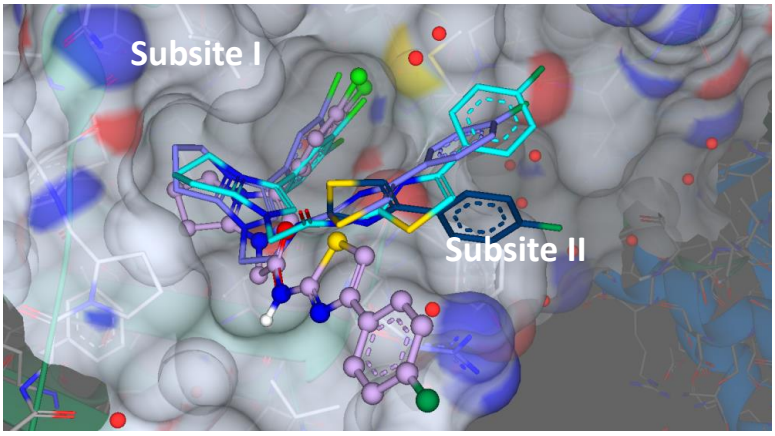

Figure 6. Overlay of representative docking poses of **H1** with the aliphatic part of the bicycle pointing into the hydrophobic cavity within the subsite I (PDB code: 5AGU).

The majority of poses converged towards those depicted in **Figure 6** and contained the 3,4-dichlorophenyl substituent buried in *subsite I* and the aliphatic part of the central bicyclic fragment buried in the hydrophobic cavity within the same subsite and 4-fluorophenyl pointing towards the *subsite II* (in **Figure 6**). There was, however, a subset of poses represented by the one depicted in purple. In this pose, unlike others, the thiazolyl and 4-fluorophenyl parts are fitted into the hydrophobic groove next to the exit from *subsite I*. This arrangement of **H1** in the protein-ligand complex is more consistent with data from STD-NMR epitope mapping. In line with data provided by STD-NMR is also the pose depicted in deep blue in **Figures 6**, **7**. It suggests the Western and central fragments of **H1** to be positioned within *subsite I* and the Eastern fragments to be pointing to the *subsite II* and not contributing greatly to binding.

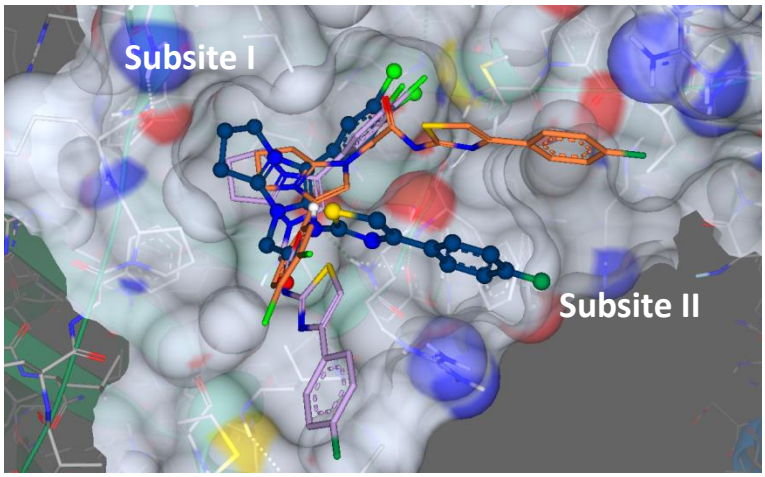

Figure 7. Superimposition of poses. Initial pose (orange) and ones derived by constrained docking (magenta and deep blue) (PDB code: 5AGU).

Visual examination of the refined poses suggested the crucial role of the Western phenyl in binding to DnaN, the productive interaction of the bicyclic fragment of the molecule to the protein was also supported. Simultaneously, the role of Eastern heterocycle and phenyl seemed to be rather nominal. This inspired us to design an additional derivative **H61** containing swapped Western and Eastern phenyls (**Figure 8**) in order to estimate the impact of relative positions of the Western and Eastern phenyls in **H1** on DnaN binding and antibacterial activity.

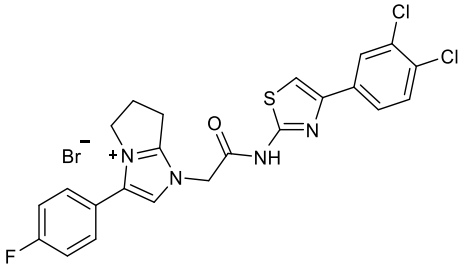

Figure 8. The structure of the swapped analogue **H61**

The reversed analogue **H61** showed an improved antitubercular activity and a slightly more potent inhibition of DNA replication *in vitro* (see **Table 8**).

Table 8. Comparison of the multiparameter performance of **H1** and its swapped analogue **H61**

Name	SPR (*RU*)		Repl. assay IC_{50} (*μM*)	MIC_{95} (*μM*)					*MTb growth inh @16 μM, %*	HepG2 IC_{50} (*μM*)
	250 μM	1 mM		*M. smegmatis*	*M. smegmatis GM^R*	*S. pneumoniae*	*S. aureus*	*E. coli ΔacrB*		
H1	**	**	150 ± 30	4	16	16	8	8	43±30	37
H61	97	**	130 ± 20	8	16	32	8	8	75±4	12.3

** - no data available

Interestingly, docking of **H61** into DnaN failed to find a solution in which its 3,4-dichloro substituted Eastern phenyl part was bound within the *subsite I* (**Figure 9**).

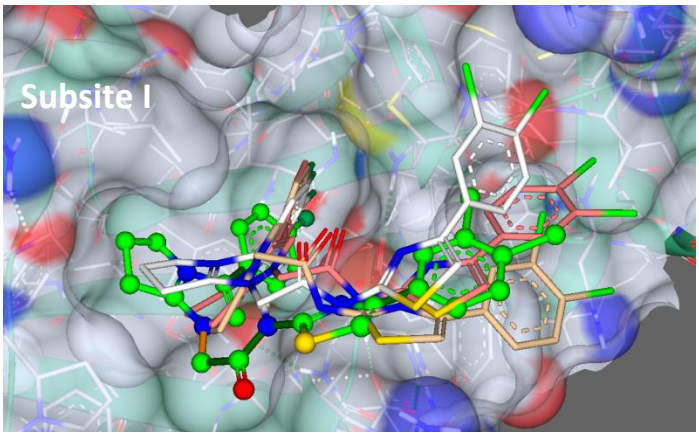

Figure 9. The overlaid representative docking poses of **H61** on *M. tb* DnaN (PDB: 5AGU).

Instead, in all solutions found, the Western 4-fluoro-substituted part of **H61** was suggested to occupy *subsite I* together with the central bicyclic fragment residing in the proximity of the hydrophobic subpocket analogously to the refined poses of **H1.** The 3,4-dichlorosubstituted phe-

nyl pointing out to the *subsite II*, but does not reach it. In view of the aforementioned predictions by modeling and overall retention of activity of the swapped analogue **H61**, the central bicyclic fragment's positioning within *subsite I* is suggested to be a more decisive factor in DnaN binding than the substitution pattern of the phenyl ring adjacent to it. However, no soaked structure of **H61** with *Rickettsia typhi* DnaN was obtained, which precludes us from making conclusions regarding the details of interaction between the swapped analogue and the β-sliding clamp.

3.2.4 Detailed testing of selected candidates on mycobacterial strains

Having established the non-aggregating concentration for most derivatives at 16 μM, compounds were tested for their ability to inhibit the growth of *Mycobacterium tuberculosis*. The performance of analogues at this concentration was featured in the respective sections above.

For compounds demonstrating the highest activity against *M. tuberculosis* in single-point growth inhibition tests, MIC_{95} values were determined (summarized in **Table 9**). From the data presented it becomes clear, that for most candidates full growth inhibition is observed at a concentration of 32 μM. For compounds **H3** and **H6,** the 95% inhibition was achieved at 16 μM, which renders them leads in this assay. However, **H6** demonstrated lower cytotoxicity (>37 μM) compared to that of **H3** (12.3 μM), making it more attractive for further development.

Table 9. MIC_{95} values of selected compounds against *M. tuberculosis* and *M. marinum*.

Name	MIC_{95} (*μM*)		HepG2 IC_{50} (*μM*)
	M. tuberculosis	*M. marimun*	
H1	**32**	**-**	**37**
H3	**16**	**16**	**12.3**
H4	**32**	**32**	**37**
H5	**32**	**-**	**37**
H6	**16**	**16**	**>37**
H10	**32**	**32**	**12.3**
H11	**32**	64	**37**
H12	**32**	**-**	**>37**
H18	**32**	**-**	**>37**
H21	N/A	64	**37**
H22	N/A	64	**37**
H43	**32**	**16**	**37**
H44	>64	**8**	**>37**
H51	N/A	**8**	**>37**
H52	64	**8**	**>37**
H53	**16**	**-**	**>37**
H54	**32**	**-**	**>37**
H64	**32**	**-**	**12.3**

N/A- MIC_{95} not achieved, - - compound not tested.

The best-performing compounds against *M. smegmatis*, *M. tuberculosis* and showing low cytotoxicity were also subjected to the minimum inhibitory concentration determination against *Mycobacterium marinum,* the species employed in the zebrafish mycobacterial infection model. The results are summarized in **Table 9**.

Thus, chimeric compounds **H51** and **H52** showed the lowest MIC_{95} values against *M. marinum;* the 2,5-disubstitution pattern in the pyridyl ring in **H44** seemed to be preferred over the 2,6 one in **H43**, while the removal of any of the two chlorine atoms from the Western phenyl was detrimental for the activity against Mycobacteria (**H21** and **H22**).

3.2.5 Activities of selected derivatives against gram-negative bacteria

Candidates that demonstrated the highest activity against the efflux-deficient *ΔacrB E. coli* strain were subsequently screened against the extended Gram-negative microorganism panel consisting of *E. coli*, *A. baumannii* and *P. aeruginosa* strains with non-impaired efflux systems. Results are summarized in the **Table 10**.

Table 10. MIC_{95} values of selected compounds against selected Gram-negative strains

Name	MIC_{95} (μM)		
	E. coli BW25113	*A. baumannii* DSM-30008	*P. aeruginosa* PA14
H1	> 128	**64**	> 128
H3	> 128	**32**	> 128
H4	> 128	> 128	> 128
H6	>128	>128	>128
H10	**128**	-	-
H14	>128	-	-
H17	>128	-	-
H21	>128	>128	>128
H31	>128	-	-
H43	>128	>128	>128
H44	>128	-	-
H45	>128	-	-
GM	>128	>128	>128
ciprofloxacin	**< 0.15**	**0.3**	**< 0.15**

- Not tested

The wild-type *E. coli* turned out to be virtually non-susceptible to the screened compounds with only **H10** demonstrating detectable MIC_{95} of 128 μM. Interestingly, another common Gram-negative pathogenic strain *A. baumannii* was found to be more susceptible, with the minimal inhibitory concentrations of only **H1** and **H3** being as high as 64 and 32 μM, respectively. Nevertheless, no activity of selected candidates against *P. aeruginosa* was demonstrated.

The stark contrast between the data presented above and previously obtained MIC_{95} values against the efflux-deficient knock-out *E. coli* strain indicates that tested compounds are substrates of the efflux transporter AcrB. The acriflavine resistance protein B is a member of the Resistance Nodulation cell Division superfamily, widely expressed by Gram-negative bacteria and conferring broad-spectrum resistance.[20] AcrB has a wide range of substrates; the primary ones are acriflavine, ethidium and berberine, with which **H1** shares apparent similarity being a flat quaternary ammonium salt (see **Figure 10**).[20]

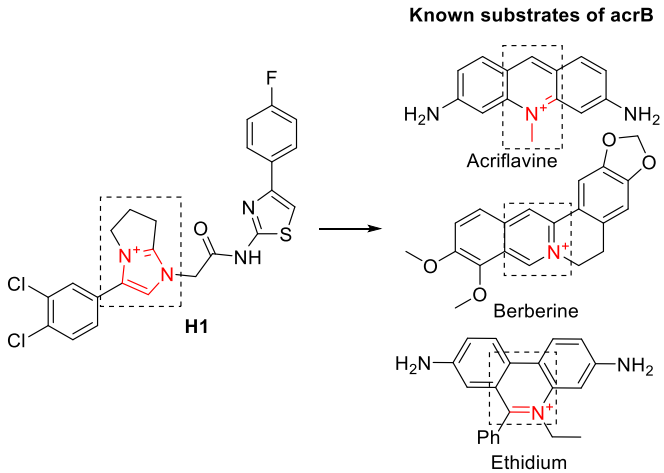

Figure 10. Illustration of molecular feature similarities between **H1** and known AcrB substrates

Nevertheless, results obtained with wild-type Gram-negative strains could be considered additional evidence, that the compound class has the mechanism of bacterial growth inhibition associated with the compounds' entry into a bacterial cell and therefore involving an intracellular target(s).

3.2.6 *In vitro* ADME properties

On the basis of DnaN binding and performance against various bacteria, selected derivatives of **H1** were subjected to *in vitro* ADME parameters determination studies (performed by Dr. Andreas Kany on the facilities of the Drug Discovery Unit at the University of Dundee, UK).

Measured parameters included: 1) Real solubility in a buffer containing 2.5% DMSO; 2) Chromatographic Hydrophobicity Index (CHI); 3) Mouse Liver microsome metabolic stability; 4) Human liver microsome metabolic stability. The results are summarized in **Tables 11-16**.

Table 11. *In vitro* ADME parameters determined for Eastern phenyl modifications

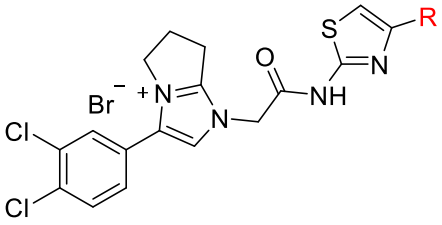

Code	Structure	Real Sol 24 h, 2.5% DMSO (μM)	ChiLogD *(CLogP)*	$t_{1/2}$ [min] / MLM Cl_{int} [ml/min/g]	$t_{1/2}$ [min] MHeps Cl_{int} [ml/min/g]
H1	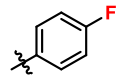	**N/D**	**3.23** ***(4.84)***	**>30 / <0.5**	**N/D**
H2		**93.3**	**3.16** ***(4.85)***	**>30 / 0.98**	**>120 / 1.66**
H3	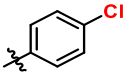	**23.3**	**3.66** ***(5.28)***	**>30 / <0.5**	**N/D**
H4	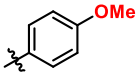	**67.4**	**3.13** ***(4.82)***	**>30 / 1.00**	**N/D**
H5	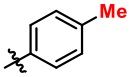	**N/D**	**3.56** ***(5.22)***	**>30 / 0.66**	**>120 / 2.21 (Rat)**
H6	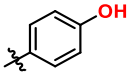	**N/D**	**N/D (4.34)**	**>30 / 0.66**	**N/D**

N/D – not determined

The highest real solubility value in the subseries was determined for the non-substituted analogue **H2** (93.3 μM). Lowest solubility – the chloro-derivative **H3** (23.3 μM), which, however, can be compensated by the introduction of heterocyclic fragments into the structure, which is showcased below. In the presented subset the observed changes in the real solubility parameter correlated with changes in the corresponding LogD values determined chromatographically.

Compounds **H1**–**H6** demonstrated long half-life in liver microsome assay (> 30 min), and therefore low yet non-uniform clearance. The increase of clearance was observed in the following row of *para*-susbstituents: -OH ≈ -Me < -H ≈ -OMe (see **Table 11**). This could be rationalized as a result of realization of different substrate-dependent metabolic degradation reactions that occur at significantly different rates, which impacts the clearance rate considerably. For **H4** the most probable primary degradation pathway is dealkylation, which presumably occurs very fast. The primary *para*-hydroxylation of the phenyl ring of **H2** seems to occur with a comparable rate to the dimethylation of **H4**. Simultaneously, the secondary *meta*-hydroxylation of the hydroxy-derivative **H6** may occur slower, which finds its reflection in the lower clearance rate compared to that of **H2** and **H4**. The degradation of the methyl derivative **H5** most likely proceeds through the oxidation of aromatic methyl to the corresponding benzylic alcohol, whose rate is comparable to that of secondary hydroxylation of **H6**, that in the end makes their clearance rates comparable.

At the same time, the measurable clearance rate of the 4-F and –Cl derivatives **H1** and **H3** is not observed because of the blocked *para*-position of the Eastern phenyl ring.

The permutation of the fluorine on the Eastern phenyl ring did not impact the LogD greatly. Simultaneously, isomeric derivatives **H10** and **H11** achieved higher solubility than any of the aforementioned *para*-substituted analogues (**Table 12**).

Table 12. *In vitro* ADME parameters determined for fluorine permutations on the Eastern phenyl

Code	Structure	Real Sol 24 h, 2.5% DMSO [μM]	ChiLogD (CLogP)	$t_{1/2}$ [min] / MLM Cl_{int} [ml/min/g]	$t_{1/2}$ [min] MHeps Cl_{int} [ml/min/g]
H1	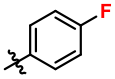	N/D	3.23 (4.84)	>30 / <0.5	N/D
H10		130.8	3.38 (4.84)	>30 / 0.84	N/D
H11	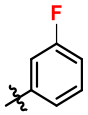	107.2	3.29 (4.84)	>30 / 0.81	>120 / 1.70

N/D – not determined

Fluorine permutation also impacted the metabolic stability: while the half-life of analogues still exceeded the upper limit of the assay (30 min), the higher clearance rate was observed for *ortho*- and *meta*-fluoro derivatives.

Among the derivatives with electron acceptors introduced on the Eastern phenyl ring the real solubility was determined only for the pyridyl analogue **H18** and rendered it the highest in the subseries. The metabolic stability of this compound was, however, determined

to be the lowest in the subseries with the half-life of 13 min and the microsomal clearance as high as 5.5 ml/min/g (see **Table 13**).

Table 13. *In vitro* ADME parameters determined for modification of Eastern phenyl

Code	Structure	Real Sol 24 h, 2.5% DMSO [µM]	ChiLogD (CLogP)	$t_{1/2}$ [min] / MLM Cl_{int} [ml/min/g]	$t_{1/2}$ [min] MHeps Cl_{int} [ml/min/g]
H1	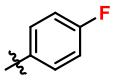	**N/D**	**3.23 (4.84)**	**>30 / <0.5**	**N/D**
H13	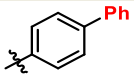	**N/D**	**4.31 (6.11)**	**>30 / <0.5**	**N/D**
H15	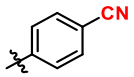	**N/D**	**2.84 (4.63)**	**>30 / <0.5**	**N/D**
H16	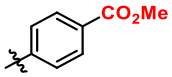	**N/D**	**3.07 (4.75)**	**>30 / 1.61**	**N/D**
H18		**197.5**	**1.85 (3.77)**	**13.22 / 5.51**	**N/D**

N/D – not determined

The dehalogenation of the Western phenyl ring had greatly impacted the lipophilicity and therefore solubility of the analogues, while the metabolic stability remained unaffected. The corresponding parameters of **H21** and **H22** demonstrate the possibility to achieve the solubility similar to that of **H18** without sacrificing the metabolic stability.

Table 14. *In vitro* ADME parameters determined for the Western phenyl modifications

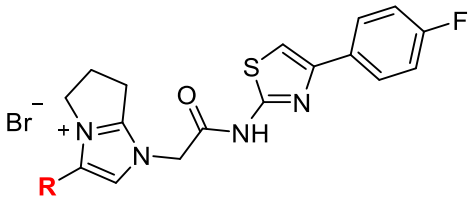

Code	Structure	Real Sol 24 h, 2.5% DMSO [µM]	ChiLogD (CLogP)	$t_{1/2}$ [min] / MLM Cl_{int} [ml/min/g]	$t_{1/2}$ [min] MHeps Cl_{int} [ml/min/g]
H1	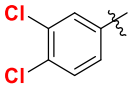	**N/D**	**3.23 (4.84)**	**>30 / <0.5**	**N/D**
H21	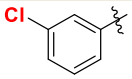	**178.9**	**2.90 (4.36)**	**>30 / <0.5**	**N/D**
H22	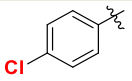	**191.7**	**N/D (4.36)**	**>30 / <0.5**	**N/D**
H23		**N/D**	**2.60 (3.84)**	**>30 / <0.5**	**N/D**

N/D – not determined

The data obtained for compounds **H43-H46** demonstrates another molecular feature that can be modified for improving solubility (**Table 15**).

Table 15. *In vitro* ADME parameters determined for Eastern heterocycle modifications

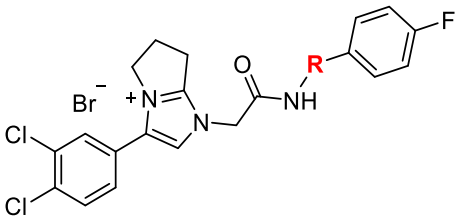

Code	Structure	Real Sol 24 h, 2.5% DMSO [µM]	ChiLogD (CLogP)	$t_{1/2}$ [min] MLM / Cl_{int} [ml/min/g]	$t_{1/2}$ [min] / MHeps Cl_{int} [ml/min/g]
H1	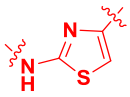	N/D	3.23 (4.84)	>30 / <0.5	N/D
H41	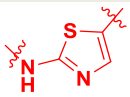	106.2	1.97 (4.84)	N/D	N/D
H42	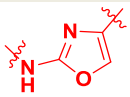	N/D	N/D (4.43)	23.94 / 3.04	N/D
H43	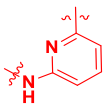	198.3	3.53 (4.41)	>30 / <0.5	N/D
H44	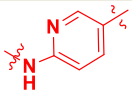	176.0	3.31 (4.41)	>30 / 1.76	>120 / 1.90 (Rat)
H45		234.7	2.89 (4.18)	>30 / <0.5 >30 / 1.44*	>120 / 1.12 (Rat)
H46	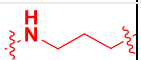	>250	2.91 (4.40)	>30 / 1.36	40.8 / 8.2 (Rat)

N/D – not determined

The modification of the Eastern heterocycle has also been shown to positively impact the candidates' susceptibility for microsomal oxidation, which is best exemplified by the case of the oxazole analogue **H42**. The metabolic stability was also slightly decreased when the original 2-amino-4-arylthiazole was replaced with 2-amino-5-arylpyridine (**H44**) and aliphatic linkers (see **H45** and **H46** in **Table 15**).

The chimeric compounds showed all in all expectable superposition of properties conferred by the combined molecular features. Thus, the swapped analogue **H61** showed no significant difference in metabolic stability in mouse liver microsomes.

Table 16. *In vitro* ADME parameters determined for chimeric molecules

Code	Real Sol 24 h, 2.5% DMSO [μM]	ChiLogD (CLogP)	$t_{1/2}$ [min] MLM Cl_{int} [ml/min/g]	$t_{1/2}$ [min] MHeps Cl_{int} [ml/min/g]
H1	**N/D**	**3.23 (4.84)**	**>30 / <0.5**	**N/D**
H61	**93.8**	**3.56 (4.84)**	**>30 / <0.5**	**N/D**
H51	**162.3**	**3.14 (4.35)**	**>30 / 1.08**	**N/D**
H53	**119.5**	**3.32 (4.85)**	**>30 / 1.09**	**98.55 / 3.38**
H54	**187.0**	**3.42 (4.34)**	**>30 / 1.54 >30 / 1.50***	**>120 / 2.65 81.9 / 4.06 (Rat)**

N/D – not determined

The chimeric compound **H51** demonstrated increased solubility, which could be attributed to the presence of the 3-Cl and 2-F substituents in the Western and Eastern phenyl rings, respectively. The diminished stability against microsomal oxidation could be caused by the simultaneous *para*-methoxy and *ortho*-fluoro substitution of the Eastern phenyl making this part of the molecule more metabolically labile.

The *bis*-*meta*-chloro (Western and Eastern phenyls) analogue of **H1** (**H53**) turned out to be more lipophilic and less soluble than **H51**, while demonstrating a similar rate of microsomal clearance. The derivative **H54**, however, demonstrated great solubility that is probably the consequence of the combination of 3-Cl substitution on the Western phenyl and the 2-amino-6-arylpyridine on the Eastern heterocycle.

Cell permeability assay

The Madin Darby Canine Kidney (MDCK) cells used in the assay were transfected with a gene MDR1, that encodes P-glycoprotein, a commonly known efflux transporter expressed in brain, kidney and intestine tissues. The MDCK permeability assay allows to estimate the candidate's ability to undergo intestinal absorption, which is indicative of oral bioavailability. The apparent permeability coefficients P_{app} and recovery percentage values for selected compounds are summarized in the **Table 17**.

Table 17. Results of the MDCK/MDR1 assay

Code	Structure	MDCK P_{app} [nm/s] (recovery, %)
H5	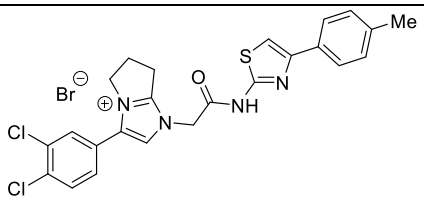	**1.17, (69%)**
H44	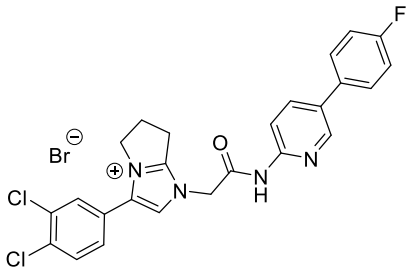	**0.47, (86%)**
H45	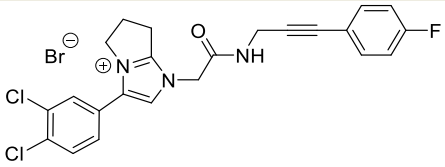	**7.73, (66%)**
H46	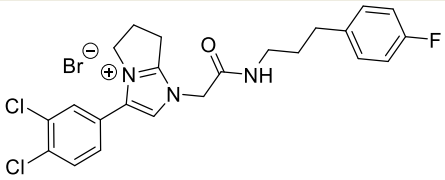	**10, (65%)**
H54	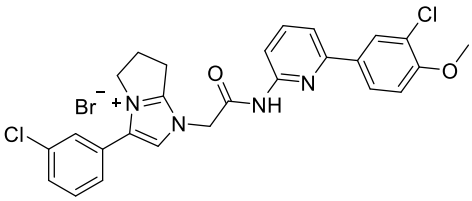	**0.92, (100%)**
Atenolol	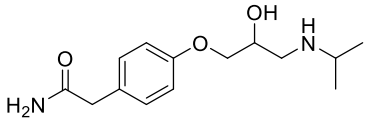	**14.9**
Bupropion	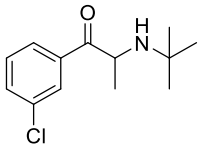	**288**

Overall, the permeability of all compounds tested turned out to be lower than that of Atenolol, which is normally used as a reference for relatively low permeability compared to Bupropion that is used as a standard of high permeability. Nevertheless, the slight positive impact on the P_{app} value within the class of compounds under investigation was associated with the non-aromatic replacement for the Eastern heterocycle: the acetylenic derivative **H45** and saturated analogue **H46** demonstrated significantly higher P_{app} among the compounds tested in MDCK

assay (7.73 and 10.00 nm/s respectively). The percentage of recovery was somewhat low (66 and 65 %), which indicates the molecules' retention in the model cells. The observed facts testify the detrimental effect of the aromaticity of the Eastern heterocycle on the compound's cell permeation, which was also found to be virtually non-dependent on the substituents of the Western and Eastern phenyl rings.

Even though the chimeric molecule **H54** demonstrated good balance between antibacterial activity and basic ADMET properties, its penetration rate was found to be extremely low even compared to other molecules tested.

According to the guidelines of the MDCK/MDR1 assay, the compounds with P_{app} values below 10 nm/s are considered poor permeators, while the good penetrating compounds typically show P_{app} values greater than 100 nm/s. In spite of our exploratory optimization effort, which yielded the compound **H46** showing permeability closer to the cutoff value, the permeability of the entire class is extremely low, with the permanent positive charge responsible for it.

Cytochrome P450 enzymes inhibition

The cytochrome P450 superfamily are oxidative enzymes involved in a multitude of biochemical pathways, associated with drug metabolism and clearance.[21] The optimized analogues were profiled for certain cytochrome P450 enzyme inhibition (summary in **Table 18**).

Table 18. Results of the CYP inhibition profiling

Code	IC_{50} (μM) on CYP subtypes					
	1A2	2C9	2C19	2D6	3A4 (DEF)	3A4 (7BQ)
H44	>20	>20	>20	3.08	>20	>20
H45	>10	> 10	>3.3 (63% @3.3 μM)	0.53	>10 (52% @10 μM)	>10 (72% @10 μM)
H46	>10 >20	>10 >20	>10 ≈20	0.056 0.048	>10 (77% @10 μM) Interference	>3.3 (49% @10 μM) >20
H53	>10	>10 (74% @10 μM)	>10 (69% @10 μM)	4.87	>10	>10
H54	>10 >20	>10 >20	6.72 14.8	>10 (58% @10 μM) 8.47	>10 interference	>10 >20

The lowest off-target activity was demonstrated by compound **H44**, for which significant inhibition was detected only for CYP 2D6. This enzyme turned out to be most inhibited by tested derivatives with the lowest IC_{50} of 0.05 μM demonstrated by the analogue **H46.**

3.3 Chemistry

The re-synthesis of the original hit compound. We synthesized compound **H1** according to the **Scheme 1**.

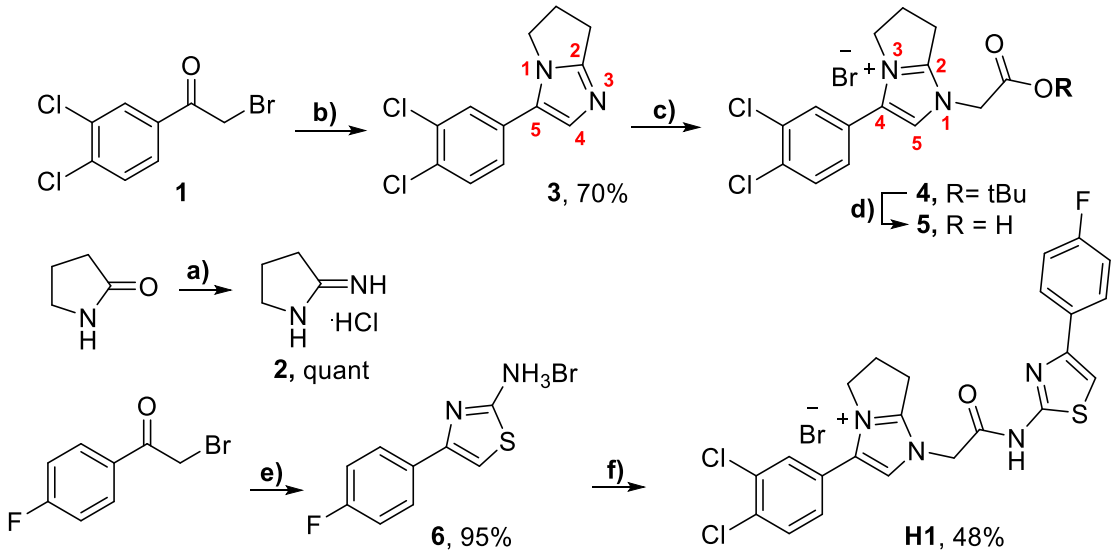

Scheme 1. The scheme used to resynthesize the original virtual hit **H1**.

Reagents and conditions: **a)** 1. Me_2SO_4 (1.0 eq), benzene, reflux, 45 min; 2. NH_4Cl, EtOH, rt, o/n; **b) 2**, K_2CO_3 (3 eq), 80 °C, DMF, 6h; **c)** Tert-butyl bromoacetate(1.5 eq), MeCN, 60 °C, o/n; **d)** CF_3CO_2H, DCM, rt, 3h; **e)** thiourea, EtOH, 4h, 80 °C; **f) 3**, T3P, pyridine.

From the chemistry viewpoint, the structure of the hit **H1** is composed of two biaryl fragments connected by a semi-flexible acetamide linker. The Eastern part of the molecule is a 4-aryl-2-aminothiazole, which can be assembled employing a robust Hantzsch method (conditions d) in **Scheme 1**). The Western portion of the molecule is represented by a di-substituted 3-aryl-6,7-dihydro-5*H*-pyrrolo[1,2-a]imidazolium salt. The linker is attached to the imidazole ring using the lone pair of the nitrogen in position 3, therefore rendering the imidazole ring permanently charged and the charge delocalized between the two nitrogen atoms.

We accomplished the synthesis of the charged part of the molecule inspired by the work of Kovtunenko *et al.*[22] and carried it out in three steps, starting from the condensation of 2-bromo-3',4'-dichloroacetophenone with an easily accessible pyrrolidin-2-imine **2** (see conditions **a)** and **b)** in **Scheme 1**). Alkylation of the resulting pyrroloimidazole **3** at the position 3 with *tert*-butyl bromoacetate yielded an imidazolium bromide salt **4**. Removal of the *tert*-butyl ester group was achieved by treatment of **4** with trifluoroacetic acid in dry DCM. Finally, the amide coupling of the acid **5** and the 2-aminothiazole **6** in mild conditions using the T3P coupling agent afforded the target molecule **H1** (conditions **c)-f)** in **Scheme 1**). It is remarkable, that synthetic sequences for Eastern and Western parts of the molecule **H1** start with an accordingly substituted 2-bromoacetophenone, which gives the possibility to vary the substitution pattern on both phenyl rings of final molecules using same starting materials.

For the synthesis of derivatives carrying variations in other parts of the molecule (Western and Eastern phenyl), the building blocks and the synthetic strategy were changed accordingly. For the synthesis of derivatives **H2-H19** the 2-aminothiazole precursors were synthesized using accordingly substituted phenacyl bromides in the Hantzsch synthesis. In order to access compounds **H21**-**H23** differently substituted phenacyl bromides were used in the sequence analogous to the synthesis of the precursor **3**. Finally, we synthesized the compounds **H51**-**H53** using the substituted phenacyl bromide building blocks to access 2-aminothiazole precursors, while in order to access **H54** the 2-aminopyridine precursor was approached analogously to compound **17** (**Scheme 4**). The detailed synthetic procedures are provided in the supplementary material.

Chemistry for the modifications of the charged bicyclic fragment. In the synthesis of compound **H31**, we accessed the central piperidino-imidazolyl ring by utilizing the piperidine-2-imine building block in a synthetic sequence analogous to that used to resynthesize the original hit.

In case of the 1,4-disubstituted triazole **H32,** we relied on the copper-catalyzed [3+2]-azide-alkyne cycloaddition reaction[23] (see **Scheme 2**).

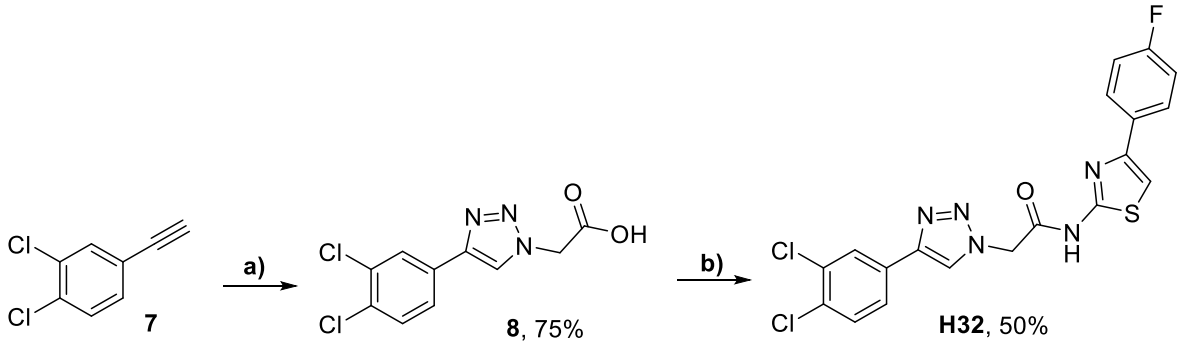

Scheme 2. The synthesis of compound **H32**.
Reagents and conditions: **a)** azidoacetic acid (1.0 eq), $CuSO_4$ (2 mol%), sodium ascorbate (4 mol%); DCM/H_2O (1:1 v/v); rt, o/n; **b)** 4-(4-fluorophenyl)-2-aminothiazole, HBTU, DIPEA; DCM; rt, o/n.

The acid **8** representing the Western part of the molecule **H32** was obtained employing the copper-catalyzed [3+2]-cycloaddition between (3,4-dichlorophenyl)-acetylene **7** and 2-azidoacetic acid. **8** was subsequently used to acylate 4-(4-fluorophenyl)-2-aminothiazole **5** employing HBTU as a coupling agent.

To obtain the cyclopenta[*c*]pyrazolic molecule **H33,** we established the following sequence (**Scheme 3**).

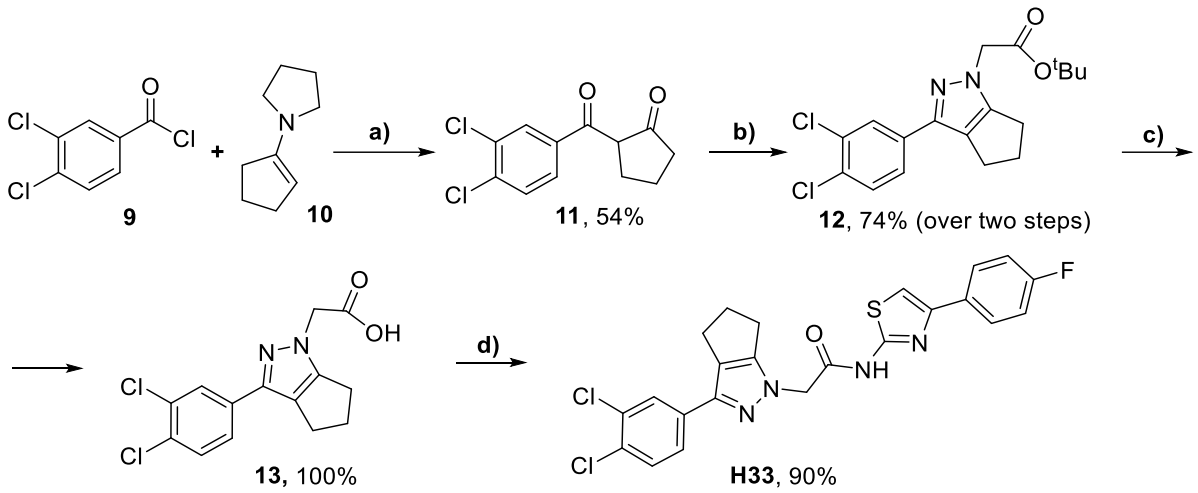

Scheme 3. The synthesis of pyrazolic analogue **H33**
Reagents and conditions: **a)** DIPEA, PhMe(anh.), 60 °C, 5 h; **b)** 1. $N_2H_4 \cdot HCl$ (1 eq), EtOH, reflux; 2. tert-butyl bromoacetate (1 eq), K_2CO_3, KI; MeCN, 70 °C, o/n; **c)** TFA, DCM; rt, 2 h; **d)** 4-(4-fluorophenyl)-2-aminothiazole, T3P, pyridine, rt, o/n.

The key intermediate in the presented synthetic route is the 1,3-dicarbonyl compound **9,** which we accessed by acylation of the enamine **10** (derived from cyclopentanone) with 3,4-dichorobenzoyl chloride **9**. The 1,3-diketone **11** is subsequently cyclized into a pyrazole, which is then alkylated by a bromoacetic acid ester to yield **12**. In the course of the alkylation, two possible isomers were formed, of which the more thermodynamically stable one prevailed. We confirmed the structure of the depicted isomer by observing the cross-peaks in the HMBC NMR spectrum (see **Supplementary material**).

Chemistry behind the modifications of the Eastern heterocycle. We accessed the precursors for the Eastern heterocycle of compounds **H41**, **H43** and **H44** by using palladium-catalyzed Suzuki coupling reactions (see **Scheme 4**). The oxazole analogue **H42** was synthesized by employing the Hantzsch approach analogous to the one used for the molecule **5.**

A Sonogashira cross-coupling reaction according to the **Scheme 5** afforded the precursors **21** and **23** for compounds **H44** and **H45**, respectively.

Coupling of obtained amines to the acid precursor **3** yielded molecules **H41–H46** (**Scheme 6**).

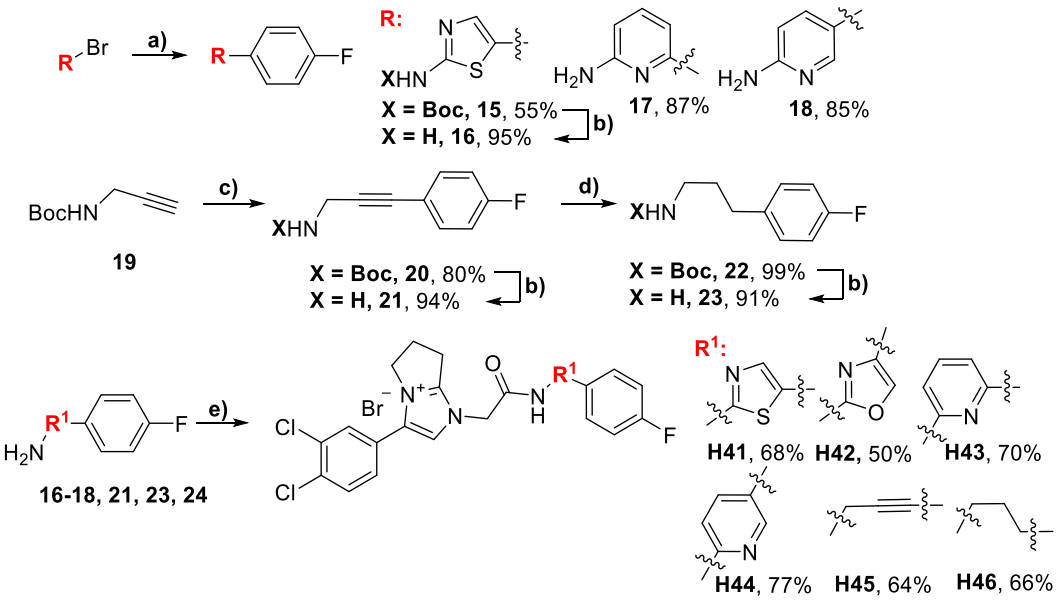

Scheme 4. Synthesis of compounds **H41-H46**

Reagents and conditions: **a)** (4-F)-PhB(OH)$_2$ (1.3 eq), [Pd(PPh$_3$)$_4$] (2 mol%), K$_3$PO$_4$ (3 eq), diox-H$_2$O, MW 150 W, 90 °C, 2 h; **b)** 4M HCl in diox., DCM, rt, 1h; **c)** 1-fluoro-4-iodobenzene (1 eq), [Pd(PPh$_3$)$_4$] (2 mol%), CuI (4 mol%), (iPr)$_2$NH, rt, o/n; **d)** H$_2$ (1 atm), Pd/C, THF, o/n; **e)** 3 (1 eq), T3P (2 eq), pyridine, rt, 2 h.

Chemistry of candidates with a modified linker. We accessed compounds with a modified/extended linker by alkylating pyrrolidinoimidazolic building blocks with appropriate carboxylic acid derivatives. We obtained the compound **H51** as a racemic mixture from optically inactive 2-bromo-*tert*-butylpropoanoate according to **Scheme 5**.

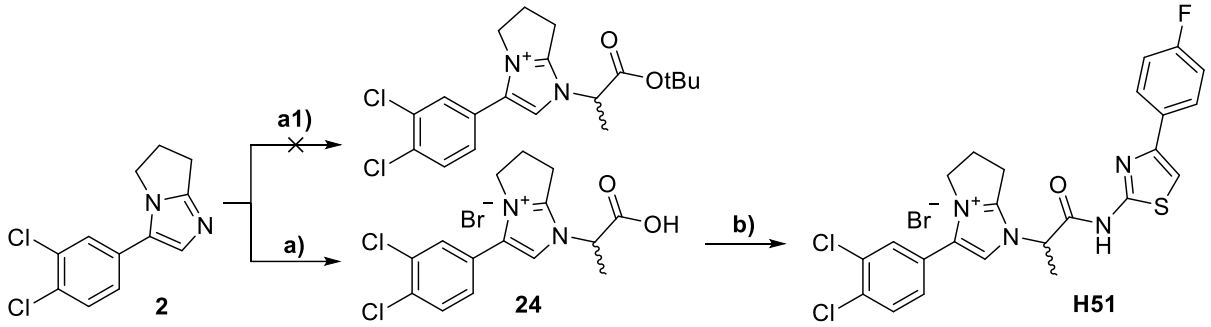

Scheme 5. The synthesis of precursors and the compound **H51**

Reagents and conditions: **a1**) Br(CH$_2$)$_2$CO$_2$tBu (5 eq), MeCN, 70 °C; **a)** 1. Ethyl 2-bromo-propanoate, KI (cat), MeCN, 70 °C, o/n.; 2. LiBr (10 eq), DIPEA (2 eq), MeCN +3% H$_2$O, rt, 2 h; **b)** 4-(4-fluorophenyl)-2-aminothiazole, T3P, pyridine, rt, 4 h.

Simultaneously, the alkylation of the imidazolinoimidazole proved to proceed sluggishly with low yields with ethyl 2-bromopropionate and other homologues of 2-bromoacetates, which precluded us from synthesizing preparative quantities of the corresponding analogues and explore possible effects of the linker elongation and substitution.

3.4 Experimental

Experimental procedures for chemical synthesis, biophysical analyses and microbiological experiments are provided in respective sections of the chapter **S3 Supplementary Material.**

3.5 Conclusions

In the course of this work, the comprehensive SAR behind the structure of the recently discovered molecule **H1** was established and summarized in **Figure 9**.

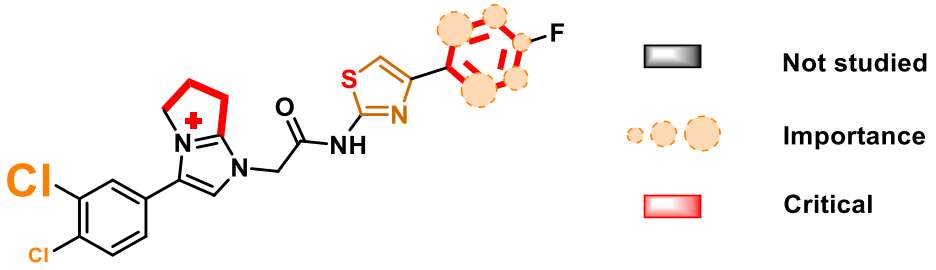

Figure 9. A graphical summary of antibacterial DnaN binding SAR for **H1** established in the present work.

The central positively charged pyrrolino-imidazolic fused ring system was found to be critical for both DnaN-binding and antibacterial activity. Along with that, these parameters of the candidates turned out to be very sensitive to modifications of the Eastern and Western ends of the molecule. Thus, the absence of the Eastern phenyl ring resulted in the abolition of DnaN binding and antibacterial activity, while the optimal substitution pattern of the ring included a strong electron-donating group in 4-position relative to the Eastern heterocycle, complemented by a moderate electron-withdrawing group(e.g –F or –Cl) at the 3- or 2- position of the same ring.

The 2-amino-4-arylthiazolic ring could be replaced by the 2-amino-5-arylaminothiazole without significant loss of antibacterial activity, while the replacement of the sulfur atom in the original **H1** structure with oxygen was found to be detrimental for both parameters. Conversely, substituting the original aminothiazole with 5- or 6-aryl-2-aminopyridines was associated with a positive impact on the compounds' DnaN binding and bacterial growth inhibition.

In the Western phenyl ring the chlorine atom in the 3rd position was demonstrated to be a more significant contributor to DnaN binding and to antibacterial activity, which partially supported the binding mode of **H1** suggested by the soaked structure of *R. typhi* sliding clamp with **H1.**

Derivatives synthesized for SAR exploration and optimization showed a reasonably improved ability to inhibit DNA replication *in vitro* (~3-fold) and the growth of various Mycobacteria, *S. aureus* and *S. pneumoniae* (2–4-fold). Simultaneously, optimized derivatives were comparably active only against efflux-deficient *E. coli*. Owing to its nature of quaternary ammonium salt, the scaffold was found to be a substrate for efflux transporters, which was demonstrated by a dramatic decrease of activity against wild-type Gram-negative strains.

Finally, we studied the ADMET properties for most of derivatives synthesized in this work, showing marked metabolic stability, and identified metabolically labile parts of the scaf-

fold. The susceptibility of certain derivatives for microsomal oxidation was associated with modifications of Eastern phenyl and heterocycle. Among the derivatives synthesized in the course of optimization we identified those inhibiting various groups of cytochrome enzymes.

Additionally, we identified the structural features of the scaffold responsible for solubility and compounds' ability to undergo intestinal absorption.

3.6 References

[1] A. Johnson, M. O'Donnell, *Annu. Rev. Biochem.* **2005**, *74*, 283–315.

[2] X. P. Kong, R. Onrust, M. O'Donnell, J. Kuriyan, *Cell* **1992**, *69*, 425–437.

[3] A. Robinson, A. J. Brzoska, K. M. Turner, R. Withers, E. J. Harry, P. J. Lewis, N. E. Dixon, *Microbiol. Mol. Biol. Rev.* **2010**, *74*, 273–297.

[4] A. Kling, P. Lukat, D. V. Almeida, A. Bauer, E. Fontaine, S. Sordello, N. Zaburannyi, J. Herrmann, S. C. Wenzel, C. König, N. C. Ammerman, M. B. Barrio, K. Borchers, F. Bordon-Pallier, M. Brönstrup, G. Courtemanche, M. Gerlitz, M. Geslin, P. Hammann, D. W. Heinz, H. Hoffmann, S. Klieber, M. Kohlmann, M. Kurz, C. Lair, H. Matter, E. Nuermberger, S. Tyagi, L. Fraisse, J. H. Grosset, S. Lagrange, R. Müller, *Science (80-.).* **2015**, *348*, 1106–1112.

[5] R. E. Georgescu, O. Yurieva, S. S. Kim, J. Kuriyan, X. P. Kong, M. O'Donnell, *Proc. Natl. Acad. Sci. U. S. A.* **2008**, *105*, 11116–11121.

[6] Z. Yin, L. R. Whittell, Y. Wang, S. Jergic, M. Liu, E. J. Harry, N. E. Dixon, J. L. Beck, M. J. Kelso, A. J. Oakley, *J. Med. Chem.* **2014**, *57*, 2799–2806.

[7] Z. Yin, L. R. Whittell, Y. Wang, S. Jergic, C. Ma, P. J. Lewis, N. E. Dixon, J. L. Beck, M. J. Kelso, A. J. Oakley, *J. Med. Chem.* **2015**, *58*, 4693–4702.

[8] A. Kling, P. Lukat, D. V. Almeida, A. Bauer, E. Fontaine, S. Sordello, N. Zaburannyi, J. Herrmann, S. C. Wenzel, C. König, N. C. Ammerman, M. B. Barrio, K. Borchers, F. Bordon-Pallier, M. Brönstrup, G. Courtemanche, M. Gerlitz, M. Geslin, P. Hammann, D. W. Heinz, H. Hoffmann, S. Klieber, M. Kohlmann, M. Kurz, C. Lair, H. Matter, E. Nuermberger, S. Tyagi, L. Fraisse, J. H. Grosset, S. Lagrange, R. Müller, *Science (80-.).* **2015**, *348*, 1106–1112.

[9] G. Wijffels, W. M. Johnson, A. J. Oakley, K. Turner, V. C. Epa, S. J. Briscoe, M. Polley, A. J. Liepa, A. Hofmann, J. Buchardt, C. Christensen, P. Prosselkov, B. P. Dalrymple, P. F. Alewood, P. A. Jennings, N. E. Dixon, D. A. Winkler, *J. Med. Chem.* **2011**, *54*, 4831–4838.

[10] P. Wolff, V. Oliéric, J. P. Briand, O. Chaloin, A. Dejaegere, P. Dumas, E. Ennifar, G. Guichard, J. Wagner, D. Y. Burnouf, *J. Med. Chem.* **2011**, *54*, 4627–4637.

[11] P. Wolff, I. Amal, V. Oliéric, O. Chaloin, G. Gygli, E. Ennifar, B. Lorber, G. Guichard, J. Wagner, A. Dejaegere, D. Y. Burnouf, *J. Med. Chem.* **2014**, *57*, 7565–7576.

[12] F. Mancini, M. Y. Unver, W. A. M. Elgaher, V. R. Jumde, A. Alhayek, P. Lukat, J. Herrmann, M. D. Witte, M. Köck, W. Blankenfeldt, R. Müller, A. K. H. Hirsch, *Chem. – A Eur. J.* **2020**, chem.202002250.

[13] J. G. Topliss, *J. Med. Chem.* **1972**, *15*, 1006–1011.

[14] M. F. Richter, B. S. Drown, A. P. Riley, A. Garcia, T. Shirai, R. L. Svec, P. J. Hergenrother, *Nature* **2017**, DOI 10.1038/nature22308.

[15] S. J. Perlmutter, E. J. Geddes, B. S. Drown, S. E. Motika, M. R. Lee, P. J. Hergenrother, *ACS Infect. Dis.* **2021**, DOI 10.1021/acsinfecdis.0c00715.

[16] M. Mayer, B. Meyer, *J. Am. Chem. Soc.* **2001**, *123*, 6108–6117.

[17] N. Schneider, G. Lange, S. Hindle, R. Klein, M. Rarey, *J. Comput. Aided. Mol. Des.* **2013**, *27*, 15–29.

[18] P. Auffinger, F. A. Hays, E. Westhof, P. Shing Ho, **2004**, *101*, 16789–16794.

[19] Z. Yin, M. J. Kelso, J. L. Beck, A. J. Oakley, *J. Med. Chem.* **2013**, *56*, 8665–8673.

[20] K. M. Pos, *Biochim. Biophys. Acta - Proteins Proteomics* **2009**, *1794*, 782–793.

[21] S. G. Sligar, *Essays Biochem.* **1999**, *34*, 71–83.

[22] V. A. Kovtunenko, K. G. Nazarenko, A. M. Demchenko, T. G. S. N. Unkiversity, **1996**, *32*, 923–927.

[23] V. V. Rostovtsev, L. G. Green, V. V. Fokin, K. B. Sharpless, *Angew. Chem. Int. Ed. Engl.* **2002**, *41*, 2596–2599.

S3 Supplementary material for Chapter 3

Topliss scheme that provided the basis for the optimization of compounds

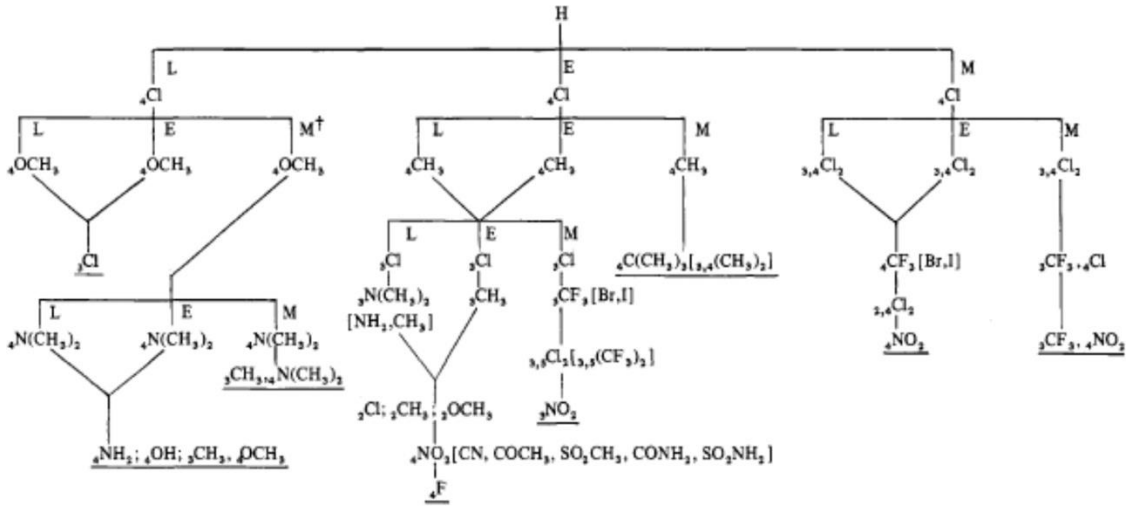

Figure S1. The Topliss method for potency optimization of aromatic ring-containing hit or lead compounds considers effects on hydrophobic, electronic and steric Hansch parameters (L = less active, E = equiactive, M = more active; descending lines indicate sequence; square brackets indicate alternates; compared to 4-H compound). Adapted from J. G. Topliss.

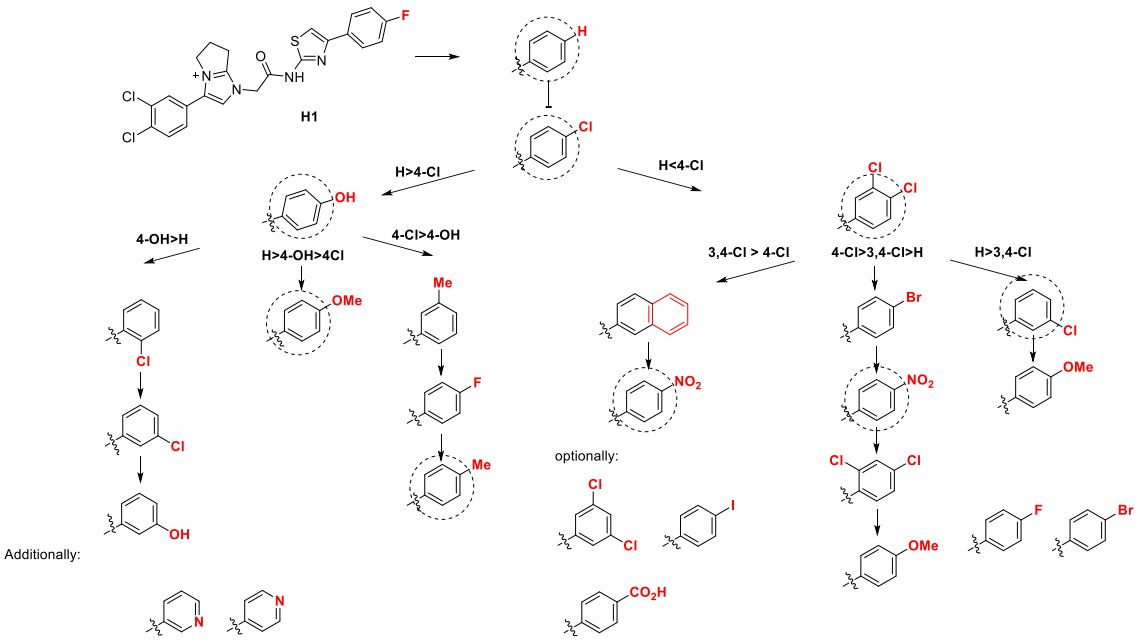

Figure S2. Matsy decision tree for the western phenyl portion of **H1.** Figure is adapted from O'Boyle et al[1]

S3.1 Experimental procedures

S3.1.1 Synthesis of the virtual hit and its derivatives

All reagents were used from commercial suppliers without further purification. Procedures were not optimized regarding yield. NMR spectra were recorded on a Bruker AV 500 (500MHz) spectrometer. Liquid chromatography-Mass spectrometry was performed on a SpectraSystems-MSQ LCMS system (Thermo Fisher, Dreieich, Germany). Flash chromatography was performed using the automated flash chromatography system CombiFlash Rf+ (Teledyne ISCO, Lincoln, NE, USA) equipped with RediSepRf silica columns (AxelSemrau, Sprockhövel Germany), Chromabond Flash C18 columns (Macherey-Nagel, Düren,Germany) or self-packed alumina flash-columns (Thermo Fischer Scientific). Purity of compounds synthesized was determined by LC-MS using the area percentage method on the UV trace recorded at a wavelength of 254 nm and found to be >95%.

General procedure of the synthesis of substituted 2-bromo-1-arylethan-1-ones

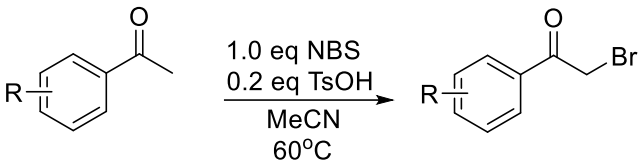

To the stirred at 60°C solution of 1-arylethan-1-one (1 eq) and 4-toluenesulfonic acid monohydrate (0.2 eq) acetonitrile (0.05 M), was added the solution of NBS (1 eq) in acetonitrile (0.05 M) dropwise over 30 minutes. The resulting mixture was stirred at 60°C for approximately 4 hours, and once TLC indicated full consumption of the starting material, the heating was stopped. The reaction mixture was concentrated *in vacuo*, the residue was taken up into the saturated aqueous solution of $NaHCO_3$ and extracted with ether (3x50ml). Combined ethereal fractions were washed with brine and dried over anhydrous sodium sulfate and concentrated *in vacuo* to afford the desired bromoacetophenones, which were used in the next step without additional purification.

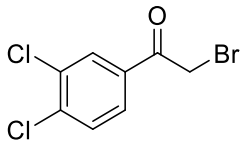

2-bromo-1-(3,4-dichlorophenyl)ethan-1-one. Obtained as white solid (8300 mg, 90%).

^{1}H NMR (500 MHz, DMSO-d_6) δ 8.21 (d, *J* = 2.1 Hz, 1H), 7.94 (dd, *J* = 8.4, 2.1 Hz, 1H), 7.83 (d, *J* = 8.4 Hz, 1H), 4.97 (s, 2H).

^{13}C NMR (126 MHz, DMSO-d_6) δ 189.99, 136.67, 134.19, 131.91, 131.21, 130.59, 128.67, 34.16.

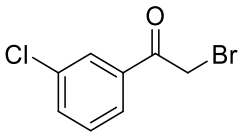

2-bromo-1-(3-chlorophenyl)ethan-1-one. Purified by column chromatography on silica (Hexane-DCM). Obtained as white solid (873 mg, 74%).

^{1}H NMR (500 MHz, Acetone-d_6) δ 8.48 (t, *J* = 1.8 Hz, 1H), 8.48 – 8.45 (m, 1H), 8.17 – 8.14 (m, 1H), 8.05 (t, *J* = 7.9 Hz, 1H), 5.27 (s, 2H).

^{13}C NMR (126 MHz, Acetone-d_6) δ 191.04, 136.99, 135.34, 134.33, 131.53, 129.37, 128.18, 32.96.

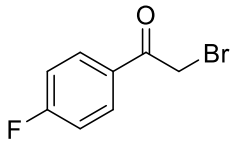

2-bromo-1-(4-fluorophenyl)ethan-1-one. Purified by column chromatography on silica (Hexane-DCM). Obtained as white solid (800 mg, 75%).

^{1}H NMR (500 MHz, $CDCl_3$) δ 8.05 – 8.00 (m, 2H), 7.19 – 7.13 (m, 2H), 4.41 (s, 2H).

^{19}F NMR (470 MHz, DMSO-d_6) δ -112.09.

^{13}C NMR (126 MHz, $CDCl_3$) δ 189.98, 166.30 (d, *J* = 256.5 Hz), 131.88 (d, *J* = 9.4 Hz), 130.48 (d, *J* = 2.8 Hz), 116.25 (d, *J* = 22.1 Hz), 30.57

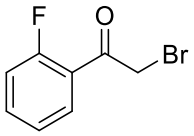

2-bromo-1-(2-fluorophenyl)ethan-1-one. Purified by column chromatography on silica (Hexane-DCM) Obtained as white solid (520 mg, 80%).

^{1}H NMR (500 MHz, $CDCl_3$) δ 7.92 (td, *J* = 7.6, 1.8 Hz, 1H), 7.59 – 7.54 (m, 1H), 7.28 – 7.23 (m, 1H), 7.16 (dd, *J* = 11.3, 8.4 Hz, 1H), 4.51 (d, *J* = 2.4 Hz, 1H).

^{19}F NMR (470 MHz, $CDCl_3$) δ -108.46.

^{13}C NMR (126 MHz, $CDCl_3$) δ 189.27 (d, *J* = 3.8 Hz), 161.87 (d, *J* = 254.7 Hz), 135.79 (d, *J* = 9.3 Hz), 131.65 (d, *J* = 2.4 Hz), 125.03 (d, *J* = 3.4 Hz), 122.92 (d, *J* = 13.0 Hz), 116.83 (d, *J* = 23.8 Hz), 36.11 (d, *J* = 10.2 Hz).

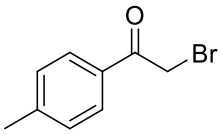

2-bromo-1-(p-tolyl)ethan-1-one. Obtained as white solid (1000 mg, 72%).

^{1}H NMR (500 MHz, $CDCl_3$) δ 7.88 (d, *J* = 8.3 Hz, 2H), 7.29 (d, *J* = 8.1 Hz, 2H), 4.43 (s, 2H), 2.42 (s, 3H).

^{13}C NMR (126 MHz, $CDCl_3$) δ 191.07, 145.14, 131.58, 129.68, 129.17, 31.09, 21.88.

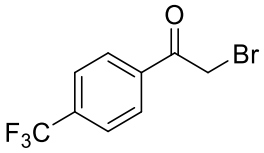

2-bromo-1-(4-(trifluoromethyl)phenyl)ethan-1-one. Obtained as white solid (825 mg, 62%).

^{1}H NMR (500 MHz, $CDCl_3$) δ 8.10 (d, *J* = 8.2 Hz, 1H), 7.77 (d, *J* = 8.2 Hz, 1H), 4.45 (s, 1H).

^{19}F NMR (470 MHz, $CDCl_3$) δ -63.27.

^{13}C NMR (126 MHz, $CDCl_3$) δ 190.56, 136.74, 135.32 (q, *J* = 32.7 Hz), 129.49, 126.10 (q, *J* = 3.6 Hz), 123.54 (q, *J* = 273.0 Hz), 30.43.

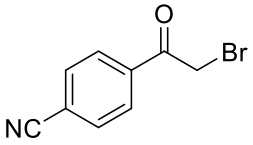

4-(2-bromoacetyl)benzonitrile. Obtained as white solid (1109 mg, quant).

^{1}H NMR (500 MHz, $CDCl_3$) δ 8.11 – 8.07 (m, 2H), 7.83 – 7.79 (m, 2H), 4.43 (s, 2H).

^{13}C NMR (126 MHz, $CDCl_3$) δ 190.22, 137.05, 132.83, 129.55, 117.78, 117.35, 30.08.

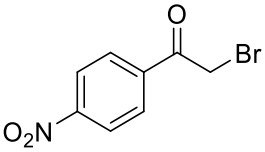

2-bromo-1-(4-nitrophenyl)ethan-1-one. Obtained as pale yellow solid (1203 mg, 98%).

^{1}H NMR (500 MHz, $CDCl_3$) δ 8.37 – 8.32 (m, 2H), 8.18 – 8.13 (m, 2H), 4.46 (s, 2H).

^{13}C NMR (126 MHz, $CDCl_3$) δ 190.03, 150.83, 138.49, 130.21, 124.18, 30.28.

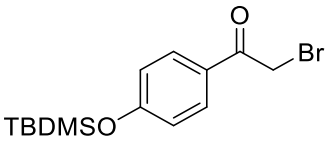

2-bromo-1-(4-hydroxyphenyl)ethan-1-one. Obtained as a white solid (498 mg, 75%).

^{1}H NMR (500 MHz, Acetone-d_6) δ 8.03 – 7.95 (m, 2H), 7.05 – 7.00 (m, 2H), 4.94 (s, 2H), 1.01 (s, J = 2.7 Hz, 9H), 0.31 – 0.26 (m, 6H).

^{13}C NMR (126 MHz, Acetone-d_6) δ 190.36, 161.56, 132.10, 131.68, 129.19, 120.99, 47.09, 32.63, 25.91, 18.83, 14.50.

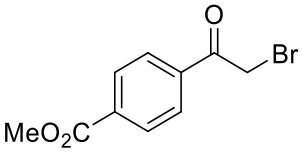

Methyl 4-(2-bromoacetyl)benzoate. Obtained as a white solid (819 mg, **64%**).

^{1}H NMR (500 MHz, $CDCl_3$) δ 8.16 – 8.13 (m, 2H), 8.05 – 8.02 (m, 2H), 4.46 (s, 2H), 3.95 (s, 3H).

^{13}C NMR (126 MHz, $CDCl_3$) δ 191.05, 166.17, 137.37, 134.85, 130.24, 129.10, 52.79, 30.89.

General procedure of the synthesis of cyclic amidoimines from lactones.

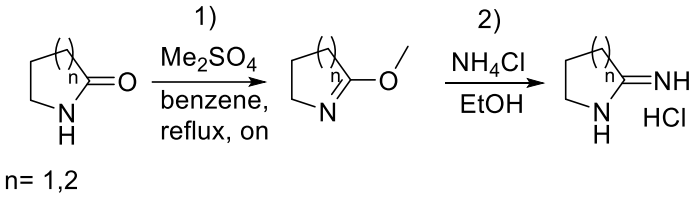

n= 1,2

Step 1. A two-necked round-bottom flask equipped with a condenser and a dripping funnel was charged with the lactone (10 mmol) in 50 ml of dry benzene. The resulting solution was brought to the reflux point, after which the addition of dimethyl sulfate was started (1 drop per 2 seconds). After the addition of dimethylsulfate was finished, the dripping funnel was replaced with a cap and the reaction mixture was refluxed for three more hours. The reaction mixture was then poured into a glass of ice-cold water and the resulting suspension was extracted three times with diethyl ether, washed with brine and dried over anhydrous sodium sulfate. The sodium sulfate was filtered off and the mother liquor was concentrated under reduced pressure. *Warning*: in order to minimize possible losses of the product due to its volatility, the solution was being concentrated under 500 mbar at 40ºC. The title methyl iminoether was obtained as clear yellowish liquid, which was used in the next step without additional purification.

Step 2. The methyl iminoether was dissolved in ethanol (0.1 M) and equimolar quantity of NH_4Cl was added to the ethanolic solution. The resulting mixture was stirred for 8 hours at room temperature. The reaction mixture was filtered through a paper filter and concentrated in vacuo to give the hydrochloric salt of the corresponding iminolactone, which can be recrystallized from ethanol if necessary.

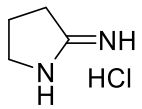

Pyrrolidine-2-imine hydrochloride. White crystals (5.5 g, 91% yield).

LC-MS: 85.05.

^{1}H NMR (500 MHz, DMSO-d_6) δ 9.12 (s, 1H), 8.86 (s, 1H), 7.37 (s, 1H), 3.51 (t, *J* = 7.1 Hz, 2H), 2.75 (t, *J* = 8.0 Hz, 2H), 2.08 – 1.98 (m, 2H).

^{13}C NMR (126 MHz, DMSO-d_6) δ 170.87, 47.08, 30.29, 20.30.

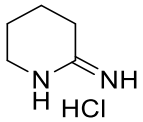

Piperidine-2-imine hydrochloride. White crystals (10.5 g, 80%).

LC-MS: 99.11

^{1}H NMR (500 MHz, DMSO-d_6) δ 9.52 (s, 1H), 8.68 (s, 1H), 8.36 (s, 1H), 3.28 – 3.23 (m, 1H), 1.73 – 1.64 (m, 2H).

^{13}C NMR (126 MHz, DMSO-d_6) δ 166.29, 40.73, 25.48, 20.28, 17.51.

General procedure of the synthesis of 3-aryl-6,7-dihydro-5H-pyrrolo[1,2-a]imidazoles.

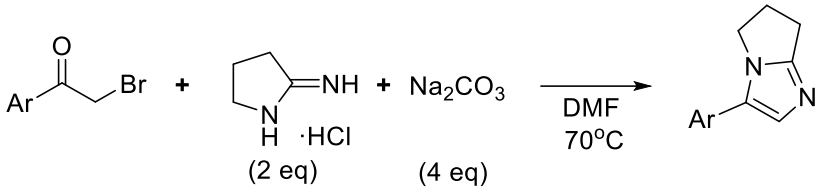

The corresponding 2-bromomethylaryl ketone (1 equivalent) is stirred in DMF together with pyrrolidine-2-imine hydrochloride (2 equivalents) and sodium carbonate (4 equivalents) at 70°C for 8 hours. The reaction mixture is then poured into tenfold volume of water, and the resulting mixture was extracted thrice with diethyl ether. The combined ethereal fractions were washed with brine, dried over anhydrous sodium sulfate, filtered and concentrated *in vacuo* to furnish the desired compound, typically of dark red colour.

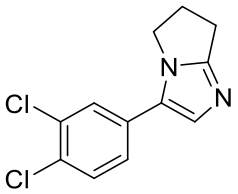

3-(3,4-dichlorophenyl)-6,7-dihydro-5H-pyrrolo[1,2-a]imidazole. Obtained as bordeaux-coloured oil solidifying upon standing (1010 mg, 86%).

LC-MS: $[M+H]^+$ 253.04

^{1}H NMR (500 MHz, DMSO-d_6) δ 7.92 (d, *J* = 2.0 Hz, 1H), 7.70 (s, 1H), 7.68 (dd, *J* = 8.4, 2.0 Hz, 1H), 7.54 (d, *J* = 8.4 Hz, 1H), 4.00 – 3.94 (m, 2H), 2.77 – 2.73 (m, 2H).

^{13}C NMR (126 MHz, DMSO-d_6) δ: 162.76, 155.35, 142.63, 136.58, 131.72, 131.09, 125.80, 124.41, 113.40, 44.85, 26.15, 22.83.

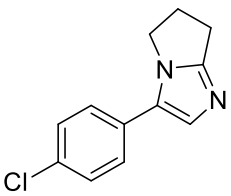

3-(4-chlorophenyl)-6,7-dihydro-5H-pyrrolo[1,2-a]imidazole. Obtained as an orange solid (270 mg, 99%).

LC-MS: $[M+H]^+$ 219.12

^{1}H NMR (500 MHz, DMSO-d_6) δ 7.75 – 7.69 (m, 2H), 7.59 (s, 1H), 7.37 – 7.34 (m, 2H), 3.98 – 3.94 (m, 2H), 2.77 – 2.73 (m, 2H), 2.54 – 2.47 (m, 2H).

^{13}C NMR (126 MHz, DMSO-d_6) δ 162.29, 154.58, 143.49, 130.06, 128.39, 125.58, 111.87, 44.31, 25.68, 22.41.

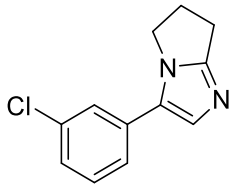

3-(3-chlorophenyl)-6,7-dihydro-5H-pyrrolo[1,2-a]imidazole. Obtained as deep red oil (400 mg, 91%).

LC-MS: $[M+H]^+$ 218.99

^{1}H NMR (500 MHz, DMSO-d_6) δ 7.76 – 7.74 (m, 1H), 7.69 – 7.66 (m, 2H), 7.35 (t, *J* = 7.9 Hz, 1H), 7.22 – 7.20 (m, 1H), 4.00 – 3.96 (m, 2H), 2.78 – 2.74 (m, 2H), 2.56 – 2.45 (m, 2H).

^{13}C NMR (126 MHz, DMSO-d_6) δ 162.32, 154.70, 143.15, 136.59, 132.90, 130.32, 123.48, 122.44, 112.48, 44.36, 25.69, 22.40.

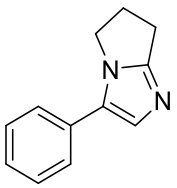

3-phenyl-6,7-dihydro-5H-pyrrolo[1,2-a]imidazole. Obtained as a light orange solid (253 mg, 69%).

LC-MS: $[M+H]^+$ 185.14

^{1}H NMR (500 MHz, DMSO-d_6) δ 7.71 (d, *J* = 7.2 Hz, 2H), 7.54 (s, 1H), 7.31 (t, *J* = 7.7 Hz, 2H), 7.15 (t, *J* = 7.4 Hz, 1H), 3.98 – 3.94 (m, 2H), 2.78 – 2.73 (m, 2H), 2.51 (p, *J* = 7.4 Hz, 2H).

^{13}C NMR (126 MHz, DMSO-d_6) δ 162.30, 154.32, 144.70, 135.37, 128.39, 125.85, 123.97, 111.29, 44.26, 25.68, 22.44.

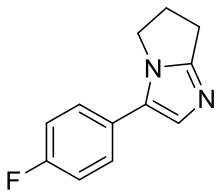

3-(4-fluorophenyl)-6,7-dihydro-5H-pyrrolo[1,2-a]imidazole. Obtained as a deep red oil, which solidified upon standing (139 mg, 67%)**.**

LC-MS: $[M+H]^+$ 203.03

^{1}H NMR (500 MHz, DMSO-d_6) δ 7.75 – 7.70 (m, 2H), 7.53 (s, 1H), 7.17 – 7.11 (m, 2H), 3.98 – 3.93 (m, 2H), 2.78 – 2.72 (m, 2H).

^{13}C NMR (126 MHz, DMSO-d_6) δ 160.69 (d, *J* = 241.9 Hz), 154.36, 143.77, 131.91, 125.67 (d, *J* = 8.0 Hz), 115.15 (d, *J* = 21.2 Hz), 111.09, 44.26, 25.65, 22.40.

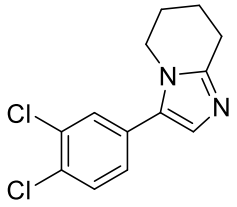

3-(3,4-dichlorophenyl)-5,6,7,8-tetrahydroimidazo[1,2-a]pyridine. Obtained as deep red solid (725 mg, 90%).

LC-MS: $[M+H]^+$ 266.89.

^{1}H NMR (500 MHz, DMSO-d_6) δ 7.91 (d, *J* = 2.0 Hz, 1H), 7.68 (dd, *J* = 8.4, 2.0 Hz, 1H), 7.63 (s, 1H), 7.56 (d, *J* = 8.4 Hz, 1H), 3.96 (t, *J* = 5.9 Hz, 2H), 2.75 (t, *J* = 6.3 Hz, 2H), 1.94 – 1.88 (m, 2H), 1.88 – 1.81 (m, 2H).

^{13}C NMR (126 MHz, DMSO-d_6) δ 145.05, 136.50, 135.70, 131.25, 130.67, 127.73, 125.41, 124.03, 116.38, 44.47, 24.06, 22.42, 20.51.

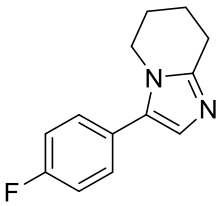

3-(4-fluorophenyl)-5,6,7,8-tetrahydroimidazo[1,2-a]pyridine. Obtained as orange solid (1200 mg, 80%).

LC-MS: $[M+H]^+$ 217.18

^{1}H NMR (500 MHz, DMSO-d_6) δ 7.75 – 7.70 (m, 2H), 7.44 (s, 1H), 7.17 – 7.11 (m, 2H), 3.96 (t, *J* = 5.9 Hz, 2H), 2.78 – 2.73 (m, 2H), 1.95 – 1.81 (m, 4H).

^{19}F NMR (470 MHz, DMSO-d_6) δ -116.18 – -117.85 (m).

^{13}C NMR (126 MHz, DMSO-d_6) δ 160.72 (d, *J* = 241.6 Hz), 144.49, 138.04, 131.47 (d, *J* = 2.8 Hz), 125.74 (d, *J* = 7.8 Hz), 115.17 (d, *J* = 21.4 Hz), 114.54, 44.31, 24.10, 22.51, 20.64.

General procedure of the the synthesis of 3-aryl-1-(2-(tert-butoxy)-2-oxoethyl)-1,5,6,7-tetrahydropyrrolo[1,2-a]imidazol-4-ium bromides

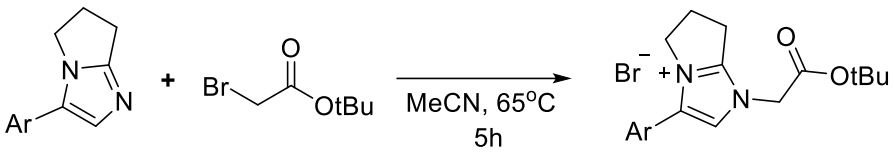

The corresponding imidazole (1 eq) together with tert-butyl bromoacetate (2 eq) is dissolved in MeCN (2.5 ml per 1 mole of the pyrrollidinoimidazole), the reaction vessel is put under nitrogen and heated up to 65ºC. After the completion of the alkylation, the volatiles are removed *in vacuo* and the residue is washed with diethyl ether to furnish the desired compound as a precipitate.

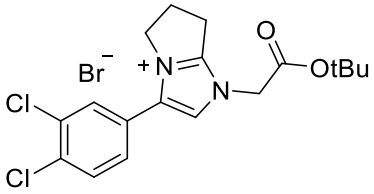

1-(2-(tert-butoxy)-2-oxoethyl)-3-(3,4-dichlorophenyl)-1,5,6,7-tetrahydropyrrolo[1,2-a]imidazol-4-ium bromide. Isolated as an orange solid (2200 mg, 91%).

LC-MS: $[M]^+$ 367.06.

^{1}H NMR (500 MHz, DMSO-d_6) δ 8.00 (s, 1H), 7.87 (d, *J* = 8.3 Hz, 1H), 7.75 (s, 1H), 7.46 (d, *J* = 8.3 Hz, 1H), 5.15 (s, 2H), 4.34 (t, *J* = 7.2 Hz, 2H), 3.24 (t, *J* = 7.4 Hz, 2H), 2.75 – 2.67 (m, 2H), 1.31 (s, 9H).

^{13}C NMR (126 MHz, DMSO-d_6) δ 165.40, 154.69, 135.32, 133.24, 132.07, 131.58, 130.65, 129.32, 126.65, 117.17, 83.45, 48.81, 48.27, 27.34, 25.11, 23.50.

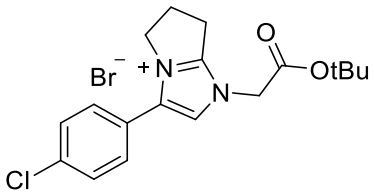

1-(2-(tert-butoxy)-2-oxoethyl)-3-(4-chlorophenyl)-1,5,6,7-tetrahydropyrrolo[1,2-a]imidazol-4-ium bromide. Obtained as a slightly orange solid (270 mg, 53%).

LC-MS: $[M]^+$ 333.10.

^{1}H NMR (500 MHz, DMSO-d_6) δ 7.95 (s, 1H), 7.69 – 7.63 (m, 2H), 7.50 – 7.46 (m, 2H), 5.10 (s, 2H), 4.37 – 4.31 (m, 2H), 3.23 (t, *J* = 7.6 Hz, 2H), 2.75 – 2.68 (m, 2H), 1.30 (s, 9H).

^{13}C NMR (126 MHz, DMSO-d_6) δ 165.23, 154.37, 136.58, 135.16, 130.83, 129.37, 124.86, 116.47, 83.29, 48.68, 48.11, 27.30, 25.06, 23.45.

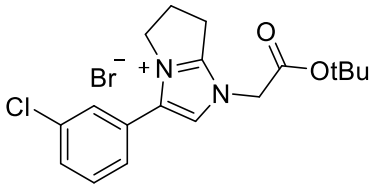

1-(2-(tert-butoxy)-2-oxoethyl)-3-(3-chlorophenyl)-1,5,6,7-tetrahydropyrrolo[1,2-a]imidazol-4-ium bromide. Obtained as a brownish solid (480 mg, 63%).

LC-MS: $[M]^+$ 333.10.

^{1}H NMR (500 MHz, DMSO-d_6) δ 7.99 (s, 1H), 7.65 (ddd, *J* = 8.1, 2.0, 1.1 Hz, 1H), 7.60 (t, *J* = 7.9 Hz, 1H), 7.54 (t, *J* = 1.8 Hz, 1H), 7.46 – 7.43 (m, 1H), 5.13 (s, 2H), 4.34 (t, *J* = 7.3 Hz, 2H), 3.24 (t, *J* = 7.6 Hz, 2H), 2.71 (p, *J* = 7.6 Hz, 2H), 1.31 (s, 9H).

^{13}C NMR (126 MHz, DMSO-d_6) δ 165.32, 154.50, 136.23, 133.86, 131.26, 130.13, 128.46, 128.01, 127.73, 116.83, 83.34, 48.73, 48.24, 27.32, 25.07, 23.44.

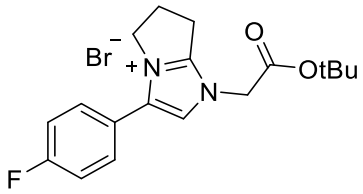

1-(2-(tert-butoxy)-2-oxoethyl)-3-(4-fluorophenyl)-1,5,6,7-tetrahydropyrrolo[1,2-a]imidazol-4-ium bromide. Obtained as a reddish solid (227 mg, 83%).

LC-MS: $[M]^+$ 317.23.

^{1}H NMR (500 MHz, DMSO-d_6) δ 7.92 (s, 1H), 7.54 – 7.50 (m, 2H), 7.46 – 7.40 (m, 2H), 5.08 (s, 2H), 4.38 – 4.31 (m, 2H), 3.24 (t, *J* = 7.6 Hz, 2H), 2.78 – 2.67 (m, 2H), 1.29 (s, 9H).

^{13}C NMR (126 MHz, DMSO-d_6) δ 165.22, 163.08 (d, *J* = 248.3 Hz), 154.09, 136.73, 131.64 (d, *J* = 9.0 Hz), 122.40 (d, *J* = 3.4 Hz), 116.30, 116.36 (d, *J* = 22.0 Hz), 83.22, 48.64, 48.03, 27.30, 25.04, 23.45.

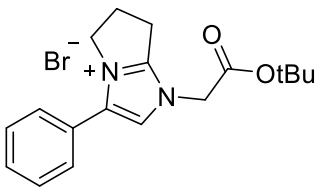

1-(2-(tert-butoxy)-2-oxoethyl)-3-phenyl-1,5,6,7-tetrahydropyrrolo[1,2-a]imidazol-4-ium bromide. Obtained as a reddish solid (420 mg, 80%).

LC-MS: $[M]^+$ 299.13.

^{1}H NMR (500 MHz, DMSO-d_6) δ 7.92 (s, *J* = 4.9 Hz, 1H), 7.56 (dd, *J* = 6.6, 3.5 Hz, 3H), 7.48 – 7.42 (m, 2H), 5.08 (s, 2H), 4.35 (t, *J* = 7.3 Hz, 2H), 3.24 (t, *J* = 7.6 Hz, 2H), 2.76 – 2.68 (m, 2H), 1.28 (s, 9H).

^{13}C NMR (126 MHz, DMSO-d_6) δ 165.27, 154.15, 137.77, 130.21, 129.30, 128.98, 125.94, 116.09, 83.21, 48.63, 48.13, 27.31, 25.06, 23.45.

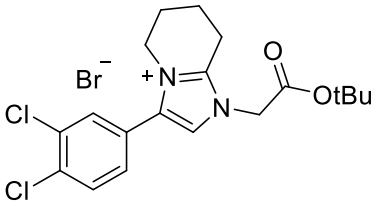

1-(2-(tert-butoxy)-2-oxoethyl)-3-(3,4-dichlorophenyl)-5,6,7,8-tetrahydro-1H-imidazo[1,2-a]pyridin-4-ium. Obtained as an orange-yellow solid (886 mg, 85%).

LC-MS: $[M]^+$ 381.14.

^{1}H NMR (500 MHz, DMSO-d_6) δ 7.98 (s, 1H), 7.88 (d, *J* = 8.3 Hz, 1H), 7.69 (d, *J* = 2.1 Hz, 1H), 7.42 (dd, *J* = 8.3, 2.1 Hz, 1H), 5.08 (s, 2H), 4.21 (t, *J* = 5.6 Hz, 2H), 3.02 (t, *J* = 6.1 Hz, 2H), 2.04 – 1.96 (m, 4H), 1.35 (s, 9H).

^{13}C NMR (126 MHz, DMSO-d_6) δ 165.51, 146.28, 133.30, 132.03, 131.59, 130.82, 129.42, 126.09, 120.37, 83.51, 46.66, 46.30, 27.47, 27.34, 20.73, 20.69, 17.50.

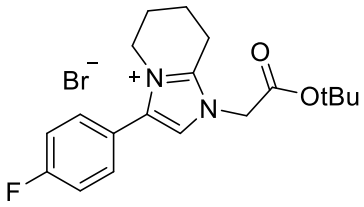

1-(2-(tert-butoxy)-2-oxoethyl)-3-(4-fluorophenyl)-5,6,7,8-tetrahydro-1H-imidazo[1,2-a]pyridin-4-ium bromide. Obtained as reddish solid (300 mg, 42%).

LC-MS: $[M]^+$ 331.27.

^{1}H NMR (500 MHz, DMSO-d_6) δ 7.84 (s, *J* = 8.1 Hz, 1H), 7.50 – 7.45 (m, 2H), 7.45 – 7.40 (m, 2H), 4.94 (s, 2H), 4.20 (t, *J* = 5.6 Hz, 2H), 2.99 (t, *J* = 6.0 Hz, 2H), 2.06 – 1.93 (m, 4H), 1.30 (s, 9H).

^{19}F NMR (470 MHz, DMSO-d_6) δ -109.25 – -110.62 (m).

^{13}C NMR (126 MHz, DMSO-d_6) δ 165.53, 163.35 (d, *J* = 248.4 Hz), 145.95, 132.48, 132.03 (d, *J* = 9.0 Hz), 122.01 (d, *J* = 2.9 Hz), 119.68, 116.63 (d, *J* = 22.1 Hz), 83.68, 46.69, 46.36, 27.51, 20.96, 20.88, 17.74.

General procedure of the removal of the tert-butyl protecting group.

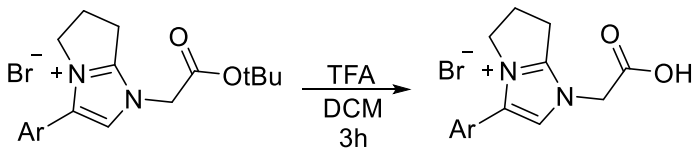

The tert-butyl protected intermediate was dissolved in dry DCM and 5 eq of TFA is added thereto. The resulting mixture was stirred for 6 hours at room temperature.

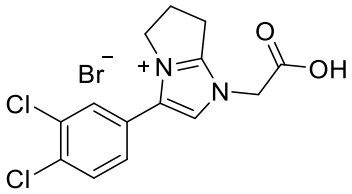

1-(carboxymethyl)-3-(3,4-dichlorophenyl)-1,5,6,7-tetrahydropyrrolo[1,2-a]imidazol-4-ium bromide. Obtained as a Bordeaux-colored solid (720 mg, 91%).

LC-MS: $[M]^+$ 310.94.

^{1}H NMR (500 MHz, MeOD) δ 7.73 – 7.69 (m, 2H), 7.63 (s, 1H), 7.43 (d, *J* = 8.3 Hz, 1H), 4.53 (s, 2H), 4.36 (t, *J* = 7.3 Hz, 2H), 3.22 (t, *J* = 7.6 Hz, 2H), 2.83 (p, *J* = 7.4 Hz, 2H).

^{13}C NMR (126 MHz, MeOD) δ 169.72, 154.25, 136.52, 134.33, 132.96, 131.24, 131.11, 128.94, 126.44, 115.77, 49.36, 24.97, 22.84.

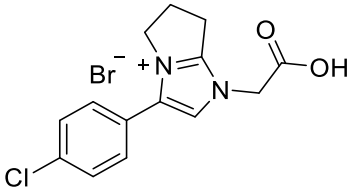

1-(carboxymethyl)-3-(4-chlorophenyl)-1,5,6,7-tetrahydropyrrolo[1,2-a]imidazol-4-ium bromide. Obtained as a dark red solid (200 mg, 85%).

LC-MS: $[M]^+$ 277.07.

^{1}H NMR (500 MHz, DMSO-d_6) δ 13.88 (s, 1H), 7.96 (s, 1H), 7.87 (d, *J* = 8.3 Hz, 2H), 7.72 (d, *J* = 8.3 Hz, 2H), 5.02 (s, 2H), 4.21 (t, *J* = 5.6 Hz, 2H), 3.02 (t, *J* = 6.1 Hz, 2H), 2.04 – 1.93 (m, 2H).

^{13}C NMR (126 MHz, DMSO-d_6) δ 167.85, 146.23, 133.27, 132.04, 131.59, 129.30, 126.09, 120.29, 48.59, 46.25, 20.75, 20.66.

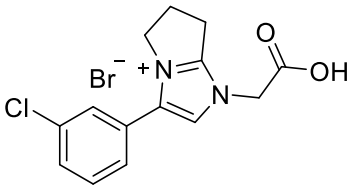

1-(carboxymethyl)-3-(3-chlorophenyl)-1,5,6,7-tetrahydropyrrolo[1,2-a]imidazol-4-ium bromide. Isolated as a brownish solid (110 mg, 98%).

LC-MS: $[M]^+$ 276.95.

^{1}H NMR (500 MHz, DMSO-d_6) δ 13.86 (br.s, 1H), 7.98 (s, 1H), 7.66 (ddd, *J* = 8.1, 2.0, 1.1 Hz, 1H), 7.61 (t, *J* = 7.8 Hz, 1H), 7.55 (t, *J* = 1.8 Hz, 1H), 7.45 – 7.42 (m, 1H), 5.09 (s, 2H), 4.38 – 4.32 (m, 2H), 3.25 (t, *J* = 7.6 Hz, 2H), 2.77 – 2.68 (m, 2H).

^{13}C NMR (126 MHz, DMSO-d_6) δ 167.79, 154.48, 136.30, 133.85, 131.25, 130.18, 128.74, 127.91, 127.65, 116.76, 48.66, 47.60, 25.07, 23.40.

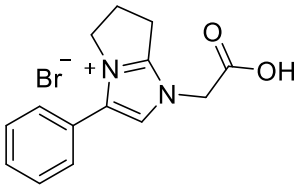

1-(carboxymethyl)-3-phenyl-1,5,6,7-tetrahydropyrrolo[1,2-a]imidazol-4-ium bromide. Obtained as orange solid (305 mg, 90%).

LC-MS: $[M]^+$ 243.10.

^{1}H NMR (500 MHz, DMSO-d_6) δ 7.90 (s, 1H), 7.60 – 7.55 (m, 3H), 7.47 – 7.42 (m, 2H), 5.00 (s, 2H), 4.35 (t, *J* = 7.3 Hz, 2H), 3.23 (t, *J* = 7.6 Hz, 2H), 2.76 – 2.67 (m, 2H).

^{13}C NMR (126 MHz, DMSO-d_6) δ 167.71, 154.14, 137.81, 130.23, 129.36, 129.01, 125.87, 115.98, 48.57, 47.53, 25.06, 23.40.

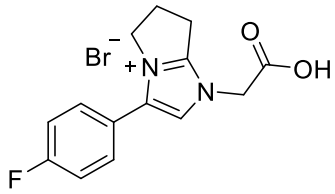

1-(carboxymethyl)-3-(4-fluorophenyl)-1,5,6,7-tetrahydropyrrolo[1,2-a]imidazol-4-ium bromide. Isolated as pale beige solid (150 mg, 77%).

LC-MS: $[M]^+$ 261.17.

^{1}H NMR (500 MHz, DMSO-d_6) δ 7.87 (s, 1H), 7.50 – 7.42 (m, 4H), 4.94 (s, 2H), 4.21 (t, *J* = 5.6 Hz, 2H), 3.01 (t, *J* = 6.1 Hz, 2H), 1.99 (s, 4H).

^{19}F NMR (470 MHz, DMSO-d_6) δ -109.25 – -111.53 (m).

^{13}C NMR (126 MHz, DMSO-d_6) δ 167.76, 163.13 (d, *J* = 248.3 Hz), 145.76, 132.31, 131.81, 131.78 (d, *J* = 8.9 Hz), 131.74, 121.84 (d, *J* = 3.4 Hz), 119.46, 116.62, 116.53 (d, *J* = 22.1 Hz), 116.44, 46.12, 46.01, 20.80, 20.66.

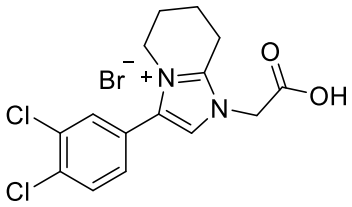

1-(carboxymethyl)-3-(3,4-dichlorophenyl)-5,6,7,8-tetrahydro-1H-imidazo[1,2-a]pyridin-4-ium bromide. Obtained as reddish solid (700 mg, 90%).

LC-MS: $[M]^+$ 324.98.

^{1}H NMR (500 MHz, DMSO-d_6) δ 13.88 (s, 1H), 7.96 (s, 1H), 7.87 (d, *J* = 8.3 Hz, 1H), 7.72 (d, *J* = 2.1 Hz, 1H), 7.42 (dd, *J* = 8.3, 2.1 Hz, 1H), 5.02 (s, 2H), 4.21 (t, *J* = 5.6 Hz, 2H), 3.02 (t, *J* = 6.1 Hz, 2H), 2.04 – 1.93 (m, 4H).

^{13}C NMR (126 MHz, DMSO-d_6) δ 167.85, 146.23, 133.27, 132.04, 131.59, 131.07, 130.97, 129.30, 126.09, 120.29, 48.59, 46.25, 20.75, 20.66, 17.51.

Synthesis of the triazolic acid (precursor of H32).

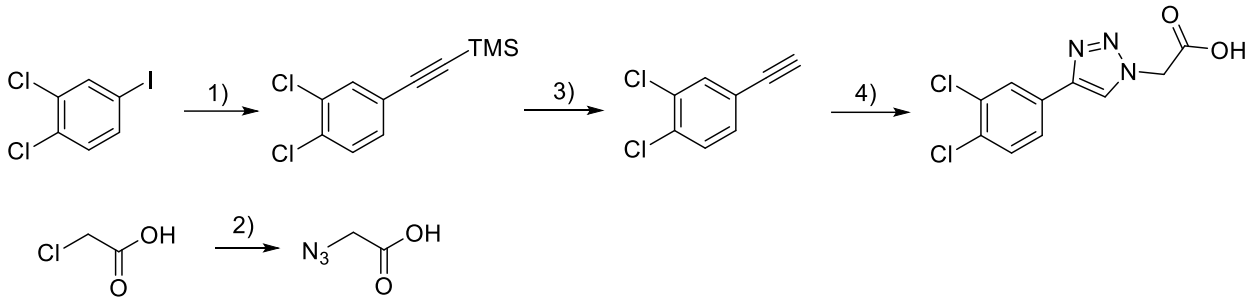

Step 1: ((3,4-dichlorophenyl)ethynyl)trimethylsilane. 1,2-dichloro-4-iodobenzene (546.0 mg, 2 mmol), trimethylsilylacetylene (236.0 mg, 2.4 mmol) and copper(I) iodide (2 mg, 0.01 mmol) were weighed into a 10-ml round-bottom flask and diisopropylamine (7 ml) was added thereto under nitrogen atmosphere. To the resulting solution $Pd(PPh_3)_2Cl_2$ (28.0 mg, 0.04 mmol) was added and the reaction mixture was stirred at 45^{o}C for 4 hours, then concentrated in vacuo. The residue was taken up in water and extracted with diethyl ether, combined ethereal fractions were washed with brine, dried over anhydrous sodium sulfate, concentrated in vacuo and subjected to flash chromatography (Hexanes), which afforded the desired product as a yellowish solid (457 mg, 94%).

^{1}H NMR (500 MHz, $CDCl_3$) δ 7.55 (s, 1H), 7.37 (d, *J* = 8.3 Hz, 1H), 7.30 – 7.26 (m, *J* = 8.0 Hz, 1H), 0.24 (s, 9H).

^{13}C NMR (126 MHz, $CDCl_3$) δ 133.73, 133.01, 132.57, 131.17, 130.40, 123.24, 102.53, 96.88, -0.07.

Step 2: Azidoacetic acid. Chloroacetic acid (474.0 mg, 5 mmol), sodium azide (975 mg, 15 mmol) and sodium iodide (50 mg, 0.33 mmol) were dissolved in DMSO (20 ml) and the resulting mixture was stirred at room temperature for 8 hours. The reaction mixture was diluted with water (100 ml), the obtained solution was acidified to pH 3 and extracted with ethyl acetate (3x40 ml). The combined organic fractions were washed with brine, dried over anhydrous sodium sulfate concentrated in vacuo to afford the desired product as a clear liquid (490 mg, 97%).

^{1}H NMR (500 MHz, $CDCl_3$) δ 8.88 (s, 1H), 3.97 (s, 2H).

^{13}C NMR (126 MHz, $CDCl_3$) δ 173.83, 50.13.

Step 3: 1,2-dichloro-4-ethynylbenzene. ((3,4-dichlorophenyl)ethynyl)trimethylsilane (457.0 mg, 1.88 mmol) was dissolved in anhydrous THF (10 ml) and to the resulting solution TBAF (1M in THF, 3.8 ml) was added. The resulting reaction mixture was stirred at room temperature overnight, then concentrated in vacuo and subjected to flash chromatography (Hexanes), which afforded the deprotected product as off-white solid (320 mg, 100%).

^{1}H NMR (500 MHz, $CDCl_3$) δ 7.57 (s, 1H), 7.40 (d, *J* = 8.3 Hz, 1H), 7.31 (d, *J* = 8.3 Hz, 1H), 3.14 (s, 1H).

^{13}C NMR (126 MHz, $CDCl_3$) δ 133.92, 133.52, 132.74, 131.38, 130.54, 122.18, 81.41, 79.37.

Step 4: 2-(4-(3,4-dichlorophenyl)-1H-1,2,3-triazol-1-yl)acetic acid. 1,2-dichloro-4-ethynylbenzene (188.0 mg, 1.1 mmol), azidoacetic acid (101.0 mg, 1 mmol) and sodium ascorbate (30.0 mg, 0.15 mmol) were dissolved in degassed DCM (10 ml) under nitrogen atmosphere. The degassed solution of copper sulfate pentahydrate (12.5 mg, 0.05 mmol) in water (10 ml) was added to the DCM solution and the resulting reaction mixture was stirred at room temperature for 4 hours. After full completion of the conversion the reaction mixture was concentrated in vacuo, the pH of the residue was adjusted to 4 and the aqueous solution was extracted with ethyl acetate. The combined organic fractions were washed with brine, dried over anhydrous sodium sulfate concentrated in vacuo to afford the desired product as white solid (240 mg, 88%).

LC-MS: $[M+H]^+$ 271.85.

^{1}H NMR (500 MHz, DMSO-d_6) δ 13.50 (s, 1H), 8.69 (s, 1H), 8.12 (s, 1H), 7.87 (d, *J* = 8.4 Hz, 1H), 7.73 (d, *J* = 8.3 Hz, 1H), 5.34 (s, 2H).

^{13}C NMR (126 MHz, DMSO-d_6) δ 144.15, 131.80, 131.34, 131.29, 130.19, 126.74, 125.23, 123.85, 50.80.

Synthesis of the pyrazolic acid (precursor of compound H33).

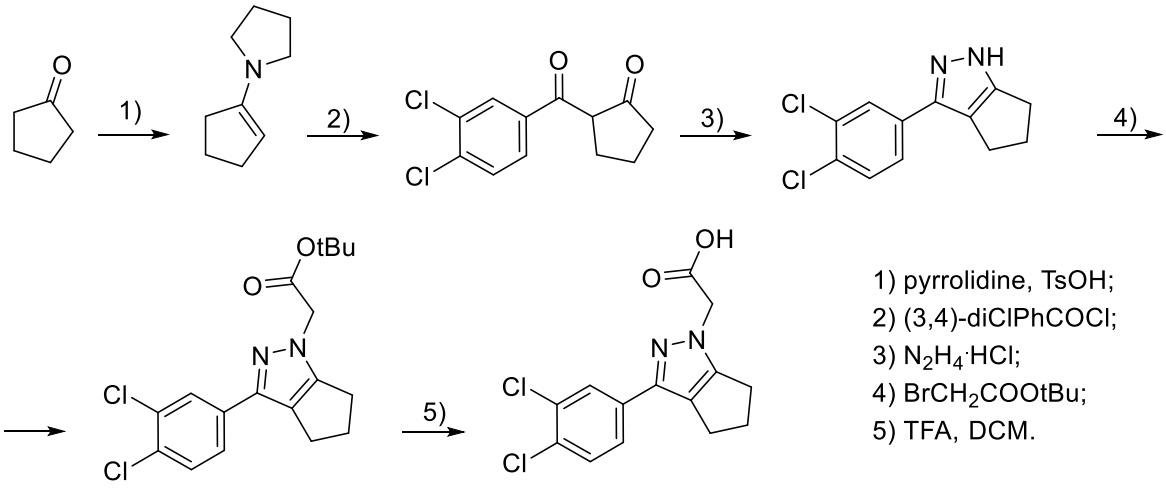

Step 1: 1-(cyclopent-1-en-1-yl)pyrrolidine (pyrrolidine enamine of cyclopentanone). Cyclopentanone (16.80 g, 0.2 mol), pyrrolidine (17.07 g, 0.24 mol) and p-toluenesulfonic acid

(40 mg, 0.23 mmol) were weighed into a 100 ml round-bottom flask and suspended in dry toluene (50 ml). The flask was equipped with a condenser, a Dean-Stark trap, and was held at reflux for 8 hours. The reaction mixture was cooled down, washed with water, dried over anhydrous sodium sulfate and evaporated. The residue was subjected to vacuum distillation and the title product was collected as a fraction with the boiling point of 85°C at 10 mm. Hg. Clear colorless liquid (21.5 g, 78%). Used in the next step directly.

Step 2: 2-(3,4-dichlorobenzoyl)cyclopentan-1-one. Into a three-necked oven-dried round bottom flask was put the enamine (5.0 g, 36.4 mmol), DIPEA (5.7 g, 43.7 mmol) and dry toluene (50 ml). The resulting solution was heated up to 40°C and the solution of 3,4-dichlorobenzoyl chloride (9.2 g, 43.7 mmol) in toluene (10 ml) was added dropwise via a dripping funnel. After the completion of the addition the reaction mixture was stirred at 40°C for an additional hour, then left at room temperature overnight. 5% aqueous HCl (25 ml) was added to the reaction mixture followed by 1 hour of reflux. The resulting reaction mixture was extracted with diethyl ether, combined ethereal fractions were washed with aq. $NaHCO_3$, brine, dried over anhydrous sodium sulfate and evaporated *in vacuo.* The resulting residue was purified by column chromatography to yield the desired product as yellowish solid (5.1 g, 54%).

^{1}H NMR (500 MHz, $CDCl_3$) δ 14.35 (s, 1H), 7.86 (d, *J* = 2.0 Hz, 1H), 7.59 (dd, *J* = 8.5, 2.0 Hz, 1H), 7.51 (d, *J* = 8.4 Hz, 1H), 2.85 (t, *J* = 7.1 Hz, 1H), 2.50 (t, *J* = 7.9 Hz, 1H), 2.04 – 1.96 (m, 1H).

^{13}C NMR (126 MHz, $CDCl_3$) δ 212.72, 193.24, 138.23, 136.11, 133.38, 130.52, 130.05, 127.29, 57.52, 37.68, 28.34, 21.31. (prevailing enol form)

Step 3: 3-(3,4-dichlorophenyl)-1,4,5,6-tetrahydrocyclopenta[c]pyrazole. The mixture of 2-(3,4-dichlorobenzoyl)cyclopentan-1-one (811 mg, 3.15 mmol) and hydrazine hydrochloride (216 mg, 0.65 mmol) was dissolved in ethanol (2 ml) and the resulting solution was stirred at 70°C overnight and then concentrated *in vacuo* to yield the crude product of reasonable purity, which was used in the next step without additional purification (800 mg, quant.)

^{1}H NMR (500 MHz, DMSO-d_6) δ 12.97 – 12.45 (br .m, 1H), 7.88 – 7.82 (m, 1H), 7.73 – 7.64 (m, 1H), 7.63 – 7.53 (m, 1H), 2.78 (t, *J* = 7.0 Hz, 2H), 2.69 – 2.59 (m, 2H), 2.48 – 2.38 (m, 2H).

^{13}C NMR (126 MHz, DMSO-d_6) δ 132.04, 131.73, 131.68, 131.56, 126.58, 125.54, 102.41, 60.24, 23.95, 23.84.

Step 4: tert-butyl 2-(3-(3,4-dichlorophenyl)-5,6-dihydrocyclopenta[c]pyrazol-1(4H)-yl)acetate. The suspension containing 3-(3,4-dichlorophenyl)-1,4,5,6-tetrahydrocyclopenta[c]pyrazole (74 mg, 0.29 mmol), tert-butyl 2-bromoacetate (63 mg, 0.32

mmol), caesium carbonate (190 mg, 0.58 mmol) and sodium iodide (10 mg, 0.07 mmol) in acetonitrile (2 ml) was stirred at 70°C overnight and then cooled down and filtered. Mother liquor was concentrated under reduced pressure and subjected to flash chromatography (Hexane-EtOAc) to yield the title product as white solid (79 mg, 74%).

^{1}H NMR (500 MHz, DMSO-d$_6$) δ 7.79 (d, *J* = 1.9 Hz, 1H), 7.72 (d, *J* = 8.4 Hz, 1H), 7.59 (dd, *J* = 8.4, 2.0 Hz, 1H), 4.88 (s, 2H), 2.81 (t, *J* = 6.9 Hz, 2H), 2.68 – 2.64 (m, 2H), 2.56 (dd, *J* = 13.7, 6.8 Hz, 2H), 1.43 (s, 9H).

^{13}C NMR (126 MHz, DMSO-d$_6$) δ 167.17, 153.03, 141.00, 134.37, 131.51, 131.09, 129.37, 126.33, 125.31, 124.35, 81.96, 52.21, 30.66, 27.70, 24.16, 23.16.

Step 5 :2-(3-(3,4-dichlorophenyl)-5,6-dihydrocyclopenta[c]pyrazol-1(4H)-yl)acetic acid. The *tert*-butyl ester (79 mg, 0.22 mmol) was dissolved in DCM (3 ml) and to the resulting solution trifluoroacetic acid (281.5 µL, 2.2 mmol was added). The reaction mixture was stirred at room temperature for 4 hours, after which concentrated and repeatedly co-evaporated with toluene to yield the desired product as a trifluoroacetic acid salt. Obtained as white solid (93 mg, quant.) and used in further steps without additional purification.

^{1}H NMR (500 MHz, DMSO-d$_6$) δ 7.79 (d, *J* = 1.9 Hz, 1H), 7.65 (d, *J* = 8.4 Hz, 1H), 7.59 (dd, *J* = 8.4, 2.0 Hz, 1H), 4.89 (s, 2H), 2.81 (t, *J* = 6.9 Hz, 2H), 2.70 – 2.64 (m, 2H), 2.56 (dd, *J* = 13.8, 6.9 Hz, 2H).

General procedure of the synthesis of substituted 4-aryl-2-amino-thiazoles.

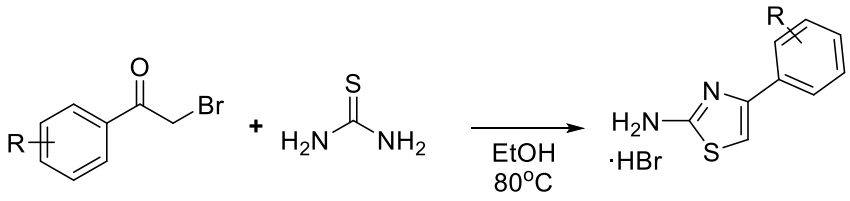

The corresponding bromoacetophenone (1 eq) is dissolved in ethanol (0.4M) together with equimolar quantity of thiourea and the resulting solution is stirred at 80°C for 8 hours. The reaction mixture is then cooled down and concentrated under reduced pressure to give the desired 2-aminothiazoles as solid hydrobromide salt.

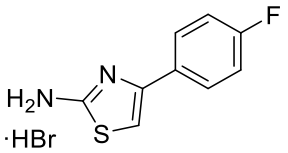

4-(4-fluorophenyl)thiazol-2-amine. Obtained as yellowish solid (545 mg, 99%).

LC-MS: $[M+H]^+$ 195.04.

^{1}H NMR (500 MHz, DMSO-d$_6$) δ: 7.82 – 7.76 (m, 2H), 7.29 (t, *J* = 8.8 Hz, 2H), 7.12 (s, 1H), 4.20 (br.s, 3H).

^{13}C NMR (126 MHz, DMSO-d_6) δ: 170.11, 162.43 (d, *J* = 247.0 Hz), 139.22, 128.24 (d, *J* = 8.7 Hz), 126.05, 116.00 (d, *J* = 22.0 Hz), 102.70.

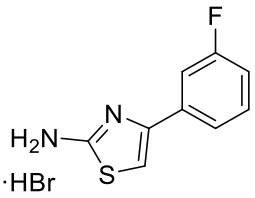

4-(3-fluorophenyl)thiazol-2-amine. Obtained as white solid (320 mg, 98%).

LC-MS: $[M+H]^+$ 195.04.

^{1}H NMR (500 MHz, DMSO-d_6) δ 7.64 – 7.58 (m, 2H), 7.52 (td, *J* = 8.0, 6.1 Hz, 1H), 7.33 (s, 1H), 7.27 – 7.22 (m, 1H).

^{13}C NMR (126 MHz, DMSO-d_6) δ 169.83, 162.32 (d, *J* = 243.4 Hz), 131.03 (d, *J* = 8.4 Hz), 121.88 (d, *J* = 2.6 Hz), 115.68 (d, *J* = 21.0 Hz), 112.61 (d, *J* = 23.7 Hz), 104.14.

^{19}F NMR (470 MHz, DMSO-d_6) δ -110.00 – -110.14 (m).

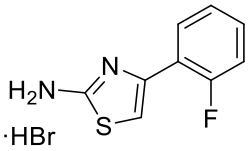

4-(2-fluorophenyl)thiazol-2-amine. Obtained as yellowish solid (500 mg, 95%).

LC-MS: $[M+H]^+$ 194.98.

^{1}H NMR (500 MHz, DMSO-d_6) δ 7.78 (td, *J* = 7.8, 1.7 Hz, 1H), 7.51 – 7.45 (m, 1H), 7.40 – 7.31 (m, 2H), 7.13 (d, *J* = 1.6 Hz, 1H).

^{19}F NMR (470 MHz, DMSO-d_6) δ -113.94 – -114.02 (m).

^{13}C NMR (126 MHz, DMSO-d_6) δ 169.86, 162.34 (d, *J* = 243.4 Hz), 140.02 (d, *J* = 14.8 Hz), 132.21 (d, *J* = 7.5 Hz), 131.05 (d, *J* = 8.4 Hz), 121.90 (d, *J* = 2.6 Hz), 115.71 (d, *J* = 20.6 Hz), 112.64 (d, *J* = 23.7 Hz), 104.17.

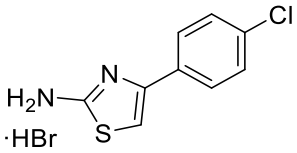

4-(4-chlorophenyl)thiazol-2-amine. Obtained as a white solid (552 mg, 95%).

LC-MS: $[M+H]^+$ 211.00.

^{1}H NMR (500 MHz, DMSO-d_6) δ 7.78 – 7.74 (m, 1H), 7.58 – 7.54 (m, 1H), 7.29 (s, 1H).

^{13}C NMR (126 MHz, DMSO-d_6) δ 170.09, 139.15, 133.72, 129.02, 128.33, 127.61, 103.64.

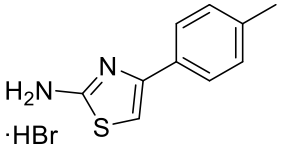

4-(p-tolyl)thiazol-2-amine. Obtained as a yellowish solid (240 mg, 94%).

LC-MS: $[M+H]^+$ 191.04.

^{1}H NMR (500 MHz, DMSO-d_6) δ 8.83 (s, 1H), 7.62 (d, *J* = 8.2 Hz, 2H), 7.30 (d, *J* = 8.1 Hz, 2H), 7.18 (s, 1H), 2.34 (s, 3H).

^{13}C NMR (126 MHz, DMSO-d_6) δ 170.17, 139.52, 139.09, 129.56, 126.24, 125.71, 101.88, 20.85.

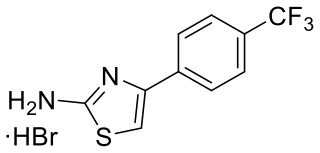

4-(4-(trifluoromethyl)phenyl)thiazol-2-amine. Obtained as slightly beige solid (950 mg, 97%).

LC-MS: $[M+H]^+$ 245.02

^{1}H NMR (500 MHz, DMSO-d_6) δ 7.97 (d, *J* = 8.2 Hz, 1H), 7.83 (d, *J* = 8.4 Hz, 1H), 7.42 (s, 1H).

^{19}F NMR (470 MHz, DMSO-d_6) δ -61.10.

^{13}C NMR (126 MHz, DMSO-d_6) δ 169.93, 140.43, 134.09, 129.46 – 128.27 (m), 127.49 – 120.62 (m), 126.47, 125.93 – 125.79 (m, *J* = 3.7 Hz), 105.40.

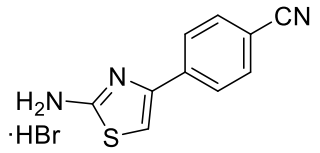

4-(2-aminothiazol-4-yl)benzonitrile. Obtained as white solid (1380 mg, 98%).

LC-MS: $[M+H]^+$ 201.92

^{1}H NMR (500 MHz, DMSO-d_6) δ 7.96 – 7.93 (m, 2H), 7.93 – 7.90 (m, 2H), 7.45 (s, 1H).

^{13}C NMR (126 MHz, DMSO-d_6) δ 169.62, 141.91, 135.36, 132.79, 126.36, 118.68, 110.54, 106.13.

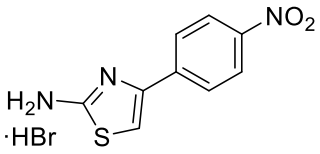

4-(4-nitrophenyl)thiazol-2-amine Obtained as orange solid (600 mg, 98%).

LC-MS: $[M+H]^+$ 201.92

^{1}H NMR (500 MHz, DMSO-d_6) δ 8.31 – 8.27 (m, 1H), 8.04 – 7.99 (m, 1H), 7.52 (s, 1H).

^{13}C NMR (126 MHz, DMSO-d_6) δ 169.76, 146.82, 141.23, 136.99, 126.72, 124.19, 107.16.

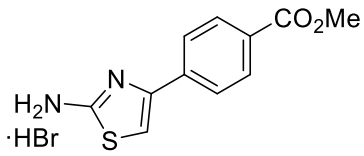

Methyl 4-(2-aminothiazol-4-yl)benzoate. Obtained as white solid (940 mg, 91%).

LC-MS: $[M+H]^+$ 222.02

^{1}H NMR (500 MHz, DMSO-d_6) δ 8.03 (d, *J* = 8.5 Hz, 1H), 7.89 (d, *J* = 8.4 Hz, 1H), 7.42 (s, 1H), 3.86 (s, 3H).

^{13}C NMR (126 MHz, DMSO-d_6) δ 170.01, 165.70, 140.00, 134.05, 129.77, 129.52, 125.97, 105.44, 52.31.

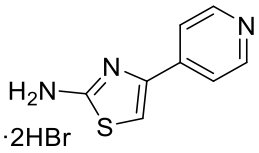

4-(pyridin-4-yl)thiazol-2-amine. Obtained as yellowish solid (320 mg, 94%).

LC-MS: $[M+H]^+$ 178.00.

^{1}H NMR (500 MHz, DMSO-d_6) δ 8.88 (d, *J* = 6.8 Hz, 2H), 8.32 (d, *J* = 6.8 Hz, 2H), 8.08 (s, 1H).

^{13}C NMR (126 MHz, DMSO-d_6) δ 169.17, 142.04, 141.86, 141.50, 122.10, 114.78.

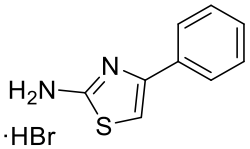

4-phenylthiazol-2-amine. Obtained as white solid (600 mg, 93%).

LC-MS: $[M+H]^+$ 177.01.

^{1}H NMR (500 MHz, DMSO-d_6) δ 8.85 (s, *J* = 92.5 Hz, 1H), 7.76 – 7.71 (m, 1H), 7.49 (t, *J* = 7.5 Hz, 1H), 7.47 – 7.40 (m, 1H), 7.25 (s, 1H).

^{13}C NMR (126 MHz, DMSO-d_6) δ 170.20, 139.59, 129.37, 129.05, 125.84, 102.85.

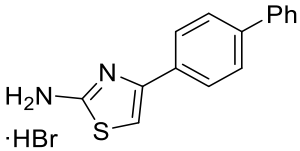

4-([1,1'-biphenyl]-4-yl)thiazol-2-amine. Obtained as a beige solid (1540 mg, 91%).

LC-MS: $[M+H]^+$ 252.91.

^{1}H NMR (500 MHz, DMSO-d_6) δ 7.87 – 7.79 (m, 4H), 7.77 – 7.72 (m, 2H), 7.50 (t, *J* = 7.7 Hz, 2H), 7.43 – 7.38 (m, 1H), 7.28 (s, 1H).

^{13}C NMR (126 MHz, DMSO-d_6) δ 170.20, 140.75, 139.32, 139.01, 129.05, 128.06, 127.96, 127.15, 126.67, 126.35, 102.91.

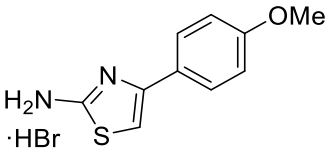

4-(4-methoxyphenyl)thiazol-2-amine. Obtained as an off-white solid (1401 mg, 97%).

LC-MS: $[M+H]^+$ 207.02.

^{1}H NMR (500 MHz, DMSO-d_6) δ 8.81 (s, 1H), 7.70 – 7.65 (m, 2H), 7.09 (s, 1H), 7.08 – 7.04 (m, 2H), 3.81 (s, 3H).

^{13}C NMR (126 MHz, DMSO-d_6) δ 170.57, 160.47, 139.93, 127.83, 122.06, 114.86, 101.06, 55.84.

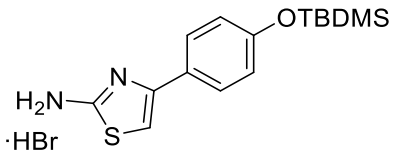

4-(4-((tert-butyldimethylsilyl)oxy)phenyl)thiazol-2-amine. Obtained as greenish crystals (475 mg, 94%).

LC-MS: $[M+H]^+$ 307.00.

^{1}H NMR (500 MHz, DMSO-d_6) δ 7.68 – 7.63 (m, 2H), 7.06 (s, 1H), 6.96 – 6.92 (m, 2H), 0.96 – 0.94 (m, 9H), 0.22 – 0.20 (m, 6H).

^{13}C NMR (126 MHz, DMSO-d_6) δ 170.03, 155.95, 130.84, 127.39, 120.32, 100.65, 30.71, 25.53, -4.54.

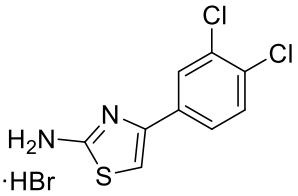

4-(3,4-dichlorophenyl)thiazol-2-amine. Obtained as white solid (96 mg, 87%).

LC-MS: $[M+H]^+$ 244.79.

^{1}H NMR (500 MHz, DMSO-d_6) δ 8.03 (d, *J* = 2.0 Hz, 1H), 7.75 (dd, *J* = 8.4, 2.0 Hz, 1H), 7.71 (d, *J* = 8.5 Hz, 1H), 7.36 (s, 1H).

^{13}C NMR (126 MHz, DMSO-d_6) δ 169.45, 141.63, 132.09, 131.57, 130.98, 130.64, 127.43, 125.83, 104.58.

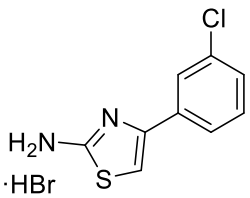

4-(3-chlorophenyl)thiazol-2-amine. Obtained as white solid (310 mg, 90%).

LC-MS: $[M+H]^+$ 211.00.

^{1}H NMR (500 MHz, DMSO-d_6) δ 7.85 (t, *J* = 1.6 Hz, 1H), 7.74 – 7.70 (m, 1H), 7.53 – 7.44 (m, 2H), 7.36 (s, 1H).

^{13}C NMR (126 MHz, DMSO-d_6) δ 169.93, 139.71, 133.75, 131.93, 130.90, 128.80, 125.56, 124.52, 104.38.

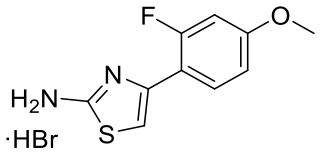

4-(2-fluoro-4-methoxyphenyl)thiazol-2-amine. Obtained as white solid (440 mg, 98%).

LC-MS: $[M+H]^+$ 225.05.

^{1}H NMR (500 MHz, DMSO-d_6) δ 8.64 (s, 1H), 7.67 (t, *J* = 8.9 Hz, 1H), 7.02 (dd, *J* = 13.4, 2.4 Hz, 1H), 6.98 (d, *J* = 1.0 Hz, 1H), 6.93 (dd, *J* = 8.7, 2.4 Hz, 1H), 3.82 (s, 3H).

^{13}C NMR (126 MHz, DMSO-d_6) δ 169.35, 161.18 (d, *J* = 11.5 Hz), 159.94 (d, *J* = 248.8 Hz), 134.87, 129.94 (d, *J* = 4.4 Hz), 110.98 (d, *J* = 2.0 Hz), 110.30 (d, *J* = 15.8 Hz), 104.68 (d, *J* = 9.2 Hz), 102.33 (d, *J* = 25.5 Hz), 56.01.

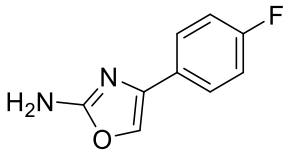

4-(4-fluorophenyl)oxazol-2-amine. Synthesized from urea (1574 mg, 26.2 mmol) and 4-fluorophenacyl bromide (569 mg, 2.6 mmol) following analogous procedure. Obtained as an off-white solid (320 mg, 69%).

LC-MS: $[M+H]^+$ 178.92.

^{1}H NMR (500 MHz, DMSO-d_6) δ 7.85 (s, 1H), 7.69 – 7.63 (m, 2H), 7.22 – 7.16 (m, 2H), 6.74 (s, 2H).

^{19}F NMR (470 MHz, DMSO-d_6) δ -114.87 – -115.01 (m).

^{13}C NMR (126 MHz, DMSO-d_6) δ 161.62, 161.31 (d, *J* = 243.6 Hz), 138.13, 128.62 (d, *J* = 2.8 Hz), 127.00 (d, *J* = 1.4 Hz), 126.58 (d, *J* = 8.1 Hz), 115.41 (d, *J* = 21.8 Hz).

Synthesis of precursors for alternative Eastern heterocycle part

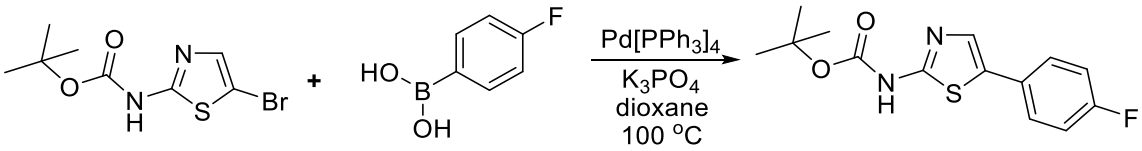

Tert-butyl (5-(4-fluorophenyl)thiazol-2-yl)carbamate was obtained as a yellowish solid (230 mg, 55%).

^{1}H NMR (500 MHz, $CDCl_3$) δ 7.49 – 7.44 (m, 3H), 7.11 – 7.06 (m, 2H), 1.60 (s, 9H).

^{19}F NMR (470 MHz, $CDCl_3$) δ -114.06.

^{13}C NMR (126 MHz, $CDCl_3$) δ 162.43 (d, *J* = 247.5 Hz), 161.66, 152.82, 136.74, 132.24, 128.12 (d, *J* = 3.4 Hz), 127.68 (d, *J* = 8.1 Hz), 116.27 (d, *J* = 22.0 Hz), 82.60, 28.43.

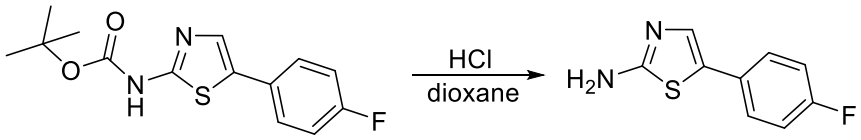

5-(4-fluorophenyl)thiazol-2-amine hydrochloride. To the solution of tert-butyl (5-(4-fluorophenyl)thiazol-2-yl)carbamate (230 mg, 0.78 mmol) in anhydrous dichloromethane (10 ml) was added the solution of hydrogen chloride (1ml, 4M in dioxane). The resulting reaction mixture was stirred 4 hours at room temperature until the conversion was complete. The mixture was then concentrated under reduced pressure to yield the product in the form of a beige-colored solid, the hydrochloric salt of the title compound.

5-(4-fluorophenyl)thiazol-2-amine <u>hydrochloride</u> was obtained as white solid (210 mg, 95%).

^{1}H NMR (500 MHz, DMSO-d_6) δ 7.47 – 7.42 (m, 2H), 7.36 (s, 1H), 7.20 – 7.14 (m, 2H).

^{19}F NMR (470 MHz, DMSO-d_6) δ -116.23 – -116.34 (m).

^{13}C NMR (126 MHz, DMSO-d_6) δ 168.56, 161.97 (d, *J* = 246.3 Hz), 127.62 (d, *J* = 8.3 Hz), 126.12 (d, *J* = 3.0 Hz), 123.14, 122.74, 116.29 (d, *J* = 22.0 Hz).

The free base was obtained by basification and subsequent extraction with ethyl acetate. **5-(4-fluorophenyl)thiazol-2-amine (<u>free base</u>):**

^{1}H NMR (500 MHz, $CDCl_3$) δ 7.40 – 7.35 (m, 2H), 7.21 (s, 1H), 7.08 – 7.02 (m, 2H), 5.21 (s, 2H).

^{13}C NMR (126 MHz, $CDCl_3$) δ 167.10, 162.20 (d, *J* = 247.3 Hz), 133.17, 128.14 (d, *J* = 3.8 Hz), 128.11, 127.51 (d, *J* = 7.8 Hz), 116.12 (d, *J* = 21.7 Hz).

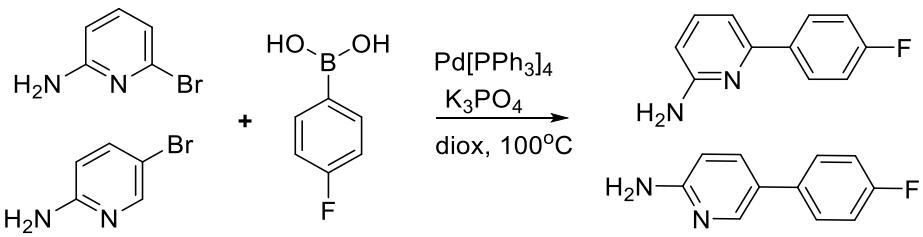

Synthesis of 5- and 6-(4-fluorophenyl)-pyridin-2-amines. The corresponding bromo-2-amine (1 eq), 4-fluorophenylboronic acid (1.5 eq), *tetrakis*-(triphenylphophine)-palladuim (3 mol%) and potassium orthophosphate (2 eq) were weighed into a 10-ml microwave vial. To the

resulted mixture was added dioxane (0.5 M) and the resulting solution was sonicated for 2 minutes, after which nitrogen was bubbled through for 10 minutes. The vial was then installed into the microwave apparatus, where it was irradiated with at 200W intensity to keep the temperature 100°C for 1.5 hours. Upon the completion of the reaction, the reaction mixture was diluted with water, extracted with ethyl acetate, washed with sodium carbonate, brine, dried over anhydrous sodium sulfate and concentrated *in vacuo*. The residue was subjected to flash column chromatography (hexane - ethyl acetate 0% →100% to furnish the desired products.

6-(4-fluorophenyl)pyridin-2-amine. Obtained as a yellowish solid (237 mg, 87%).

LC-MS: $[M+H]^+$ 189.07.

^{1}H NMR (500 MHz, $CDCl_3$) δ 7.93 – 7.88 (m, 1H), 7.53 – 7.48 (m, 1H), 7.14 – 7.08 (m, 1H), 7.04 (dd, *J* = 7.5, 0.5 Hz, 1H), 6.46 (dd, *J* = 8.1, 0.4 Hz, 1H), 4.61 (s, 1H).

^{19}F NMR (470 MHz, $CDCl_3$) δ -113.47 (s).

^{13}C NMR (126 MHz, $CDCl_3$) δ 163.37 (d, *J* = 248.0 Hz), 158.04, 154.76, 138.76, 135.37, 128.65, 128.62 (d, *J* = 8.3 Hz), 128.58, 115.57, 115.49 (d, *J* = 21.8 Hz), 115.40, 110.64, 107.20.

5-(4-fluorophenyl)pyridin-2-amine. Obtained as an orange solid (320 mg, 85%).

LC-MS: $[M+H]^+$ 189.05.

^{1}H NMR (500 MHz, DMSO-d_6) δ 8.21 (d, *J* = 2.4 Hz, 1H), 7.67 (dd, *J* = 8.6, 2.6 Hz, 1H), 7.60 – 7.55 (m, 2H), 6.51 (d, *J* = 8.6 Hz, 1H), 6.08 (s, 2H).

^{19}F NMR (470 MHz, DMSO-d_6) δ -117.00 – -117.08 (m).

^{13}C NMR (126 MHz, DMSO-d_6) δ 161.61 (d, *J* = 242.8 Hz), 159.62, 146.14, 135.81, 135.13 (d, *J* = 2.9 Hz), 127.70 (d, *J* = 7.7 Hz), 123.41, 116.08 (d, *J* = 21.3 Hz), 108.36.

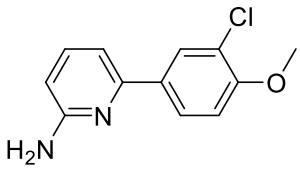

6-(3-chloro-4-methoxyphenyl)pyridin-2-amine. Obtained as yellowish solid (190 mg, 81%).

LC-MS: $[M+H]^+$ 235.07.

^{1}H NMR (500 MHz, $CDCl_3$) δ 8.01 (d, *J* = 2.2 Hz, 1H), 7.81 (dd, *J* = 8.6, 2.2 Hz, 1H), 7.47 (dd, *J* = 9.7, 6.0 Hz, 1H), 7.02 (d, *J* = 7.5 Hz, 1H), 7.00 – 6.95 (m, 1H), 6.43 (d, *J* = 8.1 Hz, 1H), 4.50 (s, 2H), 3.94 (s, 3H).

^{13}C NMR (126 MHz, $CDCl_3$) δ 158.29, 155.49, 154.48, 138.61, 133.23, 128.82, 126.19, 122.78, 111.96, 110.32, 107.05, 56.36.

Synthesis of precursors for non-cyclic Eastern heterocycle analogues

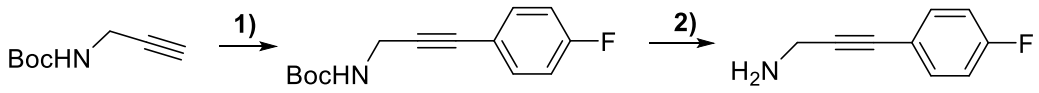

1) 4-fluoroiodobenzene, $Pd[PPh_3]_2Cl_2$, CuI
2) TFA, DCM; then $Na_2CO_{3(aq)}$

Step 1**: N-tert-butoxycabonyl-3-(4-fluorophenyl)prop-2-yn-1-amine.** In an oven-dried 25-ml Schlenk flask was weighed Boc-propargylamine (621 mg, 4 mmol), 4-fluoroiodobenzene (1332 mg, 6 mmol), $Pd[PPh_3]_2Cl_2$ (56 mg, 0.08 mmol) and CuI (30.5 mg, 0.16 mmol). The flask was evacuated – backfilled with nitrogen and 5 ml of dry THF was added to the mixture. The resulting suspension was stirred for 1 minute, after which DIPEA (1034 mg, 8 mmol) was added to it. The reaction mixture was left to stir at room temperature overnight. After completion of the reaction, the mixture was concentrated *in vacuo*, redissolved in ethyl acetate, washed with saturated sodium carbonate solution, brine and dried over anhydrous sodium sulfate. The organic solution was concentrated under reduced pressure and the residue was subjected to flash column chromatography (Hex – EtOAc 0 – 50%) to give the title compound as a clear oil, which solidified upon standing (800 mg, 80%).

^{1}H NMR (500 MHz, DMSO-d_6) δ 7.49 – 7.44 (m, 2H), 7.36 (s, 1H), 7.22 (t, *J* = 8.8 Hz, 2H), 3.97 (d, *J* = 5.4 Hz, 2H), 1.40 (s, 9H).

^{19}F NMR (470 MHz, DMSO-d_6) δ -110.99 – -111.16 (m).

^{13}C NMR (126 MHz, DMSO-d_6) δ 161.82 (d, *J* = 247.2 Hz), 155.30, 133.61 (d, *J* = 8.5 Hz), 118.81 (d, *J* = 3.2 Hz), 115.89 (d, *J* = 22.1 Hz), 87.36, 80.36, 78.28, 30.08, 28.18.

Step 2**: 3-(4-fluorophenyl)prop-2-yn-1-amine**. *N-tert*-butoxycabonyl - 3 -(4 - fluorophenyl)prop-2-yn-1-amine (225 mg, 0.90 mmol) was dissolved in 2 ml of DCM, after which the resulting solution was treated with trifluoroacetic acid (0.7 ml, 9.0 mmol). The reaction mixture was left to stir for 3 hours at room temperature, then concentrated *in vacuo* and co-evaporated with toluene. The resulting residue was taken up into the saturated sodium carbonate solution, which was then extracted with ether (2x40 ml). The combined ethereal fractions were washed with brine, dried over anhydrous sodium sulfate and concentrated *in vacuo* to give the title compound as a deep orange solidifying liquid (133 mg, 94%).

LC-MS: $[M+H]^+$ 133.09.

^{1}H NMR (500 MHz, DMSO-d_6) δ 7.47 – 7.41 (m, 2H), 7.23 – 7.17 (m, 2H), 3.49 (s, 2H).

^{19}F NMR (470 MHz, DMSO-d_6) δ -111.59 – -111.70 (m).

^{13}C NMR (126 MHz, DMSO-d_6) δ 161.66 (d, *J* = 246.6 Hz), 133.44 (d, *J* = 8.4 Hz), 119.46 (d, *J* = 3.5 Hz), 115.88 (d, *J* = 22.0 Hz), 91.96, 80.24, 31.32.

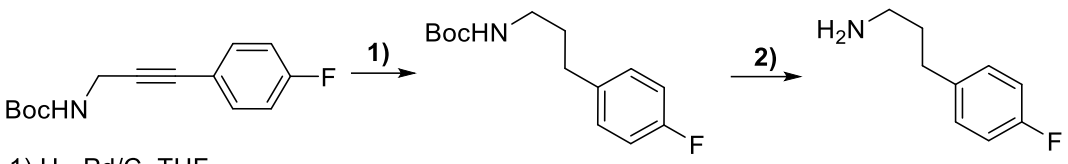

1) H_2, Pd/C, THF.
2) TFA, DCM; then $Na_2CO_{3(aq)}$

Step 1: **N-tert-butoxycabonyl-3-(4-fluorophenyl)propan-1-amine.** A 10-ml round-bottomed flask was charged with *N-tert*-butoxycabonyl-3-(4-fluorophenyl)prop-2-yn-1-amine (300 mg, 1.20 mmol), which was subsequently dissolved in THF (5 ml). To the solution formed palladium on charcoal (30 mg, 10% w/w) was added and the resulting mixture was left to stir in hydrogen atmosphere overnight. After the completion of the hydrogenation the mixture was filtered through a short pad of Celite and the resulting mother liquor was concentrated *in vacuo* to yield the title compound as a clear oil (300 mg, 99%).

^{1}H NMR (500 MHz, $CDCl_3$) δ 7.11 (dd, *J* = 8.1, 5.6 Hz, 2H), 6.95 (t, *J* = 8.6 Hz, 2H), 3.13 (dd, *J* = 12.9, 6.4 Hz, 2H), 2.59 (t, *J* = 7.7 Hz, 2H), 1.82 – 1.72 (m, 2H), 1.43 (s, 9H).

^{19}F NMR (470 MHz, $CDCl_3$) δ -117.65.

^{13}C NMR (126 MHz, $CDCl_3$) δ 161.35 (d, *J* = 243.1 Hz), 156.08, 137.25 (d, *J* = 2.6 Hz), 129.77 (d, *J* = 7.6 Hz), 115.21 (d, *J* = 21.1 Hz), 79.28, 40.16, 32.36, 31.97, 28.49.

Step 2: **3-(4-fluorophenyl)propan-1-amine**. *N-tert*-butoxycabonyl-3-(4-fluorophenyl)-propan-1-amine (360 mg, 1.42 mmol) was dissolved in 2 ml of DCM, after which the resulting solution was treated with trifluoroacetic acid (1.6 ml, 14.2 mmol). The reaction mixture was left to stir for 3 hours at room temperature, then concentrated *in vacuo* and co-evaporated with toluene. The resulting residue was taken up into the saturated sodium carbonate solution, which was then extracted with ether (2x50 ml). The combined ethereal fractions were washed with brine, dried over anhydrous sodium sulfate and concentrated *in vacuo* to give the title compound as a brownish liquid (200 mg, 91%).

LC-MS: $[M+H]^+$ 154.14.

^{1}H NMR (500 MHz, DMSO-d_6) δ 7.25 – 7.19 (m, 2H), 7.07 (t, *J* = 8.5 Hz, 2H), 4.88 (s, 2H), 2.92 (s, 1H), 2.63 – 2.52 (m, 3H), 1.71 – 1.59 (m, 2H).

^{19}F NMR (470 MHz, DMSO-d_6) δ -117.82 (d, *J* = 29.2 Hz).

^{13}C NMR (126 MHz, DMSO-d_6) δ 161.00 (d, *J* = 240.9 Hz), 138.54, 130.44 (d, *J* = 7.9 Hz), 115.32 (d, *J* = 20.9 Hz), 49.21, 33.93, 32.00.

Synthesis of final compounds

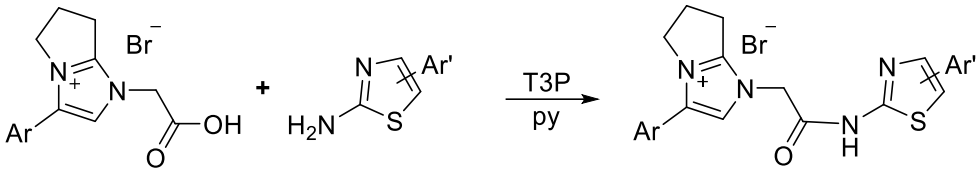

General procedure for amide coupling. The acid (1 eq) and the corresponding amine (1 eq) were weighed into a 4-ml glass vial and dissolved in a minimum amount of anhydrous pyridine. The resulting mixture was stirred at room temperature for 5 minutes, after which put onto ice. After cooling down the 50% solution of propylphosphonic anhydride (2eq) was added thereto in a dropwise fashion and the reaction mixture was left to stir in an ice bath for 15 minutes. After this, the cooling was removed and the mixture was stirred at room temperature until the completion of the reaction. The reaction progress was monitored by HPLC-MS. Once the reaction was complete, the reaction mixture was quenched with water and extracted with DCM. The organic extracts were merged, dried over anhydrous sodium sulfate and concentrated in vacuo. If not stipulated otherwise, the residue obtained was subjected to the purification by flash chromatography using neutral alumina as a stationary phase (DCM-MeOH 0% → 10%) or preparative HPLC (H_2O – MeCN 5% → 100%).

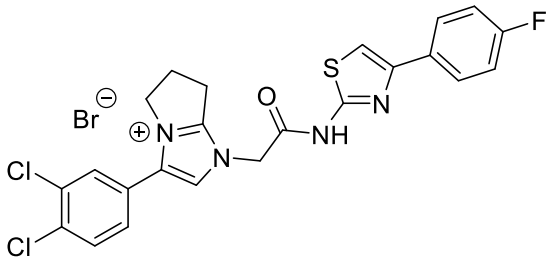

Compound **H1.** Isolated as off-white solid (55 mg, 48%).

^{1}H NMR (500 MHz, DMSO-d_6) δ: 8.01 (s, 1H), 7.92 – 7.88 (m, 2H), 7.83 (d, J = 8.4 Hz, 1H), 7.78 (d, J = 2.0 Hz, 1H), 7.52 (s, 1H), 7.46 (dd, J = 8.3, 2.1 Hz, 1H), 7.24 (t, J = 8.9 Hz, 2H), 5.13 (s, 2H), 4.37 (t, J = 7.3 Hz, 2H), 3.27 (t, J = 7.6 Hz, 2H), 2.78 – 2.69 (m, 2H).

^{19}F NMR (470 MHz, DMSO-d_6) δ: -114.67.

^{13}C NMR (126 MHz, DMSO-d_6) δ 165.24, 161.64 (d, *J* = 244.3 Hz), 154.80, 149.62, 147.66, 135.47, 133.15, 131.95, 131.48, 131.23 (d, *J* = 2.1 Hz), 131.14, 129.34, 127.58 (d, *J* = 8.0 Hz), 126.46, 116.84, 115.49 (d, *J* = 21.4 Hz), 107.62, 49.37, 48.65, 25.13, 23.60.

HRMS (ESI): calculated for $[C_{23}H_{18}Cl_2FN_4OS]^+$: 487.0557, found 487.0556.

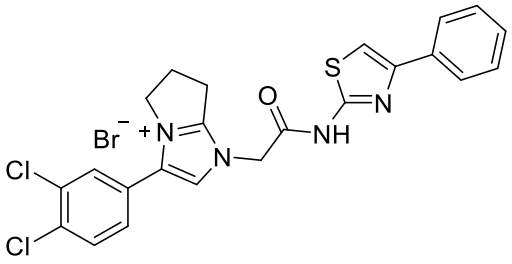

Compound **H2**. Isolated as white solid (50 mg, 75%).

^{1}H NMR (500 MHz, MeOD) δ 7.87 (d, *J* = 7.4 Hz, 2H), 7.73 (s, 1H), 7.72 – 7.68 (m, 2H), 7.43 – 7.34 (m, 4H), 7.29 (t, *J* = 7.3 Hz, 1H), 4.43 (t, *J* = 7.3 Hz, 2H), 2.92 – 2.83 (m, 2H).

^{13}C NMR (126 MHz, MeOD) δ 156.54, 138.12, 136.17, 135.98, 134.52, 132.89, 132.64, 130.50, 129.63, 128.86, 127.26, 127.05, 117.74, 108.95, 50.03, 26.45, 24.65.

HRMS (ESI): calculated for $[C_{23}H_{19}Cl_2N_4OS]^+$: 469.0651, found: 469.0650.

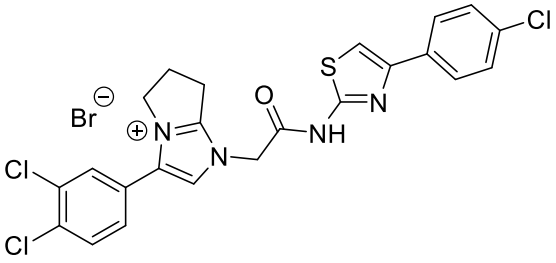

Compound **H3**. Isolated as slightly beige solid (50 mg, 42%).

^{1}H NMR (500 MHz, DMSO-d_6) δ 12.78 (s, 1H), 8.01 (s, 1H), 7.92 – 7.89 (m, 2H), 7.86 (d, *J* = 8.3 Hz, 1H), 7.77 (s, 1H), 7.76 (d, *J* = 2.1 Hz, 1H), 7.53 – 7.49 (m, 2H), 7.44 (dd, *J* = 8.3, 2.1 Hz, 1H), 5.24 (s, 2H), 4.41 – 4.36 (m, 2H), 3.28 (t, *J* = 7.6 Hz, 2H), 2.79 – 2.70 (m, 2H).

^{13}C NMR (126 MHz, DMSO-d_6) δ 164.55, 157.62, 155.48, 148.34, 135.86, 133.79, 133.26, 132.96, 132.45, 131.99, 131.72, 129.96, 129.33, 127.88, 126.67, 117.50, 110.09, 49.22, 48.85, 25.60, 24.09.

HRMS (ESI): calculated for $[C_{23}H_{18}Cl_3N_4OS]^+$: 503.0261, found 503.0261.

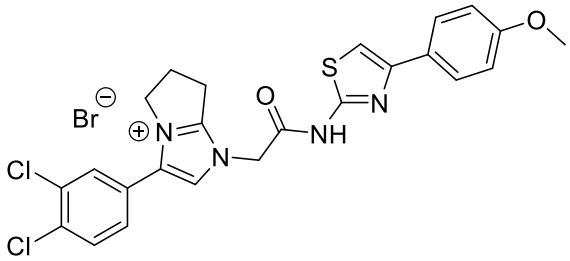

Compound **H4**. Isolated as white solid (30 mg, 26%).

^{1}H NMR (500 MHz, DMSO-d_6) δ 8.01 (s, 1H), 7.85 (d, *J* = 8.3 Hz, 1H), 7.82 – 7.78 (m, 2H), 7.77 (d, *J* = 2.0 Hz, 1H), 7.48 (s, 1H), 7.44 (dd, *J* = 8.3, 2.1 Hz, 1H), 7.00 – 6.94 (m, 2H),

5.18 (d, *J* = 16.3 Hz, 2H), 4.38 (t, *J* = 7.3 Hz, 2H), 3.78 (s, 3H), 3.30 – 3.24 (m, 3H), 2.78 – 2.69 (m, 2H).

^{13}C NMR (126 MHz, DMSO-d_6) δ 164.34, 159.03, 154.95, 148.85, 135.43, 133.26, 131.98, 131.52, 131.22, 129.43, 127.01, 126.32, 116.99, 114.11, 106.49, 55.17, 48.73, 46.11, 25.15, 23.65, 18.76.

HRMS (ESI): calculated for $[C_{24}H_{21}Cl_2N_4O_2S]^+$: 499.0757, found: 499.0757.

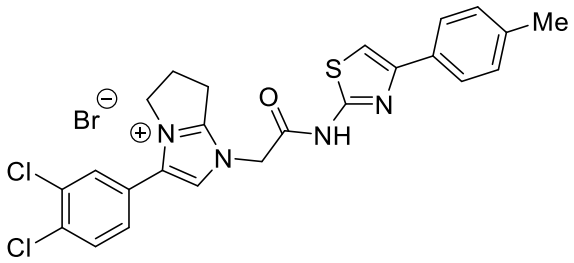

Compound **H5**. Isolated as slightly beige solid (64 mg, 57%).

^{1}H NMR (500 MHz, MeOD) δ 7.73 (d, *J* = 7.9 Hz, 2H), 7.72 (s, 1H), 7.66 (d, *J* = 8.3 Hz, 1H), 7.65 (s, 1H), 7.44 (dd, *J* = 8.3, 2.0 Hz, 1H), 7.16 (d, *J* = 8.1 Hz, 2H), 7.09 (s, 1H), 4.38 (t, *J* = 7.3 Hz, 2H), 3.28 (t, *J* = 7.6 Hz, 2H), 2.87 – 2.80 (m, 2H), 2.33 (s, 3H).

^{13}C NMR (126 MHz, MeOD) δ 171.16, 169.72, 156.13, 150.27, 138.17, 138.00, 135.69, 134.35, 134.31, 132.77, 132.44, 130.41, 130.07, 127.79, 126.96, 117.15, 107.25, 49.74, 26.39, 24.51, 21.21.

HRMS (ESI): calculated for $[C_{24}H_{21}Cl_2N_4O_2S]^+$: 483.0808, found: 483.0807.

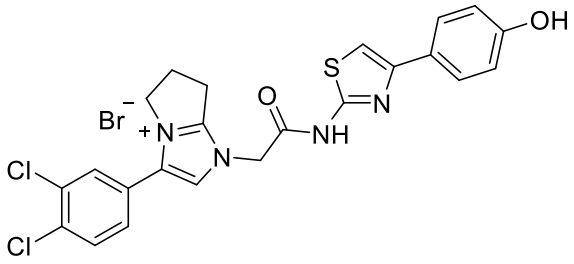

Compound **H6** was obtained from TBDMS-protected 4-(4-hydroxyphenyl)-2-aminothiazolyl hydrobromide. After the completion of the amide coupling, the reaction mixture was quenched byADDINg aqueous HBr (1 ml, 0.15 M) and stirring the mixture. After successful removal of the silyl protecting group in acidic medium, the reaction mixture was concentrated in vacuo and subsequently subjected the purification by preparative HPLC. Isolated as white fluffy solid (50 mg, 75%).

^{1}H NMR (500 MHz, DMSO-d_6) δ 12.73 (s, 1H), 9.66 (s, 1H), 8.01 (s, 1H), 7.85 (d, *J* = 8.3 Hz, 1H), 7.76 (d, *J* = 2.0 Hz, 1H), 7.68 (d, *J* = 8.6 Hz, 2H), 7.45 – 7.40 (m, 2H), 6.81 (d, *J* = 8.7 Hz, 2H), 5.23 (s, 2H), 4.38 (t, *J* = 7.3 Hz, 2H), 3.27 (t, *J* = 7.6 Hz, 2H), 2.78 – 2.69 (m, 2H).

^{13}C NMR (126 MHz, DMSO-d_6) δ 163.92, 157.46, 155.01, 149.47, 135.41, 133.31, 131.99, 131.54, 131.25, 129.47, 127.10, 126.25, 125.31, 117.04, 115.48, 105.89, 48.76, 48.44, 25.15, 23.66.

HRMS (ESI): calculated for $[C_{23}H_{19}Cl_2N_4O_2S]^+$: 485.0600, found: 485.0600.

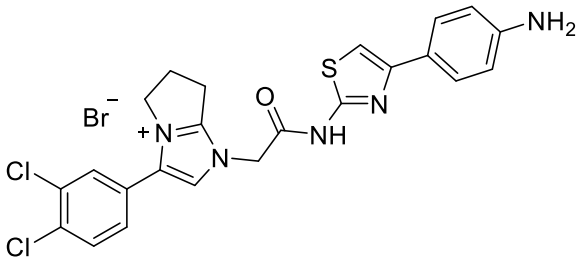

Compound H7 was obtained by means of selective reduction of the compound **H14**. **Procedure:** to the solution of the nitroderivative **H14** (10 mg, 0.017 mmol) in 1 ml of the solvent mixture MeOH/THF/H_2O (6/2/2 v/v) and the resulting solution was heated up to 45^{o}C. After that, $Na_2S_2O_4$ (11 mg, 0.060 mmol) was added to the reaction mixture, which was then left to stir at 45^{o}C for 30 minutes. After the HPLC-MS indicated the full consumption of the starting material, the reaction mixture was quenched byADDINg 1 ml of saturated aqueous Na_2CO_3 and diluted with DCM. The organic fraction was separated, dried over anhydrous sodium sulfate, concentrated in vacuo and subjected to the purification by preparative HPLC. Isolated as white solid (5 mg, 20%)

^{1}H NMR (500 MHz, DMSO-d_6) δ 8.34 (s, 1H), 7.99 (s, 1H), 7.84 (d, *J* = 8.4 Hz, 1H), 7.82 (d, *J* = 2.0 Hz, 1H), 7.53 – 7.48 (fm, 3H), 6.96 (s, 1H), 6.54 (d, *J* = 8.5 Hz, 2H), 4.91 (s, 2H), 4.37 (t, *J* = 7.4 Hz, 2H), 3.28 – 3.22 (m, 2H), 2.77 – 2.69 (m, 2H).

HRMS (ESI): calculated for $[C_{23}H_{20}Cl_2N_5OS]^+$: 484.0760, found: 499.0757.

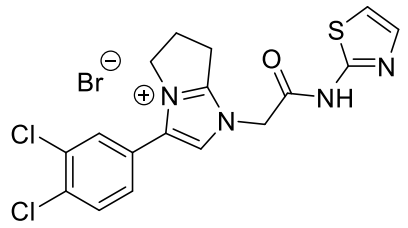

Compound **H8.** Isolated as clear, vitrifying solid (35 mg, 52%).

^{1}H NMR (500 MHz, MeOD) δ 7.74 (s, 1H), 7.70 (d, *J* = 8.3 Hz, 1H), 7.68 (d, *J* = 2.1 Hz, 1H), 7.42 (d, *J* = 3.7 Hz, 1H), 7.39 (dd, *J* = 8.3, 2.1 Hz, 1H), 7.12 (d, *J* = 3.7 Hz, 1H), 5.50 (s, 2H), 4.46 – 4.38 (m, 2H), 2.91 – 2.83 (m, 2H).

^{13}C NMR (126 MHz, MeOD) δ 166.78, 156.49, 138.45, 138.07, 137.57, 136.08, 134.45, 132.85, 132.61, 130.50, 127.32, 117.70, 114.64, 108.07, 50.00, 26.44, 24.63.

HRMS (ESI): calculated for $[C_{17}H_{15}Cl_2N_4OS]^+$: 393.0338, found: 393.0334.

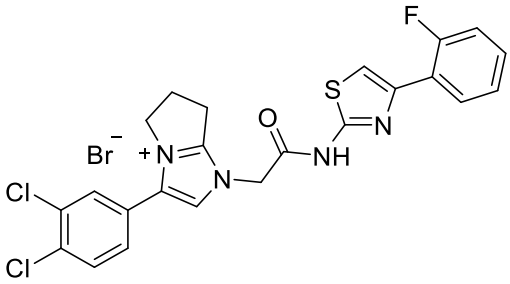

Compound **H10.** Isolated as white solid (70 mg, 70%).

^{1}H NMR (500 MHz, DMSO-d_6) δ 8.06 – 7.99 (m, 2H), 7.86 – 7.81 (m, 2H), 7.51 (d, *J* = 7.2 Hz, 1H), 7.37 (d, *J* = 2.3 Hz, 1H), 7.35 – 7.30 (m, 1H), 7.30 – 7.24 (m, 3H), 5.09 (s, 2H), 4.37 (t, *J* = 7.0 Hz, 3H), 3.27 (s, 2H), 2.77 – 2.68 (m, 2H).

^{19}F NMR (470 MHz, DMSO-d_6) δ -114.63 – -114.81 (m).

^{13}C NMR (126 MHz, DMSO-d_6) δ 166.27, 162.35, 159.61 (d, *J* = 248.4 Hz), 154.73, 142.20, 135.58, 133.07, 131.97, 131.51, 131.10, 129.39 (d, *J* = 3.0 Hz), 129.26, 128.91 (d, *J* = 8.2 Hz), 126.69, 124.65 (d, *J* = 2.8 Hz), 122.59 (d, *J* = 11.0 Hz), 122.63, 122.54, 116.70, 116.05 (d, *J* = 22.2 Hz), 111.71 (d, *J* = 13.8 Hz), 50.04, 48.61, 25.14, 23.56.

HRMS (ESI):: calculated for $[C_{23}H_{18}Cl_2FN_4OS]^+$: 487.0557, found 487.0555.

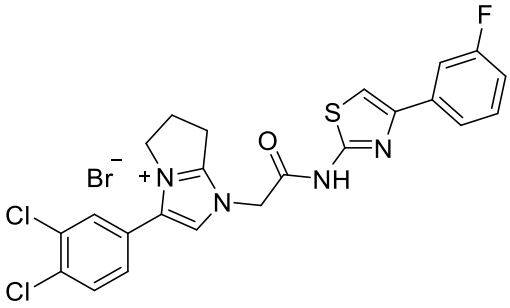

Compound **H11.** Isolated as beige solid (71 mg, 71%).

^{1}H NMR (500 MHz, DMSO-d_6) δ 8.01 (s, 1H), 7.83 (d, *J* = 8.3 Hz, 1H), 7.80 (d, *J* = 1.2 Hz, 1H), 7.73 (d, *J* = 7.8 Hz, 1H), 7.68 – 7.64 (m, *J* = 7.1 Hz, 1H), 7.51 (d, *J* = 7.6 Hz, 1H), 7.44 (dt, *J* = 14.3, 7.2 Hz, 1H), 7.12 (td, *J* = 8.5, 2.4 Hz, 1H), 5.23 (s, 1H), 4.37 (t, *J* = 7.1 Hz, 1H), 3.29 (s, 1H), 2.78 – 2.67 (m, 1H).

^{19}F NMR (470 MHz, DMSO-d_6) δ -113.09 – -113.31 (m).

^{13}C NMR (126 MHz, DMSO-d_6) δ 165.60, 162.60 (d, *J* = 242.5 Hz), 160.80, 154.88, 147.39 (d, *J* = 2.5 Hz), 137.07 (d, *J* = 8.2 Hz), 135.56, 133.12, 131.97, 131.53, 131.12, 130.69 (d, *J* = 8.5 Hz), 129.31, 126.57, 121.66 (d, *J* = 2.0 Hz), 116.83, 114.22 (d, *J* = 21.0 Hz), 112.17 (d, *J* = 22.8 Hz), 109.22, 49.48, 48.67, 25.14, 23.59.

HRMS (ESI):: calculated for $[C_{23}H_{18}Cl_2FN_4OS]^+$: 487.0557, found 487.0555.

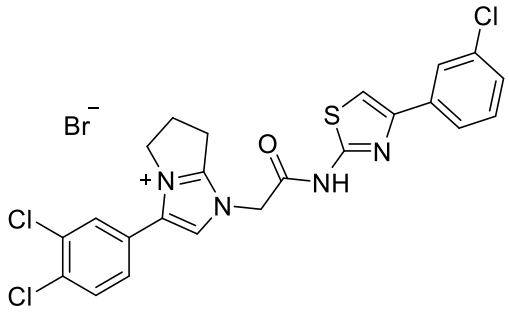

Compound **H12.** Isolated as white solid (22.0 mg, 44%).

^{1}H NMR (500 MHz, DMSO-d_6) δ 12.86(s, 1H), 7.85 (s, 1H), 7.75 (s, 1H),), 7.72 (t, *J* = 8.3 Hz, 1H), 7.70 (d, *J* = 2.1 Hz, 1H), 7.54 (t, *J* = 1.8 Hz, 1H), 7.47 (t, *J* = 8.1 Hz, 1H), 7.42-7.38 (m, 2H), 7.40 (dd, *J* = 8.3, 2.1 Hz), 5.20 (s, 2H), 4.34 (t, *J* = 7.2 Hz, 1H), 3.28 (t, *J* = 7.2 Hz, 2H), 2.79 – 2.66 (m, 2H).

^{13}C NMR (126 MHz, DMSO-d_6) δ 164.29, 154.05, 147.44, 136.30, 135.50, 133.90, 133.822, 131.70, 131.56, 131.00, 129.08, 127.87, 127.70, 126.66, 124.37, 124.33, 117.02, 110.34, 54.97, 48.75, 48.33, 25.12, 23.50.

HRMS (ESI): calculated for $[C_{23}H_{18}Cl_3N_4OS]^+$: 503.0261/505.0232, found 503.0264/ 505.0228.

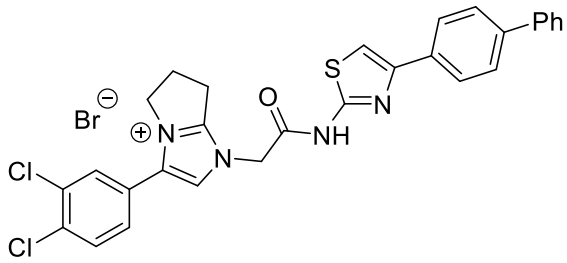

Compound **H13.** Isolated as beige solid (44 mg, 35%).

^{1}H NMR (500 MHz, MeOD) δ 7.96 (d, *J* = 8.3 Hz, 1H), 7.73 (s, 1H), 7.70 (dd, *J* = 5.1, 3.1 Hz, 1H), 7.68 – 7.63 (m, 2H), 7.47 – 7.38 (m, 2H), 7.34 (ddd, *J* = 8.5, 2.1, 1.1 Hz, 1H), 4.43 (t, *J* = 7.3 Hz, 1H), 3.36 – 3.32 (m, 3H), 2.92 – 2.83 (m, 1H).

^{13}C NMR (126 MHz, MeOD) δ 168.90, 155.06, 140.56, 140.29, 136.73, 134.68, 133.78, 133.08, 131.46, 131.21, 129.08, 128.49, 127.01, 126.71, 126.64, 126.40, 126.10, 126.01, 125.95, 116.23, 48.58, 25.04, 23.22.

HRMS (ESI):: calculated for $[C_{29}H_{23}Cl_2N_4OS]^+$: 545.0964, found 545.0964.

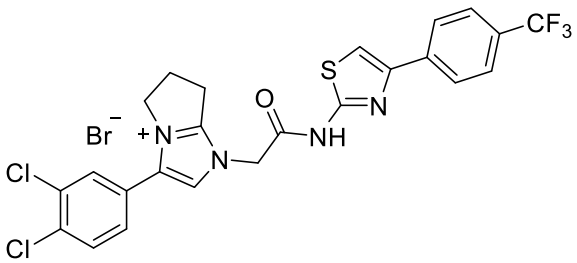

Compound **H14.** Isolated as white solid (38.5 mg, 63%).

^{1}H NMR (500 MHz, DMSO-d_6) δ 8.08 – 8.04 (m, *J* = 8.0 Hz, 1H), 7.99 (s, 1H), 7.85 – 7.81 (m, *J* = 7.6 Hz, 2H), 7.74 – 7.69 (m, *J* = 8.3 Hz, 1H), 7.56 – 7.49 (m, *J* = 12.3 Hz, 1H), 4.86 (s, 2H), 4.37 (t, *J* = 7.0 Hz, 2H), 3.28 – 3.22 (m, 2H), 2.78 – 2.68 (m, 2H).

^{19}F NMR (470 MHz, DMSO-d_6) δ -60.71 (s).

^{13}C NMR (126 MHz, DMSO-d_6) δ 167.28, 154.43, 146.47, 139.35, 135.58, 132.95, 131.90, 131.40, 131.01, 129.15, 127.01, 126.80, 125.92, 125.39 (q, *J* = 2.6 Hz), 116.46, 109.60, 108.98, 50.85, 48.47, 25.08, 23.43.

HRMS (ESI):: calculated for $[C_{24}H_{18}Cl_2F_3N_4OS]^+$: 537.0525, found 537.0525

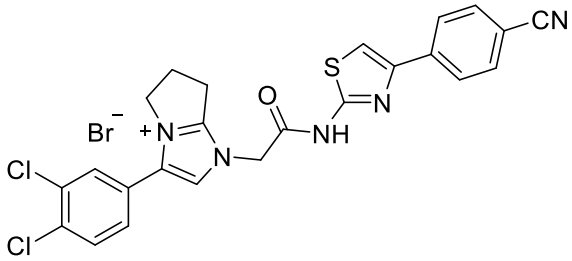

Compound **H15.** Isolated as white solid (44 mg, 43%).

^{1}H NMR (500 MHz, DMSO-d_6) δ 8.08 – 8.04 (m, 1H), 8.02 (s, 1H), 7.88 (d, *J* = 8.5 Hz, 1H), 7.87 – 7.84 (m, 1H), 7.80 (d, *J* = 2.1 Hz, 1H), 7.47 (dd, *J* = 8.3, 2.1 Hz, 1H), 5.13 (s, 1H), 4.38 (t, *J* = 7.3 Hz, 1H), 3.27 (t, *J* = 7.6 Hz, 1H), 2.79 – 2.71 (m, 1H).

^{13}C NMR (126 MHz, DMSO-d_6) δ 165.99, 155.27, 147.36, 139.15, 135.92, 133.62, 133.25, 132.41, 131.96, 131.61, 129.80, 126.92, 126.67, 119.47, 117.31, 112.02, 110.10, 107.20, 49.81, 49.12, 25.59, 24.04.

HRMS (ESI): calculated for $[C_{24}H_{18}Cl_2N_5OS]^+$: 494.0604, found 494.0603.

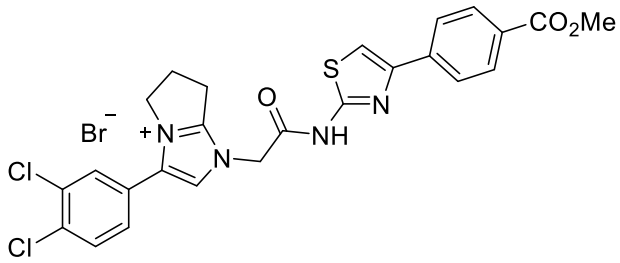

Compound **H16.** Isolated as white solid (102 mg, 33%).

^{1}H NMR (500 MHz, DMSO-d_6) δ 8.03 – 7.96 (m, 5H), 7.84 (d, *J* = 8.4 Hz, 1H), 7.79 (d, *J* = 2.0 Hz, 1H), 7.73 (s, 1H), 7.47 (dd, *J* = 8.4, 2.0 Hz, 1H), 5.09 (s, 2H), 4.42 – 4.32 (m, 2H), 3.85 (s, 3H), 3.26 (t, *J* = 7.6 Hz, 2H), 2.78 – 2.68 (m, 2H).

^{13}C NMR (126 MHz, DMSO-d_6) δ 166.07, 165.79, 154.79, 149.67, 147.43, 139.07, 135.51, 133.16, 131.99, 131.53, 131.16, 129.73, 129.34, 128.16, 126.56, 125.73, 116.83, 110.46, 52.16, 49.65, 48.67, 25.16, 23.61.

HRMS (ESI):: calculated for $[C_{25}H_{21}Cl_2N_4O_3S]^+$: 527.0706, found 527.0705.

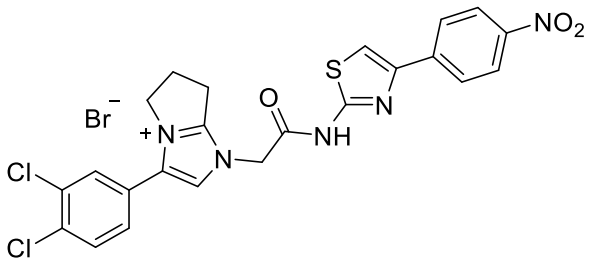

Compound **H17.** Isolated as yellow solid (77 mg, 63%).

^{1}H NMR (500 MHz, MeOD) δ 8.23 (d, *J* = 8.8 Hz, 2H), 8.09 (d, *J* = 8.8 Hz, 2H), 7.71 (d, *J* = 2.0 Hz, 1H), 7.67 (s, 1H), 7.66 (d, *J* = 8.8 Hz, 1H), 7.50 (s, 1H), 7.43 (dd, *J* = 8.3, 2.0 Hz, 1H), 4.40 (t, *J* = 7.3 Hz, 2H), 3.28 (t, *J* = 7.7 Hz, 2H), 2.89 – 2.81 (m, 2H).

^{13}C NMR (126 MHz, MeOD) δ 171.57, 170.32, 156.14, 147.93, 147.88, 143.15, 138.18, 135.72, 134.32, 132.77, 132.45, 130.38, 127.75, 127.47, 124.87, 117.23, 112.31, 54.81, 49.77, 26.41, 24.51.

HRMS (ESI): calculated for $[C_{23}H_{18}Cl_2N_5O_3S]^+$: 514.0502, found 514.0504.

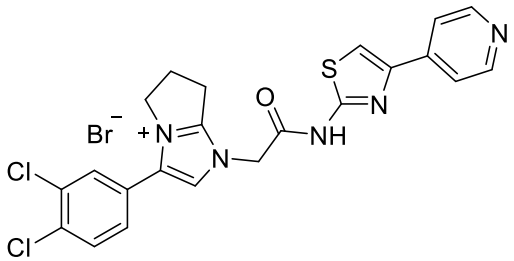

Compound **H18.** Isolated as white solid (69 mg, 69%).

^{1}H NMR (500 MHz, DMSO-d_6) δ 8.60 (dd, *J* = 4.5, 1.6 Hz, 1H), 8.02 (s, 1H), 7.91 (s, 1H), 7.85 (d, *J* = 8.4 Hz, 1H), 7.81 (dd, *J* = 4.5, 1.6 Hz, 1H), 7.80 (d, *J* = 2.1 Hz, 1H), 5.12 (s, 1H), 4.38 (t, *J* = 7.3 Hz, 1H), 3.27 (t, *J* = 7.6 Hz, 1H), 2.78 – 2.70 (m, 1H).

^{13}C NMR (126 MHz, DMSO-d_6) δ 166.08, 155.25, 150.65, 146.67, 141.70, 135.92, 133.61, 132.41, 131.96, 131.60, 129.79, 126.93, 120.36, 117.29, 112.56, 55.41, 49.88, 49.11, 25.59, 24.04.

HRMS (ESI): calculated for $[C_{22}H_{19}Cl_2N_5OS]^{2+}$: 235.5338, found: 235.5335; calculated for $[C_{22}H_{18}Cl_2N_5OS]^+$ 470.0604, found 470.0601.

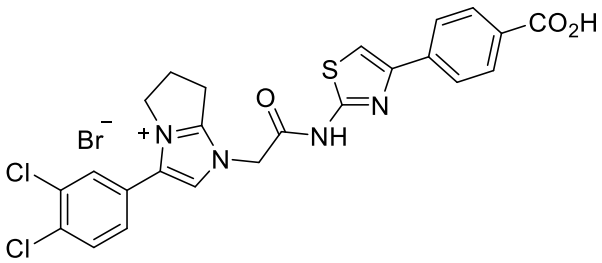

Compound **H19** was obtained by hydrolysis of the methyl ester (compound **H13**).

Procedure: the compound **H16** (51.3 mg, 0.0843 mmol) was dissolved in a mixture of acetonitrile and water (510 µl, 2% water v/v), after which DIPEA (44 µl, 0.253 mmol) and LiBr (73.2 mg, 0.843 mmol) were added thereto. The progress of the reaction was monitored by HPLC-MS and once it had indicated the full consumption of the starting material, the reaction was quenched by adding aqueous HBr (500 µl of 1M solution, 0.5 mmol). The resulting mixture was then concentrated in vacuo and subjected to the purification by preparative HPLC. The title compound was isolated as slightly beige solid (20 mg, 40%).

^{1}H NMR (500 MHz, DMSO-d_6) δ 8.31 (s, 1H), 8.00 (s, 1H), 7.95 (s, 5H), 7.85 (d, *J* = 8.4 Hz, 1H), 7.82 (d, *J* = 2.0 Hz, 1H), 7.57 (s, 1H), 7.50 (dd, *J* = 8.4, 2.1 Hz, 1H), 4.99 (s, 2H), 4.38 (t, *J* = 7.3 Hz, 3H), 3.29 – 3.22 (m, 5H), 2.74 (dt, *J* = 15.2, 7.5 Hz, 3H).

^{13}C NMR (126 MHz, DMSO-d_6) δ 167.99, 166.89, 164.66, 155.06, 147.96, 138.95, 135.99, 133.50, 132.39, 131.92, 131.52, 130.12, 129.68, 127.12, 126.06, 125.76, 117.07, 109.56, 50.63, 49.01, 25.56, 23.94.

HRMS (ESI): calculated for $[C_{24}H_{19}Cl_2N_4O_3S]^+$: 513.0549, found 513.0550.

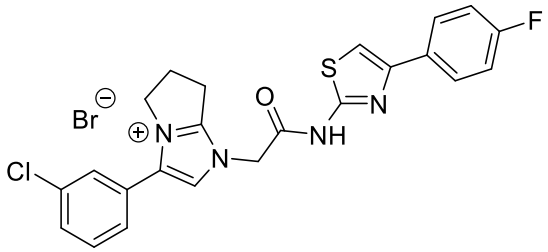

Compound **H21.** Obtained as slightly orange solid (71 mg, 66%).

^{1}H NMR (500 MHz, DMSO-d_6) δ 7.97 (s, 1H), 7.87 (dd, *J* = 8.5, 5.7 Hz, 2H), 7.63 – 7.54 (m, 3H), 7.48 (d, *J* = 7.5 Hz, 1H), 7.23 (s, 1H), 7.18 (t, *J* = 8.8 Hz, 2H), 4.82 (s, 2H), 4.37 (t, *J* = 7.2 Hz, 2H), 3.25 (t, *J* = 7.6 Hz, 2H), 2.73 (p, J =7.5 Hz, 2H).

^{13}C NMR (126 MHz, DMSO-d_6) δ 167.64, 161.72 (d, *J* = 243.3 Hz), 154.80, 149.75, 147.39, 136.95, 134.23, 132.82 (d, *J* = 2.6 Hz), 131.56, 130.37, 129.30, 128.71, 128.10, 127.77 (d, *J* = 8.0 Hz), 116.56, 115.63 (d, *J* = 21.3 Hz), 106.29, 51.37, 48.87, 25.53, 23.93.

HRMS (ESI): calculated for $[C_{23}H_{19}ClFN_4OS]^+$: 453.0947, found 453.0943

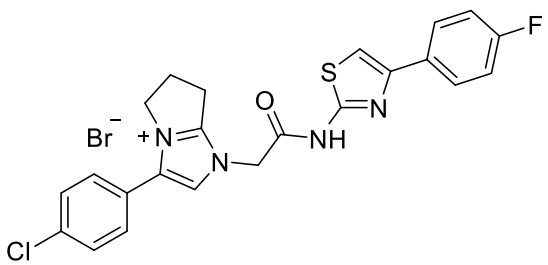

Compound **H22** Isolated as white solid (65 mg, 63%).

^{1}H NMR (500 MHz, DMSO-d_6) δ 7.96 (s, 1H), 7.93 – 7.90 (m, 2H), 7.69 (s, 1H), 7.67 – 7.63 (m, 2H), 7.47 – 7.43 (m, 2H), 7.29 – 7.25 (m, 2H), 5.21 (s, 2H), 4.38 (t, *J* = 7.3 Hz, 2H), 3.28 – 3.24 (m, 4H), 2.78 – 2.70 (m, 2H).

^{13}C NMR (126 MHz, DMSO-d_6) δ 164.13, 161.87 (d, *J* = 245.3 Hz), 157.25, 155.95, 154.85, 148.06, 136.66, 135.28, 131.11, 129.48, 127.72 (d, *J* = 8.1 Hz), 124.54, 116.42, 115.69 (d, *J* = 21.5 Hz), 108.60, 48.69, 48.29, 25.12, 23.66.

HRMS (ESI): calculated for $[C_{23}H_{19}ClFN_4OS]^+$: 453.0947, found 453.0944.

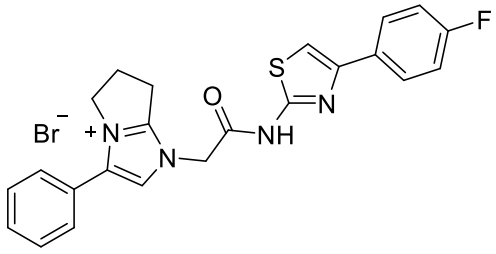

Compound **H23.** Obtained as slightly beige solid (40 mg, 62%).

^{1}H NMR (500 MHz, DMSO-d_6) δ 7.89 – 7.84 (m, 3H), 7.56 – 7.48 (m, 5H), 7.16 (t, *J* = 8.9 Hz, 2H), 7.11 (s, 1H), 4.69 (s, 2H), 4.36 (t, *J* = 7.3 Hz, 2H), 3.24 (t, *J* = 7.6 Hz, 2H), 2.76 – 2.69 (m, 2H).

^{19}F NMR (470 MHz, DMSO-d_6) δ -116.14 – -116.38 (m).

^{13}C NMR (126 MHz, DMSO-d_6) δ 167.99, 161.10 (d, *J* = 242.5 Hz), 160.75, 153.96, 146.64, 138.00, 132.80 (d, *J* = 2.7 Hz), 129.91, 129.11 (d, *J* = 28.6 Hz), 127.21 (d, *J* = 7.9 Hz), 126.38, 115.12, 114.95, 105.07, 51.29, 48.24, 25.04, 23.47.

HRMS (ESI): Calculated for $[C_{23}H_{20}FN_4OS]^+$ 419.1336, found: 419.1334

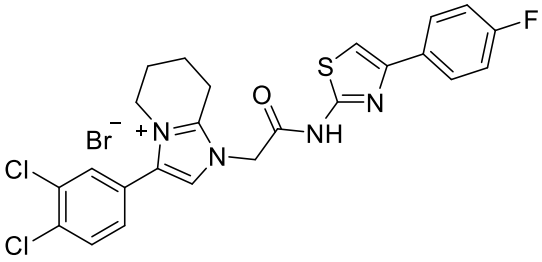

Compound **H31.** Obtained as a yellowish solid (41 mg, 42%).

^{1}H NMR (500 MHz, MeOD) δ 8.44 (s, 1H), 7.93 – 7.88 (m, 2H), 7.73 – 7.71 (m, 2H), 7.66 (d, *J* = 2.0 Hz, 1H), 7.41 (s, 1H), 7.38 (dd, *J* = 8.3, 2.0 Hz, 1H), 7.15 – 7.10 (m, 2H), 5.11 (s, 2H), 4.30 (t, *J* = 5.7 Hz, 2H), 3.10 (t, *J* = 6.1 Hz, 2H), 2.22 – 2.10 (m, 4H).

^{19}F NMR (470 MHz, MeOD) δ -114.73 – -118.62 (m).

^{13}C NMR (126 MHz, MeOD) δ 165.20, 164.05 (d, *J* = 246.2 Hz), 158.60, 150.48, 148.40, 136.34, 134.58, 133.64, 133.00, 132.72, 132.08 (d, *J* = 3.0 Hz), 130.63, 129.00 (d, *J* = 8.2 Hz), 126.72, 121.25, 116.40 (d, *J* = 21.8 Hz), 109.08, 48.09, 47.94, 22.34, 22.25, 19.16.

HRMS (ESI): Calculated for $[C_{24}H_{20}Cl_2FN_4OS]^+$ 501.0713, found: 501.0714.

Synthesis of the 1,4-triazolic analogue H32

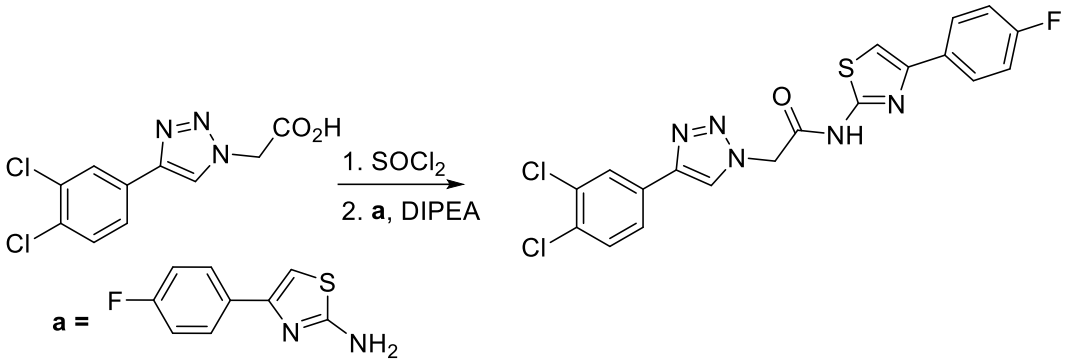

Compound (H32). (27.2 mg, 0.1 mmol) was suspended in anhydrous DCM (1.5 ml) and oxalyl chloride (25 µL, 0.15 mmol) was added thereto. The resulting mixture was refluxed for 1 hour and then evaporated under reduced pressure yielding a yellowish residue, which was re-suspended in anhydrous DCM (1 ml). To the resulting suspension was added DIPEA (25 µL, 0.15 mmol) and 4-(4-fluorophenyl)thiazol-2-amine (19.4 mg, 0.1 mmol), after which the reaction mixture was stirred at room temperature for 5 hours. The reaction mixture was concentrated in vacuo and subjected to RP chromatography (C18 column, H_2O-MeCN), which afforded the title product as white solid (22 mg, 50%).

LC-MS $[M+H]^+$: 448.22.

^{1}H NMR (500 MHz, DMSO-d_6) δ 12.80 (s, 1H), 8.78 (s, *J* = 6.0 Hz, 1H), 8.15 (d, *J* = 1.9 Hz, 1H), 7.92 – 7.88 (m, 2H), 7.74 (d, *J* = 8.4 Hz, 1H), 7.65 (dd, *J* = 8.7, 5.3 Hz, 2H), 7.26 (t, *J* = 8.8 Hz, 2H), 5.58 (s, *J* = 11.6 Hz, 2H).

^{19}F NMR (470 MHz, DMSO-d_6) δ -114.09 – -114.18 (m).

^{13}C NMR (126 MHz, DMSO-d6) δ 164.57, 161.61 (d, *J* = 244.9 Hz), 156.28, 144.15, 134.26 (d, *J* = 5.8 Hz), 131.80, 131.29, 130.71, 130.21, 127.81 (d, *J* = 8.0 Hz), 126.77, 125.24, 124.15, 116.18 (d, *J* = 21.8 Hz), 51.71.

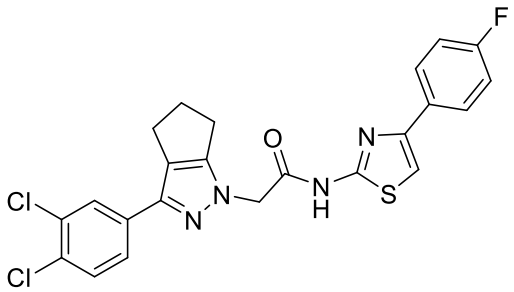

Compound **H33** Purified by flash chromatography on silica (Cyclohexane-EtOAc). Obtained as white solid (60 mg, 90%).

^{1}H NMR (500 MHz, DMSO-d_6) δ 12.74 (s, 1H), 7.98 – 7.92 (m, 1H), 7.80 (d, *J* = 1.9 Hz, 1H), 7.68 – 7.64 (m, 1H), 7.60 (dd, *J* = 8.4, 1.9 Hz, 1H), 7.31 – 7.25 (m, 1H), 5.13 (s, 2H), 2.84 (t, *J* = 7.0 Hz, 1H), 2.74 (t, *J* = 7.3 Hz, 1H), 2.63 – 2.55 (m, 1H).

^{19}F NMR (470 MHz, DMSO-d_6) δ -113.51 – -115.57 (m).

^{13}C NMR (126 MHz, DMSO-d_6) δ 166.03, 161.87 (d, *J* = 244.7 Hz), 157.52, 153.62, 148.01, 141.32, 134.34, 131.52, 131.10, 130.80 (d, *J* = 2.7 Hz), 129.42, 127.76 (d, *J* = 8.2 Hz), 126.36, 125.34, 124.30, 115.72 (d, *J* = 21.7 Hz), 108.38, 52.59, 30.64, 24.20, 23.30.

HRMS (ESI): Calculated for $[C_{23}H_{18}Cl_2FN_4OS]^+$ 487.0557, found 487.0555.

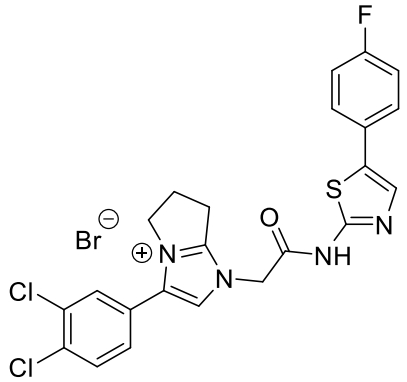

Compound **H41.** Obtained as white solid (44 mg, 68%).

^{1}H NMR (500 MHz, DMSO-d_6) δ 7.98 (s, 1H), 7.83 (dd, *J* = 6.7, 5.2 Hz, 2H), 7.57 (s, 1H), 7.54 – 7.47 (m, 3H), 7.16 (t, *J* = 8.9 Hz, 2H), 4.79 (s, 2H), 4.36 (t, *J* = 7.2 Hz, 2H), 3.23 (t, *J* = 7.6 Hz, 3H), 2.76 – 2.68 (m, 2H).

^{19}F NMR (470 MHz, DMSO-d_6) δ -116.23 – -116.33 (m).

^{13}C NMR (126 MHz, DMSO-d_6) δ 168.48, 167.99, 160.98 (d, *J* = 242.6 Hz), 154.79, 136.05, 134.20, 133.33, 132.35, 131.85, 131.39, 131.00 (d, *J* = 2.0 Hz), 129.57, 127.38, 127.01 (d, *J* = 7.9 Hz), 126.65, 116.79, 116.18 (d, *J* = 21.5 Hz), 51.78, 48.86, 25.53, 23.88.

HRMS (ESI):: calculated for $[C_{23}H_{18}Cl_2FN_4OS]^+$: 487.0557, found 487.0552.

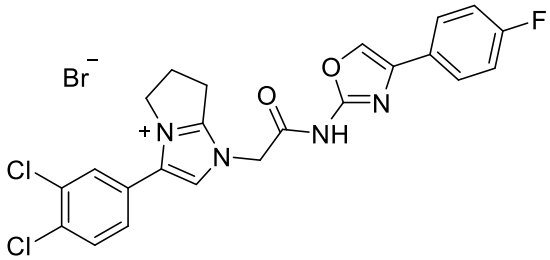

Compound **H42.** Obtained as a reddish solid (44 mg, 50%).

^{1}H NMR (500 MHz, MeOD) δ 7.86 (s, 1H), 7.77 – 7.68 (m, 5H), 7.48 (dd, *J* = 8.3, 1.9 Hz, 1H), 7.10 (t, *J* = 8.8 Hz, 2H), 5.50 (s, 1H), 4.40 (t, *J* = 7.3 Hz, 2H), 2.90 – 2.81 (m, 2H).

^{19}F NMR (470 MHz, MeOD) δ -116.51.

^{13}C NMR (126 MHz, MeOD) δ 168.92, 162.26 (d, *J* = 245.3 Hz), 154.75, 136.77, 134.80, 132.96, 131.35, 131.29, 129.01, 128.07, 126.40, 126.75 (d, *J* = 1.5 Hz), 126.63 (d, *J* = 8.4 Hz), 115.70, 114.96 (d, *J* = 22.0 Hz), 48.69, 24.99, 23.06.

LC-MS:$[M]^+$ 471.26

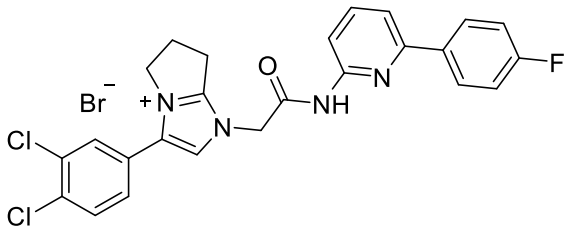

Compound **H43**. Obtained as slightly orange solid (60 mg, 70 %).

^{1}H NMR (500 MHz, DMSO-d_6) δ 11.02 (s, 1H), 8.15 – 8.06 (m, 2H), 7.96 – 7.82 (m, 3H), 7.77 (d, *J* = 2.0 Hz, 1H), 7.75 – 7.69 (m, 1H), 7.45 (dd, *J* = 8.3, 2.0 Hz, 1H), 7.34 (t, *J* = 8.8 Hz, 2H), 5.22 (s, 2H), 4.43 – 4.32 (m, 2H), 2.73 (dd, *J* = 14.4, 7.1 Hz, 2H).

^{13}C NMR (126 MHz, DMSO-d_6) δ 162.96 (d, *J* = 246.4 Hz), 154.91, 153.91, 150.69, 139.76, 135.47, 135.35, 134.41 (d, *J* = 2.8 Hz), 133.27, 131.98, 131.55, 131.19, 129.47, 128.78 (d, *J* = 8.4 Hz), 126.38, 116.93, 116.39, 115.65 (d, *J* = 21.4 Hz), 112.23, 49.03, 48.70, 24.96.

HRMS (ESI):: calculated for $[C_{25}H_{20}Cl_2FN_4O]^+$ 481.0993, found 481.0993.

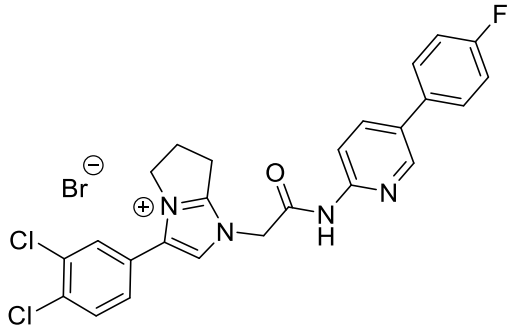

Compound **H44.** Obtained as off-white solid (95 mg, 77%).

^{1}H NMR (500 MHz, DMSO-d_6) δ 11.17 (s, 1H), 8.68 (d, *J* = 2.3 Hz, 1H), 8.13 (dd, *J* = 8.7, 2.5 Hz, 1H), 7.87 (d, *J* = 8.3 Hz, 1H), 7.77 (td, *J* = 6.0, 2.1 Hz, 3H), 7.45 (dd, *J* = 8.3, 2.1 Hz, 1H), 7.36 – 7.30 (m, 2H), 5.22 (s, 2H), 4.38 (t, *J* = 7.3 Hz, 2H), 3.28 (t, *J* = 7.6 Hz, 2H), 2.79 – 2.70 (m, 2H).

^{19}F NMR (470 MHz, DMSO-d_6) δ -114.64 – -114.71 (m).

^{13}C NMR (126 MHz, DMSO-d_6) δ 164.82, 162.56 (d, *J* = 245.0 Hz), 155.44, 150.65, 146.43, 136.92, 135.86, 133.69, 133.46 (d, *J* = 2.9 Hz), 132.44, 132.01, 131.62, 131.41, 129.89, 129.02 (d, *J* = 8.2 Hz), 126.86, 117.42, 116.44 (d, *J* = 21.4 Hz), 113.91, 49.49, 49.17, 25.62, 24.09.

HRMS (ESI): Calculated for $[C_{25}H_{20}Cl_2FN_4O]^+$:481.0993, found 481.0992

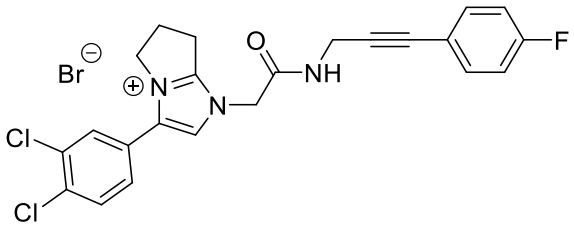

Compound **H45** Obtained as slightly yellow solid (39 mg, 64%).

^{1}H NMR (500 MHz, DMSO-d$_6$) δ 9.54 (s, 1H), 8.51 (s, 1H), 7.98 (s, 1H), 7.78 (d, *J* = 8.3 Hz, 1H), 7.74 (d, *J* = 1.8 Hz, 1H), 7.48 – 7.41 (m, 3H), 7.27 – 7.21 (m, 2H), 4.98 (s, 2H), 4.34 (t, *J* = 7.2 Hz, 2H), 4.13 (d, *J* = 5.2 Hz, 2H), 3.22 (t, *J* = 7.3 Hz, 2H), 2.70 (dt, *J* = 14.7, 7.4 Hz, 2H).

^{19}F NMR (470 MHz, DMSO-d$_6$) δ -110.63 – -110.70 (m).

^{13}C NMR (126 MHz, DMSO-d$_6$) δ 164.76, 161.99 (d, $^{1}J_{C\text{-}F}$ = 247.3 Hz), 154.81, 133.77 (d, $^{3}J_{C\text{-}F}$ = 8.4 Hz), 135.43, 133.18, 131.99, 131.44, 131.00, 129.38, 126.46, 118.53 (d, $^{4}J_{C\text{-}F}$ = 3.1 Hz), 116.04 (d, $^{2}J_{C\text{-}F}$ = 22.1 Hz), 116.94, 85.85, 80.99, 48.68, 48.44, 29.02, 25.14, 23.53.

HRMS (ESI): calculated for $[C_{23}H_{19}Cl_2FN_3O]^+$ 442.0884, found 442.0880.

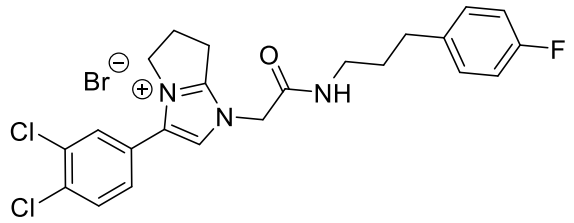

Compound **H46** Obtained as brownish solid (80 mg, 66%).

^{1}H NMR (500 MHz, DMSO-d$_6$) δ 8.65 (t, *J* = 5.5 Hz, 1H), 7.97 (s, 1H), 7.82 (d, *J* = 8.3 Hz, 1H), 7.73 (d, *J* = 2.1 Hz, 1H), 7.46 (dd, *J* = 8.3, 2.1 Hz, 1H), 7.21 – 7.16 (m, 2H), 7.12 – 7.07 (m, 2H), 4.91 (s, 2H), 4.34 (t, *J* = 7.3 Hz, 2H), 3.22 (t, *J* = 7.6 Hz, 2H), 3.03 (dd, *J* = 12.7, 6.7 Hz, 2H), 2.74 – 2.67 (m, 2H), 2.49 – 2.45 (m, 2H), 1.64 – 1.55 (m, 2H).

^{19}F NMR (470 MHz, DMSO-d$_6$) δ -116.96 – -118.75 (m).

^{13}C NMR (126 MHz, DMSO-d$_6$) δ 164.51 (s), 160.66 (d, $^{1}J_{C\text{-}F}$ = 240.9 Hz), 154.72, 137.56 (d, $^{4}J_{C\text{-}F}$ = 3.2 Hz), 135.39, 133.20, 131.97, 131.49, 130.97, 130.07 (d, $^{3}J_{C\text{-}F}$ = 7.7 Hz), 129.46, 126.54, 116.88, 115.01 (d, $^{2}J_{C\text{-}F}$ = 20.8 Hz), 48.66, 48.60, 38.23, 31.35, 30.68, 25.14, 23.50.

HRMS (ESI): calculated for $[C_{23}H_{23}Cl_2FN_3O]^+$ 446.1197, found 446.1191.

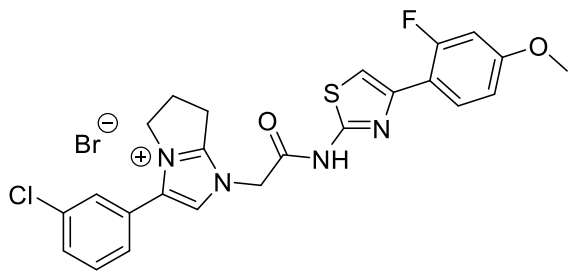

Compound **H51.** Obtained as a white solid (69 mg, 74%).

^{1}H NMR (500 MHz, DMSO-d_6) δ 8.01 (s, 1H), 7.91 (t, *J* = 9.0 Hz, 1H), 7.65 – 7.62 (m, 1H), 7.59 (t, *J* = 7.8 Hz, 1H), 7.56 (t, *J* = 1.7 Hz, 1H), 7.42 (d, *J* = 7.5 Hz, 1H), 7.35 (d, *J* = 2.1 Hz, 1H), 6.94 (dd, *J* = 13.5, 2.4 Hz, 1H), 6.89 (dd, *J* = 8.8, 2.5 Hz, 1H), 5.18 (s, 2H), 4.38 (t, *J* = 7.3 Hz, 2H), 3.81 (s, 3H), 3.27 (t, *J* = 7.6 Hz, 3H), 2.79 – 2.69 (m, 2H).

^{19}F NMR (470 MHz, DMSO-d_6) δ -112.18 – -112.31 (m).

^{13}C NMR (126 MHz, DMSO-d_6) δ 164.88, 160.26 (d, *J* = 248.5 Hz), 159.96 (d, *J* = 11.3 Hz), 154.85, 142.73, 136.37, 133.85, 131.30, 130.24, 129.84 (d, *J* = 5.2 Hz), 129.02, 127.87, 127.85, 116.67, 114.74, 114.65, 110.72 (d, *J* = 2.2 Hz), 110.45 (d, *J* = 12.1 Hz), 102.13 (d, *J* = 25.9 Hz), 55.78, 49.02, 48.70, 25.18, 23.67.

HRMS (ESI): Calculated for $[C_{24}H_{21}ClFN_4O_2S]^+$ 483.1052, found 483.1049.

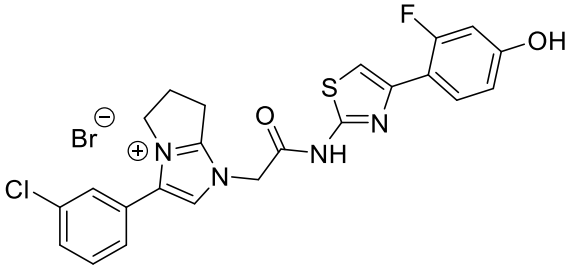

Compound **H52.** Obtained as a white solid (9.5 mg, 86%).

^{1}H NMR (500 MHz, MeOD) δ 7.87 (t, *J* = 8.9 Hz, 1H), 7.71 (s, 1H), 7.57 (d, *J* = 8.3 Hz, 1H), 7.54 – 7.49 (m, 2H), 7.38 (d, *J* = 7.7 Hz, 1H), 7.26 (d, *J* = 2.2 Hz, 1H), 6.64 (dd, *J* = 8.6, 2.4 Hz, 1H), 6.58 (dd, *J* = 13.3, 2.3 Hz, 1H), 4.43 (t, *J* = 7.3 Hz, 2H), 2.91 – 2.84 (m, 2H).

^{19}F NMR (470 MHz, MeOD) δ -114.76 – -114.96 (m, *J* = 10.5 Hz).

^{13}C NMR (126 MHz, MeOD) δ 165.65, 162.37 (d, *J* = 248.3 Hz), 160.01 (d, *J* = 12.3 Hz), 158.95, 156.44, 145.39 (d, *J* = 1.3 Hz), 139.00, 136.33, 132.08, 131.92, 131.35 (d, *J* = 5.2 Hz), 130.83, 129.15, 128.76, 117.53, 114.87 (d, *J* = 12.0 Hz), 112.52 (d, *J* = 2.2 Hz), 111.02, 110.91, 103.95 (d, *J* = 25.0 Hz), 50.02, 26.43, 24.64.

HRMS (ESI): Calculated for $[C_{23}H_{19}ClFN_4O_2S]^+$ 469.0896, found 469.0894.

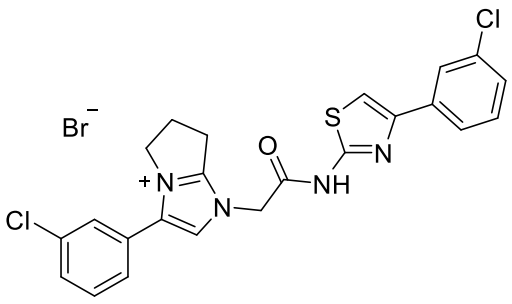

Compound **H53.** Obtained as white solid (40 mg, 40 %).

LC-MS $[M]^+$: 469.08.

^{1}H NMR (500 MHz, DMSO-d_6) δ 12.89 (s, 1H), 8.01 (s, 1H), 7.94 (t, *J* = 1.7 Hz, 1H), 7.88 – 7.83 (m, 2H), 7.65 – 7.61 (m, 1H), 7.59 (t, *J* = 7.8 Hz, 1H), 7.54 (t, *J* = 1.7 Hz, 1H), 7.47 (t, *J* = 7.9 Hz, 1H), 7.42 – 7.38 (m, 2H), 5.27 (s, 2H), 4.38 (t, *J* = 7.3 Hz, 2H), 3.28 (t, *J* = 7.6 Hz, 2H), 2.79 – 2.70 (m, 2H).

^{13}C NMR (126 MHz, DMSO-d_6) δ 164.30, 154.93, 147.44, 136.30, 136.00, 133.81, 133.62, 131.26, 130.76, 130.25, 129.01, 127.87, 127.70, 127.66, 125.37, 124.23, 116.76, 110.29, 54.93, 48.72, 48.49, 25.14, 23.66.

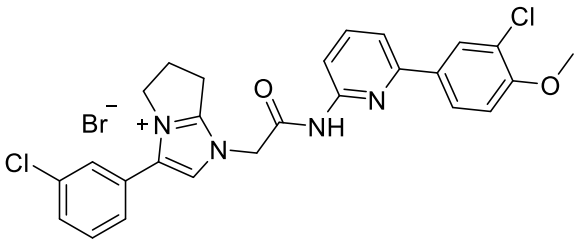

Compound **H54.** Obtained as an off-white solid (110 mg, 71 %).

LC-MS $[M]^+$: 493.28

^{1}H NMR (500 MHz, DMSO-d_6) δ 11.04 (s, 1H), 8.18 (s, 1H), 8.02 (d, *J* = 8.8 Hz, 1H), 8.00 (s, 1H), 7.90 – 7.84 (m, 2H), 7.77 – 7.72 (m, 1H), 7.65 – 7.62 (m, 1H), 7.60 (t, *J* = 7.8 Hz, 1H), 7.55 (d, *J* = 1.7 Hz, 1H), 7.42 (d, *J* = 7.4 Hz, 1H), 7.27 (d, *J* = 8.7 Hz, 1H), 5.22 (s, 2H), 4.38 (t, *J* = 7.3 Hz, 2H), 3.92 (s, 3H), 3.27 (t, *J* = 7.6 Hz, 2H), 2.79 – 2.68 (m, 2H).

^{13}C NMR (126 MHz, DMSO-d_6) δ 164.48, 155.45, 154.95, 153.18, 150.68, 139.81, 136.39, 133.88, 131.36, 131.19, 130.29, 129.01, 127.92, 127.86, 126.52, 121.59, 116.68, 115.91, 112.93, 112.04, 56.38, 49.04, 48.72, 25.20, 23.65.

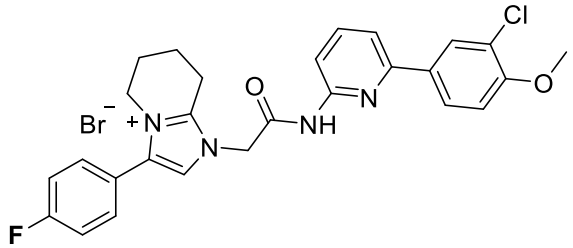

Obtained as reddish solid (35 mg, 70%).

LC-MS $[M]^+$: 491.35

^{1}H NMR (500 MHz, DMSO-d_6) δ 8.14 (d, *J* = 2.0 Hz, 1H), 7.99 (dd, *J* = 8.6, 2.0 Hz, 1H), 7.86 (s, 1H), 7.79 – 7.71 (m, *J* = 14.1, 6.0 Hz, 2H), 7.58 (d, *J* = 5.4 Hz, 1H), 7.54 (dd, *J* = 8.6, 5.4 Hz, 2H), 7.43 (t, *J* = 8.8 Hz, 2H), 7.24 (d, *J* = 8.7 Hz, 1H), 4.96 (s, 2H), 4.23 (t, *J* = 5.6 Hz, 2H), 3.04 (t, *J* = 6.1 Hz, 2H), 2.01 (dd, *J* = 25.2, 5.1 Hz, 4H).

^{13}C NMR (126 MHz, DMSO-d_6) δ 164.73, 164.07, 163.09 (d, *J* = 247.5 Hz), 162.10, 155.12, 152.87, 145.92, 138.79, 132.52, 131.87 (d, *J* = 8.9 Hz), 127.70, 126.26, 122.09 (d, *J* = 3.3 Hz), 121.44, 119.01, 116.46 (d, *J* = 22.1 Hz), 112.79, 56.28, 48.28, 46.04, 20.93, 17.66.

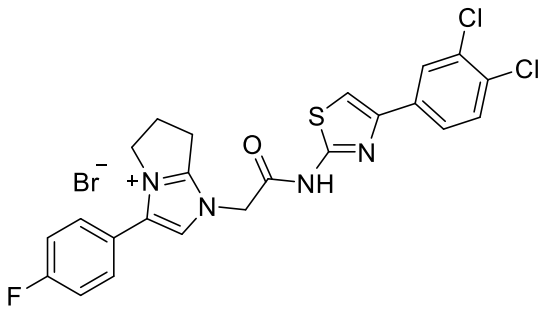

Compound **H61**. Obtained as an off-white solid (66 mg, 57%).

^{1}H NMR (500 MHz, DMSO-d_6) δ 8.11 – 8.08 (m, *J* = 4.9, 1.7 Hz, 2H), 7.91 (s, 1H), 7.85 (dd, *J* = 8.4, 2.0 Hz, 1H), 7.54 – 7.50 (m, 2H), 7.42 (dt, *J* = 8.8, 4.8 Hz, 2H), 4.95 (s, 2H), 4.37 (t, *J* = 7.3 Hz, 2H), 3.24 (t, *J* = 7.6 Hz, 2H), 2.77 – 2.69 (m, 2H).

HRMS (ESI): Calculated for $[C_{23}H_{18}Cl_2FN_4OS]^+$ 487.0557, found 487.0557.

Isomers of pyrazolic precursor

There are two cross-peaks corresponding to the methylene group's protons shift of the compound **8**: one correlates the proton signal with the ester's carbonyl (at 167.6 ppm), while the other – with a carbon atom at the position indicated on the figure above. Out of two alternatives, the shift of 153.2 ppm corresponds to the C-5 atom of the pyrazole, which is supported by correlations of this carbon signal with those belonging to the methylenes of the fused ring (see figure above).

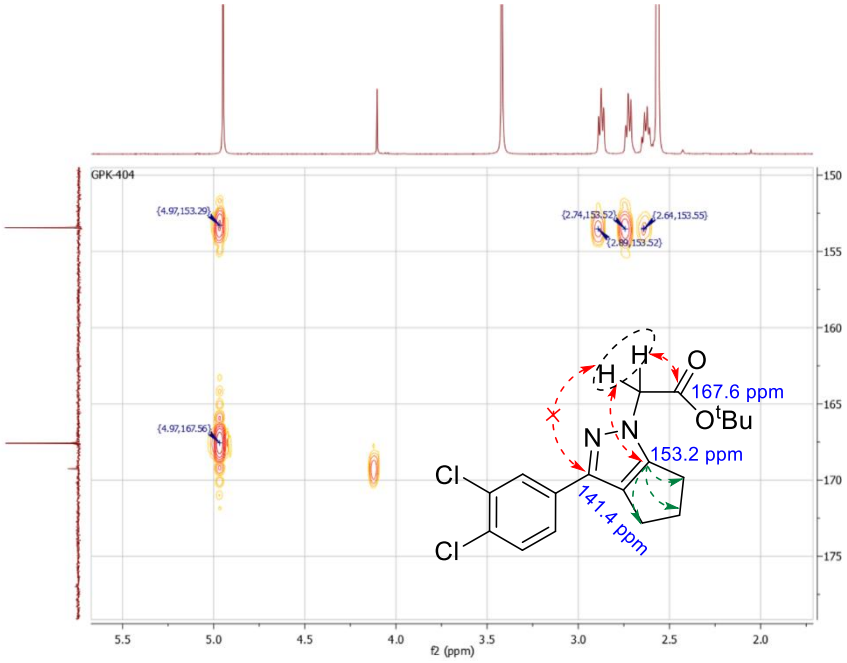

Figure S3. Excerpt from the HMBC NMR spectrum of the precursor of compound **H33** and a schematic representation of the ^{1}H-^{13}C multiple bond correlations observed.

HRMS spectra

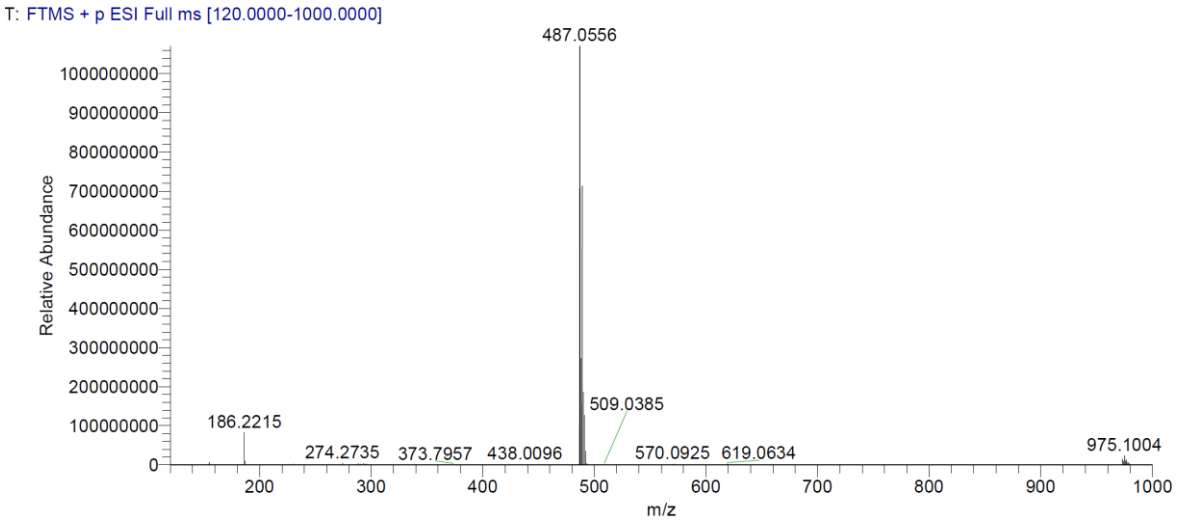

Figure S4. The HRMS spectrum of compound **H1**

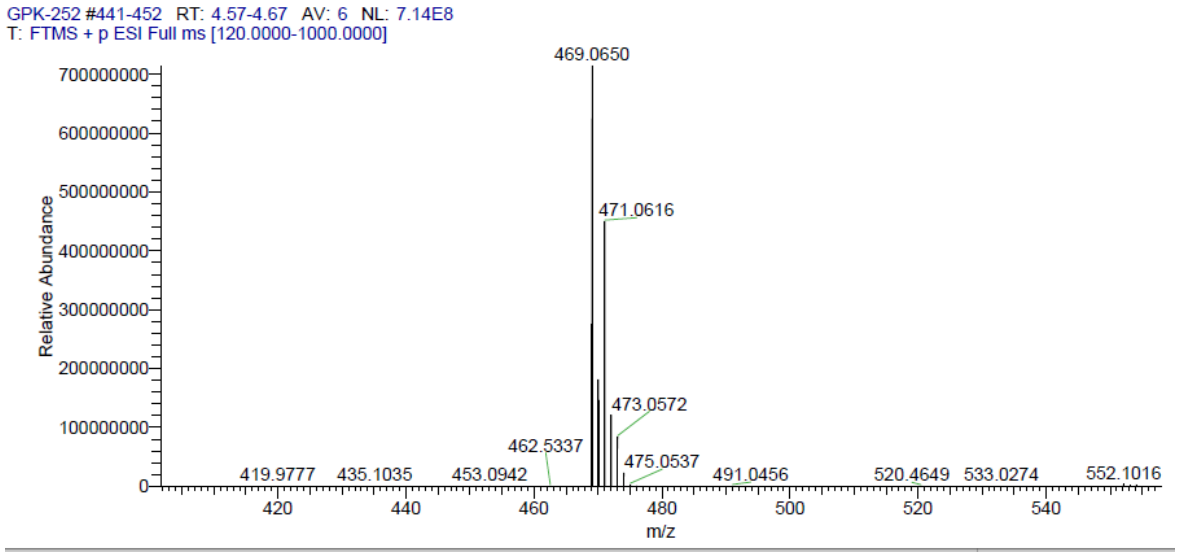

Figure S5. The HRMS spectrum of compound **H2**

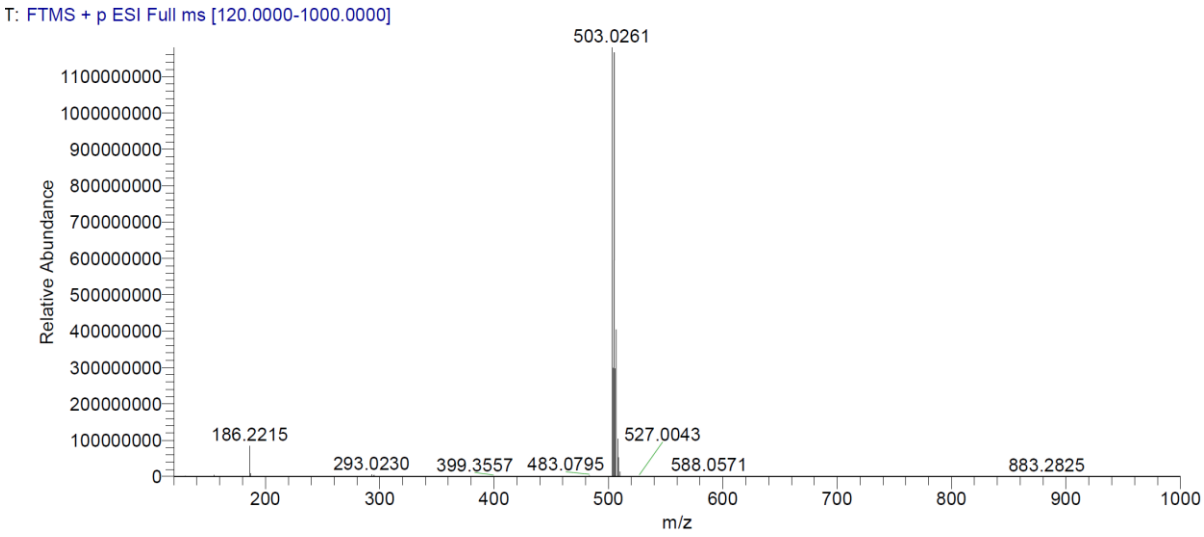

Figure S6. The HRMS spectrum of compound **H3**

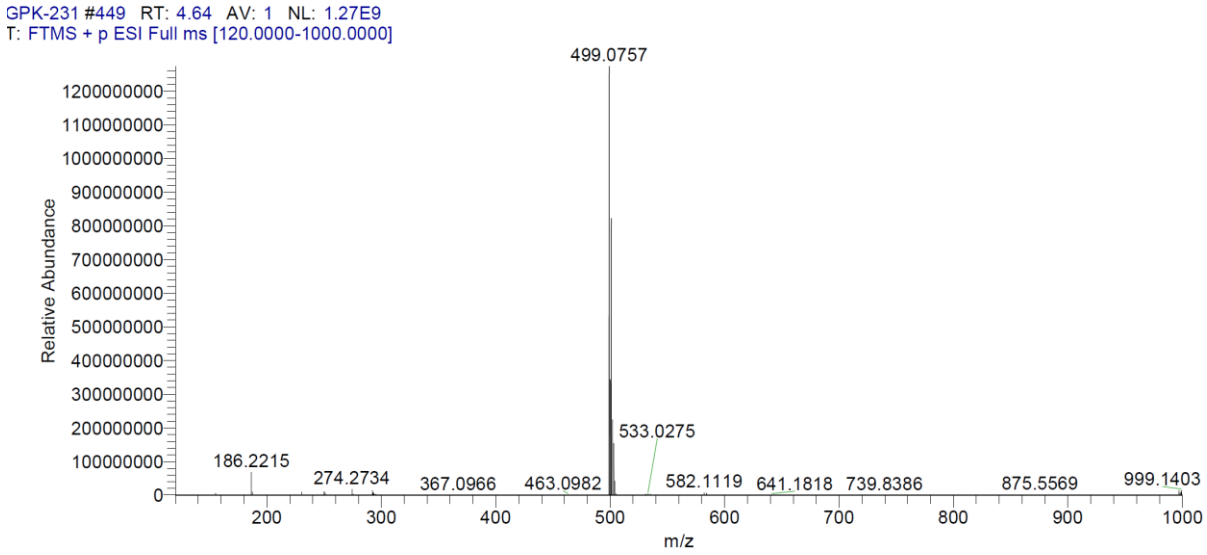

Figure S7. The HRMS spectrum of compound **H4**

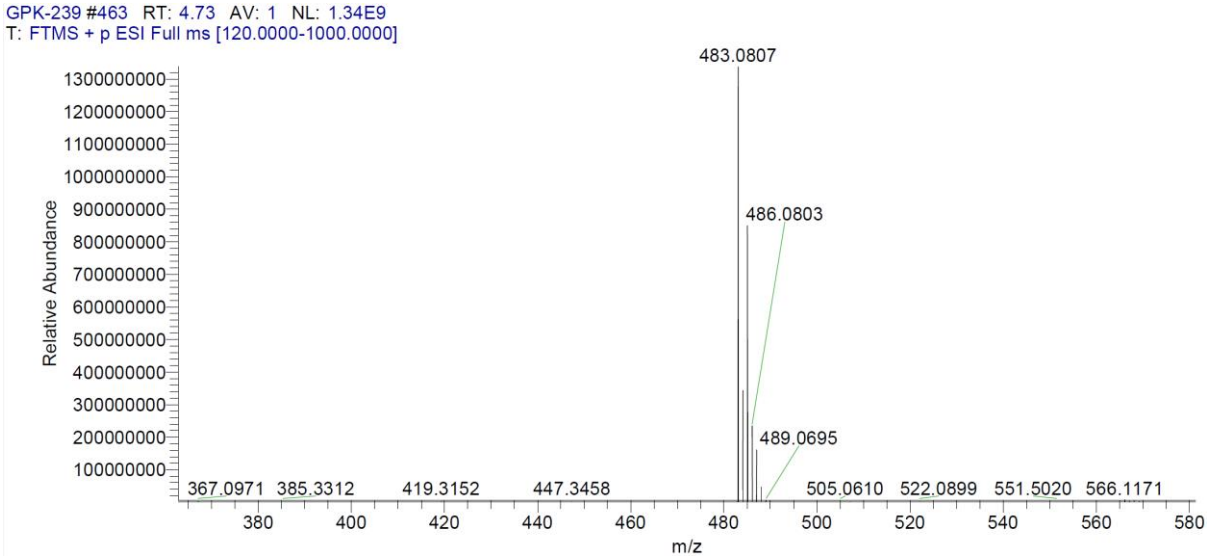

Figure S8. The HRMS spectrum of compound **H5**

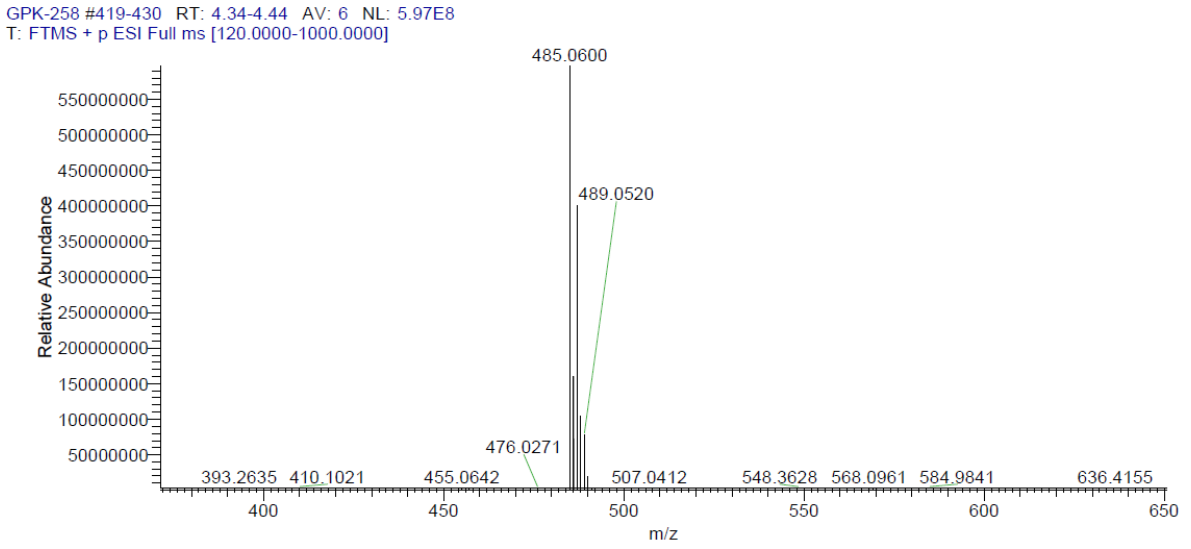

Figure S9. The HRMS spectrum of compound **H6**

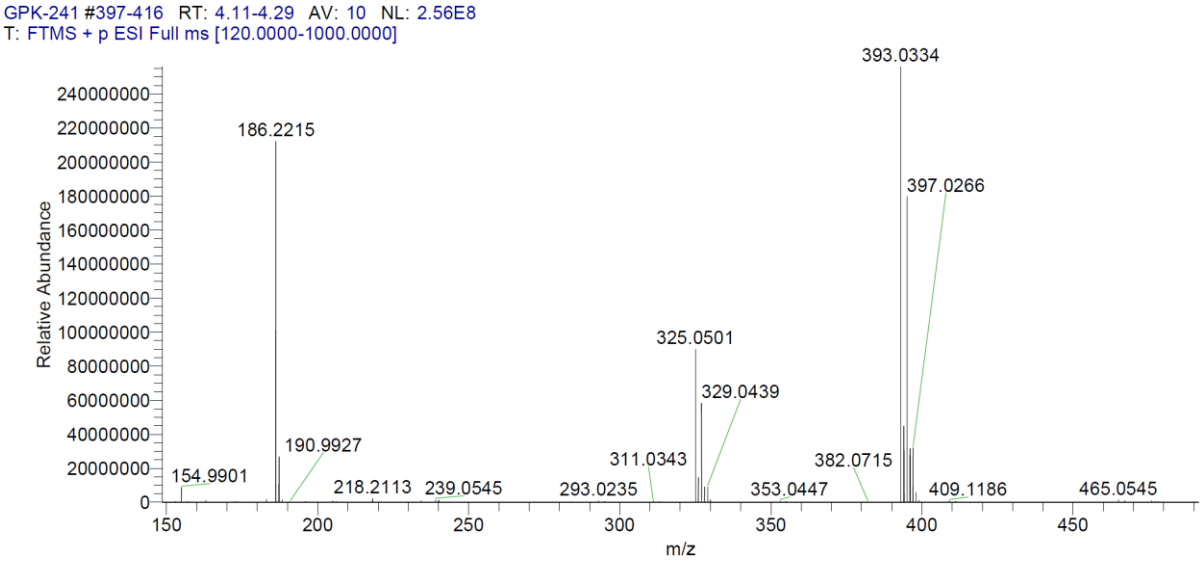

Figure S11. The HRMS spectrum of compound **H8**

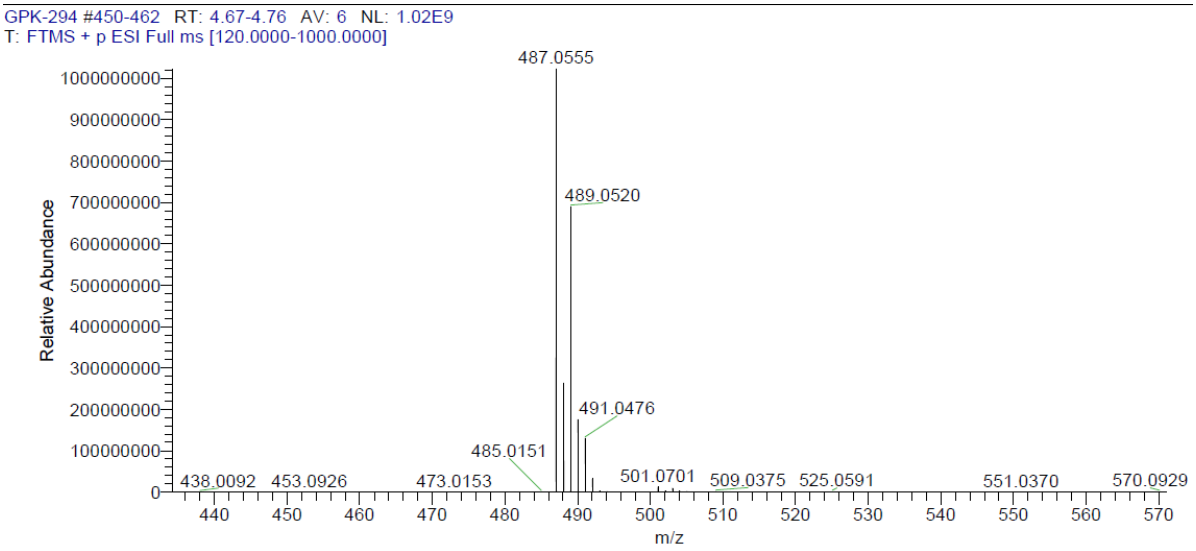

Figure S12. The HRMS spectrum of compound **H10**

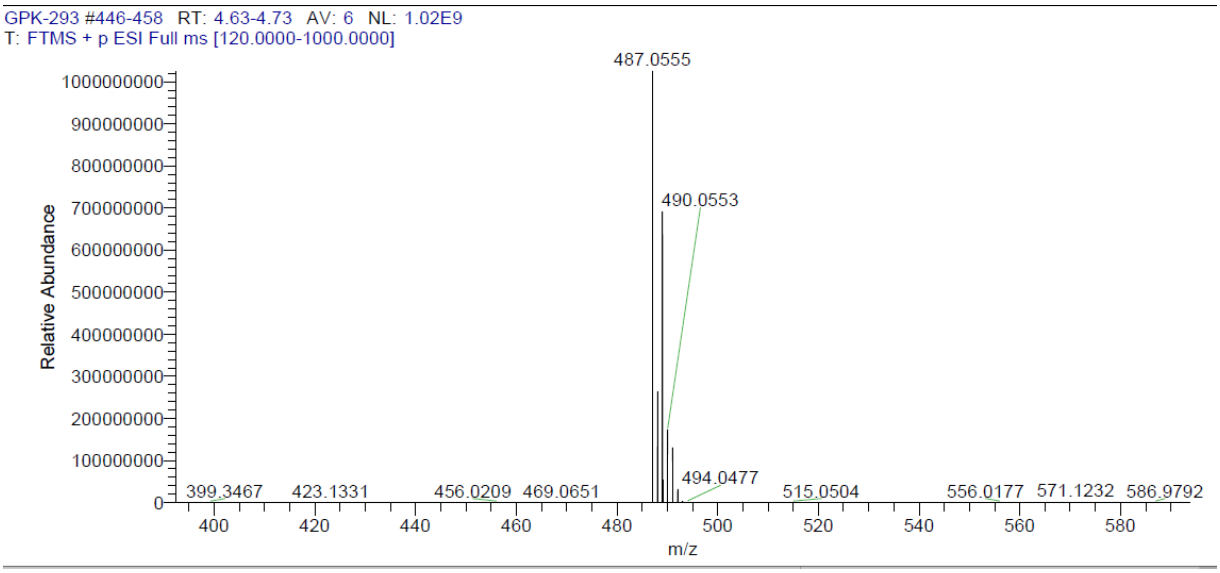

Figure S13. The HRMS spectrum of compound **H11**

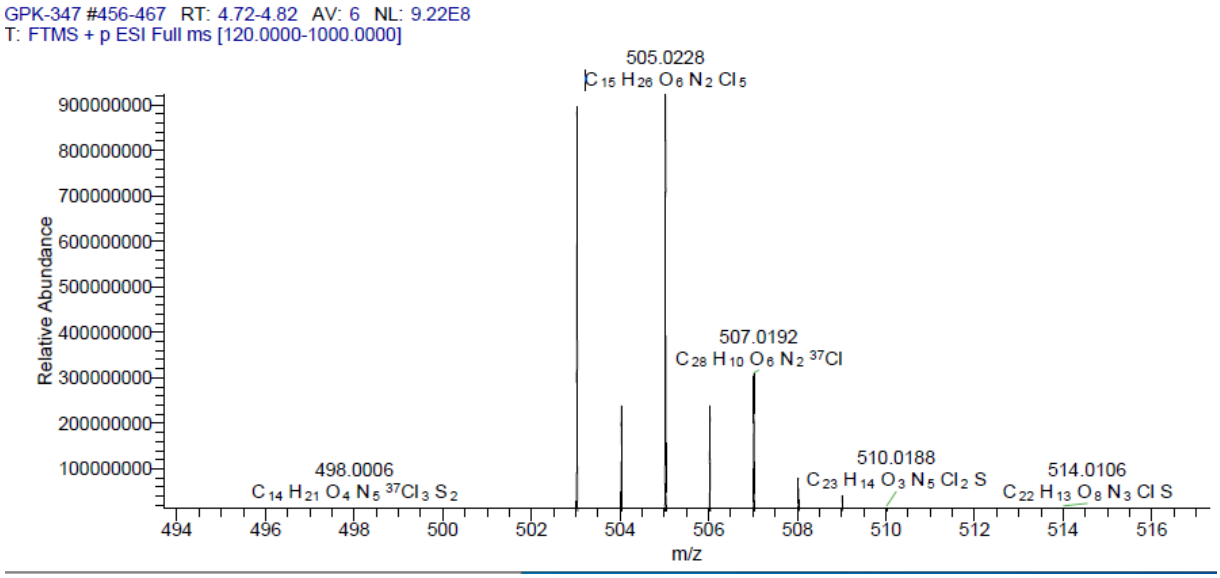

Figure S14. A fragment of HRMS spectrum of compound **H12**

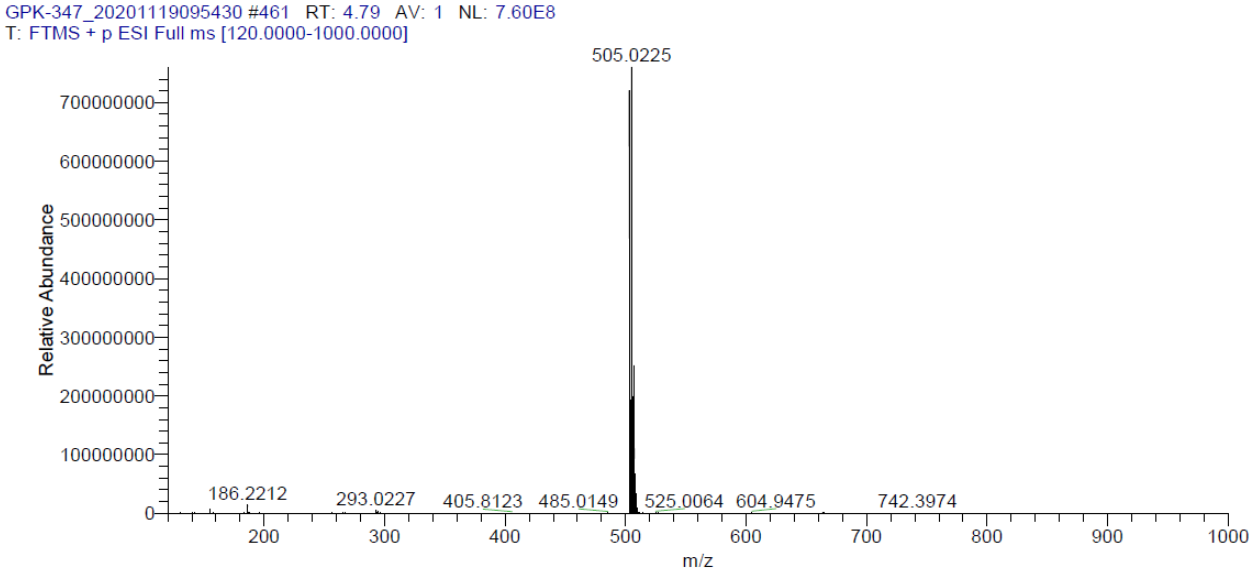

Figure S15. The HRMS spectrum of compound **H12**

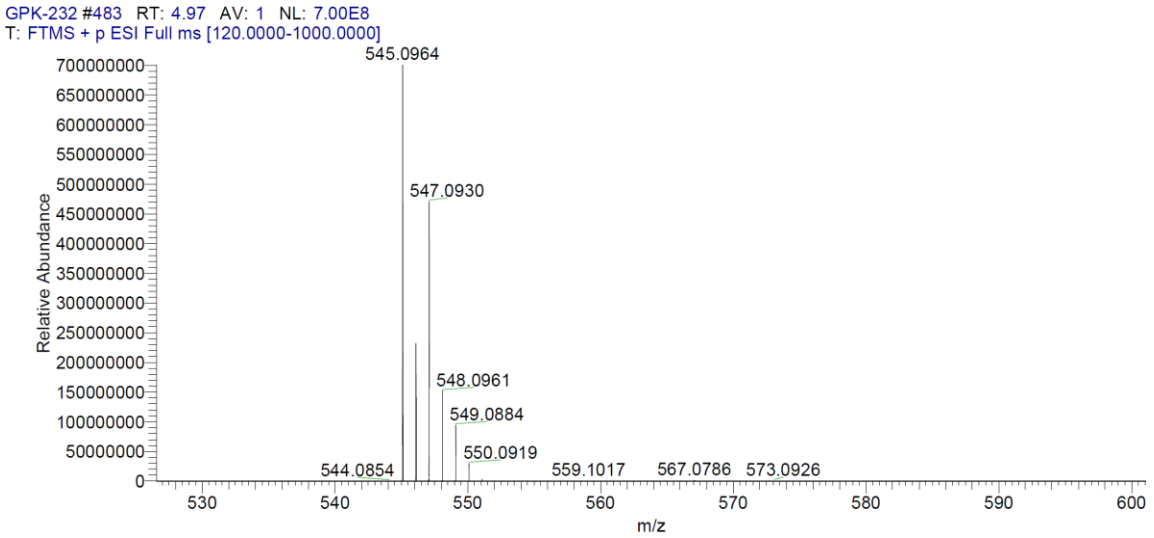

Figure S16. The HRMS spectrum of compound **H13**

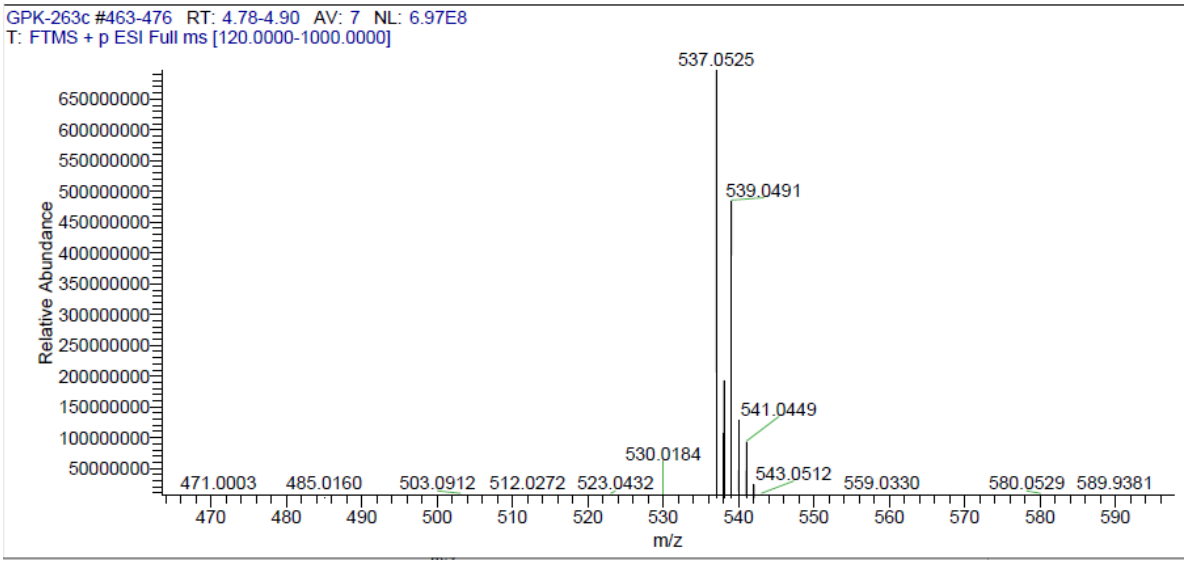

Figure S17. The HRMS spectrum of compound **H14**

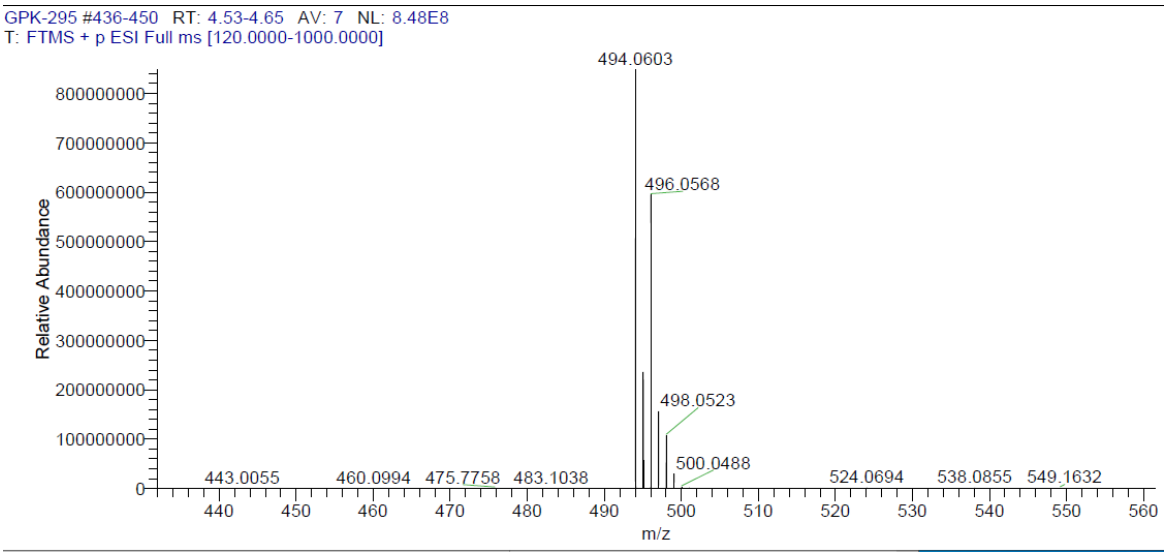

Figure S18. The HRMS spectrum of compound **H15**

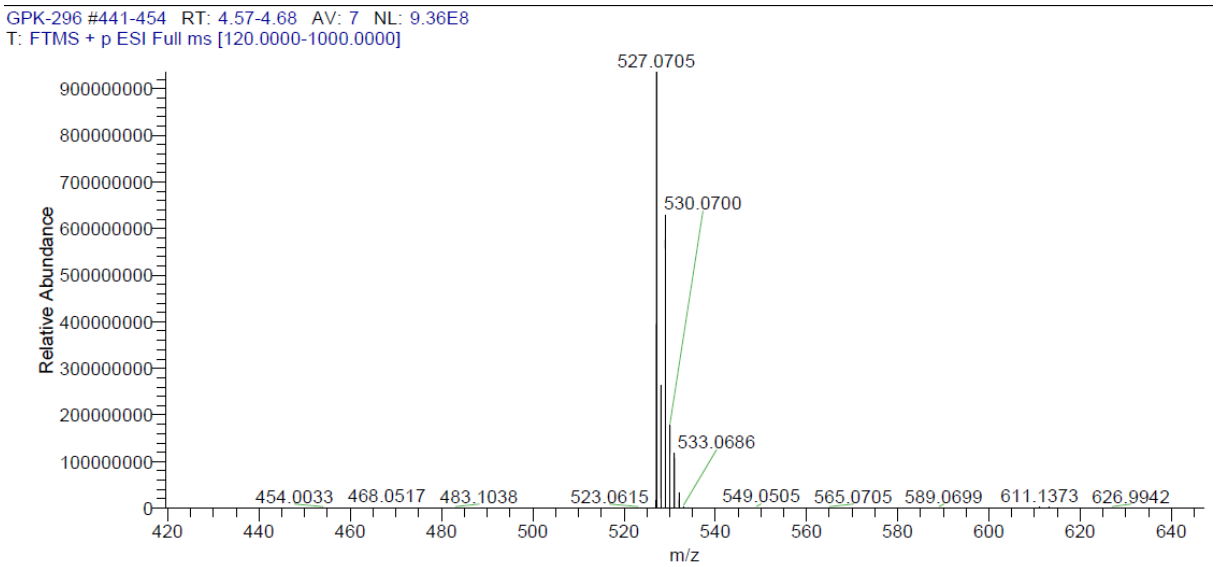

Figure S19. The HRMS spectrum of compound **H16**

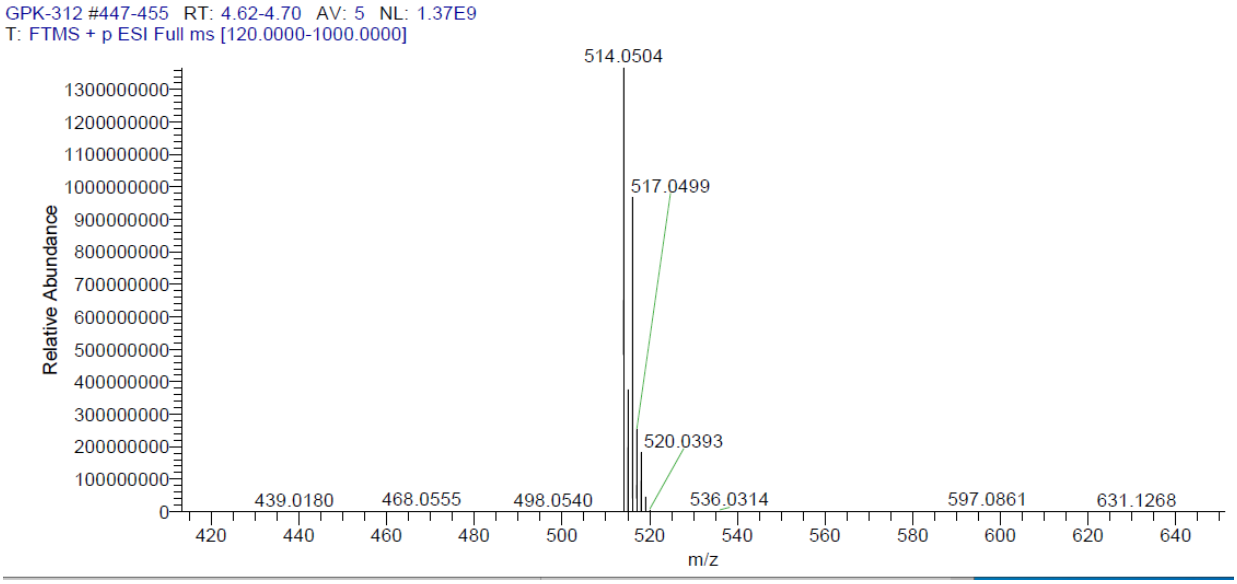

Figure S20. The HRMS spectrum of compound **H17**

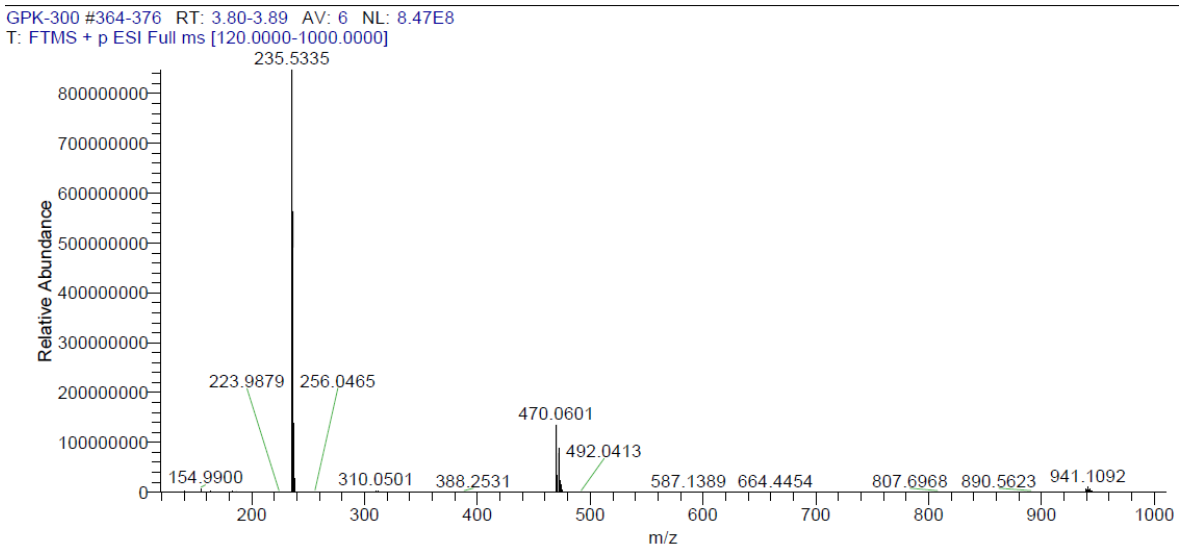

Figure S21. The HRMS spectrum of compound **H18**

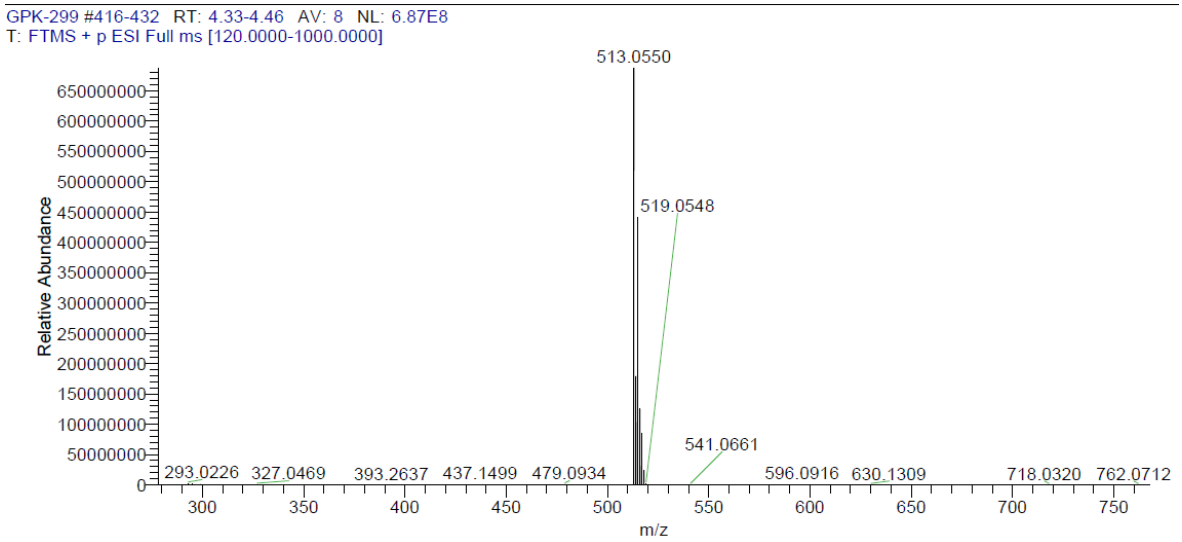

Figure S22. The HRMS spectrum of compound **H19**

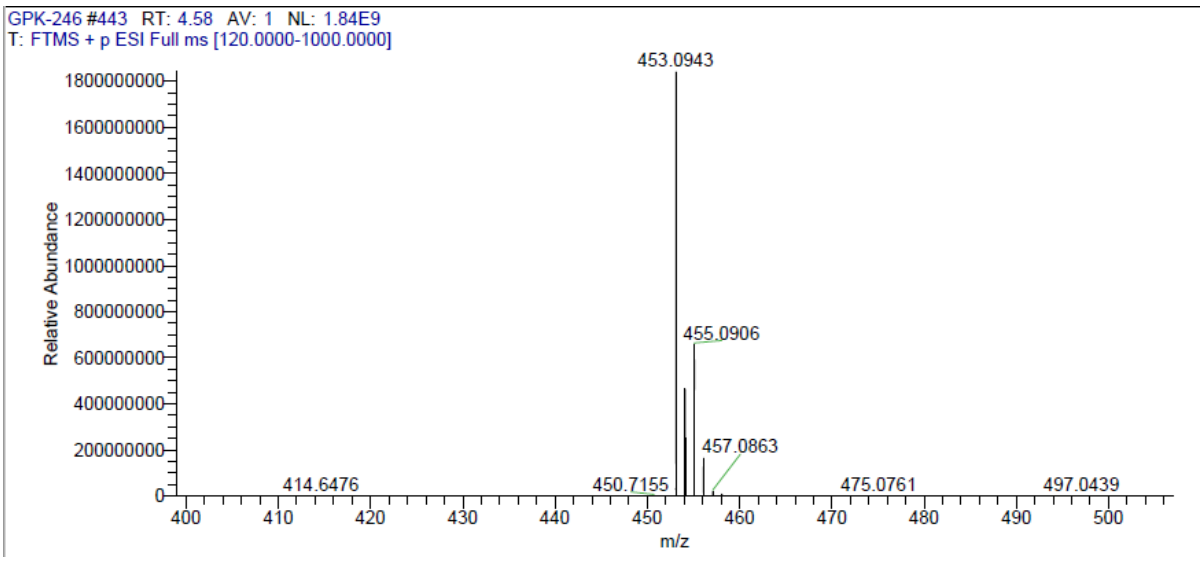

Figure S23. The HRMS spectrum of compound **H21**

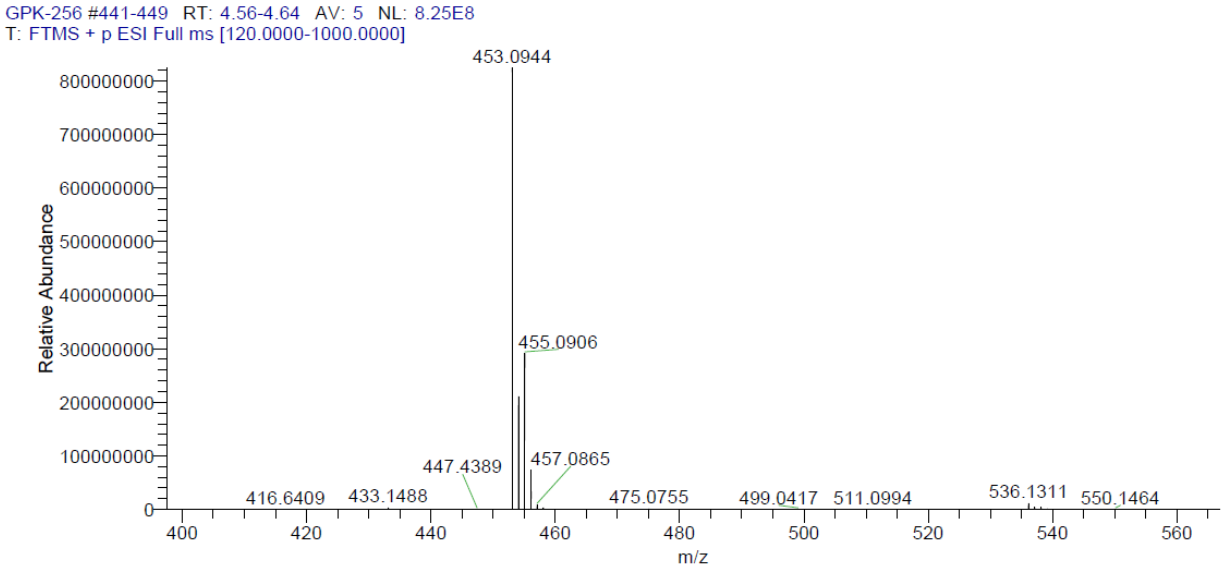

Figure S24. The HRMS spectrum of compound **H22**

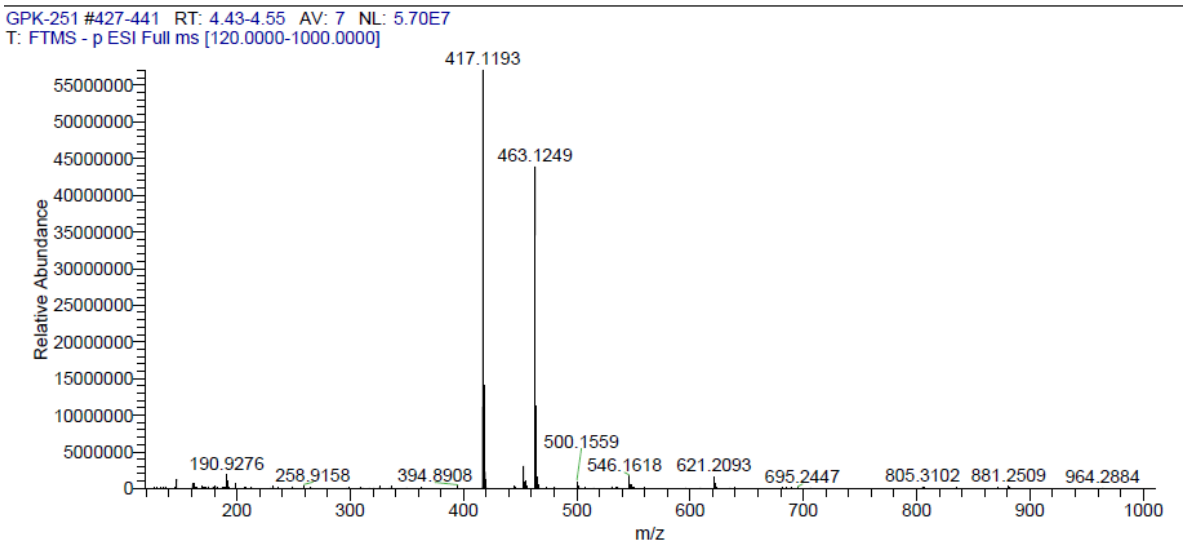

Figure S25. The HRMS spectrum of compound **H23**

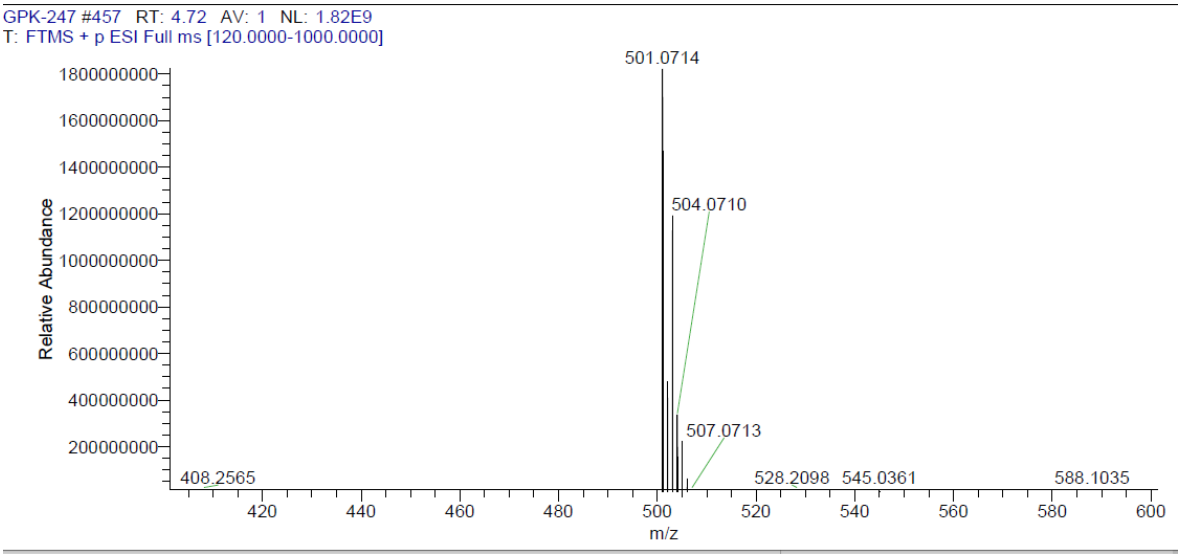

Figure S26. The HRMS spectrum of compound **H31**

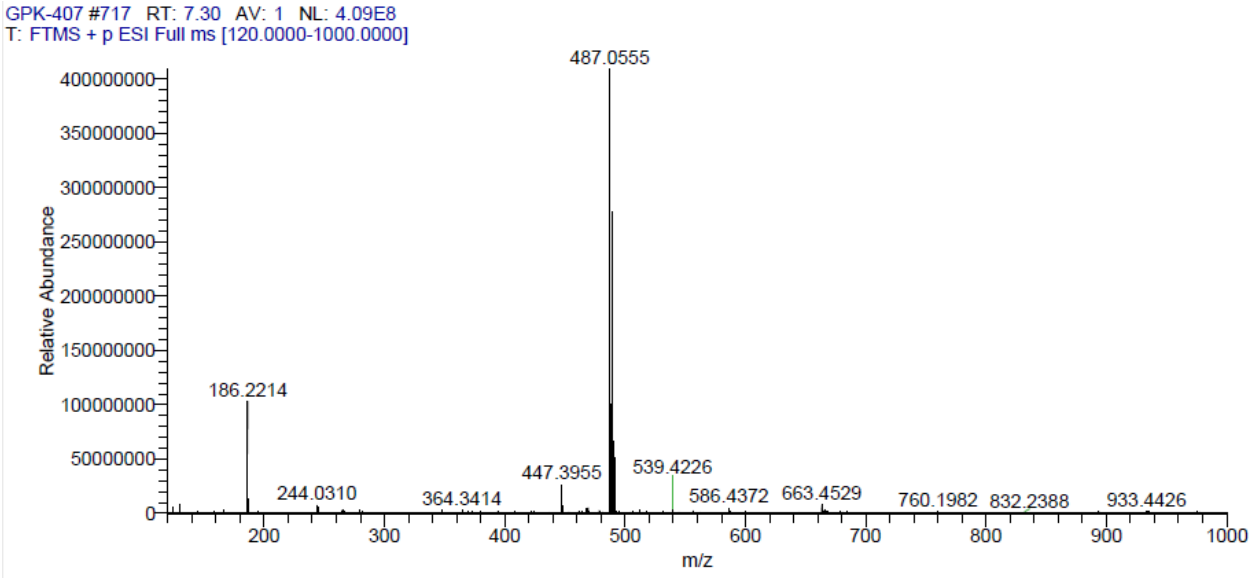

Figure S27. The HRMS spectrum of compound **H33**

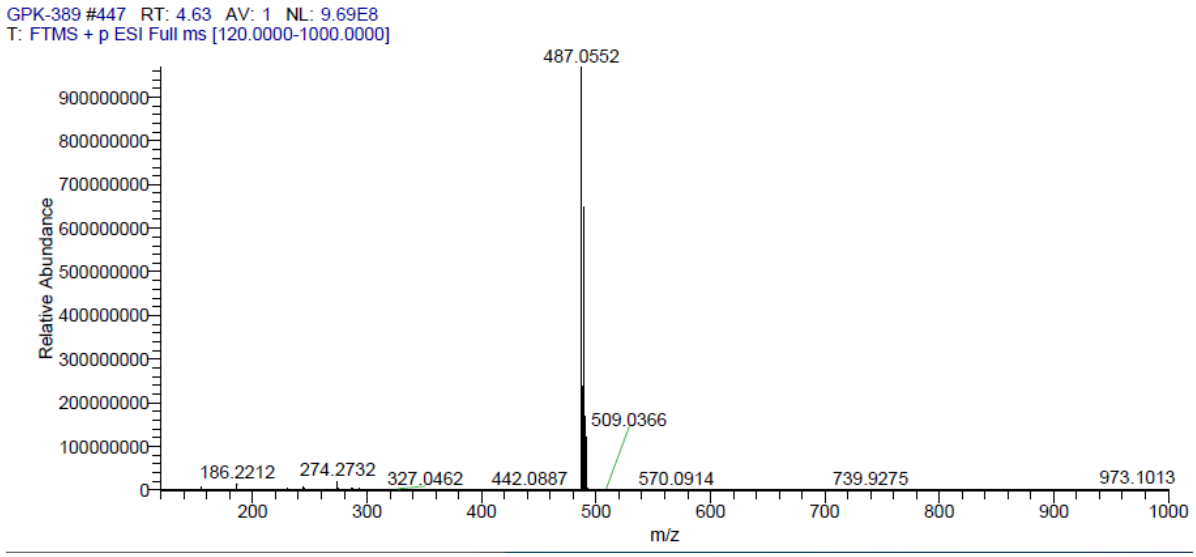

Figure S28. The HRMS spectrum of compound **H41**

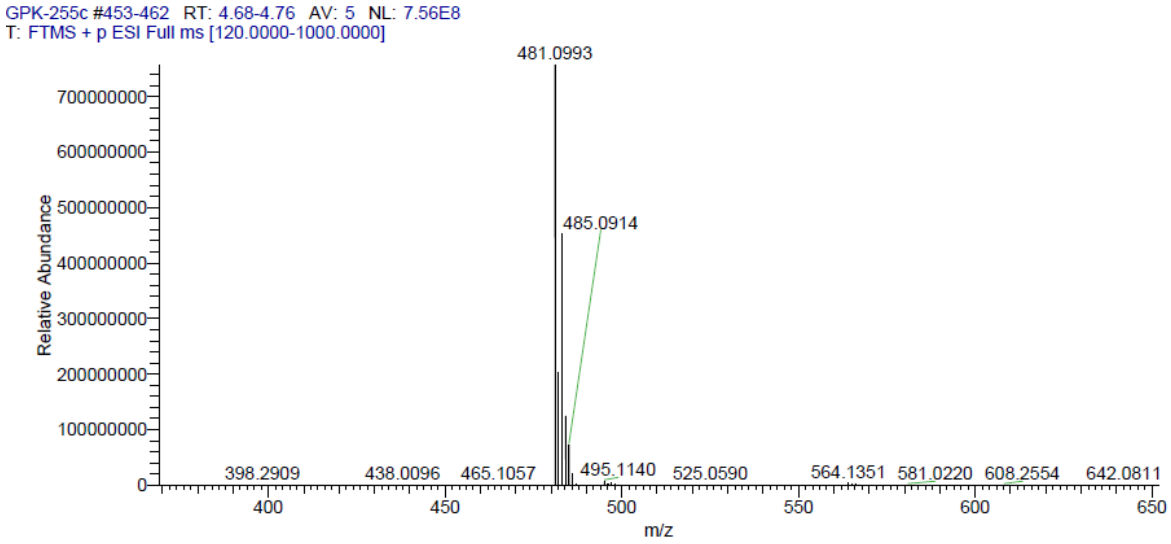

Figure S29. The HRMS spectrum of compound **H43**

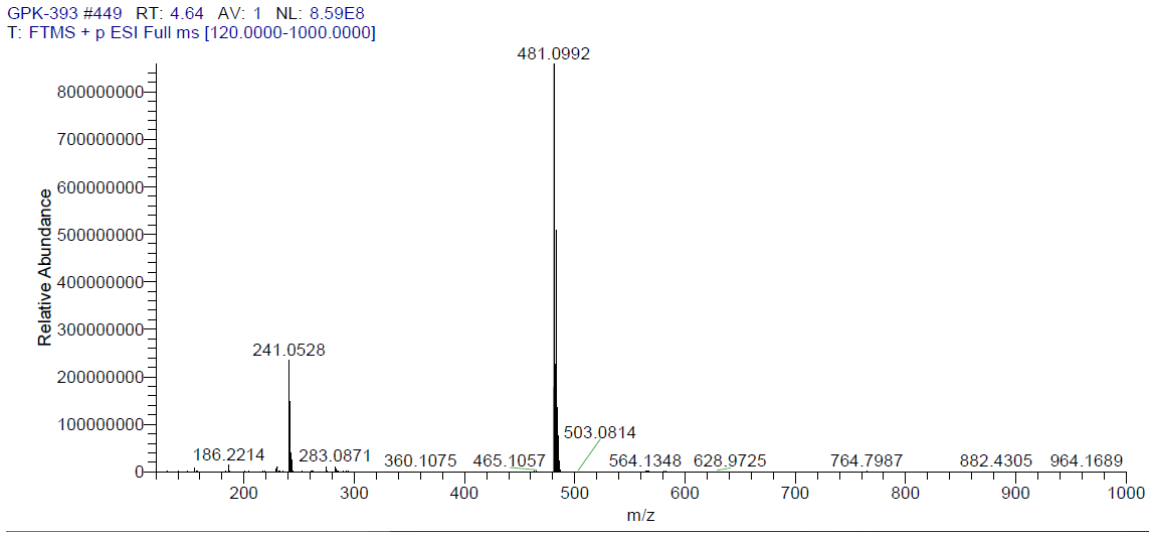

Figure S30. The HRMS spectrum of compound **H44**

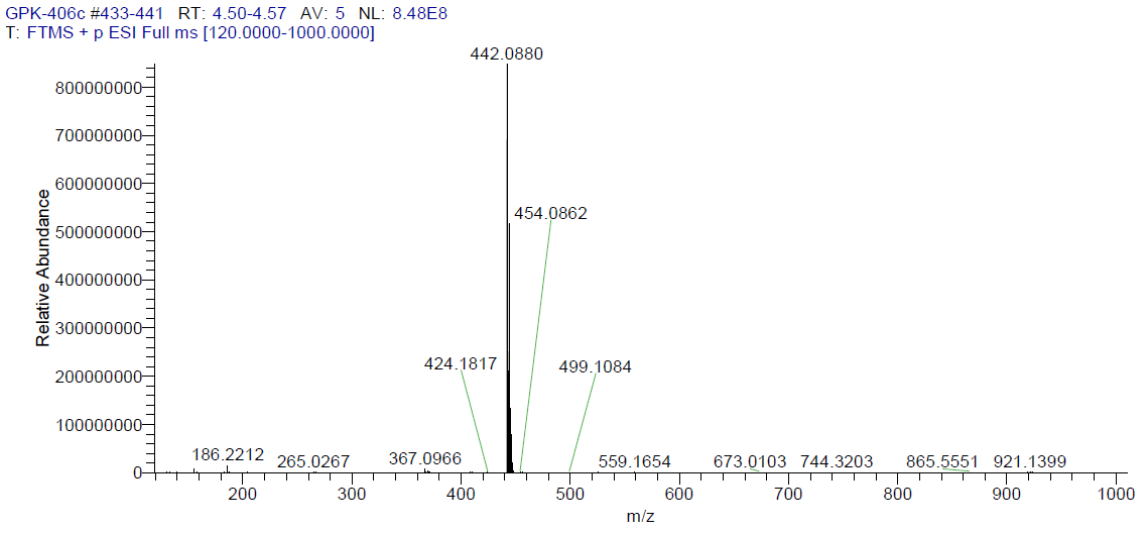

Figure S31. The HRMS spectrum of compound **H45**

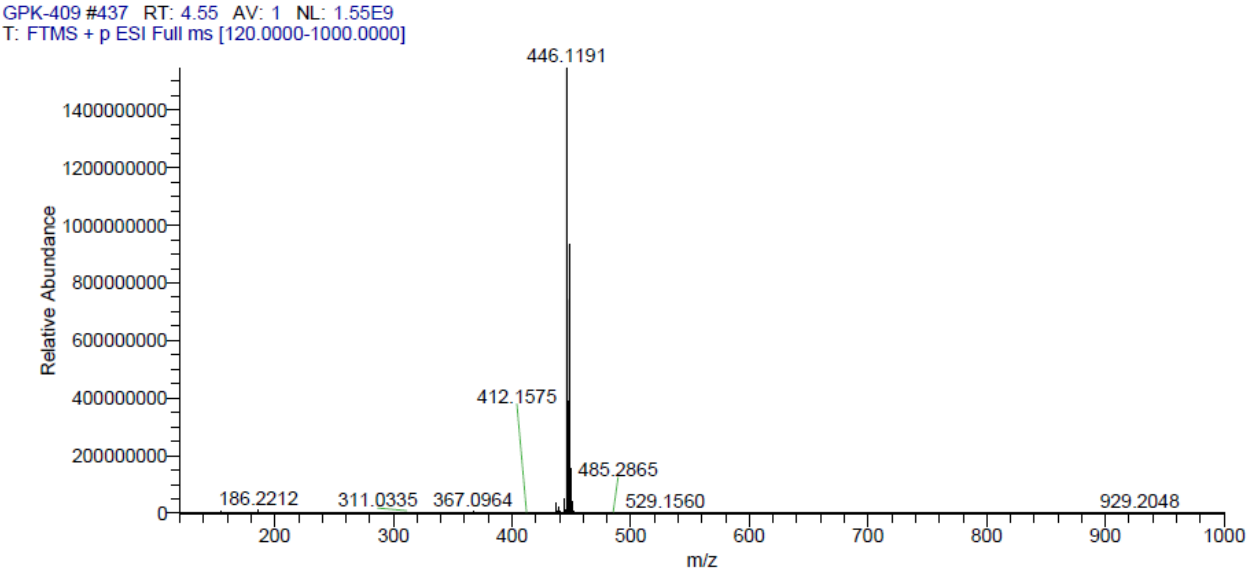

Figure S32. The HRMS spectrum of compound **H46**

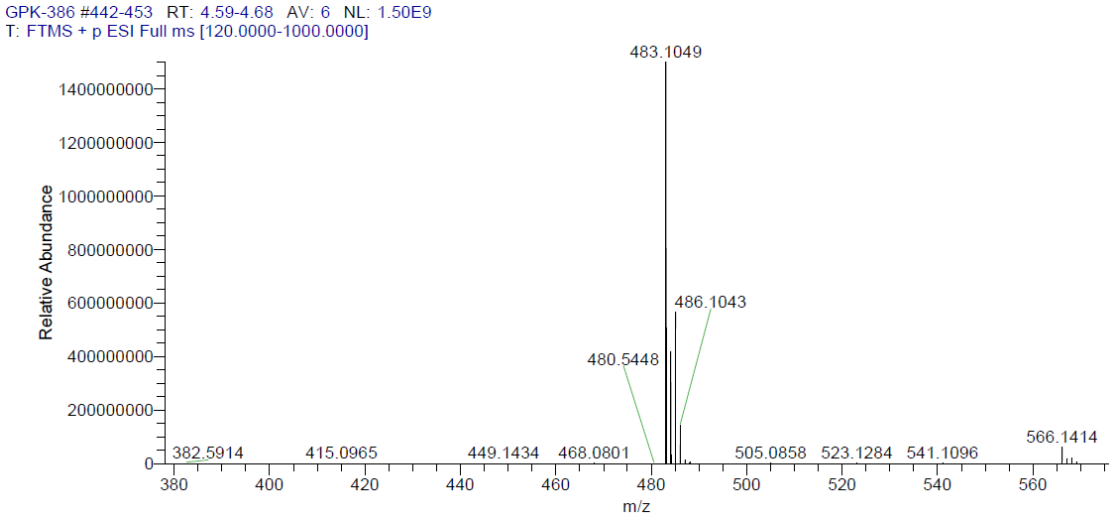

Figure S33. The HRMS spectrum of compound **H51**

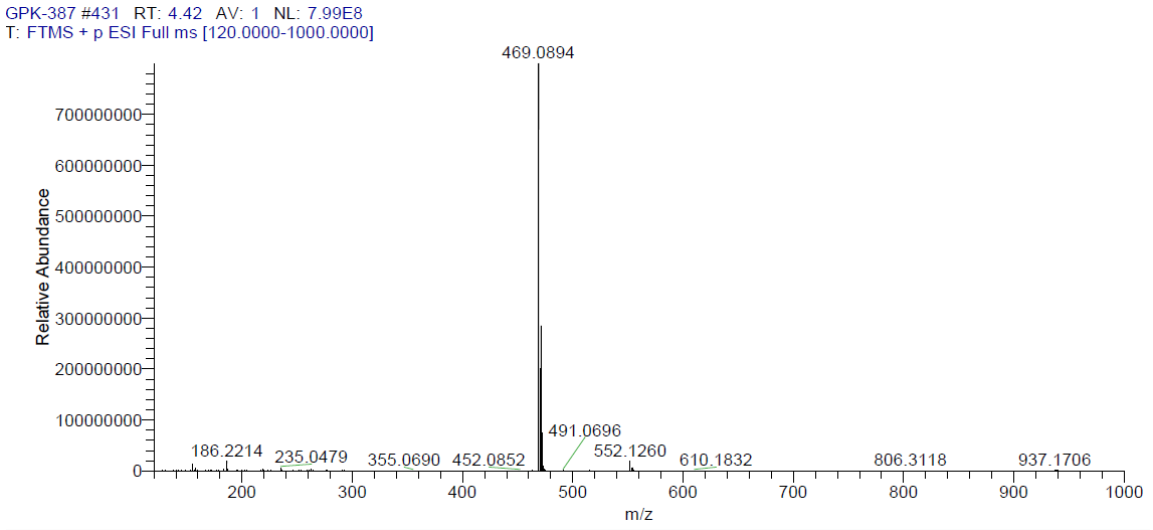

Figure S34. The HRMS spectrum of compound **H52**

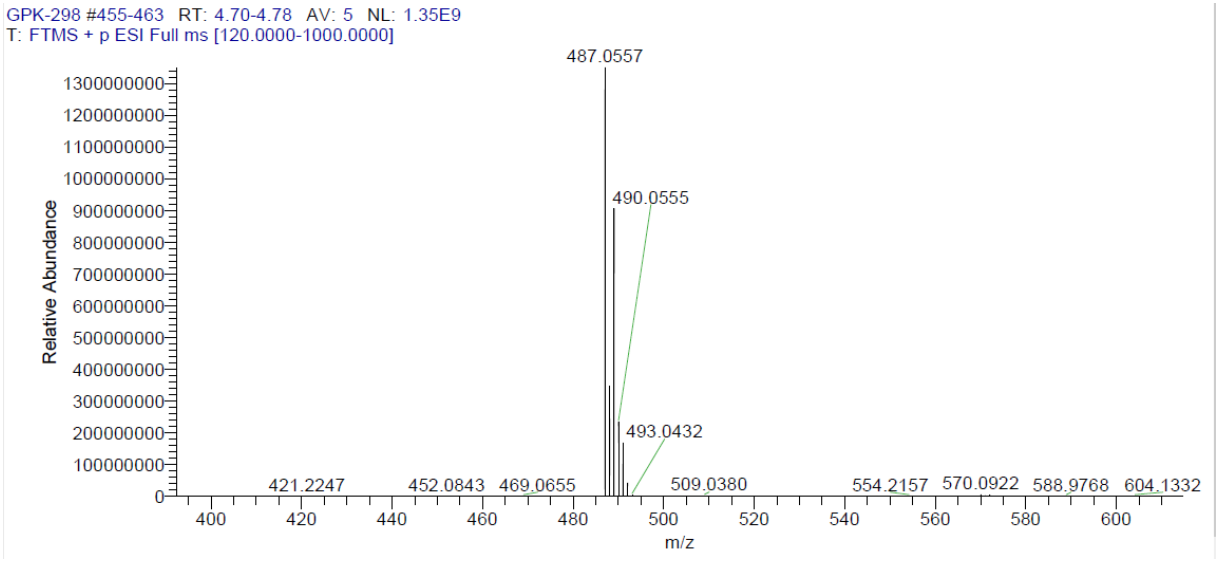

Figure S35. The HRMS spectrum of compound **H61**

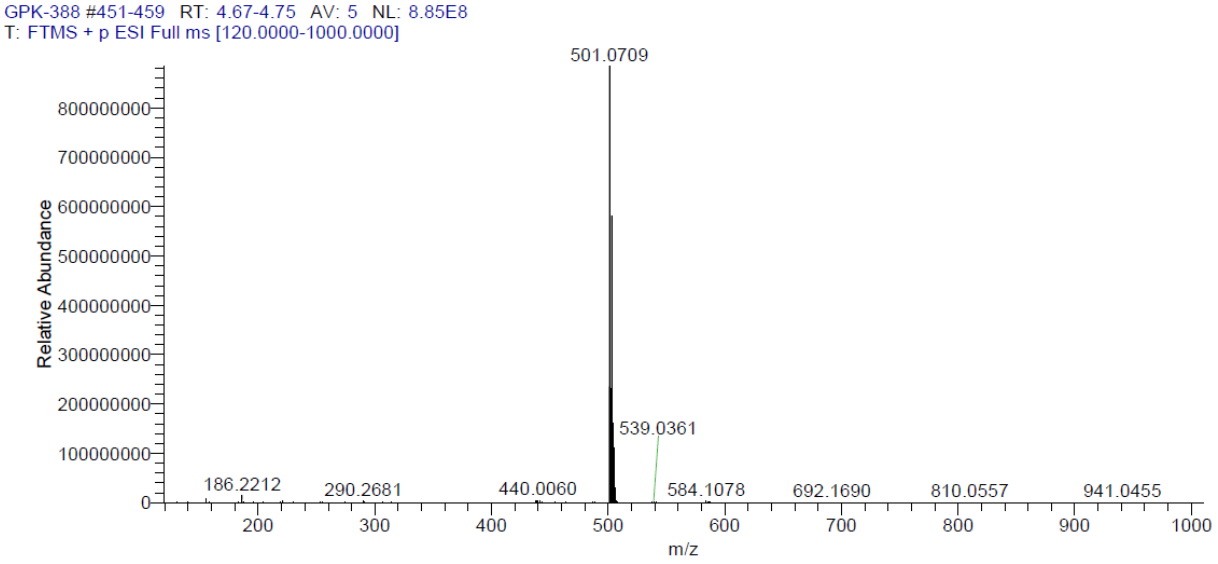

FigureSXX. The HRMS spectrum of compound **GPK-388**

S3.1.2 Experimental procedure for STD-NMR measurements

The STD-NMR experiments were recorded at 298 K on a Bruker Fourier spectrometer (500 MHz). The samples contained a 20-fold excess of compound being screened (100 μM) over *M. tuberculosis* sliding clamp protein (10 mg/ml stock solution in the HEPES/NaOH buffer, pH 7.5, 150 mM NaCl, 5.0 μM being the final concentration of DnaN). The compounds for screening were used as stock solutions in DMSO-d_6, which were mixed with the screening buffer (50 mM Tris(hydroxymethyl)-aminomethane (Tris), 5 mM $MgCl_2$, pH = 6.8 in D_2O), and certain quantity of DMSO-d_6 to reach the final concentration of 5% DMSO-d_6. To the resulting solution the protein sample (or DnaN stock buffer in H_2O) was added and the obtained solution was carefully mixed and transferred into an NMR tube. The final volume of the sample was 250 μl.

All experiments were performed using the *stddiffesgp.3* pulse program by Bruker. Blank spectrum was recorded in order to establish the parameters at which no residual compound peaks were visible. The screening experiments were all recorded with a carrier set at 0 ppm for the on-resonance and −40 ppm for the off-resonance irradiation. Selective protein saturation was carried out at 2 s (D20 parameter in TopSpin) by using a train of 50 ms Gauss-shaped pulses, each separated by a 1 s delay (D1 parameter in TopSpin). The number of scans was 512.

The difference spectrum was obtained by algebraic subtraction of the on-resonance spectrum from the off-resonance spectrum after automatic phase correction.

The relative difference in intensity of signals due to saturation transfer (relative STD effect) was estimated using the following formula:

$$\text{STDeffect} = (I_0 - I_{sat})/I_0 \qquad (1)$$

(where I_{sat} is the intensity of the signal of interest in the on-resonance NMR spectrum, and I_0 is the intensity of the signal in the off-resonance NMR spectrum). The STDeffect was used to estimate the contribution of the particular proton group into binding with DnaN and to infer the binding epitope for the compounds tested.

The spectra obtained are provided below (**Figure S40** and **Figure S41**).

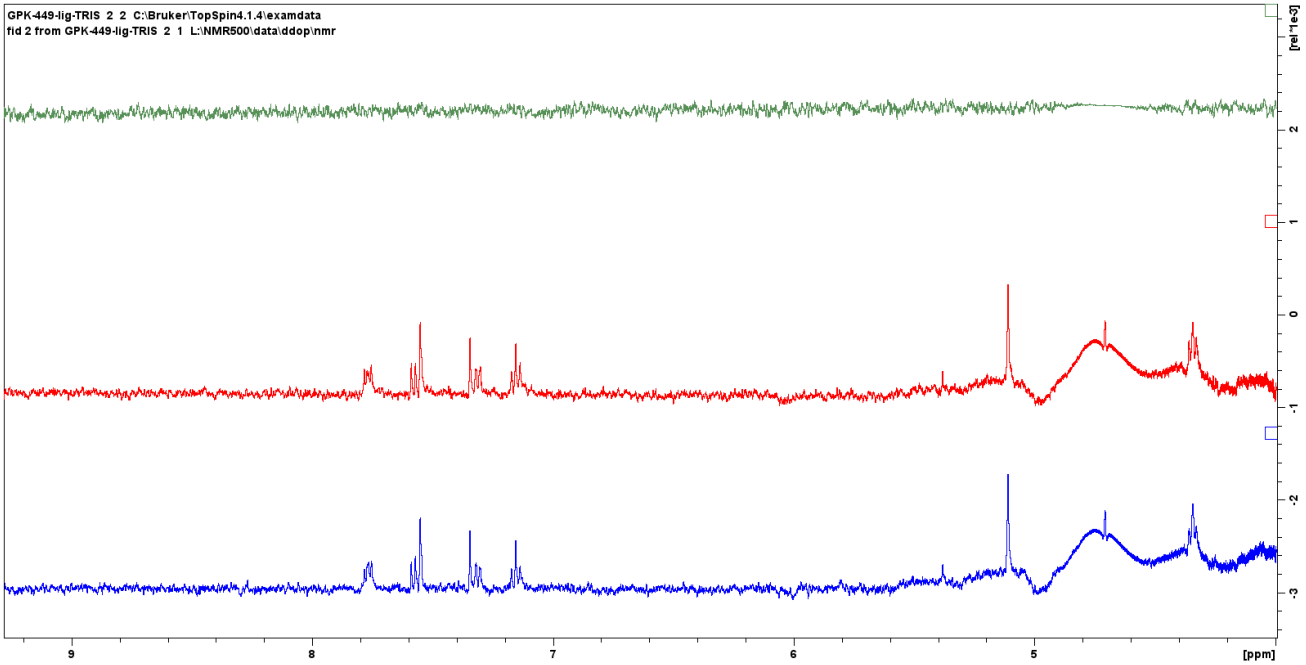

Figure S40. A section of a blank STD-NMR spectrum obtained for **H1** alone. Off-resonance spectrum is depicted in **blue**, on-resonance spectrum - in **red**, difference spectrum - in **green**.

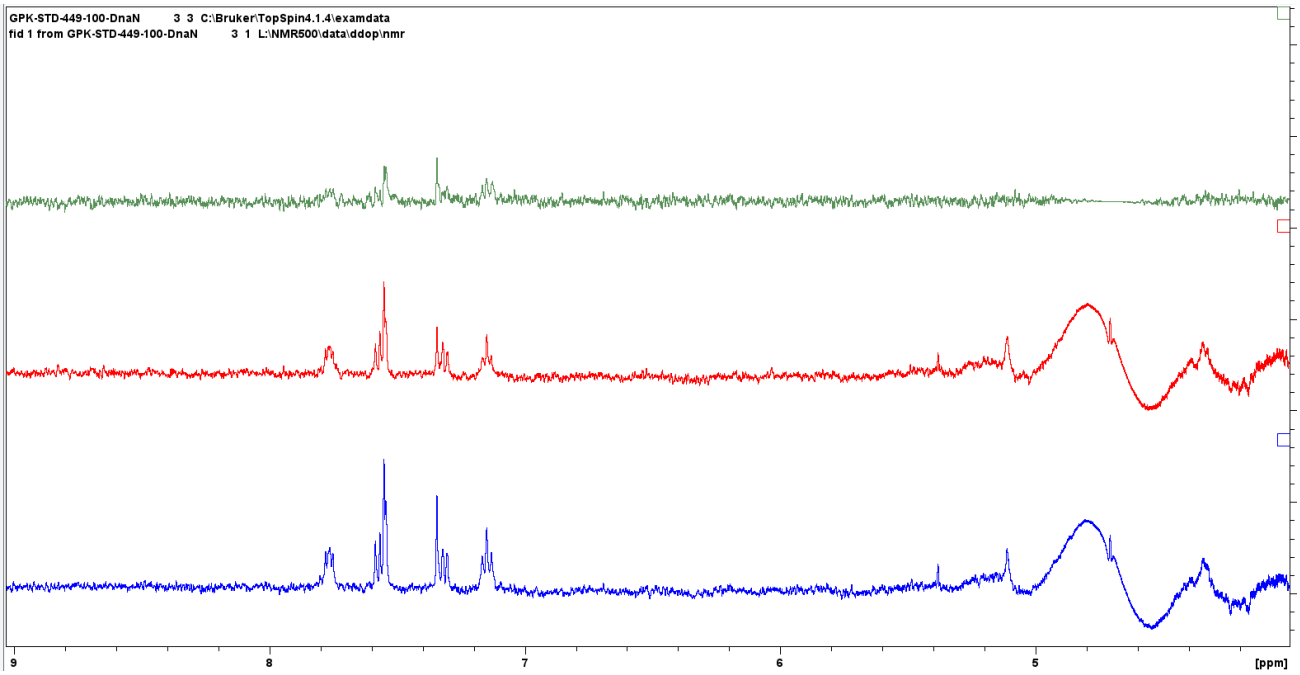

Figure S41.. A section of an STD-NMR spectrum obtained for **H1** in the presence of *M.tb* DnaN. Off-resonance spectrum is depicted in **blue**, on-resonance spectrum - in **red**, difference spectrum - in **green**.

S3.1.3 Experimental procedures for ADMET testing

The experiments described below were performed at the Drug Discovery Unit (DDU) at the University of Dundee, the United Kingdom.

CHI LogD Determination.

The chromatographic hydrophobicity index (CHI) was determined according the method previously described.[2] Briefly, test compounds were prepared as 0.5 mM solutions in 50:50 acetonitrile/water and analyzed by reversed-phase HPLC-UV (wavelength 254 nm) using a Phenomenex Luna C18 100 Å, 150 × 4.6 mm, 5 μm column with a gradient of aqueous phase (50 mM ammonium acetate (pH 7.4)) and mobile phase (acetonitrile). By plotting the retention time of a set of reference compounds against known CHI values, the CHI value of test compounds was calculated according to their retention time.

Intrinsic clearance (CL_{int})

The procedure was carried out as reported previously.[3] Test compound (0.5 μM) was incubated with female CD1 mouse liver microsomes (Xenotech LLC TM; 0.5 mg/mL 50 mM potassium phosphate buffer, pH 7.4) and the reaction started with addition of excess NADPH (8 mg/mL 50 mM potassium phosphate buffer, pH7.4). Immediately, at time zero, then at 3, 6, 9, 15 and 30 minutes an aliquot (50 μL) of the incubation mixture was removed and mixed with acetonitrile (100 μL) to stop the reaction. Internal standard was added to all samples, the samples centrifuged to sediment precipitated protein and the plates then sealed prior to UPLC-MS/MS analysis using a Quattro Premier XE (Waters Corporation, USA).

XLfit (idbs, UK) was used to calculate the exponential decay and consequently the rate constant (k) from the ratio of peak area of test compound to internal standard at each time-point. The rate of intrinsic clearance (CLint) of each test compound was then calculated using the following calculation:

CL_{int}(mL/min/g liver) = k x V x Microsomal protein yield.

Where V (mL/mg protein) is the incubation volume/mg protein added and microsomal protein yield is taken as 52.5 mg protein/g liver. Verapamil (0.5 μM) was used as a positive control to confirm acceptable assay performance.

Permeability Across MDCK-MDR1 Cell Monolayers

Permeability was determined as reported previously.[4] MDR1-MDCK monolayers were grown to confluence on collagen-coated, microporous, polycarbonate membranes in 12-well Costar Transwell plates. Data are considered valid for a specific assay plate if TEER values are < 1400 $\Omega.cm^2$, the P_{app} of propanolol is between 10-30 x 10^{-6} cm/s and the P_{app} of atenolol is < 0.5 x 10^{-6} cm/s. The permeability assay buffer was Hanks Balanced Salt Solution containing 10 mM HEPES and 15 mM glucose at a pH of 7.4. A known p-glycoprotein inhibitor cyclosporin A

(CSA) was also added to the assay buffer at 10 microM. The dosing solution concentrations of the test compounds were 5.0 micro M in the assay buffer. All cell monolayers were first pre-incubated for 30 minutes with assay buffer to saturate any P-glycoprotein sites with test compound. After 30 minutes, the buffer was removed, replaced with fresh buffer, and time was recorded as 0. Cell monolayers were dosed on the apical side (A-to-B) or basolateral side (B-to-A) and incubated at 37°C with 5% CO_2 in a humidified incubator. After 2 hours, aliquots were taken from the receiver chambers. Samples were taken from the donor chamber at 0 and 2 hours. Each determination was performed in duplicate. The lucifer yellow flux was also measured for each monolayer to ensure no damage was inflicted to the cell monolayers during the flux period. All samples were assayed by LC/MS/MS using electrospray ionization.

The apparent permeability, P_{app}, and percent recovery were calculated as follows:

$$Papp = (dCr/dt) \times Vr/(A \times C_0) \quad (1)$$

$$\text{Percent Recovery} = 100 \times ((Vr \times Cr^{final}) + (Vd \times Cd^{final}))/(Vd \times CN) \quad (2)$$

where,

dCr/dt is the slope of the cumulative concentration in the receiver compartment versus time in microM s^{-1}.

Vr is the volume of the receiver compartment in cm^3.

Vd is the volume of the donor compartment in cm^3.

A is the area of the cell monolayer (1.13 cm^2 for 12-well Transwell).

C0 is the measured concentration of the donor chamber at time 0 in microM.

CN is the nominal concentration of the dosing solution in microM.

Cr^{final} is the cumulative receiver concentration in microM at the end of the incubation period.

Cd^{final} is the concentration of the donor in microM at the end of the incubation period.

Metabolic Stability—Pooled Human Cryopreserved Hepatocyte Incubations

The analysis was performed as reported previously.[5] Test compounds and positive controls (verapamil, 7-ethoxycoumarin (7-EC) and 7-hydroxycoumarin (7-HC)) were incubated at 0.5 _M in pooled cryopreserved hepatocytes. Total incubation volume was 400 _L. Procedure: Cells were thawed and added to cryopreserved hepatocyte recovery media, centrifuged (100_ g, 10 min, 22 _C), counted and diluted in WME (37 _C, bubbled with 5% CO_2:95% O_2). To initiate reactions, 200 _L of drug working solution (1 _M) was added to 200 _L cell suspension (0.5 million cells mL^{-1}). Samples were mixed and 20 _L sampled immediately and added to 80 _L ACN containing donepezil (IS, 50 ng mL^{-1}) in a 96 deep-well 2 mL plate. Plates were incubated at 37 _C with 5% CO_2 with agitation at 95 rpm. Further aliquots were taken at 3, 6, 9, 15, 30, 45,

60 min. Samples were diluted with 100 _L of water/ACN (80:20 v/v) and centrifuged (2800 rpm, 10 min, 22 _C) prior to UPLC/MS.

MS analysis. Each SCRA was incubated at least in triplicate but additional incubations were carried out across a number of analytical batches, giving greater replication and a greater understanding of system variability. Differing values for hepatocyte cell density are reported in the literature. Intrinsic clearance and predicted in vivo clearance rates calculated using an alternative hepatocyte cell density is provided in Section S7 of the supplementary information, to aid comparison of data between publications. Rate constants (k, min^{-1}) and half-lives ($t_{1/2}$) were calculated using XLfit 5.3.1 add-in (IDBS, Surrey, UK) for Microsoft Excel 2013, version 15.0 (Microsoft, Redmond,WA, US), calculated from plots of analyte/IS peak area ratio against time. Microsomal intrinsic clearance (CLint micr) (pHLM data) and intrinsic clearance (CLint) scaled to whole-liver dimensions for humans (pHLM and pHHeps data) were calculated from k, liver and body weight estimates and scaling factors.[6],[7],[8] Hepatic clearance (CLH) and extraction ratios (EH) were estimated based on the corresponding human CLint values, fraction unbound and estimates of liver blood flow rate (human 21 mL min^{-1} kg^{-1}).[7],[9],[10] The equations used for in vitro intrinsic clearance calculations and human *in vivo* clearance estimation were as described by Baranczewski et al. (2006)[7] Rane, Wilkinson & Shand (1977)[9] and Obach *et al*. (1997).[10]

***In Vivo* Pharmacokinetics in mice**.

Experiments were performed as described previously.[11] Test compound 15 was dosed intravenously or orally by gavage as a solution at 3 or 10mg free base/kg respectively (dose volume, 5 or 10 mL/kg respectively; dose vehicle (IV), 5% (v/v) dimethyl sulfoxide (DMSO), 95% Saline, dose vehicle (PO),1% carboxy methyl cellulose, 99% Saline to female CD-1 (n = 3). Blood samples were taken from each mouse at 0.08, 0.25, 0.5, 1, 2, 4, 6, 8, and 24 h post dose and mixed with two volumes of distilled water. After suitable sample preparation, the concentration of test compound in blood was determined by UPLC-MS/MS using a Quattro Premier XE (Waters, USA). Pharmacokinetic parameters were derived from the mean blood concentration time curve using PK solutions software v 2.0 (Summit Research Services, USA).

S3.1.4 Experimental procedures and results of co-crystallization and soaking

Production of R. typhi DnaN Protein. The plasmid containing the gene encoding for *R. typhi* DnaN with an N-terminal hexahistine tag was obtained from the Seattle Structural Genomics Center for Infectious Disease (SSGCID; Center Reference ID of the construct: RityA.17987.a). The protein was expressed in *E. coli* BL21 (DE3) in ZYM-5052 auto-inducing medium[12] at 20°C for 20-24 h. The cell pellet was resuspended in a buffer containing 20 mM HEPES/NaOH pH 7.5, 150 mM NaCl, one tablet of complete EDTA-free protease inhibitor cocktail (Roche) and lysed by sonication. The protein was isolated from the supernatant after centrifugation for 1 h at 100,000 x g using a 5 ml HisTrap HP column (Cytiva) and eluted from the column using a linear gradient with increasing imidazole concentration. Gel filtration was carried out using a HiLoad 16/600 Superdex 200 pg column (GE Healthcare) in 20 mM HEPES/NaOH pH 7.5, 150 mM NaCl. The peak fractions were concentrated and flash-frozen in liquid nitrogen for crystallization screening.

Crystallization and ligand soaking. Crystallization trials were set up at room temperature with a Crystal Gryphon crystallization robot (Art Robbins Instruments) in Intelli 96-3 plates (Art Robbins Instruments) with 200 nl protein solution at different concentrations and 200 nl reservoir solution. Initial hits were optimized by a randomized screening approach and optimized crystals were obtained after a few days in 25 % (w/v) PEG 1500, 0.175 M NH_4Cl, 0.1 M BIS-TRIS pH 8.0. Soaking trials were carried out with various concentrations and durations. Successful soaking of H1 into *R. typhi* DnaN could be achieved with 2 mM of the compound (and 10 % (v/v) DMSO, respectively) for 12 h. After harvesting, crystals were cryo-protected by addition of 10% (v/v) (2R,3R)-2,3-butanediol.

Data collection and processing. Data collection for was performed at beamline P11 at the Petra III storage ring (Deutsches Elektronen-Synchrotron, Hamburg, Germany)[13] at a temperature of 100 K. Data processing was carried out using the AutoPROC[14] toolbox (Global Phasing) executing XDS[15] ,Pointless[16] and Aimless[17].

Structure determination, refinement, and model building. The structure was determined by molecular replacement using the available structure of *R. typhi* from the PDB (6D46) as a search-model for Phaser[18] from the Phenix suite[19]. The structural model was built using Coot[20] and crystallographic refinement was performed with Phenix.refine[21] including the addition of hydrogens in riding positions and TLS-refinement. 5% of random reflections were flagged for the calculation of R_{free}. The model of *R. typhi* DnaN in complex with compound H1 was at 2.2 Å resolution refined to R/R_{free} of 18/23% in space group C2. Data collection and refinement statistics are summarized in **Tab S1** below.

Table S1: Data collection & Refinement Statistics.

Structure	*R. typhi* DnaN & **H1**
PDB-ID:	**XXXX**
Data collection	
Beamline	DESY P11
Wavelength (Å)	1.03
Space group	C2
Cell dimensions	
a, *b*, *c* (Å)	148.29, 41.49, 83.05
α, β, γ (°)	90.00, 120.73, 90.00
Resolution (Å)[a]	41.46 – 2.20 (2.27 – 2.20)
R_{merge} (%)[a]	12.1 (99.9)
R_{pim} (%)[a]	6.2 (55.0)
$I/\sigma I^{a}$	7.7 (2.2)
Completeness (%)[a]	100.0 (100.0)
Redundancy[a]	4.6 (4.7)
$CC_{1/2}$ (%)[a]	99.5 (77.1)
Refinement	
Resolution (Å)	2.20
No. reflections	22434
R_{work}/ R_{free} (%)	17.93/22.82
No. atoms	3159
Protein	3009
Ligand/ion	32
Water	118
B-factors (Å^2)	49.44
Protein	49.34
Ligand/ion	56.69
Water	49.99
R.m.s deviations	
Bond lengths (Å)	0.004
Bond angles (°)	0.660
Ramachandran statistics (%)	
Favored	96.78
Allowed	3.22
Outliers	0.00
Clashscore (MolProbity)	4.69
MolProbity score	1.44

S3.1.5 Experimental procedure for SPR measurements

SPR analyses were performed on a Biacore X100 system (GE Healthcare). The *M. smegmatis-DnaN* protein was diluted to 50 µg/mL in 10 mM sodium acetate buffer (pH 4.5) and immobilized on a CM5 (or CM7) sensor chip by standard amine coupling resulting in a protein level of approximately 1700-2200 response units (RU). Manual run was performed for small fragments with an injection rate of 60 sec at two concentrations for each compound (125 and 250 µM). After the compounds were prepared, they were centrifuged and the supernatant was included in the SPR run. Resonance units (RU) representing the change in resonance angle which is proportional to the number of molecules binding was reported for all the compounds. 1 RU equals $1 \cdot 10^{-6}$ RIU (refractive index units). The compounds were tested at 125 and 250 µM in 5% DMSO.

The theoretical maximal RU (Rmax) was determined as follows: Rmax = molecular weight (MW) Analyte (Da) ÷ MWLigand (Da) × immobilized ligand density (RU) × stoichiometric ratio (number of binding sites per ligand). The MW values for *M. smegmatis* DnaN protein is 42,113 Da

S3.1.6 Experimental procedures and results of MIC and cytotoxicity assays

MIC determination

All microorganisms used in this study were obtained from the German Collection of Microorganisms and Cell Cultures (DSMZ), the Coli Genetic Stock Center (CGSC), or were part of our internal collection, and were handled according to standard procedures. *S. aureus*, *E. coli*, *E. faecium* and *E. faecalis* were inoculated in cation-adjusted Mueller Hinton Broth (Sigma Aldrich) and incubated under shaking conditions overnight at 37 °C, and for 48 h for *M. smegmatis*. *S. pneumoniae* was cultured without shaking under microaerophilic conditions (5% CO2) overnight at 37 °C. *S. aureus*, *E.coli*, *E. faecium*, and *E. faecalis* were subcultured on CASO agar plates, *M. smegmatis* and *S. pneumoniae* were subcultured on Middlebrook 7H10 agar plates (M7H10) with 10% oleic acid albumindextrose-catalase OADC Enrichment and 5% sheep blood agar plates, respectively, and incubated for 24 h at their optimal growth temperature. Single colonies of the bacterial strains were suspended in 0.9% NaCl and McFarland was adjusted to 0.5 using a Densitometer. The bacterial suspension was diluted 1:100 in the corresponding broth to achieve a final inoculum of approximately 10^4 CFU/mL. Serial dilutions of compounds (0.06 to 128 µM) were prepared in sterile 96-well plates and the bacterial suspension was added. Growth inhibition was assessed after overnight incubation (24–48 h) at 30–37 °C. Minimum inhibitory concentration (MIC) was determined as the lowest compound concentration where no visible growth was observed. *M. smegmatis* GM^R was cultured in Middlebrook 7H9 minimal media

(7H9) supplemented with 10% oleic acid albumindextrose-catalase OADC Enrichment, with 25 µg/mL GM.

Cytotoxicity evaluation (IC_{50})

HepG2 cells (human hepatoblastoma cell line; ACC 180, DSMZ) were cultured under conditions recommended by the depositor and cells were propagated in Dulbecco's modified Eagle medium (DMEM) supplemented with 10% fetal bovine serum (FBS). For determining the antiproliferative activity of test compounds, cells were seeded at 6×10^3 cells per well of 96-well plates in 120 µL complete medium. After 2 h of equilibration, compounds were added in serial dilution in 60 µL complete medium. Compounds, as well as the solvent control and doxorubicin as reference, were tested as duplicates in two independent experiments. After 5 d incubation, 20 µL of 5 mg/mL MTT (thiazolyl blue tetrazolium bromide) in PBS was added per well and cells were further incubated for 2 h at 37 °C. The medium was then discarded and cells were washed with 100 µL PBS before adding 100 µL 2-propanol/10 N HCl (250:1) in order to dissolve formazan granules. The absorbance at 570 nm was measured using a microplate reader (Tecan Infinite M200Pro), and cell viability was expressed as percentage relative to the respective solvent control. IC_{50} were determined by sigmoidal curve fitting using GraphPad PRISM 8 (GraphPad Software, San Diego, CA, USA).

S3.1.7 Experimental procedure for DLS measurements

Compounds were analyzed for aggregate formation using dynamic light scattering (DLS) on a zetasizer Nano ZS90 (Malvern Instruments Ltd, Worcestershire, UK) as recently described).[22] Disposable cuvettes (3.2 ml, 67.758, Sarstedt AG & Co, Nümbrecht, Germany) were filled with a total sample volume of 50 µl and equilibrated to 25 °C for 60 s prior to the experiments. Analyses were performed in the absence or presence of compounds using 7H9 medium supplemented with 10% OADC and 1% DMSO. Count rate data for all samples were determined from 3 measurements of 3 cycles of 10 seconds each. The count rate at high scattering intensities is reduced by an automatic attenuator, so the derived count rate, which is corrected with the attenuation factor, was used as a measure for the degree of aggregate formation. Derived count rate values of the compounds were compared with the derived count rate of the medium at the concentrations as indicated. This allowed the determination of the highest sample concentration at which the respective compound was not yet present with an increased degree of aggregate formation.

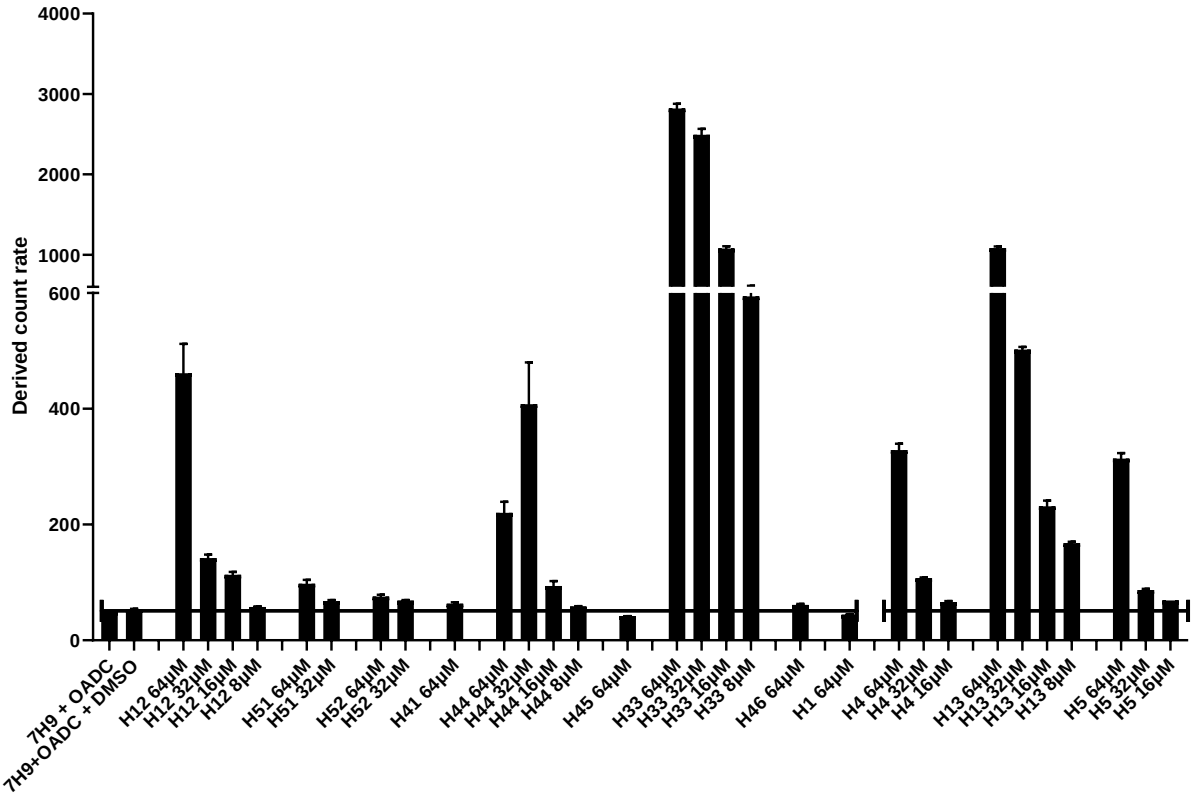

Figure S42. Derived count rate for representative classes of compounds that were subjected to tests against *M.tuberculosis*

S3.1.8 Experimental procedure for *M. tuberculosis* growth analysis in liquid culture

Bacteria

M. tuberculosis (M. tb) strain H37Rv (ATCC 25618) carrying a mCherry-expressing plasmid (pCherry10)[23] was cultured in 7H9 complete medium (BD Difco; Becton Dickinson) supplemented with oleic acid-albumin-dextrose-catalase (OADC, 10%; BD), 0.2% glycerol, and 0.05% Tween80 as previously described. At mid-log phase (OD_{600} = 0.4) cultures were harvested and frozen in aliquots at −80◦C.[24]

M. tuberculosis growth analysis in liquid culture

Frozen aliquots of mCherry-Mtb H37Rv were thawed and centrifuged (3700×g, 10 minutes). Supernatants were discarded and bacteria thoroughly resuspended in 7H9 medium (10% OADC) in the absence of glycerol and Tween80 by use of a syringe and a 26-gauge syringe needle. The bacterial suspension was passed in and out of the syringe about 10 times. Compounds were tested in 2 fold dilutions starting at 64µM in triplicates (2×10e6 bacteria, volume 100µl) for their anti-tubercular activity using 96-well flat clear bottom black polystyrene microplates (Corning® CellBIND®, New York, USA). Each plate was prepared with rifampicin (National Reference Center, Borstel) as reference compound. Plates were sealed with an air-permeable membrane (Porvair Sciences, Wrexham, UK) in a 37°C incubator with mild agitation (TiMix5, Edmund Bühler, Germany), as previously described.[22] Bacterial growth was measured as relative light units (RLU) from the fluorescence intensity obtained at an excitation wavelength

of 575 nm and emission wave length of 635 nm (microplate reader, Synergy 2, BioTek Instruments, Vermont, USA) at the indicated time points. Obtained values were normalized to RLU values of the solvent control (DMSO)-treated bacteria set to 100%) and MIC_{95} of each compound was determined. MIC_{95} was defined as the minimum concentration of the compound required to achieve a reduction in fluorescence by 95%. Obtained MIC values were validated by a visual Resazurin microtiter assay (REMA)[25] by adding 30 µL of 0,02% Resazurin (Cayman) solution to each well followed by another 20 h of culture without agitation.

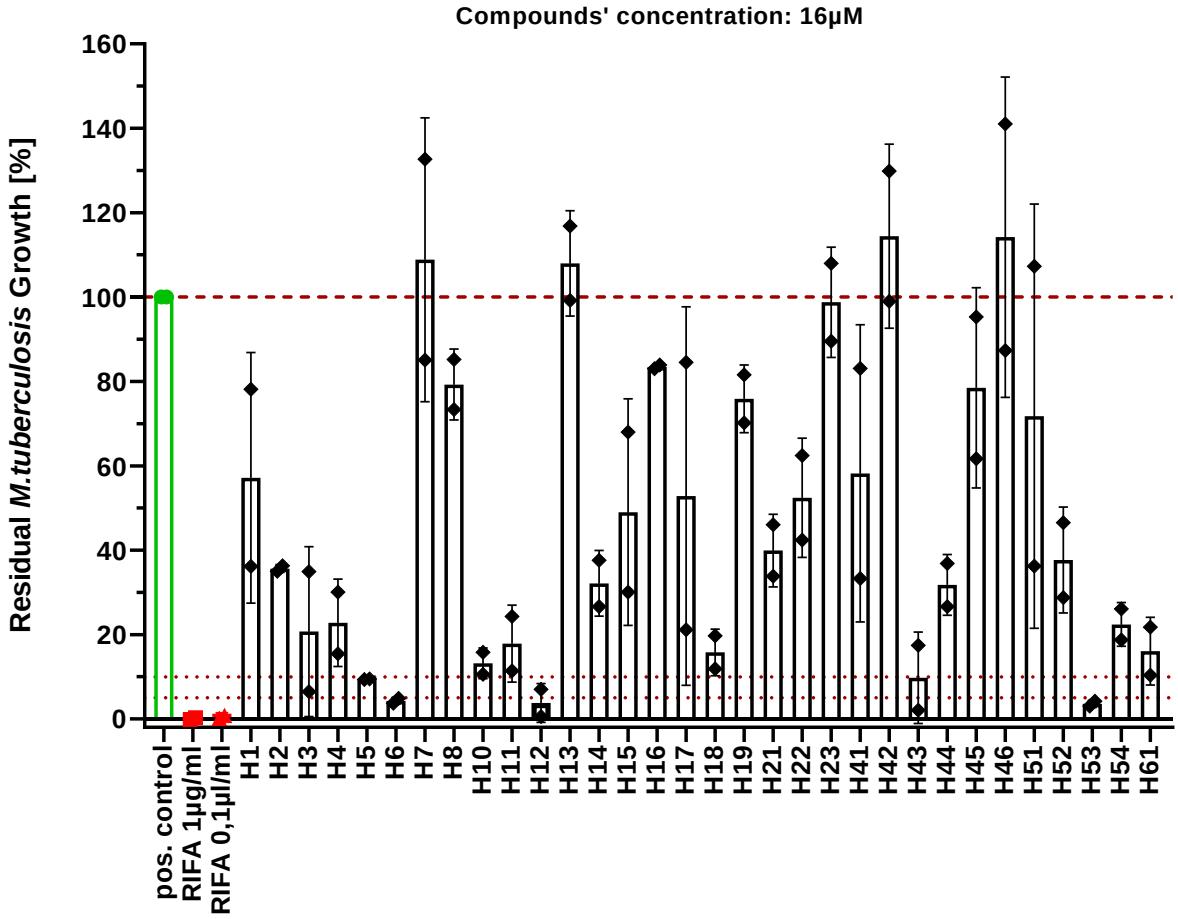

Figure S43. Residual growth of *M. tuberculosis* in the presence of 16 µM of compounds.

Based on the obtained results, the highly active and non-aggregating compounds were selected for serial dilution experiments in order to determine respective MIC_{95} values (**Figure S44**).

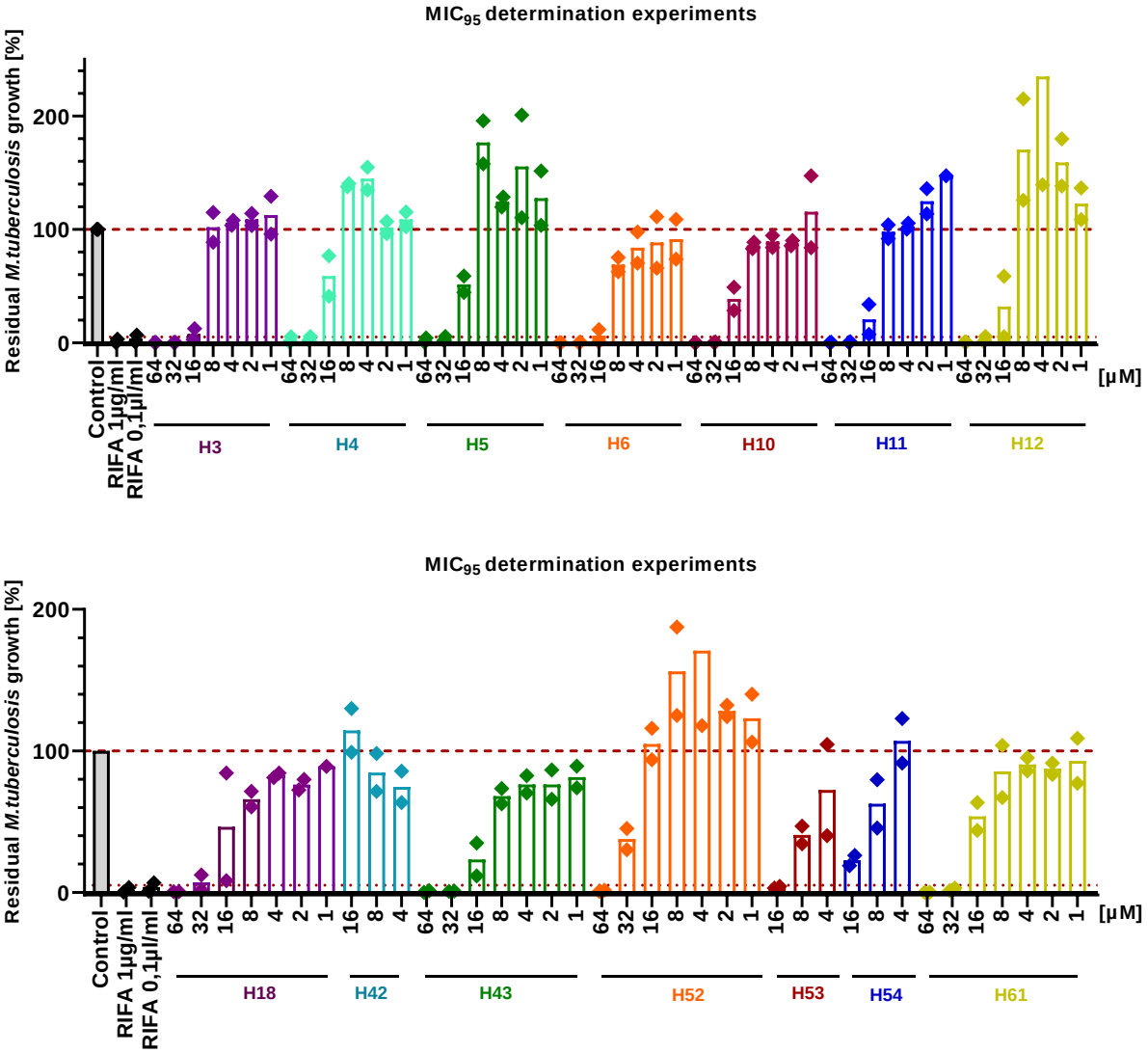

Figure S44. Results of serial dilution experiments performed for chosen compounds.

S3.2 References

[1] N. M. O'Boyle, J. Boström, R. A. Sayle, A. Gill, *J. Med. Chem.* **2014**, *57*, 2704–2713.

[2] * Klára Valkó, and Chris Bevan, D. Reynolds, *Anal. Chem.* **1997**, *69*, 2022–2029.

[3] S. Patterson, S. Wyllie, L. Stojanovski, M. R. Perry, F. R. C. Simeons, S. Norval, M. Osuna-Cabello, M. De Rycker, K. D. Read, A. H. Fairlamb, *Antimicrob. Agents Chemother.* **2013**, *57*, 4699–4706.

[4] E. Milner, J. Sousa, B. Pybus, V. Melendez, S. Gardner, K. Grauer, J. Moon, D. Carroll, J. Auschwitz, M. Gettayacamin, P. Lee, S. Leed, W. McCalmont, S. Norval, A. Tungtaeng, Q. Zeng, M. Kozar, K. D. Read, Q. Li, G. Dow, *Eur. J. Drug Metab. Pharmacokinet.* **2011**, *36*, 151–158.

[5] A. M. Brandon, L. H. Antonides, J. Riley, O. Epemolu, D. A. McKeown, K. D. Read, C. McKenzie, *Molecules* **2021**, *26*, DOI 10.3390/molecules26051396.

[6] A. B. Davidsen, M. Mardal, K. Linnet, *AAPS J.* **2019**, *21*, 1–9.

[7] P. Baranczewski, A. Stańczak, K. Sundberg, R. Svensson, Å. Wallin, J. Jansson, P. Garberg, H. Postlind, *Pharmacol. Reports* **2006**, *58*, 453–472.

[8] P. Obach, R.S.; Baxter, J.G.; Liston, T.E.; Silber, B.M.; Jones, B.C.; MacIntyre, F.; Range, D.J.; Wastall, *J. Pharmacol. Exp. Ther* **1997**, 46–58.

[9] D. . Rane, A.;Wilkinson, G.R.; Shand, *J. Pharmacol. Exp. Ther.* **1977**, 420–424.

[10] R. S. Obach, *Drug Metab. Dispos.* **1999**, 1350–1359.

[11] P. C. Ray, M. Huggett, P. A. Turner, M. Taylor, L. A. T. Cleghorn, J. Early, A. Kumar, S. A. Bonnett, L. Flint, D. Joerss, J. Johnson, A. Korkegian, S. Mullen, A. L. Moure, S. H. Davis, D. Murugesan, M. Mathieson, N. Caldwell, C. A. Engelhart, D. Schnappinger, O. Epemolu, F. Zuccotto, J. Riley, P. Scullion, L. Stojanovski, L. Massoudi, G. T. Robertson, A. J. Lenaerts, G. Freiberg, D. J. Kempf, T. Masquelin, P. A. Hipskind, J. Odingo, K. D. Read, S. R. Green, P. G. Wyatt, T. Parish, *ACS Omega* **2021**, *6*, 2284–2311.

[12] F. W. Studier, *Protein Expr. Purif.* **2005**, *41*, 207–234.

[13] A. Burkhardt, T. Pakendorf, B. Reime, J. Meyer, P. Fischer, N. Stübe, S. Panneerselvam, O. Lorbeer, K. Stachnik, M. Warmer, P. Rödig, D. Göries, A. Meents, *Eur. Phys. J. Plus* **2016**, *131*, DOI 10.1140/epjp/i2016-16056-0.

[14] C. Vonrhein, C. Flensburg, P. Keller, A. Sharff, O. Smart, W. Paciorek, T. Womack, G. Bricogne, *Acta Crystallogr D Biol Crystallogr* **2011**, *67*, 293–302.

[15] W. Kabsch, IUCr, *Acta Crystallogr D Biol Crystallogr* **2010**, *66*, 125–132.

[16] P. Evans, IUCr, *Acta Crystallogr D Biol Crystallogr* **2005**, *62*, 72–82.

[17] P. R. Evans, G. N. Murshudov, *Acta Crystallogr D Biol Crystallogr* **2013**, *69*, 1204–1214.

[18] A. J. McCoy, R. W. Grosse-Kunstleve, P. D. Adams, M. D. Winn, L. C. Storoni, R. J. Read, *J Appl Crystallogr* **2007**, *40*, 658–674.

[19] P. D. Adams, P. V. Afonine, G. Bunkóczi, V. B. Chen, I. W. Davis, N. Echols, J. J. Headd, L. W. Hung, G. J. Kapral, R. W. Grosse-Kunstleve, A. J. McCoy, N. W. Moriarty, R. Oeffner, R. J. Read, D. C. Richardson, J. S. Richardson, T. C. Terwilliger, P. H. Zwart, *Acta Crystallogr D Biol Crystallogr* **2010**, *66*, 213–221.

[20] P. Emsley, B. Lohkamp, W. G. Scott, K. Cowtan, *Acta Crystallogr D Biol Crystallogr* **2010**, *66*, 486–501.

[21] P. V. Afonine, R. W. Grosse-Kunstleve, N. Echols, J. J. Headd, N. W. Moriarty, M. Mustyakimov, T. C. Terwilliger, A. Urzhumtsev, P. H. Zwart, P. D. Adams, *Acta Crystallogr D Biol Crystallogr* **2012**, *68*, 352–367.

[22] R. P. Jumde, M. Guardigni, R. M. Gierse, A. Alhayek, D. Zhu, Z. Hamid, S. Johannsen, W. A. M. Elgaher, P. J. Neusens, C. Nehls, J. ¨ Org Haupenthal, N. Reiling, A. K. H. Hirsch, **2021**, DOI 10.1039/d1sc00330e.

[23] A. Zelmer, P. Carroll, N. Andreu, K. Hagens, J. Mahlo, N. Redinger, B. D. Robertson, S. Wiles, T. H. Ward, T. Parish, J. Ripoll, G. J. Bancroft, U. E. Schaible, *J. Antimicrob. Chemother.* **2012**, *67*, 1948–1960.

[24] K. Kolbe, L. Möckl, V. Sohst, J. Brandenburg, R. Engel, S. Malm, C. Bräuchle, O. Holst, T. K. Lindhorst, N. Reiling, *Chembiochem* **2017**, *18*, 1172–1176.

[25] S. G. Franzblau, M. A. Degroote, S. H. Cho, K. Andries, E. Nuermberger, I. M. Orme, K. Mdluli, I. Angulo-Barturen, T. Dick, V. Dartois, A. J. Lenaerts, *Tuberculosis (Edinb).* **2012**, *92*, 453–488.

4. Fragment-based discovery of novel mycobacterial β-sliding clamp inhibitors

Uladzislau Hapko[1,2], Sari Rasheed[2], Walid Elgaher[1,2], Jennifer Herrmann[2], Rolf Müller[1,2] Anna K. H. Hirsch[1,2]

[1]Department of Pharmacy, Saarland University, Unversitätscampus C2.3, 66123, Saarbrücken, Germany
[2]Helmholtz Institute for Pharmaceutical Research Saarland, Unversitätscampus E8.1, 66123, Saarbrücken, Germany

Abstract

The discovery of a highly active fragment-sized hit binding to the β-sliding clamp (DnaN) of *Mycobacterium tuberculosis* is reported. The screening of a commercial fragment library with MST and hit validation using SPR and STD-NMR yielded seven hits, of which we prioritized one scaffold for further elaboration.
We describe herein successful SAR establishment and optimization of the binding affinity of fragments for DnaN and antibacterial activity against Mycobacteria and Gram-positive bacteria. Additionally, growing attempts of optimized fragments leading to further improved binding to DnaN are outlined.

4.1 Introduction

Mycobacterium tuberculosis is known to be the causative agent of tuberculosis in mammals.[1,2] The extensive use of various classes of antibiotics for the treatment of infections rendered the emergence of multi- and extensively drug-resistant *M. tuberculosis* inevitable, and this is becoming one of the major concerns for the global healthcare system. The aforementioned fact necessitates the intensification of efforts focused on the discovery of novel classes of antibiotics with unprecedented modes of action.

One of the targets that can be addressed in the context of novel antibacterial discovery is the bacterial β-sliding clamp (DnaN). DnaN has an essential function in bacterial cells being the processivity factor for various DNA-polymerases as a part of the bacterial replisome.[3] The β-sliding clamp encircles the DNA and assures the firm tethering of a partnering DNA-polymerase by involving it into a tight (K_d 10^{-6} – 10^{-8}) protein-protein interaction.[4,5] Inhibiting the protein-protein interaction between the DnaN and partnering DNA-polymerases can be envisaged as a novel and efficient mechanism of action for the next generation of antibiotics given the conserved structure of DnaN throughout bacterial species[6] and high sequence dissimilarity to its orthologue PCNA found in eukaryotes.[7]

The β-sliding clamp protein, however, has been a target for a wealth of small-molecule hit discovery and optimization attempts undertaken by various groups.[8,9,10,11,12,13] Nevertheless, the small-molecule inhibitors discovered so far as a result of fragment-based screening and optimization campaigns have either lacked broad-spectrum antibacterial activity or demonstrated no activity against Mycobacteria.[10,11,12,13]

Hereby we report the discovery and attempts of exploratory optimization of fragment-sized *M. tubercuosis* DnaN binders active against Mycobacteria and certain ESKAPE species alike.

4.2 Results and discussion

4.2.1 Identification and validation of fragment hits.

For finding initial hits, we screened the Maybridge Ro3 (rule of three) library (Thermo Fischer Scientific) consisting of 350 Ro3 criteria consistent (MW ≤ 300, cLogP ≤ 3.0, $H_{acc} \leq 3$, $H_{don} \leq 3$, $N_{rot.bonds} \leq 3$, PSA ≤ 60 Å^2) molecules, which we subjected to microscale thermophoresis (MST) single-point screening (c = 500 µM) for *M. tuberculosis* DnaN binding, followed by validation using surface plasmon resonance (SPR). For the validated hits, affinity to the sliding clamp was determined in the form of the dissociation constant (K_d). The two-step screening-validation effort yielded **seven** hits (2% hit rate) active in both assays at a given concentration. The structures and parameters of the validated hits are given in **Table 1**.

Table 1. Structure, binding affinity and ligand efficiency (LE) of fragment hits validated by Surface Plasmon Resonance (SPR).

Compound	Structure	Molecular weight	SPR K_d (µM)	LE
Fr1	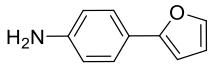	159.19	**58±2**	**0.48**
Fr2	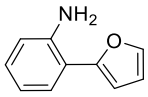	159.19	**170±10**	**0.43**
Fr3	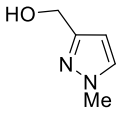	112.13	**200±40**	**0.63**
Fr4	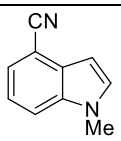	156.19	410±20	0.39
Fr5	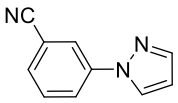	169.19	≈1000	0.32
Fr6	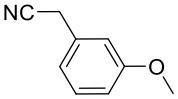	147.18	≈1500	0.35
Fr7		82.11	>1500	n.d

LE – ligand efficiency, **n.d** – not determined

Compounds **Fr1**–**Fr4** showed K_d values ranging from 58 to 410 µM, while dissociation constants of **Fr5**–**Fr7** clearly exceeded 1 mM. Fragments **Fr1**, **Fr2** and **Fr3** also became clear

favorites based on their ligand efficiency values. Nevertheless, the seven fragments were subjected to cross-validation using Saturation Transfer Difference NMR (STD-NMR).

4.2.2 Cross-validation of hits by STD-NMR and their binding epitope mapping

We cross-validated fragment hits **Fr1**-**Fr7** via STD-NMR measurements of mixtures, which were assembled based on the proton shifts of individual fragments so that the overlap of signals is minimized (see spectra in Supplementary information, Figures **S1-S16**). Having assigned observed signals to the corresponding structures, we found proton signals belonging to **Fr1** and **Fr2** to demonstrate most prominent intensities in difference spectra, which correlated with the fragments' (relatively) high affinities determined by SPR. We observed lower intensities in the difference spectra for the protons belonging to **Fr4** and **Fr5**, which also correlated with their average affinities to the sliding clamp, cross-validating these structures as binders. Conversely, the lack of proton signals of **Fr3**, **Fr6** and **Fr7** in the corresponding difference spectra ultimately disqualified them as DnaN binders.

We additionally determined relative STD effects of all proton groups of interest (**Figure 1**) to support the ranking of poses suggested by modeling of validated hits using group epitope mapping.[14]

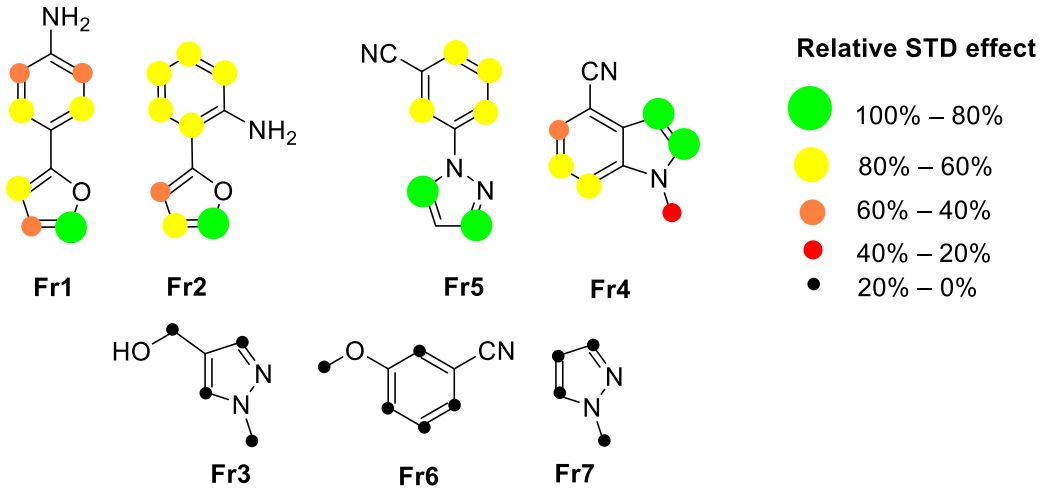

Figure 1. STD-NMR effects of molecules **Fr1-Fr7**.

Based on the behavior of fragments in the three biophysical DnaN binding assays, we decided to focus our exploratory optimization effort on regioisomers **Fr1** and **Fr2** because of their high affinities to DnaN (as demonstrated by SPR and STD-NMR) and ligand efficiencies.

4.2.3 Modeling of structures Fr1 and Fr2

According to the relative STD effect demonstrated by protons belonging to **Fr1**, the proton at C5 atom of the furan ring forms the tightest contact with the fragment's binding site of the DnaN protein, while the contact of the neighboring proton at C4 with the protein's surface is less tight. Simultaneously, all other proton groups within the structure of **Fr1** (C3 protons on the fu-

ran ring and two groups of aromatic protons on the phenyl ring) form even less tight contacts with the protein surface with the relative level of STD effect about 50% (see **Figure 2**).

Out of several poses predicted by docking using SeeSAR 10.1 and prioritized by the HYDE scoring function[15,16] the one depicted in **Figure 2** matched the constraints imposed by observed STD-NMR signal intensities very well. In this pose, **Fr1** resides in *subsite I* of *M. tuberculosis* DnaN, the furan ring is buried deep in a hydrophobic pocket found within the subsite and the aniline part of the molecule is suggested to make mainly hydrophobic contacts within the *subsite I.*

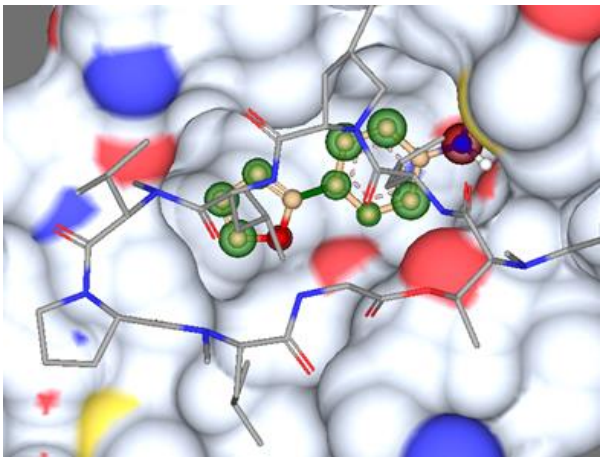

Figure 2. Predicted binding pose of **Fr1** (free base form), fitting STD-NMR observations, at subsite I of *Mycobacterium. tuberculosis* DnaN–GM (gray) cocrystal structure (PDB ID: 5AGU).[17]

The STD-NMR epitope mapping for the structure **Fr2** supports the pose depicted in **Figure 3**, where the 2-phenyl furan scaffold is positioned differently compared to that of **Fr1**. The furan ring is buried at an end of *subsite I* occupied by the aniline ring of **Fr1**, while the *ortho*-aniline ring of **Fr2** is partially exposed to the solution with its amino group. This aniline amino group is also suggested to form a hydrogen bond with the backbone of Arg-184. The protons on the opposite side of the phenyl ring point into a hydrophobic subpocket within *subsite I* without forming tight contact with the protein.

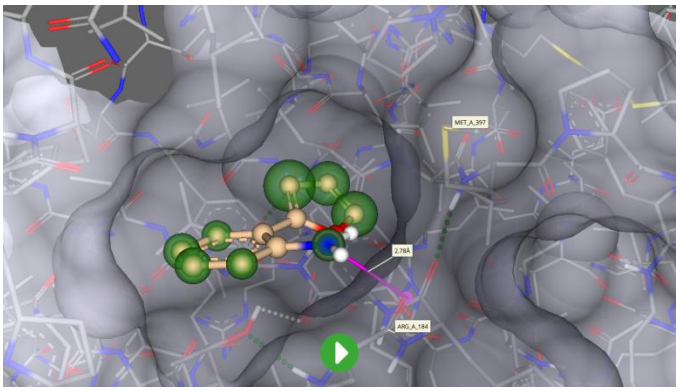

Figure 3. Predcited binding pose of **Fr2** (free base form) at subsite I of *M. tuberculosis* DnaN–GM cocrystal structure (PDB ID: 5AGU).[17]

In spite of seemingly plausible suggestions of docking studies supported by STD-NMR, the real binding modes of fragments **Fr1** and **Fr2** could be different from suggested ones and, furthermore, those could change owing to dynamicity of the protein–ligand complex upon the introduction of additional substituents into fragment hits during exploratory optimization. Therefore, we set out to explore various substitution patterns of the parent structures testing hypotheses, which are inspired by both STD-NMR and docking studies of **Fr1** and **Fr2** and their predicted interaction modes with *M. tuberculosis* DnaN.

4.2.4 Fragment optimization

We used SPR to assess binding affinity for DnaN and performed MIC tests against a panel of representative Mycobacteria (*Mycobacterium smegmatis MC^{2}155*, *Mycobacterium smegmatis MC^{2}155 GM^R* - in-house mutant strain, resistant to griselimycin), Gram-positive (*Streptococcus pneumoniae DSM20566, Staphylococcus aureus Newman)* and Gram-negative (*Escherichia coli ΔacrB)* bacteria to keep track of antibacterial activities of the derivatives originating from structures **Fr1** and **Fr2**.

Regioisomers of Fr1 and Fr2. Since fragments **Fr1** and **Fr2** are regioisomers, we synthesized the fragment **3** to complement the collection of possible isomers and evaluate the importance of the amino group at different positions on the phenyl ring (**Table 2**).

Table 2. DnaN binding and antibacterial activity of **Fr1** and **Fr2** analogues.

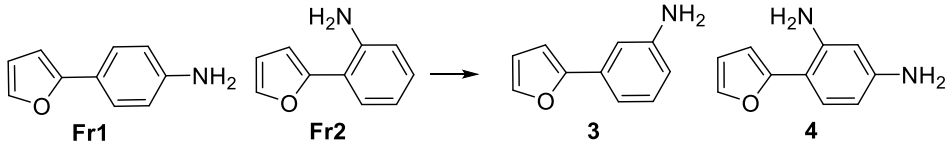

Name	SPR (*RU*)		MIC$_{95}$ (*μM*)				
	125 μM	250 μM	*M. smegmatis*	*M. smegmatis GM^r*	*S. pneumoniae*	*S. aureus*	*E.coli ΔacrB*
Fr1	**7**	**15**	**2**	**2**	> 128	> 128	> 128
Fr2	**12**	**34**	**32**	**32**	**8**	**32**	**64**
3	--	**42**	**32**	**32**	**32**	**64**	**128**
4	0	0	> 128	> 128	> 128	> 128	> 128

-- no data available.

The SPR responses of both *ortho*- and *meta*-isomers of **Fr1** were more than twice higher than that of **Fr1,** which indicates better affinity of **Fr2** and **3** for DnaN. Simultaneously, fragment **Fr1** demonstrated extraordinary activity against *M. smegmatis* (MIC = 2 *μM* in both wild-type and resistant strains) from the very beginning, while its isomers **Fr2** and **3** had modest activity. However, activity of **Fr2** and **3** turned out to be not limited to *M. smegmatis* as the positional isomers of **Fr1** were also active against other bacteria in the screening panel (**Table 2**). This disconnect between the β-clamp binding and antibacterial activity, along with the absence

of attenuation of the fragments' activity against the mutant *M. smegmatis* strain, which overexpresses the DnaN gene, suggests that the mechanism of action also involves interaction with targets besides the sliding clamp.

With an idea to combine the positive impacts of the amino groups in compounds **Fr1** and **Fr2**, we synthesized compound **4**, which surprisingly failed to show any DnaN binding and antibacterial activity, rendering the 1,3-diamino substitution pattern of the phenyl ring unfavorable.

Exploratory optimization of Fr1

***Replacements for the 2-furan*.** To probe for the response to changing the original 2-furyl substituent, we synthesized a small library of corresponding analogues of **Fr1**.

The first part focuses on the replacement of the 2-furyl ring with various five-membered heterocycles. The performance of the analogues is summarized in **Table 3**.

Table 3. DnaN binding and antibacterial activity of **Fr1** analogues carrying various aryl groups.

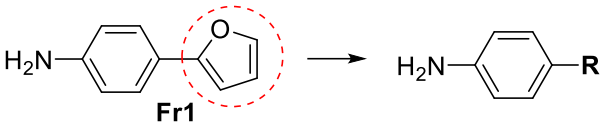

Name	R	SPR (*RU*)		*MIC*$_{95}$ (*μM*)				
		125 μM	250 μM	*M. smegmatis*	*M. smegmatis GM*^{r}	*S. pneumoniae*	*S. aureus*	*E.coli ΔacrB*
Fr1	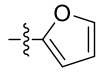	**7**	**15**	**2**	**2**	> 128	> 128	> 128
5	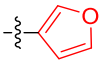	0	0	**1**	**1**	128	> 128	> 128
6	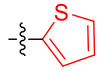	**9**	**16**	**0.5**	**1**	128	> 128	> 128
7	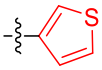	**68**	**137**	**0.5**	**0.5**	> 128	> 128	> 128
8	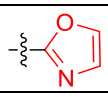	0	0	**16**	**16**	**128**	> 128	> 128
9	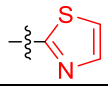	0	0	**32**	**32**	> 128	> 128	> 128
10	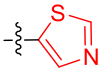	**20**	**4**	**4**	**4**	> 128	> 128	> 128
11	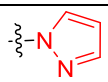	0	0	**8**	**8**	> 128	> 128	> 128
12	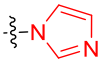	--	**8**	> 128	> 128	> 128	> 128	> 128
13	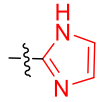	--	**18**	> 128	> 128	> 128	> 128	> 128
14	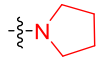	0	0	> 128	> 128	> 128	> 128	> 128
15	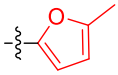	0	0	**16**	**16**	> 128	> 128	> 128
16	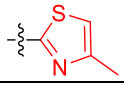	0	**2**	**16**	**16**	> 128	> 128	> 128

-- no data available.

We found the 3-thienyl derivative **7** to give the highest SPR response and antibacterial activity. Although its isomer **6** showed DnaN binding comparable to that of **Fr1**, it showed similar antibacterial activity, which was attenuated in the case of mutant *M. smegmatis*. Simultaneously, compound **5** unexpectedly turned out to be a non-binder according to SPR, still demonstrating high activity against both strains of *M. smegmatis*, which can be attributed to off-target interaction. The same considerations may hold true for analogues **8**, **9**, and **11**.

Incorporation of nitrogen in position 3 of the heterocycle is generally not favorable (compounds **8** and **9**). Exceptionally, the isomeric thiazole **10** showed improved DnaN binding com-

pared to its progenitor **6**, which, however, was not reflected in an increase in antibacterial activity.

Nitrogen-based hetarenes (**11**, **12** and **13**) were not productive and resulted in significant loss of target binding compared to the parent molecule **1** and abolition of antibacterial effect, which was retained only in the case of pyrazole **11** (not corroborated by DnaN binding).

On the other hand, the introduction of methyl into the position forming the tightest contact with DnaN according to STD-NMR was shown to be deleterious binding affinity (**15**), and led to a 4-fold drop in antibacterial activity. These observations can be considered a confirmation of an insight provided by a relative STD effect at the C5 position of furan.

Six-membered ring replacements of the 2-furan. The second part of the analogue library containing possible replacements of the furan ring in **Fr1** comprised variously substituted 4-aminno biphenyls. The binding and antibacterial activity of the analogues are summarized in **Table 4**.

The biphenyl analogue **17** showed somewhat diminished SPR response, while its activity against *M. smegmatis* was two times higher compared to parent furan **Fr1**. This data can be interpreted in favor of the tolerance of the replacement of the furan ring with a larger phenyl one.

Within the aforementioned library a series of fluorine-containing biphenyls were designed to probe for space-filling possibilities within the hydrophobic binding pocket originally presumed to be occupied by a furan ring. While the introduction of fluorine into the positions 2' and 4' did not lead to any improvements, the substitution of the 3'-position resulted in a significant increase in SPR response in the case of derivative **19**, that also maintained a high activity against *M. smegmatis*. However, the attempt to further increase the size of substituent at the same position in **26** and **27** only led to a decrease in SPR response of the derivatives as well as their antibacterial activities.

Table 4. DnaN binding and antibacterial activity of **Fr1** analogues carrying various aryl groups.

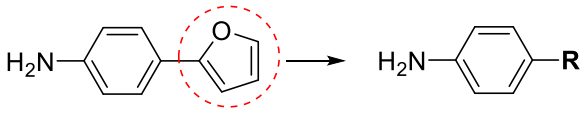

Fr1

Name	R	SPR (*RU*)		*MIC*$_{95}$ *(μM)*				
		125 μM	250 μM	*M. smegmatis*	*M. smegmatis GM*^{r}	*S. pneumoniae*	*S. aureus*	*E.coli ΔacrB*
Fr1		**7**	**15**	**2**	**2**	> 128	> 128	> 128
17	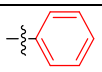	**4**	**14**	**1**	**1**	> 128	> 128	> 128
18	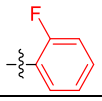	**7**	**18**	**2**	**4**	> 128	> 128	> 128
19	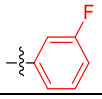	**26**	**57**	**2**	**2**	> 128	> 128	> 128
20	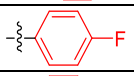	**--**	**16**	**2**	**4**	> 128	> 128	> 128
21	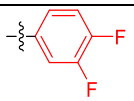	**2**	**5**	**2**	**2**	> 128	> 128	> 128
22	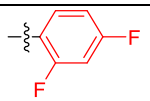	**9**	**18**	**16**	**16**	> 128	> 128	> 128
23	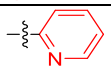	**11**	**31**	**16**	**16**	> 128	> 128	> 128
24	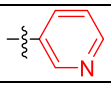	**0**	**5**	**--**	**--**	--	--	--
25	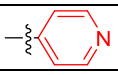	**0**	**0**	128	>128	>128	>128	>128
26	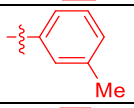	**8**	**18**	**16**	**32**	> 128	> 128	> 128
27	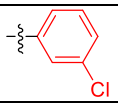	**0**	**0**	>128	>128	**64**	**64**	**64**

-- No data available.

The loss of DnaN binding observed for pyridine derivatives **24** and **25** served as additional indication of the hydrophobic character of the pocket accommodating the furan portion of the fragment hit **Fr1**.

Function of the aniline group. In order to shed light on the influence of amino groups in fragments **Fr1** and **Fr2** on their DnaN binding and antibacterial activities, we tested phenolic analogues **28** and **31** (**Table 5**).

The total loss of activity against *M. smegmatis* accompanied by the increase of SPR response demonstrated by compound **28** suggested the aniline moiety to be responsible for the an-

tibacterial effect. Simultaneously, no dramatic decrease of antibacterial activity resulted from the replacement of the amino group with hydroxyl in the structure of **Fr2** (compound **31**).

Table 5. SPR responses and antibacterial activity of oxy-analogues of **Fr1** and **Fr2**.

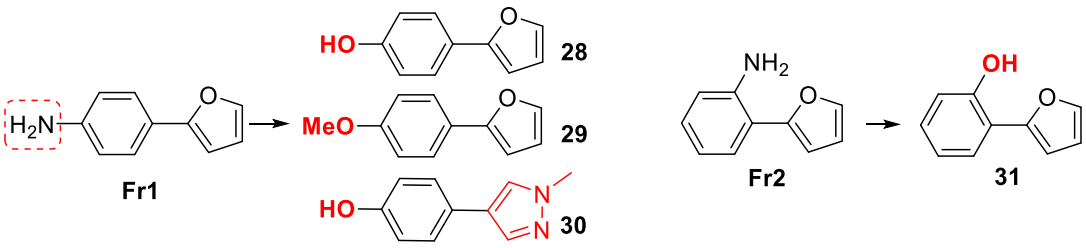

Name	SPR (*RU*)		MIC$_{95}$ (*μM*)				
	125 μM	250 μM	*M. smegmatis*	*M. smegmatis GM^r*	*S. pneumoniae*	*S. aureus*	*E.coli ΔacrB*
Fr1	**7**	**15**	**2**	**2**	> 128	> 128	> 128
Fr2	**12**	**34**	**32**	**32**	**8**	**32**	**64**
28	--	**28**	> 128	> 128	**64**	> 128	> 128
29	--	--	**64**	**64**	**16**	**64**	**128**
30	**17**	**41**	> 128	> 128	> 128	> 128	> 128
31	--	**35**	**64**	**64**	**32**	**64**	> 128

-- No data available

The *O*-methylation of **28** afforded **29**, which showed inconclusive SPR behavior (presumably because of dramatically reduced solubility) yet detectable activity against microorganisms in the testing panel. Replacing the original 2-furyl moiety with an *N*-methyl-pyrazole ring in the phenol **28** led to a significant increase in DnaN binding. This substitution of the furan moiety demonstrated promising potential.

Combining amine permutations with 3-thienyl. The replacement of 2-furyl group with 3-thienyl for **Fr1** was demonstrated to be associated with the highest increase of SPR response and improvement of activity against *M. smegmatis*. To evaluate the effect of the same replacement in the regioisomers of **Fr1** (**Fr2** and **3**), we synthesized their 3-thienyl analogues **32** and **33** (**Table 6**).

In case of the modification of **Fr2**, its binding ability remained essentially unchanged in **32**, while for **3** it resulted in total loss of binding to DnaN. A similar trend was observed for antibacterial activity: as a result of furan replacement the activity was diminished in both cases.

Table 6. SPR responses and antibacterial activity of 3-thienyl-substituted analogues of **Fr2** and **3**.

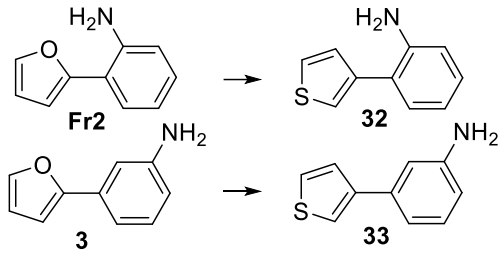

Name	SPR (*RU*)		MIC$_{95}$ *(μM)*				
	125 μM	250 μM	*M. smegmatis*	*M. smegmatis GM^r*	*S. pneumoniae*	*S. aureus*	*E.coli ΔacrB*
Fr2	**12**	**34**	**32**	**32**	**8**	**32**	**64**
3	**--**	**42**	**32**	**32**	**32**	**64**	**128**
32	**--**	**28**	> 128	> 128	> 128	> 128	> 128
33	0	0	**64**	**64**	> 128	> 128	> 128

-- No data available

Overall, the binding to β-clamp of **Fr1** and **Fr2**, seems to be much more tolerant to modifications than that of the other positional isomer **3**. For this reason, our major SAR exploration and optimization efforts will be concentrated around the structures of **Fr1** and **Fr2**.

***Substitutions in 2-position of the phenyl ring*.** According to the relative transfer difference intensities revealed by STD-NMR measurements, the phenyl protons next to the amino group in **Fr1** were in a looser contact with the β-clamp, which calls for the introduction of substituents next to the aniline moiety (see **Table 7** for synthesized analogues).

Table 7. SPR responses and antibacterial activity of *ortho*- substituted analogues of **Fr1**.

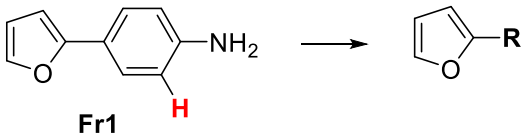

Fr1

Name	R	SPR (*RU*)		MIC$_{95}$ (*μM*)				
		125 μM	250 μM	*M. smegmatis*	*M. smegmatis GM^r*	*S. pneumoniae*	*S. aureus*	*E.coli ΔacrB*
Fr1	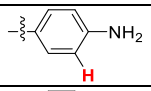	**7**	**15**	**2**	**2**	> 128	> 128	> 128
34	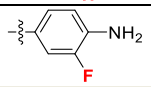	**20**	**42**	**32**	**32**	**64**	>128	>128
35	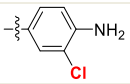	**--**	**43**	**32**	**32**	**64**	>128	>128
36	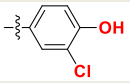	**--**	**5**	**128**	**128**	**128**	**64**	**128**
37	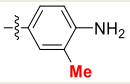	**7**	**19**	**32**	**32**	**16**	**64**	>128
38	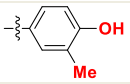	**--**	**19**	**128**	**128**	**64**	**128**	**128**
39	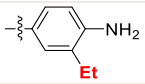	**--**	**29**	**64**	**64**	**16**	**64**	>128
40	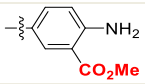	**1**	**10**	**64**	**64**	**32-64**	**64**	**64**
41	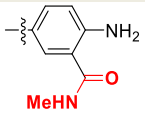	**14**	**35**	**64**	**64**	**16**	**128**	> 128
42	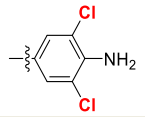	**--**	**107**	**16**	**128**	> 128	**128**	**128**
43	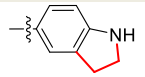	**--**	**--**	**8**	**8-16**	**1**	**4**	**32**
44	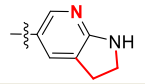	**--**	**22**	**64**	**32**	**64**	**32**	**64**
45	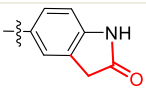	**--**	**--**	**128**	> 128	> 128	> 128	> 128

-- No data available

Overall, this *ortho*-position appears to be highly sensitive to the introduction of small substituents. Thus, the fluoro- and chloro-derivatives of **Fr1 34** and **35** demonstrated considerably better DnaN binding, while slightly more bulky methyl- and ethyl-derivatives **37** and **39** showed more modest improvement of target binding, which indicates the limited ability of the binding site to accommodate larger substituents at this position. The introduction of chlorines into both available *ortho*-positions resulted in **42**, which showed the highest SPR response in the series together with the very clear shift in the activity against wild-type and mutant *M. smegmatis.*

These observations validate **42** as a stronger DnaN binder and its antibacterial action is likely mainly due to DnaN inhibition.

The phenolic analogues of **35** and **37** had shown contradictory behavior in screening: while the *ortho*-cresol **38** showed similar DnaN binding, its *ortho*-Cl analogue **36** demonstrated a significantly decreased SPR response. However, both analogues showed the same decrease in antibacterial activity compared to the corresponding anilines **35** and **37**, which could be associated exclusively with the presence of an aniline amino group in the structures.

The cyclized derivatives **43**–**45** were inspired by the *ortho*-ethyl derivative **39**. Surprisingly, the conformational restriction of the ethyl group in **43** was associated with significantly improved activity against the entire microorganism panel (**Table 7**). However, the IC_{50} exhibited by this compound in the HepG2 cell viability test was 0.5 μM, which indicates that its cytotoxicity may be the cause of the improved antibacterial activity. At the same time, more polar analogues **44** and **45** demonstrated much more modest activity against bacteria.

Substitutions in 3-position. Having established the preferred nature for the substituents directly next to the amino group, we evaluated a small series of substitutions in the 3-position of the phenyl ring in compound **Fr1** as depicted below (**Table 8**).

We introduced a methyl group into **Fr1** making **46** to probe for tolerance of additional substituents in this position of the ring. This resulted in a two-fold improvement of the compound's response in SPR, while the activity against *M. smegmatis* dropped significantly from 2 μM to 32 μM.

Table 8. SPR responses and antibacterial activity of compounds substituted in 3-position of **Fr1.**

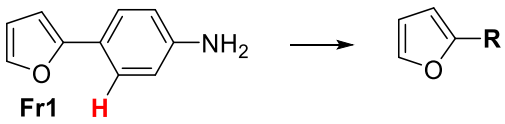

Name	R	SPR (*RU*)		MIC$_{95}$ (*μM*)				
		125 μM	250 μM	*M. smegmatis*	*M. smegmatis GM^r*	*S. pneumoniae*	*S. aureus*	*E.coli ΔacrB*
Fr1	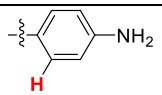	**7**	**15**	**2**	**2**	> 128	> 128	> 128
46	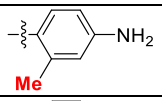	**14**	**35**	**32**	**32**	**128**	>128	>128
47	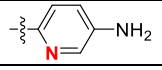	**4**	**15**	**8**	**8**	> 128	> 128	> 128
48	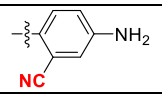	--	**47**	**8**	**8**	> 128	**64**	> 128

-- No data available

The introduction of pyridine nitrogen in the same position was well-tolerated: we observed only an insignificant drop in SPR response with the simultaneous decrease in corresponding MIC

values from 2 to 8 μM. The position was also substituted with cyano group in compound **48**. As a result, the binding to DnaN increased along with the activity against *M. smegmatis* (MIC = 8 μM).

Double substitutions of positions 2-, 3-, 5- and 6. To explore the possibilities of combining positive impacts from simultaneous *ortho*- and *meta*- substitutions, we synthesized a number of derivatives carrying fairly small substituents at those positions (**Table 9**).

Table 9. SPR responses and antibacterial activity of doubly substituted analogues of **Fr1**.

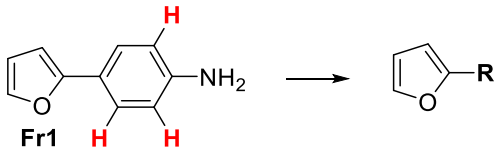

Name	R	SPR (*RU*)		MIC$_{95}$ (*μM*)				
		125 μM	250 μM	*M. smegmatis*	*M. smegmatis GM^r*	*S. pneumoniae*	*S. aureus*	*E.coli ΔacrB*
Fr1	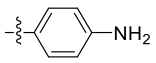	**7**	**15**	**2**	**2**	> 128	> 128	> 128
49	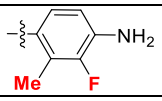	--	--	**64**	**128**	**16**	**32**	~128
50	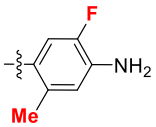	--	--	**16**	**32**	**32**	**64**	> 128
51	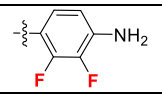	--	--	**64**	**128**	**32**	**32**	> 128
52	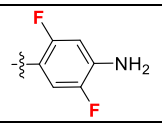	--	--	**64**	**128**	**16**	**32**	~128

- No data available

Two variants of substituent combinations inspired by compounds **34** and **46** gave positional isomers **49** and **50**, of which the latter showed improved antibacterial activity compared to both of its progenitors. The introduction of two fluorines into **Fr1** following the same logic (**51**, **52**), however, failed to deliver derivatives with improved antibacterial activity.

It is remarkable that compounds **49**–**52** did not give reproducible response in SPR experiments. This could be attributed to their increased lipophilicity caused by the simultaneous introduction of both methyl and fluoro substituents, which perhaps adversely impacted the analogues' aqueous solubility.

Combining positive impacts of some prior modifications. Taking into account the tolerance of the introduction of the Me-group into the 2-position in **29**, we introduced it into the structures **7** and **17**, obtaining analogues **54** and **53**, respectively. Surprisingly, the *ortho*-Me

compound **54** showed a significant decrease in SPR response compared to **7** as well as decrease in ability to inhibit the growth of *M. smegmatis* (**Table 10**).

The decrease of DnaN binding following the introduction of chlorine in **55** caused the decrease in antibacterial activity to 8 μM.

Table 10. SPR responses and antibacterial activity of substituted analogues of **7** and **17**.

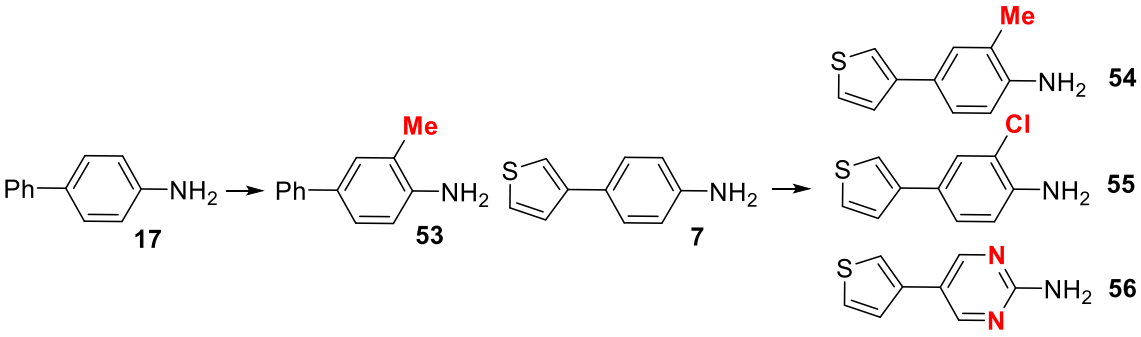

Name	SPR (*RU*)		MIC$_{95}$ (*μM*)				
	125 μM	250 μM	*M. smegmatis*	*M. smegmatis GM^r*	*S. pneumoniae*	*S. aureus*	*E.coli ΔacrB*
7	**68**	**137**	**0.5**	**0.5**	> 128	> 128	> 128
17	**4**	**14**	**1**	**1**	> 128	> 128	> 128
53	**0**	**1**	**8**	**8–16**	> 128	> 128	> 128
54	**10**	**25**	**4**	**4**	> 128	> 128	> 128
55	**--**	**64**	**8**	**8**	> 128	> 128	> 128
56	**0**	**2**	> 128	> 128	> 128	> 128	> 128

-- No data available

We synthesized compound **56** with the idea to decrease the lipophilicity of **7** and probe for tolerance of this type of substitution at this particular position of the phenyl ring. Derivative **56** barely showed any binding and antibacterial activity, making this type of derivatization unfavorable.

Refining the predicted binding pose of Fr1

Correlating slight modifications of **Fr1** structure with the change in the binding affinity for DnaN makes it possible to reconsider the presumed binding pose of **Fr1**. In the light of the observed positive impact of substitutions on the phenyl ring, we suggest the orientation of **Fr1** on **Figure 4** to better fit the experimental binding data.

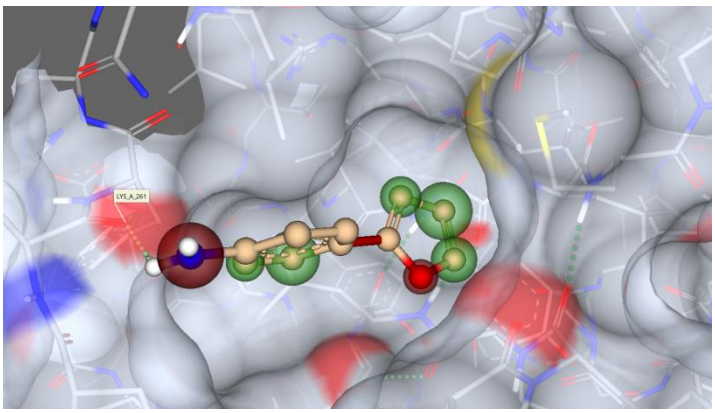

Figure 4. More plausible presumed binding mode of **Fr1** and its derivatives.

In the aforementioned docking solution, the amino group of **Fr1** projects out of the *subsite I* and the furan ring is suggested to be buried deeper in the subsite. The *ortho*- and *meta*-positions of the phenyl ring are presented with space within *subsite I* just enough to accommodate aforementioned substituents consisting of 1 to 4 heavy atoms.

Simultaneously, the suggested orientation of the amino group of **Fr1** towards solution makes it possible to support the growing attempts using this vector with modeling.

***Growing attempts for Fr1*.** The extensions of the original $–NH_2$ group were supported by modeling and capitalized on docking poses akin to that provided on **Figure 4**, which suggested the amino group pointing towards the solution from the *subsite I*.

Table 11. SPR responses and antibacterial activity of grown derivatives of **Fr1.**

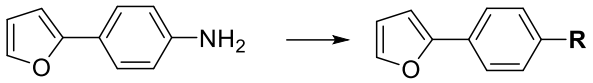

Fr1

Name	R	SPR (*RU*)		MIC$_{95}$ (*μM*)				
		125 μM	250 μM	*M. smegmatis*	*M. smegmatis GM^r*	*S. pneumoniae*	*S. aureus*	*E. coli ΔacrB*
Fr1	**-NH$_2$**	**7**	**15**	**2**	**2**	> 128	> 128	> 128
57	**-NHBz**	--	**76**	> 128	> 128	> 128	> 128	> 128
58	**-NHSO$_2$Ph**	--	**25**	> 128	> 128	> 128	> 128	> 128
59	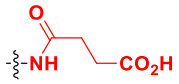	--	--	> 128	> 128	> 128	> 128	> 128
60	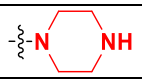	--	--	**64**	**64**	**8**	**16**	**128**
61		--	--	**64**	**128**	**16**	**32**	**128**
62	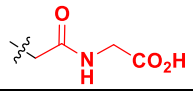	--	--	**32**	**32**	**32**	**4–8**	> 128
63	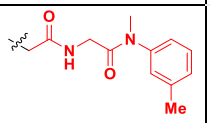	--	**44**	**128**	**64**	**64**	> 128	**128**

-- No data available

The benzoylation, benzosulfonylation and succinylation of the amino group were supposed to probe for available interactions at the extension site: hydrophobic/water displacement in case of **57** and **58,** and hydrogen bond donors in case of **59**. The benzoylated **Fr1** showed significantly increased SPR response and lost activity against *M. smegmatis*; the same trend (though to a lesser extent) was displayed by the sulfonylated analogue **58**.

Slight extension of the amino group by converting it into piperazine **60** was aimed at involving the side chain of Arg-184 into hydrogen bonding, while the acetylated derivative **61** precluded this supposed interaction. Although the binding to DnaN monitored by SPR turned out to be non-conclusive, the antibacterial activity of **60** was slightly higher, which could be interpreted as indirect evidence of better engagement of **60** with the target protein.

The extension **62** was designed to have analogous functions with **59** as the topological distance from the phenyl ring to the free carboxyl was kept the same. Derivative **62** was, however, equipped with a more hydrophilic linker, which was supposed to increase the compound's polarity and solubility - the compound had unfortunately shown inconclusive DnaN binding with modest antibacterial activity.

The amide **63** was designed on the basis of modeling of **62** into the *subsite I* of *M. tuberculosis* DnaN, which suggested the new hydrophobic interactions to take place on the protein surface adjacent to *subsite I*. Interestingly, **63** demonstrated modest SPR response and antibacterial activity, which turned out to be slightly higher in the case of resistant *M. smegmatis* mutants. This disconnect indicates potential absence of a causal relationship between DnaN inhibition by **63** and its antibacterial activity.

Summary for Fr1 derivatives with positive impact on DnaN affinity and antibacterial activity.

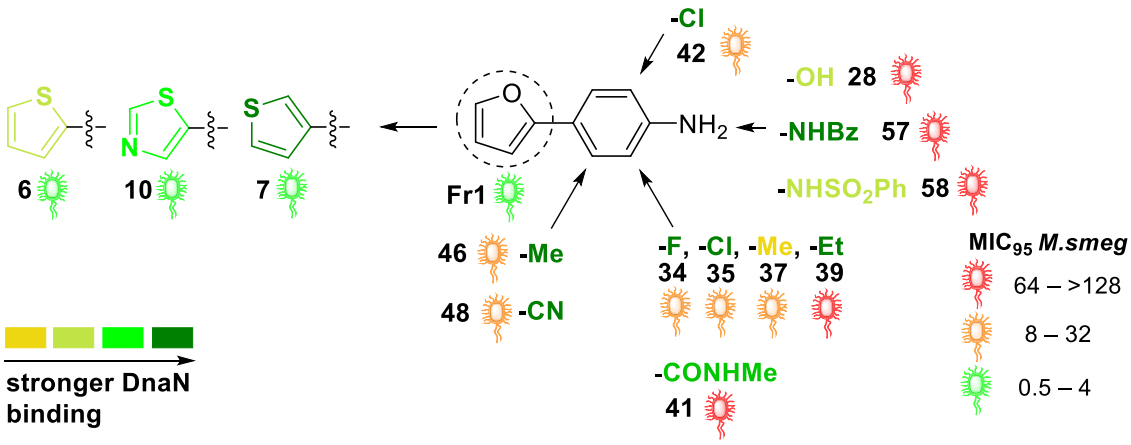

Figure 5. Graphical summary of positive impacts on DnaN binding and antibacterial activity associated with introduction of certain substitutions in **Fr1** structure.

The molecular features of the original structure of **Fr1** were comprehensively explored and the following structure–activity relationships (SAR) were established.

- The best binding to DnaN was achieved with a 3-thienyl in place of the original 2-furyl ring.
- The amino group has no significant importance for targeting protein binding; however, it can be responsible for the antibacterial effect as shown by the majority of active derivatives.
- The introduction of relatively small (1 to 4 heavy atoms) substituents into positions of the phenyl ring adjacent to the NH_2 group and next to the furan ring is tolerated and was shown to lead to gains in both DnaN binding and antibacterial activity. This can be associated with more efficient occupation of *subsite I* of β-sliding clamp and/or binding driven by entropy gains.
- The two above-mentioned modifications of **Fr1** structure, however, were found to be non-combinable, confirming a non-additive SAR.
- The extension attempts undertaken at the position of the amine in the original structure were shown to provide gains in DnaN binding (compounds **57** and **58**), while antibacterial activity of grown substances was negatively affected.

Exploratory optimization of Fr2

Based on the docking pose of **Fr2** depicted in **Figure 3**, we first aimed at exploring the substitution possibilities at positions across the phenyl ring in order to obtain experimental validation for the calculated pose. Second, we undertook the growing attempts based on the amino group of **Fr2** in order to explore the possibilities of targeting other subsites of DnaN.

Substitution of 4-position of the phenyl ring. According to previously mentioned STD-NMR measurements (**Figure 1**) and modeling (**Figure 3**), the proton in this position does not form a tight contact with DnaN and thereby creates the opportunity for substitution (**Table 12**).

Table 12. SPR responses and antibacterial activity of 3-substituted analogues of **Fr2**.

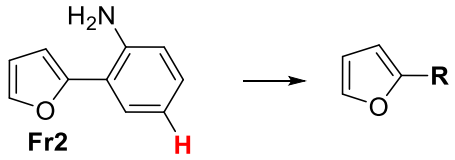

Name	R	SPR (RU)		*MIC95 (μM)*				
		125 μM	250 μM	*M. smegmatis*	*M. smegmatis GMr*	*S. pneumoniae*	*S. aureus*	*E.coli ΔacrB*
Fr2	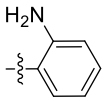	**12**	**34**	**32**	**32**	**8**	**32**	**64**
64	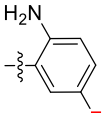	--	--	**64**	**64**	**16**	**32**	**128**
65		--	**2**	**128**	**128**	**64**	**128**	> 128
66	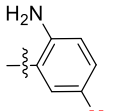	--	**37**	> 128	> 128	**64**	**64**	**64**
67	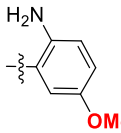	--	**35**	> 128	> 128	**64**	**64**	> 128
68	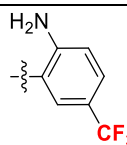	--	**0**	**64**	**64**	**32**	**64**	**64**
69	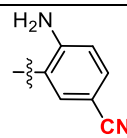	--	**28**	> 128	> 128	**64**	**32**	> 128

-- No data available

Overall, the size and electronic nature of substituent in this position had virtually no influence on the analogues' binding affinity with the exceptions of Cl- and CF_3- moieties, which had

significantly attenuated SPR response relative to the corresponding derivatives. Simultaneously, all substituted analogues demonstrated almost no antibacterial activity: only the marginal activity was detected for F-, Cl- and -CF_3 substituted derivatives. Therefore, the appropriate substitutions at this position could be made for increasing fragment's binding and combined with other substitutions.

Outstanding performance of compound 65 in STD-NMR analysis

Based on the suggested docking pose and relatively favorable HYDE scoring[15] (**Figure 6B**), the compound **65** was chosen to be subjected to single-point STD-NMR measurements in the presence of *M. tuberculosis* DnaN protein. In spite of relatively weak binding by SPR, compound **65** showed high proton signals intensities in its STD-NMR difference spectrum. The relative intensities in the difference spectrum are depicted in **Figure 6A** and are in good accordance with the presumed binding mode of **65** (**Figure 6B**). The respective spectra are provided in Supplementary material (Figures **S16**–**S17**).

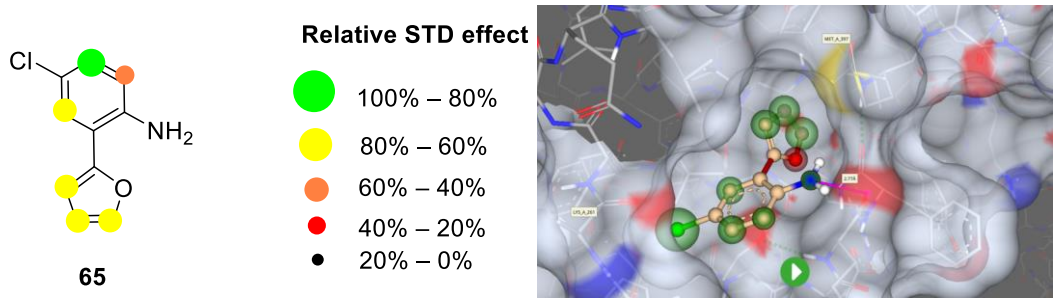

Figure 6. A) Relative intensities of protons in **65 B)** Predicted pose of **65** in *subsite I* (PDB code: 5AGU).[17]

This derivative of **Fr2** was therefore taken into consideration because of its outstanding performance in the STD-NMR DnaN binding test, which was consistent with the docking pose we previously capitalized on. Moreover, its substitution pattern inspired the exploration of **Fr2** derivatives whose substitution patterns closely resembled the one of compound **65**.

Substitution in both meta-positions within the Fr2 structure. According to the modeling and STD-NMR, the position 3 of the phenyl ring of **Fr2** could be used for the exploration of growing possibilities.

The introduction of fluorine and chlorine atoms into the 5-position of the phenyl ring resulted in diminution of DnaN binding and antibacterial activity of **70** and **71**. The antibacterial activity of the methoxy-derivative **72** was also almost lost, however, its SPR response increased significantly (**Table 13**).

Table 13. SPR responses and antibacterial activity of 3- and 5-substituted analogs of **Fr2.**

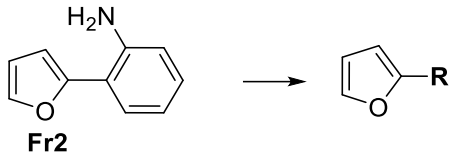

Name	R	SPR (*RU*)		MIC$_{95}$ (*μM*)				
		125 μM	250 μM	*M. smegmatis*	*M. smegmatis GM^r*	*S. pneumoniae*	*S. aureus*	*E. coli ΔacrB*
Fr2	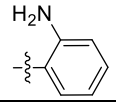	**12**	**34**	**32**	**32**	**8**	**32**	**64**
70	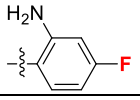	**12**	**26**	128	128	64	128	> 128
71	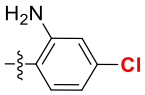	--	**10**	128	128	128	128	> 128
72	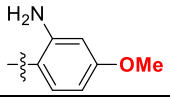	--	**65**	>128	>128	>128	>128	>128
73	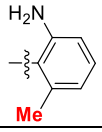	--	**33**	> 128	> 128	> 128	> 128	> 128
74		--	**37**	>128	>128	**64**	**64**	>128
75	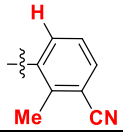	--	**54**	> 128	>128	>128	>128	> 128

-- No data available

An exploration of the possibilities of substitution at the 3-position of the phenyl ring by methyl and cyano groups revealed large tolerance of these moieties at that position, which was reflected in the retention of SPR responses by compounds **73** and **74**. The antibacterial activity was, however, completely abolished in both cases.

In order to estimate the potential additive effect of a combination of substitution patterns of **69** and **74**, we synthesized compound **75** that carried the methyl and nitrile moieties and was devoid of the amino group. It nevertheless showed a 1.5-fold increase in DnaN binding compared to **Fr2**, which underscored non-principal importance of amino group in this fragment class and the possibility of further development based on this substitution pattern.

Substitution of both 4- and 5- positions within the Fr2 phenyl ring. Aiming at combining our findings associated with a positive impact on **Fr2** DnaN binding, we synthesized certain **Fr2** analogues containing substitutions at both 4- and 5- positions (**Table 14**).

Table 14. Analogues combining successful substitutions in the phenyl ring of **Fr2**.

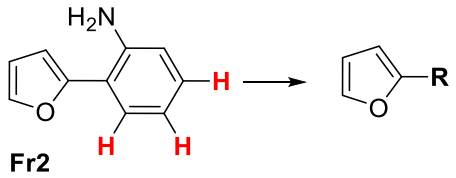

Fr2

Name	R	SPR (*RU*)		MIC$_{95}$ (*μM*)				
		125 μM	250 μM	*M. smegmatis*	*M. smegmatis GM^r*	*S. pneumoniae*	*S. aureus*	*E. coli ΔacrB*
Fr2	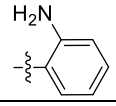	**12**	**34**	**32**	**32**	**8**	**32**	**64**
76	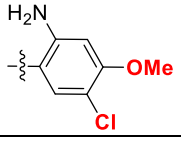	--	**11**	> 128	> 128	> 128	> 128	> 128
77	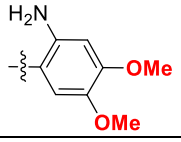	--	--	**128**	> 128	**32**	**32**	> 128
78	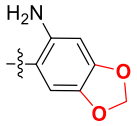	--	--	**64**	**64**	**16**	**8**	~128
79	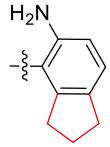	--	**72**	**64**	>128	**32**	**32**	>128

-- No data available

The case of **76** exemplified the superposition of detrimental (4-Cl in **65**) and positive (5-OMe in **72**) impacts associated with these analogues of **Fr2** showing considerable decrease of SPR response and complete loss of antibacterial activity. The combination of two methoxy groups placed in *para*- and *meta*- positions gave rise to a better-performing derivative **77** with fairly weak activity against *M. smegmatis*. The dioxole analogue of **77** – compound **78** – had demonstrated slightly better overall antibacterial activity compared to **77**, which could potentially indicate improved steric compatibility of **78** with the corresponding region of *subsite I* relative to its progenitor.

The only derivative in the series carrying a substitution pattern formally similar to that of **75** was indane **79,** which demonstrated the greatest SPR response in the series along with slight antibacterial activity. This was also accompanied by an increase in MIC values against the mutant *M. smegmatis* strain, which serves as evidence of DnaN-mediated antibacterial action mechanism.

Modifications of the indane 79. In order to explore the possibilities of further improvement of DnaN binding of **79**, we equipped it with groups that were previously shown to have a positive impact on DnaN binding in the case of **Fr1** (**Table 15**).

Table 15. SPR responses and antibacterial activity of **79** derivatives.

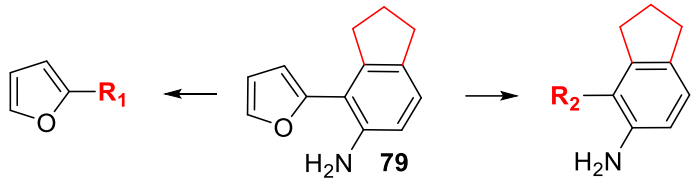

Name	R1, R2	SPR (*RU*)		*MIC95 (μM)*				
		125 μM	250 μM	*M. smegmatis*	*M. smegmatis GMr*	*S. pneumoniae*	*S. aureus*	*E. coli ΔacrB*
79	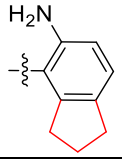	--	**72**	**64**	**>128**	**32**	**32**	>128
80	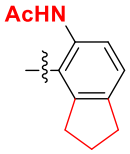	--	--	**32**	**64**	**8**	**8**	**128**
81	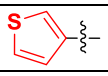	--	**38**	> 128	> 128	> 128	> 128	> 128
82	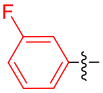	--	--	**128**	> 128	> 128	> 128	> 128

-- No data available

In order to estimate the contribution of the free amino group and explore the possibilities of growing in its direction, we synthesized the acetylated derivative **80**. In spite of non-conclusive SPR behavior, **80** demonstrated improved activity against the panel of microorganisms, which was complemented by the difference in activities against wild-type and mutant *M. smegmatis* strains. The replacements of the furan ring by 3-thienyl and 3-fluorophenyl groups, however, led to significant diminution of DnaN binding of **81** and **82** and their respective antibacterial activities, probably owing to the compounds' decreased solubility.

Growing Fr2 from the amino group

We explored the possibilities for growing in the direction of the amino group of **Fr2** independently using the original structure of **Fr2** (**Table 16**).

Table 16. SPR responses and antibacterial activity of grown **Fr2** derivatives.

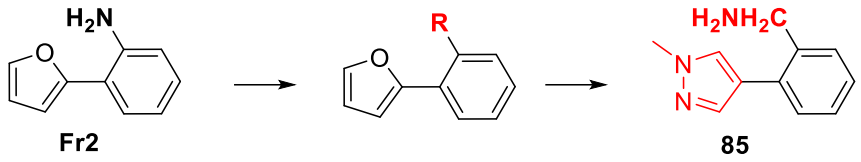

Name	R	SPR (*RU*)		MIC$_{95}$ (*μM*)				
		125 μM	250 μM	*M. smegmatis*	*M. smegmatis GM^r*	*S. pneumoniae*	*S. aureus*	*E.coli ΔacrB*
Fr2	-NH$_2$	**12**	**34**	**32**	**32**	**8**	**32**	**64**
83	-NHBz	--	**12**	128	128	128	> 128	> 128
84		--	**27**	**64**	**64**	**32**	**64**	**128**
85	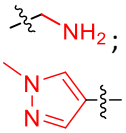	--	**21**	> 128	> 128	> 128	> 128	> 128
86		--	**51**	> 128	> 128	> 128	> 128	128
87	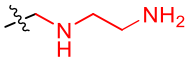	--	**0**	> 128	> 128	> 128	> 128	> 128
88	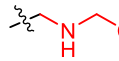	--	--	**32**	**32**	**16**	**32**	**64**
89	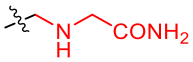	--	**13**	> 128	> 128	> 128	> 128	> 128
90	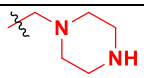	--	**1**	128	> 128	> 128	> 128	> 128
91	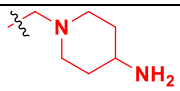	--	**26**	> 128	> 128	> 128	> 128	> 128

-- No data available

The benzoylated derivative **83** showed diminished binding response together with a loss of antibacterial activity, which halted further acylation-based extensions. Keeping in mind the presumed importance of the amino group, we tested the aminomethyl derivative **84**, which had, in spite of lowered antibacterial activity, largely retained DnaN binding. Surprisingly, its acetylated derivative **86** demonstrated even better binding to the target protein, which was, however, not supported by antibacterial activity.

Nevertheless, further extension attempts expressed in the synthesis of compounds **87**–**89** proved not productive as no improvements in DnaN binding were achieved. The SPR binding of **88** was found to be inconclusive and the HepG2 IC$_{50}$ of this compound was determined to be 6.7 μM (data not shown). Therefore, the antibacterial activity of **88** most likely originates from its cytotoxicity rather than the engagement with the β-sliding clamp.

The grown derivatives containing piperazine (**90**) and 4-aminopiperidine (**91**) fragments had also not shown any improvements in binding or antibacterial activity.

Growing 65 from the amino group

The presumed orientation of the molecule **65** in the *subsite I* and its activity in STD-NMR DnaN binding assay inspired us to undertake growing from the amino group of **65**. Nevertheless, taking into account the relatively high lipophilicity of **65** we first tried to replace the furan ring with of *N*-methyl-3-pyrazole, which gave rise to compound **92.** It had nevertheless no effect on performance compared to the original structure (**Table 17**).

Table 17. SPR responses and antibacterial activity of derivatives of **65** with extensions of its amino group.

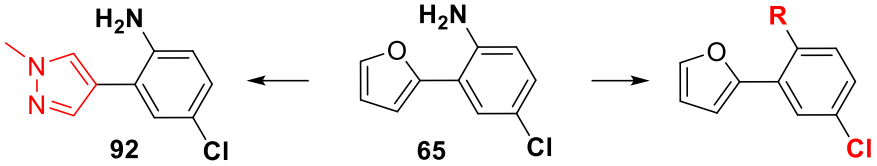

Name	R	SPR (*RU*)		MIC$_{95}$ (*μM*)				
		125 μM	250 μM	*M. smegmatis*	*M. smegmatis GM^r*	*S. pneumoniae*	*S. aureus*	*E. coli ΔacrB*
65	-NH_2	--	**2**	**128**	**128**	**64**	**128**	**> 128**
92	-NH_2; 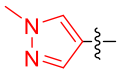		**3**	> 128	> 128	> 128	> 128	> 128
93	**-NHAc**		**0**	> 128	> 128	> 128	> 128	> 128
94	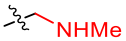		--	> 128	> 128	> 128	> 128	> 128
95	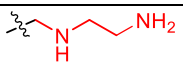		**8**	**128**	**128**	**128**	> 128	> 128
96	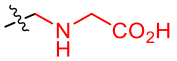		**10**	> 128	> 128	> 128	> 128	> 128
97	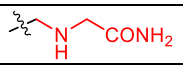		**32**	> 128	> 128	> 128	> 128	> 128
98	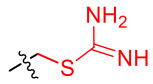		**36**	**32**	**64**	**32**	**128**	**64**
99	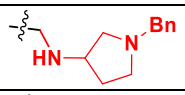		**2**	**64**	**32-64**	**32**	**128**	**128**
100	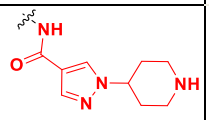		**19**	> 128	> 128	>128	> 128	> 128
101	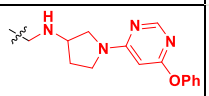		**30**	> 128	> 128	> 128	> 128	> 128

-- No data available

The effect of the acylation of amino group in **93** was detrimental for both binding and antibacterial activity. The replacement of the original amine with various substituted methylamine moieties in **94**–**97** proved not particularly productive with only acetamide **97** showing appreciable DnaN binding without concomitant antibacterial activity.

The extended isothiourea **98** had shown moderate antibacterial activity, the relevance of which to DnaN binding was corroborated by the compound's SPR response and the detectable attenuation of activity against the mutant strain of *M. smegmatis*. Simultaneously, **98** did not demonstrate any cytotoxicity on the HepG2 cell line, which makes this compound best in the subseries. The observed improvements in antibacterial activity could be attributed to the positive charge conferred by the isothiouronium moiety, which is predicted to improve the compounds' penetration through bacterial cell walls.[18]

The design of other grown derivatives **99**–**101** was inspired by modeling and capitalized on the aforementioned pose of **65** in *subsite I*, which turned out to be invalid. For this reason, the detectable binding shown by these compounds could be regarded as coincidental and not be considered a signal for further optimization.

Short summary on Fr2 optimization

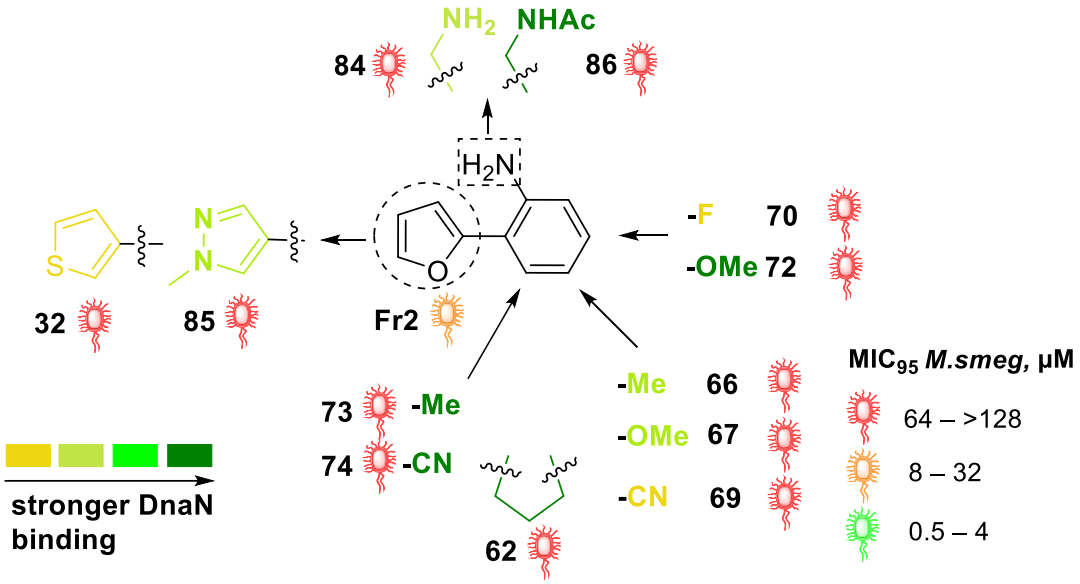

Figure 7. Graphical summary of beneficial substitutions introduced into the structure of **Fr2**.

- The introduction of small substituents on the phenyl ring of **Fr2** was found to be either tolerable or beneficial for both DnaN binding and antibacterial activity.
- In spite of dominating effect in STD-NMR competition experiments, the chloro-substituted derivative **65** and most of its grown derivatives had not shown superior binding to DnaN and antibacterial effects.
- Introduction of substituents in the *para*-position relative to the furan ring was also shown to be beneficial in almost all cases.
- Introduction of two substituents at adjacent positions of the phenyl ring was found to deliver derivatives with significantly higher DnaN affinities, which can account for better space filling within the *subsite I* of DnaN.

- The amino group belonging to the original structure was shown to not have critical importance for the **Fr2** binding affinity for DnaN.
- Growing in the direction of the amino group delivered compounds with higher affinities for DnaN.
- All aforementioned conclusions further validate the binding pose of **Fr2** suggested by docking (**Figure 3**)

Exploratory optimization and growing of compound 3

In the light of our previous findings regarding the presumed binding poses of **Fr1** and **Fr2**, we relied on the similarly oriented pose of **3** depicted in **Figure 8** and planned exploration and optimization of **3** accordingly.

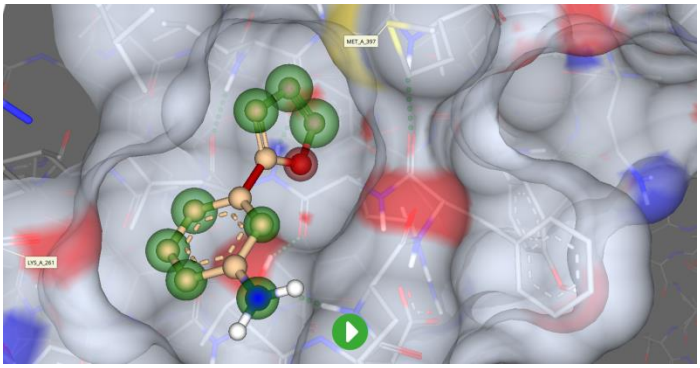

Figure 8. Docking pose of fragment **3** (free base) in the *subsite I* of *M.tuberculosis* DnaN (PDB code: 5AGU).[17]

Based on the previously attempted replacements of the furan ring with 3-thienyl in **33** and 2-thienyl in **6**, we synthesized compound **102** to assess the impact of 2-thienyl group in case of structure **3** together with a number of derivatives carrying substituents on the phenyl ring (**Table 18**).

Table 18. SPR responses and antibacterial activity of derivatives of **3** with various substitutions.

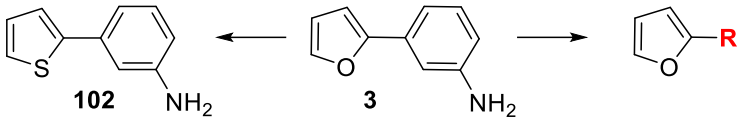

Name	R	SPR (*RU*)		MIC$_{95}$ (*μM*)				
		125 μM	250 μM	*M. smegmatis*	*M. smegmatis GM^r*	*S. pneumoniae*	*S. aureus*	*E. coli ΔacrB*
3	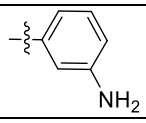		**42**	**32**	**32**	**32**	**64**	**128**
102		**42**	**91**	**16**	**16**	> 128	> 128	> 128
103	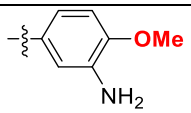		**40**	> 128	> 128	> 128	> 128	> 128
104	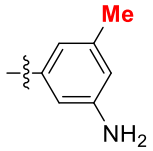	**0**	**5**	**8**	**16**	**64**	> 128	> 128
105	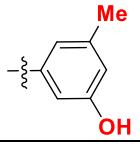	**0**	**--**	128	128	128	**64**	**32**

-- No data available

The 2-thienyl derivative **102** showed a substantial increase in SPR response together with the strain-specific decrease in MIC values against *M. smegmatis* compared to **3**. Introducing the methoxy group in the *ortho*- position in **103** barely influenced the DnaN binding, while the activity against bacteria was nullified. Simultaneously, the introduction of a *meta*-methyl substituent into **3** following the similar rationale for **1** and **2** yielded **104**, which demonstrated marginal DnaN binding along with increased antibacterial activity compared to **3**. The oxy-analogue of compound **104** had, however, shown inconclusive binding and only marginal antibacterial activity, which underscores the importance of the role played by the amino group in endowing this class of molecules with antibacterial activity.

Growing from the amino group

The grown derivatives **106** and **107** were inspired by modeling and designed in a way that the aryl group is flexibly attached to the amino group of parent fragment **3** and pointing in the direction of *subsite II*.

Table 19. SPR responses and antibacterial activity of grown derivatives of **3**.

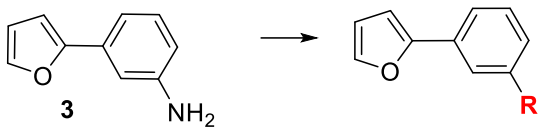

Name	R	SPR (*RU*)		MIC$_{95}$ (*μM*)				
		125 μM	250 μM	*M. smegmatis*	*M. smegmatis GM^r*	*S. pneumoniae*	*S. aureus*	*E. coli ΔacrB*
3	-NH_2		**42**	**32**	**32**	**32**	**64**	**128**
106	-**NHBn**	--	**16**	**32**	**32**	> 128	> 128	> 128
107	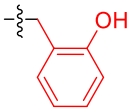	--	**0**	> 128	> 128	**32**	**64**	**64**

-- No data available

Both grown derivatives showed a considerable decrease in DnaN binding by SPR, yet the bacterial growth inhibitory ability remained essentially the same in the case of **106** compared to that of compound **3**. The hydroxy-substituted analogue of **106** had shown no DnaN binding and activity against *M. smegmatis*, which could account for a possible mismatch between the introduced hydroxyl and its supposed binding site within DnaN. Nevertheless, we demonstrated that placing relatively big substituents in the *meta*-position can be tolerated (to a certain extent), which inspired another series of grown derivatives addressing this position of **3**.

3-aryl benzylamines. Substitutions on the phenyl ring

Addressing the necessity to replace the original aniline group because of its presumed cytotoxicity and therefore positive influence on antibacterial activity combined with the intention to perform fragment growing in the same position prompted us to test the benzylamino derivative **108** and several of its substituted analogues (**Tables 20-21**).

Table 20. SPR responses and antibacterial activity of benzylamines designed on the basis of **3**

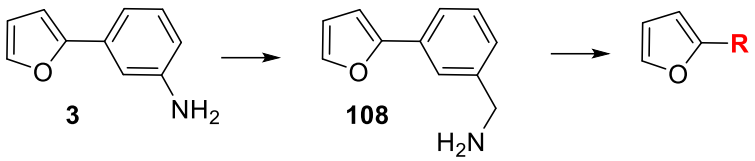

Name	R	SPR (*RU*)		MIC$_{95}$ (*μM*)				
		125 μM	250 μM	*M. smegmatis*	*M. smegmatis GM^r*	*S. pneumoniae*	*S. aureus*	*E. coli ΔacrB*
3	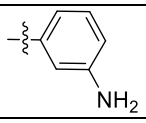		**42**	**32**	**32**	**32**	**64**	**128**
108	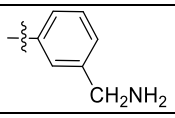		--	**4**	**4**	**64**	**16**	**32-64**
109	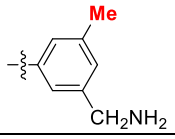		**27**	**64**	**64**	**32**	**128**	**128**
110	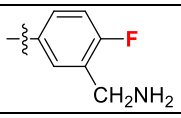		**42**	**64**	**64**	**16**	**64**	**128**

-- No data available

In spite of misbehavior on the SPR chip[1], the benzylamine **108** showed considerably improved activity against all bacterial strains in the testing panel, which could not be attributed to the presence of the aniline moiety anymore. Exploration of performance of substituted analogues **109** and **110** revealed the positive impact of the 6-fluorine on the fragment's DnaN binding behavior and a slight disadvantage of the 5-methyl substitution. The substantial drop caused by the substitutions on the phenyl ring of **108** were roughly equal in both cases.

3-Aryl benzylamines. Furan substitutions

We introduced 3-thienyl and *N*-methyl-4-pyrazolic replacements for the original furan in **111** and **112** based on their presumed beneficial impact on the compounds' target binding as was demonstrated previously (**Table 21**).

[1] Negative response values were observed

Table 21. SPR responses and antibacterial activity of analogues of compound **108**

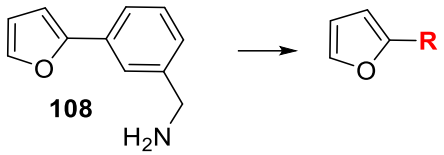

Name	R	SPR (*RU*)		MIC$_{95}$ (*μM*)				
		125 μM	250 μM	*M. smegmatis*	*M. smegmatis GM^r*	*S. pneumoniae*	*S. aureus*	*E. coli ΔacrB*
108			--	**4**	**4**	**64**	**16**	**32-64**
111	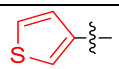		**4**	> 128	> 128	> 128	> 128	> 128
112	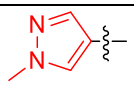		**30**	> 128	> 128	> 128	> 128	> 128

-- No data available

Surprisingly, the thienyl analogue **111** demonstrated a low SPR response and no antibacterial activity, which rendered the introduction of the 3-thienyl ring unfavorable in the case of 3-benzylic amines. Conversely, the pyrazole **112** showed good DnaN binding, which was, however, not supported by antibacterial activity.

Growing attempts of 3-arylbenzylamine 108

In order to further explore possibilities of growing, we synthesized a series of derivatives using the benzylamine **108** as a template. Our growing attempts supported by modeling gave rise to a number of derivatives which can be formally subdivided into several subclasses: *N*-acylated (**113-115**), *N*-alkylated (**116**, **117, 120, 121**) and *N*-arylated (**118**, **119**) benzylamines (**Table 22**).

Table 22.SPR responses and antibacterial activity of grown **108** derivatives.

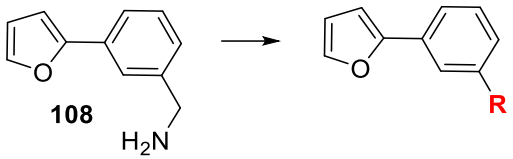

Name	R	SPR (*RU*)		MIC$_{95}$ (*μM*)				
		125 μM	250 μM	*M. smegmatis*	*M. smegmatis GM^r*	*S. pneumoniae*	*S. aureus*	*E.coli ΔacrB*
108			--	**4**	**4**	**64**	**16**	**32-64**
113			**10**	> 128	> 128	> 128	> 128	> 128
114	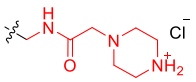		--	**16**	**16-32**	> 128	> 128	**64-128**
115	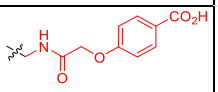		**70**	> 128	> 128	**64**	> 128	> 128
116	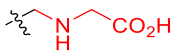		**23**	> 128	> 128	> 128	> 128	> 128
117	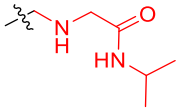		**98**	> 128	128	> 128	> 128	> 128
118	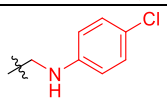		--	>128	>128	>128	>128	>128
119	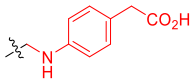		**41**	> 128	> 128	**64**	**64**	>128
120	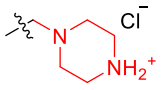		**15**	**64**	**64**	**32**	**8**	> 128
121	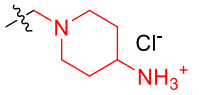		--	>128	**128**	> 128	> 128	> 128

-- No data available

First, we extended the benzylamine **108** by synthesizing the acetylated derivative **113**. Although **113** has shown only modest DnaN binding and no antibacterial activity, its further elongated derivative **114** exhibited a characteristic shift in activity against the mutant strain of *M. smegmatis*. The grown derivative **115** had surprisingly demonstrated considerable improvement in SPR response yet accompanied by scarcely detectable antibacterial activity.

The second approach implied growing by connecting alkyl chains to the benzylic amino group of **108**. As a result, the amino acid **116** was synthesized first, with an idea to perform further growing by taking advantage of amide-coupling chemistry, which was implemented in **118.** Even though both representatives of the class **116** and (especially) **117** had shown relatively

good binding to DnaN, their activity against microorganisms in the testing panel remained undetected.

The 3-arylated benzylamine **118** had demonstrated dramatically diminished solubility, which could account for its non-conclusive behavior during SPR measurements. The derivative **119,** however, demonstrated a high SPR response probably owing to better solubility or the involvement of the free carboxyl moiety in hydrogen bonding. Both arylated derivatives had, however, not shown antibacterial activity.

Analogous to the previously implemented extensions of **Fr1** and **Fr2,** we synthesized piperazine **121** and 4-aminopiperidine **122** as extensions of **108**. The piperazine derivative **121** showed low yet measurable DnaN binding and marginal antibacterial activity, while the aminopiperidine **122** did not demonstrate any appreciable activity.

Miscellaneous grown substituted benzylamines

Finally, we synthesized several derivatives of the benzylamine **108** whose structures were inspired by *in silico* modeling (**Table 23**).

Table 23. SPR responses and antibacterial activity of miscellaneous grown derivatives of **108**.

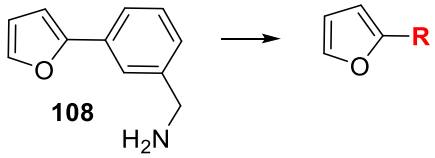

Name	R	SPR (*RU*)		MIC$_{95}$ (*μM*)				
		125 μM	250 μM	*M. smegmatis*	*M. smegmatis GM^r*	*S. pneumoniae*	*S. aureus*	*E. coli ΔacrB*
108			--	**4**	**4**	**64**	**16**	**32-64**
122	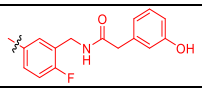		**70**	**> 128**	**> 128**	**> 128**	**> 128**	**> 128**
123	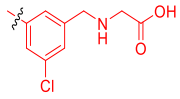		--	**64**	**64**	**16**	**8-16**	**> 128**

-- No data available

The compound **122** is a grown derivative of **110**, which demonstrated the best SPR binding in the series without activity against bacteria. The *N*-benzylated glycine **123** possessing a *meta*-Cl substituent in the phenyl ring had inconclusive SPR data, while exhibiting some activity against almost all bacteria in the testing panel.

Graphical summary on modifications of 3 with positive impact

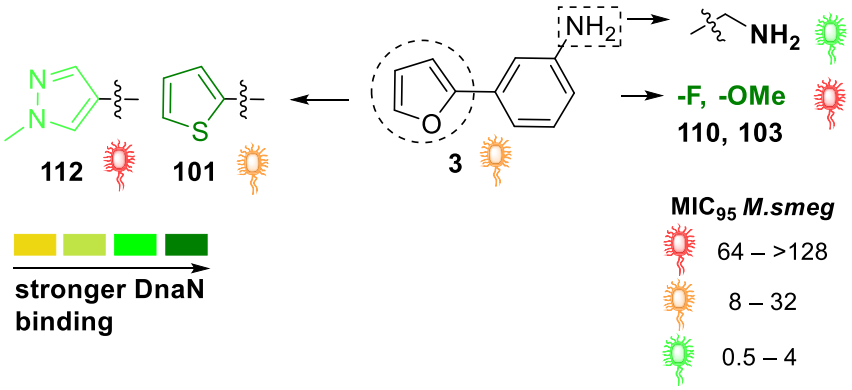

Figure 10. Summary of beneficial modifications of structure **3**.

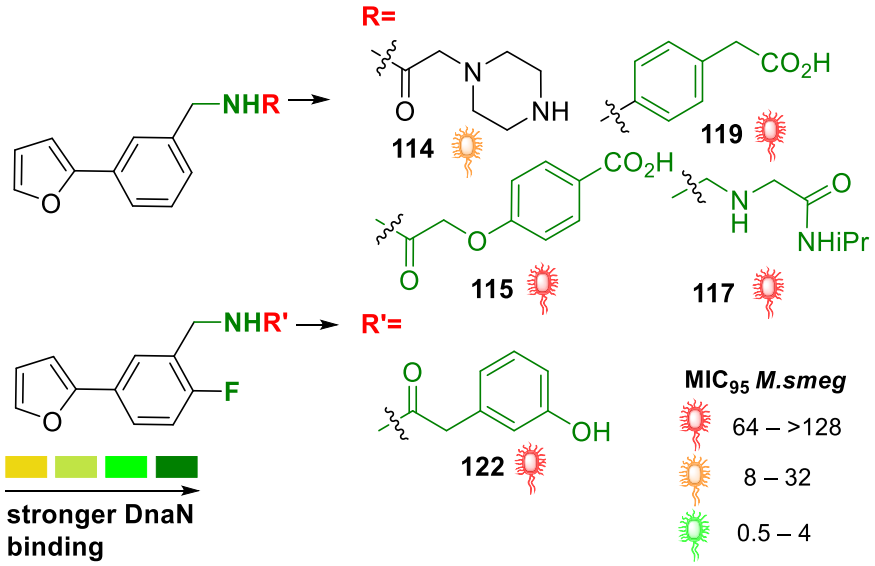

Figure 11. Summary of beneficial appendages on the derivatives of **3**.

- The replacements of furan in **3** was with 2-thienyl and 4-(1-methyl)-pyrazyl were found beneficial for DnaN binding and antibacterial activity in case of the thienyl group.
- Replacing the original amino group with aminomethyl group resulted in great improvement in antibacterial activity (as illustrated in **Figures 10** and **11**).
- Derivatives with highest SPR responses were discovered as a result of growing attempts based on the substituted benzylamines **108** and **109.**
- Nevertheless, for most grown derivatives showing improved binding to DnaN, antibacterial activity is either not observed or marginal, which could be associated with their poor bacterial cell wall penetration ability.

4.3 Chemistry

The synthesis of **Fr1**, **Fr2**, **3** and their further derivatives is provided below following the logic and chronology of their SAR exploration. In most cases the connection of the rings into biaryl scaffold was performed using a certain type of Pd-catalyzed cross-coupling (**Fr1**, **Fr2**, **3**, **4** in **Scheme 1**; **5-7**, **9**, **10, 15,** and **17-27** in **Scheme 2**) or nucleophilic aromatic substitution, followed by reduction (**11**, **14** in **Scheme 3**).

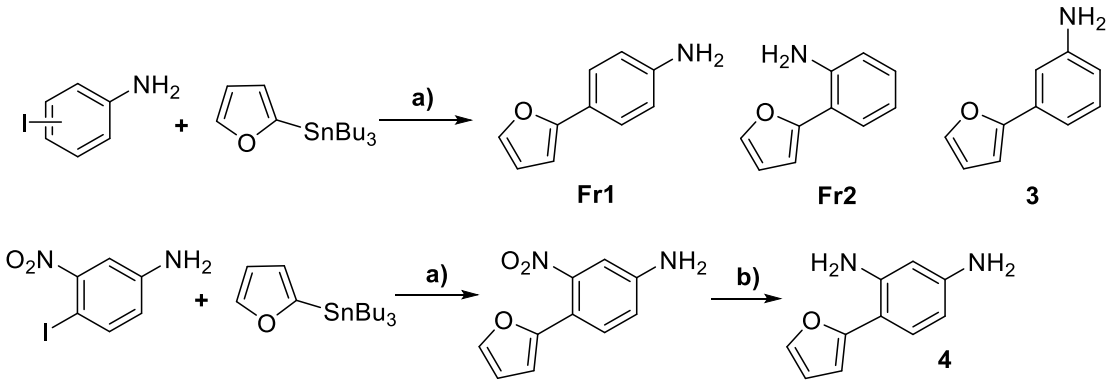

Scheme 1. Synthesis of initial fragments **Fr1** and **Fr2** and their first derivatives.
Conditions: **a) [**$Pd(PPh_3)_4$] (0.03 eq), PhMe (0.5M), 110 °C, o/n; **b)** H_2, Pd/C, EtOH (0.25 M).

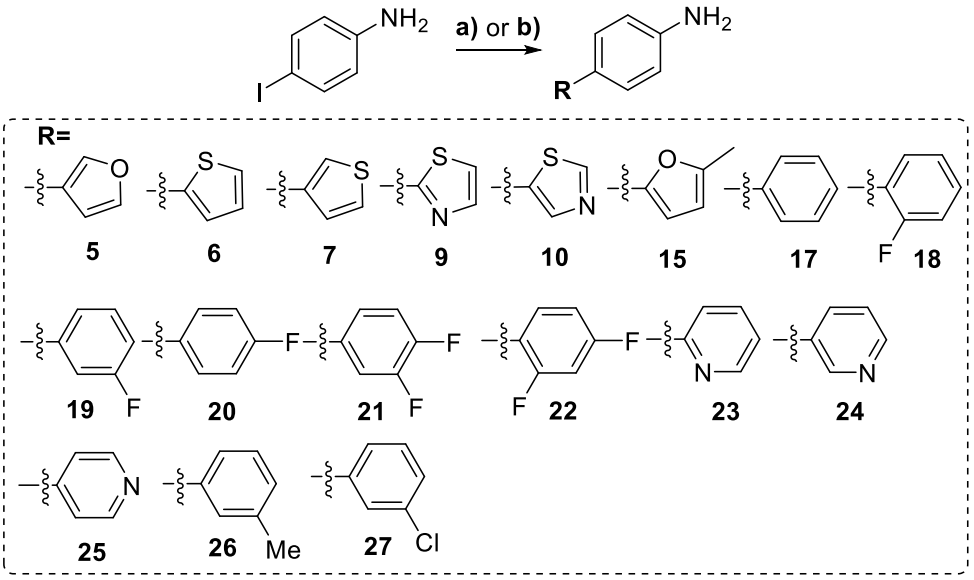

Scheme 2. Synthesis of **Fr1** analogues containing the furan ring replacements
Conditions: **a) R**$B(OH)_2$ (1.2 eq), **[**$Pd(PPh_3)_4$] (0.03 eq), K_2CO_3 (3.0 eq), PhMe/EtOH/H_2O (7:2:1 v/v), 120 °C (MW), 30 min; **b) R**BPin (1.2 eq), **[**$Pd(PPh_3)_4$] (0.03 eq), K_2CO_3 (3.0 eq), dioxane/H_2O (9:1 v/v), 120 °C (MW), 30 min.

In the case of 5-aryloxazole **8** and 2-arylimidazole **13** the heterocycles were assembled through a sequence of reactions starting from 4-nitrobenzaldehyde (**8** and **13** in **Scheme 3**) including reduction to corresponding aromatic amines.

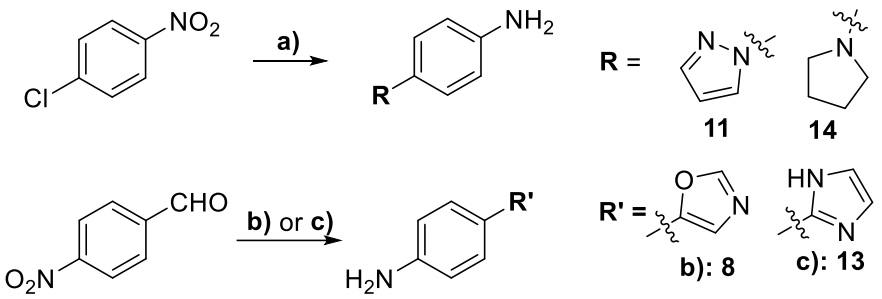

Scheme 3. Incorporation of miscellaneous heterocycles into the structure of **Fr1**
Conditions: **a) 1.** RH (2.0 eq), K_2CO_3 (2.0 eq), DMSO (0.4 M), 100 °C o/n; **2.** H_2, Pd/C, EtOH (0.25 M). **b)** 1. TosMIC. **c)** 1. 1,2-ethylenediamine; 2. $PhI(OAc)_2$**; 3.** H_2, Pd/C, EtOH (0.25 M).

Analogues of positional isomers **Fr2** and **3** containing the thiophene ring **32** and **33** were prepared using Suzuki cross-coupling reaction as illustrated in **Scheme 4.**

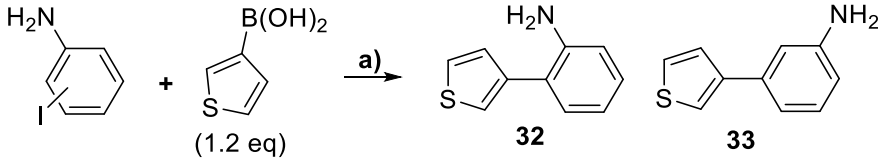

Scheme 4. Synthesis of positional isomers of **7**
Conditions: **a) [**$Pd(PPh_3)_4$] (0.03 eq), K_2CO_3 (3.0 eq), PhMe/EtOH/H_2O (7:2:1 v/v), 120 °C (MW), 30 min

Structures **28**–**31** were also accessed using Stille of Suzuki cross-coupling reactions (**Scheme 5**).

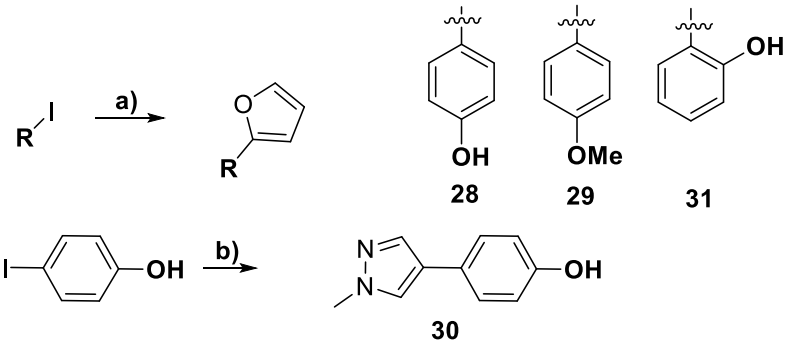

Scheme 5. Synthesis of substituted oxy-analogues of **Fr1**
Conditions:**a) [**$Pd(PPh_3)_4$] (0.03 eq), PhMe (0.5M), 110 °C, o/n; **b)** 4-(1-methylimidazolyl)-BPin (1.2 eq), **[**$Pd(PPh_3)_4$] (0.03 eq), K_2CO_3 (3.0 eq), diox/H_2O (9:1 v/v), 120 °C (MW), 30 min.

Derivatives of **Fr1** carrying diverse substitution patterns on their phenyl rings were synthesized utilizing corresponding aryl halogenides and Stille coupling with 2-furyl-tributylstannane (**34**–**52** in **Scheme 6**). The synthesis of methylamide **41** via aminolysis of the mehyl ester **40** was successful.

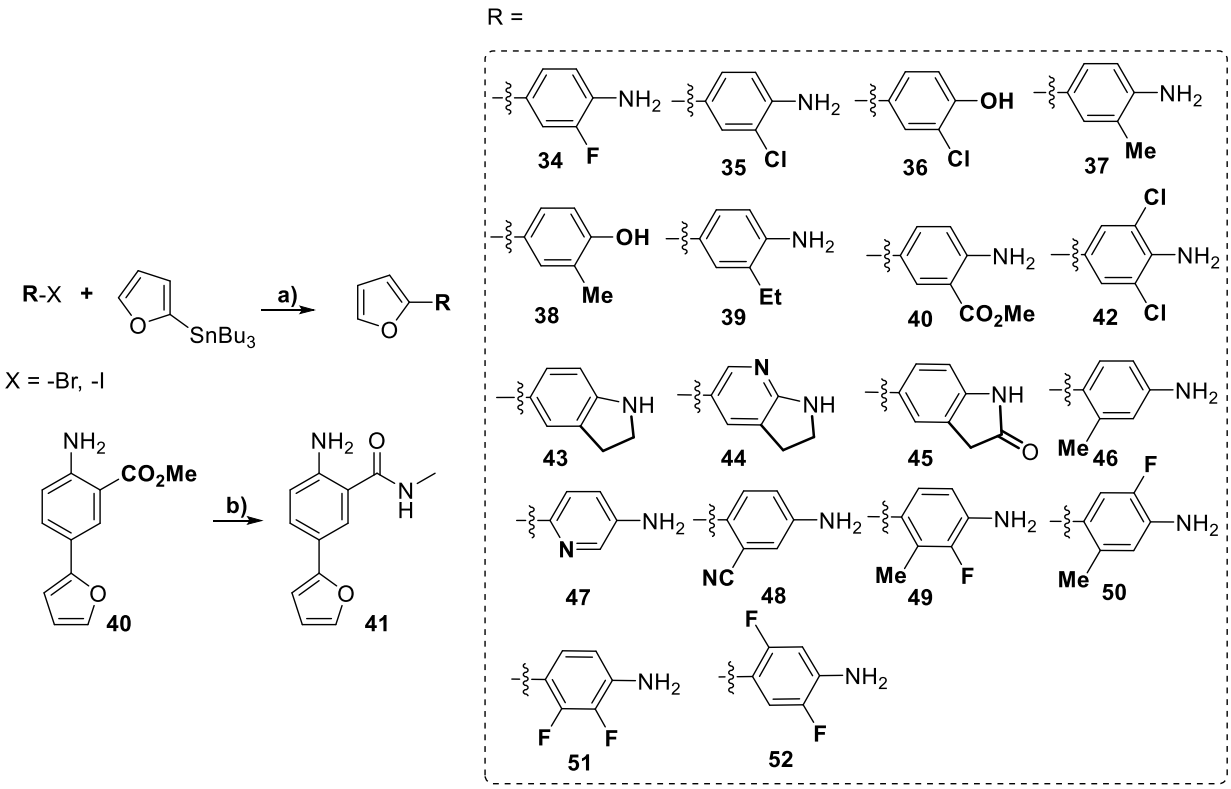

Scheme 6. Synthesis of **Fr1** derivatives substituted on the phenyl ring
Conditions: **a) [**$Pd(PPh_3)_4$] (0.03 eq), PhMe (0.5 M), 110 °C, o/n; **b)** $MeNH_2$ (aq., 0.5M), 90 °C, sealed vessel, 8 hours.

Fr1 derivatives including 3-thienyl or phenyl substituents and miscellaneous substitution patterns were synthesized using Suzuki cross coupling, making use of boronic acids and appropriate aryl halides (**Scheme 7**).

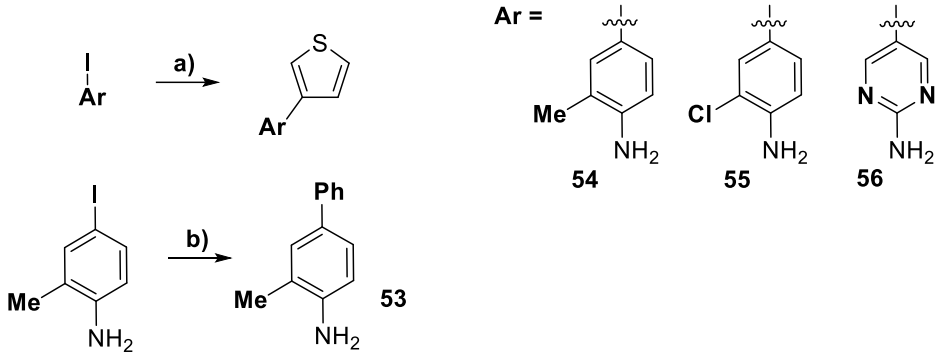

Scheme 7. Synthesis of **Fr1** derivatives with combined substitution patterns
Conditions: **a)** (3-thienyl)-$B(OH)_2$ (1.2 eq), **[**$Pd(PPh_3)_4$] (0.03 eq), K_2CO_3 (3.0 eq), PhMe/EtOH/H_2O (7:2:1 v/v), 120 °C (MW), 30 min **b)** $PhB(OH)_2$ (1.2 eq), **[**$Pd(PPh_3)_4$] (0.03 eq), K_2CO_3 (3.0 eq), PhMe/EtOH/H_2O (7:2:1 v/v), 120 °C (MW), 30 min.

Synthesis of grown derivatives of **Fr1.**

Since grown derivatives of **Fr1** are members of a number of separate subclasses (*N*-acylated/sulfonylated derivatives and miscellaneous extended derivatives), their syntheses will be addressed separately.

Compounds **57**, **58** and **59** were synthesized using **Fr1** and corresponding acylating or sulfonylating agents as starting materials (**Scheme 8**). The piperazine derivatives **60** and **61** were accessed by constructing the biaryl system using commercially available *tert*-butyl 4-(4-bromophenyl)piperazine-1-carboxylate and Stille cross-coupling, followed by the deprotection and acetylation (**Scheme 8**).

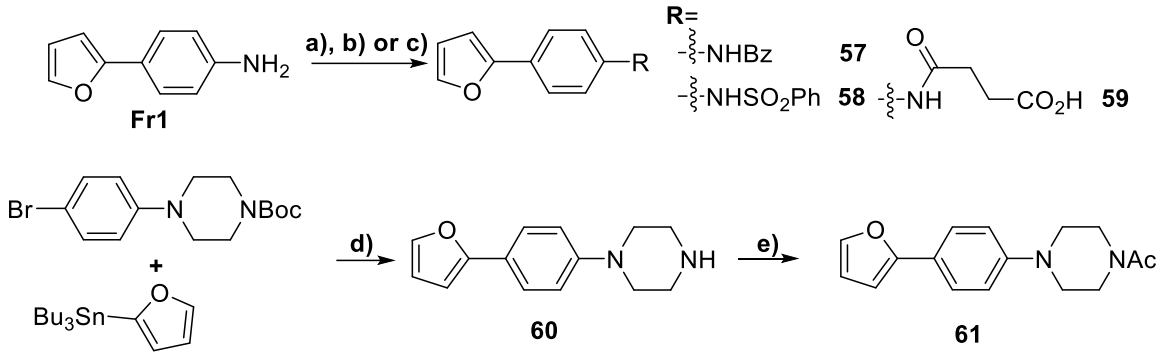

Scheme 8. Syntheses of grown derivatives of **Fr1**
Conditions: **a)** PhCOCl (1.05 eq), pyridine (0.3 M), rt, o/n; **b)** $PhSO_2Cl$ (1.05 eq), pyridine (0.3 M), rt, o/n; **c)** succinic anhydride (1.2 eq), Et_3N (2.0 eq), THF (0.25 M), rt, o/n; **d) 1. [**$Pd(PPh_3)_4$] (0.03 eq), PhMe (0.5M), 110 °C, o/n; **2.** HCl (1M in diox), rt, 2 h. **e)** Ac_2O (1.05 eq), Et_3N (2.0 eq), THF (0.3 M), rt, o/n.

The further extended derivatives **62** and **63** were obtained starting from commercially available 4-iodophenylacetic acid, which was coupled to ethyl glycinate using EDC as activating agent. The synthesized amide was subjected to Stille coupling with (1-furyl)-tributyl stannane, which gave rise to **I1**. After ethyl ester deprotection under basic conditions and coupling of the carboxylic acid **62** with *N*,3-dimethylaniline using HBTU, the grown amide **63** was obtained (**Scheme 9**).

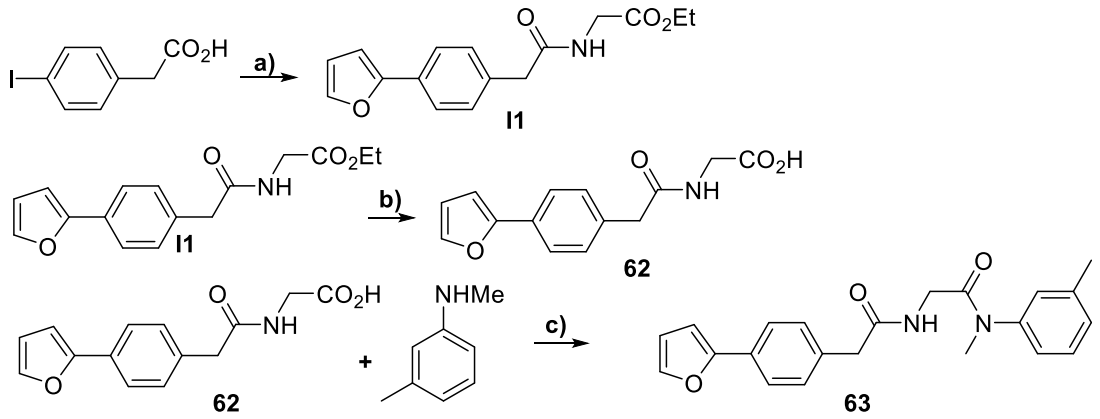

Scheme 9. Syntheses of grown derivatives of **Fr1**
Conditions: **a) 1.** glycine ethyl ester hydrochloride (1.1 eq), 7-aza-HOBt (1.1 eq), EDC·HCl (1.5 eq), TEA (5.0 eq), DMF; **2. [**$Pd(PPh_3)_4$] (0.03 eq), PhMe (0.5 M), 110 °C, **b)** NaOH (15.0 eq), H_2O-THF (1:1 v/v, 0.15 M); **c)** HBTU (1.05 eq), DIPEA (3.0 eq), DMF.

Synthesis of derivatives of **Fr2.** We synthesized substituted derivatives of **Fr2 64–76** utilizing cross-coupling reactions and appropriate aryl halides as starting materials (**Scheme 10**).

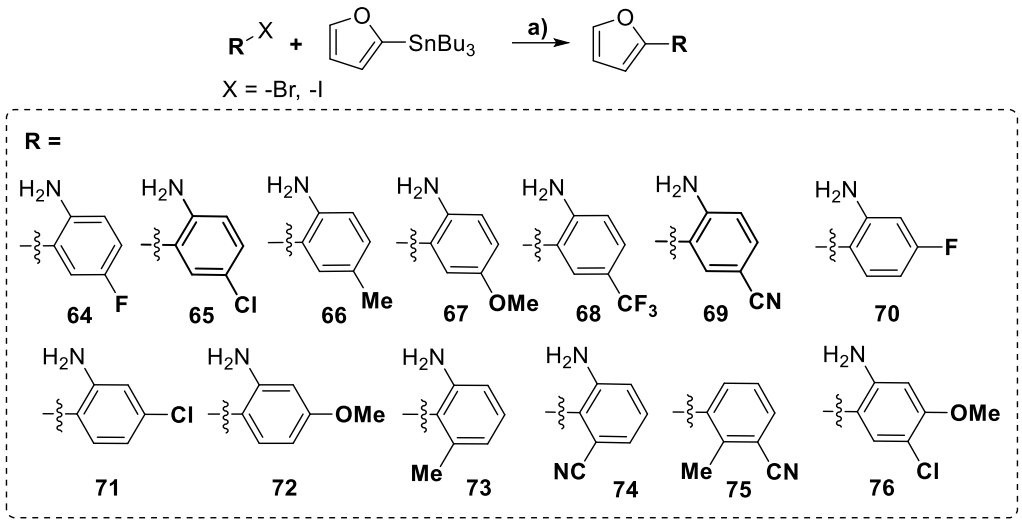

Scheme 10. Synthesis of **Fr2** derivatives carrying substituents on their phenyl rings
Conditions: **a) [**$Pd(PPh_3)_4$] (0.03 eq), PhMe (0.5M), 110 °C, o/n.

The synthesis of certain doubly substituted **Fr2** derivatives (**77**–**82**) was preceded by the preparation of corresponding precursor aryl halides via bromination of substituted arenes under various conditions (**Scheme 11, a)**, **c)**). The brominated arenes were functionalized under the Stille cross-coupling conditions with tributyl(furan-2-yl)stannane to yield desired **Fr2** derivatives.

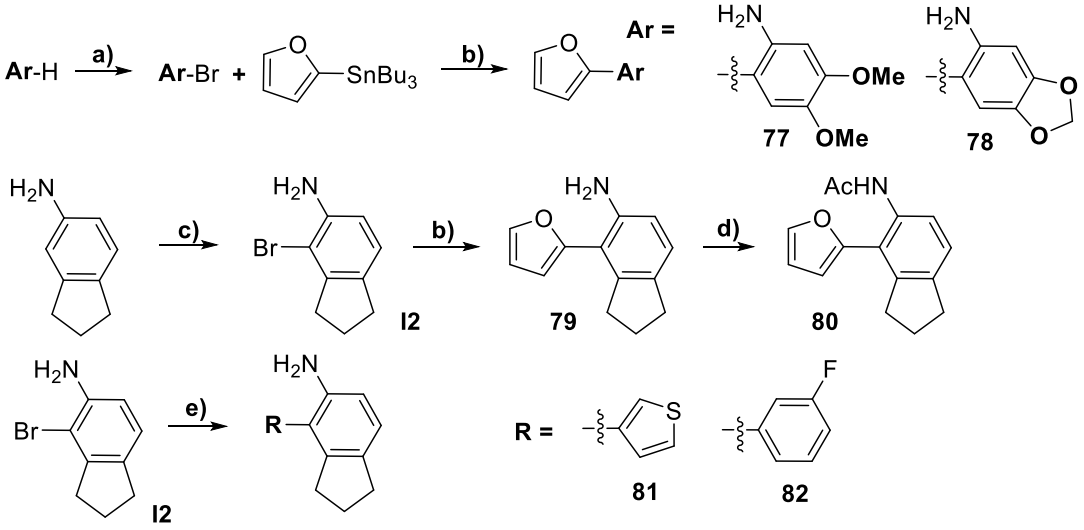

Scheme 11. Synthesis of compounds **77**-**82** and their precursors.
Conditions: **a)** NBS (1.05 eq), MeCN (0.25 M), 55 °C, 4h**; b) [**$Pd(PPh_3)_4$] (0.03 eq), PhMe (0.5M), 110 °C, o/n; **c) 1.** Br_2 (2.0 eq), AcOH (0.2 M), rt, 30 min; **2.** $SnCl_2$ (1.1 eq), HCl (conc.), rt, 1 h. **d)** Ac_2O (1.05 eq), Et_3N (2.0 eq), THF (0.3 M), rt, o/n; **e) R**$B(OH)_2$ (1.2 eq), **[**$Pd(PPh_3)_4$] (0.03 eq), K_2CO_3 (3.0 eq), PhMe/EtOH/H_2O (7:2:1 v/v), 120 °C (MW), 30 min.

Synthesis of grown derivatives of **Fr2.** The benzoylated derivative **83** was synthesized by simple acylation of **Fr2.** For the synthesis of benzylamine derivatives **84**–**86** Boc-protected 3-bormobenzylamine **I3** was cross-coupled with the (2-furyl)-tributylstannane and (1-methyl)-4-pyrazolyl boronic acid, deprotected (**84** and **85**) and acetylated (**86**, **Scheme 12**).

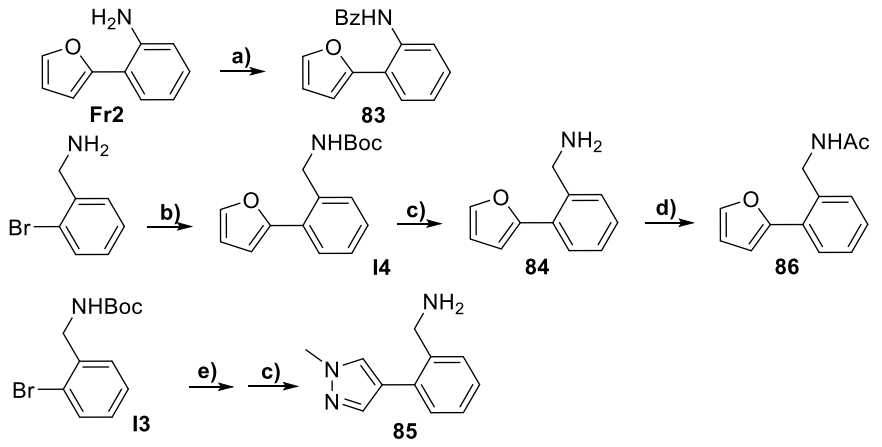

Scheme 12. Synthesis of grown derivatives **83-86**of **Fr2**

Conditions: **a)** PhCOCl (1.05 eq), pyridine (0.3 M), rt, o/n; **b) 1.** Boc_2O (1.05 eq), Et_3N (2.0 eq), THF (0.5 M), rt, o/n; **2. [**$Pd(PPh_3)_4$] (0.03 eq), PhMe (0.5 M), 110 °C, o/n; **c)** HCl (1M in diox), rt, 2h; **d)** Ac_2O (1.05 eq), Et_3N (2.0 eq), THF (0.3 M), rt, o/n; **e)** 4-(1-methylimidazolyl)-BPin (1.2 eq), **[**$Pd(PPh_3)_4$] (0.03 eq), K_2CO_3 (3.0 eq), di-ox/H_2O (9:1 v/v), 120 °C (MW), 30 min.

The other grown derivatives of **Fr2 87–89** were accessed using reductive amination of 2-furylbenzaldehyde **I5** with corresponding primary or secondary amines (**Scheme 13**). **Fr2** derivatives **90** and **91** were obtained by reductive amination of 2-bromobenzaldehyde with corresponding Boc-protected piperazine or 4-aminopiperidine followed by the Stille cross-coupling and deprotection (see **Scheme 13** below).

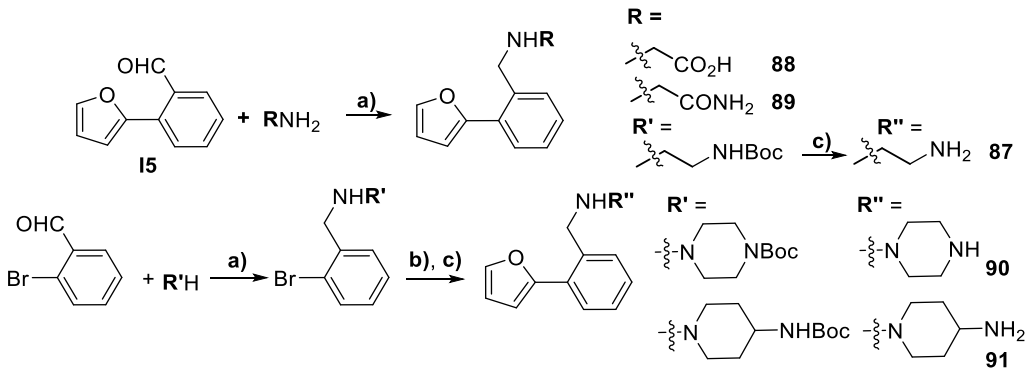

Scheme 13. Synthesis of grown derivatives of **Fr2 -** substituted benzylamines.

Conditions: **a)** $NaBH(OAc)_3$ (1.5 eq), THF (0.3 M); **b)** (2-furyl)-trbutylstannane (1.2 eq.), **[**$Pd(PPh_3)_4$] (0.03 eq), PhMe (0.5M), 110 °C, o/n; **c)** HCl (1M in diox), rt, 2 h.

Derivatives of **65.** The analogue of **65** containing the pyrazole ring (**92**) was accessed by Suzuki cross-coupling of 2-bromo-4-chloro aniline with appropriate boronic acid pinacol ester. Certain grown derivatives of **65** were synthesized by *N*-acylation under various conditions (**b)**, **c)** in **Scheme 14**).

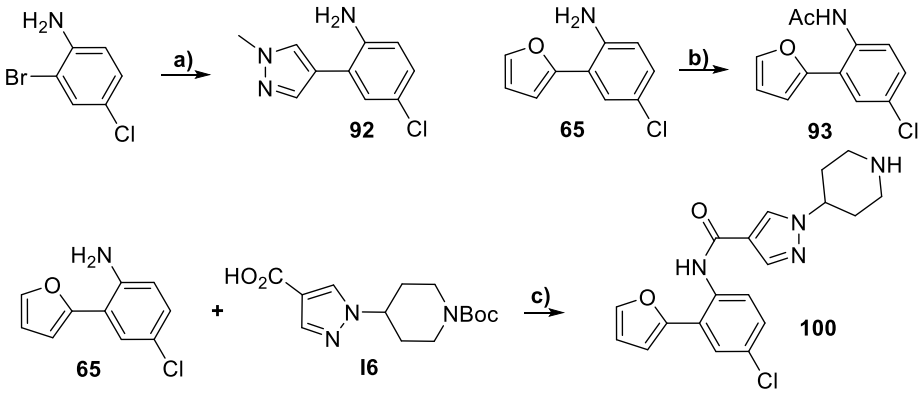

Scheme 14. Synthesis of grown derivatives of **65**
Conditions: **a)** 4-(1-methylimidazolyl)-BPin (1.2 eq), **[**$Pd(PPh_3)_4$] (0.03 eq), K_2CO_3 (3.0 eq), diox/H_2O (9:1 v/v), 120 ºC (MW), 30 min **b)** Ac_2O (1.05 eq), Et_3N (2.0 eq), THF (0.3 M), rt, o/n; **c) 1.**T3P (2.0 eq), pyridine (0.3 M), 0–25 ºC, 3h; **2.** HCl (1M in diox), rt, 2 h.

Chlorobenzylamine derivatives were yielded by reductive amination of the chloro furanbenzaldehyde **I5** with corresponding amines (**Scheme 15**).

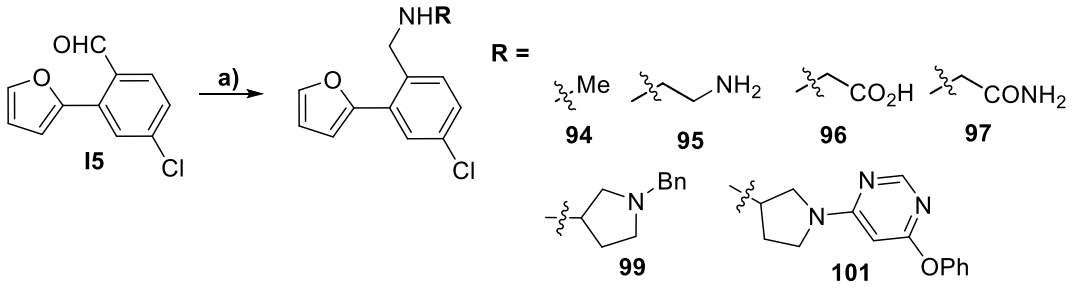

Scheme 15. Synthesis of substituted grown chlorobenzylamines
Conditions: **a)** **R**NH_2 (1.0 eq), $NaBH(OAc)_3$ (1.5 eq), THF (0.3 M).

The isothiourea derivative **98** was synthesized by alkylation of thiourea with the substituted benzyl bromide **I7** (**Scheme 16**).

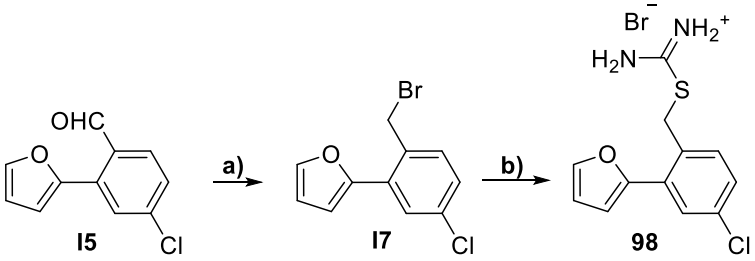

Scheme 16. Synthesis of substituted grown chlorobenzylamines
Conditions: **a) 1.** $NaBH_4$ (2.0 eq), EtOH:THF (0.5 M, 1:1 v/v); **2.** CBr_4 (2.0 eq), PPh_3 (2.0 eq), DCM (0.2 M), rt, o/n. **b)** thiourea (1.0 eq), EtOH (0.3 M), rt, o/n.

Synthesis of derivatives of **3.** Analogous to its positional isomers **Fr1** and **Fr2**, the substituted derivatives of **3** were accessed by employing Stille coupling of aryl bromides and 2-furyltributylstannane (**103**–**105** in **Scheme 17**).

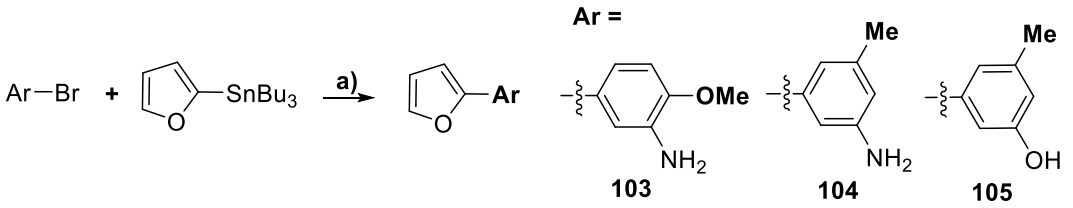

Scheme 17. Synthesis of substituted derivatives of **3**
Conditions: **a)** [$Pd(PPh_3)_4$] (0.03 eq), PhMe (0.5 M), 110 ºC, o/n.

The first grown derivatives of **3** were obtained by reductive amination using **3** and appropriate benzaldehydes (**106**, **107** in **Scheme 18**).

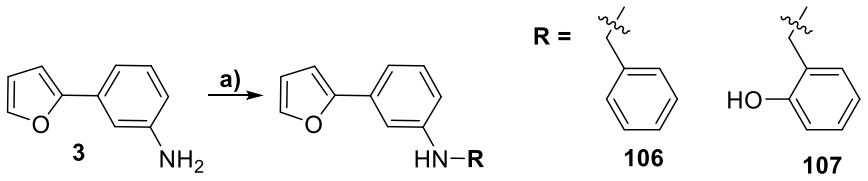

Scheme 18. Synthesis of first grown **3** derivatives
Conditions: **a) R**CHO (0.95 eq), $NaBH(OAc)_3$ (1.5 eq), THF (0.3 M).

Substituted benzylamines **108**–**112** were accessed using corresponding aryl bromides in cross-coupling reactions with appropriate arylstannanes or boronic acids (see conditions **a)-c)** in **Scheme 19**).

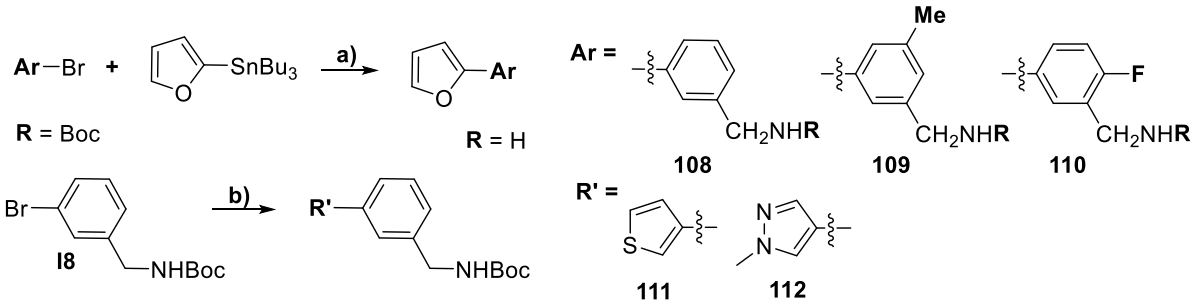

Scheme 19. Synthesis of various 3-arylbenzylamine derivatives
Conditions: **a) 1. [**$Pd(PPh_3)_4$] (0.03 eq), PhMe (0.5M), 110 ºC, o/n; **2.** HCl (1M in diox), rt, 2 h. **b) 1. R**BPin or **R**$B(OH)_2$ (1.2 eq), **[**$Pd(PPh_3)_4$] (0.03 eq), K_2CO_3 (3.0 eq), diox/H_2O (9:1 v/v), 120 ºC (MW), 30 min; **2.** HCl (1M in diox), rt, 2 h.

Grown acylated derivatives of **3 114**–**116** were obtained by *N*-acetylation with acetic anhydride (**113**) or bromoacetyl bromide and further substitution of the *N*-bromoacetyl intermediate **I9** as depicted below (**Scheme 20**). The derivative **122** was obtained by the EDC-promoted acylation of **110** with (3-hydroxyphenyl)-acetic acid.

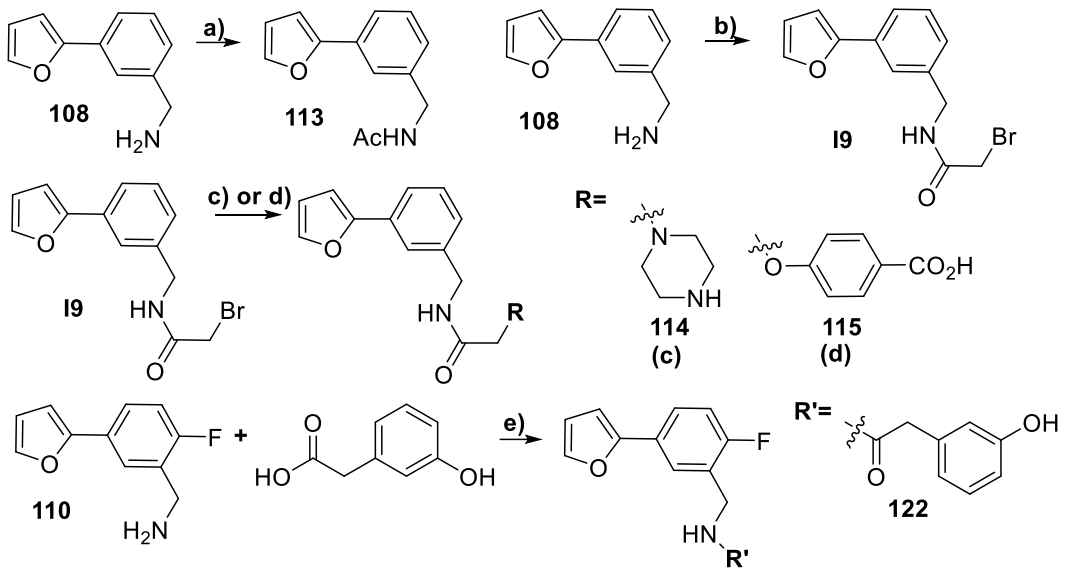

Scheme 20. Synthesis of substituted grown acylated derivatives of **108**

Conditions: **a)** Ac_2O (1.05 eq), Et_3N (2.0 eq), THF (0.3 M), rt, o/n; **b)** Bromoacetyl bromide (1.05 eq), Et_3N (2.0 eq), dichloroethane (0.15 M), 0 °C, 1h; **c) 1.** *N*-Boc-piperazine (1.0 eq), DiPEA (2.0 eq), MeCN (0.2 M) 70 °C, o/n; **2.** HCl (1M in diox), rt, 2h. **d) 1**. Ethyl 4-hydroxybenzoate (1.0 eq), K_2CO_3 (1.5 eq), MeCN (0.2 M) 80 °C, o/n **2.** HCl (1M in diox), rt, 2 h; **e)** EDC·HCl (1.05 eq), HOBt (1.05 eq), DiPEA (4.0 eq), DMF (1.0 M), rt, o/n.

The alkylated derivatives of **116–121** were obtained using reductive amination of the aryl benzaldehyde with corresponding amines (**Scheme 21**).

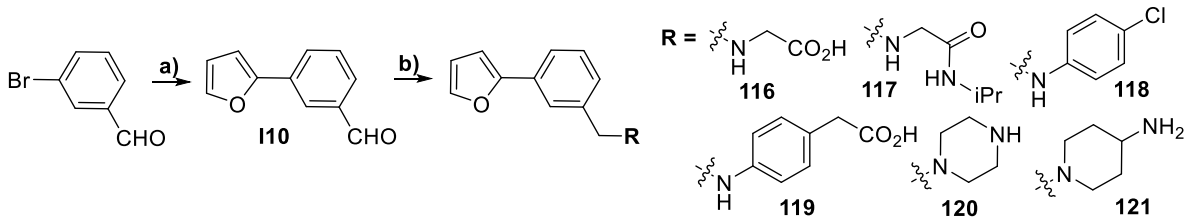

Scheme 21. Synthesis of *N*-alkylated and arylated derivatives of 3-(1-furyl)-benzylamine **108**

Conditions: **a) (**1-furyl)-tribytylstannane (1.3 eq), [$Pd(PPh_3)_4$] (0.03 eq), PhMe (0.5M), 110 °C, o/n; **b) R**H (1.05 eq), $NaBH(OAc)_3$ (1.5 eq), THF (0.3 M).

Finally, the variously substituted 3-(1-furyl)-benzylamines **123-125** were synthesized in a similar manner to previously mentioned **108** derivatives by making use of reductive amination (**Scheme 22**).

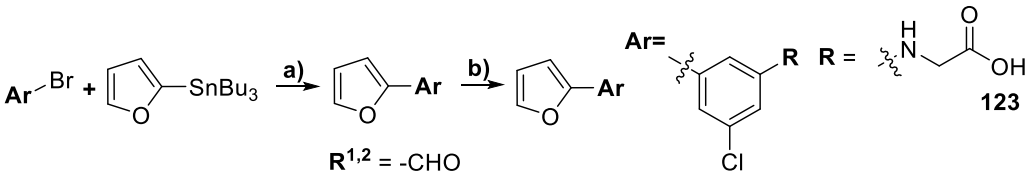

Scheme 22. Synthesis of miscellaneously substituted *N*-alkylated derivatives of 3-(1-furyl)-benzylamine **108**.

Conditions: **a)** [$Pd(PPh_3)_4$] (0.03 eq), PhMe (0.5M), 110 °C, o/n; **b) R**H (1.05 eq), $NaBH(OAc)_3$ (1.5 eq), THF (0.3 M).

4.4 Experimental

4.4.1 Synthesis procedures and characterization of fragments are provided in the respective section of the Supplementary material.

4.4.2 The STD-NMR spectra acquisition procedure

The STD-NMR experiments were recorded at 298 K on a Bruker Fourier spectrometer (500 MHz). The samples contained a 25-fold excess of compound being screened (250 μM) over *M. tuberculosis* sliding clamp protein (10 mg/mL stock solution in the HEPES/NaOH buffer, pH 7.5, 150 mM NaCl, 10.0 μM being the final concentration of DnaN). The compounds for screening were used as stock solutions in DMSO-d_6, which were mixed with the screening buffer (phosphate buffer c= 0.1 M, pH = 6.8 in D_2O), and a certain quantity of DMSO-d_6 to reach the final concentration of 5% (v/v) DMSO-d_6. To the resulting solution the protein sample (or DnaN stock buffer in H_2O) was added, and the obtained solution was carefully mixed and transferred into an NMR tube. The final volume of the sample was 250 μL.

All experiments were performed using the *stddiffesgp.3* pulse program by Bruker. A blank spectrum was recorded in order to establish the parameters at which no residual compound peaks were visible. The screening experiments were all recorded with a carrier set at 0 ppm for the on-resonance and −40 ppm for the off-resonance irradiation. Selective protein saturation was carried out at 2 s (D20 parameter in TopSpin) by using a train of 50 ms Gauss-shaped pulses, each separated by a 1 s delay (D1 parameter in TopSpin). The number of scans was 512.

The difference spectrum was obtained by algebraic subtraction of the on-resonance spectrum from the off-resonance spectrum after automatic phase correction.

The relative difference in intensity of signals due to saturation transfer (relative STD effect) was estimated using the following formula:

$$\text{STDeffect} = (I_0 - I_{sat})/I_0 \qquad (1)$$

(where I_{sat} is the intensity of the signal of interest in the on-resonance NMR spectrum, and I_0 is the intensity of the signal in the off-resonance NMR spectrum). The STD effect was used to estimate the contribution of the particular proton group into binding with DnaN and to infer the binding epitope for the compounds tested.

Calculations for group epitope mapping were done as described by Mayer *et al.*[14]

The STD-NMR spectra with assignments are provided in the Supplementary material (Figures **S1**-**S18**).

4.4.3 MIC determination

All microorganisms used in this study were obtained from the German Collection of Microorganisms and Cell Cultures (DSMZ), the Coli Genetic Stock Center (CGSC), or were part of

our internal collection, and were handled according to standard procedures. *S. aureus*, *E. coli*, *E. faecium* and *E. faecalis* were inoculated in cation-adjusted Mueller Hinton Broth (Sigma Aldrich) and incubated under shaking conditions overnight at 37 °C, and for 48 h for *M. smegmatis*. *S. pneumoniae* was cultured without shaking under microaerophilic conditions (5% CO2) overnight at 37 °C. *S. aureus*, *E.coli*, *E. faecium*, and *E. faecalis* were subcultured on CASO agar plates, *M. smegmatis* and *S. pneumoniae* were subcultured on Middlebrook 7H10 agar plates (M7H10) with 10% oleic acid albumindextrose-catalase OADC Enrichment and 5% sheep blood agar plates, respectively, and incubated for 24 h at their optimal growth temperature. Single colonies of the bacterial strains were suspended in 0.9% NaCl and McFarland was adjusted to 0.5 using a Densitometer. The bacterial suspension was diluted 1:100 in the corresponding broth to achieve a final inoculum of approximately 10^4 CFU/mL. Serial dilutions of compounds (0.06 to 128 µM) were prepared in sterile 96-well plates and the bacterial suspension was added. Growth inhibition was assessed after overnight incubation (24–48 h) at 30–37 °C. Minimum inhibitory concentration (MIC) was determined as the lowest compound concentration where no visible growth was observed. *M. smegmatis* GM^R was cultured in Middlebrook 7H9 minimal media (7H9) supplemented with 10% oleic acid albumindextrose-catalase OADC Enrichment, with 25 µg/mL GM.

4.4.4 Cytotoxicity evaluation (IC_{50})

HepG2 cells (human hepatoblastoma cell line; ACC 180, DSMZ) were cultured under conditions recommended by the depositor and cells were propagated in Dulbecco's modified Eagle medium (DMEM) supplemented with 10% fetal bovine serum (FBS). For determining the antiproliferative activity of test compounds, cells were seeded at 6×10^3 cells per well of 96-well plates in 120 µL complete medium. After 2 h of equilibration, compounds were added in serial dilution in 60 µL complete medium. Compounds, as well as the solvent control and doxorubicin as reference, were tested in duplicate in two independent experiments. After 5 days of incubation, 20 µL of 5 mg/mL MTT (thiazolyl blue tetrazolium bromide) in PBS was added per well, and the cells were further incubated for 2 h at 37 °C. The medium was then discarded and cells were washed with 100 µL PBS before adding 100 µL 2-propanol/10 N HCl (250:1) in order to dissolve formazan granules. The absorbance at 570 nm was measured using a microplate reader (Tecan Infinite M200Pro), and cell viability was expressed as percentage relative to the respective solvent control. IC_{50} were determined by sigmoidal curve fitting using GraphPad PRISM 8 (GraphPad Software, San Diego, CA, USA).

4.5 Conclusions

In the course of this chapter, we explored the SAR within one of the most promising scaffolds of previously discovered fragment DnaN inhibitors.

Owing to the structure of the fragment hits, the SAR of three positional isomers (**Fr1**, **Fr2** and **3**) were explored independently.

As a result of the described exploratory optimization, which nevertheless was not supported by structural data, we have suggested, refined and confirmed plausible binding poses of **Fr1** and **Fr2**. These poses guided our growing attempts, some of which were successful and provided fragment derivatives with significantly improved DnaN binding. Still, structural data in the form of a co-crystal structure of **Fr1**, **Fr2, 3** or their derivatives would be highly instrumental for supporting more advanced hit-to-lead optimization.

As an outlook, combining beneficial modifications discovered in the course of SAR studies centered around the structures of **Fr1**, **Fr2** and **3** could potentially yield even stronger DnaN binders useful for further structural biology studies.

4.6 References

(1) van Ingen, J.; Rahim, Z.; Mulder, A.; Boeree, M. J.; Simeone, R.; Brosch, R.; van Soolingen, D. Characterization of Mycobacterium Orygis as M. Tuberculosis Complex Subspecies - Volume 18, Number 4—April 2012 - Emerging Infectious Diseases Journal - CDC. *Emerg. Infect. Dis.* **2012**, *18* (4), 653–655. https://doi.org/10.3201/EID1804.110888.

(2) Gordon, S. V.; Parish, T. Microbe Profile: Mycobacterium Tuberculosis: Humanity's Deadly Microbial Foe. *Microbiol. (United Kingdom)* **2018**, *164* (4), 437–439. https://doi.org/10.1099/MIC.0.000601/CITE/REFWORKS.

(3) Robinson, A.; J. Causer, R.; E. Dixon, N. Architecture and Conservation of the Bacterial DNA Replication Machinery, an Underexploited Drug Target. *Curr. Drug Targets* **2012**, *13* (3), 352–372. https://doi.org/10.2174/138945012799424598.

(4) Burnouf, D. Y.; Olieric, V.; Wagner, J.; Fujii, S.; Reinbolt, J.; Fuchs, R. P. P.; Dumas, P. Structural and Biochemical Analysis of Sliding Clamp/Ligand Interactions Suggest a Competition Between Replicative and Translesion DNA Polymerases. *J. Mol. Biol.* **2004**, *335* (5), 1187–1197. https://doi.org/10.1016/J.JMB.2003.11.049.

(5) Wolff, P.; Oliéric, V.; Briand, J. P.; Chaloin, O.; Dejaegere, A.; Dumas, P.; Ennifar, E.; Guichard, G.; Wagner, J.; Burnouf, D. Y. Structure-Based Design of Short Peptide Ligands Binding onto the E. Coli Processivity Ring. *J. Med. Chem.* **2011**, *54* (13), 4627–4637. https://doi.org/10.1021/jm200311m.

(6) Kong, X. P.; Onrust, R.; O'Donnell, M.; Kuriyan, J. Three-Dimensional Structure of the β Subunit of E. Coli DNA Polymerase III Holoenzyme: A Sliding DNA Clamp. *Cell* **1992**, *69* (3), 425–437. https://doi.org/10.1016/0092-8674(92)90445-I.

(7) Acharya, S.; Dahal, A.; Bhattarai, H. K. Evolution and Origin of Sliding Clamp in Bacteria, Archaea and Eukarya. *PLoS One* **2021**, *16* (8 August), 1–17. https://doi.org/10.1371/journal.pone.0241093.

(8) Georgescu, R. E.; Yurieva, O.; Kim, S. S.; Kuriyan, J.; Kong, X. P.; O'Donnell, M. Structure of a Small-Molecule Inhibitor of a DNA Polymerase Sliding Clamp. *Proc. Natl. Acad. Sci. U. S. A.* **2008**, *105* (32), 11116–11121. https://doi.org/10.1073/pnas.0804754105.

(9) Wijffels, G.; Johnson, W. M.; Oakley, A. J.; Turner, K.; Epa, V. C.; Briscoe, S. J.; Polley, M.; Liepa, A. J.; Hofmann, A.; Buchardt, J.; Christensen, C.; Prosselkov, P.; Dalrymple, B. P.; Alewood, P. F.; Jennings, P. A.; Dixon, N. E.; Winkler, D. A. Binding Inhibitors of the Bacterial Sliding Clamp by Design. *J. Med. Chem.* **2011**, *54* (13), 4831–4838. https://doi.org/10.1021/jm2004333.

(10) Yin, Z.; Whittell, L. R.; Wang, Y.; Jergic, S.; Liu, M.; Harry, E. J.; Dixon, N. E.; Beck, J. L.; Kelso, M. J.; Oakley, A. J. Discovery of Lead Compounds Targeting the Bacterial Sliding Clamp Using a Fragment-Based Approach. *J. Med. Chem.* **2014**, *57* (6), 2799–2806. https://doi.org/10.1021/jm500122r.

(11) Yin, Z.; Wang, Y.; Whittell, L. R.; Jergic, S.; Liu, M.; Harry, E.; Dixon, N. E.; Kelso, M. J.; Beck, J. L.; Oakley, A. J. DNA Replication Is the Target for the Antibacterial Effects of Nonsteroidal Anti-Inflammatory Drugs. *Chem. Biol.* **2014**, *21* (4), 481–487. https://doi.org/10.1016/j.chembiol.2014.02.009.

(12) Yin, Z.; Whittell, L. R.; Wang, Y.; Jergic, S.; Ma, C.; Lewis, P. J.; Dixon, N. E.; Beck, J. L.; Kelso, M. J.; Oakley, A. J. Bacterial Sliding Clamp Inhibitors That Mimic the Sequential Binding Mechanism of Endogenous Linear Motifs. *J. Med. Chem.* **2015**, *58* (11), 4693–4702. https://doi.org/10.1021/acs.jmedchem.5b00232.

(13) Mancini, F.; Unver, M. Y.; Elgaher, W. A. M.; Jumde, V. R.; Alhayek, A.; Lukat, P.; Herrmann, J.; Witte, M. D.; Köck, M.; Blankenfeldt, W.; Müller, R.; Hirsch, A. K. H. Protein-Templated Hit Identification via an Ugi Four-Component Reaction. *Chem. – A Eur. J.* **2020**, chem.202002250. https://doi.org/10.1002/chem.202002250.

(14) Mayer, M.; Meyer, B. Group Epitope Mapping by Saturation Transfer Difference NMR to Identify Segments of a Ligand in Direct Contact with a Protein Receptor. *J. Am. Chem. Soc.* **2001**, *123* (25), 6108–6117. https://doi.org/10.1021/JA0100120/ASSET/IMAGES/LARGE/JA0100120F00011.JPEG.

(15) Reulecke, I.; Lange, G.; Albrecht, J.; Klein, R.; Rarey, M. Towards an Integrated Description of Hydrogen Bonding and Dehydration: Decreasing False Positives in Virtual Screening with the HYDE Scoring Function. *ChemMedChem* **2008**, *3* (6), 885–897. https://doi.org/10.1002/CMDC.200700319.

(16) Schneider, N.; Lange, G.; Hindle, S.; Klein, R.; Rarey, M. A Consistent Description of HYdrogen Bond and DEhydration Energies in Protein-Ligand Complexes: Methods behind the HYDE Scoring Function. *J. Comput. Aided. Mol. Des.* **2013**, *27* (1), 15–29. https://doi.org/10.1007/S10822-012-9626-2/FIGURES/9.

(17) Kling, A.; Lukat, P.; Almeida, D. V.; Bauer, A.; Fontaine, E.; Sordello, S.; Zaburannyi, N.; Herrmann, J.; Wenzel, S. C.; König, C.; Ammerman, N. C.; Barrio, M. B.; Borchers, K.; Bordon-Pallier, F.; Brönstrup, M.; Courtemanche, G.; Gerlitz, M.; Geslin, M.; Hammann, P.; Heinz, D. W.; Hoffmann, H.; Klieber, S.; Kohlmann, M.; Kurz, M.; Lair, C.; Matter, H.; Nuermberger, E.; Tyagi, S.; Fraisse, L.; Grosset, J. H.; Lagrange, S.; Müller, R. Targeting DnaN for Tuberculosis Therapy Using Novel Griselimycins. *Science (80-.).* **2015**, *348* (6239).

(18) Perlmutter, S. J.; Geddes, E. J.; Drown, B. S.; Motika, S. E.; Lee, M. R.; Hergenrother, P. J. Compound Uptake into E. Coli Can Be Facilitated by N-Alkyl Guanidiniums and Pyridiniums. *ACS Infect. Dis.* **2021**. https://doi.org/10.1021/acsinfecdis.0c00715.

S4 Supplementary material to Chapter 4

S4.1 Experimental procedures

S4.1.1 Synthesis of the fragment molecules

All reagents were used from commercial suppliers without further purification. Procedures were not optimized regarding yield. Microwave experiments were performed in the Anton Paar® Monowave 400 microwave reactor. Reactions were carried out in sealed pressure-proof vials with magnetic stirring. NMR spectra were recorded on a Bruker AV 500 (500MHz) spectrometer, the chemical shifts are provided in ppm. Liquid chromatography-Mass spectrometry measurements was performed on a SpectraSystems-MSQ LCMS system (Thermo Fisher, Dreieich, Germany). Flash chromatography was performed using the automated flash chromatography system CombiFlash Rf+ (Teledyne ISCO, Lincoln, NE, USA) equipped with RediSepRf silica columns (AxelSemrau, Sprockhövel Germany), Chromabond Flash C18 columns (Macherey-Nagel, Düren,Germany) or self-packed alumina flash-columns (Thermo Fischer Scientific). Purity of compounds synthesized was determined by LC-MS using the area percentage method on the UV trace recorded at a wavelength of 254 nm and found to be >95%.

General procedure I (Stille coupling). To a stirred degassed solution of the corresponding aryl halogenide (1.0 eq) and $Pd[PPh_3]_4$ (0.03 eq) in dry toluene (0.3 M) was added 2-(Tri-n-butylstannyl)furan (1.1 eq) and the reaction mixture was heated up to 110 ^oC and stirred at that temperature for 6 hours. After the full conversion of the starting material the reaction mixture was concentrated *in vacuo*, taken up into same volume of ethyl acetate, washed with saturated aqueous solution of sodium fluoride, brine, dried over anhydrous sodium sulfate and concentrated *in vacuo.* The residue was subjected to purification by flash chromatography on silica (Hex:DCM 0-100% DCM over 18 min, 18 ml/min, 12 g silica) to yield the desired cross-coupled product.

General procedure II (Suzuki coupling). A degassed solution of the corresponding aryl halogenide (1.00 eq), $Pd[PPh_3]_4$ (0.03 eq), a boronic acid (1.30 eq) and an inorganic base (3.0 eq) in the mixture of toluene, ethanol and water (7:2:1 v/v/v, 0.4M) was subjected to microwave impact at 140 ^oC for 10 min, which was repeated if necessary. The crude reaction mixture was diluted with double volume of ethyl acetate and the organic phase was washed with saturated aqueous $NaHCO_3$, brine, dried over anhydrous sodium sulfate and concentrated *in vacuo.* The resulting residue was purified by means of flash chromatography on silica to yield the desired cross-coupled product.

General procedure III (S_NAr). A stirred solution of corresponding aryl halogenide (1.0 eq), suitable inorganic base (3.00 eq) and the nucleophile (1.50 eq) in DMSO was heated up to

100 ^{o}C and stirred at this temperature for 8 hours. The reaction mixture was allowed to cool down to room temperature and poured into ice-cold water (4x volume of the reaction mixture). The precipitate formed was filtered off, dried on air and used in the next steps without additional purification.

General procedure IV (reductive amination). To the ice-cold stirred solution of corresponding aldehyde (1.00 eq) and amine (1.00 eq) in the appropriate anhydrous solvent (0.3 M) was added sodium triacetoxyborohydride or sodium borohydride (2.00 eq) portionwise over two minutes, after which the resulting reaction mixture was stirred at 0 ^{o}C for ten minutes and allowed to warm up to room temperature. The reaction was quenched by adding excess of aqueous $NaHCO_3$, pH of the aqueous phase was set to 6 and it was extracted with ethyl acetate. The combined organic fractions were washed with brine, dried over anhydrous sodium sulfate and concentrated *in vacuo.* The residue was subjected to purification by flash column chromatography to yield the desired product.

General procedure V (nitro-group reduction by hydrogenation). The solution of a corresponding nitro-compound containing palladium on charcoal (10% m/m, 20 wt.% Pd) was stirred under hydrogen atmosphere for four hours, after which the reaction mixture was filtered through a short pad of Celite. The resulting mother liquor was concentrated *in vacuo* to obtain corresponding amine, which was used further without additional purification.

General procedure VI (-*Boc* protection group installation). To the stirred solution of the amine and the base in appropriate solvent was added Boc_2O (1.1 eq) at 0^{o}C. The reaction mixture was stirred at room temperature for 5 hours, after which it was diluted with aqueous sodium hydrocarbonate solution (1/5 from the volume of the reaction mixture) and the resulting solution was extracted with ethyl acetate, the combined organic fractions were washed with brine, dried over anhydrous Na_2SO_4 and concentrated *in vacuo*. The protected amine was purified using flash chromatography if necessary.

General procedure VII (-*Boc* protection group removal). To the solution of the respective Boc-protected amine in anhydrous DCM was added HCl (2.0 M solution in dioxane, 20 eq.) and the resulting mixture was stirred at room temperature for two hours. The reaction mixture was concentrated *in vacuo* and the resulting residue was purified by recrystallization or chromatography if necessary.

General procedure VIII (electrophilic bromination using NBS). To the solution of the corresponding substituted benzene (1.0 eq) in DMF at 0^{o}C was added NBS (1.1 eq) upon vigorous stirring. The resulting reaction mixture was stirred for a specified amount of time, after which diluted with water (10x the volume of the reaction mixture), extracted with a specified organic solvent, washed with brine, dried over anhydrous Na_2SO_4 and concentrated *in vacuo*.

The resulting residue was used in further transformations without additional purification if not specified otherwise.

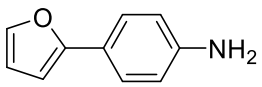

Fr1

Fr1 4-(furan-2-yl)aniline was synthesized from 4-iodo aniline (2.11 g, 9.66 mmol), $Pd[PPh_3]_4$ (330 mg, 0.29 mmol), and 2-(Tri-n-butylstannyl)furan (3.80 g, 10.6 mmol) following **General procedure I** to obtain the title compound as slightly brown solid (1.01 g, 6.28 mmol, 65% yield).

LC-MS: $[M+H]^+$ 160.18

^{1}H NMR (500 MHz, DMSO-d_6) δ 7.56 (dd, *J* = 1.8, 0.7 Hz, 1H), 7.37 – 7.32 (m, 2H), 6.60 – 6.56 (m, 2H), 6.53 (dd, *J* = 3.3, 0.7 Hz, 1H), 6.48 (dd, *J* = 3.3, 1.8 Hz, 1H), 5.28 (s, 2H).

^{13}C NMR (126 MHz, $CDCl_3$) δ 154.72, 145.95, 141.01, 125.35, 122.15, 115.27, 111.56, 102.52.

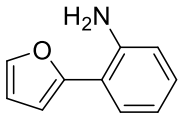

Fr2

Fr2 2-(furan-2-yl)aniline was synthesized from 2-iodo aniline (1.37 g, 6.30 mmol), $Pd[PPh_3]_4$ (215 mg, 0.18 mmol), and 2-(Tri-n-butylstannyl)furan (2.47 g, 6.90 mmol) following **General procedure I** to obtain the title compound as off-white solid (720 mg, 4.52 mmol, 76% yield).

LC-MS: $[M+H]^+$ 160.14

^{1}H NMR (500 MHz, $CDCl_3$) δ 7.51 – 7.50 (m, 1H), 7.48 (dd, *J* = 7.8, 1.5 Hz, 1H), 7.12 (td, *J* = 8.1, 1.5 Hz, 1H), 6.82 – 6.77 (m, 1H), 6.75 (dd, *J* = 8.1, 0.8 Hz, 1H), 6.59 – 6.57 (m, 1H), 6.51 (dd, *J* = 3.3, 1.8 Hz, 1H), 4.36 (s, 2H).

^{13}C NMR (126 MHz, $CDCl_3$) δ 153.6, 143.3, 141.4, 128.9, 127.80, 118.5, 116.8, 116.3, 111.5, 106.5.

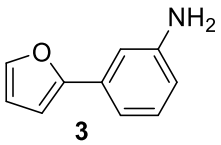

3

3 3-(furan-2-yl)aniline was synthesized from 3-iodo aniline (1.14 g, 5.22 mmol), $Pd[PPh_3]_4$ (175 mg, 0.15 mmol), and 2-(Tri-n-butylstannyl)furan (2.05 g, 5.72 mmol) following

General procedure I to obtain the title compound as a colorless solid (590 mg, 3.70 mmol, 71% yield).

LC-MS: $[M+H]^+$ 160.13

^{1}H NMR (500 MHz, $CDCl_3$) δ 7.45 (d, *J* = 1.3 Hz, 1H), 7.17 (t, *J* = 7.8 Hz, 1H), 7.10 – 7.07 (m, 1H), 7.03 – 7.02 (m, 1H), 6.61 (d, *J* = 3.2 Hz, 1H), 6.59 (dd, *J* = 2.3, 0.9 Hz, 1H), 6.46 (dd, *J* = 3.3, 1.8 Hz, 1H), 3.71 (s, 2H).

^{13}C NMR (126 MHz, $CDCl_3$) δ 154.2, 146.80, 142.0, 131.9, 129.7, 114.60, 114.4, 111.6, 110.4, 105.1.

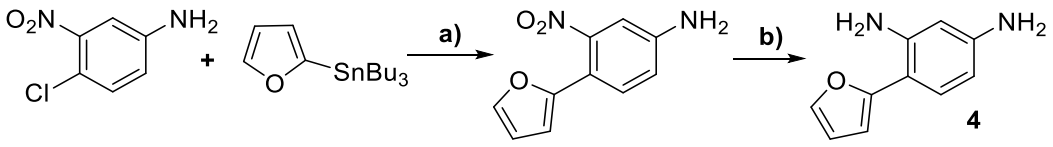

Scheme 1. Synthesis of compound **4**

(Step a) 4-(furan-2-yl)-3-nitroaniline was synthesized from 4-chloro-3-nitroaniline (300 mg, 1.72 mmol), $Pd[PPh_3]_4$ (60 mg, 0.05 mmol), and 2-(Tri-n-butylstannyl)furan (680 mg, 1.90 mmol) following **General procedure I** to obtain the title compound as a yellowish solid (130 mg, 0.64 mmol, 37% yield).

^{1}H NMR (500 MHz, DMSO-d_6) δ 8.27 (d, *J* = 2.7 Hz, 1H), 7.94 (dd, *J* = 9.1, 2.7 Hz, 1H), 7.80 (d, *J* = 1.7 Hz, 1H), 6.95 (d, *J* = 3.4 Hz, 1H), 6.87 (d, *J* = 9.1 Hz, 1H), 6.77 (s, 2H), 6.66 (dd, *J* = 3.4, 1.8 Hz, 1H).

^{13}C NMR (126 MHz, DMSO-d_6) δ 151.2, 150.1, 143.1, 136.8, 125.1, 123.7, 115.8, 113.5, 112.3, 108.6.

(Step b) 4 4-(furan-2-yl)benzene-1,3-diamine was synthesized using **General procedure VI** from 4-(furan-2-yl)-3-nitroaniline (60 mg, 0.29 mmol), palladium on charcoal (6 mg). The desired aniline was obtained as brownish solid (51 mg, 0.29 mmol, quant. yield).

^{1}H NMR (500 MHz, DMSO-d_6) δ 7.67 (d, *J* = 1.4 Hz, 1H), 6.78 (d, *J* = 2.6 Hz, 1H), 6.64 (d, *J* = 3.3 Hz, 1H), 6.59 – 6.55 (m, 2H), 6.40 (dd, *J* = 8.4, 2.6 Hz, 1H), 4.45 (s, 4H).

^{13}C NMR (126 MHz, DMSO-d_6) δ 152.7, 141.2, 139.5, 135.2, 118.1, 116.1, 115.8, 111.8, 111.6, 106.4.

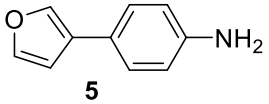

5

5 4-(furan-3-yl)aniline was synthesized from 4-iodo aniline (84 mg, 0.4 mmol), $Pd[PPh_3]_4$ (8 mg, 7 μmol), 3-furanylboronic acid (109 mg, 0.98 mmol) and KF (87 mg, 1.5 mmol) using dioxane (1.5 mL) as solvent and following **General procedure II**. The title compound was iso-

lated by flash chromatography (Hex:DCM 0-100% DCM over 18 min, 18 mL/min, 12 g silica) as slightly beige solid (43 mg, 0.27 mmol, 68% yield).

LC-MS: $[M+H]^+$ 160.18

^{1}H NMR (500 MHz, $CDCl_3$) δ 7.66 – 7.64 (m, 1H), 7.52 (t, *J* = 1.7 Hz, 1H), 7.20 (dd, *J* = 7.6, 1.5 Hz, 1H), 7.14 – 7.10 (m, 1H), 6.79 (td, *J* = 7.5, 1.2 Hz, 1H), 6.76 (dd, *J* = 8.0, 1.0 Hz, 1H), 6.64 (dd, *J* = 1.8, 0.8 Hz, 1H).

^{13}C NMR (126 MHz, $CDCl_3$) δ 145.6, 143.5, 137.4, 127.1, 126.55, 123.1, 115.6, 108.9.

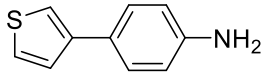

7

7 4-(thiophen-2-yl)aniline was synthesized from 4-bromoaniline (172 mg, 1.00 mmol), 3-thiphenylboronic acid (192 mg, 1.50 mmol), $Pd[PPh_3]_4$ (12 mg, 10 μmol) and KF (174 mg, 3.00 mmol) using dioxane (4.0 mL) as solvent and following **General procedure II**. The title compound was isolated by flash chromatography (Hex:EA 0-100% EA over 15 min, 18 mL/min, 12 g silica) as beige solid (168 mg, 0.96 mmol, 96% yield).

LC-MS: $[M+H]^+$ 176.08

^{1}H NMR (500 MHz, $CDCl_3$) δ 7.46 – 7.12 (m, 5H), 6.91 – 6.53 (m, 2H), 3.62 (s, 2H).

^{13}C NMR (126 MHz, $CDCl_3$) δ 145.7, 142.6, 127.6, 126.8, 126.3, 126.0, 118.2, 115.5.

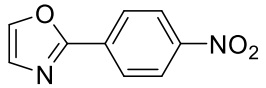

2-(4-nitrophenyl)oxazole. 4-nitrobenzaldehyde (302 mg, 2.00 mmol), TosMIC (390 mg, 2.00 mmol) and K_2CO_3 (415 mg, 6.00 mmol) were dissolved in methanol (10.0 mL) and the resulting reaction mixture was stirred under nitrogen atmosphere at 80°C for 8 hours. The mixture was concentrated *in vacuo* and the residue was taken up into water (40 mL). The aqueous fraction was extracted with ethyl acetate (3x25 mL), washed with brine, dried over anhydrous $MgSO_4$ and evaporated to yield the desired product as brownish solid (358 mg, 1.88 mmol, 94% yield).

LC-MS: $[M+H]^+$ 191.05

^{1}H NMR (500 MHz, DMSO-d_6) δ 8.62 (s, 1H), 8.36 – 8.32 (m, 2H), 8.02 (s, 1H), 8.02 – 7.99 (m, 2H).

^{13}C NMR (126 MHz, DMSO-d_6) δ 153.5, 148.7, 146.8, 133.3, 125.7, 125.0, 124.6.

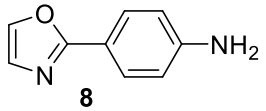

8

8 4-(oxazol-2-yl)aniline was synthesized following the **General procedure VI** from 2-(4-nitrophenyl)oxazole (350 mg, 1.86 mmol) and palladium on charcoal (40 mg), which were sus-

pended in EtOH (10.0 mL). The desired aniline was obtained as light-yellow solid (295 mg, 1.86 mmol, quant. yield).

LC-MS: $[M+H]^+$ 161.20

^{1}H NMR (500 MHz, DMSO-d_6) δ 8.24 (s, 1H), 7.38 – 7.34 (m, 2H), 7.29 (s, 1H), 6.64 – 6.58 (m, 2H), 5.45 (s, 1H).

NMR data is in accordance with literature.[1]

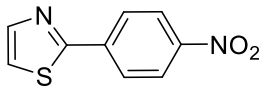

2-(4-nitrophenyl)thiazole was synthesized using 2-bromothiazole (164 mg, 1.01 mmol), 4,4,5,5-tetramethyl-2-(4-nitrophenyl)-1,3,2-dioxaborolane (261 mg, 1.05 mmol), $Pd[PPh_3]_4$ (35 mg, 30 μmol), K_2CO_3(553 mg, 4.00 mmol) and following the **General procedure II.** The desired product was obtained as pale yellow solid (107 mg, 0.52 mmol, 52% yield).

LC-MS: $[M+H]^+$ 207.06

^{1}H NMR (500 MHz, $CDCl_3$) δ 8.34 – 8.29 (m, 2H), 8.18 – 8.12 (m, 2H), 7.97 (d, *J* = 3.2 Hz, 1H), 7.49 (d, *J* = 3.2 Hz, 1H).

NMR data is in accordance with literature.[2]

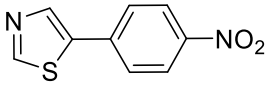

5-(4-nitrophenyl)thiazole was synthesized using 5-bromothiazole (164 mg, 1.0 mmol), 4,4,5,5-tetramethyl-2-(4-nitrophenyl)-1,3,2-dioxaborolane (261 mg, 1.05 mmol), $Pd[PPh_3]_4$ (35 mg, 30 μmol), K_2CO_3(553 mg, 4.00 mmol) and following the **General procedure II.** The desired product was obtained as pale yellow solid (205 mg, 0.99 mmol, 99% yield).

LC-MS: $[M+H]^+$ 207.11

^{1}H NMR (500 MHz, $CDCl_3$) δ 8.88 (s, 1H), 8.31 – 8.26 (m, 2H), 8.23 (d, *J* = 7.6 Hz, 1H), 7.77 – 7.71 (m, 2H).

NMR data is in accordance with literature.[3]

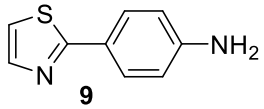

9

9 4-(thiazol-2-yl)aniline was synthesized from 2-(4-nitrophenyl)thiazole (103 mg, 0.50 mmol) and palladium on charcoal (10.0 mg) suspended in EtOH (3.0 mL) and following the **General procedure VI.** The desired compound was isolated as beige solid (85 mg, 0.48 mmol, 96% yield).

LC-MS: $[M+H]^+$ 177.10

^{1}H NMR (500 MHz, $CDCl_3$) δ 7.74-7.71 (m, 2H), 7.60 (d, 1H), 7.49 (d, 1H), 6.62-6.59 (m, 2H), 5.63(s, 2H).

NMR data is in accordance with literature.[4]

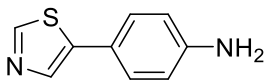

10

10 4-(thiazol-5-yl)aniline was synthesized from 5-(4-nitrophenyl)thiazole (202 mg, 0.98 mmol) and palladium on charcoal (20.0 mg) suspended in EtOH (5.0 mL) according to **General procedure VI** and obtained as yellowish solid (149 mg, 0.97 mmol, 98% yield)

LC-MS: $[M+H]^+$ 177.05

^{1}H NMR (500 MHz, $CDCl_3$) δ 7.91 – 7.86 (m, 2H), 7.80 (d, *J* = 3.3 Hz, 1H), 7.25 (d, *J* = 3.3 Hz, 1H), 7.06 – 7.01 (m, 2H).

NMR data is in accordance with literature.[4]

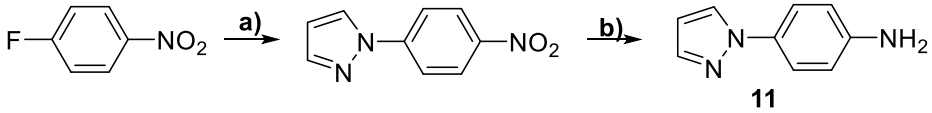

11

Scheme 2. Synthesis of compound **11**

Step a): 1-(4-nitrophenyl)-1H-pyrazole was synthesized from 4-nitrofluorobenzene (282 mg, 2.00 mmol), pyrazole (204 mg, 3.00 mmol) and Cs_2CO_3 (1.30 g, 4.00 mmol) using DMSO (4.0 mL) as solvent and following the **General procedure III**. The diluted with water reaction mixture was extracted with ethyl acetate (4x20 mL), washed with brine, dried over anhydrous $MgSO_4$ and concentrated *in vacuo* to afford the desired product as a yellowish solid (370 mg, 1.98 mmol, 98% yield), which was used in further transformation without additional purification.

LC-MS: $[M+H]^+$ 190.06

^{1}H NMR (500 MHz, DMSO-d6) δ 8.72 (d, *J* = 2.6 Hz, 1H), 8.39 – 8.34 (m, 2H), 8.15 – 8.11 (m, 2H), 7.89 (d, *J* = 1.6 Hz, 1H), 6.66 (dd, *J* = 2.5, 1.8 Hz, 1H).

^{13}C NMR (126 MHz, DMSO-d6) δ 144.78, 144.10, 142.86, 128.91, 125.46, 118.49, 109.43.

Step b): 11 4-(1H-pyrazol-1-yl)aniline was synthesized from 1-(4-nitrophenyl)-1H-pyrazole (100 mg, 0.53 mmol) and palladium on charcoal (10 mg) suspended in EtOH (5.0 mL) following **General procedure VI**. The desired aniline was isolated as white solid (80 mg, 0.50 mmol, 95% yield).

LC-MS: $[M+H]^+$ 160.08

^{1}H NMR (500 MHz, DMSO-d6) δ 8.18 (dd, *J* = 2.4, 0.4 Hz, 1H), 7.60 (d, *J* = 1.4 Hz, 1H), 7.45 – 7.39 (m, 1H), 6.66 – 6.60 (m, 1H), 6.44 – 6.40 (m, 1H), 5.20 (s, 2H).

^{13}C NMR (126 MHz, DMSO-d6) δ 147.42, 139.48, 129.84, 126.87, 120.06, 113.97, 106.65.

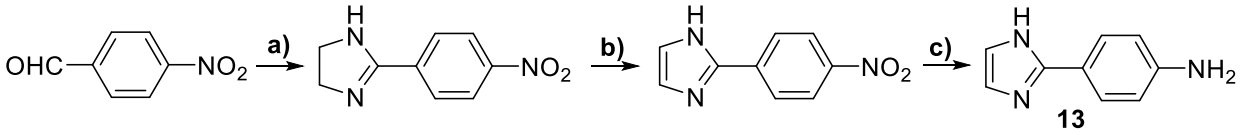

Scheme 3. Synthesis of compound **13**

Step a): 2-(4-nitrophenyl)-4,5-dihydro-1H-imidazole. 4-nitrobenaldehyde (450 mg, 2.98 mmol) and ethylenediamine (196 mg, 3.27 mmol) were suspended in *tert*-butanol (25.0 ml) and the mixture was left to stir for 90 minutes at room temperature. To the resulting yellow suspension K_2CO_3 (1234.0 mg, 8.93 mmol) and I_2 (944.1 mg, 3.72 mmol) were added and the reaction mixture was stirred at 80^{o}C under nitrogen atmosphere for 3.5 hours, after which the heating was removed and the reaction was quenched by adding saturated aqueous solution of sodium sulfite (10.0 ml). The volatiles from the resulting mixture were removed under reduced pressure and the aqueous residue was extracted with chloroform (2x40 mL), the combined organic fractions were washed with saturated aqueous $NaHCO_3$, brine, dried over anhydrous $MgSO_4$ and concentrated *in vacuo* to yield the desired imidazoline (430.0 mg, 2.25 mmol, 75% yield), which was used in the next step without additional purification.

LC-MS: $[M+H]^+$ 192.11

^{1}H NMR (500 MHz, $CDCl_3$) δ 8.29 – 8.25 (m, 2H), 7.97 – 7.93 (m, 2H), 3.86 (s, 4H).

NMR data is in accordance with literature.[5]

Step b): 2-(4-nitrophenyl)-1H-imidazole. 2-(4-nitrophenyl)-4,5-dihydro-1H-imidazole (429 mg, 2.25 mmol), diacetoxyiodobenzene (797 mg, 2.47 mmol) and K_2CO_3 (341 mg, 2.47 mmol) were suspended in DMSO (20.0 mL) and the resulting mixture was stirred at room temperature overnight. The reaction mixture was diluted with water (200.0 mL) and extracted with ethyl acetate (3x50 mL). The combined organic fractions were washed with brine, dried over anhydrous Na_2SO_4 and evaporated *in vacuo* to yield the residue, which was subjected to flash chromatography (Hex:EA 0-100% EA, over 25 min, 22 mL/min, 24 g silica, in 100% EA), which afforded the desired compound as yellow solid (210 mg, 1.11 mmol, 49%).

LC-MS: $[M+H]^+$ 190.09

^{1}H NMR (500 MHz, DMSO-d_6) δ 12.96 (s, 1H), 8.34 – 8.30 (m, 2H), 8.20 – 8.16 (m, 2H), 7.42 (dd, J = 2.0, 0.9 Hz, 1H), 7.16 (s, 1H).

^{13}C NMR (126 MHz, DMSO-d_6) δ 146.4, 143.6, 136.6, 130.4, 125.4, 124.3, 119.7.

Step c): 13 4-(1H-imidazol-2-yl)aniline was obtained following the **General procedure VI** from 2-(4-nitrophenyl)-1H-imidazole (60 mg, 0.32 mmol) and palladium on charcoal (10 mg)

suspended in EtOH (3.0 mL). The desired aniline was obtained as slightly reddish solid (51 mg, 0.32 mmol, quant. yield).

LC-MS: $[M+H]^+$ 160.18

^{1}H NMR (500 MHz, MeOD) δ 7.61 – 7.57 (m, 2H), 7.04 (s, 2H), 6.78 – 6.73 (m, 2H), 3.35 (s, 2H).

^{13}C NMR (126 MHz, MeOD) δ 150.3, 148.9, 127.7, 122.7, 120.4, 116.1.

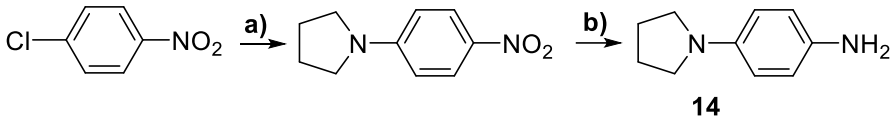

14

Scheme 4. Synthesis of compound **14**

Step a): 1-(4-nitrophenyl)pyrrolidine was obtained from 1-chloro-4-nitrobenzene (630 mg, 4.00 mmol), pyrrolidine (427 mg, 6.00 mmol) and K_2CO_3 (8.00 g, 57.8 mmol) using DMF (55.0 mL) as a solvent and following the **General procedure III.** The obtained precursor was used in the next step without additional purification.

LC-MS: $[M+H]^+$ 192.04

Step b): 14 4-(pyrrolidin-1-yl)aniline was synthesized following the **General procedure VI** from crude 1-(4-nitrophenyl)pyrrolidine (1.00 g of the precipitate) and palladium on charcoal (90 mg), which were suspended in ethanol (20.0 mL). The residue obtained after the concentration of mother liquor was purified by flash chromatography (DCM:MeOH 0-10% DCM over 15 min, 25 mL/min, 24 g silica), which afforded the desired aniline as slightly purple solid (420 mg, 2.80 mmol, 55% yield).

LC-MS: $[M+H]^+$ 163.17

^{1}H NMR (500 MHz, DMSO-d_6) δ 9.87 (s, 3H), 7.16 (d, *J* = 8.8 Hz, 2H), 6.59 (d, *J* = 8.5 Hz, 2H), 4.72 (s, 3H), 3.22 (t, *J* = 6.5 Hz, 4H), 1.98 – 1.93 (m, 4H).

NMR data is in accordance with literature.[6]

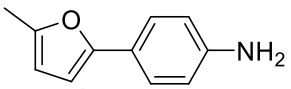

15

15 4-(5-methylfuran-2-yl)aniline was synthesized from 4-iodoaniline (55 mg, 0.25 mmol), 2-(2-Furanyl)-4,4,5,5-tetramethyl-1,3,2-dioxaborolane (55 mg, 0.27 mmol), $Pd[PPh_3]_4$ (6 mg, 5.0 μmol) and K_2CO_3 (138 mg, 1.00 mmol) using the mixture of dioxane (2.0 mL) and water (1.0 mL) as solvent and following the **General procedure II.** The desired product was purified by flash chromatography (Hex:EA 0-10% EA over 15 min, 18 mL/min, 12 g silica) and obtained as slightly beige solid (36 mg, 0.21 mmol, 84% yield).

LC-MS: $[M+H]^+$ 174.13

^{1}H NMR (500 MHz, $CDCl_3$) δ 7.44 – 7.42 (m, 2H), 6.70 – 6.66 (m, 2H), 6.32 (d, *J* = 3.1 Hz, 1H), 6.01 – 5.98 (m, 1H), 3.71 (s, 2H), 2.34 (s, 3H).

^{13}C NMR (126 MHz, $CDCl_3$) δ 153.0, 150.8, 145.5, 124.9, 122.6, 115.3, 107.5, 103.4, 13.8.

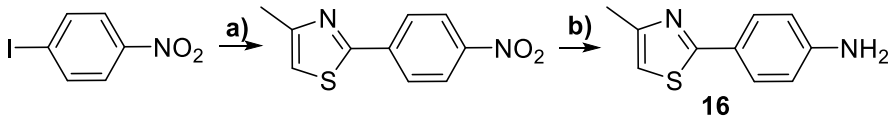

16

Scheme 5. Synthesis of compound **16**

Step a): 4-methyl-2-(4-nitrophenyl)thiazole. 4-iodoaniline (498 mg, 2.00 mmol), 4-methylthiazole (198 mg, 2.00 mmol), $Pd(OAc)_2$ (22 mg, 0.10 mmol) and CuI (76 mg, 0.40 mmol) were weighed into a glass vial in argon atmosphere and suspended in anhydrous and de-gassed DMF (5.0 ml). The resulting reaction mixture was stirred at 140 °C for 8 hours, after which it was diluted with water and extracted with ethyl acetate (3x30 mL). The combined organic fractions were washed with saturated $NaHCO_3$ solution, brine, dried over anhydrous Na_2SO_4 and concentrated *in vacuo*. The residue was purified by flash chromatography (Hex:EA 0-100% EA over 19 min, 18 mL/min, 12 g silica) and obtained as orange solid (260.0 mg, 1.20 mmol, 60% yield).

LC-MS: $[M+H]^+$ 221.13

^{1}H NMR (500 MHz, $CDCl_3$) δ 8.32 – 8.26 (m, 2H), 8.15 – 8.06 (m, 2H), 7.04 (d, *J* = 0.9 Hz, 1H), 2.55 (d, *J* = 0.9 Hz, 3H).

NMR and MS data are in accordance with literature.[7]

Step b): 16 4-(4-methylthiazol-2-yl)aniline was synthesized following the **General procedure VI** from 4-methyl-2-(4-nitrophenyl)thiazole (250 mg, 1.14 mmol) and palladium on charcoal (25 mg). The desired compound was obtained as beige solid (214 mg, 98% yield).

LC-MS: $[M+H]^+$ 191.25

^{1}H NMR (500 MHz, $CDCl_3$) δ 7.76 – 7.71 (m, 2H), 6.74 (d, *J* = 0.9 Hz, 1H), 6.71 – 6.67 (m, 2H), 3.87 (s, 2H), 2.47 (d, *J* = 0.9 Hz, 3H).

^{13}C NMR (126 MHz, DMSO-d6) δ 163.59, 154.34, 147.82, 138.58, 126.95, 124.54, 117.42, 16.84.

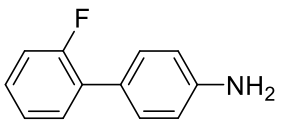

18

18 2'-fluoro-[1,1'-biphenyl]-4-amine was synthesized from 4-iodo aniline (110 mg, 0.50 mmol), $Pd[PPh_3]_4$ (17 mg, 15 μmol), (2-fluorophenyl)-boronic acid (133 mg, 0.70 mmol) and K_3PO_4 (318 mg, 1.50 mmol) using dioxane (2.0 mL) as solvent and following **General procedure II**. The desired compound was isolated by flash chromatography (Hex:DCM 0-100% DCM

over 15 min, 18 mL/min, 12 g silica) and obtained as colorless solid (71 mg, 0.38 mmol, 77% yield).

LC-MS: $[M+H]^+$ 188.11

^{1}H NMR (500 MHz, $CDCl_3$) δ 7.42 – 7.35 (m, 3H), 7.23 (ddd, *J* = 9.7, 4.7, 2.2 Hz, 1H), 7.16 (td, *J* = 7.5, 1.2 Hz, 1H), 7.11 (ddd, *J* = 10.9, 8.1, 1.2 Hz, 1H), 6.77 – 6.74 (m, 2H), 3.73 (s, 2H).

^{13}C NMR (126 MHz, $CDCl_3$) δ 159.91 (d, *J* = 246.5 Hz), 146.18, 130.43 (d, *J* = 3.7 Hz), 130.14 (d, *J* = 3.2 Hz), 129.19 (d, *J* = 13.1 Hz), 128.07 (d, *J* = 8.2 Hz), 126.07, 124.36 (d, *J* = 3.7 Hz), 116.13 (d, *J* = 23.0 Hz), 115.13.

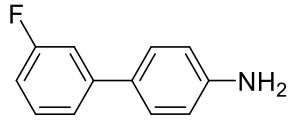

19

19 3'-fluoro-[1,1'-biphenyl]-4-amine was synthesized using 4-iodoaniline (109 mg, 0.50 mmol), (3-fluorophenyl)-boronic acid (84 mg, 0.6 mmol), $Pd[PPh_3]_4$ (25 mg, 22 μmol) and K_2CO_3 (207 mg, 1.50 mmol), using the mixture of dioxane (3.0 mL) and water (1.0 mL) as solvent and following the **General Procedure II**. The desired compound was isolated by flash chromatography (Hex:DCM 0-100% DCM over 15 min, 18 mL/min, 12 g silica) and obtained as colorless solid (59 mg, 0.32 mmol, 63% yield).

LC-MS: $[M+H]^+$ 188.12

^{1}H NMR (500 MHz, $CDCl_3$) δ 7.46 – 7.37 (m, 5H), 7.12 – 7.07 (m, 1H), 6.75 (d, *J* = 7.5 Hz, 2H), 4.00 (s, 2H).

NMR is in accordance with literature data.[8]

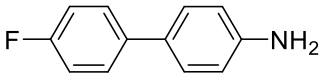

20

20 4'-fluoro-[1,1'-biphenyl]-4-amine was synthesized from 4-iodoaniline (110 mg, 0.50 mmol), $Pd[PPh_3]_4$ (17 mg, 15 μmol), (4-fluorophenyl)-boronic acid (133 mg, 0.98 mmol) and K_3PO_4 (318 mg, 1.50 mmol) using dioxane (2.0 mL) as solvent and following **General procedure II**. The desired compound was isolated by flash chromatography (Hex:DCM 0-100% DCM over 15 min, 18 mL/min, 12 g silica) and obtained as colorless solid (88 mg, 0.47 mmol, 94% yield).

LC-MS: $[M+H]^+$ 188.09

^{1}H NMR (500 MHz, $CDCl_3$) δ 7.50 – 7.45 (m, 2H), 7.37 – 7.33 (m, 2H), 7.11 – 7.05 (m, 2H), 6.77 – 6.73 (m, 2H), 3.73 (s, 2H).

^{13}C NMR (126 MHz, $CDCl_3$) δ 162.00 (d, *J* = 244.7 Hz), 145.93, 137.45 (d, *J* = 3.2 Hz), 130.81, 128.03, 127.98 (d, *J* = 7.9 Hz), 115.57 (d, *J* = 21.2 Hz), 115.54.

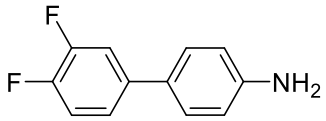

21

21 3',4'-difluoro-[1,1'-biphenyl]-4-amine was synthesized from 4-iodoaniline (110 mg, 0.50 mmol), $Pd[PPh_3]_4$ (17 mg, 15 μmol), (3,4-difluorophenyl)-boronic acid (133 mg, 0.98 mmol) and K_3PO_4 (318 mg, 1.50 mmol) using dioxane (2.0 mL) as solvent and following **General procedure II**. The desired compound was isolated by flash chromatography (Hex:DCM 0-100% DCM over 15 min, 18 mL/min, 12 g silica) and obtained as yellowish solid (71 mg, 0.35 mmol, 69% yield).

LC-MS: $[M+H]^+$ 206.06

^{1}H NMR (500 MHz, DMSO-d6) δ 7.57 (ddd, *J* = 12.4, 7.7, 1.8 Hz, 1H), 7.43 – 7.34 (m, 4H), 6.64 – 6.61 (m, 2H), 5.30 (s, 2H).

NMR is in accordance with literature data.[8]

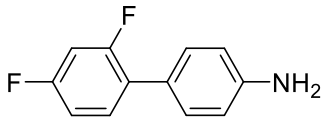

22

22 2',4'-difluoro-[1,1'-biphenyl]-4-amine was synthesized from 4-iodoaniline (110 mg, 0.50 mmol), $Pd[PPh_3]_4$ (17 mg, 15 μmol), (2,4-difluorophenyl)-boronic acid (133 mg, 0.98 mmol) and K_3PO_4 (318 mg, 1.50 mmol) using dioxane (2.0 mL) as solvent and following **General procedure II**. The desired compound was isolated by flash chromatography (Hex:DCM 0-100% DCM over 15 min, 18 mL/min, 12 g silica) and obtained as brownish solid (64 mg, 0.31 mmol, 62% yield).

LC-MS: $[M+H]^+$ 206.06

^{1}H NMR (500 MHz, DMSO-d6) δ 7.63 (dd, *J* = 4.9, 2.9 Hz, 1H), 7.56 (dd, *J* = 2.8, 1.2 Hz, 1H), 7.29 (dd, *J* = 4.9, 1.2 Hz, 1H), 7.11 (dd, *J* = 7.5, 1.4 Hz, 1H), 7.06 – 6.97 (m, 1H), 6.76 (dd, *J* = 8.0, 0.8 Hz, 1H), 6.61 (td, *J* = 7.5, 1.0 Hz, 1H), 4.86 (s, 2H).

^{13}C NMR (126 MHz, DMSO-d6) δ 145.23, 139.85, 129.70, 128.16, 128.02, 126.29, 122.09, 120.75, 116.63, 115.45.

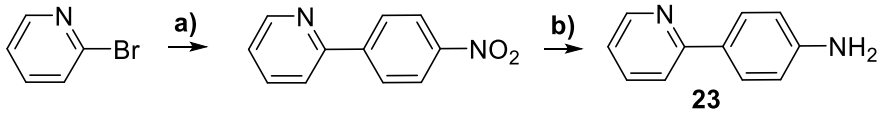

23

Scheme 6. Synthesis of compound **23**

Step a): 2-(4-nitrophenyl)pyridine was synthesized from 2-bromopyridine (516 mg, 2.00 mmol), 4,4,5,5-tetramethyl-2-(4-nitrophenyl)-1,3,2-dioxaborolane (523 mg, 2.10 mmol),

$Pd[PPh_3]_4$ (70 mg, 60 μmol) and K_2CO_3 (553 mg, 8.00 mmol), using the mixture of dioxane (3.0 mL) and water (1.0 mL) as solvent and following the **General Procedure II**. The desired compound was isolated by flash chromatography (Hex:EA 0-100% EA over 15 min, 18 mL/min, 12 g silica) and obtained as scarlet solid (300 mg, 1.50 mmol, 75% yield).

LC-MS: $[M+H]^+$ 201.28

^{1}H NMR (500 MHz, $CDCl_3$) δ 8.77 – 8.74 (m, 1H), 8.36 – 8.32 (m, 2H), 8.21 – 8.16 (m, 2H), 7.86 – 7.79 (m, 2H), 7.35 (ddd, *J* = 6.7, 4.8, 2.0 Hz, 1H).

NMR is in accordance with literature data.[9]

Step b): 23 4-(pyridin-2-yl)aniline was synthesized using 2-(4-nitrophenyl)pyridine (150 mg, 0.75 mmol) and palladium on charcoal (15 mg) suspended in EtOH (5.0 mL) and following **General procedure VI**. The desired product was obtained as yellowish solid (125 mg, 0.73 mmol, 98% yield).

LC-MS: $[M+H]^+$ 171.14

^{1}H NMR (500 MHz, $CDCl_3$) δ 8.62 (ddd, *J* = 4.8, 1.7, 0.9 Hz, 1H), 7.86 – 7.80 (m, 2H), 7.70 – 7.66 (m, 1H), 7.63 (dt, *J* = 8.0, 1.1 Hz, 1H), 7.12 (ddd, *J* = 7.2, 4.8, 1.2 Hz, 1H), 6.79 – 6.75 (m, 2H), 3.82 (s, 2H).

NMR is in accordance with literature data.[9]

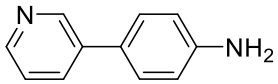

24

24 4-(pyridin-3-yl)-aniline was synthesized from 4-iodoaniline (219 mg, 1.00 mmol), pyridin-3-ylboronic acid (147 mg, 1.20 mmol), $Pd[PPh_3]_4$ (35 mg, 30 μmol) and K_2CO_3 (414 mg, 3.00 mmol), using the mixture of dioxane (6.0 mL) and water (2.0 mL) as solvent and following the **General Procedure II**. The desired compound was isolated by flash chromatography (Hex:EA 0-100% EA over 16 min, 18 mL/min, 12 g silica) and obtained as off-white solid (127 mg, 0.75 mmol, 75% yield).

LC-MS: $[M+H]^+$ 171.10

^{1}H NMR (500 MHz, $CDCl_3$) δ 8.79 (dd, *J* = 2.4, 0.7 Hz, 1H), 8.50 (dd, *J* = 4.8, 1.6 Hz, 1H), 7.80 (ddd, *J* = 7.9, 2.3, 1.7 Hz, 1H), 7.43 – 7.38 (m, 2H), 7.31 (ddd, *J* = 7.9, 4.8, 0.8 Hz, 1H), 6.80 – 6.76 (m, 2H), 3.80 (s, 2H).

^{13}C NMR (126 MHz, $CDCl_3$) δ 147.86, 147.56, 146.73, 136.70, 133.61, 128.20, 128.02, 123.60, 115.65.

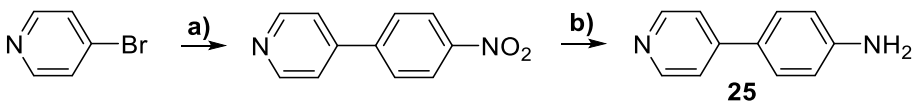

25

Scheme 7. Synthesis of compound **25**

Step a): 4-(4-nitrophenyl)-pyridine was synthesized from 4-bromopyridinium hydrochloride (97 mg, 0.5 mmol), (4-nitrophenyl)-boronic acid pinacol ester (174 mg, 0.70 mmol), $Pd[PPh_3]_4$ (29 mg, 25 μmol) and K_3PO_4 (212 mg, 1.00 mmol), using the mixture of dioxane (3.4 mL) and water (0.1 mL) as solvent and following the **General Procedure II**. The desired compound was isolated by flash chromatography (Hex:EA 0-100% EA over 12 min, 18 mL/min, 12 g silica) and obtained as slightly orange solid (70 mg, 0.35 mmol, 70% yield).

LC-MS: $[M+H]^+$ 201.18

^{1}H NMR (500 MHz, DMSO-d6) δ 8.73 (d, *J* = 6.0 Hz, 2H), 8.36 (t, *J* = 5.6 Hz, 2H), 8.10 (d, *J* = 8.8 Hz, 2H), 7.82 (d, *J* = 6.1 Hz, 2H).

^{13}C NMR (126 MHz, DMSO-d6) δ 150.55, 147.85, 144.81, 143.58, 128.35, 124.25, 121.69.

Step b): 25 4-(pyridin-4-yl)aniline was synthesized using 4-(4-nitrophenyl)-pyridine (60 mg, 0.32 mmol) and palladium on charcoal (6 mg) suspended in EtOH (3.0 mL) and following **General procedure VI**. The desired aniline was obtained as yellowish solid (54 mg, 0.32 mmol, 99% yield).

LC-MS: $[M+H]^+$ 171.10

^{1}H NMR (500 MHz, DMSO-d6) δ 8.47 (d, *J* = 5.9 Hz, 2H), 7.55 (d, *J* = 6.0 Hz, 2H), 7.53 (d, *J* = 8.5 Hz, 2H), 6.66 (d, *J* = 8.5 Hz, 2H), 5.51 (s, 2H).

^{13}C NMR (126 MHz, DMSO-d6) δ 150.25, 149.91, 147.17, 127.45, 123.38, 119.42, 114.05.

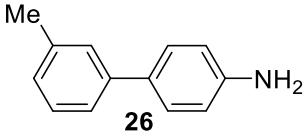

26

26 3'-methyl-[1,1'-biphenyl]-4-amine was synthesized using 4-iodoaniline (109 mg, 0.50 mmol), m-tolylboronic acid (82 mg, 0.6 mmol), $Pd[PPh_3]_4$ (20 mg, 25.0 μmol) and K_2CO_3 (207 mg, 1.50 mmol), using the mixture of dioxane (3.0 mL) and water (1.0 mL) as solvent and following the **General Procedure II**. The desired compound was isolated by flash chromatography (Hex:DCM 0-100% DCM over 15 min, 18 mL/min, 12 g silica) and obtained as colorless solid (64 mg, 0.35 mmol, 70% yield).

LC-MS: $[M+H]^+$ 184.17

^{1}H NMR (500 MHz, $CDCl_3$) δ 7.43 – 7.39 (m, 2H), 7.36 – 7.32 (m, 2H), 7.29 (t, *J* = 7.5 Hz, 1H), 7.09 (d, *J* = 7.3 Hz, 1H), 6.79 – 6.73 (m, 2H), 3.72 (s, 2H), 2.40 (s, 3H).

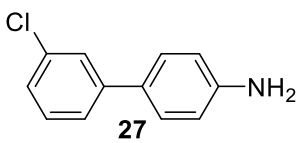

27

27 3'-chloro-[1,1'-biphenyl]-4-amine was synthesized using 4-iodoaniline (110 mg, 0.50 mmol), (3-cholophenyl)-boronic acid (109 mg, 0.70 mmol), $Pd[PPh_3]_4$ (29 mg, 25 μmol) and K_3PO_4 (318 mg, 1.50 mmol), using dioxane (2.0 mL) as solvent and following the **General Procedure II**. The desired compound was isolated by flash chromatography (Hex:DCM 0-100% DCM over 16 min, 18 mL/min, 12 g silica) and obtained as white solid (66 mg, 0.33 mmol, 66% yield).

LC-MS: $[M+H]^+$ 204.17, 206.16

^1H NMR (500 MHz, $CDCl_3$) δ 7.51 (t, *J* = 1.8 Hz, 1H), 7.42 – 7.37 (m, 3H), 7.31 (t, *J* = 7.8 Hz, 1H), 7.25 – 7.21 (m, 1H), 6.78 – 6.73 (m, 2H), 3.77 (s, 2H).

^{13}C NMR (126 MHz, $CDCl_3$) δ 146.51, 143.15, 134.66, 130.15, 130.00, 128.15, 126.58, 126.31, 124.59, 115.50.

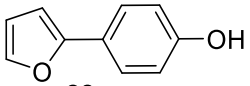

28

28 4-(furan-2-yl)phenol was obtained from 4-iodophenol (220 mg, 1.00 mmol), $Pd[PPh_3]_4$ (30 mg, 26 μmol), and 2-(Tri-n-butylstannyl)furan (464 mg, 1.30 mmol) following **General procedure I** to obtain the title compound as white crystalline solid (128 mg, 0.80 mmol, 80% yield).

^1H NMR (500 MHz, $CDCl_3$) δ 7.58 – 7.54 (m, 2H), 7.43 – 7.41 (m, 1H), 6.87 – 6.83 (m, 2H), 6.51 (d, *J* = 3.3 Hz, 1H), 6.44 (dd, *J* = 3.3, 1.8 Hz, 1H), 4.77 (s, 1H).

NMR data is in accordance with literature.[10]

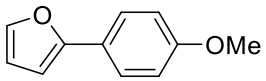

29

29 2-(4-methoxyphenyl)furan was synthesized from 4-iodoanisol (117 mg, 0.50 mmol), $Pd[PPh_3]_4$ (17 mg, 15 μmol), and 2-(Tri-n-butylstannyl)furan (232 mg, 0.65 mmol) following **General procedure I** . The title compound was obtained as white solid (44 mg, 0.23 mmol, 46% yield).

^1H NMR (500 MHz, $CDCl_3$) δ 7.62 – 7.58 (m, 2H), 7.43 – 7.42 (m, 1H), 6.94 – 6.90 (m, 2H), 6.51 (d, *J* = 3.3 Hz, 1H), 6.44 (dd, *J* = 3.3, 1.8 Hz, 1H), 3.84 (s, 3H).

NMR data is in accordance with literature.[11]

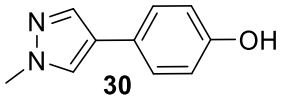

30

30 4-(1-methyl-1H-pyrazol-4-yl)phenol **GPK-102** was synthesized using 4-iodophenol (110 mg, 0.5 mmol), 1-methyl-4-(4,4,5,5-tetramethyl-1,3,2-dioxaborolan-2-yl)-1H-pyrazole (114 mg, 0.55 mmol), $Pd[PPh_3]_4$ (29 mg, 25 μmol) and K_2CO_3 (207 mg , 1.5 mmol) following the

General Procedure II. The title compound was isolated by flash chromatography (Hex:EA 0-100% EA over 15 min, 18 mL/min, 12 g silica) as white solid (52 mg, 0.3 mmol, 60% yield).

LC-MS: $[M+H]^+$ 175.10

^{1}H NMR (500 MHz, $CDCl_3$) δ 7.76 (s, 1H), 7.61 (s, 1H), 7.49 – 7.44 (m, 2H), 7.36 (dd, *J* = 10.7, 4.8 Hz, 2H), 7.22 (t, *J* = 7.4 Hz, 1H), 3.95 (s, 3H).

^{13}C NMR (126 MHz, $CDCl_3$) δ 136.91, 132.77, 128.99, 127.04, 126.49, 125.65, 123.39, 39.25.

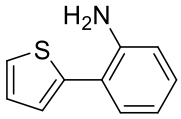

2-(thiophen-2-yl)aniline was synthesized from 2-iodoaniline (220.0 mg, 1.0 mmol), $Pd[PPh_3]_4$ (11.6 mg, 10 μmol), (2-thienyl)-boronic acid (192.0 mg, 1.5 mmol) and K_2CO_3 (174.0 mg, 3.0 mmol) using the mixture of dioxane (2.0 mL) and water (0.5 mL) as solvent and following **General procedure II**. The desired compound was isolated by flash chromatography (Hex:DCM 0-100% DCM over 20 min, 18 mL/min, 12 g silica) and obtained as off-white solid (105.0 mg, 0.6 mmol, 60 % yield).

LC-MS: $[M+H]^+$ 177.06

^{1}H NMR (500 MHz, $CDCl_3$) δ 7.35 (dd, *J* = 5.1, 0.6 Hz, 1H), 7.28 (dd, *J* = 7.6, 1.5 Hz, 1H), 7.20 (dd, *J* = 3.5, 0.6 Hz, 1H), 7.16 (dd, *J* = 7.7, 1.4 Hz, 1H), 7.12 (dd, *J* = 5.1, 3.8 Hz, 1H).

^{13}C NMR (126 MHz, $CDCl_3$) δ 144.19, 141.23, 131.14, 129.17, 127.68, 125.94, 125.37, 120.11, 118.69, 115.99.

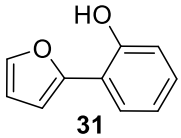

31

31 2-(furan-2-yl)phenol was synthesized from 2-bromophenol (259 mg, 1.50 mmol), $Pd[PPh_3]_4$ (86 mg, 75 μmol) and 2-(Tri-n-butylstannyl)furan (464 mg, 1.30 mmol) following **General procedure I** to obtain the title compound as white crystalline solid (150 mg, 0.93 mmol, 62% yield).

^{1}H NMR (500 MHz, $CDCl_3$) δ 7.51 – 7.50 (m, 1H), 7.48 (dd, *J* = 7.8, 1.5 Hz, 1H), 7.12 (td, *J* = 8.1, 1.5 Hz, 1H), 6.82 – 6.77 (m, 1H), 6.75 (dd, *J* = 8.1, 0.8 Hz, 1H), 6.59 – 6.57 (m, 1H), 6.51 (dd, *J* = 3.3, 1.8 Hz, 1H), 4.36 (s, 2H).

^{13}C NMR (126 MHz, $CDCl_3$) δ 153.6, 143.3, 141.4, 128.9, 127.80, 118.5, 116.8, 116.3, 111.5, 106.5.

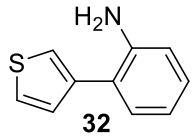

32

32 2-(thiophen-3-yl)aniline was synthesized from 2-iodoaniline (110 mg, 0.50 mmol), $Pd[PPh_3]_4$ (17 mg, 15 μmol), (3-thienyl)-boronic acid (90 mg, 0.70 mmol) and KF (87 mg, 1.5 mmol) using dioxane (2.0 mL) as solvent and following **General procedure II**. The desired compound was isolated by flash chromatography (Hex:DCM 0-100% DCM over 15 min, 18 mL/min, 12 g silica) and obtained as off-white solid (44 mg, 0.25 mmol, 50% yield).

LC-MS: $[M+H]^+$ 176.04

^{1}H NMR (500 MHz, $CDCl_3$) δ 7.51 – 7.50 (m, 1H), 7.48 (dd, *J* = 7.8, 1.5 Hz, 1H), 7.12 (td, *J* = 8.1, 1.5 Hz, 1H), 6.82 – 6.77 (m, 1H), 6.75 (dd, *J* = 8.1, 0.8 Hz, 1H), 6.59 – 6.57 (m, 1H), 6.51 (dd, *J* = 3.3, 1.8 Hz, 1H), 4.36 (s, 2H).

^{13}C NMR (126 MHz, $CDCl_3$) δ 153.6, 143.3, 141.4, 128.9, 127.80, 118.5, 116.8, 116.3, 111.5, 106.5.

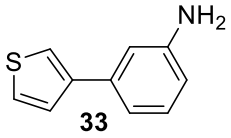

33

33 3-(thiophen-3-yl)aniline was synthesized from 3-iodoaniline (110 mg, 0.50 mmol), $Pd[PPh_3]_4$ (17 mg, 15 μmol), (3-thienyl)-boronic acid (90.0 mg, 0.70 mmol) and KF (87 mg, 1.50 mmol) using dioxane (2.0 mL) as solvent and following **General procedure II**. The desired compound was isolated by flash chromatography (Hex:DCM 0-100% DCM over 15 min, 18 mL/min, 12 g silica) and obtained as off-white solid (62 mg, 0.36 mmol, 71% yield).

LC-MS: $[M+H]^+$ 176.02

^{1}H NMR (500 MHz, DMSO-d6) δ 7.65 (dd, *J* = 2.9, 1.3 Hz, 1H), 7.59 (dd, *J* = 5.0, 2.9 Hz, 1H), 7.40 (dd, *J* = 5.0, 1.3 Hz, 1H), 7.04 (t, *J* = 7.8 Hz, 1H), 6.86 (t, *J* = 1.9 Hz, 1H), 6.84 – 6.81 (m, 1H), 6.50 (ddd, *J* = 7.9, 2.2, 0.8 Hz, 1H), 5.09 (s, 2H).

^{13}C NMR (126 MHz, DMSO-d6) δ 149.03, 142.34, 135.72, 129.34, 126.70, 126.13, 120.09, 113.98, 112.98, 111.51.

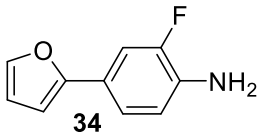

34

34 2-fluoro-4-(furan-2-yl)aniline was synthesized from 2-fluoro-4-iodoaniline (237 mg, 1.00 mmol), $Pd[PPh_3]_4$ (58 mg, 50 μmol), and 2-(Tri-n-butylstannyl)furan (535 mg, 1.5 mmol) following **General procedure I** to obtain the title compound as slightly brown solid (124 mg, 0.7 mmol, 70% yield).

LC-MS: $[M+H]^+$ 178.17

^{1}H NMR (500 MHz, $CDCl_3$) δ 7.40 (d, *J* = 1.2 Hz, 1H), 7.31 (dd, *J* = 12.2, 1.9 Hz, 1H), 7.26 (dd, *J* = 8.0, 1.7 Hz, 2H), 6.80 – 6.75 (m, 1H), 6.46 (d, *J* = 3.3 Hz, 1H), 6.43 (dd, *J* = 3.3, 1.8 Hz, 1H), 3.78 (s, 2H).

^{19}F NMR (470 MHz, $CDCl_3$) δ -135.17 – -135.22 (m).

^{13}C NMR (126 MHz, $CDCl_3$) δ 153.61 (d, *J* = 2.6 Hz), 151.78 (d, *J* = 238.3 Hz), 141.45, 133.94 (d, *J* = 13.2 Hz), 122.57 (d, *J* = 7.3 Hz), 120.34 (d, *J* = 2.9 Hz), 117.06 (d, *J* = 3.8 Hz), 111.70, 111.25 (d, *J* = 20.5 Hz), 103.45.

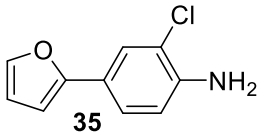

35

35 2-fluoro-4-(furan-2-yl)aniline was synthesized from 4-bromo-2-chloroaniline (206 mg, 1.00 mmol), $Pd[PPh_3]_4$ (15 mg, 13 μmol), and 2-(Tri-n-butylstannyl)furan (536 mg, 1.5 mmol) following **General procedure I** to obtain the title compound as slightly green solid (123 mg, 0.64 mmol, 64% yield).

LC-MS: $[M+H]^+$ 194.06, 196.00

^{1}H NMR (500 MHz, $CDCl_3$) δ 7.58 (d, *J* = 2.0 Hz, 1H), 7.40 (dd, *J* = 1.8, 0.7 Hz, 1H), 7.38 (dd, *J* = 8.3, 2.0 Hz, 1H), 6.77 (d, *J* = 8.3 Hz, 1H), 6.46 (dd, *J* = 3.3, 0.7 Hz, 1H), 6.43 (dd, *J* = 3.3, 1.8 Hz, 1H), 4.17 – 4.04 (m, 2H).

NMR data is in accordance with literature.[12]

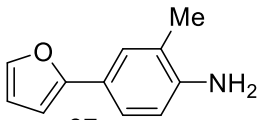

37

37 4-(furan-2-yl)-2-methylaniline was synthesized from 4-bromo-2-methylaniline (186 mg, 1.00 mmol), $Pd[PPh_3]_4$ (58 mg, 50 μmol), and 2-(Tri-n-butylstannyl)furan (535 mg, 1.5 mmol) following **General procedure I** to obtain the title compound as green-yellow solid (64 mg, 0.37 mmol, 37% yield).

LC-MS: $[M+H]^+$ 174.12

^{1}H NMR (500 MHz, $CDCl_3$) δ 7.39 (s, 2H), 7.36 (dd, *J* = 8.2, 1.6 Hz, 1H), 6.68 (d, *J* = 8.2 Hz, 1H), 6.42 (dt, *J* = 3.3, 2.6 Hz, 1H), 3.67 (s, 2H).

^{13}C NMR (126 MHz, $CDCl_3$) δ 154.89, 144.25, 140.94, 126.41, 123.08, 122.50, 122.16, 115.14, 111.55, 102.43, 17.58.

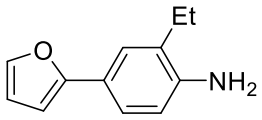

39

39 2-ethyl-4-(furan-2-yl)aniline was synthesized from 4-bromo-2-ethylaniline (200 mg, 1.00 mmol), $Pd[PPh_3]_4$ (58 mg, 50 μmol), and 2-(Tri-n-butylstannyl)furan (535 mg, 1.5 mmol) following **General procedure I** to obtain the title compound as beige-colored solid (161 mg, 0.86 mmol, 86% yield).

LC-MS: $[M+H]^+$ 188.12

^{1}H NMR (500 MHz, $CDCl_3$) δ 7.40 (d, *J* = 2.0 Hz, 1H), 7.39 (dd, *J* = 1.8, 0.6 Hz, 1H), 7.36 (dd, *J* = 8.2, 2.0 Hz, 1H), 6.69 (d, *J* = 8.2 Hz, 1H), 6.45 (d, *J* = 3.3 Hz, 1H), 6.42 (dd, *J* = 3.3, 1.8 Hz, 1H), 3.69 (s, 2H), 2.55 (q, *J* = 7.5 Hz, 2H), 1.29 (t, *J* = 7.5 Hz, 3H).

^{13}C NMR (126 MHz, $CDCl_3$) δ 155.00, 143.68, 140.94, 128.25, 124.45, 122.96, 122.33, 115.60, 111.55, 102.43, 24.25, 13.13.

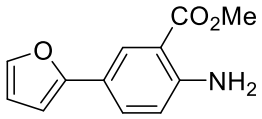

40

40 methyl 2-amino-5-(furan-2-yl)benzoate was synthesized from methyl 2-amino-5-bromobenzoate (1.15g, 5.00 mmol), $Pd[PPh_3]_4$ (140 mg, 0.25 mmol), and 2-(Tri-n-butylstannyl)furan (2.68 g, 7.50 mmol) following **General procedure I** to obtain the title compound as a light yellow solid (597 mg, 2.75 mmol, 55% yield).

LC-MS: $[M+H]^+$ 218.09

^{1}H NMR (500 MHz, $CDCl_3$) δ 8.18 (d, *J* = 2.1 Hz, 1H), 7.58 (dd, *J* = 8.6, 2.2 Hz, 1H), 7.41 (dd, *J* = 1.7, 0.6 Hz, 1H), 6.69 (d, *J* = 8.6 Hz, 1H), 6.47 (dd, *J* = 3.3, 0.6 Hz, 1H), 6.44 (dd, *J* = 3.3, 1.8 Hz, 1H), 5.81 (s, 2H), 3.90 (s, 3H).

^{13}C NMR (126 MHz, $CDCl_3$) δ 168.57, 153.94, 149.80, 141.20, 130.14, 126.77, 120.16, 117.18, 111.63, 110.80, 102.79, 51.82.

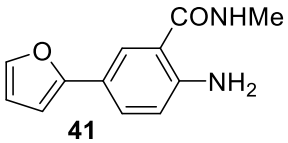

41

41 2-amino-5-(furan-2-yl)-N-methylbenzamide. To the aqueous solution of methylamine (1.0 mL, 40% wt.) was added methyl 2-amino-5-(furan-2-yl)benzoate (108 mg, 0.50 mmol) and the obtained reaction mixture was stirred at 80^{o}C under nitrogen atmosphere for 8 hours. The resulting reaction mixture was concentrated *in vacuo* to afford the title compound as yellowish solid (95 mg, 0.44 mmol, 88% yield), which was further used without additional purification.

LC-MS: $[M+H-CH_4N]^+$ 186.12

^{1}H NMR (500 MHz, $CDCl_3$) δ 7.63 (d, *J* = 2.0 Hz, 1H), 7.49 (dd, *J* = 8.5, 2.0 Hz, 1H), 7.40 (dd, *J* = 1.5, 1.0 Hz, 1H), 6.70 (d, *J* = 8.5 Hz, 1H), 6.46 – 6.42 (m, 2H), 3.00 (d, *J* = 4.9 Hz, 3H).

NMR data is in accordance with literature.[13]

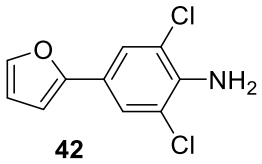

42

42 2,6-dichloro-4-(furan-2-yl)aniline was synthesized from 4-bromo-2,6-dichloroaniline (200 mg, 1.00 mmol), $Pd[PPh_3]_4$ (25 mg, 22 μmol), and 2-(Tri-n-butylstannyl)furan (428 mg, 1.20 mmol) following **General procedure I** to obtain the title compound as off-white solid (125 mg, 0.55 mmol, 55% yield).

LC-MS: $[M+H]^+$ 227.92, 229.95.

^{1}H NMR (500 MHz, Acetone-d6) δ 7.59 – 7.55 (m, 3H), 6.75 (d, *J* = 3.4 Hz, 1H), 6.51 (dd, *J* = 3.4, 1.8 Hz, 1H), 5.31 (s, 2H).

^{13}C NMR (126 MHz, Acetone-d6) δ 152.86, 142.98, 141.30, 124.23, 122.16, 120.12, 112.77, 105.14.

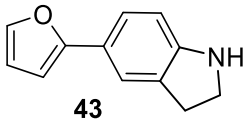

43

43 5-(furan-2-yl)-indoline was synthesized from 5-bromoindoline (99 mg, 0.5 mmol), $Pd[PPh_3]_4$ (29 mg, 25 μmol), and 2-(Tri-n-butylstannyl)furan (223 mg, 0.63 mmol) following **General procedure I** to obtain the title compound as brownish solid (98 mg, 0.5 mmol, 99% yield).

LC-MS: $[M+H]^+$ 186.17

^{1}H NMR (500 MHz, $CDCl_3$) δ 7.44 (s, 1H), 7.38 (s, 1H), 7.36 (dd, *J* = 8.1, 1.3 Hz, 1H), 6.64 (d, *J* = 8.1 Hz, 1H), 6.42 (d, *J* = 1.2 Hz, 2H), 3.60 (t, *J* = 8.4 Hz, 2H), 3.06 (t, *J* = 8.4 Hz, 2H).

^{13}C NMR (126 MHz, $CDCl_3$) δ 155.23, 151.33, 140.82, 129.87, 123.70, 122.36, 120.76, 111.54, 109.28, 102.23, 47.56, 29.78.

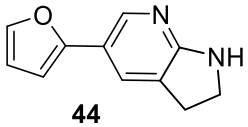

44

44 5-(furan-2-yl)-2,3-dihydro-1H-pyrrolo[2,3-b]pyridine was synthesized from 5-bromo-2,3-dihydro-1H-pyrrolo[2,3-b]pyridine (200 mg, 1.00 mmol), $Pd[PPh_3]_4$ (25 mg, 22 μmol), and 2-(Tri-n-butylstannyl)furan (428 mg, 1.20 mmol) following **General procedure I.**

The title compound was isolated by flash chromatography (Hex:EA 0-100% EA over 15 min, 18 mL/min, 12 g silica) as beige-colored solid (134 mg, 0.72 mmol, 72% yield).

LC-MS: $[M+H]^+$ 187.02

^{1}H NMR (500 MHz, DMSO-d6) δ 8.07 – 8.04 (m, 1H), 7.61 (d, *J* = 1.3 Hz, 1H), 7.53 (d, *J* = 1.3 Hz, 1H), 6.63 (d, *J* = 3.1 Hz, 1H), 6.61 (s, 1H), 6.50 (dd, *J* = 3.3, 1.8 Hz, 1H), 3.53 – 3.47 (m, 2H), 3.00 (t, *J* = 8.5 Hz, 2H).

^{13}C NMR (126 MHz, DMSO-d6) δ 164.31, 152.48, 141.52, 141.41, 126.66, 122.48, 115.92, 111.73, 102.65, 43.50, 26.76.

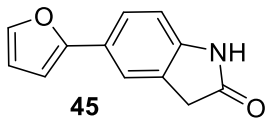

45

45 5-(furan-2-yl)-indolin-2-one was synthesized from 5-bromo-indolin-2-one (106 mg, 0.50 mmol), $Pd[PPh_3]_4$ (29 mg, 25 μmol), and 2-(Tri-n-butylstannyl)furan (223 mg, 0.63 mmol) following **General procedure I.** The title compound was isolated by flash chromatography (Hex:EA 0-100% EA over 17 min, 18 mL/min, 12 g silica) as white crystalline solid (99 mg, 0.49 mmol, 98% yield).

LC-MS: $[M+H]^+$ 200.24

^{1}H NMR (500 MHz, DMSO-d6) δ 10.47 (s, 1H), 7.68 – 7.66 (m, 1H), 7.55 (s, 1H), 7.52 (d, *J* = 8.1 Hz, 1H), 6.85 (d, *J* = 8.1 Hz, 1H), 6.77 (d, *J* = 3.3 Hz, 1H), 6.54 (dd, *J* = 3.2, 1.8 Hz, 1H), 3.52 (s, 2H).

^{13}C NMR (126 MHz, DMSO-d6) δ 176.30, 153.47, 143.18, 142.03, 126.59, 124.03, 122.98, 119.93, 111.95, 109.32, 103.90, 35.75.

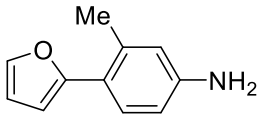

46

46 4-(furan-2-yl)-3-methylaniline was synthesized from 4-bromo-3-methylaniline (372 mg, 2.00 mmol), $Pd[PPh_3]_4$ (70 mg, 60.0 μmol), and 2-(Tri-n-butylstannyl)-furan (1.07 g, 3.00 mmol) following **General procedure I** to obtain the title compound as a colorless solid (277 mg, 1.60 mmol, 80% yield).

LC-MS: $[M+H]^+$ 174.12

^{1}H NMR (500 MHz, $CDCl_3$) δ 7.47 (d, *J* = 8.0 Hz, 1H), 7.44 (dd, *J* = 1.7, 0.6 Hz, 1H), 6.59 – 6.55 (m, 2H), 6.46 (dd, *J* = 3.3, 1.8 Hz, 1H), 6.37 – 6.35 (m, 1H), 3.69 (s, 2H), 2.40 (s, 3H).

^{13}C NMR (126 MHz, $CDCl_3$) δ 154.28, 145.94, 140.84, 136.30, 128.74, 121.48, 117.42, 112.85, 111.21, 106.51, 21.89.

NMR data is in accordance with literature.[14]

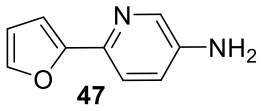

47

47 6-(furan-2-yl)pyridin-3-amine was synthesized from 6-bromopyridin-3-amine (173 mg, 1.00 mmol), $Pd[PPh_3]_4$ (50 mg, 50 μmol), and 2-(Tri-n-butylstannyl)-furan (464 mg, 1.30 mmol) following **General procedure I** to obtain the title compound as a off-white solid (133 mg, 0.83 mmol, 83% yield).

LC-MS: $[M+H]^+$ 161.10

^{1}H NMR (500 MHz, DMSO-d6) δ 7.93 (d, *J* = 2.3 Hz, 1H), 7.64 (dd, *J* = 1.7, 0.7 Hz, 1H), 7.40 (d, *J* = 8.5 Hz, 1H), 6.95 (dd, *J* = 8.5, 2.7 Hz, 1H), 6.71 (dd, *J* = 3.3, 0.7 Hz, 1H), 6.53 (dd, *J* = 3.3, 1.8 Hz, 1H), 5.51 (s, 2H).

NMR data is in accordance with literature.[15]

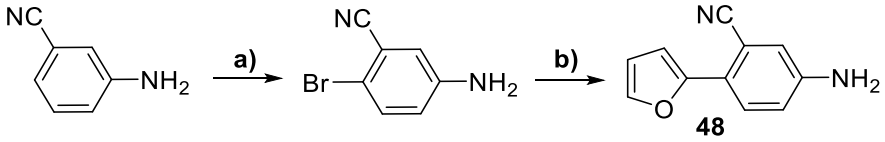

48

Scheme 8. Synthesis of compound **48**

Step a): 5-amino-2-bromobenzonitrile. To the stirred solution of 3-aminobenzonitrile (550 mg, 4.65 mmol) in DMF (6.0 mL) was added dropwise the solution of N-bromosuccinimide (828 mg, 4.88 mmol) in DMF (6.0 mL) over 30 min. at room temperature, after which the reaction mixture was stirred at room temperature overnight. The reaction mixture was diluted with water (200 mL), extracted with ethyl acetate (3x50 mL) and concentrated *in vacuo*. The resulting residue was re-dissolved in DCM (40 mL), the precipitate was filtered off, mother liquor was concentrated and purified by flash chromatography (Hex:EA 0-100% EA over 15 min, 18 mL/min, 12 g silica) to yield the desired compound as off-white solid (395 mg, 2.00 mmol, 43% yield).

LC-MS: [M+H] 196.98, 198.98

^{1}H NMR (500 MHz, DMSO-d6) δ 7.40 (d, *J* = 8.8 Hz, 1H), 6.95 (d, *J* = 2.8 Hz, 1H), 6.79 (dd, *J* = 8.8, 2.8 Hz, 1H), 5.78 (s, 2H).

^{13}C NMR (126 MHz, DMSO-d6) δ 179.88, 149.25, 133.80, 120.51, 118.61, 118.21, 114.54, 107.91, 29.99.

Step b): 48 5-amino-2-(furan-2-yl)benzonitrile was synthesized from 5-amino-2-bromobenzonitrile (196 mg, 1.00 mmol), $Pd[PPh_3]_4$ (57 mg, 49 μmol), and 2-(Tri-n-butylstannyl)-furan (500 mg, 1.40 mmol) following **General procedure I** and using flash chromatography (Hex:EA 0-100% EA over 15 min, 18 mL/min, 12 g silica) to obtain the title compound as a brownish solid (74 mg, 0.40 mmol, 40% yield).

LC-MS: 185.07

^{1}H NMR (500 MHz, DMSO-d6) δ 7.74 (d, *J* = 1.4 Hz, 1H), 7.55 (d, *J* = 8.4 Hz, 1H), 6.95 – 6.89 (m, 2H), 6.85 (d, *J* = 3.4 Hz, 1H), 6.60 (dd, *J* = 3.3, 1.8 Hz, 1H), 5.83 (s, 2H).

^{13}C NMR (126 MHz, DMSO-d6) δ 150.57, 148.62, 142.43, 127.61, 119.98, 119.11, 118.66, 117.22, 111.95, 106.86, 106.21.

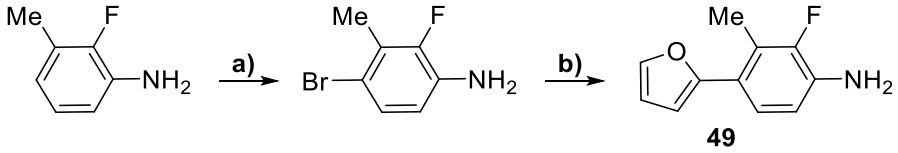

Scheme 9. Synthesis of compound **49**

Step a): 4-bromo-2-fluoro-3-methylaniline. To the stirred solution of 2-fluoro-3-methylaniline (458 mg, 3.66 mmol) in DMF (5.0 mL) was added dropwise the solution of N-bromosuccinimide (684 mg, 3.84 mmol) in DMF (10.0 mL) over 30 min. upon cooling the reaction mixture to 0°C, after which the reaction mixture was stirred at room temperature for 2 hours. The reaction mixture was diluted with water (250 mL), extracted with ethyl acetate (2x100 mL) and concentrated *in vacuo*. The resulting residue was concentrated and purified by flash chromatography (Hex:DCM 0-100% DCM over 18 min, 22 mL/min, 24g silica) to yield the desired compound as off-white solid (395 mg, 1.94 mmol, 53% yield).

LC-MS: $[M+H]^+$ 204.09, 206.08.

^{1}H NMR (500 MHz, DMSO-d6) δ 7.05 (dd, *J* = 8.6, 1.0 Hz, 1H), 6.56 (t, *J* = 9.0 Hz, 1H), 5.23 (s, 2H), 2.19 (d, *J* = 2.6 Hz, 3H).

^{19}F NMR (470 MHz, DMSO-d6) δ -133.10, -133.12.

^{13}C NMR (126 MHz, DMSO-d6) δ 148.92 (d, *J* = 239.0 Hz), 136.02 (d, *J* = 13.9 Hz), 127.21 (d, *J* = 3.6 Hz), 123.77 (d, *J* = 16.4 Hz), 114.60 (d, *J* = 5.3 Hz), 108.58 (d, *J* = 4.3 Hz), 14.46 (d, *J* = 4.7 Hz).

Step b): 49 2-fluoro-4-(furan-2-yl)-3-methylaniline was synthesized from 4-bromo-2-fluoro-3-methylaniline (100.0 mg, 0.49 mmol), $Pd[PPh_3]_4$ (29.0 mg, 25 μmol), and 2-(Tri-n-butylstannyl)-furan (219.0 mg, 0.6 mmol) following **General procedure I** which afforded the title compound as colorless solid (80.0 mg, 0.42 mmol, 85% yield).

LC-MS: $[M+H]^+$ 192.18.

^{1}H NMR (500 MHz, Acetone-d6) δ 7.56 (d, *J* = 1.7 Hz, 1H), 7.18 (dd, *J* = 8.4, 1.0 Hz, 1H), 6.74 (dd, *J* = 11.0, 6.5 Hz, 1H), 6.50 (dd, *J* = 3.3, 1.9 Hz, 1H), 6.43 (d, *J* = 3.3 Hz, 1H), 4.79 (s, 2H), 2.31 (d, *J* = 2.5 Hz, 3H).

^{19}F NMR (470 MHz, Acetone-d6) δ -140.49 (d, *J* = 9.2 Hz).

^{13}C NMR (126 MHz, Acetone-d6) δ 154.36 (d, *J* = 3.6 Hz), 150.56 (d, *J* = 233.3 Hz), 142.06, 136.63 (d, *J* = 14.6 Hz), 124.11 (d, *J* = 3.6 Hz), 122.53 (d, *J* = 15.3 Hz), 121.20 (d, *J* = 3.6 Hz), 114.40 (d, *J* = 4.9 Hz), 112.05, 107.53, 12.37 (d, *J* = 7.3 Hz).

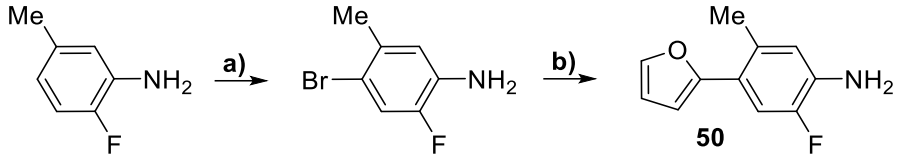

Scheme 10. Synthesis of compound **50**

Step a): 4-bromo-2-fluoro-5-methylaniline. To the stirred solution of 2-fluoro-5-methylaniline (500 mg, 4.00 mmol) in DMF (4.0 mL) was added dropwise the solution of N-bromosuccinimide (712 mg, 4.00 mmol) in DMF (8.0 mL) over 15 min. at room temperature and vigorous stirring, after which the reaction mixture was stirred at room temperature for 4 hours. The reaction mixture was diluted with water (250 mL), extracted with ethyl acetate (3x50 mL) and concentrated *in vacuo*. The resulting residue was concentrated and used in further steps without additional purification. Snow-white solid (720 mg, 3.50 mmol, 88% yield).

LC-MS: $[M+H]^+$ 204.09, 206.09.

^{1}H NMR (500 MHz, DMSO-d6) δ 7.27 (dd, *J* = 8.4, 2.9 Hz, 1H), 6.96 (td, *J* = 8.6, 2.9 Hz, 1H), 6.79 (dd, *J* = 8.9, 5.4 Hz, 1H), 5.16 (s, 2H).

^{19}F NMR (470 MHz, DMSO-d6) δ -127.82 – -127.93 (m).

^{13}C NMR (126 MHz, DMSO-d6) δ 153.89 (d, *J* = 234.9 Hz), 129.37, 128.68, 118.91 (d, *J* = 25.0 Hz), 116.02 (d, *J* = 8.0 Hz), 115.68 (d, *J* = 22.0 Hz), 21.51.

Step b): 50 2-fluoro-4-(furan-2-yl)-5-methylaniline was synthesized from 4-bromo-2-fluoro-5-methylaniline (102 mg, 0.5 mmol), $Pd[PPh_3]_4$ (29 mg, 25 μmol), and 2-(Tri-n-butylstannyl)-furan (219 mg, 0.6 mmol) following **General procedure I** which afforded the title compound as white solid (63 mg, 0.33 mmol, 66% yield).

LC-MS: $[M+H]^+$ 192.16.

^{1}H NMR (500 MHz, DMSO-d6) δ 7.65 (d, *J* = 1.7 Hz, 1H), 7.21 (d, *J* = 12.8 Hz, 1H), 6.64 (d, *J* = 9.3 Hz, 1H), 6.53 (dd, *J* = 3.3, 1.8 Hz, 1H), 6.48 (d, *J* = 3.3 Hz, 1H), 5.28 (s, 2H), 2.28 (s, 3H).

^{19}F NMR (470 MHz, DMSO-d6) δ -138.89 – -138.98 (m).

^{13}C NMR (126 MHz, DMSO-d6) δ 152.54 (d, *J* = 2.0 Hz), 148.79 (d, *J* = 234.8 Hz), 141.29, 135.71 (d, *J* = 12.9 Hz), 130.31 (d, *J* = 2.6 Hz), 118.23 (d, *J* = 4.7 Hz), 117.66 (d, *J* = 6.5 Hz), 112.83 (d, *J* = 19.7 Hz), 111.61, 106.60, 20.95.

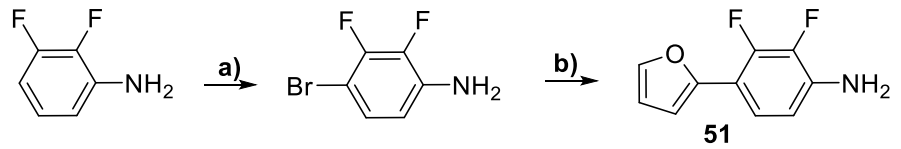

Scheme 11. Synthesis of compound **51**

Step a): 4-bromo-2,3-difluoroaniline. To the stirred solution of 2,3-difluoroaniline (516 mg, 4.00 mmol) in DMF (10.0 mL) was added N-bromosuccinimide (748 mg, 4.20 mmol) in a

portionwise manner over 15 min. at 0°C and vigorous stirring, after which the reaction mixture was stirred at room temperature for 2 hours. The reaction mixture was diluted with water (250 mL), extracted with ethyl acetate (3x50 mL) and concentrated *in vacuo.* The resulting residue was concentrated and used in further steps without additional purification. White solid (700 mg, 3.41 mmol, 84% yield).

LC-MS: $[M+H]^+$ 208.09, 210.08

^{1}H NMR (500 MHz, DMSO-d6) δ 7.11 (ddd, *J* = 9.2, 7.4, 2.1 Hz, 1H), 6.55 (td, *J* = 8.8, 1.9 Hz, 1H), 5.70 (s, 2H).

^{19}F NMR (470 MHz, DMSO-d6) δ -133.93 (dd, *J* = 21.1, 7.1 Hz), -157.20 (dd, *J* = 21.0, 8.6 Hz).

^{13}C NMR (126 MHz, DMSO-d6) δ 147.58 (d, *J* = 241.4 Hz), 147.49 (d, *J* = 241.3 Hz), 139.88 (d, *J* = 15.3 Hz), 137.96 (d, *J* = 15.0 Hz), 127.02 (d, *J* = 3.5 Hz), 112.25 – 112.12 (m).

Step b): 51 2,3-difluoro-4-(furan-2-yl)aniline was synthesized from 4-bromo-2,3-difluoroaniline (100 mg, 0.48 mmol), $Pd[PPh_3]_4$ (28 mg, 24 μmol), and 2-(Tri-n-butylstannyl)-furan (215 mg, 0.6 mmol) following **General procedure I** which afforded the title compound as colorless solid (78 mg, 0.4 mmol, 83% yield).

LC-MS: $[M+H]^+$ 196.14

^{1}H NMR (500 MHz, Acetone-d6) δ 7.58 (d, *J* = 1.4 Hz, 1H), 7.31 (td, *J* = 8.7, 2.0 Hz, 1H), 6.72 (td, *J* = 8.5, 1.7 Hz, 1H), 6.61 (t, *J* = 3.4 Hz, 1H), 6.54 (dd, *J* = 3.3, 1.8 Hz, 1H), 5.18 (s, 2H).

^{19}F NMR (470 MHz, Acetone) δ -143.40 (dd, *J* = 17.9, 7.0 Hz), -163.61 (dd, *J* = 17.6, 8.0 Hz).

^{13}C NMR (126 MHz, Acetone-d6) δ 149.03 – 148.95 (m), 148.52 (dd, *J* = 247.6, 12.1 Hz), 142.40, 140.60 (dd, *J* = 237.4, 14.4 Hz), 138.52 (dd, *J* = 9.9, 2.4 Hz), 121.37 (t, *J* = 4.1 Hz), 112.66, 112.41 (t, *J* = 3.3 Hz), 109.65 (d, *J* = 9.9 Hz), 107.80 (d, *J* = 9.7 Hz).

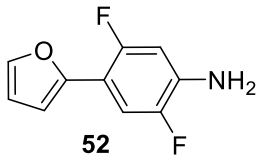

52

52 2,5-difluoro-4-(furan-2-yl)aniline was synthesized from 4-bromo-2,5-difluoroaniline (104 mg, 0.50 mmol), $Pd[PPh_3]_4$ (29 mg, 25 μmol), and 2-(Tri-n-butylstannyl)-furan (200 mg, 0.56 mmol) following **General procedure I** which afforded the title compound as colorless solid (76 mg, 0.4 mmol, 78% yield)

LC-MS: $[M+H]^+$ 196.14

^{1}H NMR (500 MHz, DMSO-d6) δ 7.68 (s, 1H), 7.31 (dd, *J* = 12.0, 6.9 Hz, 1H), 6.61 (dd, *J* = 12.8, 7.5 Hz, 1H), 6.58 – 6.55 (m, 2H), 5.70 (s, 2H).

^{19}F NMR (470 MHz, DMSO-d6) δ -119.59 (td, *J* = 14.0, 7.3 Hz), -139.71 – -139.80 (m).

^{13}C NMR (126 MHz, DMSO-d6) δ 154.62 (d, *J* = 241.7 Hz), 147.53 – 147.43 (m), 146.75 (d, *J* = 233.4 Hz), 141.64, 137.41 (dd, *J* = 15.4, 12.3 Hz), 111.99, 111.36 (dd, *J* = 22.8, 5.7 Hz), 106.92 (d, *J* = 9.6 Hz), 105.15 (dd, *J* = 15.4, 7.2 Hz), 102.48 (dd, *J* = 27.2, 5.2 Hz).

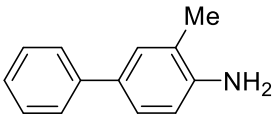

53

53 3-methyl-[1,1'-biphenyl]-4-amine was synthesized from 4-bromo-2-methylaniline (112 mg, 0.60 mmol), phenylboronic acid (95 mg, 0.78 mmol), $Pd[PPh_3]_4$ (21 mg, 18 μmol) and K_2CO_3 (249 mg, 1.8 mmol), using the mixture of dioxane (3.0 mL) and water (1.0 mL) as solvent and following the **General Procedure II**. The desired compound was isolated by flash chromatography (Hex:DCM 0-100% DCM over 15 min, 18 mL/min, 12 g silica) as colorless solid (72 mg, 0.4 mmol, 66% yield).

LC-MS: $[M+H]^+$ 184.18

^{1}H NMR (500 MHz, $CDCl_3$) δ 7.56 – 7.51 (m, 2H), 7.42 – 7.35 (m, *J* = 10.7, 4.7 Hz, 2H), 7.33 – 7.26 (m, 2H), 7.25 (s, 2H), 6.75 (dd, *J* = 8.0, 3.2 Hz, 1H), 3.67 (s, 2H), 2.24 (s, *J* = 2.8 Hz, 3H).

NMR and MS data is in accordance with literature.[16]

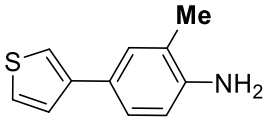

54

54 2-methyl-4-(thiophen-3-yl)aniline was synthesized from 4-bromo-2-methylaniline (93 mg, 0.5 mmol), (3-thienyl)-boronic acid (96 mg, 0.75 mmol), $Pd[PPh_3]_4$ (12 mg, 10 μmol) and KF (87 mg, 1.5 mmol), using dioxane (1.5 mL) as solvent and following the **General Procedure II**. The desired compound was isolated by flash chromatography (Hex:DCM 0-100% DCM over 15 min, 18 mL/min, 12 g silica) as colorless solid (52 mg, 0.3 mmol, 55% yield).

^{1}H NMR (500 MHz, $CDCl_3$) δ 7.35 – 7.31 (m, 3H), 7.31 – 7.28 (m, 2H), 6.74 (d, *J* = 8.1 Hz, 1H), 4.01 (s, 2H), 2.23 (s, 3H).

^{13}C NMR (126 MHz, $CDCl_3$) δ 142.66, 132.97, 129.70, 128.82, 126.35, 125.91, 125.26, 118.15, 115.46, 17.68.

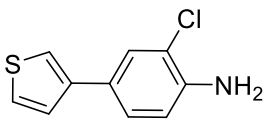

55

55 2-chloro-4-(thiophen-3-yl)aniline was synthesized from 4-bromo-2-chloroaniline (310 mg, 1.50 mmol), (3-thienyl)-boronic acid (288 mg, 2.30 mmol), $Pd[PPh_3]_4$ (35 mg, 30 μmol) and KF (262 mg, 4.50 mmol), using dioxane (5.0 mL) as solvent and following the **General Procedure II**. The desired compound was isolated by flash chromatography (Hex:EA 0-100% EA over 15 min, 18 mL/min, 12 g silica) as white solid (235 mg, 1.13 mmol, 75% yield).

LC-MS: $[M+H]^+$ 210.00, 212.00.

^{1}H NMR (500 MHz, $CDCl_3$) δ 7.42 (d, *J* = 2.0 Hz, 1H), 7.27 (dd, *J* = 4.8, 3.1 Hz, 1H), 7.24 – 7.20 (m, 3H), 6.70 (d, *J* = 8.3 Hz, 1H), 3.99 (s, 2H).

^{13}C NMR (126 MHz, $CDCl_3$) δ 142.05, 141.31, 127.58, 127.43, 126.30, 126.07, 125.93, 119.68, 118.85, 116.16.

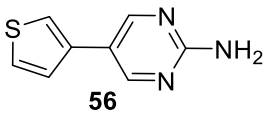

56

56 5-(thiophen-3-yl)pyrimidin-2-amine was synthesized from 5-bromopyrimidin-2-amine (174 mg, 1.00 mmol), (3-thienyl)-boronic acid (180 mg, 1.40 mmol), $Pd[PPh_3]_4$ (34 mg, 30 μmol) and KF (174 mg, 3.00 mmol), using dioxane (3.0 mL) as solvent and following the **General Procedure II**. The desired compound was isolated by flash chromatography (Hex:EA 0-100% EA over 15 min, 18 mL/min, 12 g silica) as white solid (101 mg, 0.57 mmol, 57% yield).

LC-MS: $[M+H]^+$ 178.06

^{1}H NMR (500 MHz, DMSO-d6) δ 8.62 (s, 2H), 7.77 (dd, *J* = 2.9, 1.3 Hz, 1H), 7.63 (dd, *J* = 5.0, 2.9 Hz, 1H), 7.52 (dd, *J* = 5.0, 1.3 Hz, 1H), 6.72 (s, 2H).

NMR data is in accordance with literature.[17]

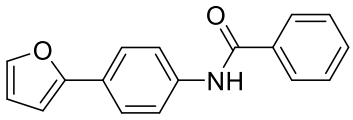

57

57 N-(4-(furan-2-yl)phenyl)benzamide. To a solution containing 4-(furan-2-yl)-aniline (80 mg, 0.5 mmol), pyridine (43 mg, 0.55 mmol) and catalytic amounts of DMAP in DCM (4.0 mL) was added benzoyl chloride (77 mg, 0.55 mmol) upon cooling with ice bath and vigorous stirring. The resulting mixture was stirred at room temperature overnight, quenched by adding aqueous solution of $NaHCO_3$ (1 mL), diluted with water (20 mL) and extracted with EtOAc (3x20 mL). The combined organic fractions were washed with brine, dried over anhydrous sodium sulfate and concentrated *in vacuo.* The residue was subjected to purification by flash column chromatography (Hex:EA 0-100% EA over 15 min, 18 L/min, 12 g silica) which afforded the desired product as white crystals (75 mg, 0.28 mmol, 57%).

LC-MS: $[M+H]^+$ 264.00

^{1}H NMR (500 MHz, DMSO-d6) δ 10.34 (s, 1H), 7.96 (dd, *J* = 5.2, 3.3 Hz, 2H), 7.87 – 7.85 (m, 2H), 7.72 (dd, *J* = 1.7, 0.5 Hz, 1H), 7.71 – 7.67 (m, 2H), 7.63 – 7.57 (m, 1H), 7.56 – 7.51 (m, 2H), 6.87 (dd, *J* = 3.3, 0.5 Hz, 1H), 6.58 (dd, *J* = 3.3, 1.8 Hz, 1H).

^{13}C NMR (126 MHz, DMSO-d6) δ 165.56, 153.04, 142.47, 138.52, 134.90, 131.61, 128.40, 127.67, 125.84, 123.82, 120.50, 112.04, 104.94.

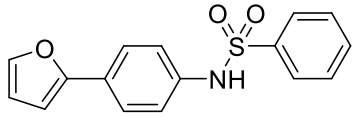

58

58 N-(4-(furan-2-yl)phenyl)benzenesulfonamide. To a solution containing 4-(furan-2-yl)-aniline (80 mg, 0.5 mmol) and pyridine (120 mg, 1.50 mmol) in DCM (4.0 mL) was added benzenesulfonyl chloride (115 mg, 0.65 mmol) upon cooling with ice bath and vigorous stirring. The resulting reaction mixture was stirred at room temperature for 6 hours, then diluted with saturated aqueous $NaHCO_3$, extracted with ethyl acetate (3x20 mL), the combined organic fractions were washed with brine, dried over anhydrous $MgSO_4$, concentrated *in vacuo*. The desired product was isolated by flash chromatography (DCM:EA 0-100% EA over 14 min, 18 mL/min, 12 g silica) as white solid (86 mg, 0.29 mmol, 58% yield).

LC-MS: $[M+H]^+$ 299.87

^{1}H NMR (500 MHz, $CDCl_3$) δ 7.77 (dt, *J* = 8.6, 1.6 Hz, 2H), 7.56 – 7.51 (m, 3H), 7.44 – 7.42 (m, 2H), 7.10 – 7.06 (m, 2H), 6.59 (dd, *J* = 6.2, 5.7 Hz, 2H), 6.45 (dd, *J* = 3.4, 1.8 Hz, 1H).

^{13}C NMR (126 MHz, $CDCl_3$) δ 153.22, 142.33, 139.05, 135.31, 133.26, 129.22, 128.63, 127.36, 124.89, 122.42, 111.88, 105.22.

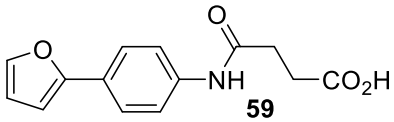

59

59 4-((4-(furan-2-yl)phenyl)amino)-4-oxobutanoic acid. To a solution containing 4-(furan-2-yl)-aniline (63 mg, 0.4 mmol) and triethylamine (120 mg, 1.20 mmol) in chloroform (1.0 mL) was added succinic anhydride (40 mg, 0.4 mmol) at room temperature. The resulting reaction mixture was stirred for 8 hours, then diluted with 1M aqueous HCl (500 μL) extracted with ethyl acetate (3x10 mL), the combined organic fractions were dried over anhydrous $MgSO_4$, concentrated *in vacuo* and subjected to reversed-phase flash chromatography (H_2O-MeCN 10-100% MeCN over 12 min, 13 mL/min, 14 g C18), which afforded the desired acylated product as white solid after lyophilization (94 mg, 0.26 mmol, 65% yield).

LC-MS: $[M+H]^+$ 259.96

^{1}H NMR (500 MHz, MeOD) δ 7.64 – 7.61 (m, 2H), 7.60 – 7.57 (m, 2H), 7.52 (d, *J* = 1.3 Hz, 1H), 6.68 (d, *J* = 3.2 Hz, 1H), 6.49 (dd, *J* = 3.4, 1.8 Hz, 1H).

^{13}C NMR (126 MHz, MeOD) δ 176.33, 172.83, 155.10, 143.07, 139.20, 128.18, 125.15, 121.20, 112.67, 105.32, 32.37, 29.99.

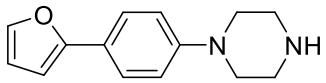

60

60 1-(4-(furan-2-yl)phenyl)piperazine was synthesized from 1-(4-bromophenyl)-piperazine (964 mg, 4.00 mmol), Pd[PPh$_3$]$_4$ (230 mg, 0.20 mmol), and 2-(Tri-n-butylstannyl)-furan (1.86 g, 5.20 mmol) following **General procedure I**. The desired compound was isolated by flash chromatography (DCM:MeOH 0-10% DCM over 19 min, 25 mL/min, 24 g silica). Slightly yellow solid (550 mg, 2.40 mmol, 60% yield).

LC-MS: [M+H]$^{+}$ 229.22

^{1}H NMR (500 MHz, DMSO-d6) δ 7.63 (d, *J* = 1.6 Hz, 1H), 7.53 (d, *J* = 8.8 Hz, 2H), 6.96 (d, *J* = 8.9 Hz, 2H), 6.70 (d, *J* = 3.3 Hz, 1H), 6.52 (dd, *J* = 3.3, 1.8 Hz, 1H), 3.15 – 3.10 (m, 4H), 2.91 – 2.86 (m, 4H).

^{13}C NMR (126 MHz, DMSO-d6) δ 153.59, 150.59, 141.62, 124.42, 121.17, 115.20, 111.84, 103.21, 48.38, 45.13.

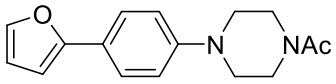

61

61 1-(4-(4-(furan-2-yl)phenyl)piperazin-1-yl)ethan-1-one was synthesized by acylation of 1-(4-bromophenyl)-piperazine (10 mg, 44 μmol) with Ac$_2$O (6.0 mg, 59 μmol) in the presence of DiPEA (11 mg, 85 μmol) and using DCM (1.5 mL) as a solvent. The solvent was evaporated *in vacuo* and the residue was purified by flash chromatography (DCM:EA 0-100% EA, over 15 min, 12 mL/min, 4 g silica) that delivered the desired compound as white solid (10 mg, 37 μmol, 84% yield).

LC-MS: [M+H]$^{+}$ 271.19

^{1}H NMR (500 MHz, DMSO-d6) δ 7.71 (d, *J* = 1.7 Hz, 1H), 7.62 (d, *J* = 8.8 Hz, 2H), 7.06 (d, *J* = 8.9 Hz, 2H), 6.78 (d, *J* = 3.3 Hz, 1H), 6.59 (dd, *J* = 3.3, 1.8 Hz, 1H), 3.67 – 3.61 (m, 4H), 3.30 – 3.25 (m, 2H), 3.23 – 3.19 (m, 2H), 2.11 (s, *J* = 2.9 Hz, 3H).

^{13}C NMR (126 MHz, DMSO-d6) δ 168.75, 153.95, 150.41, 142.19, 124.93, 122.07, 116.12, 112.33, 103.89, 48.65, 48.27, 45.81, 41.02, 21.68.

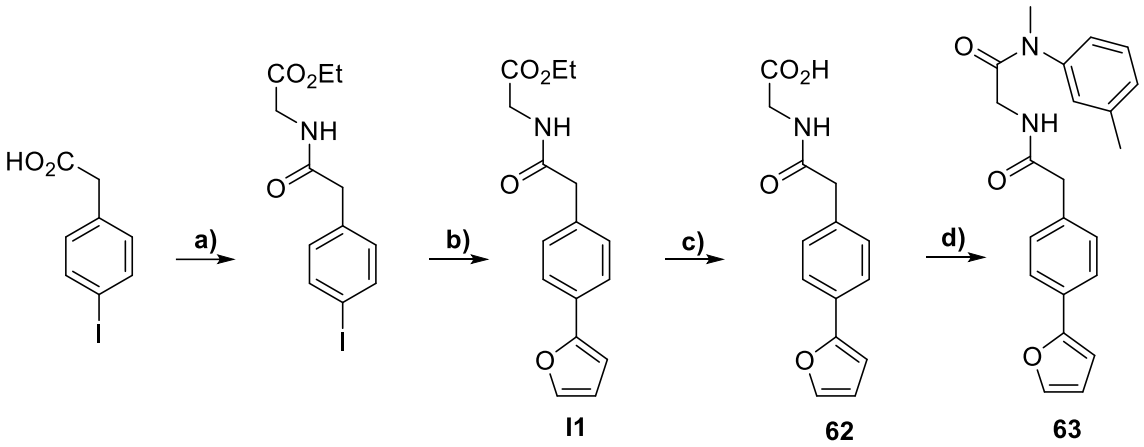

Scheme 12. Synthesis of compounds **62** and **63**

Step a): Ethyl (2-(4-iodophenyl)acetyl)glycinate. To the stirred solution of 2-(4-iodophenyl)acetic acid (1.05 g, 4.00 mmol), 7-aza-HOBt (599 mg, 4.40 mmol) and TEA (2.02 g, 20.0 mmol) in anhydrous DMF (20.0 mL) was added EDC·HCl (1.15 g, 6.00 mmol) in portions upon cooling over 10 min. The resulting solution was stirred for 15 min, after which glycine ethyl ester hydrochloride (614 mg, 4.41 mmol) was added to it in a portionwise manner. The resulting solution was stirred for 1 hour at room temperature, then at 50°C for another hour, after which it was diluted with water (300 mL), extracted with EtOAc (3x50 mL), the combined organic fractions were washed with water, brine, dried over anhydrous Na_2SO_4 and concentrated *in vacuo*. The desired product was isolated using flash chromatography (DCM:MeOH 0-10% over 22 min, 24 mL/min, 24 g silica) as white solid (1.00 g, 2.88 mmol, 72% yield).

LC-MS: $[M+H]^+$ 348.01

^{1}H NMR (500 MHz, DMSO-d6) δ 8.49 (t, *J* = 5.8 Hz, 1H), 7.68 – 7.62 (m, 2H), 7.10 – 7.06 (m, 2H), 4.07 (q, *J* = 7.1 Hz, 2H), 3.82 (d, *J* = 5.9 Hz, 2H), 3.44 (s, 2H), 1.16 (t, *J* = 7.1 Hz, 3H).

^{13}C NMR (126 MHz, DMSO-d6) δ 170.26, 169.81, 136.92, 135.90, 131.49, 92.25, 60.40, 41.27, 40.80, 14.04.

Step b): I1 Ethyl (2-(4-(furan-2-yl)phenyl)acetyl)glycinate was synthesized from ethyl (2-(4-iodophenyl)acetyl)glycinate (729 mg, 2.10 mmol), $Pd[PPh_3]_4$ (73 mg, 63 μmol) and 2-(Tri-n-butylstannyl)-furan (975 mg, 2.73 mmol) following **General procedure I**, which afforded the title compound after separation by flash chromatography (Hex:EA 0-100% over 25 min, 24 mL/min, 24 g silica) as colorless solid (504 mg, 1.75 mmol, 83% yield).

^{1}H NMR (500 MHz, DMSO-d6) δ 8.50 (t, *J* = 5.8 Hz, 1H), 7.72 (d, *J* = 1.4 Hz, 1H), 7.65 – 7.61 (m, 2H), 7.32 (d, *J* = 8.3 Hz, 2H), 6.90 (d, *J* = 3.3 Hz, 1H), 6.58 (dd, *J* = 3.4, 1.8 Hz, 1H), 4.08 (q, *J* = 7.1 Hz, 2H), 3.84 (d, *J* = 5.9 Hz, 2H), 3.50 (s, 2H), 1.17 (t, *J* = 7.1 Hz, 3H).

^{13}C NMR (126 MHz, DMSO-d6) δ 170.53, 169.87, 153.03, 142.71, 135.36, 129.55, 128.65, 123.31, 112.02, 105.47, 60.40, 41.62, 40.83, 14.05.

Step c): 62 (2-(4-(furan-2-yl)phenyl)acetyl)glycine was synthesized by saponification of ethyl (2-(4-(furan-2-yl)phenyl)acetyl)glycinate (400 mg, 1.40 mmol) with NaOH (112 mg, 22.8 mmol) using the mixture of THF (6.0 mL) and water (6.0 mL) as solvent. After full consumption of the starting material and adjustment of pH of the reaction mixture to 7 it was extracted with EtOAc (3x15 mL), the combined organic fractions were washed with brine, dried over anhydrous Na_2SO_4 and concentrated *in vacuo* to give the desired product as fluffy white solid (300 mg, 1.15 mmol, 82% yield).

^{1}H NMR (500 MHz, DMSO-d6) δ 12.54 (s, 1H), 8.39 (t, *J* = 5.7 Hz, 1H), 7.72 (d, *J* = 1.4 Hz, 1H), 7.62 (d, *J* = 8.2 Hz, 2H), 7.32 (d, *J* = 8.2 Hz, 2H), 6.90 (d, *J* = 3.3 Hz, 1H), 6.58 (dd, *J* = 3.3, 1.8 Hz, 1H), 3.77 (d, *J* = 5.9 Hz, 2H), 3.50 (s, 2H).

^{13}C NMR (126 MHz, DMSO-d6) δ 171.31, 170.37, 153.05, 142.71, 135.46, 129.60, 128.63, 123.31, 112.04, 105.47, 41.67, 40.77.

Step d): 63 2-(2-(4-(furan-2-yl)phenyl)acetamido)-N-methyl-N-(m-tolyl)acetamide. To the stirred solution of **62** (60 mg, 0.23 mmol) and DIPEA (89 mg, 0.7 mmol) in anhydrous DMF (1.0 mL) was added HBTU (104 mg, 0.28 mmol) at 0^{o}C. The resulting solution was stirred for 20 min at room temperature, after which *N*,3-dimethylaniline (27 mg, 0.22 mmol) was added thereto. The reaction mixture was stirred for 3 hour at room temperature, then after which it was diluted with water (20 mL), extracted with EtOAc (3x10 mL), the combined organic fractions were washed with water, brine, dried over anhydrous Na_2SO_4 and concentrated *in vacuo*. The desired product was isolated using flash chromatography (DCM:MeOH 0-10% over 14 min, 19 mL/min, 12 g silica) as white solid (54 g, 0.15 mmol, 67% yield).

^{1}H NMR (500 MHz, $CDCl_3$) δ 7.65 (d, *J* = 8.1 Hz, 2H), 7.46 (s, 1H), 7.34 – 7.24 (m, 3H), 7.17 (d, *J* = 7.4 Hz, 1H), 6.94 (d, *J* = 7.6 Hz, 2H), 6.63 (d, *J* = 3.2 Hz, 1H), 6.51 (s, 1H), 6.46 (dd, *J* = 3.1, 1.7 Hz, 1H), 3.71 (d, *J* = 4.1 Hz, 2H), 3.57 (s, 2H), 3.23 (s, 3H), 2.35 (s, 3H).

^{13}C NMR (126 MHz, $CDCl_3$) δ 170.72, 168.19, 153.75, 142.18, 141.62, 140.53, 133.75, 130.12, 130.09, 129.81, 129.66, 127.78, 124.43, 124.16, 111.77, 105.19, 43.43, 42.33, 38.73, 37.60.

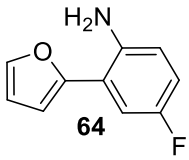

64

64 4-fluoro-2-(furan-2-yl)aniline was synthesized from 2-bromo-4-fluoroaniline (115 mg, 0.6 mmol), $Pd[PPh_3]_4$ (21 mg, 18 μmol) and 2-(Tri-n-butylstannyl)-furan (257 mg, 0.72 mmol) following **General procedure I** to obtain the title compound as beige solid (95 mg, 0.54 mmol, 90% yield).

LC-MS: $[M+H]^+$ 178.14

^{1}H NMR (500 MHz, DMSO-d6) δ 7.74 (d, *J* = 1.7 Hz, 1H), 7.22 (dd, *J* = 10.3, 3.0 Hz, 1H), 6.89 (td, *J* = 8.5, 3.0 Hz, 1H), 6.84 (d, *J* = 3.4 Hz, 1H), 6.80 (dd, *J* = 8.9, 5.2 Hz, 1H), 6.61 (dd, *J* = 3.4, 1.8 Hz, 1H), 5.19 (s, 2H).

^{13}C NMR (126 MHz, DMSO-d6) δ 154.38 (d, *J* = 231.3 Hz), 151.13 (d, *J* = 2.0 Hz), 141.99, 140.87 (d, *J* = 1.3 Hz), 117.66 (d, *J* = 7.9 Hz), 115.11 (d, *J* = 7.6 Hz), 115.07 (d, *J* = 22.2 Hz), 111.95, 111.76, 107.49.

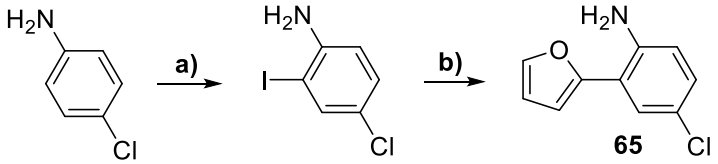

Scheme 13. Synthesis of compound **65**

Step a): 4-chloro-2-iodoaniline. 4-chloroaniline (500 mg, 3.92 mmol) was suspended in the mixture of toluene (0.3 mL) and water (10.3 mL), after which iodine (784 mg, 3.09 mmol) and $NaHCO_3$ (519 mg, 6.17 mmol) were added simultaneously and in a portionwise manner over the period of 30 minutes. The resulting mixture was stirred at room temperature for 3 hours and poured into ice-cold water (150 mL). The yellowish precipitate was filtered off and used in the next step without additional purification (890 mg, 3.53 mmol, 90% yield).

^{1}H NMR (500 MHz, $CDCl_3$) δ 7.60 (d, *J* = 2.3 Hz, 1H), 7.10 (dd, *J* = 8.6, 2.4 Hz, 1H), 6.66 (d, *J* = 8.6 Hz, 1H), 4.09 (s, 2H).

^{13}C NMR (126 MHz, $CDCl_3$) δ 145.67, 137.92, 129.39, 123.30, 115.12, 83.59.

Step b): 65 4-chloro-2-(furan-2-yl)aniline was synthesized using 4-chloro-2-iodoaniline (295 mg, 1.00 mmol), $Pd[PPh_3]_4$ (58 mg, 50 μmol), and 2-(Tri-n-butylstannyl)furan (467 mg, 1.30 mmol) following **General procedure I** to obtain the title compound as slightly brown solid (120 mg, 0.62 mmol, 62% yield).

LC-MS: $[M+H]^+$ 194.16, 196.14.

^{1}H NMR (500 MHz, $CDCl_3$) δ 7.52 – 7.49 (m, 1H), 7.44 (d, *J* = 2.4 Hz, 1H), 7.04 (dd, *J* = 8.6, 2.5 Hz, 1H), 6.67 (d, *J* = 8.6 Hz, 1H), 6.60 (d, *J* = 3.4 Hz, 1H), 6.51 (dd, *J* = 3.4, 1.8 Hz, 1H), 4.35 (s, 2H).

^{13}C NMR (126 MHz, $CDCl_3$) δ 152.26, 141.86, 128.57, 127.11, 123.19, 118.04, 117.46, 111.63, 107.33.

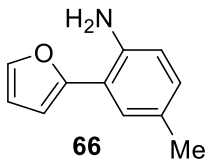

66 2-(furan-2-yl)-4-methylaniline was synthesized using 2-iodo-4-methylaniline (250 mg, 1.07 mmol), $Pd[PPh_3]_4$ (56 mg, 50 μmol), and 2-(Tri-n-butylstannyl)furan (500 mg, 1.40 mmol)

following **General procedure I** to obtain the title compound as brownish solid (132 mg, 0.76 mmol, 71% yield).

LC-MS: $[M+H]^+$ 174.12

^{1}H NMR (500 MHz, $CDCl_3$) δ 7.49 (dd, *J* = 1.8, 0.7 Hz, 1H), 7.29 (d, *J* = 1.4 Hz, 1H), 6.93 (dd, *J* = 8.1, 1.6 Hz, 1H), 6.67 (d, *J* = 8.1 Hz, 1H), 6.57 (dd, *J* = 3.3, 0.6 Hz, 1H), 6.50 (dd, *J* = 3.3, 1.8 Hz, 1H), 4.21 (s, 2H), 2.27 (s, 3H).

NMR data is in accordance with literature.[18]

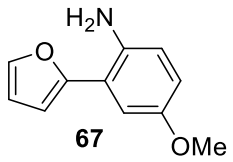

67

67 2-(furan-2-yl)-4-methoxyaniline was synthesized from 2-iodo-4-methoxyaniline (125 mg, 0.50 mmol), $Pd[PPh_3]_4$ (18 mg, 15 μmol), and 2-(Tri-n-butylstannyl)furan (214 mg, 0.60 mmol) following **General procedure I** to obtain the title compound as brownish solid (74 mg, 0.39 mmol, 78% yield).

LC-MS: $[M+H]^+$ 190.08

^{1}H NMR (500 MHz, DMSO-d6) δ 7.72 (d, *J* = 1.7 Hz, 1H), 7.00 (d, *J* = 2.9 Hz, 1H), 6.78 (d, *J* = 3.4 Hz, 1H), 6.76 (d, *J* = 8.8 Hz, 1H), 6.70 (dd, *J* = 8.7, 2.9 Hz, 1H), 6.60 (dd, *J* = 3.4, 1.8 Hz, 1H), 4.87 (s, 2H), 3.68 (s, 3H).

^{13}C NMR (126 MHz, DMSO-d6) δ 152.07, 150.95, 141.58, 138.32, 117.93, 115.33, 115.28, 111.66, 110.63, 106.95, 55.33.

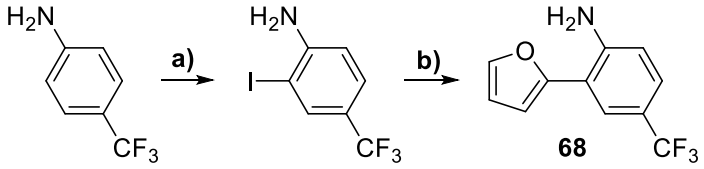

68

Scheme 14. Synthesis of compound **68**

Step a): 2-iodo-4-(trifluoromethyl)aniline. To the stirred solution of 4-(trifluoromethyl)-aniline (500 mg, 3.1 mmol) in MeOH (5.0 mL) at 0°C was dropwise added the solution of ICl (556 mg, 3.4 mmol) in DCM (5.0 mL) over 25 min. The resulting solution was stirred at room temperature for 2 hours, after which saturated aqueous Na_2CO_3 (10.0 mL) solution was added. The resulting mixture was extracted with EtOAc (3x50 mL), the combined organic fractions were washed with brine, dried over anhydrous Na_2SO_4 and concentrated *in vacuo*. The resulting residue was used further without additional purification. Orange solid (609 mg, 2.12 mmol, 68%).

LC-MS: $[M+H]^+$ 287.94

^{1}H NMR (500 MHz, $CDCl_3$) δ 7.87 (d, *J* = 1.1 Hz, 1H), 7.37 (dd, *J* = 8.4, 1.6 Hz, 1H), 6.74 (d, *J* = 8.4 Hz, 1H), 4.42 (s, 2H).

^{13}C NMR (126 MHz, $CDCl_3$) δ 149.59, 136.22 (q, *J* = 3.9 Hz), 126.57 (q, *J* = 3.5 Hz), 123.53 (q, *J* = 271.0 Hz), 121.46 (q, *J* = 33.3 Hz), 113.51, 82.15.

Step b): 68 2-(furan-2-yl)-4-(trifluoromethyl)aniline was synthesized from 2-iodo-4-(trifluoromethyl)aniline (175 mg, 0.61 mmol), $Pd[PPh_3]_4$ (21 mg, 18 μmol), and 2-(Tri-n-butylstannyl)furan (283 mg, 0.8 mmol) following **General procedure I** to obtain the title compound as yellowish solid (110 mg, 0.48 mmol, 79% yield).

^{1}H NMR (500 MHz, $CDCl_3$) δ 7.70 (s, 1H), 7.53 (d, *J* = 1.6 Hz, 1H), 7.32 (dd, *J* = 8.4, 1.7 Hz, 1H), 6.76 (d, *J* = 8.5 Hz, 1H), 6.64 (d, *J* = 3.4 Hz, 1H), 6.53 (dd, *J* = 3.3, 1.9 Hz, 1H), 4.69 (s, *J* = 42.1 Hz, 2H).

^{13}C NMR (126 MHz, $CDCl_3$) δ 152.22, 145.89, 141.81, 125.60 (q, *J* = 3.6 Hz), 125.03 (q, *J* = 3.9 Hz), 123.55, 120.19 (q, *J* = 32.9 Hz), 116.16, 115.42, 111.54, 107.24.

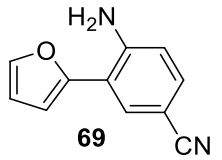

69

69 4-amino-3-(furan-2-yl)benzonitrile was synthesized from 4-amino-3-iodobenzonitrile (122 mg, 0.50 mmol), $Pd[PPh_3]_4$ (87 mg, 75 μmol) and 2-(Tri-n-butylstannyl)furan (214 mg, 1.95 mmol) following **General procedure I** to obtain the title compound white solid (47 mg, 0.25 mmol, 51% yield).

LC-MS: $[M+H]^+$ 185.11.

^{1}H NMR (500 MHz, $CDCl_3$) δ 7.70 (d, *J* = 1.9 Hz, 1H), 7.52 (d, *J* = 1.7 Hz, 1H), 7.32 (dd, *J* = 8.4, 1.9 Hz, 1H), 6.71 (d, *J* = 8.4 Hz, 1H), 6.61 (d, *J* = 3.4 Hz, 1H), 6.55 – 6.51 (m, 1H), 4.94 (s, 2H).

^{13}C NMR (126 MHz, $CDCl_3$) δ 151.51, 147.03, 142.15, 132.34, 132.07, 119.94, 116.50, 115.93, 111.74, 107.63, 100.43.

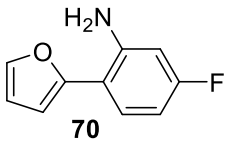

70

70 5-fluoro-2-(furan-2-yl)aniline was synthesized from 2-bromo-5-fluoroaniline (285 mg, 1.50 mmol), $Pd[PPh_3]_4$ (17 mg, 15 μmol) and 2-(Tri-n-butylstannyl)furan (696 mg, 1.95 mmol) following **General procedure I** to obtain the title compound white solid (183 mg, 1.04 mmol, 69% yield).

LC-MS: $[M+H]^+$ 178.17

^{1}H NMR (500 MHz, $CDCl_3$) δ 7.50 – 7.47 (m, 1H), 7.39 (dd, *J* = 8.6, 6.4 Hz, 1H), 6.51 – 6.46 (m, 3H), 6.44 (dd, *J* = 10.6, 2.5 Hz, 1H), 4.46 (s, 2H).

NMR data is in accordance with literature.[19]

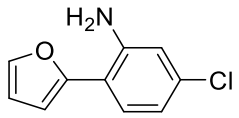

71

71 5-chloro-2-(furan-2-yl)aniline was synthesized from 5-chloro-2-iodoaniline (500.0 mg, 1.97 mmol), $Pd[PPh_3]_4$ (114.0 mg, 98 μmol) and 2-(Tri-n-butylstannyl)furan (704.2 mg, 1.97 mmol) following **General procedure I** to obtain the title compound white solid (206 mg, 1.06 mmol, 54% yield).

LC-MS: $[M+H]^+$ 194.06, 196.00.

^{1}H NMR (500 MHz, $CDCl_3$) δ 7.49 (d, *J* = 1.3 Hz, 1H), 7.37 (d, *J* = 8.2 Hz, 1H), 6.76 – 6.72 (m, 2H), 6.56 – 6.54 (m, 1H), 6.51 (dd, *J* = 3.4, 1.8 Hz, 1H), 4.44 (s, 2H).

^{13}C NMR (126 MHz, $CDCl_3$) δ 152.74, 144.37, 141.61, 134.30, 128.86, 118.58, 116.30, 114.76, 111.57, 106.77.

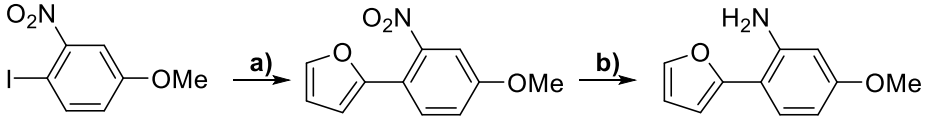

72

Scheme 15. Synthesis of compound **72**

Step a): 2-(4-methoxy-2-nitrophenyl)furan was synthesized from 1-iodo-4-methoxy-2-nitrobenzene (419 mg, 1.5 mmol), $Pd[PPh_3]_4$ (52 mg, 45 μmol) and 2-(Tri-n-butylstannyl)furan (696 mg, 1.95 mmol) following **General procedure I** to obtain the title compound as yellow oil solidifying upon storage (240 mg, 1.1 mmol, 73% yield).

LC-MS: $[M+H]^+$ 220.09

^{1}H NMR (500 MHz, $CDCl_3$) δ 7.60 (d, *J* = 8.7 Hz, 1H), 7.48 – 7.46 (m, 1H), 7.22 (d, *J* = 2.6 Hz, 1H), 7.11 (dd, *J* = 8.7, 2.6 Hz, 1H), 6.55 (d, *J* = 3.4 Hz, 1H), 6.47 (dd, *J* = 3.4, 1.8 Hz, 1H), 3.88 (s, 3H).

^{13}C NMR (126 MHz, $CDCl_3$) δ 159.44, 148.67, 148.38, 143.27, 130.49, 118.46, 117.17, 111.79, 109.05, 108.53, 56.07.

Step b): 72 2-(furan-2-yl)-5-methoxyaniline was synthesized using **General procedure VI** from 2-(4-methoxy-2-nitrophenyl)furan (219 mg, 1.0 mmol), palladium on charcoal (20.0 mg) suspended in EtOH (3.0 mL). After the purification by flash chromatography (Hex:$CHCl_3$ 0-100% $CHCl_3$ over 22 min, 18 mL/min, 12 g silica) the desired aniline was obtained as dark brownish solid (70 mg, 0.37 mmol, 37% yield).

LC-MS: $[M+H]^+$ 190.13

^{1}H NMR (500 MHz, $CDCl_3$) δ 7.46 (dd, *J* = 1.8, 0.7 Hz, 1H), 7.37 (d, *J* = 8.6 Hz, 1H), 6.48 (dd, *J* = 3.3, 1.8 Hz, 1H), 6.44 (dd, *J* = 3.3, 0.7 Hz, 1H), 6.38 (dd, *J* = 8.6, 2.5 Hz, 1H), 6.28 (d, *J* = 2.5 Hz, 1H), 4.35 (s, 2H), 3.79 (s, 3H).

^{13}C NMR (126 MHz, $CDCl_3$) δ 160.49, 153.67, 144.84, 140.89, 129.21, 111.37, 109.95, 105.28, 104.85, 101.55, 55.33.

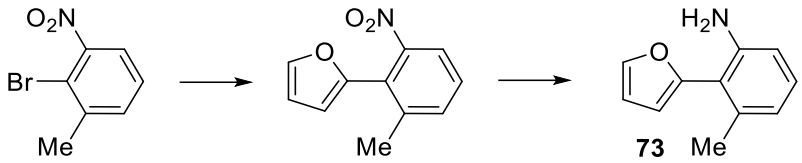

Scheme 16. Synthesis of compound **73**

2-(2-methyl-6-nitrophenyl)furan was synthesized from 2-bromo-1-methyl-3-nitrobenzene (222 mg, 1.10 mmol), $Pd[PPh_3]_4$ (30 mg, 26 μmol) and 2-(Tri-n-butylstannyl)furan (499 mg, 1.33 mmol) following **General procedure I** to obtain the title compound as yellow solid (179 mg, 0.9 mmol, 88% yield).

^{1}H NMR (500 MHz, $CDCl_3$) δ 7.64 (d, *J* = 8.0 Hz, 1H), 7.53 (dd, *J* = 1.7, 0.5 Hz, 1H), 7.50 – 7.47 (m, 1H), 7.39 (t, *J* = 7.9 Hz, 1H), 6.52 (dd, *J* = 3.3, 1.9 Hz, 1H), 6.47 – 6.45 (m, 1H), 2.37 (s, 3H).

^{13}C NMR (126 MHz, $CDCl_3$) δ 150.67, 146.88, 143.31, 140.25, 134.14, 128.98, 124.63, 121.53, 111.31, 110.97, 20.65.

73 2-(furan-2-yl)-3-methylaniline was synthesized from 2-(2-methyl-6-nitrophenyl)furan (50 mg, 0.25 mmol) and palladium on charcoal (5 mg) suspended in EtOH (2.0 mL) following the **General Procedure VI**. The desired compound was obtained as slightly beige solid (43 mg, 0.25 mmol, 99% yield).

LC-MS: $[M+H]^+$ 174.13

^{1}H NMR (500 MHz, $CDCl_3$) δ 7.54 (dd, *J* = 1.8, 0.7 Hz, 1H), 7.07 (dd, *J* = 9.8, 5.8 Hz, 1H), 6.66 (d, *J* = 7.5 Hz, 1H), 6.60 (d, *J* = 8.0 Hz, 1H), 6.52 (dd, *J* = 3.2, 1.9 Hz, 1H), 6.42 (dd, *J* = 3.2, 0.7 Hz, 1H), 2.19 (s, 3H).

^{13}C NMR (126 MHz, DMSO-d6) δ 157.65, 153.25, 142.57, 139.34, 131.28, 115.28, 115.15, 111.93, 107.43, 105.51, 21.10.

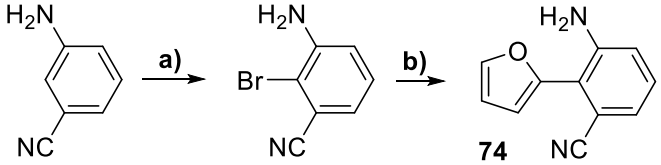

Scheme 17. Synthesis of compound **74**

Step a): 3-amino-2-bromobenzonitrile. To the stirred solution of 3-aminobenzonitrile (472 mg, 4.00 mmol) in dioxane (6.4 mL) was added dropwise the solution of N-bromosuccinimide (715 mg, 4.04 mmol) in dioxane (3.2 mL) over 30 min. at room temperature,

after which the reaction mixture was stirred for additional 30 min. The reaction mixture was concentrated *in vacuo* and the resulting residue was subjected to flash chromatography (Hex:EA 0-100% EA over 15 min, 18 mL/min, 12 g silica) to afford the desired compound as slightly yellow solid (395. mg, 2.00 mmol, 50% yield).

^{1}H NMR (500 MHz, $CDCl_3$) δ 7.18 (t, *J* = 7.9 Hz, 1H), 7.05 (d, *J* = 7.5 Hz, 1H), 6.94 (d, *J* = 8.2 Hz, 1H), 4.34 (s, 2H).

^{13}C NMR (126 MHz, $CDCl_3$) δ 145.43, 128.61, 123.94, 119.37, 117.84, 116.43, 110.50.

74 3-amino-2-(furan-2-yl)benzonitrile was synthesized from 3-amino-2-bromobenzonitrile (100 mg, 0.51 mmol), $Pd[PPh_3]_4$ (30 mg, 26 μmol) and 2-(Tri-n-butylstannyl)furan (217 mg, 0.61 mmol) following **General procedure I** to obtain the title compound as yellow solid (72 mg, 0.39 mmol, 77% yield).

LC-MS: $[M+H]^+$ 185.11

^{1}H NMR (500 MHz, $CDCl_3$) δ 7.59 (d, *J* = 1.7 Hz, 1H), 7.18 (t, *J* = 7.8 Hz, 1H), 7.14 – 7.09 (m, 1H), 6.92 (dd, *J* = 8.1, 1.0 Hz, 1H), 6.90 (d, *J* = 3.4 Hz, 1H), 6.59 (dd, *J* = 3.4, 1.9 Hz, 1H), 4.48 (s, 2H).

^{13}C NMR (126 MHz, $CDCl_3$) δ 148.55, 145.45, 142.83, 129.35, 127.80, 123.88, 120.32, 119.14, 117.82, 111.96, 111.81.

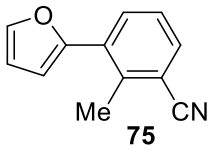

75

75 3-(furan-2-yl)-2-methylbenzonitrile was synthesized from 3-bromo-2-methylbenzonitrile (196 mg, 1.00 mmol), $Pd[PPh_3]_4$ (35 mg, 30 μmol) and 2-(Tri-n-butylstannyl)furan (464 mg, 1.30 mmol) following **General procedure I** to obtain the title compound as yellow solid (147 mg, 0.80 mmol, 80% yield).

^{1}H NMR (500 MHz, $CDCl_3$) δ 7.87 (dd, *J* = 7.9, 0.7 Hz, 1H), 7.57 (dd, *J* = 7.6, 0.8 Hz, 1H), 7.55 (d, *J* = 1.7 Hz, 1H), 7.34 (t, *J* = 7.8 Hz, 1H), 6.61 (d, *J* = 3.4 Hz, 1H), 6.54 (dd, *J* = 3.4, 1.8 Hz, 1H), 2.70 (s, 3H).

^{13}C NMR (126 MHz, $CDCl_3$) δ 151.66, 142.79, 138.32, 131.88, 131.66, 126.61, 118.52, 114.64, 111.76, 110.36, 19.85.

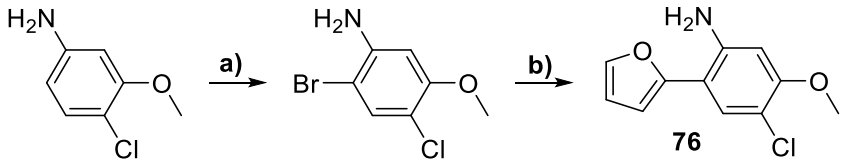

76

Scheme 18. Synthesis of compound **76**

Step a): 2-bromo-4-chloro-5-methoxyaniline. To the solution of 4-chloro-3-methoxyaniline (405 mg, 2.57 mmol) in DMF (13.0 mL) was added N-bromosuccinimide (471

mg, 2.65 mmol) portionwise at 0°C and the reaction mixture was stirred vigorously for 10 min. After that the reaction was quenched by adding saturated aqueous solution of Na_2SO_3 (5.0 mL), and the resulting mixture was further diluted with ice-cold water (150 mL), extracted with DCM (3x40 mL). The combined organic fractions were washed with brine, dried over anhydrous $MgSO_4$ and evaporated to yield the residue, which was purified by flash chromatography (Hex:DCM 0-100% DCM over 18 min, 24 mL/min, 24 g silica), that afforded the desired product as a beige solid (440 mg, 1.86 mmol, 72% yield).

^{1}H NMR (500 MHz, $CDCl_3$) δ 7.36 (s, 1H), 6.34 (s, 1H), 4.08 (s, 2H), 3.83 (s, 3H).

^{13}C NMR (126 MHz, $CDCl_3$) δ 155.22, 143.85, 132.81, 112.04, 99.68, 99.43, 56.33.

Step b): 76 4-chloro-2-(furan-2-yl)-5-methoxyaniline was synthesized from 2-bromo-4-chloro-5-methoxyaniline (118 mg, 0.50 mmol), $Pd[PPh_3]_4$ (17 mg, 15 μmol) and 2-(Tri-n-butylstannyl)furan (217 mg, 0.61 mmol) following **General procedure I** to obtain the title compound as white solid (68 mg, 0.30 mmol, 61% yield).

LC-MS: $[M+H]^+$ 224.11, 226.08

^{1}H NMR (500 MHz, $CDCl_3$) δ 7.46 (d, *J* = 1.6 Hz, 1H), 7.43 (s, 1H), 6.49 (dd, *J* = 3.2, 1.9 Hz, 1H), 6.46 (d, *J* = 3.3 Hz, 1H), 6.29 (s, 1H), 4.41 (s, 2H), 3.87 (s, 3H).

^{13}C NMR (126 MHz, $CDCl_3$) δ 155.24, 152.43, 143.36, 141.25, 128.98, 111.90, 111.52, 109.97, 105.88, 100.44, 56.19.

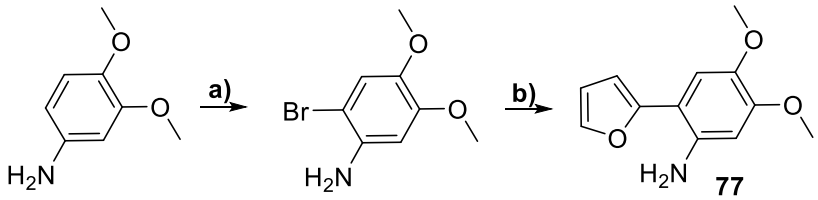

Scheme 19. Synthesis of compound **77**

Step a): 2-bromo-4,5-dimethoxyaniline was synthesized from 3,4-dimethoxyaniline (766 mg, 5.00 mmol), NBS (908 mg, 5.10 mmol) and using DMF (15.0 mL) as solvent following the **General procedure VIII**. The desired product was obtained as yellowish solid (950 mg, 4.10 mmol, 82% yield).

LC-MS: $[M+H]^+$ 232.09, 234.09.

^{1}H NMR (500 MHz, DMSO-d6) δ 6.89 (s, 1H), 6.50 (s, 1H), 4.83 (s, 2H), 3.67 (s, 3H), 3.63 (s, 3H).

^{13}C NMR (126 MHz, DMSO-d6) δ 149.43, 140.71, 140.10, 116.52, 100.43, 96.40, 56.58, 55.35.

Step b): 77 2-(furan-2-yl)-4,5-dimethoxyaniline was synthesized from 2-bromo-4,5-dimethoxyaniline (50 mg, 0.21 mmol), $Pd[PPh_3]_4$ (7.0 mg, 6 μmol) and 2-(Tri-n-butylstannyl)-

furan (78 mg, 0.22 mmol) following **General procedure I** to obtain the title compound as dark beige solid (32 mg, 0.15 mmol, 70% yield).

LC-MS: $[M+H]^+$ 220.21.

^{1}H NMR (500 MHz, DMSO-d6) δ 7.65 (d, *J* = 1.7 Hz, 1H), 6.97 (s, 1H), 6.61 (d, *J* = 3.3 Hz, 1H), 6.55 (dd, *J* = 3.3, 1.8 Hz, 1H), 6.47 (s, 1H), 4.96 (s, 2H), 3.71 (s, 3H), 3.68 (s, 3H).

^{13}C NMR (126 MHz, DMSO-d6) δ 152.44, 149.66, 140.69, 140.59, 139.25, 111.54, 111.06, 106.32, 105.04, 101.12, 56.34, 55.19.

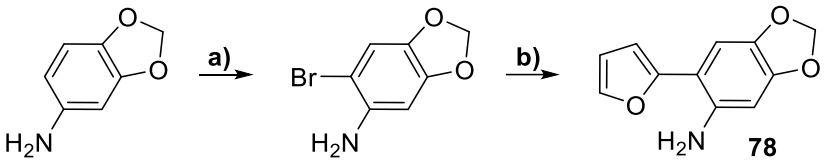

Scheme 19. Synthesis of compound **78**

Step a): 6-bromobenzo[d][1,3]dioxol-5-amine was synthesized from benzo[d][1,3]dioxol-5-amine (686 mg, 5.0 mmol), NBS (907 mg, 5.1 mmol) and using DMF (15.0 mL) as solvent following the **General procedure VIII**. The desired product was obtained as white solid (970 mg, 4.51 mmol, 90% yield).

LC-MS: $[M+H]^+$ 216.08, 218.08

^{1}H NMR (500 MHz, DMSO-d6) δ 6.94 (s, 1H), 6.47 (s, 1H), 5.88 (s, 2H), 4.93 (s, 2H).

^{13}C NMR (126 MHz, DMSO-d6) δ 147.52, 140.74, 138.86, 111.37, 100.82, 96.98, 96.44.

Step b): 78 6-(furan-2-yl)benzo[d][1,3]dioxol-5-amine was synthesized from 6-bromobenzo[d][1,3]dioxol-5-amine (108 mg, 0.50 mmol), $Pd[PPh_3]_4$ (29 mg, 25 μmol) and 2-(Tri-n-butylstannyl)-furan (232 mg, 0.65 mmol) following **General procedure I** to obtain the title compound as dark beige solid (77 mg, 0.38 mmol, 76% yield).

^{1}H NMR (500 MHz, DMSO-d6) δ 7.65 (d, *J* = 1.7 Hz, 1H), 6.94 (s, 1H), 6.61 (d, *J* = 3.3 Hz, 1H), 6.55 (dd, *J* = 3.3, 1.8 Hz, 1H), 6.47 (s, 1H), 5.88 (s, 2H), 4.93 (s, 2H),

^{13}C NMR (126 MHz, DMSO-d6) δ 152.44, 149.66, 147.52, 140.74, 138.86, 122.72, 113.66, 111.37, 100.82, 96.98, 96.44.

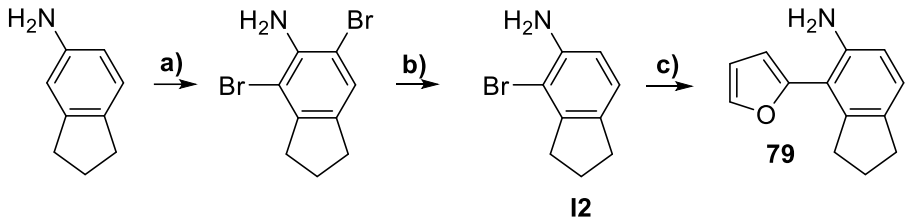

Scheme 20. Synthesis of compound **79**

Step a): 4,6-dibromo-2,3-dihydro-1H-inden-5-amine. To the solution of 2,3-dihydro-1H-inden-5-amine (3.01 g, 22.5 mmol) in acetic acid (100.0 mL) was added the solution of bromine (27.0 g, 168 mmol) in acetic acid (20.0 mL) and the resulting solution was stirred for 2 h at

room temperature, after which the reaction was quenched by adding saturated aqueous $Na_2S_2O_3$ solution (in small portions, until the mixture was discolored). The pH of the resulting mixture was adjusted to 7 by adding solid Na_2CO_3, after which it was extracted with EtOAc (3x200 mL). The combined organic fractions were washed with brine, dried over anhydrous Na_2SO_4 and concentrated *in vacuo*. This resulted in 5.0 g (crude) as slightly yellow solid, which was used in the next step without additional purification.

LC-MS: $[M+H]^+$ 289.95, 291.96, 293.94

^{1}H NMR (500 MHz, DMSO-d6) δ 2.85 (t, *J* = 7.4 Hz, 2H), 2.75 (t, *J* = 7.4 Hz, 2H), 1.97 (p, *J* = 7.5 Hz, 1H).

^{13}C NMR (126 MHz, DMSO-d6) δ 144.76, 140.79, 133.95, 127.09, 105.88, 105.61, 35.03, 32.90, 24.45.

Step b): I2 4-bromo-2,3-dihydro-1H-inden-5-amine. To the solution of 4,6-dibromo-2,3-dihydro-1H-inden-5-amine (3.20 g, 11.0 mmol) in the mixture of acetic acid (16.0 mL) and concentrated HCl (12.0 mL) was added $SnCl_2$ (2.80 g, 14.7 mmol). The resulting solution was stirred for 1.5 h at 95°C in an oil bath. The pH value of the reaction mixture was adjusted to 8 by adding saturated sodium hydroxide solution and the resulting solution was extracted with DCM (2x100 mL), the combined organic fractions were washed with 1M sodium hydroxide solution (25 mL), dried over anhydrous Na_2SO_4 and concentrated *in vacuo*. The crude residue was purified using flash chromatography (Hex:DCM 0-100% DCM over 20 min, 22 mL/min, 24 g silica) to furnish the product as beige solid (1.38 g, 6.50 mmol, 59%).

LC-MS: $[M+H]^+$ 212.11, 214.11

^{1}H NMR (500 MHz, $CDCl_3$) δ 6.94 (d, *J* = 7.8 Hz, 1H), 6.58 (d, *J* = 7.8 Hz, 1H), 3.96 (s, 2H), 2.93 (t, *J* = 5.4 Hz, 2H), 2.90 (t, *J* = 5.5 Hz, 2H).

^{13}C NMR (126 MHz, $CDCl_3$) δ 145.47, 142.30, 135.06, 123.58, 114.00, 107.58, 35.20, 33.50, 24.88.

Step c): 79 4-(furan-2-yl)-2,3-dihydro-1H-inden-5-amine was synthesized from 4-bromo-2,3-dihydro-1H-inden-5-amine (106 mg, 0.50 mmol), $Pd[PPh_3]_4$ (30 mg, 26 μmol) and 2-(Tri-n-butylstannyl)-furan (232 mg, 0.65 mmol) following **General procedure I** to obtain the title compound as grayish solid (70 mg, 0.35 mmol, 70% yield).

^{1}H NMR (500 MHz, $CDCl_3$) δ 7.50 (d, *J* = 0.7 Hz, 1H), 7.00 (d, *J* = 8.0 Hz, 1H), 6.59 (d, *J* = 8.0 Hz, 1H), 6.51 (dd, *J* = 2.6, 1.4 Hz, 1H), 6.48 (d, *J* = 3.3 Hz, 1H), 4.13 (s, 2H), 2.92 (t, *J* = 7.4 Hz, 2H), 2.84 (t, *J* = 7.4 Hz, 2H), 2.03 (p, *J* = 7.4 Hz, 2H).

^{13}C NMR (126 MHz, $CDCl_3$) δ 151.82, 143.92, 142.91, 141.22, 134.49, 124.95, 114.68, 113.66, 111.02, 109.15, 33.90, 32.49, 25.75.

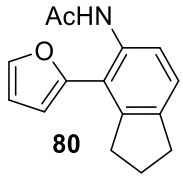

80

80 N-(4-(furan-2-yl)-2,3-dihydro-1H-inden-5-yl)acetamide was synthesized by acylation 4-(furan-2-yl)-2,3-dihydro-1H-inden-5-amine (10 mg, 50 μmol) with Ac_2O (5 mg, 50 μmol) in the presence of DiPEA (13 mg, 100 μmol) and using DCM (1.0 mL) as a solvent. The solvent was evaporated *in vacuo* and the residue was purified by flash chromatography (DCM:EA 0-100% EA, over 15 min, 12 mL/min, 4 g silica) that yielded the title compound as white solid (11 mg, 45 μmol, 90% yield).

LC-MS: $[M+H]^+$ 242.23

^{1}H NMR (500 MHz, DMSO-d6) δ 9.24 (s, 1H), 7.76 (s, 1H), 7.23 (d, *J* = 7.9 Hz, 1H), 7.18 (d, *J* = 7.9 Hz, 1H), 6.61 – 6.59 (m, 2H), 2.93 (t, *J* = 7.3 Hz, 2H), 2.87 (t, *J* = 7.4 Hz, 2H), 2.04 – 1.98 (m, 2H), 1.96 (s, 3H).

^{13}C NMR (126 MHz, DMSO-d6) δ 168.53, 149.92, 142.67, 142.39, 141.63, 132.93, 125.44, 123.74, 122.72, 111.25, 109.88, 33.31, 32.18, 25.03, 23.20.

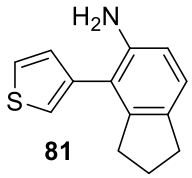

81

81 4-(thiophen-3-yl)-2,3-dihydro-1H-inden-5-amine was synthesized from **4-bromo-2,3-dihydro-1H-inden-5-amine** (215 mg, 1.00 mmol), $Pd[PPh_3]_4$ (50 mg, 43 μmol), 3-thienylboronic acid (168 mg, 1.3 mmol) and KF (174 mg, 3.0 mmol) using dioxane (2.0 mL) as solvent and following **General procedure II**. The product was isolated by flash chromatography (Hex:DCM 0-100% DCM over 15 min, 18 mL/min, 12 g silica) as brownish solid (200 mg, 0.93 mmol, 93% yield).

LC-MS: $[M+H]^+$ 216.18.

^{1}H NMR (500 MHz, $CDCl_3$) δ 7.42 (dd, *J* = 4.9, 3.0 Hz, 1H), 7.27 – 7.26 (m, 1H), 7.14 (dd, *J* = 4.9, 1.0 Hz, 1H), 7.01 (d, *J* = 7.9 Hz, 1H), 6.61 (d, *J* = 7.9 Hz, 1H), 3.60 (s, 2H), 2.86 (t, *J* = 7.3 Hz, 2H), 2.69 (t, *J* = 7.4 Hz, 2H), 1.99 (p, *J* = 7.4 Hz, 2H).

^{13}C NMR (126 MHz, $CDCl_3$) δ 144.52, 142.80, 138.02, 134.23, 128.90, 125.86, 124.18, 123.44, 119.60, 113.79, 33.07, 32.68, 25.78.

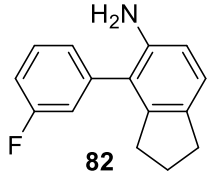

82

82 4-(3-fluorophenyl)-2,3-dihydro-1H-inden-5-amine was synthesized from **4-bromo-2,3-dihydro-1H-inden-5-amine** (106 mg, 0.50 mmol), $Pd[PPh_3]_4$ (50 mg, 43 μmol), 3-fluorophenyl boronic acid (105 mg, 0.75 mmol) and K_3PO_4 (212 mg, 1.00 mmol) using dioxane (2.0 mL) as solvent and following **General procedure II**. The product was isolated by flash chromatography (Hex:DCM 0-100% DCM over 15 min, 18 mL/min, 12 g silica) as light brown solid (100 mg, 0.44 mmol, 88 % yield).

LC-MS: $[M+H]^+$ 228.21.

^{1}H NMR (500 MHz, DMSO-d6) δ 7.51 – 7.44 (m, 1H), 7.15 (td, *J* = 8.7, 2.5 Hz, 1H), 7.12 – 7.06 (m, 2H), 6.91 (d, *J* = 8.0 Hz, 1H), 6.57 (d, *J* = 8.0 Hz, 1H), 4.37 (s, 2H), 2.75 (t, *J* = 7.3 Hz, 2H), 2.53 – 2.50 (m, 2H), 1.88 (p, *J* = 7.4 Hz, 2H).

^{19}F NMR (470 MHz, DMSO-d6) δ -112.94 – -113.02 (m).

^{13}C NMR (126 MHz, DMSO-d6) δ 162.39 (d, *J* = 243.8 Hz), 143.31, 142.44, 140.61 (d, *J* = 7.7 Hz), 131.30, 130.59 (d, *J* = 8.6 Hz), 125.59 (d, *J* = 2.5 Hz), 123.92, 121.68, 116.12 (d, *J* = 20.6 Hz), 113.71, 113.53, 32.21, 31.96, 25.16.

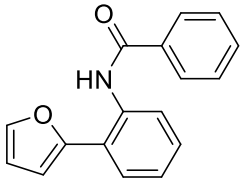

83

83 N-(2-(furan-2-yl)phenyl)benzamide. To the solution containing 2-(furan-2-yl)-aniline (80 mg, 0.50 mmol), pyridine (43 mg, 0.55 mmol) and catalytic amounts of DMAP in DCM (4.0 mL) was added benzoyl chloride (78 mg, 0.55 mmol) upon cooling with ice bath and vigorous stirring. The resulting mixture was stirred at room temperature overnight, quenched by adding aqueous solution of $NaHCO_3$ (1 mL), diluted with water (20 mL) and extracted with EtOAc (3x20 mL). The combined organic fractions were washed with brine, dried over anhydrous sodium sulfate and concentrated *in vacuo.* The residue was subjected to purification by flash column chromatography (Hex:EA 0-100% EA over 15 min, 18 L/min, 12 g silica) which afforded the desired product as white crystals (75 mg, 0.28 mmol, 57%).

LC-MS: $[M+H]^+$ 263.97

^{1}H NMR (500 MHz, $CDCl_3$) δ 9.39 (s, 1H), 8.56 (d, *J* = 8.3 Hz, 1H), 7.94 – 7.87 (m, 2H), 7.60 – 7.54 (m, 3H), 7.54 – 7.45 (m, 3H), 7.41 – 7.37 (m, 1H), 7.18 (td, *J* = 7.7, 1.2 Hz, 1H), 6.66 (d, *J* = 3.4 Hz, 1H), 6.57 (dd, *J* = 3.4, 1.9 Hz, 1H).

^{13}C NMR (126 MHz, DMSO-d6) δ 165.56, 153.04, 142.47, 138.52, 134.90, 131.61, 128.40, 127.67, 125.84, 123.82, 120.50, 112.04, 104.94.

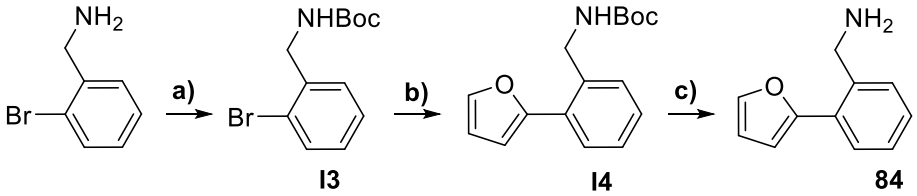

Scheme 21. Synthesis of compound **84**

Step a): I3 *tert*-butyl (2-bromobenzyl)carbamate was synthesized from 2-bromobenzylamine (2.50 g, 13.4 mmol), Boc_2O (3.23 g, 14.8 mmol), DIPEA (3.47 mg, 26.9 mmol) following the **General procedure VI** to obtain the protected amine as white solid (3.54 g, 12.4 mmol, 90% yield).

LC-MS: $[M+H]^+$ 271.06, 273.07

^{1}H NMR (500 MHz, $CDCl_3$) δ 7.43 (s, 1H), 7.41 – 7.38 (m, 1H), 7.23 – 7.17 (m, 2H), 4.86 (s, 1H), 4.29 (d, *J* = 5.8 Hz, 2H), 1.46 (s, 9H).

NMR data is in accordance with literature.[20]

Step b): I4 *tert*-butyl (2-(furan-2-yl)benzyl)carbamate was synthesized from *tert*-butyl (2-bromobenzyl)carbamate (200 mg, 0.70 mmol), $Pd[PPh_3]_4$ (16 mg, 13 μmol) and 2-(Tri-n-butylstannyl)-furan (287 mg, 0.80 mmol) following **General procedure I** to obtain the title compound as white solid (190 mg, 0.70 mmol, 99% yield).

LC-MS: $[M+H]^+$ 217.97

^{1}H NMR (500 MHz, $CDCl_3$) δ 7.62 – 7.58 (m, 1H), 7.53 (dd, *J* = 1.8, 0.6 Hz, 1H), 7.44 (s, 1H), 7.34 – 7.28 (m, 2H), 6.56 (d, *J* = 3.3 Hz, 1H), 6.51 (dd, *J* = 3.4, 1.8 Hz, 1H), 4.97 (s, 1H), 4.49 (d, *J* = 5.7 Hz, 2H), 1.45 (s, 9H).

^{13}C NMR (126 MHz, $CDCl_3$) δ 155.99, 153.45, 142.55, 135.50, 129.90, 129.77, 128.34, 128.15, 127.73, 111.67, 108.58, 79.57, 43.60, 28.58.

Step c): 84 (2-(furan-2-yl)phenyl)methanamine was synthesized from *tert*-butyl (2-(furan-2-yl)benzyl)carbamate (130 mg, 0.70 mmol) and HCl_{diox} (c= 4M, 500 μL) using DCM (4.0 mL) as solvent and following **General procedure VII**, which afforded the desired amine in the form of a hydrochloride (147 mg, 0.70 mmol, quant. yield).

LC-MS: $[M+H]^+$ 174.13

^{1}H NMR (500 MHz, DMSO-d6) δ 8.38 (s, 3H), 7.85 (dd, *J* = 1.8, 0.5 Hz, 1H), 7.71 (dd, *J* = 7.7, 1.5 Hz, 1H), 7.57 (dd, *J* = 7.5, 1.3 Hz, 1H), 7.47 (td, *J* = 7.5, 1.6 Hz, 1H), 7.43 (td, *J* = 7.4, 1.6 Hz, 1H), 6.88 (dd, *J* = 3.4, 0.5 Hz, 1H), 6.68 (dd, *J* = 3.4, 1.8 Hz, 1H), 4.23 (s, 2H).

^{13}C NMR (126 MHz, DMSO-d6) δ 152.20, 144.18, 130.43, 130.35, 130.16, 129.30, 128.55, 128.16, 112.41, 109.99, 41.08.

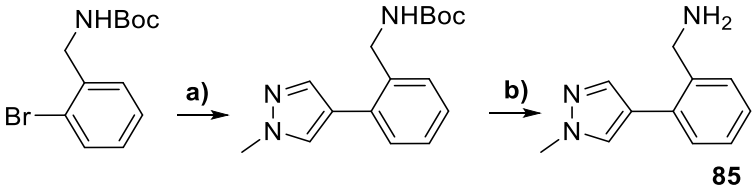

85

Scheme 22. Synthesis of compound **85**

Step a): *tert*-butyl (2-(1-methyl-1H-pyrazol-4-yl)benzyl)carbamate was synthesized from *tert*-butyl (2-bromobenzyl)carbamate (143 mg , 0.50 mmol), 1-methyl-4-(4,4,5,5-tetramethyl-1,3,2-dioxaborolan-2-yl)-1H-pyrazole (125 mg , 0.6 mmol), $Pd[PPh_3]_4$ (17 mg, 15 μmol) and K_2CO_3 (138 mg, 1.0 mmol) and following the **General procedure II** to isolate the desired product as slightly yellow solid (184 mg, 0.49 mmol, 97% yield).

^{1}H NMR (500 MHz, $CDCl_3$) δ 7.57 (s, 1H), 7.46 (s, 1H), 7.41 – 7.36 (m, 1H), 7.34 – 7.27 (m, 3H), 4.71 (s, 1H), 4.38 (d, *J* = 4.9 Hz, 2H), 3.95 (s, 3H), 1.45 (s, 9H).

^{13}C NMR (126 MHz, $CDCl_3$) δ 155.85, 138.95, 135.75, 132.16, 130.08, 129.08, 128.76, 127.74, 127.40, 121.01, 43.18, 39.18, 28.53, 24.99.

Step b): 85 (2-(1-methyl-1H-pyrazol-4-yl)phenyl)methanamine was synthesized from *tert*-butyl (2-(furan-2-yl)benzyl)carbamate (90 mg, 0.30 mmol) and HCl_{diox} (400 μL) using DCM (3.5 mL) as solvent and following **General procedure VII**, which afforded the desired amine in the form of a double hydrochloride (80 mg, 0.30 mmol, quant. yield).

LC-MS: $[M+H-NH_2]^+$ 171.09.

^{1}H NMR (500 MHz, DMSO-d6) δ 8.54 (s, 3H), 7.97 (s, 1H), 7.65 – 7.60 (m, 2H), 7.40 – 7.34 (m, 3H), 4.07 (q, *J* = 5.8 Hz, 2H), 3.90 (s, 3H).

^{13}C NMR (126 MHz, DMSO-d6) δ 138.24, 132.51, 131.15, 130.04, 129.79, 128.80, 128.44, 126.96, 119.44, 43.63, 38.65.

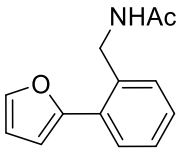

86

86 *N*-(2-(furan-2-yl)benzyl)acetamide was synthesized by acylation of (2-(furan-2-yl)phenyl)-methanamine hydrochloride (40 mg, 0.19 mmol), with Ac_2O (22 mg, 0.21 mmol) in the presence of TEA (92 mg, 0.82 mmol) and using THF (3.0 mL) as a solvent. After 4 hours of stirring at room temperature the reaction was quenched by adding aqueos $NaHCO_3$ (0.5 mL). The volatiles were evaporated *in vacuo* and the residue was purified by flash chromatography (DCM:EA 0-100% EA, over 15 min, 12 mL/min, 4 g silica), which afforded the desired product as beige solid (37 mg, 0.17 mmol, 89% yield).

LC-MS: $[M+H]^+$ 216.15

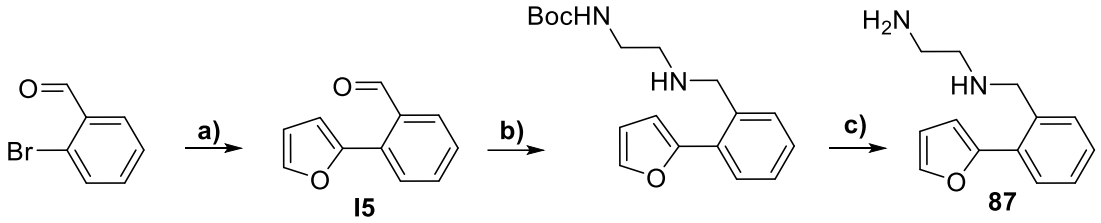

Scheme 23. Synthesis of compound **87**

Step a): I5 2-(furan-2-yl)benzaldehyde was synthesized from 2-bromobenzaldehyde (555 mg, 3.0 mmol), $Pd[PPh_3]_4$ (17 mg, 15 μmol) and 2-(Tri-n-butylstannyl)-furan (1.07 mg, 3.00 mmol) following **General procedure I** to obtain the title compound as white solid (316 mg, 1.81 mmol, 61% yield).

^{1}H NMR (500 MHz, $CDCl_3$) δ 10.38 (d, *J* = 0.8 Hz, 1H), 7.98 (dd, *J* = 7.9, 1.4 Hz, 1H), 7.69 (dd, *J* = 7.9, 1.2 Hz, 1H), 7.65 – 7.58 (m, 2H), 7.48 – 7.41 (m, 1H), 6.64 (dd, *J* = 3.4, 0.8 Hz, 1H), 6.57 (dd, *J* = 3.4, 1.8 Hz, 1H).

^{13}C NMR (126 MHz, $CDCl_3$) δ 192.57, 151.22, 144.15, 134.05, 133.72, 133.24, 128.53, 128.22, 128.14, 112.09, 111.42.

Step b): *tert*-butyl (2-((2-(furan-2-yl)benzyl)amino)ethyl)carbamate was synthesized from 2-(furan-2-yl)benzaldehyde (103 mg, 0.60 mmol), N-Boc-ethylenediamine (96 mg, 0.60 mmol) and $NaBH_4$ (11 mg, 0.30 mmol) using anhydrous MeOH (6.0 mL) as solvent and following the **General procedure IV** to isolate the desired product as white solid (163 mg, 0.52 mmol, 86% yield).

LC-MS: $[M\text{-}tBu]^{\cdot+}$ 261.02.

^{1}H NMR (500 MHz, $CDCl_3$) δ 7.63 – 7.58 (m, 1H), 7.55 – 7.51 (m, 1H), 7.39 (dd, *J* = 8.2, 5.9 Hz, 1H), 7.32 – 7.28 (m, 2H), 6.60 (d, *J* = 3.3 Hz, 1H), 6.52 – 6.49 (m, 1H), 4.95 (s, 1H), 3.91 (s, 2H), 3.23 (t, *J* = 12.0 Hz, 2H), 2.79 – 2.70 (m, 2H), 1.44 (s, 9H).

^{13}C NMR (126 MHz, $CDCl_3$) δ 156.23, 153.62, 142.37, 136.89, 130.30, 130.28, 128.42, 128.06, 127.46, 111.59, 108.54, 52.23, 48.67, 28.56.

Step c): 87 N1-(2-(furan-2-yl)benzyl)ethane-1,2-diamine was obtained from tert-butyl (2-((2-(furan-2-yl)benzyl)amino)ethyl)carbamate (150 mg, 0.47 mmol) and HCl_{diox} (c = 4 M, 600 μL) using DCM (5.0 mL) as solvent and following **General procedure VII**, which afforded the desired amine in the form of a double hydrochloride (115 mg, 0.45 mmol, 95% yield).

LC-MS: $[M+H]^+$ 217.12.

^{1}H NMR (500 MHz, DMSO-d6) δ 7.86 (d, *J* = 1.7 Hz, 1H), 7.77 (d, *J* = 7.1 Hz, 1H), 7.57 (d, *J* = 7.6 Hz, 1H), 7.51 (t, *J* = 7.2 Hz, 1H), 7.44 (dt, *J* = 7.5, 3.8 Hz, 1H), 6.97 (d, *J* = 3.4 Hz, 1H), 6.69 (dd, *J* = 3.4, 1.8 Hz, 1H), 4.43 (s, 2H), 3.31 (t, *J* = 6.9 Hz, 2H), 3.20 (t, *J* = 6.9 Hz, 2H).

^{13}C NMR (126 MHz, DMSO-d6) δ 151.84, 143.88, 131.11, 130.14, 129.56, 128.16, 127.77, 112.08, 109.66, 49.18, 44.34, 35.40.

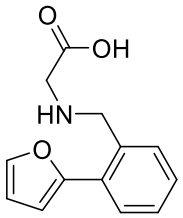

88

88 (2-(furan-2-yl)benzyl)glycine was synthesized from 2-(furan-2-yl)benzaldehyde (100 mg, 0.58 mmol), glycine (44 mg, 0.58 mmol) and $NaBH_4$ (11 mg, 0.29 mmol) using anhydrous MeOH (4.0 mL) as solvent and following the **General procedure IV** to isolate the desired product as white solid (110 mg, 0.52 mmol, 56% yield).

LC-MS: $[M+H]^+$ 232.12

^{1}H NMR (500 MHz, DMSO-d6) δ 7.79 (d, *J* = 1.6 Hz, 1H), 7.68 – 7.62 (m, 1H), 7.62 – 7.57 (m, 1H), 7.37 – 7.31 (m, 3H), 6.78 (d, *J* = 3.3 Hz, 1H), 6.64 – 6.60 (m, 1H), 5.28 (t, *J* = 5.5 Hz, 1H), 4.64 (d, *J* = 5.5 Hz, 3H).

^{13}C NMR (126 MHz, DMSO-d6) δ 151.71, 142.89, 138.36, 128.23, 127.85, 127.48, 127.01, 126.37, 111.87, 109.36, 61.36.

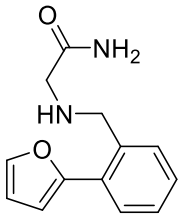

89

89 2-((2-(furan-2-yl)benzyl)amino)acetamide was synthesized from 2-(furan-2-yl)benzaldehyde (100 mg, 0.58 mmol), glycinamide (65 mg, 0.58 mmol) and $NaBH_4$ (11 mg, 0.3 mmol) using anhydrous MeOH (4.0 mL) as solvent and following the **General procedure IV** to isolate the desired product as white solid (44 mg, 0.19 mmol, 32% yield).

^{1}H NMR (500 MHz, DMSO-d6) δ 7.79 (d, *J* = 1.7 Hz, 1H), 7.68 – 7.64 (m, 1H), 7.63 – 7.58 (m, 1H), 7.38 – 7.31 (m, 2H), 6.78 (d, *J* = 3.4 Hz, 1H), 6.62 (dd, *J* = 3.3, 1.8 Hz, 1H), 5.29 (t, *J* = 5.5 Hz, 1H), 4.64 (d, *J* = 5.5 Hz, 2H).

^{13}C NMR (126 MHz, DMSO-d6) δ 152.16, 143.34, 138.81, 128.68, 128.30, 127.93, 127.46, 126.82, 112.32, 109.82, 61.81.

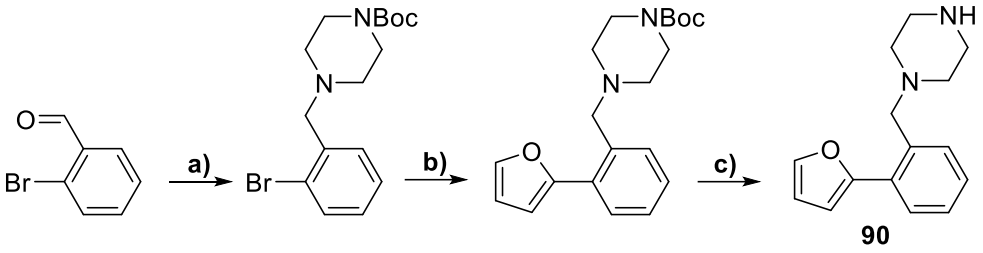

Scheme 24. Synthesis of compound **90**

Step a): *tert*-butyl 4-(2-bromobenzyl)piperazine-1-carboxylate was synthesized from 2-bromobenzaldehyde (925 mg, 5.00 mmol), N-Boc-piperazine (978 mg, 5.25 mmol) and $NaBH(OAc)_3$ (1.41 g, 6.65 mmol) using anhydrous DCM (25.0 mL) as solvent and following the **General procedure IV** to isolate the desired product by flash chromatography (Hex:EA 0-100% EA over 20 min, 24 mL/min, 24 g silica) as white solid (888 mg, 2.50 mmol, 50% yield).

LC-MS: $[M+H]^+$ 355.05. 358.16

^{1}H NMR (500 MHz, Acetone-d6) δ 7.58 (d, *J* = 8.0 Hz, 1H), 7.54 (d, *J* = 7.6 Hz, 1H), 7.36 (dd, *J* = 10.8, 4.2 Hz, 1H), 7.20 (td, *J* = 7.8, 1.6 Hz, 1H), 3.60 (s, 2H), 3.40 (s, 4H), 2.47 – 2.41 (m, 4H), 1.43 (s, 9H).

^{13}C NMR (126 MHz, Acetone-d6) δ 155.12, 138.53, 133.66, 131.95, 129.74, 128.41, 125.20, 79.61, 62.49, 60.64, 53.79, 28.64.

Step b): *tert*-butyl 4-(2-(furan-2-yl)benzyl)piperazine-1-carboxylate was synthesized from *tert*-butyl 4-(2-bromobenzyl)piperazine-1-carboxylate (343 mg, 1.00 mmol), $Pd[PPh_3]_4$ (57 mg, 49 μmol) and 2-(Tri-n-butylstannyl)-furan (464 mg, 1.30 mmol) following **General procedure I** to obtain the title compound slightly beige solid (323 mg, 0.94 mmol, 94% yield).

LC-MS: $[M+H]^+$ 343.15

^{1}H NMR (500 MHz, Acetone-d6) δ 7.70 – 7.62 (m, 2H), 7.51 (d, *J* = 7.5 Hz, 1H), 7.39 – 7.33 (m, 1H), 7.31 (t, *J* = 7.4 Hz, 1H), 6.86 (d, *J* = 3.3 Hz, 1H), 6.56 (dd, *J* = 3.0, 2.0 Hz, 1H), 3.62 (s, 2H), 3.37 (s, 4H), 2.43 – 2.37 (m, 4H), 1.43 (s, 9H).

^{13}C NMR (126 MHz, Acetone-d6) δ 154.14, 152.76, 142.32, 134.61, 131.16, 131.01, 127.74, 127.31, 127.27, 111.48, 109.63, 78.59, 67.17, 60.63, 52.64, 27.65.

Step c): 90 1-(2-(furan-2-yl)benzyl)piperazine was synthesized by deprotection of *tert*-butyl 4-(2-(furan-2-yl)benzyl)piperazine-1-carboxylate (323 mg, 0.94 mmol) with HCl_{diox} (1.0 mL) using DCM (5.0 mL) as solvent and following **General procedure VII**, which afforded the desired amine in the form of a dihydrochloride (296 mg, 0.94 mmol, 99% yield).

LC-MS: $[M+H]^+$ 243.01

^{1}H NMR (500 MHz, MeOD) δ 7.67 (dd, *J* = 8.0, 1.3 Hz, 2H), 7.51 (dd, *J* = 7.5, 1.0 Hz, 1H), 7.39 (td, *J* = 7.6, 1.4 Hz, 1H), 7.34 (td, *J* = 7.5, 1.4 Hz, 1H), 6.77 (d, *J* = 3.3 Hz, 1H), 6.56

(dd, *J* = 3.3, 1.8 Hz, 1H), 3.91 (s, 2H), 3.24 – 3.10 (m, 3H), 2.41 (t, *J* = 11.6 Hz, 2H), 2.07 – 1.99 (m, 2H), 1.72 (qd, *J* = 12.4, 3.9 Hz, 2H).

^{13}C NMR (126 MHz, MeOD) δ 154.37, 143.82, 132.78, 132.68, 129.40, 129.30, 128.83, 112.59, 110.44, 60.99, 52.11, 40.38, 30.39.

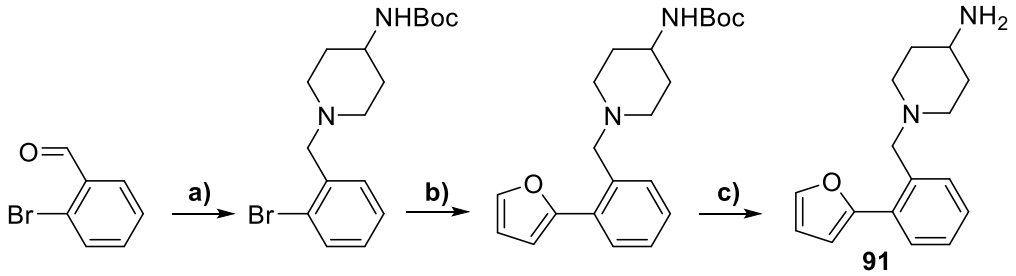

Scheme 25. Synthesis of compound **91**

Step a): *tert*-butyl (1-(2-bromobenzyl)piperidin-4-yl)carbamate was synthesized from 2-bromobenzaldehyde (925 mg, 5.00 mmol), *tert*-butyl piperidin-4-ylcarbamate (1.05 g, 5.25 mmol) and $NaBH(OAc)_3$ (1.41 mg, 6.65 mmol) using anhydrous DCM (25.0 mL) as solvent and following the **General procedure IV** to isolate the desired product by flash chromatography (DCM:MeOH 0-10% MeOH over 25 min, 24 mL/min, 24 g silica) as white solid (816 mg, 2.21 mmol, 44% yield).

LC-MS: $[M+H]^+$ 369.15, 371.13.

^{1}H NMR (500 MHz, DMSO-d6) δ 7.58 (dd, *J* = 8.0, 1.0 Hz, 1H), 7.44 (dd, *J* = 7.6, 1.6 Hz, 1H), 7.36 (td, *J* = 7.5, 1.0 Hz, 1H), 7.19 (td, *J* = 7.7, 1.7 Hz, 1H), 6.77 (d, *J* = 7.8 Hz, 1H), 3.49 (s, 2H), 3.33 (s, 2H), 3.28 – 3.19 (m, 1H), 2.76 (d, *J* = 11.8 Hz, 2H), 2.05 (dd, *J* = 11.5, 9.9 Hz, 2H), 1.67 (d, *J* = 11.2 Hz, 2H), 1.37 (s, 9H).

^{13}C NMR (126 MHz, DMSO-d6) δ 154.84, 137.66, 132.47, 130.73, 128.79, 127.55, 123.88, 77.43, 61.21, 52.24, 47.43, 31.89, 28.27.

Step b): *tert*-butyl (1-(2-(furan-2-yl)benzyl)piperidin-4-yl)carbamate was synthesized from *tert*-butyl (1-(2-bromobenzyl)piperidin-4-yl)carbamate (355 mg, 1.00 mmol), $Pd[PPh_3]_4$ (57 mg, 49 μmol) and 2-(Tri-n-butylstannyl)-furan (464 mg, 1.30 mmol) following **General procedure I** to obtain the title compound slightly beige solid (250 mg, 0.70 mmol, 70% yield).

LC-MS: $[M+H]^+$ 357.23.

^{1}H NMR (500 MHz, DMSO-d6) δ 7.78 (d, *J* = 1.5 Hz, 1H), 7.63 (dd, *J* = 7.6, 1.4 Hz, 1H), 7.46 – 7.42 (m, 1H), 7.35 (td, *J* = 7.4, 1.5 Hz, 1H), 7.31 (td, *J* = 7.4, 1.5 Hz, 1H), 6.82 (d, *J* = 3.3 Hz, 1H), 6.76 (d, *J* = 7.7 Hz, 1H), 6.61 (dd, *J* = 3.3, 1.8 Hz, 1H), 3.51 (s, *J* = 7.7 Hz, 2H), 3.27 – 3.18 (m, 1H), 2.76 (d, *J* = 11.5 Hz, 2H), 1.98 (t, *J* = 11.1 Hz, 2H), 1.67 (d, *J* = 11.0 Hz, 2H), 1.37 (s, 9H), 1.35 – 1.29 (m, 2H).

^{13}C NMR (126 MHz, DMSO-d6) δ 154.85, 151.96, 142.80, 134.80, 130.69, 130.31, 127.32, 127.29, 127.22, 111.79, 109.80, 77.43, 60.23, 52.04, 47.58, 31.93, 28.27.

Step c): 91 1-(2-(furan-2-yl)benzyl)piperidin-4-amine was synthesized by deprotection of *tert*-butyl (1-(2-(furan-2-yl)benzyl)piperidin-4-yl)carbamate (100 mg, 0.28 mmol) with $HCl_{di\text{-}ox}$ (0.5 mL) using DCM (4.5 mL) as solvent and following **General procedure VII**, which afforded the desired amine in the form of a dihydrochloride as white solid (92 mg, 0.28 mmol, 99% yield).

LC-MS: $[M+H]^+$ 257.04.

^{1}H NMR (500 MHz, DMSO-d6) δ 7.93 (d, *J* = 1.5 Hz, 1H), 7.87 (d, *J* = 7.6 Hz, 1H), 7.74 – 7.71 (m, 1H), 7.53 (dd, *J* = 10.9, 4.3 Hz, 1H), 7.44 (td, *J* = 7.6, 1.0 Hz, 1H), 6.96 (d, *J* = 3.4 Hz, 1H), 6.68 (dd, *J* = 3.4, 1.8 Hz, 1H), 4.49 (d, *J* = 4.9 Hz, 2H), 3.29 (d, *J* = 5.0 Hz, 2H), 3.13 – 3.02 (m, 2H), 2.13 – 1.93 (m, 6H).

^{13}C NMR (126 MHz, DMSO-d6) δ 152.04, 144.08, 133.26, 131.38, 129.98, 128.33, 128.28, 125.77, 112.03, 109.92, 57.49, 50.11, 45.08, 26.92.

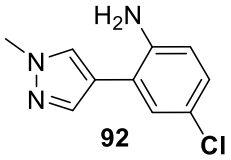

92

92 4-chloro-2-(1-methyl-1H-pyrazol-4-yl)aniline was synthesized from 4-chloro-2-bromoaniline (103 mg, 0.50 mmol), $Pd[PPh_3]_4$ (17 mg, 15 μmol), (1-methyl-1H-pyrazol-4-yl)boronic acid pinacol ester (125 mg, 0.60 mmol) and K_2CO_3 (138 mg, 1.00 mmol) following **General procedure II** to isolate the title compound by flash chromatography (Hex:EA 0-100% EA over 15 min, 18 mL/min, 12 g silica) as beige solid (120 mg, 0.62 mmol, 62% yield).

LC-MS: 208.13, 210.14.

^{1}H NMR (500 MHz, $CDCl_3$) δ 7.67 (s, *J* = 3.7 Hz, 1H), 7.56 (s, 1H), 7.14 (d, *J* = 2.5 Hz, 1H), 7.04 (dd, *J* = 8.5, 2.5 Hz, 1H), 6.68 (d, *J* = 8.5 Hz, 1H), 3.96 (s, 3H), 3.80 (s, 2H).

^{13}C NMR (126 MHz, $CDCl_3$) δ 142.54, 138.53, 129.40, 128.80, 127.76, 123.41, 120.27, 119.01, 116.92, 39.28.

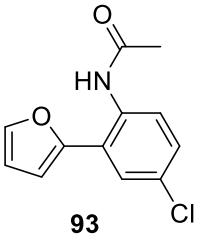

93

93 N-(4-chloro-2-(furan-2-yl)phenyl)acetamide was synthesized by acetylation of **65** (50 mg, 0.26 mmol) with Ac_2O (32 mg, 0.31 mmol) in the presence of TEA (52 mg, 0.52 mmol) and using DCM (3.0 mL) as a solvent. The solvent was evaporated *in vacuo* and the residue was purified by flash chromatography (DCM:EA 0-100% EA, over 15 min, 12 mL/min, 4 g silica) to yield the desired product as slightly yellow solid (62 mg, 0.26 mmol, 84% yield).

^{1}H NMR (500 MHz, $CDCl_3$) δ 7.85 (d, *J* = 2.4 Hz, 1H), 7.49 (d, *J* = 1.7 Hz, 1H), 7.34 (dd, *J* = 8.4, 2.4 Hz, 1H), 7.10 (d, *J* = 8.4 Hz, 1H), 6.54 (d, *J* = 3.5 Hz, 1H), 6.48 (dd, *J* = 3.5, 1.8 Hz, 1H), 2.28 (s, 3H).

^{13}C NMR (126 MHz, $CDCl_3$) δ 172.90, 149.16, 143.62, 135.51, 133.46, 131.82, 130.67, 128.83, 127.67, 112.25, 109.86, 26.88.

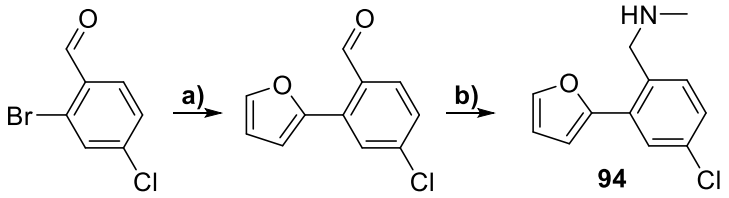

Scheme 26. Synthesis of compound **94**

Step a): 4-chloro-2-(furan-2-yl)benzaldehyde was synthesized from 2-bromo-4-chlorobenzaldehyde (658 mg, 3.00 mmol), $Pd[PPh_3]_4$ (173 mg, 0.15 mmol) and 2-(Tri-n-butylstannyl)-furan (1.07 g, 3.00 mmol) following **General procedure I** to obtain the title compound as white solid (446 mg, 2.16 mmol, 72% yield).

^{1}H NMR (500 MHz, $CDCl_3$) δ 10.35 (s, 1H), 7.92 (d, *J* = 8.4 Hz, 1H), 7.68 (d, *J* = 2.0 Hz, 1H), 7.63 (d, *J* = 1.7 Hz, 1H), 7.40 (dd, *J* = 8.4, 1.9 Hz, 1H), 6.68 (d, *J* = 3.4 Hz, 1H), 6.58 (dd, *J* = 3.4, 1.8 Hz, 1H).

^{13}C NMR (126 MHz, $CDCl_3$) δ 191.28, 149.85, 144.66, 140.15, 134.74, 131.37, 129.83, 128.42, 128.26, 112.36, 112.31.

Step b): 94 1-(4-chloro-2-(furan-2-yl)phenyl)-N-methylmethanamine GPK-519 HCl was synthesized from 4-chloro-2-(furan-2-yl)-benzaldehyde (26 mg, 0.12 mmol), $MeNH_2$ (40% aqueous solution, 50 mg, 0.6 mmol), $NaBH_4$ (25 mg, 0.6 mmol) using MeOH (3.0 mL) as solvent and following the **General procedure IV**. The desired amine was isolated as free base and converted into the hydrochloride from – white solid (21 mg, 0.08 mmol, 70% yield).

^{1}H NMR (500 MHz, DMSO-d6) δ 9.40 (s, 2H), 7.91 (d, *J* = 1.6 Hz, 1H), 7.81 (d, *J* = 2.2 Hz, 1H), 7.69 (d, *J* = 8.4 Hz, 1H), 7.50 (dd, *J* = 8.4, 2.2 Hz, 1H), 7.09 (d, *J* = 3.4 Hz, 1H), 6.70 (dd, *J* = 3.4, 1.8 Hz, 1H), 4.31 (s, 2H), 2.60 (s, 3H).

^{13}C NMR (126 MHz, DMSO-d6) δ 150.38, 144.46, 133.93, 133.26, 131.86, 127.63, 126.80, 112.16, 110.81, 49.23, 32.51.

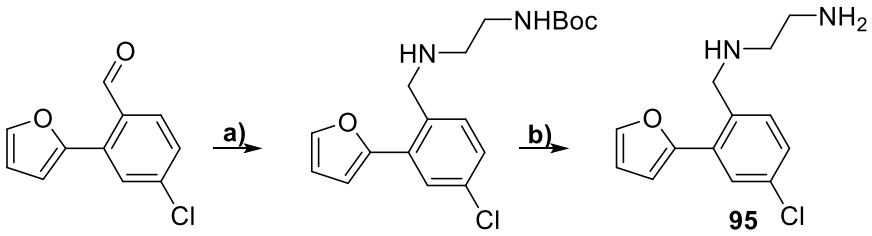

Scheme 27. Synthesis of compound **95**

Step a): *tert*-butyl (2-((4-chloro-2-(furan-2-yl)benzyl)amino)ethyl)carbamate was synthesized from 4-chloro-2-(furan-2-yl)benzaldehyde (124 mg, 0.60 mmol), N-Boc-ethylenediamine (96 mg, 0.60 mmol) and $NaBH_4$ (12 mg, 0.3 mmol) using anhydrous MeOH (6.0 mL) as solvent and following the **General procedure IV** the desired product was isolated as white solid (94 mg, 0.27 mmol, 45% yield).

LC-MS: $[M+H]^+$ 351.22, 353.23.

^{1}H NMR (500 MHz, DMSO-d6) δ 7.82 (d, *J* = 1.6 Hz, 1H), 7.63 (d, *J* = 2.3 Hz, 1H), 7.56 (d, *J* = 8.3 Hz, 1H), 7.36 (dd, *J* = 8.3, 2.3 Hz, 1H), 6.90 (d, *J* = 3.3 Hz, 1H), 6.75 (t, *J* = 5.3 Hz, 1H), 6.64 (dd, *J* = 3.3, 1.8 Hz, 1H), 3.79 (s, 2H), 3.03 (q, *J* = 6.1 Hz, 2H), 2.57 (t, *J* = 6.4 Hz, 2H), 1.36 (s, 9H).

^{13}C NMR (126 MHz, DMSO-d6) δ 155.64, 150.47, 143.45, 135.89, 131.37, 131.09, 127.05, 126.07, 112.02, 110.58, 77.47, 50.50, 48.71, 28.25.

Step b): 95 *N*1-(4-chloro-2-(furan-2-yl)benzyl)ethane-1,2-diamine was synthesized from *tert*-butyl (2-((4-chloro-2-(furan-2-yl)benzyl)amino)ethyl)carbamate (70 mg, 0.3 mmol), and HCl_{diox} (400 µL) using DCM (3.0 mL) as solvent and following **General procedure VII**, which afforded the desired amine in the form of a double hydrochloride (28 mg, 0.09 mmol, 29% yield).

LC-MS: $[M+H]^+$ 251.02, 253.07.

^{1}H NMR (500 MHz, DMSO-d6) δ 7.96 (d, *J* = 1.6 Hz, 1H), 7.81 (d, *J* = 2.2 Hz, 1H), 7.76 (d, *J* = 8.4 Hz, 1H), 7.50 (dd, *J* = 8.4, 2.2 Hz, 1H), 7.11 (d, *J* = 3.4 Hz, 1H), 6.70 (dd, *J* = 3.4, 1.8 Hz, 1H), 4.33 (s, 2H), 3.33 – 3.29 (m, 2H), 3.23 (t, *J* = 6.0 Hz, 2H).

^{13}C NMR (126 MHz, DMSO-d6) δ 150.34, 144.49, 133.77, 133.13, 131.83, 127.56, 126.68, 112.11, 110.89, 48.40, 44.55, 35.61.

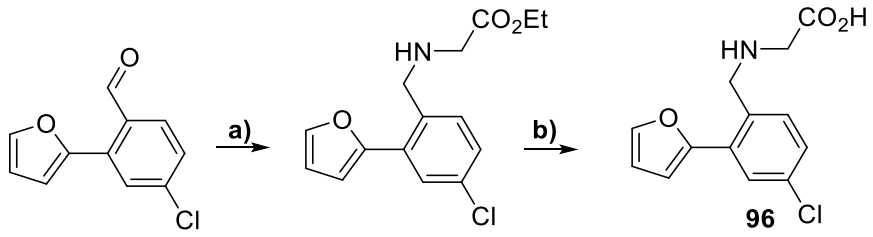

Scheme 28. Synthesis of compound **96**

Step a): Ethyl (4-chloro-2-(furan-2-yl)benzyl)glycinate was synthesized from 4-chloro-2-(furan-2-yl)benzaldehyde (150 mg, 0.73 mmol), glycine ethyl ester hydrochloride (101 mg, 0.73 mmol), TEA (74 mg, 0.73 mmol) and $NaBH(OAc)_3$ (308 mg, 1.45 mmol) using anhydrous MeOH (6.0 mL) as solvent and following the **General procedure IV** the desired product was isolated as white solid (99 mg, 0.34 mmol, 47% yield).

LC-MS: $[M+H]^+$ 294.04, 296.07.

^{1}H NMR (500 MHz, DMSO-d_6) δ 7.82 (d, *J* = 1.9 Hz, 1H), 7.64 (d, *J* = 2.3 Hz, 1H), 7.55 (d, *J* = 8.3 Hz, 1H), 7.37 (dd, *J* = 8.3, 2.3 Hz, 1H), 6.95 (d, *J* = 3.3 Hz, 1H), 6.64 (dd, *J* = 3.4, 1.8 Hz, 1H), 4.08 (q, *J* = 7.1 Hz, 2H), 3.85 (s, 2H), 3.36 (s, 2H), 1.18 (t, *J* = 7.1 Hz, 3H).

^{13}C NMR (126 MHz, DMSO-d_6) δ 172.06, 150.40, 143.49, 135.27, 131.56, 131.52, 131.16, 127.16, 126.12, 112.05, 110.64, 59.96, 49.90, 49.72, 14.12.

Step b): 96 (4-chloro-2-(furan-2-yl)benzyl)glycine was synthesized by saponification of ethyl (4-chloro-2-(furan-2-yl)benzyl)glycinate (99 mg, 0.34 mmol), 2M NaOH (0.6 mL) and using THF (0.6 mL) as solvent. The resulting reaction mixture was stirred for 4 hours, after which it was diluted with water (10 mL) and its pH was adjusted to 7 by adding 1M HCl. The resulting solution was extracted with EtOAc (3x15 mL) and to the combined organic fractions 2M solution of HCl in diethyl ether (100 μL) was added and the resulting precipitate was filtered off to afford the desired product as a hydrochloride (100 mg, 0.33 mmol, 95% yield).

LC-MS: $[M+H]^+$ 266.05, 268.04.

^{1}H NMR (500 MHz, DMSO-d6) δ 7.83 (s, 1H), 7.68 (d, *J* = 1.9 Hz, 1H), 7.57 (d, *J* = 8.3 Hz, 1H), 7.40 (dd, *J* = 8.3, 2.0 Hz, 1H), 6.99 (d, *J* = 3.2 Hz, 1H), 6.65 (d, *J* = 1.3 Hz, 1H), 3.98 (s, 2H), 3.25 (s, 2H).

^{13}C NMR (126 MHz, DMSO-d6) δ 150.39, 143.72, 133.15, 133.13, 132.14, 131.90, 131.36, 127.28, 126.30, 112.09, 110.68, 49.77, 49.43.

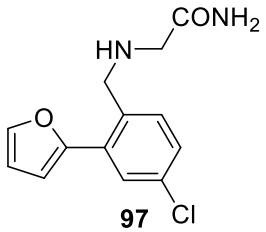

97

97 2-((4-chloro-2-(furan-2-yl)benzyl)amino)acetamide was synthesized from 4-chloro-2-(furan-2-yl)benzaldehyde (50 mg, 0.24 mmol), glycinamide (101 mg, 0.73 mmol) and $NaBH(OAc)_3$ (103 mg, 0.48 mmol) using anhydrous MeOH (3.0 mL) as solvent and following the **General procedure IV** the desired product was isolated as white solid (11 mg, 0.04 mmol, 17% yield).

LC-MS: $[M+H]^+$ 265.03, 266.99.

^{1}H NMR (500 MHz, DMSO-d6) δ 7.82 (d, *J* = 1.6 Hz, 1H), 7.65 (d, *J* = 2.2 Hz, 1H), 7.58 (d, *J* = 8.3 Hz, 1H), 7.38 (dd, *J* = 8.3, 2.3 Hz, 1H), 7.27 (s, 1H), 7.03 (s, 1H), 6.91 (d, *J* = 3.4 Hz, 1H), 6.64 (dd, *J* = 3.3, 1.8 Hz, 1H), 3.82 (s, 2H), 3.09 (s, 2H).

^{13}C NMR (126 MHz, DMSO-d6) δ 173.09, 150.47, 143.52, 135.32, 131.54, 131.37, 131.11, 127.18, 126.19, 112.05, 110.58, 51.31, 50.33.

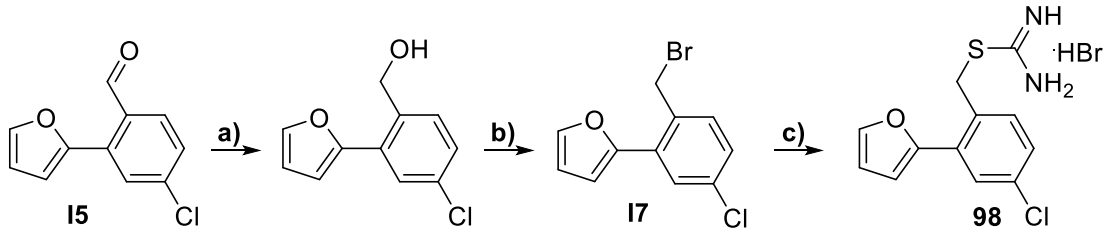

Scheme 29. Synthesis of compound **98**

Step a): (4-chloro-2-(furan-2-yl)phenyl)methanol was synthesized by the reduction of 4-chloro-2-(furan-2-yl)benzaldehyde (206 mg, 1.00 mmol) with $NaBH_4$ (19 mg, 0.5 mmol) in the THF/EtOH mixture (2.5 mL + 2.5 mL). The title compound was obtained as colorless solid (207 mg, 0.99 mmol, 99% yield).

^{1}H NMR (500 MHz, DMSO-d6) δ 7.79 (d, *J* = 1.6 Hz, 1H), 7.68 – 7.62 (m, 1H), 7.62 – 7.57 (m, 1H), 7.37 – 7.31 (m, 3H), 6.78 (d, *J* = 3.3 Hz, 1H), 6.64 – 6.60 (m, 1H), 5.28 (t, *J* = 5.5 Hz, 1H), 4.64 (d, *J* = 5.5 Hz, 3H).

^{13}C NMR (126 MHz, DMSO-d6) δ 151.71, 142.89, 138.36, 128.23, 127.85, 127.48, 127.01, 126.37, 111.87, 109.36, 61.36.

Step b): 2-(2-(bromomethyl)-5-chlorophenyl)furan. To the solution of (4-chloro-2-(furan-2-yl)phenyl)methanol (88 mg, 0.4 mmol) in DCM (5.0 mL) were added CBr_4 (280 mg, 0.8 mmol) and PPh_3 (221 mg, 0.8 mmol) and the resulting mixture was stirred for 2 hours at room temperature. The reaction mixture was diluted with water (15 mL), extracted with DCM (2x10 mL), washed with brine, dried over anhydrous sodium sulfate and concentrated *in vacuo.* Purification by flash column chromatography (Hex:DCM 0-30% DCM over 12 min, 18 mL/min, 12 g silica) yielded the desired product as colorless solid (98 mg, 0.36 mmol, 90% yield).

^{1}H NMR (500 MHz, DMSO-d_6) δ 7.89 (d, *J* = 1.7 Hz, 1H), 7.71 (d, *J* = 2.3 Hz, 1H), 7.59 (d, *J* = 8.3 Hz, 1H), 7.41 (dd, *J* = 8.3, 2.3 Hz, 1H), 7.07 (d, *J* = 3.4 Hz, 1H), 6.70 (dd, *J* = 3.4, 1.8 Hz, 1H), 4.92 (s, 2H).

^{13}C NMR (126 MHz, DMSO-d_6) δ 110.75, 112.27, 126.76, 127.82, 131.23, 132.51, 133.62, 133.82, 144.09, 149.90.

Step c): 98 4-chloro-2-(furan-2-yl)benzyl carbamimidothioate hydrobromide. To the stirred solution of 2-(2-(bromomethyl)-5-chlorophenyl)furan (60 mg, 0.22 mmol) in acetonitrile (2.0 mL) was added thiourea (17 mg, 0.22 mmol), after which the reaction mixture was heated up to 60^{o}C and stirred at this temperature for 1 hour. The reaction mixture was concentrated *in vacuo* and the residue was resuspended in diethyl ether, which gave a white precipitate that was collected (75 mg, 0.22 mmol, 95% yield).

LC-MS: $[M+H]^+$ 266.98, 269.01

^{1}H NMR (500 MHz, DMSO-d6) δ 9.20 (s, 2H), 9.02 (s, 2H), 7.88 (d, *J* = 1.7 Hz, 1H), 7.76 (d, *J* = 2.3 Hz, 1H), 7.56 (d, *J* = 8.3 Hz, 1H), 7.44 (dd, *J* = 8.3, 2.3 Hz, 1H), 7.05 (d, *J* = 3.4 Hz, 1H), 6.70 (dd, *J* = 3.4, 1.8 Hz, 1H), 4.71 (s, 2H).

^{13}C NMR (126 MHz, DMSO-d6) δ 168.97, 150.29, 144.24, 133.47, 133.20, 131.51, 129.21, 127.91, 127.19, 112.31, 110.67, 33.48.

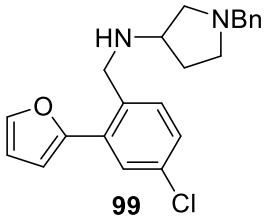

99

99 1-benzyl-N-(4-chloro-2-(furan-2-yl)benzyl)pyrrolidin-3-amine was synthesized from 4-chloro-2-(furan-2-yl)benzaldehyde (50 mg, 0.24 mmol), 1-benzylpyrrolidin-3-amine (43 mg, 0.24 mmol) and $NaBH(OAc)_3$ (103 mg, 0.48 mmol) using anhydrous MeOH (2.0 mL) as solvent and following the **General procedure IV**. The desired product was isolated by flash chromatography (DCM:MeOH 0-10% MeOH over 16 min, 18 mL/min, 12 g silica) as white solid (56 mg, 0.15 mmol, 63% yield).

LC-MS: $[M+H]^+$ 367.24, 369.24

^{1}H NMR (500 MHz, DMSO-d6) δ 7.80 (d, *J* = 1.6 Hz, 1H), 7.63 (d, *J* = 2.3 Hz, 1H), 7.57 (d, *J* = 8.3 Hz, 1H), 7.37 (dd, *J* = 8.3, 2.3 Hz, 1H), 7.33 – 7.30 (m, 4H), 7.28 – 7.22 (m, 1H), 6.94 (d, *J* = 3.4 Hz, 1H), 6.63 (dd, *J* = 3.3, 1.8 Hz, 1H), 3.82 (q, *J* = 13.9 Hz, 2H), 3.62 (q, *J* = 13.0 Hz, 2H), 3.31 (td, *J* = 11.8, 5.0 Hz, 1H), 2.73 (dd, *J* = 9.5, 6.8 Hz, 1H), 2.61 (dd, *J* = 15.0, 8.4 Hz, 1H), 2.56 – 2.51 (m, 1H), 2.39 (dd, *J* = 9.6, 5.0 Hz, 1H), 2.00 (td, *J* = 14.2, 7.9 Hz, 1H), 1.59 (dq, *J* = 8.0, 5.5 Hz, 1H).

^{13}C NMR (126 MHz, DMSO-d6) δ 163.77, 150.48, 143.45, 138.25, 134.80, 131.82, 131.12, 128.60, 128.11, 127.11, 126.93, 126.12, 111.93, 110.44, 59.27, 59.25, 56.50, 52.29, 48.74, 30.84.

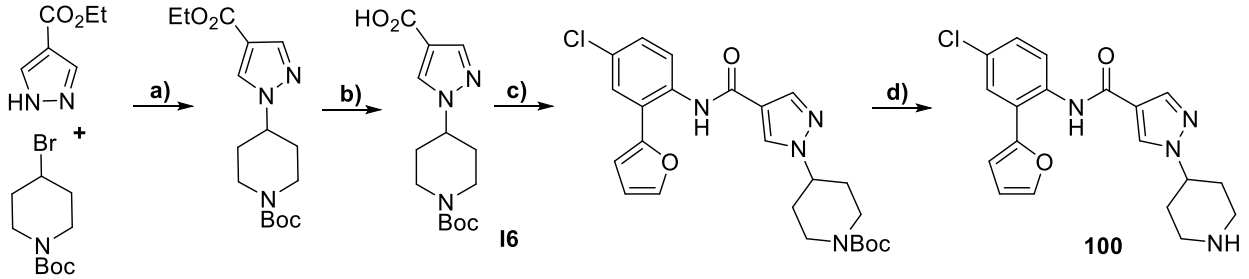

Scheme 30. Synthesis of compound **100**

Step a): *tert*-butyl 4-(4-(ethoxycarbonyl)-1H-pyrazol-1-yl)piperidine-1-carboxylate. The solution containing *tert*-butyl 4-bromopiperidine-1-carboxylate (594 mg, 2.25 mmol), ethyl 1H-pyrazole-4-carboxylate (182 mg, 1.3 mmol) and Cs_2CO_3 (1.27 g, 3.90 mmol) in DMF (5.0

mL) was subjected to microwave irradiation (150 W, 100°C, 30 min). The resulting mixture was diluted with water (50 mL), extracted with EtOAc (3x30 mL), the combined organic fractions were washed with brine, dried over anhydrous Na_2SO_4 and concentrated *in vacuo*. The desired product was isolated by flash chromatography (DCM-EA 0-100% EA over 16 min, 18 mL/min, 12 g silica) as clear viscous oil (350 mg, 1.1 mmol, 83% yield).

LC-MS: $[M+H\text{-}tBu]^+$ 324.26

^{1}H NMR (500 MHz, Acetone-d6) δ 8.19 (s, 1H), 7.82 (s, 1H), 4.46 (tt, *J* = 11.5, 4.1 Hz, 1H), 4.23 (q, *J* = 7.1 Hz, 2H), 4.22 – 4.13 (m, 2H), 2.94 (s, 2H), 2.12 – 2.06 (m, 2H), 1.98 – 1.87 (m, 2H), 1.46 (s, 9H), 1.29 (t, *J* = 7.1 Hz, 3H).

^{13}C NMR (126 MHz, Acetone-d6) δ 163.39, 155.07, 141.03, 132.06, 115.44, 79.82, 60.42, 60.36, 43.81, 43.17, 32.99, 28.65.

Step b): I6 1-(1-(tert-butoxycarbonyl)piperidin-4-yl)-1H-pyrazole-4-carboxylic acid was synthesized by saponification of *tert*-butyl 4-(4-(ethoxycarbonyl)-1H-pyrazol-1-yl)piperidine-1-carboxylate (30 mg, 0.09 mmol) with LiOH (4.0 M, 1.0 mL) using THF (1.0 mL) as solvent. After full consumption of the starting material the pH of the reaction mixture was adjusted to 7 by adding 1M HCl and the resulting mixture was extracted with EtOAc (3x10 mL). The combined organic fractions were dried over anhydrous Na_2SO_4, and concentrated *in vacuo* to afford the product as colorless solid (15 mg, 0.05 mmol, 56% yield).

LC-MS: $[M+H]^+$ 268.11.

^{1}H NMR (500 MHz, $CDCl_3$) δ 7.99 (s, 1H), 7.98 (s, 1H), 4.37 – 4.18 (m, 3H), 2.90 (s, 2H), 2.16 (d, *J* = 12.3 Hz, 2H), 1.91 (qd, *J* = 12.4, 4.4 Hz, 2H), 1.48 (s, 9H).

^{13}C NMR (126 MHz, $CDCl_3$) δ 167.46, 154.70, 141.62, 131.18, 113.96, 80.30, 60.01, 43.09, 42.35, 28.55.

Step c): *tert*-butyl 4-(4-((4-chloro-2-(furan-2-yl)phenyl)carbamoyl)-1H-pyrazol-1-yl)-piperidine-1-carboxylate was synthesized by acylation of **65** (6.0 mg, 30 μmol) using 1-(1-(tert-butoxycarbonyl)piperidin-4-yl)-1H-pyrazole-4-carboxylic acid (8.9 mg, 30 μmol) and T3P (19 mg, 60 μmol) and pyridine (0.7 mL). The product was isolated using flash chromatography (DCM:MeOH 0-10% MeOH over 10 min, 18 mL/min, 4 g silica) as white solid (6.0 mg, 12 μmol, 40% yield).

^{1}H NMR (500 MHz, $CDCl_3$) δ 8.97 (s, 1H), 8.44 (d, *J* = 8.9 Hz, 1H), 8.01 (s, 1H), 7.81 (s, 1H), 7.63 (d, *J* = 1.3 Hz, 1H), 7.54 (d, *J* = 2.4 Hz, 1H), 7.30 (dd, *J* = 8.9, 2.4 Hz, 1H), 6.69 (d, *J* = 3.4 Hz, 1H), 6.60 (dd, *J* = 3.3, 1.8 Hz, 1H), 4.35 – 4.19 (m, 3H), 2.91 (s, 2H), 2.16 (d, *J* = 11.7 Hz, 2H), 1.93 (qd, *J* = 12.3, 4.3 Hz, 2H), 1.48 (s, 9H).

^{13}C NMR (126 MHz, $CDCl_3$) δ 160.49, 154.68, 151.67, 142.82, 137.21, 133.08, 129.68, 129.32, 128.89, 127.24, 123.51, 121.64, 119.19, 112.40, 109.22, 80.25, 60.06, 42.74, 32.34, 28.56.

Step d): 100 N-(4-chloro-2-(furan-2-yl)phenyl)-1-(piperidin-4-yl)-1H-pyrazole-4-carboxamide was synthesized from its previously obtained Boc-protected derivative (5.0 mg, 10 μmol) and HCl (4M in dioxane, 100 μL) using DCM (1.0 mL) as solvent and following **General procedure VII**, which afforded the desired amine in the form of a double hydrochloride (3.0 mg, 0.09 mmol, 42% yield) as a result of preparative HPLC.

^{1}H NMR (500 MHz, $CDCl_3$) δ 8.87 (s, 1H), 8.40 (d, *J* = 8.9 Hz, 1H), 8.01 (s, 1H), 7.81 (s, 1H), 7.63 (d, *J* = 1.3 Hz, 1H), 7.54 (d, *J* = 2.4 Hz, 1H), 7.30 (dd, *J* = 8.9, 2.4 Hz, 1H), 6.69 (d, *J* = 3.4 Hz, 1H), 6.60 (dd, *J* = 3.3, 1.8 Hz, 1H), 4.40 – 4.22 (m, 3H), 2.89 (s, 2H), 2.16 (d, *J* = 11.7 Hz, 2H), 1.90 (qd, *J* = 12.3, 4.3 Hz, 2H).

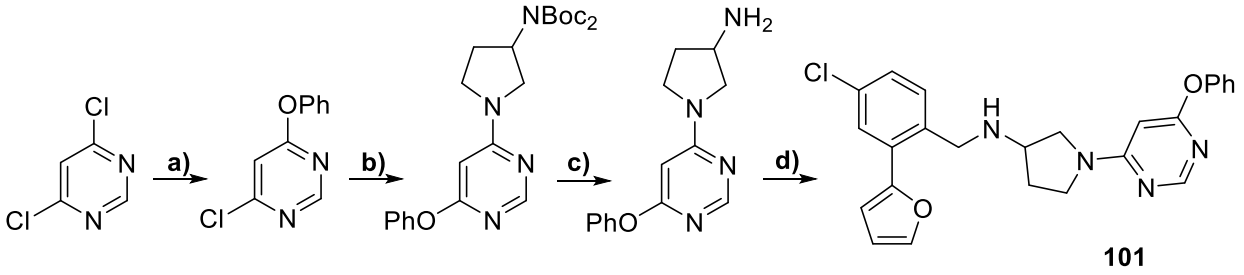

Scheme 31. Synthesis of compound **101**

Step a): 4-chloro-6-phenoxypyrimidine was synthesized from 4,6-dischloropyrimidine (150 mg, 1.00 mmol), phenol (99 mg, 1.06 mmol) and Cs_2CO_3 (326 mg, 1.00 mmol) using MeCN (2.0 mL) as a solvent and following **General procedure III.** The crude desired product (200 mg) was used in the next step without additional purification.

LC-MS**:** $[M+H]^+$ 207.10.

Step b): *tert*-butyl (tert-butoxycarbonyl)(1-(6-phenoxypyrimidin-4-yl)pyrrolidin-3-yl)carbamate was synthesized following the **General procedure III** was synthesized using crude 4-chloro-6-phenoxypyrimidine (100 mg, 0.48 mmol), *tert*-butyl (tert-butoxycarbonyl)(pyrrolidin-3-yl)carbamate (139 mg, 0.48 mmol) and DIPEA (125 mg, 0.97 mmol) as starting materials and anhydrous MeCN (1.0 mL) as solvent following **General procedure III**. The desired product was isolated by flash chromatography (Hex-Et_2O 0-90% Et_2O over 15 min, 18 mL/min, 12 g silica) as white solid (190 mg, 0.42 mmol, 85% yield over two steps).

LC-MS: $[M+H]^+$ 457.28

^{1}H NMR (500 MHz, $CDCl_3$) δ 8.31 (s, 1H), 7.40 (t, *J* = 7.9 Hz, 2H), 7.22 (t, *J* = 7.4 Hz, 1H), 7.12 (d, *J* = 7.7 Hz, 2H), 5.66 (s, 1H), 4.89 (p, *J* = 8.2 Hz, 1H), 3.58 (dd, *J* = 11.3, 6.2 Hz, 1H), 3.44 – 3.34 (m, 1H), 2.45 (s, 1H), 1.45 (s, 3H), 1.42 (s, 18H).

^{13}C NMR (126 MHz, $CDCl_3$) δ 169.80, 162.25, 158.23, 153.26, 153.01, 129.84, 125.35, 121.61, 86.42, 83.14, 54.67, 52.12, 43.76, 28.51, 28.13.

Step c): 1-(6-phenoxypyrimidin-4-yl)pyrrolidin-3-amine GPK-545 was synthesized from *tert*-butyl (tert-butoxycarbonyl)(1-(6-phenoxypyrimidin-4-yl)pyrrolidin-3-yl)carbamate (122 mg, 0.27 mmol), HCl (4M in dioxane, 250 µL) and using anhydrous DCM (2.0 mL) as solvent and following the **General procedure VII,** which afforded the desired product (33 mg, 0.1 mmol, 37% yield) as white solid after isolation using preparative HPLC.

LC-MS: $[M+H]^+$ 257.11

^{1}H NMR (500 MHz, DMSO-d6) δ 8.34 (s, 1H), 8.17 (s, 1H), 7.42 (t, *J* = 7.9 Hz, 2H), 7.23 (t, *J* = 7.4 Hz, 1H), 7.12 (d, *J* = 7.8 Hz, 2H), 5.88 (s, 1H), 3.73 (s, 1H), 3.69 – 3.24 (m, 4H), 2.15 (s, 1H), 1.90 (s, 1H).

^{13}C NMR (126 MHz, DMSO-d6) δ 168.85, 164.97, 161.86, 157.56, 152.94, 129.65, 124.94, 121.41, 86.34, 52.29, 44.32, 31.22.

Step d): 101 N-(4-chloro-2-(furan-2-yl)benzyl)-1-(6-phenoxypyrimidin-4-yl)pyrrolidin-3-aminewas synthesized using 4-chloro-2-(furan-2-yl)benzaldehyde (21 mg, 0.1 mmol), 1-(6-phenoxypyrimidin-4-yl)pyrrolidin-3-amine hydrochloride (33 mg, 0.1 mmol), DIPEA (26 mg, 0.2 mmol) and $NaBH(OAc)_3$ (32 mg, 0.15 mmol) as starting materials and following **General procedure IV.** The desired product was isolated using preparative HPLC (H_2O (+ 0.1 HCO_2H) - MeCN (+ 0.1 HCO_2H) 0-100% MeCN over 30 min) as a colorless solid (11 mg, 0.06 mmol, 60% yield).

LC-MS**:** $[M+H]^+$ 447.18.

^{1}H NMR (500 MHz, $CDCl_3$) δ 8.32 (s, *J* = 5.5 Hz, 1H), 7.60 (d, *J* = 2.2 Hz, 1H), 7.50 (d, *J* = 1.5 Hz, 1H), 7.42 – 7.35 (m, 3H), 7.26 – 7.20 (m, 2H), 7.13 (d, *J* = 7.7 Hz, 2H), 6.65 (d, *J* = 3.3 Hz, 1H), 6.47 (s, 1H), 5.66 (s, 1H), 3.94 (q, *J* = 13.1 Hz, 2H), 3.49 (s, 2H), 2.16 (td, *J* = 12.8, 6.8 Hz, 1H), 1.88 (s, 1H), 1.59 (s, 2H), 1.32 – 1.23 (m, 1H).

^{13}C NMR (126 MHz, $CDCl_3$) δ 169.76, 162.39, 158.25, 153.24, 152.04, 142.87, 134.92, 133.31, 131.76, 131.72, 129.83, 128.09, 127.93, 125.35, 121.59, 111.82, 109.60, 86.36, 52.36, 50.31, 31.81, 29.83.

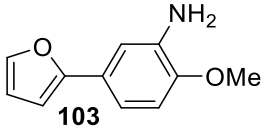

103

103 5-(furan-2-yl)-2-methoxyaniline was synthesized from 5-bromo-2-methoxyaniline (202 mg, 1.00 mmol), $Pd[PPh_3]_4$ (58 mg, 50 µmol), and 2-(Tri-n-butylstannyl)furan (536 mg, 1.50 mmol) following the **General procedure I** and isolated as a colorless solid (80.0 mg, 0.42 mmol, 42% yield).

LC-MS: $[M+H]^+$ 190.11.

^{1}H NMR (500 MHz, $CDCl_3$) δ 7.41 (d, *J* = 1.3 Hz, 1H), 7.09 – 7.03 (m, 2H), 6.80 (d, *J* = 8.1 Hz, 1H), 6.48 (d, *J* = 3.2 Hz, 1H), 6.43 (dd, *J* = 3.3, 1.8 Hz, 1H), 3.87 (s, 3H).

NMR data is in accordance with literature.[21]

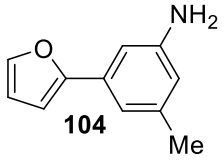

104

104 3-(furan-2-yl)-5-methylaniline was synthesized from 3-bromo-5-methylaniline (186 mg, 1.00 mmol), $Pd[PPh_3]_4$ (35 mg, 30 μmol), and 2-(Tri-n-butylstannyl)furan (536 mg, 1.5 mmol) following the **General procedure I** and isolated as a colorless solid (104 mg, 0.60 mmol, 60% yield).

LC-MS: $[M+H]^+$ 174.12.

^{1}H NMR (500 MHz, $CDCl_3$) δ 7.44 (dd, *J* = 1.7, 0.6 Hz, 1H), 6.93 (d, *J* = 0.5 Hz, 1H), 6.84 (d, *J* = 1.5 Hz, 1H), 6.59 (dd, *J* = 3.3, 0.6 Hz, 1H), 6.45 (dd, *J* = 3.4, 1.8 Hz, 1H), 6.44 (s, 1H), 3.65 (s, 2H), 2.30 (s, 3H).

^{13}C NMR (126 MHz, $CDCl_3$) δ 154.33, 146.71, 141.85, 139.61, 131.79, 115.41, 115.28, 111.63, 107.79, 104.94, 21.60.

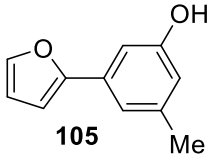

105

105 3-(furan-2-yl)-5-methylphenol was synthesized from 3-bromo-5-methylphenol (188 mg, 1.00 mmol), $Pd[PPh_3]_4$ (35 mg, 30 μmol), and 2-(Tri-n-butylstannyl)furan (464 mg, 1.30 mmol) following the **General procedure I** and isolated as a colorless crystals (146 mg, 0.84 mmol, 84% yield).

LC-MS: $[M+H]^+$ 175.09.

^{1}H NMR (500 MHz, Acetone-d6) δ 7.58 (s, 2H), 7.56 (d, *J* = 1.7 Hz, 1H), 6.75 (d, *J* = 3.4 Hz, 1H), 6.51 (dd, *J* = 3.4, 1.8 Hz, 1H), 5.31 (s, 2H), 2.83 (s, 1H).

NMR data is in accordance with literature.[22]

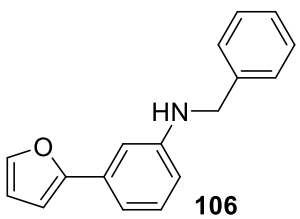

106

106 N-benzyl-3-(furan-2-yl)aniline was synthesized from **3** (56.0 mg , 0.35 mmol), benzaldehyde (35 mg, 0.32 mmol) and $NaBH(OAc)_3$ (81 mg, 0.38 mmol) using dichloroethane (1.0 mL) as solvent and following the **General procedure IV.** The desired product was isolated by flash chromatography (Hex:Et_2O 0-100% Et_2O over 15 min, 18 mL/min, 12 g silica) as colorless solid (38 mg, 0.15 mmol, 43% yield).

LC-MS: $[M+H]^+$ 250.02.

^1H NMR (500 MHz, $CDCl_3$) δ 7.44 (dd, *J* = 1.7, 0.6 Hz, 1H), 7.41 – 7.33 (m, 4H), 7.31 – 7.27 (m, 1H), 7.18 (t, *J* = 7.9 Hz, 1H), 7.05 – 7.03 (m, 1H), 7.00 – 6.98 (m, 1H), 6.58 (dd, *J* = 3.3, 0.6 Hz, 1H), 6.55 (ddd, *J* = 8.1, 2.4, 0.8 Hz, 1H), 6.45 (dd, *J* = 3.3, 1.8 Hz, 1H), 4.38 (s, 2H).

^{13}C NMR (126 MHz, $CDCl_3$) δ 154.49, 148.52, 141.94, 139.43, 131.92, 129.72, 128.82, 127.72, 127.45, 113.68, 112.21, 111.66, 108.23, 105.01, 48.49.

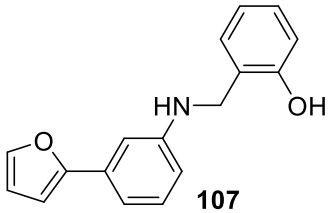

107

107 2-(((3-(furan-2-yl)phenyl)amino)methyl)phenol was synthesized from **3** (80 mg, 0.5 mmol), 2-hydroxybenzaldehyde (56 mg, 0.45 mmol) and $NaBH(OAc)_3$ (116 mg, 0.55 mmol) using dichloroethane (2.0 mL) as solvent and following the **General procedure IV.** The desired product was isolated by flash chromatography (Hex:Et_2O 0-100% Et_2O over 15 min, 18 mL/min, 12 g silica) as colorless solid (78 mg, 0.29 mmol, 59% yield).

LC-MS: $[M+H]^+$ 264.20

^1H NMR (500 MHz, $CDCl_3$) δ 7.44 (dd, *J* = 1.7, 0.5 Hz, 1H), 7.26 – 7.20 (m, 4H), 7.20 – 7.15 (m, *J* = 7.1, 1.3 Hz, 2H), 6.91 – 6.87 (m, *J* = 8.5, 5.6, 1.9 Hz, 2H), 6.74 (ddd, *J* = 7.5, 2.3, 1.6 Hz, 1H), 6.60 (dd, *J* = 3.3, 0.5 Hz, 1H), 6.45 (dd, *J* = 3.4, 1.8 Hz, 1H), 4.45 (s, 2H).

^{13}C NMR (126 MHz, $CDCl_3$) δ 156.80, 153.89, 147.66, 142.26, 132.07, 129.85, 129.46, 128.95, 122.99, 120.28, 116.81, 116.64, 115.01, 111.78, 111.21, 105.45, 48.74.

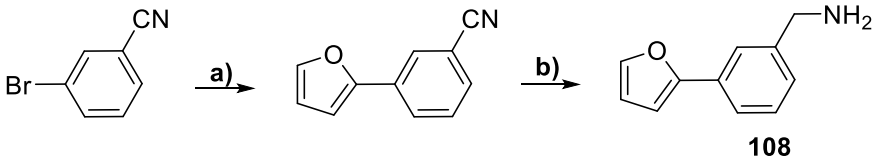

108

Scheme 32. Synthesis of compound **108**

Step a): 3-(furan-2-yl)benzonitrile was synthesized from 3-bromobenzonitrile (546 mg, 3.00 mmol), $Pd[PPh_3]_4$ (170 mg, 150 μmol), and 2-(Tri-n-butylstannyl)furan (1.29 g, 3.60 mmol) following the **General procedure I** and isolated as yellowish crystals (335 mg, 1.98 mmol, 66% yield).

^{1}H NMR (500 MHz, DMSO-d6) δ 8.17 (t, *J* = 1.5 Hz, 1H), 8.04 – 7.98 (m, 1H), 7.83 (d, *J* = 1.3 Hz, 1H), 7.76 – 7.71 (m, 1H), 7.63 (t, *J* = 7.8 Hz, 1H), 7.18 (d, *J* = 3.4 Hz, 1H), 6.65 (dd, *J* = 3.4, 1.8 Hz, 1H).

NMR data is in accordance with literature.[23]

Step b): 108 (3-(furan-2-yl)phenyl)methanamine. To the stirred solution of 3-(furan-2-yl)benzonitrile (85 mg, 0.5 mmol) and anhydrous $NiCl_2$ (65 mg, 0.5 mmol) in anhydrous EtOH (1.0 mL) was added $NaBH_4$ (57 mg, 1.5 mmol) in portions, after which the reaction mixture was stirred at room temperature for 15 minutes. The reaction was quenched by adding water (5 mL) and its pH was adjusted to 8 by adding 1M NaOH, after which it was extracted with EtOAc (3x10 mL), the combined organic fractions were washed with brine, dried over anhydrous Na_2SO_4 and concentrated *in vacuo* to give the desired product as off-white solid (27 mg, 0.15 mmol, 30% yield).

LC-MS: $[M\text{-}NH_2]^{\cdot+}$ 157.10

^{1}H NMR (500 MHz, MeOD) δ 7.69 (s, 1H), 7.58 (d, *J* = 7.8 Hz, 1H), 7.54 (d, *J* = 1.4 Hz, 1H), 7.35 (t, *J* = 7.7 Hz, 1H), 7.24 (d, *J* = 7.6 Hz, 1H), 6.77 (d, *J* = 3.3 Hz, 1H), 6.51 (dd, *J* = 3.4, 1.8 Hz, 1H), 3.83 (s, 2H).

^{13}C NMR (126 MHz, DMSO-d6) δ 153.22, 142.73, 142.50, 137.0, 130.25, 128.22, 122.50, 119.87, 112.03, 105.65, 45.59.

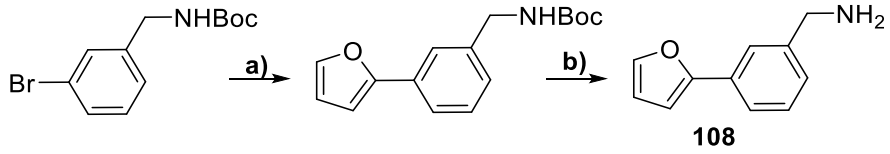

Scheme 33. Alternative synthesis of compound **108**

Step a): *tert*-butyl (3-(furan-2-yl)benzyl)carbamate was synthesized from ***tert*-butyl (3-bromobenzyl)carbamate** (430 mg, 1.50 mmol), $Pd[PPh_3]_4$ (86 mg, 74 μmol), and 2-(Tri-n-butylstannyl)furan (589 mg, 1.60 mmol) following the **General procedure I** and isolated as a white solid (423 mg, 1.50 mmol, 98% yield).

Step b): (3-(furan-2-yl)phenyl)methanamine was synthesized from the Boc-protected 3-(2-furyl)-benzylamine (406 mg, 1.49 mmol), HCl (4M in dioxane, 1.85 mL), using anhydrous DCM (5.0 mL) as solvent and following **General procedure VII**. The deprotected amine was isolated in the form of hydrochloride as white solid (252 mg, 1.49 mmol, 98% yield).

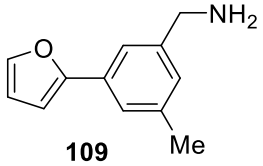

109 (3-(furan-2-yl)-5-methylphenyl)methanamine was synthesized from (3-bromo-5-methylphenyl)methanamine hydrochloride (126 mg, 0.53 mmol), $Pd[PPh_3]_4$ (30 mg, 27 μmol),

TEA (54 mg, 0.53 mmol) and 2-(Tri-n-butylstannyl)furan (285 mg, 0.80 mmol) following the **General procedure I** and isolated as brownish solid (335 mg, 1.98 mmol, 66% yield).

LC-MS: $[M+H]^{\cdot+}$181.11

^{1}H NMR (500 MHz, $CDCl_3$) δ 7.47 – 7.44 (m, 2H), 7.39 (s, 1H), 7.05 (s, 1H), 6.65 (dd, *J* = 3.3, 0.5 Hz, 1H), 6.46 (dd, *J* = 3.3, 1.8 Hz, 1H), 3.88 (s, 2H), 2.37 (s, 3H).

^{13}C NMR (126 MHz, DMSO-d6) δ 153.22, 142.73, 141.97, 137.93, 130.25, 127.44, 122.50, 119.87, 112.03, 105.65, 44.59, 21.02.

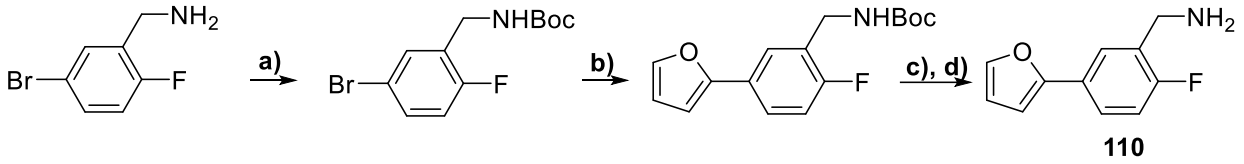

Scheme 34. Synthesis of compound **110**

Step a): *tert*-butyl (5-bromo-2-fluorobenzyl)carbamate. (5-bromo-2-fluorophenyl)methylammonium hydrochloride (361 mg, 1.50 mmol) and triethylamine (304 mg, 3.00 mmol) were dissolved in DCM (8.0 mL) and to the resulting solution Boc_2O (328 mg, 1.50 mmol) was added in a portionwise manner. The resulting solution was stirred at room temperature for 8 hours, evaporated to dryness and subjected to flash chromatography (Hex:DCM 0-100% DCM over 18 min, 18 mL/min, 12 g silica) which afforded the protected product as white solid (433 mg, 1.43 mmol, 95% yield).

LC-MS: $[M+H]^+$ 304.17, 306.16

^{1}H NMR (500 MHz, $CDCl_3$) δ 7.45 (dd, *J* = 6.6, 2.4 Hz, 1H), 7.35 (ddd, *J* = 8.5, 4.5, 2.5 Hz, 1H), 6.92 (t, *J* = 9.1 Hz, 1H), 4.33 (d, *J* = 5.7 Hz, 2H), 1.45 (s, 9H).

^{19}F NMR (470 MHz, DMSO-d6) δ -120.77 – -120.89 (m).

^{13}C NMR (126 MHz, $CDCl_3$) δ 159.99 (d, *J* = 246.5 Hz), 155.85, 132.49 (d, *J* = 4.4 Hz), 131.98 (d, *J* = 8.2 Hz), 128.42 (d, *J* = 16.9 Hz), 117.24 (d, *J* = 23.0 Hz), 116.85 (d, *J* = 2.9 Hz), 80.09, 38.36, 28.50.

Step b): *tert*-butyl (2-fluoro-5-(furan-2-yl)benzyl)carbamate was synthesized from *tert*-butyl (5-bromo-2-fluorobenzyl)carbamate (324 mg, 1.11 mmol), $Pd[PPh_3]_4$ (64 mg, 55 μmol), and 2-(Tri-n-butylstannyl)furan (476 mg, 1.33 mmol) following **General procedure I** to obtain the title compound as white solid (238 mg, 0.82 mmol, 74% yield).

^{1}H NMR (500 MHz, $CDCl_3$) δ 7.62 (dd, *J* = 7.1, 2.2 Hz, 1H), 7.55 (ddd, *J* = 8.4, 4.9, 2.3 Hz, 1H), 7.45 (d, *J* = 1.2 Hz, 1H), 7.05 (dd, *J* = 9.6, 8.7 Hz, 1H), 6.58 (d, *J* = 3.2 Hz, 1H), 6.46 (dd, *J* = 3.3, 1.8 Hz, 1H), 4.92 (s, 1H), 4.43 – 4.30 (m, *J* = 4.9 Hz, 2H), 1.46 (s, *J* = 6.8 Hz, 9H).

Step c): (2-fluoro-5-(furan-2-yl)phenyl)methanaminium chloride was synthesized from tert-butyl (2-fluoro-5-(furan-2-yl)benzyl)carbamate (238 mg, 0.82 mmol), $HCl_{(diox)}$(5.0 ml, 5.0 mmol), using DCM (10.0 mL) as solvent and following **General Procedure VII**. The desired

compound was obtained in the form of a hydrochloric salt as white crystals (185 mg, 0.82 mmol, 99% yield).

LC-MS: $[M\text{-}NH_2]^{\cdot+}$ 175.08.

^{1}H NMR (500 MHz, DMSO-d6) δ 8.08 (br.s, 2H), 7.94 (dd, *J* = 7.1, 2.2 Hz, 1H), 7.79 (d, *J* = 1.3 Hz, 1H), 7.75 (ddd, *J* = 8.5, 4.9, 2.3 Hz, 1H), 7.37 – 7.31 (m, 1H), 6.93 (d, *J* = 3.3 Hz, 1H), 6.62 (dd, *J* = 3.4, 1.8 Hz, 1H), 4.08 (s, 2H).

^{19}F NMR (470 MHz, DMSO-d6) δ -118.62 – -118.73 (m).

^{13}C NMR (126 MHz, DMSO-d6) δ 159.37 (d, *J* = 247.5 Hz), 151.89, 143.18, 127.04 (d, *J* = 3.4 Hz), 126.22 (d, *J* = 3.4 Hz), 125.45 (d, *J* = 8.4 Hz), 122.66 (d, *J* = 15.7 Hz), 116.09 (d, *J* = 22.3 Hz), 112.22, 106.09, 35.85 (d, *J* = 4.1 Hz).

Step d): 110 (2-fluoro-5-(furan-2-yl)phenyl)methanamine was obtained from the corresponding hydrochloride salt (see above) by treatment with 2M NaOH solution and extraction with EtOAc.

LC-MS: $[M+H]^+$ 192.19

^{1}H NMR (500 MHz, $CDCl_3$) δ 7.65 (dd, *J* = 7.1, 2.2 Hz, 1H), 7.53 (ddd, *J* = 8.4, 4.9, 2.3 Hz, 1H), 7.45 (dd, *J* = 1.7, 0.6 Hz, 1H), 7.05 (dd, *J* = 9.7, 8.6 Hz, 1H), 6.60 (d, *J* = 3.3 Hz, 1H), 6.46 (dd, *J* = 3.4, 1.8 Hz, 1H), 3.94 (s, 2H), 0.92 (t, *J* = 7.3 Hz, 4H).

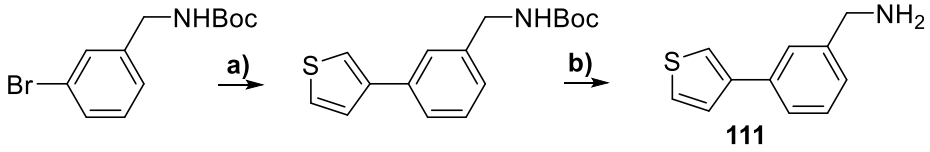

111

Scheme 35. Synthesis of compound **111**

Step a): *tert*-butyl (3-(thiophen-3-yl)benzyl)carbamate was synthesized from *tert*-butyl (3-bromobenzyl)carbamate (105 mg, 0.37 mmol), $Pd[PPh_3]_4$ (8.5 mg, 7 μmol), (3-thienyl)-boronic acid (70 mg, 0.55 mmol) and KF (87 mg, 1.1 mmol) using dioxane (2.0 mL) as solvent and following **General procedure II**. The desired compound was isolated by flash chromatography (Hex:DCM 0-100% DCM over 15 min, 18 mL/min, 12 g silica) and obtained as off-white solid (100 mg, 0.34 mmol, 93% yield).

LC-MS: $[M+H\text{-}tBu]^+$ 233.94, $[M\text{-}(NHCO\mathit{tBu})]^+$ 173.03

^{1}H NMR (500 MHz, Acetone-d6) δ 7.71 (dd, *J* = 2.9, 1.3 Hz, 1H), 7.65 (s, 1H), 7.60 – 7.55 (m, 2H), 7.51 (dd, *J* = 5.0, 1.2 Hz, 1H), 7.36 (t, *J* = 7.6 Hz, 1H), 7.24 (d, *J* = 7.6 Hz, 1H), 6.54 (s, 1H), 4.32 (d, *J* = 6.3 Hz, 2H), 1.43 (s, *J* = 15.7 Hz, 9H).

^{13}C NMR (126 MHz, Acetone-d6) δ 156.90, 143.07, 141.93, 136.68, 129.77, 127.45, 127.03, 126.88, 126.09, 125.63, 121.28, 78.84, 44.79, 28.67.

111 (3-(thiophen-3-yl)phenyl)methanamine was synthesized by deprotection of ***tert*-butyl (3-(thiophen-3-yl)benzyl)carbamate** (100 mg, 0.34 mmol) with HCl_{diox} (300 μL) using

DCM (3.0 mL) as solvent and following **General procedure VII**, which afforded the desired amine in the form of a hydrochloride after a recrystallization from ethanol (48 mg, 0.21 mmol, 62% yield).

LC-MS: $[M\text{-}NH_2]^+$ 172.99

^{1}H NMR (500 MHz, DMSO-d6) δ 8.23 (s, 3H), 7.88 (d, *J* = 12.4 Hz, 2H), 7.74 (d, *J* = 7.4 Hz, 1H), 7.69 (s, 1H), 7.57 (d, *J* = 4.6 Hz, 1H), 7.46 (t, *J* = 7.6 Hz, 1H), 7.37 (d, *J* = 7.4 Hz, 1H), 4.08 (s, 2H).

^{13}C NMR (126 MHz, DMSO-d6) δ 172.67, 140.97, 135.44, 134.77, 129.27, 127.48, 126.64, 126.07, 121.37, 54.26.

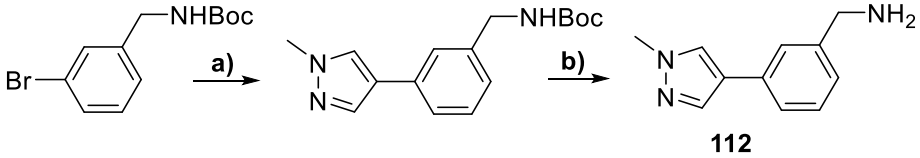

112

Scheme 36. Synthesis of compound **112**

Step a): *Tert*-butyl (3-(1-methyl-1H-pyrazol-4-yl)benzyl)carbamate was synthesized from *tert*-butyl (3-bromobenzyl)carbamate (143 mg, 0.50 mmol), $Pd[PPh_3]_4$ (20 mg, 17 μmol), (1-methyl-1H-pyrazol-4-yl)boronic acid pinacol ester (125 mg, 0.60 mmol) and K_2CO_3 (207 mg, 1.50 mmol) following the **General procedure II** to isolate the title compound by flash chromatography (DCM:EA 0-100% EA over 14min, 18 mL/min, 12 g silica) as white solid (115 mg, 0.40 mmol, 80% yield).

LC-MS: $[M+H]^+$ 288.09

^{1}H NMR (500 MHz, $CDCl_3$) δ 7.75 (s, 1H), 7.61 (s, 1H), 7.39 – 7.35 (m, 2H), 7.32 (t, *J* = 7.8 Hz, 1H), 7.14 (d, *J* = 7.3 Hz, 1H), 4.33 (d, *J* = 5.5 Hz, 2H), 3.95 (s, 3H), 1.47 (s, 9H).

^{13}C NMR (126 MHz, $CDCl_3$) δ 156.07, 139.64, 136.93, 133.13, 129.30, 127.15, 125.64, 124.81, 124.66, 123.12, 44.85, 39.26, 28.56.

Step b): 112 (3-(1-methyl-1H-pyrazol-4-yl)phenyl)methanamine was synthesized by deprotection of *tert*-butyl (3-(1-methyl-1H-pyrazol-4-yl)benzyl)carbamate (56 mg, 0.19 mmol) with HCl_{diox} (150 μL) using DCM (1.0 mL) as solvent and following **General procedure VII**, which afforded the desired amine in the form of a dihydrochloride - slightly beige solid (47 mg, 0.19 mmol, 99% yield).

LC-MS: $[M+H]^+$ 188.01, $[M\text{-}NH_2]^+$ 170.96

^{1}H NMR (500 MHz, DMSO-d6) δ 8.38 (s, 2H), 8.13 (s, 1H), 7.86 (d, *J* = 0.4 Hz, 1H), 7.74 (s, 1H), 7.56 (d, *J* = 7.8 Hz, 1H), 7.39 (t, *J* = 7.7 Hz, 1H), 7.28 (d, *J* = 7.7 Hz, 1H), 4.02 (q, *J* = 5.8 Hz, 2H), 3.87 (s, 3H).

^{13}C NMR (126 MHz, DMSO-d6) δ 136.04, 134.64, 132.94, 129.18, 127.90, 126.27, 125.42, 124.87, 121.49, 42.28, 24.99.

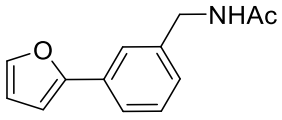

113

113 *N*-(3-(furan-2-yl)benzyl)acetamidewas synthesized by acylation of (3-(furan-2-yl)phenyl)methanamine hydrochloride (41 mg, 0.19 mmol) using Ac_2O (22 mg, 0.22 mmol), DIPEA (76 mg, 0.59 mmol) and THF (2.0 mL) as solvent. The reaction mixture was stirred for 2 hours at room temperature, quenched by adding saturated $NaHCO_3$ solution. The resulting mixture was extracted with EtOAc, the combined organic fractions were dried over anhydrous Na_2SO_4 and evaporated *in vacuo* to give the desired product (41 mg, 0.19 mmol, 100% yield) as white solid.

^{1}H NMR (500 MHz, $CDCl_3$) δ 7.36 – 7.27 (m, 5H), 6.71 (d, *J* = 8.1 Hz, 1H), 3.68 (s, 2H), 2.22 (s, 3H).

^{13}C NMR (126 MHz, $CDCl_3$) δ 170.09, 153.64, 142.37, 138.77, 131.45, 129.27, 126.97, 123.31, 123.16, 111.85, 105.53, 43.89, 23.48.

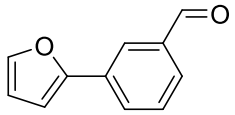

I10

3-(furan-2-yl)benzaldehyde was synthesized from 3-bromobenzaldehyde (555 mg, 3.0 mmol), $Pd[PPh_3]_4$ (31 mg, 27 μmol) and 2-(Tri-n-butylstannyl)furan (1.28 g, 3.60 mmol) following the **General procedure I** and isolated as brownish solid (320 mg, 1.85 mmol, 62% yield).

^{1}H NMR (500 MHz, $CDCl_3$) δ 10.06 (s, 1H), 8.17 (t, *J* = 1.6 Hz, 1H), 7.95 – 7.91 (m, 1H), 7.77 (dt, *J* = 7.6, 1.3 Hz, 1H), 7.56 (t, *J* = 7.7 Hz, 1H), 7.52 (d, *J* = 1.6 Hz, 1H), 6.77 (d, *J* = 3.4 Hz, 1H), 6.52 (dd, *J* = 3.4, 1.8 Hz, 1H).

^{13}C NMR (126 MHz, DMSO-d6) δ 193.06, 151.78, 143.66, 136.78, 131.12, 129.85, 129.01, 128.08, 124.13, 112.32, 107.21.

NMR data is in accordance with literature.[24]

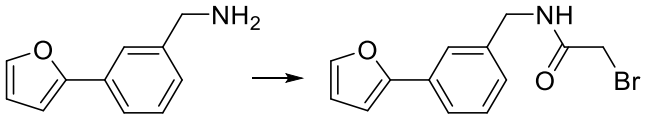

108 **I9**

Scheme 37. Synthesis of compound **I9**

I9 2-bromo-N-(3-(furan-2-yl)benzyl)acetamide. To the stirred solution containing (3-(furan-2-yl)phenyl)methanamine hydrochloride (206 mg, 0.99 mmol), DIPEA (254.6 mg, 1.97 mmol) and catalytic amount of DMAP in dry DCM (10.0 mL) was added dropwise 2-bromoacetyl chloride (170 mg, 1.08 mmol) at 0°C. The reaction mixture was kept at 0°C for 20 minutes, after which it was stirred at room temperature for 1.5 hours. The reaction mixture was

diluted with ice-cold water (120 mL), extracted with DCM (3x40 mL), the combined organic fractions were washed with brine, dried over anhydrous Na_2SO_4 and concentrated *in vacuo* to afford the desired product as yellowish solid (161 mg, 0.55 mmol, 56% yield).

^{1}H NMR (500 MHz, $CDCl_3$) δ 7.63 – 7.59 (m, 2H), 7.48 (s, 1H), 7.37 (t, *J* = 7.5 Hz, 1H), 7.19 (d, *J* = 7.4 Hz, 1H), 6.90 (s, 1H), 6.68 (d, *J* = 3.3 Hz, 1H), 6.50 – 6.47 (m, 1H), 4.53 (d, *J* = 5.8 Hz, 2H), 4.13 (s, 2H).

^{13}C NMR (126 MHz, $CDCl_3$) δ 166.02, 153.53, 142.44, 137.85, 131.55, 129.39, 126.84, 123.39, 123.28, 111.87, 105.63, 43.96, 42.77.

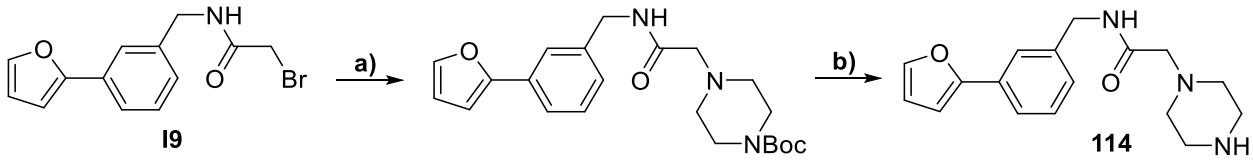

I9 **114**

Scheme 38. Synthesis of compound **114**

Step a): *tert*-butyl 4-(2-((3-(furan-2-yl)benzyl)amino)-2-oxoethyl)piperazine-1-carboxylate. To the stirred solution of N-Boc-piperazine (45 mg, 0.2 mmol), DIPEA (52 mg, 0.4 mmol) and catalytic amount of KI in MeCN (1.0 mL) at 70°C was added the solution of 2-bromo-N-(3-(furan-2-yl)benzyl)acetamide (59 mg, 0.2 mmol) in MeCN (1.0 mL), after which the resulting reaction mixture was stirred at 70°C for 8 hours. The reaction mixture was evaporated to dryness and the resulting residue was subjected to flash chromatography (DCM:MeOH 0-5% MeOH over 15 min, 18 mL/min, 12 g silica) to afford the desired product as white solid (79 mg, 0.2 mmol, 99% yield)

LC-MS: $[M+H]^+$ 400.24

^{1}H NMR (500 MHz, Acetone-d6) δ 8.03 (s, 1H), 7.68 – 7.54 (m, 3H), 7.36 (t, *J* = 7.7 Hz, 1H), 7.22 (d, *J* = 7.6 Hz, 1H), 6.84 (d, *J* = 3.3 Hz, 1H), 6.55 (dd, *J* = 3.3, 1.8 Hz, 1H), 4.46 (d, *J* = 6.3 Hz, 2H), 3.41 (s, 4H), 3.04 (s, 2H), 2.48 (d, *J* = 4.5 Hz, 4H), 1.42 (s, 9H).

^{13}C NMR (126 MHz, Acetone-d6) δ 170.09, 155.01, 154.62, 143.38, 141.62, 131.86, 129.78, 127.39, 123.41, 123.05, 112.73, 106.26, 79.62, 62.50, 54.05, 42.93, 28.54.

Step b): 114 *tert*-butyl 4-(2-((3-(furan-2-yl)benzyl)amino)-2-oxoethyl)piperazine-1-carboxylate was synthesized by deprotection of *tert*-butyl 4-(2-((3-(furan-2-yl)benzyl)amino)-2-oxoethyl)piperazine-1-carboxylate (79 mg, 0.19 mmol) with HCl_{diox} (250 μL) using DCM (2.0 mL) as solvent and following **General procedure VII**, which afforded the desired amine in the form of a dihydrochloride - slightly purple solid after a recrystallization from ethanol (61 mg, 0.16 mmol, 85% yield).

LC-MS: $[M+H]^+$ 300.2

^{1}H NMR (500 MHz, DMSO-d6) δ 9.25 – 9.19 (m, 1H), 7.83 (d, *J* = 1.4 Hz, 1H), 7.71 – 7.64 (m, 2H), 7.46 (q, *J* = 7.5 Hz, 1H), 7.28 (t, *J* = 6.3 Hz, 1H), 7.03 – 7.00 (m, 1H), 6.69 – 6.67

(m, 1H), 4.46 (dd, *J* = 15.2, 5.9 Hz, 2H), 3.76 (dtd, *J* = 7.5, 5.7, 1.2 Hz, 1H), 3.38 – 3.10 (m, 8H).

^{13}C NMR (126 MHz, DMSO-d6) δ 143.48, 130.92, 130.83, 129.54, 129.46, 127.01, 126.89, 122.71, 112.59, 106.47, 80.37, 66.82, 51.86, 49.43, 28.40.

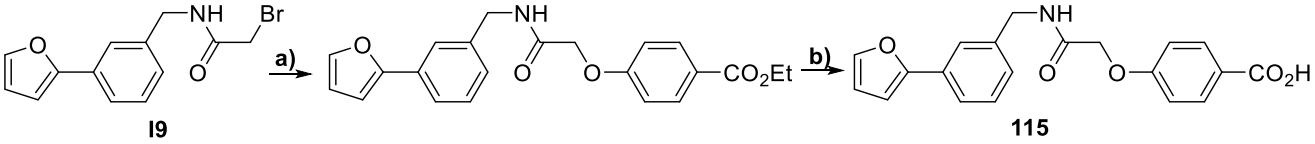

I9 **115**

Scheme 39. Synthesis of compound **115**

Step a): Ethyl 4-(2-((3-(furan-2-yl)benzyl)amino)-2-oxoethoxy)benzoate. The solution containing 2-bromo-N-(3-(furan-2-yl)benzyl)acetamide (29 mg, 0.1 mmol), 4-hydroxybenzoic acid (17 mg, 0.1 mmol), K_2CO_3 (21 mg, 0.15 mmol) and catalytic amount of NaI in MeCN (2.0 mL) was heated up to 70^{o}C and stirred at this temperature overnight. The reaction mixture was concentrated *in vacuo* and subjected to flash chromatography (Hex:EA 0-100% EA over 16 min, 14 mL/min, 4 g silica), which afforded the product as white solid (35 mg, 0.1 mmol, 99% yield).

LC-MS: $[M+H]^+$ 380.02

^{1}H NMR (500 MHz, $CDCl_3$) δ 7.98 – 7.93 (m, 2H), 7.56 – 7.50 (m, 2H), 7.42 – 7.39 (m, 1H), 7.29 (t, *J* = 7.5 Hz, 1H), 7.11 (d, *J* = 7.4 Hz, 1H), 6.90 – 6.86 (m, 2H), 6.58 (d, *J* = 3.4 Hz, 1H), 6.40 (dd, *J* = 3.3, 1.8 Hz, 1H), 4.56 (s, 2H), 4.52 (d, *J* = 6.0 Hz, 2H), 4.28 (q, *J* = 7.1 Hz, 2H), 1.31 (t, *J* = 7.1 Hz, 3H).

Step b): 115 4-(2-((3-(furan-2-yl)benzyl)amino)-2-oxoethoxy)benzoic acid was obtained by saponification of ethyl 4-(2-((3-(furan-2-yl)benzyl)amino)-2-oxoethoxy)benzoate (37.4 mg, 0.1 mmol) with 2 M LiOH (1.0 mL) and using THF (2.5 mL) as solvent. Colorless solid (30 mg, 0.085 mmol, 85% yield).

LC-MS: $[M+H]^+$ 352.15

^{1}H NMR (500 MHz, $CDCl_3$) δ 7.98 – 7.93 (m, 2H), 7.56 – 7.50 (m, 2H), 7.42 – 7.39 (m, 1H), 7.29 (t, *J* = 7.5 Hz, 1H), 7.11 (d, *J* = 7.4 Hz, 1H), 6.90 – 6.86 (m, 2H), 6.58 (d, *J* = 3.4 Hz, 1H), 6.40 (dd, *J* = 3.3, 1.8 Hz, 1H), 4.56 (s, 2H), 4.52 (d, *J* = 6.0 Hz, 2H).

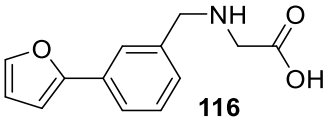

116

116 (3-(furan-2-yl)benzyl)glycine. To the solution containing glycine (34 mg, 0.4 mmol) in MeOH (340 μL) and 2M NaOH (240 μL) was added the solution of 3-(furan-2-yl)benzaldehyde (86 mg, 0.5 mmol) in MeOH (390 μL) and the resulting mixture was stirred at room temperature for 30 minutes. To the reaction mixture was added $NaBH_4$ (58 mg, 1.5 mmol) in two portions with a 2-minutes interval upon cooling in an ice bath, after which the reaction

mixture was stirred at room temperature for 2 hours. The volatiles were distilled off *in vacuo*, pH of the aqueous phase was adjusted to 5 and it was extracted with Et_2O (2x20 mL). The combined ethereal fractions were concentrated *in vacuo*, the residue was recrystallized from water to give the title product as white fluffy solid (90 mg, 0.39 mmol, 86% yield).

LC-MS: $[M+H]^+$ 232.16

^{1}H NMR (500 MHz, DMSO-d6) δ 7.79 (s, 1H), 7.77 (d, *J* = 1.2 Hz, 1H), 7.67 (d, *J* = 7.8 Hz, 1H), 7.43 (t, *J* = 7.7 Hz, 1H), 7.33 (d, *J* = 7.6 Hz, 1H), 6.94 (d, *J* = 3.3 Hz, 1H), 6.61 (dd, *J* = 3.4, 1.8 Hz, 1H), 3.99 (s, 2H), 3.14 (s, 2H).

^{13}C NMR (126 MHz, DMSO-d6) δ 168.53, 152.71, 143.17, 134.84, 130.53, 129.15, 128.50, 124.49, 123.33, 112.20, 106.25, 50.13, 49.02.

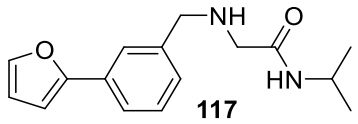

117

117 2-((3-(furan-2-yl)benzyl)amino)-N-isopropylacetamide. To the stirred solution (3-(furan-2-yl)benzyl)glycine (23 mg, 0.1 mmol), DIPEA (26 mg, 0.2 mmol) and HATU (46 mg, 0.12 mmol) in anhydrous DCM (1.0 mL) was added isopropylamine (6.5 mg, 0.11 mmol). The reaction mixture was stirred for 8 hours, after which it was evaporated *in vacuo* and subjected to flash chromatography (DCM:MeOH 0-10% MeOH over 12 min, 14 mL/min, 4 g silica), which afforded the product as colorless crystals) (22 mg, 0.08 mmol, 81% yield).

LC-MS: $[M+H]^+$ 273.21

^{1}H NMR (500 MHz, $CDCl_3$) δ 7.64 (s, 1H), 7.61 (d, *J* = 7.9 Hz, 1H), 7.47 (dd, *J* = 1.7, 0.6 Hz, 1H), 7.37 (t, *J* = 7.7 Hz, 1H), 7.21 (d, *J* = 7.7 Hz, 1H), 6.89 (d, *J* = 7.6 Hz, 1H), 6.68 (dd, *J* = 3.4, 0.6 Hz, 1H), 6.48 (dd, *J* = 3.4, 1.8 Hz, 1H), 4.08 – 4.02 (m, 1H), 3.89 (s, 2H), 3.41 (s, 2H).

^{13}C NMR (126 MHz, $CDCl_3$) δ 153.61, 142.42, 131.55, 129.33, 128.16, 127.47, 123.86, 123.46, 111.91, 105.61, 55.94, 51.51, 41.31, 38.76.

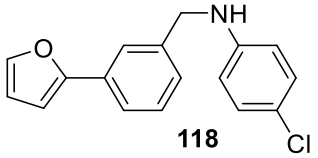

118

118 4-chloro-N-(3-(furan-2-yl)benzyl)aniline was synthesized from 3-(furan-2-yl)benzaldehyde (50 mg, 0.3 mmol), 4-chloroaniline (41 mg, 0.3 mmol) and $NaBH(OAc)_3$ (74 mg, 0.3 mmol) using anhydrous dichloroethane (1.0 mL) as solvent and following **General procedure IV** to isolate the desired product by flash chromatography (Hex:EA 0-100% EA over 14 min, 19 mL/min, 12 g silica) as colorless solid (40 mg, 0.14 mmol, 48% yield).

LC-MS: $[M+H]^+$ 284.13, 286.16

^{1}H NMR (500 MHz, $CDCl_3$) δ 7.67 (s, 1H), 7.59 (d, *J* = 7.8 Hz, 1H), 7.49 – 7.44 (m, 1H), 7.36 (t, *J* = 7.7 Hz, 1H), 7.24 (d, *J* = 7.6 Hz, 1H), 7.13 – 7.09 (m, 2H), 6.66 (dd, *J* = 3.4, 0.5 Hz, 1H), 6.59 – 6.54 (m, 2H), 6.47 (dd, *J* = 3.4, 1.8 Hz, 1H), 4.33 (s, 2H).

^{13}C NMR (126 MHz, $CDCl_3$) δ 153.83, 146.72, 142.32, 139.60, 131.43, 129.22, 126.46, 123.01, 122.86, 122.33, 114.10, 111.83, 105.44, 48.51.

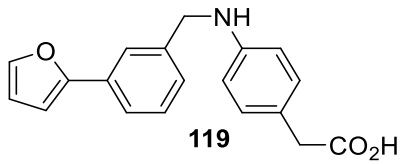

119

119 2-(4-((3-(furan-2-yl)benzyl)amino)phenyl)acetic acid was synthesized from 3-(furan-2-yl)benzaldehyde (75 mg, 0.50 mmol), 4'-aminophenylacetic acid (95 mg, 0.55 mmol) and $NaBH(OAc)_3$ (318 mg, 1.5 mmol) using anhydrous dichloroethane (5.0 mL) as solvent and following **General procedure IV** to isolate the desired product by flash chromatography (Hex:EA 0-100% EA over 14 min, 19 mL/min, 12 g silica) as colorless solid (95 mg, 0.3 mmol, 59% yield).

LC-MS: $[M+H]^+$ 308.02

^{1}H NMR (500 MHz, $CDCl_3$) δ 7.68 (s, 1H), 7.58 (d, *J* = 7.8 Hz, 1H), 7.48 – 7.46 (m, 1H), 7.35 (t, *J* = 7.7 Hz, 1H), 7.08 (t, *J* = 5.6 Hz, 2H), 6.65 (d, *J* = 3.3 Hz, 1H), 6.64 – 6.59 (m, 2H), 6.47 (dd, *J* = 3.4, 1.8 Hz, 1H), 4.34 (s, 2H), 3.53 (s, 2H).

^{13}C NMR (126 MHz, $CDCl_3$) δ 175.96, 153.91, 147.48, 142.28, 139.98, 131.37, 130.35, 129.18, 126.56, 122.95, 122.92, 122.34, 113.19, 111.81, 105.38, 48.53, 39.98.

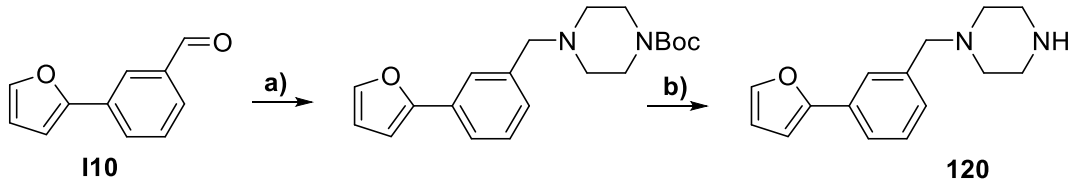

I10 **120**

Scheme 40. Synthesis of compound **120**

Step a): *tert*-butyl 4-(3-(furan-2-yl)benzyl)piperazine-1-carboxylate was synthesized from 3-(furan-2-yl)benzaldehyde (100 mg, 0.58 mmol), *N*-Boc-piperidine (113 mg, 0.61 mmol) and $NaBH(OAc)_3$ (164 mg, 0.77 mmol) using anhydrous DCM (4.0 mL) as solvent and following the **General procedure IV** to isolate the desired product by flash chromatography (Hex:EA 0-100% EA over 20 min, 19 mL/min, 12 g silica) as white solid (110 mg, 0.32 mmol, 55% yield).

LC-MS: $[M+H]^+$ 343.22

^{1}H NMR (500 MHz, Acetone-d6) δ 7.71 (s, 1H), 7.64 – 7.59 (m, 2H), 7.37 (t, *J* = 7.7 Hz, 1H), 7.27 (d, *J* = 7.6 Hz, 1H), 6.85 (d, *J* = 3.0 Hz, 1H), 6.55 (dd, *J* = 3.4, 1.8 Hz, 1H), 3.55 (s, 2H), 3.40 (s, 4H), 2.42 – 2.36 (m, 4H), 1.43 (s, 9H).

^{13}C NMR (126 MHz, Acetone-d6) δ 154.13, 153.81, 142.40, 139.14, 130.89, 128.67, 128.02, 124.05, 122.37, 111.76, 105.29, 78.58, 62.43, 54.08, 52.80, 27.65.

Step b): 120 1-(3-(furan-2-yl)benzyl)piperazine was synthesized by deprotection of tert-butyl 4-(3-(furan-2-yl)benzyl)piperazine-1-carboxylate (110 mg, 0.32 mmol) with HCl_{diox} (200 µL) using DCM (3.0 mL) as solvent and following **General procedure VII**, which afforded the desired amine in the form of a dihydrochloride (98 mg, 0.31 mmol, 99% yield).

LC-MS: $[M+H]^+$ 243.02

^{1}H NMR (500 MHz, DMSO-d6) δ 8.36 (s, 1H), 7.75 (d, *J* = 1.3 Hz, 1H), 7.63 (s, 1H), 7.59 (d, *J* = 7.8 Hz, 1H), 7.37 (t, *J* = 7.7 Hz, 1H), 7.22 (d, *J* = 7.6 Hz, 1H), 6.94 (d, *J* = 3.3 Hz, 1H), 6.59 (dd, *J* = 3.3, 1.8 Hz, 1H), 3.52 (s, 2H), 2.91 (d, *J* = 4.3 Hz, 4H), 2.47 (s, 4H).

^{13}C NMR (126 MHz, DMSO-d6) δ 165.41, 152.98, 142.91, 138.40, 130.31, 128.83, 128.09, 123.81, 122.30, 112.08, 105.91, 61.93, 50.95, 43.57.

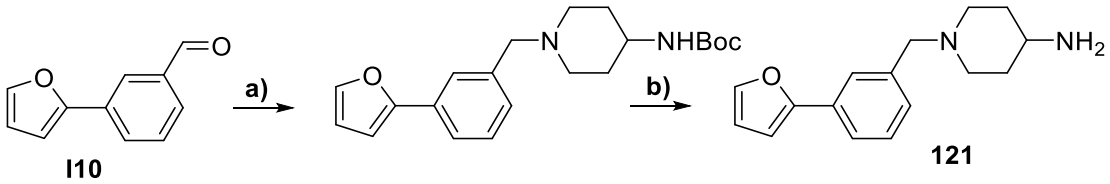

Scheme 41. Synthesis of compound **121**

Step a): tert-butyl (1-(3-(furan-2-yl)benzyl)piperidin-4-yl)carbamate was synthesized from 3-(furan-2-yl)benzaldehyde (105 mg, 0.61 mmol), *tert*-butyl piperidin-4-ylcarbamate (128 mg, 0.64 mmol) and $NaBH(OAc)_3$ (172 mg, 0.81 mmol) using anhydrous DCM (5.0 mL) as solvent and following the **General procedure IV** to isolate the desired product by flash chromatography (DCM:MeOH 0-10% MeOH over 25 min, 24 mL/min, 12 g silica) as white solid (128 mg, 0.36 mmol, 59% yield).

LC-MS: $[M+H]^+$ 357.20

^{1}H NMR (500 MHz, Acetone-d6) δ 7.69 (s, 1H), 7.62 (d, *J* = 1.1 Hz, 1H), 7.59 (d, *J* = 7.8 Hz, 1H), 7.35 (t, *J* = 7.7 Hz, 1H), 7.25 (d, *J* = 7.6 Hz, 1H), 6.85 – 6.81 (m, 1H), 6.54 (dd, *J* = 3.3, 1.8 Hz, 1H), 5.85 (d, *J* = 5.2 Hz, 1H), 3.51 (s, 2H), 3.37 (s, 1H), 2.84 (d, *J* = 11.7 Hz, 2H), 2.11 – 2.06 (m, 2H), 1.82 (d, *J* = 11.7 Hz, 2H), 1.51 (qd, *J* = 12.0, 3.7 Hz, 2H), 1.38 (s, 9H).

^{13}C NMR (126 MHz, Acetone-d6) δ 155.99, 154.86, 143.33, 140.87, 131.80, 129.58, 128.87, 124.89, 123.20, 112.72, 106.18, 78.46, 63.49, 53.41, 48.94, 33.29, 28.72.

Step b): 121 1-(3-(furan-2-yl)benzyl)piperidin-4-amine was synthesized by deprotection of *tert*-butyl (1-(3-(furan-2-yl)benzyl)piperidin-4-yl)carbamate (100 mg, 0.28 mmol) with HCl_{diox} (200 µL) using DCM (3.0 mL) as solvent and following **General procedure VII**, which afforded the desired amine in the form of a dihydrochloride (92 mg, 0.28 mmol, quant. yield).

LC-MS: $[M+H]^+$ 257.08

^{1}H NMR (500 MHz, DMSO-d6) δ 7.75 (d, *J* = 1.5 Hz, 1H), 7.63 (s, 1H), 7.60 (d, *J* = 7.8 Hz, 1H), 7.37 (t, *J* = 7.7 Hz, 1H), 7.22 (d, *J* = 7.6 Hz, 1H), 6.94 (d, *J* = 3.3 Hz, 1H), 6.59 (dd, *J* = 3.3, 1.8 Hz, 1H), 3.54 (s, 2H), 2.98 (ddd, *J* = 15.2, 11.1, 3.9 Hz, 1H), 2.86 (d, *J* = 11.9 Hz, 2H), 2.06 (dd, *J* = 13.9, 8.5 Hz, 2H), 1.89 (d, *J* = 10.6 Hz, 2H), 1.58 (qd, *J* = 12.1, 3.6 Hz, 2H).

^{13}C NMR (126 MHz, DMSO-d6) δ 152.98, 142.94, 138.51, 130.32, 128.86, 128.07, 123.77, 122.37, 112.09, 105.93, 61.37, 50.81, 47.59, 29.46.

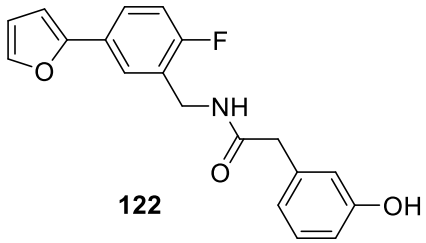

122

122 *N*-(2-fluoro-5-(furan-2-yl)benzyl)-2-(3-hydroxyphenyl)acetamide. To the stirred solution of 2-(3-hydroxyphenyl)acetic acid (27 mg, 0.17 mmol), 7-aza-HOBt (24 mg, 0.17 mmol) and TEA (67 mg, 0.67 mmol) in anhydrous DMF (1.5 mL) was added EDC·HCl (34 mg, 0.18 mmol). The resulting solution was stirred for 15 min, after which (2-fluoro-5-(furan-2-yl)phenyl)methanamine hydrochloride (40 mg, 0.17 mmol) was added to it. The reaction mixture was stirred for 8 hours at room temperature, then diluted with water (20 mL), extracted with EtOAc (3x20 mL), the combined organic fractions were washed with water, brine, dried over anhydrous Na_2SO_4 and concentrated *in vacuo*. The desired product was isolated using flash chromatography (Hex:EA 0-10% EA over 18 min, 18mL/min, 12 g silica) as white solid (50 mg, 0.15 mmol, 90% yield).

LC-MS: $[M+H]^+$ 326.05

^{1}H NMR (500 MHz, $CDCl_3$) δ 7.54 – 7.48 (m, 2H), 7.44 (d, *J* = 1.2 Hz, 1H), 7.20 (td, *J* = 7.5, 1.1 Hz, 1H), 7.04 – 6.99 (m, 1H), 6.54 (d, *J* = 3.2 Hz, 1H), 6.45 (dd, *J* = 3.4, 1.8 Hz, 1H), 5.89 (s, 1H), 4.48 (d, *J* = 6.0 Hz, 2H), 3.56 (s, *J* = 11.9 Hz, 2H).

^{19}F NMR (470 MHz, $CDCl_3$) δ -120.37 – -120.45 (m).

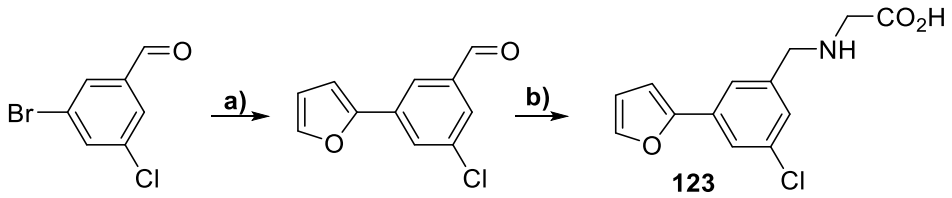

123

Scheme 42. Synthesis of compound **124**

3-chloro-5-(furan-2-yl)benzaldehyde was synthesized from 3-bromo-5-chlorobenzaldehyde (439 mg 2.00 mmol), $Pd[PPh_3]_4$ (115 mg, 0.1 mmol) and 2-(Tri-n-butylstannyl)furan (857 mg, 1.76 mmol) following the **General procedure I** and isolated as shiny white solid (364 mg, 1.85 mmol, 88% yield).

^{1}H NMR (500 MHz, DMSO-d6) δ 10.03 (s, 1H), 8.17 (t, *J* = 1.4 Hz, 1H), 8.09 (t, *J* = 1.8 Hz, 1H), 7.86 (d, *J* = 1.7 Hz, 1H), 7.84 – 7.82 (m, 1H), 7.27 (d, *J* = 3.4 Hz, 1H), 6.68 (dd, *J* = 3.4, 1.8 Hz, 1H).

^{13}C NMR (126 MHz, DMSO-d6) δ 191.99, 150.44, 144.37, 138.44, 134.81, 132.98, 128.10, 127.24, 122.52, 112.57, 108.74.

123 (3-chloro-5-(furan-2-yl)benzyl)glycine

LC-MS: $[M+H]^{+}$ 265.96, 268.01

^{1}H NMR (500 MHz, DMSO-d6) δ 7.86 – 7.82 (m, 1H), 7.82 – 7.78 (m, 1H), 7.77 – 7.70 (m, 1H), 7.51 (d, *J* = 9.7 Hz, 1H), 7.09 (dd, *J* = 12.6, 3.3 Hz, 1H), 6.87 (s, 1H), 6.66 – 6.63 (m, 1H), 3.64 – 3.57 (m, 2H).

^{13}C NMR (126 MHz, DMSO-d6) δ 171.06, 151.23, 143.88, 143.77, 136.46, 133.77, 132.28, 128.12, 123.31, 112.38, 107.82, 45.21, 43.10.

S4.1.2 STD-NMR experiments

Primary fragment hit screen (Fr1-Fr7)

1. Mixture of Fr1, Fr2, Fr3 and Fr5. The composition of the first mixture of fragments was chosen on the basis of minimal overlapping of their proton signals in ^{1}H NMR spectra. The concentration of every fragment used was set to 50 μM.

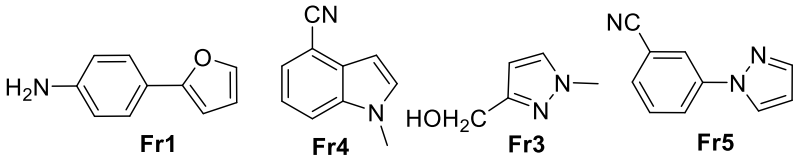

Figure S1. Structures of fragments **Fr1**, **Fr2**, **Fr3** and **Fr5**.

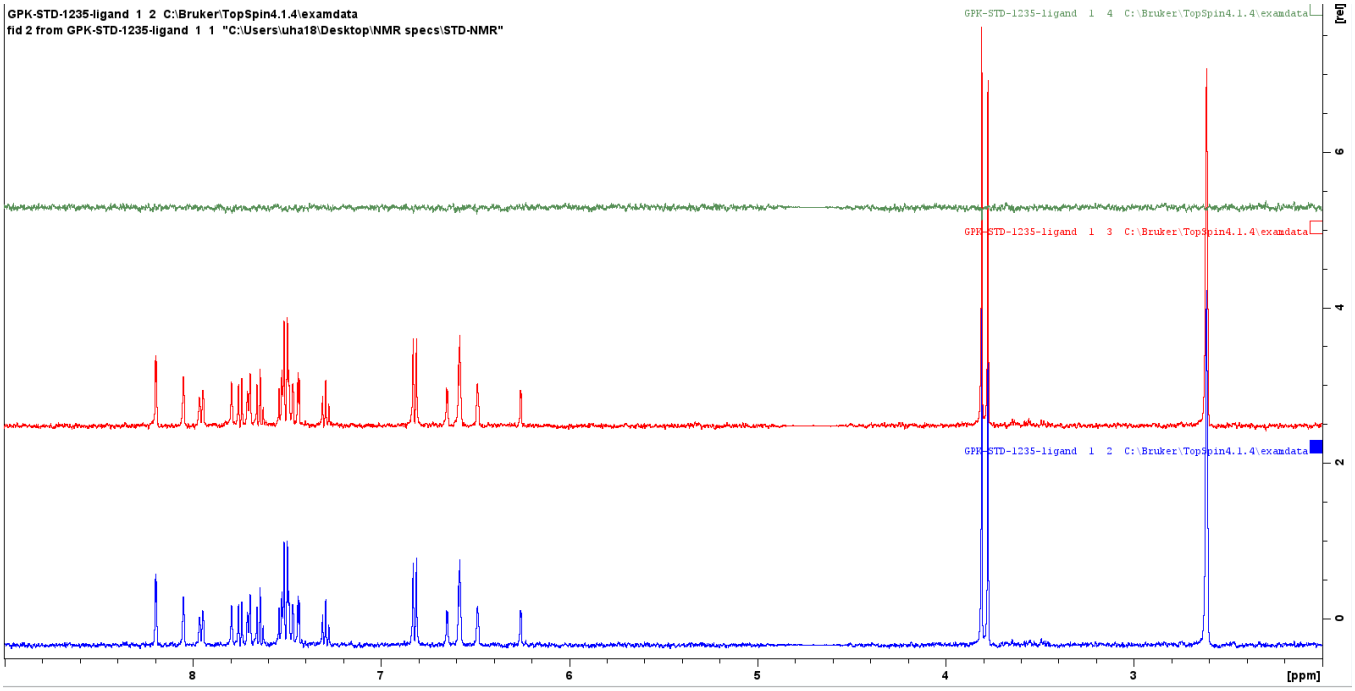

Figure S2. Overlay of the on-resonance (blue), off-resonance (red) and the difference spectrum (green) of the mixture containing **Fr1**, **Fr2**, **Fr3** and **Fr5** in the absence of DnaN.

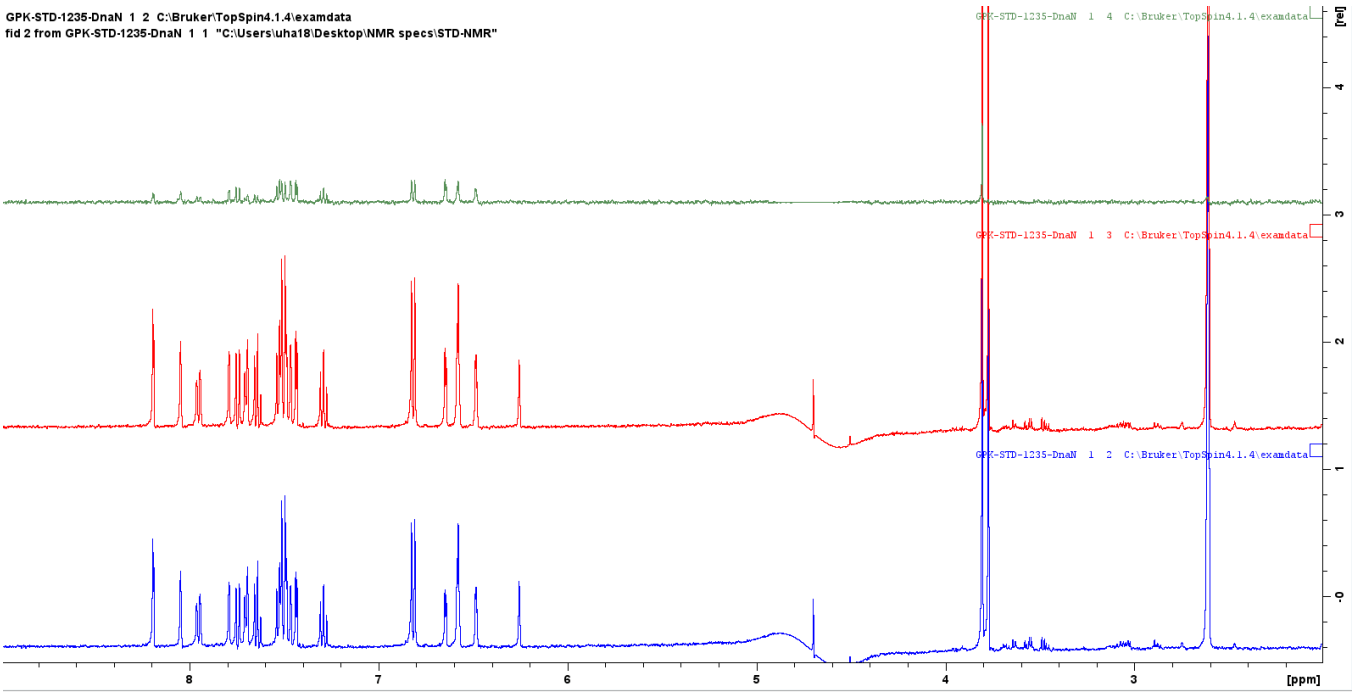

Figure S3. Overlay of the on-resonance (**blue**), off-resonance (**red**) and the difference spectrum (**green**) of the mixture of **Fr1**, **Fr2**, **Fr3** and **Fr5** in the presence of DnaN.

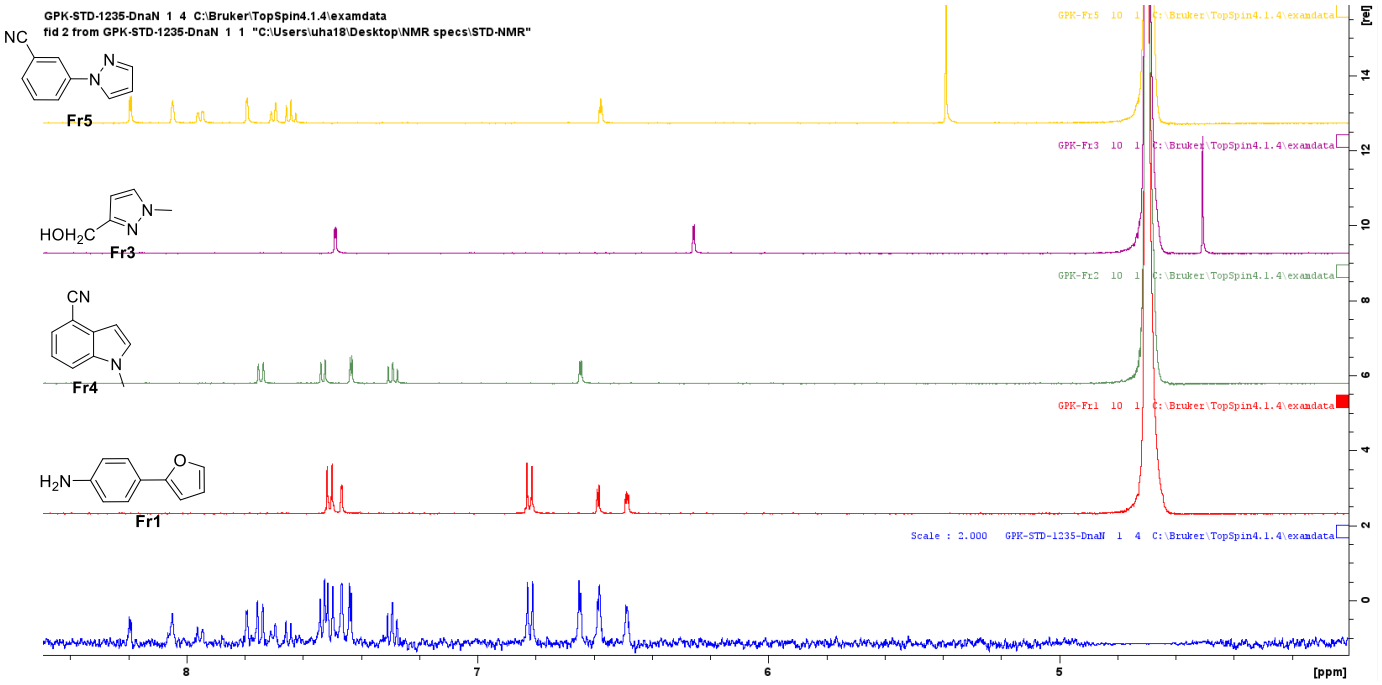

Figure S4. Overlay of the difference spectrum depicted on **Figure S3** (blue) and individual spectra of **Fr1** (**red**), **Fr2** (**green**), **Fr3** (**magenta**) and **Fr5** (**yellow**) acquired in the same buffer.

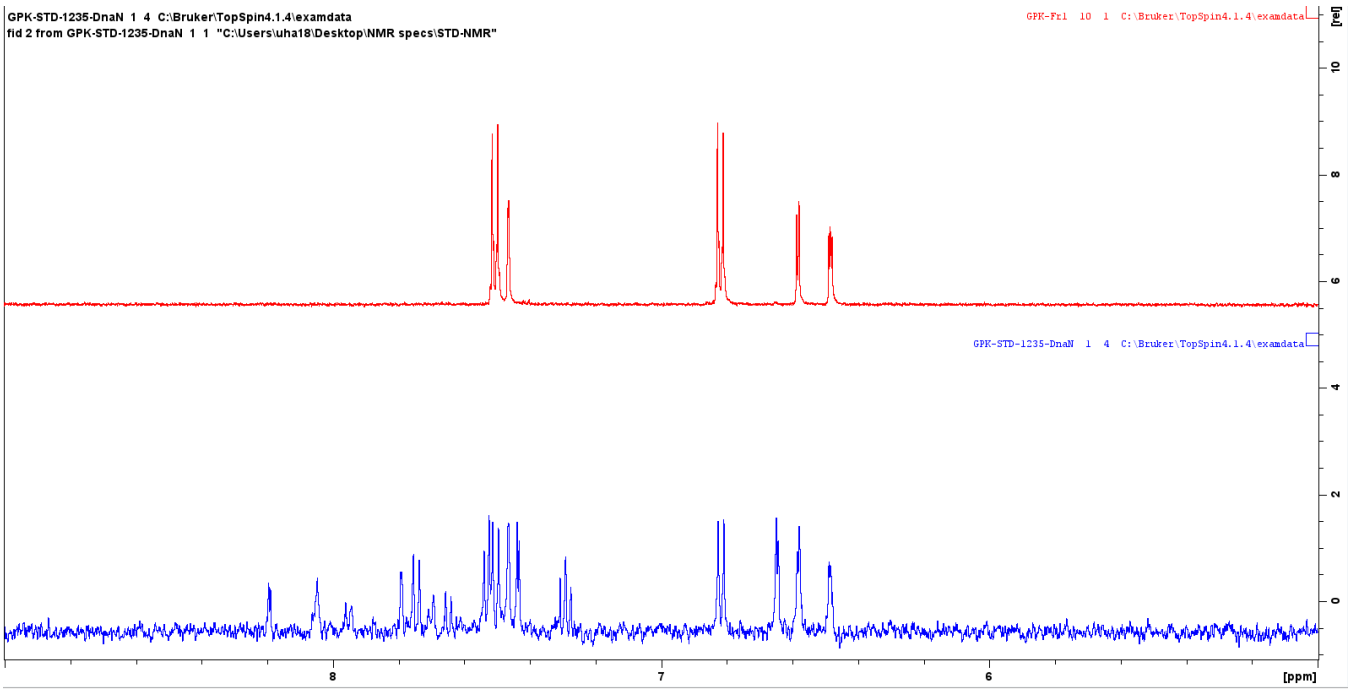

Figure S5. Overlay of the difference spectrum (**blue**) and individual spectrum of **Fr1** (**red**)

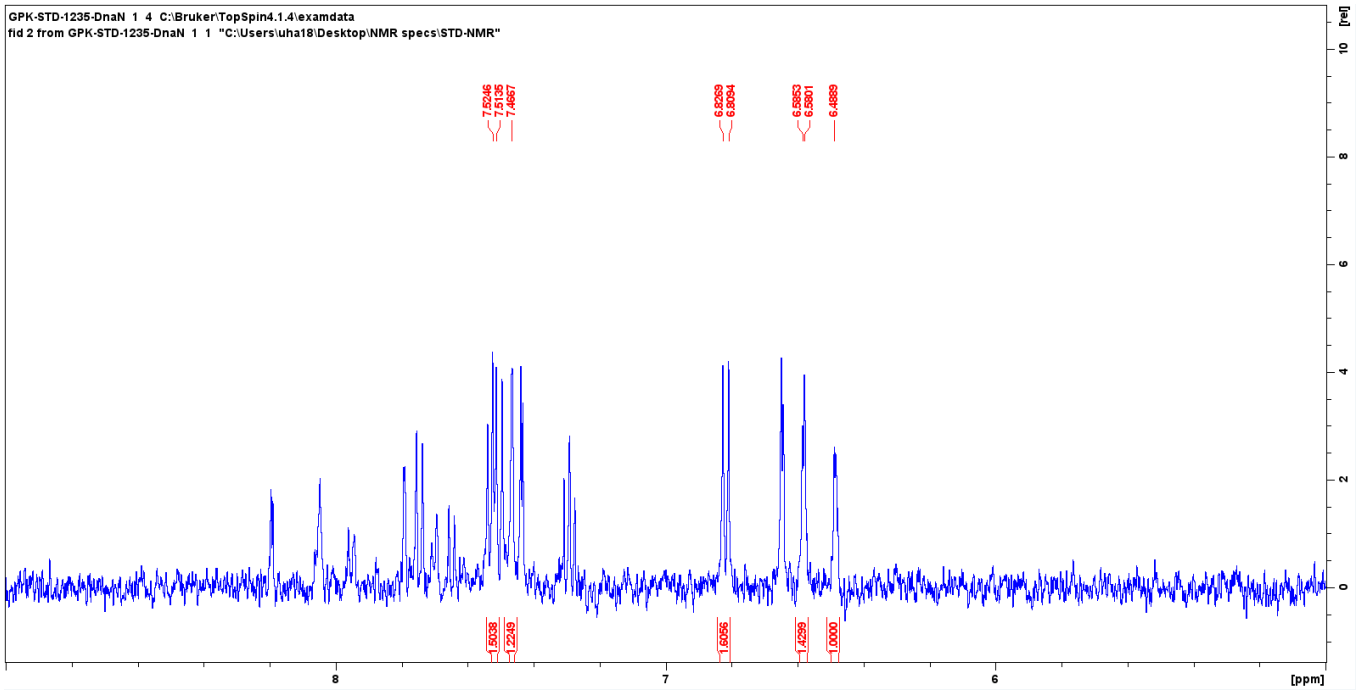

Figure S6. Peak-picked and integrated signals in the difference spectrum belonging to **Fr1**

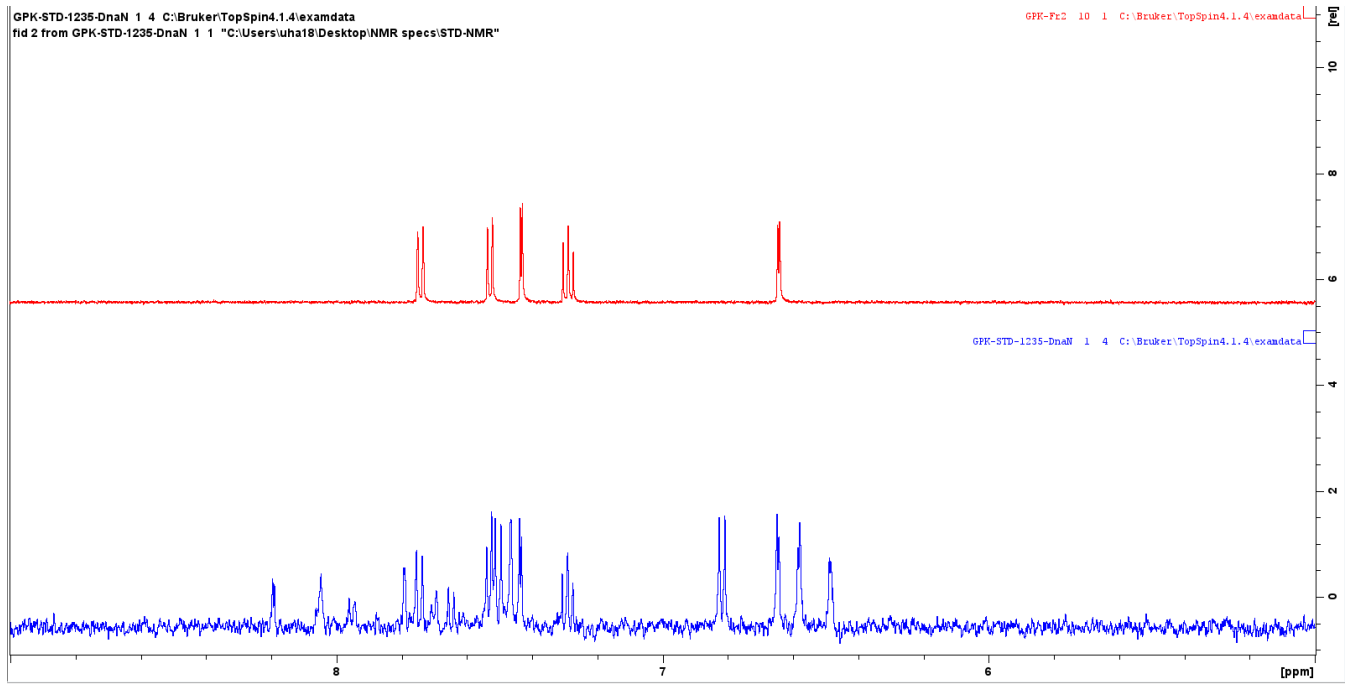

Figure S7. Overlay of the difference spectrum (**blue**) and individual spectrum of **Fr4** (**red**)

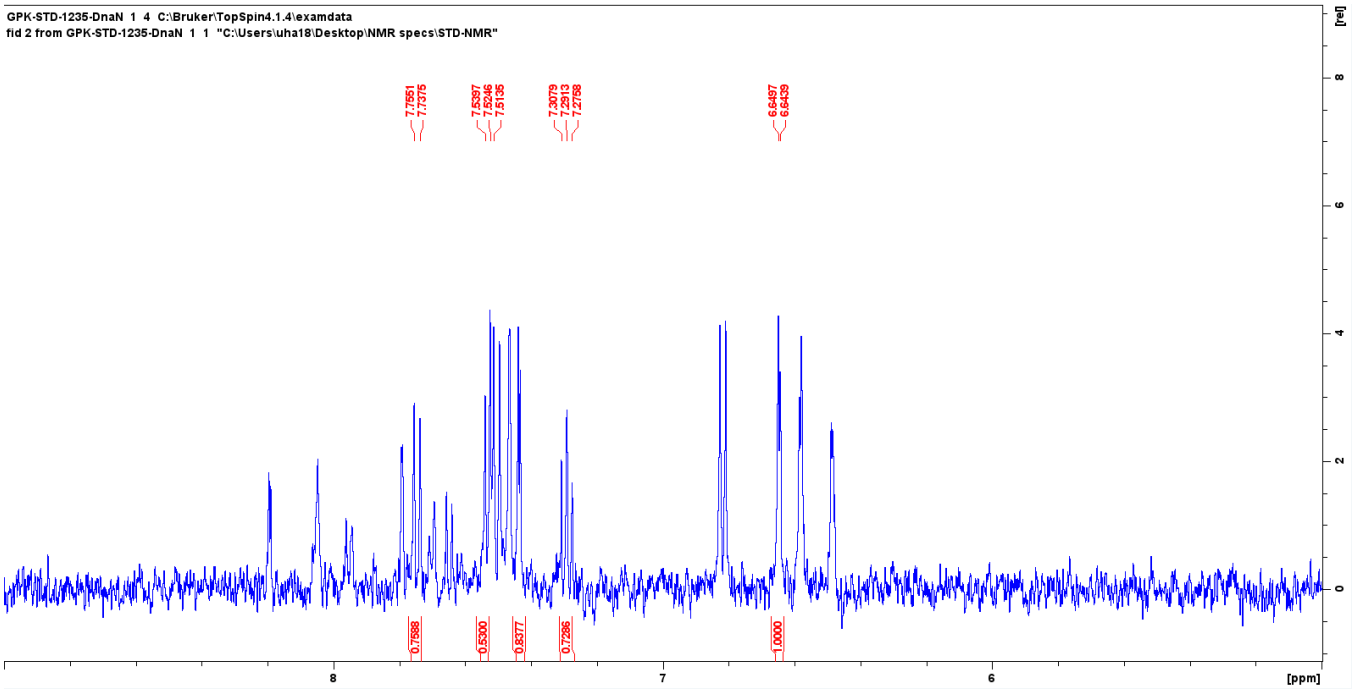

Figure S8. Peak-picked and integrated signals in the difference spectrum belonging to **Fr4**

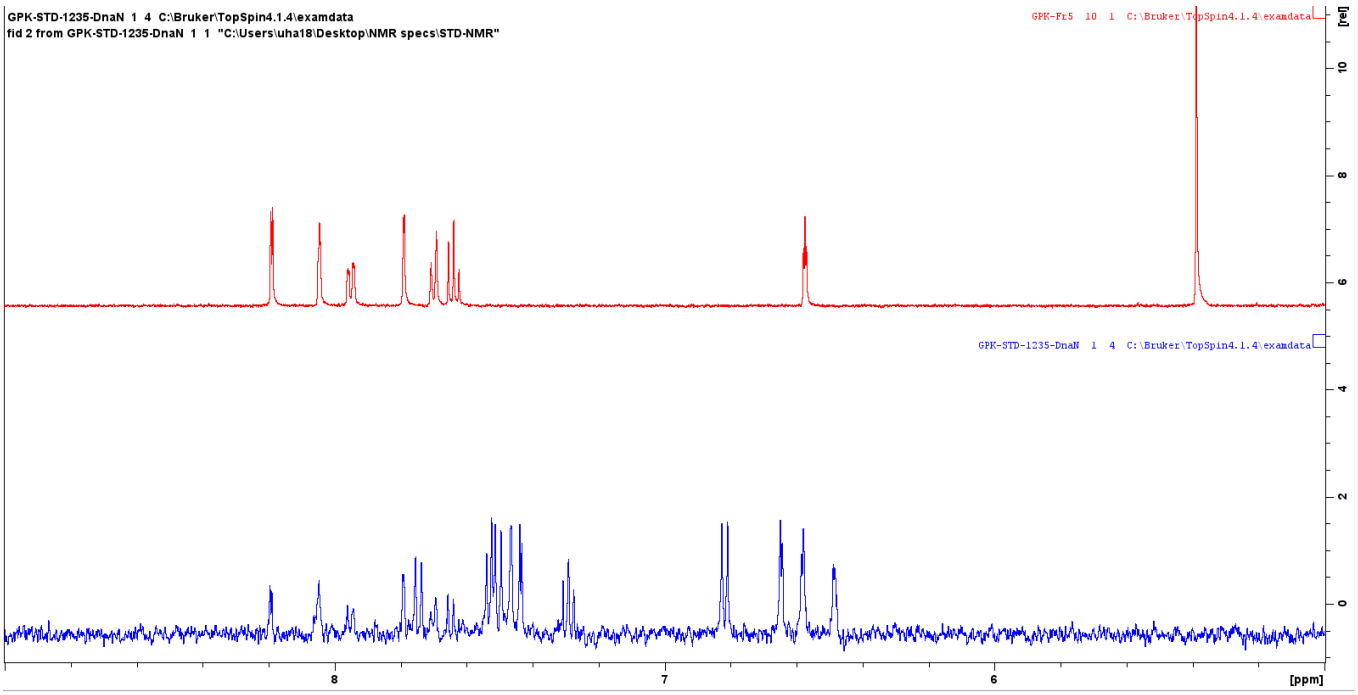

Figure S9. Overlay of the difference spectrum (blue) and an individual spectrum of **Fr5** (red)

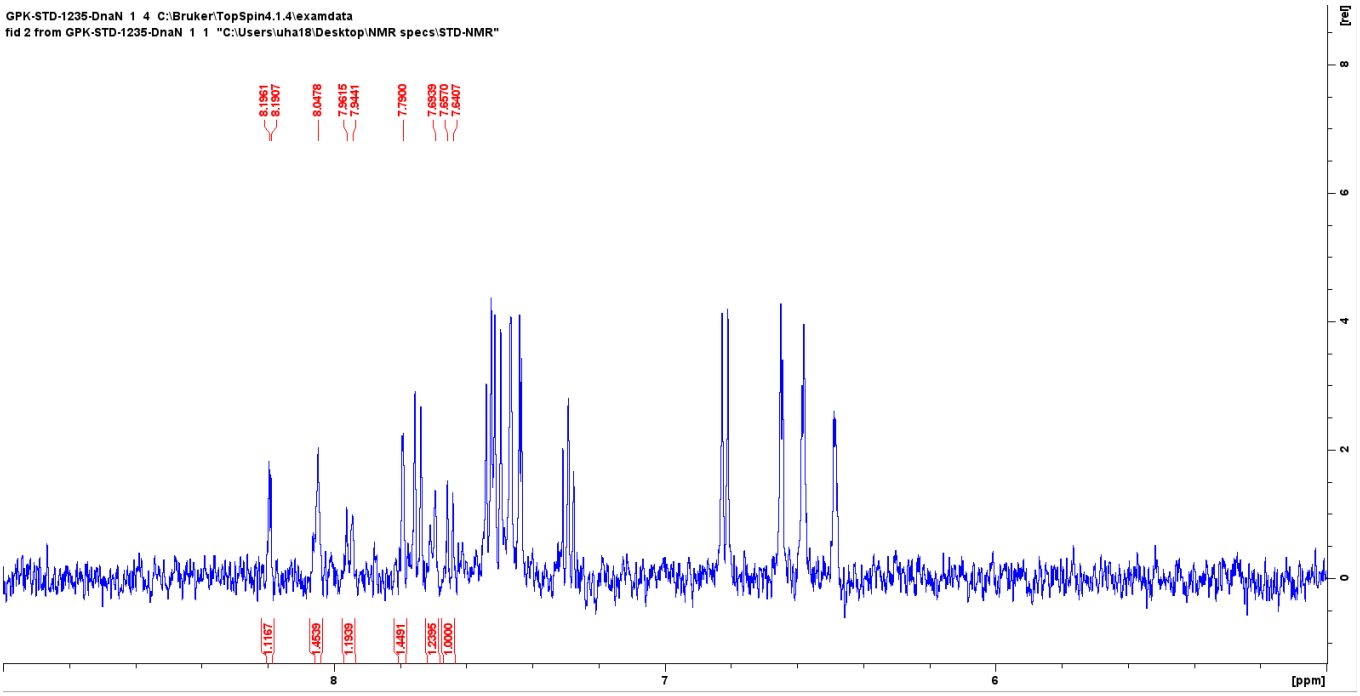

Figure S10. Peak-picked and integrated signals in the difference spectrum belonging to **Fr5**

2. **Mixture of Fr4, Fr6 and Fr7.** The second mixture of fragments consisted of the molecules **Fr4**, **Fr6** and **Fr7**. The concentration of every molecule used was 50 μM.

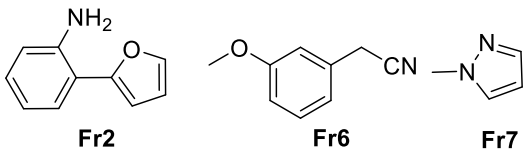

Figure S11. Structures of fragments **Fr4**, **Fr6**, and **Fr7**.

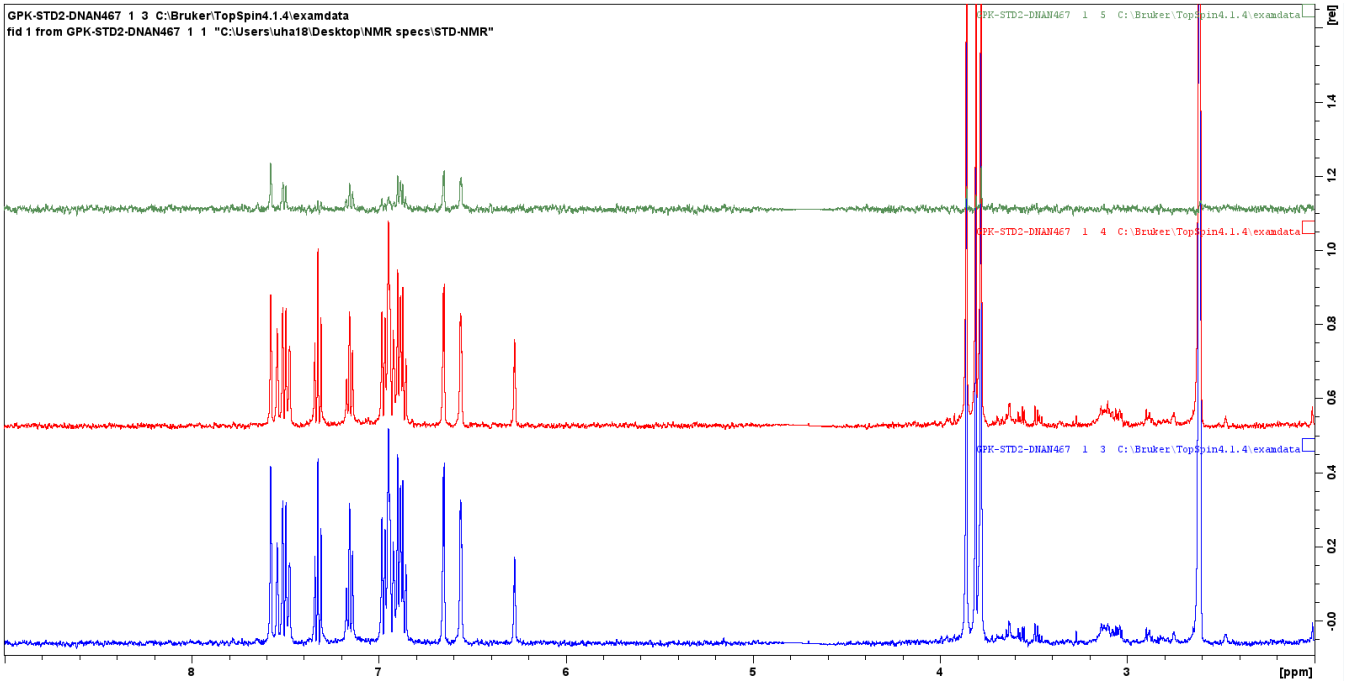

Figure S12. Overlay of the on-resonance (blue), off-resonance (red) and the difference spectrum (green) of the mixture containing **Fr2**, **Fr6**, and **Fr7**.

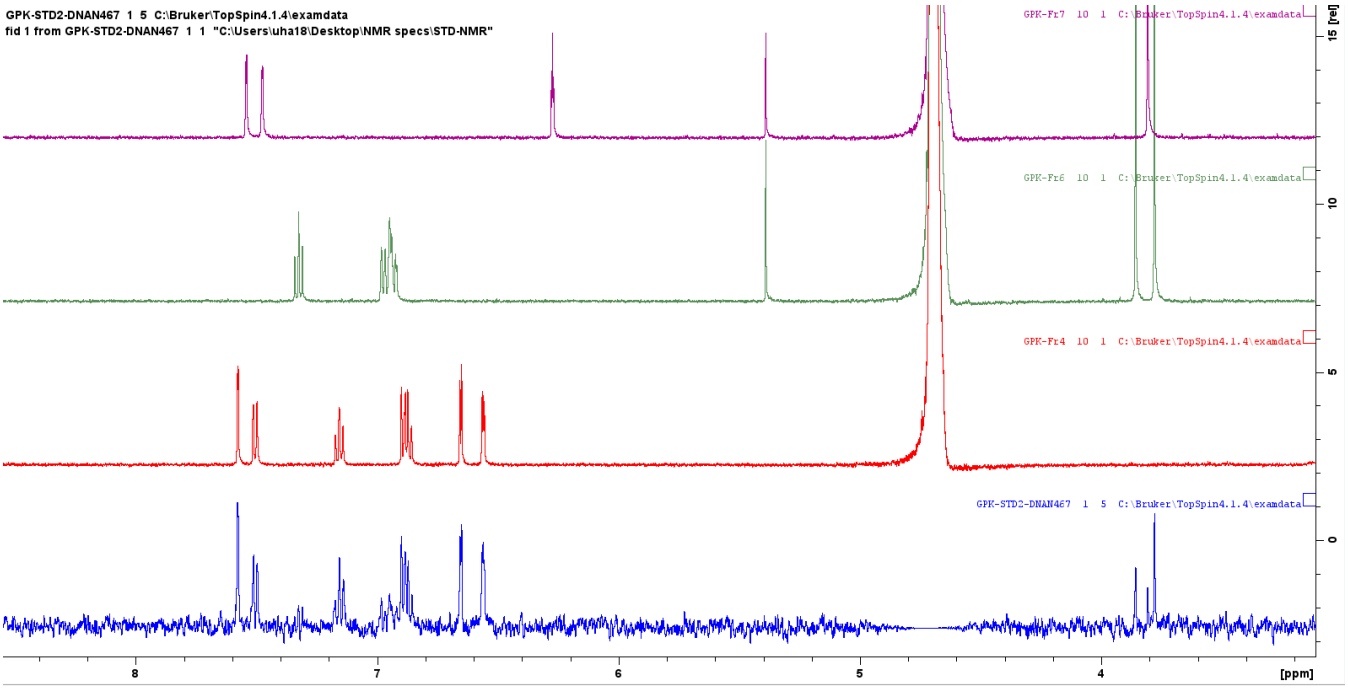

Figure S13. Overlay of the difference spectrum (**blue**) and individual spectra of **Fr2** (**red**), **Fr6** (**green**), **Fr7** (magenta).

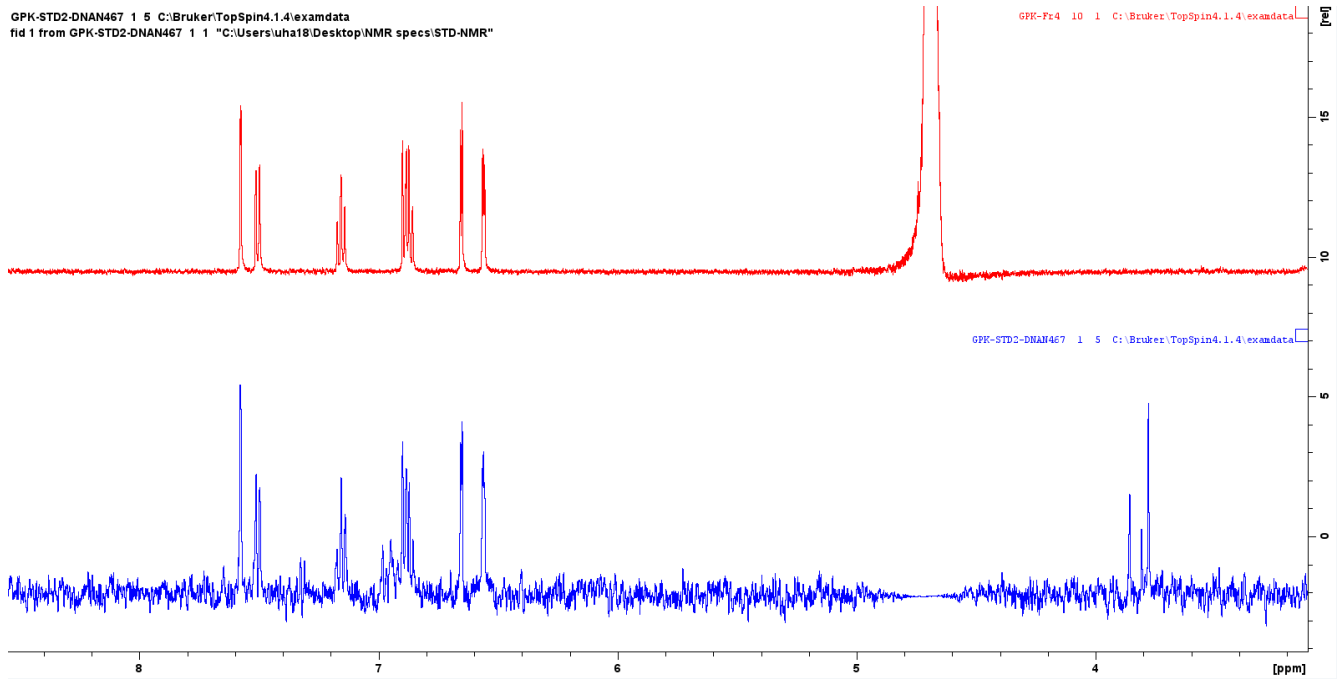

Figure S14. Overlay of the difference spectrum (**blue**) and an individual spectrum of **Fr2** (**red**)

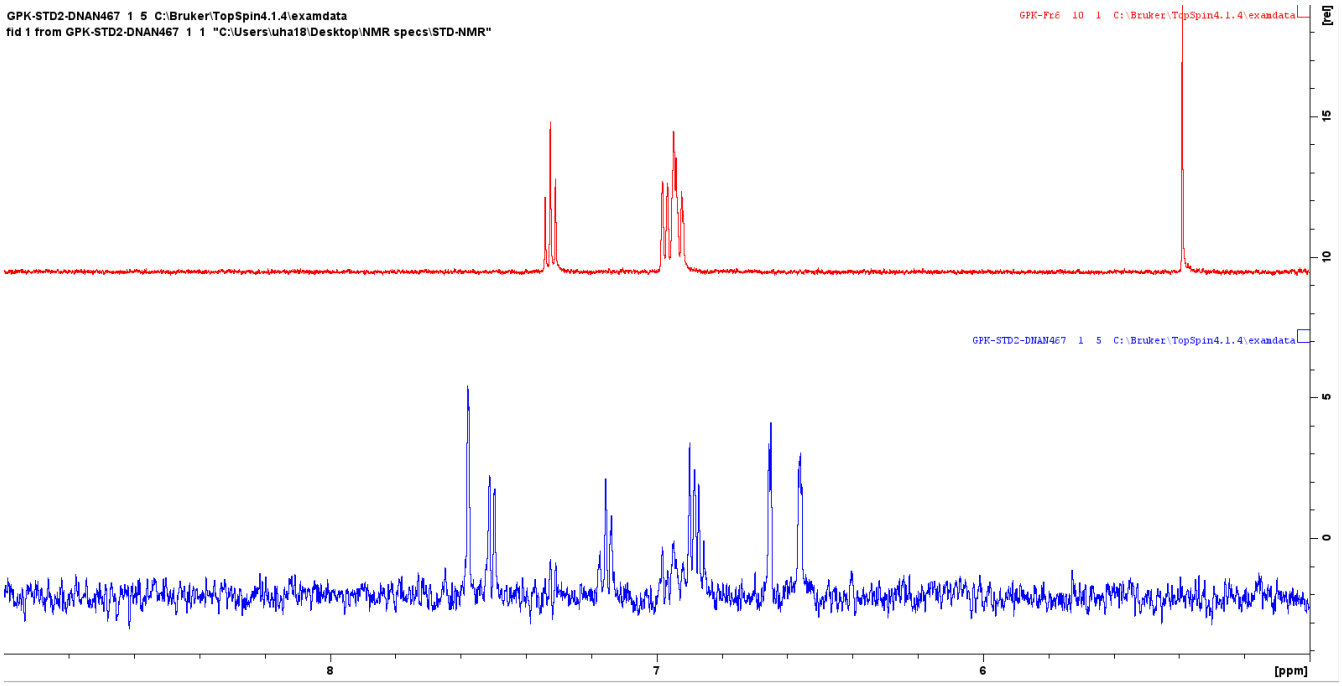

FigureS15. Overlay of the difference spectrum (blue) and an individual spectrum of **Fr6** (red)

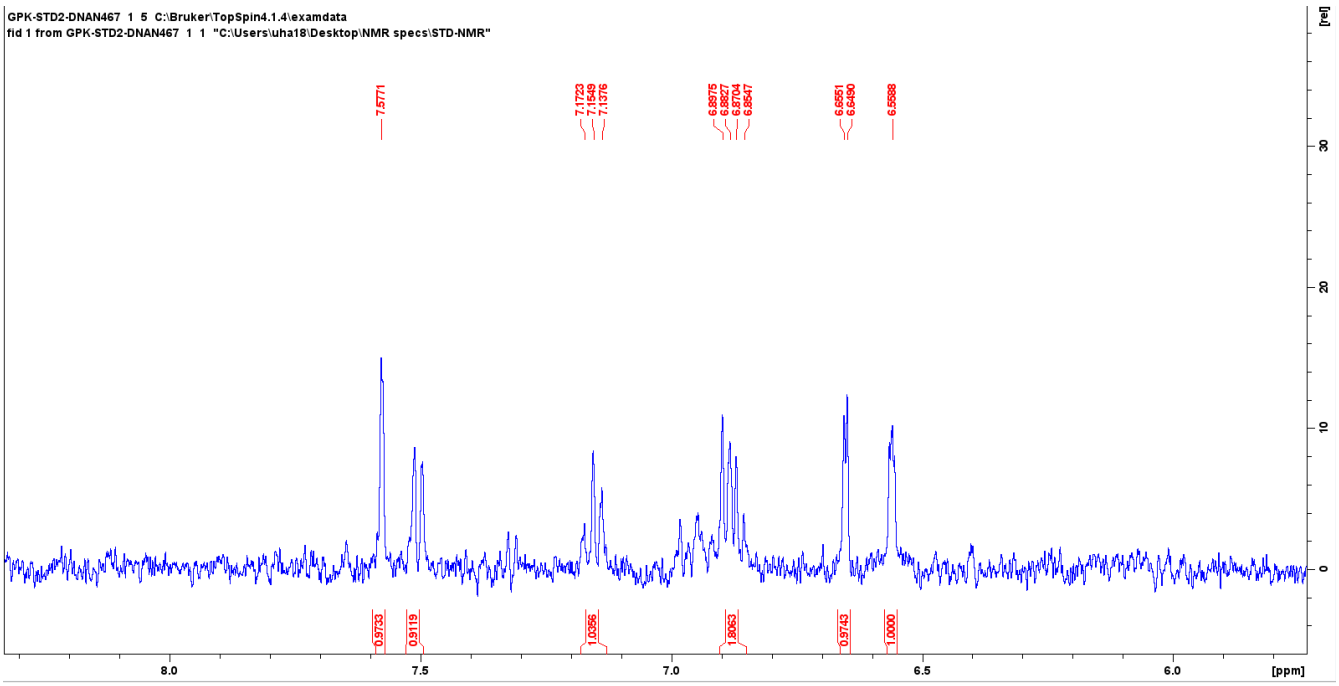

Figure S16. Peak-picked and integrated signals in the difference spectrum belonging to **Fr2**

STD-NMR measurements of compound 65. Because of the limited solubility the compound's concentration in the assay was set to 100 µM.

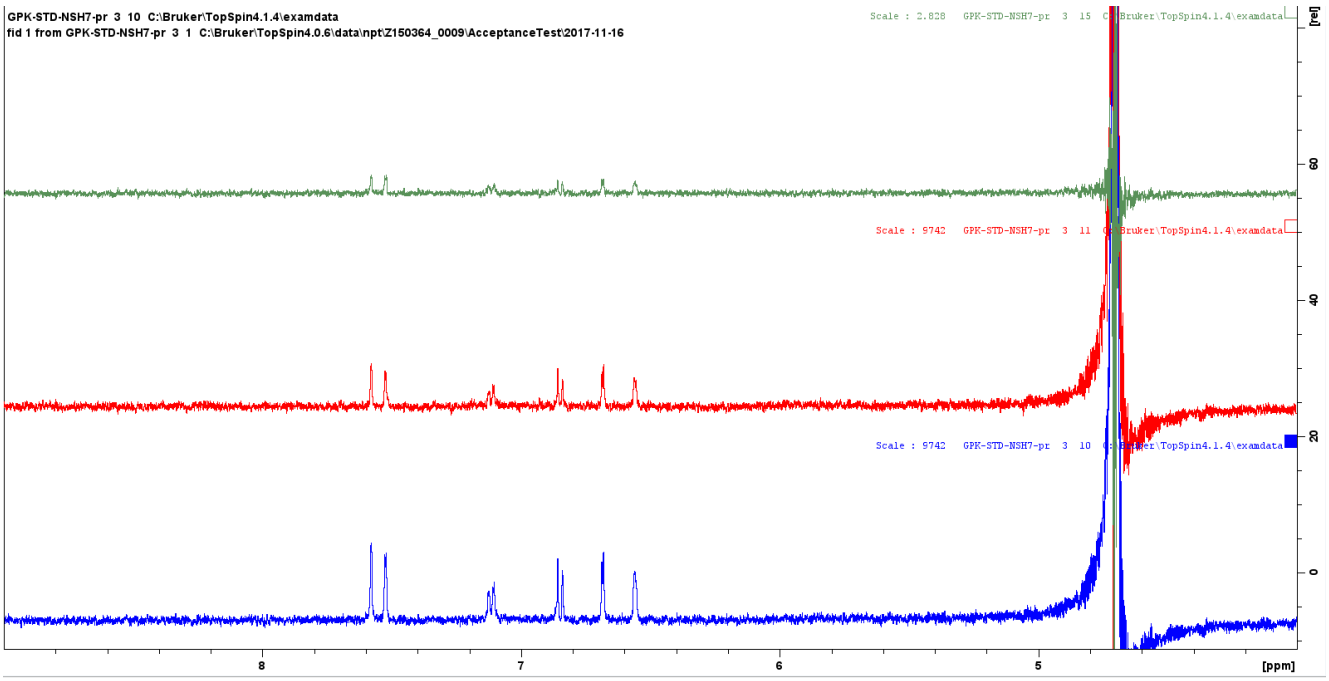

Figure S17. Overlay of the on-resonance (**blue**), off-resonance (**red**) and the difference spectrum (**green**) of **65.**

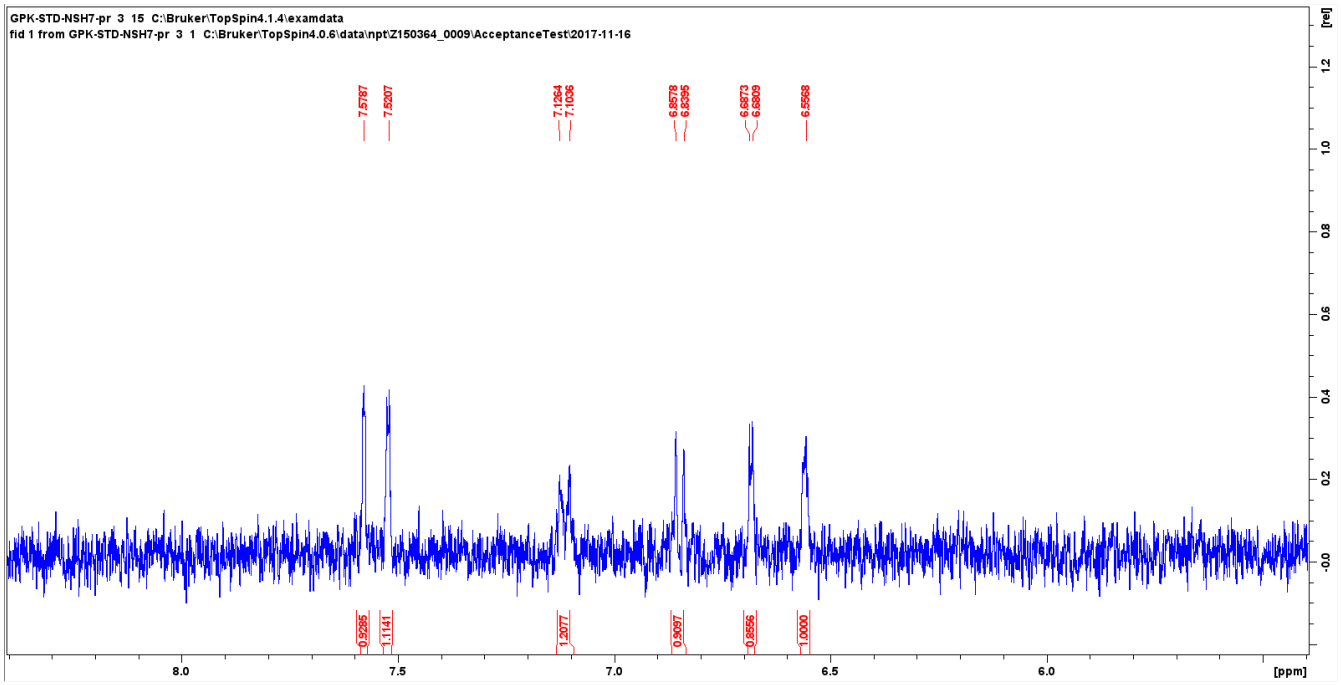

Figure S18. Peak-picked and integrated difference spectrum of **65**

S4.3 References

[1] C. Verrier, T. Martin, C. Hoarau, F. Marsais, *J. Org. Chem.* **2008**, *73*, 7383–7386.

[2] J. Ahmed, P. Sreejyothi, G. Vijaykumar, A. Jose, M. Raj, S. K. Mandal, *Chem. Sci.* **2017**, *8*, 7798–7806.

[3] S. Tani, T. N. Uehara, J. Yamaguchi, K. Itami, *Chem. Sci.* **2013**, *5*, 123–135.

[4] N. Primas, A. Bouillon, J. C. Lancelot, H. El-Kashef, S. Rault, *Tetrahedron* **2009**, *65*, 5739–5746.

[5] J. Chen, Z. Wang, C. M. Li, Y. Lu, P. K. Vaddady, B. Meibohm, J. T. Dalton, D. D. Miller, W. Li, *J. Med. Chem.* **2010**, *53*, 7414–7427.

[6] H. Gao, Z. Zhou, D. H. Kwon, J. Coombs, S. Jones, N. E. Behnke, D. H. Ess, L. Kürti, *Nat. Chem. 2016 97* **2016**, *9*, 681–688.

[7] J. Gu, C. Cai, *RSC Adv.* **2015**, *5*, 56311–56315.

[8] A. M. Birch, S. Groombridge, R. Law, A. G. Leach, C. D. Mee, C. Schramm, *J. Med. Chem.* **2012**, *55*, 3923–3933.

[9] C. Beinat, T. Reekie, S. D. Banister, J. O'Brien-Brown, T. Xie, T. T. Olson, Y. Xiao, A. Harvey, S. O'Connor, C. Coles, A. Grishin, P. Kolesik, J. Tsanaktsidis, M. Kassiou, *Eur. J. Med. Chem.* **2015**, *95*, 277–301.

[10] D. P. Hari, P. Schroll, B. König, *J. Am. Chem. Soc.* **2012**, *134*, 2958–2961.

[11] K. Rybicka-Jasińska, B. König, D. Gryko, *European J. Org. Chem.* **2017**, *2017*, 2104–2107.

[12] C. Y. Long, S. F. Ni, M. H. Su, X. Q. Wang, W. Tan, *ACS Catal.* **2020**, *10*, 13641–13649.

[13] D. Le Grand, M. Gosling, U. Baettig, P. Bahra, K. Bala, C. Brocklehurst, E. Budd, R. Butler, A. K. Cheung, H. Choudhury, S. P. Collingwood, B. Cox, H. Danahay, L. Edwards, B. Everatt, U. Glaenzel, A. L. Glotin, P. Groot-Kormelink, E. Hall, J. Hatto, C. Howsham, G. Hughes, A. King, J. Koehler, S. Kulkarni, M. Lightfoot, I. Nicholls, C. Page, G. Pergl-Wilson, M. O. Popa, R. Robinson, D. Rowlands, T. Sharp, M. Spendiff, E. Stanley, O. Steward, R. J. Taylor, P. Tranter, T. Wagner, H. Watson, G. Williams, P. Wright, A. Young, D. A. Sandham, *J. Med. Chem.* **2021**, *64*, 7241–7260.

[14] H. J. Park, D. H. Jung, K. H. Park, *Res. Chem. Intermed.* **2018**, *44*, 7657–7664.

[15] E. Řezníčková, T. Gucký, V. Kováčová, H. Ajani, R. Jorda, V. Kryštof, *Eur. J. Med. Chem.* **2019**, *182*, DOI 10.1016/J.EJMECH.2019.111663.

[16] F. Wang, R. Tanaka, Z. Cai, Y. Nakayama, T. Shiono, *Appl. Organomet. Chem.* **2015**, *29*, 771–776.

[17] E. A. Lindsey, R. J. Worthington, C. Alcaraz, C. Melander, *Org. Biomol. Chem.* **2012**, *10*, 2552–2561.

[18] V. Pirovano, E. Brambilla, S. Rizzato, G. Abbiati, M. Bozzi, E. Rossi, *J. Org. Chem.* **2019**, *84*, 5150–5166.

[19] V. Pirovano, A. Caselli, A. Colombo, C. Dragonetti, M. Giannangeli, E. Rossi, E. Brambilla, *ChemCatChem* **2020**, *12*, 5250–5255.

[20] Y. Yamamoto, Y. Nakanishi, K. ichi Yamada, K. Tomioka, *Tetrahedron* **2018**, *74*, 5309–5318.

[21] C. J. Novotny, S. Pollari, J. H. Park, M. A. Lemmon, W. Shen, K. M. Shokat, *Nat. Chem. Biol. 2016 1211* **2016**, *12*, 923–930.

[22] G. Yu, D. L. J. Clive, *J. Org. Chem.* **2016**, *81*, 8470–8484.

[23] L. Wang, J. Shen, S. Yang, W. Liu, Q. Chen, M. He, *Green Chem.* **2018**, *20*, 1290–1296.

[24] A. S. Demir, Ö. Reis, M. Emrullahoglu, *J. Org. Chem.* **2003**, *68*, 578–580.

5 Overarching Conclusion and Outlook

In conclusion, we utilized a virtual screening with further exploratory optimization to identify promising DnaN inhibitors, focusing around the structure of compound **H1**. Using STD-NMR, docking, X-ray crystallography and data pertaining the performance of analogues in SPR experiments, replisome assay and MIC tests, we elucidated the details of **H1**'s interaction with the DnaN protein and established crucial features of the scaffold associated with its DnaN affinity and antibacterial activity.

While derivatives of **H1** exhibited significant activity against Mycobacteria and Gram-positive bacteria, they did not affect efflux-competent Gram-negative pathogens (*E. coli*, *K. pneumonia*, *P. aeruginosa*). The chemotype discovered shows promise; however, further optimization is required to achieve more detailed understanding of its action mechanism.

Moving forward, it is crucial to delve deeper into the mechanism of antibacterial action of the chemotype representatives. The charged nature of these compounds suggests the possibility of multiple modes of action, both intracellularly by inhibiting DnaN (and possibly other relevant targets) and extracellularly akin to quaternary ammonium salts. Elucidating these mechanisms and dissecting their contributions into net antibacterial effect would enhance our understanding of the origins of compounds' inhibitory action and would be instrumental in driving further optimization efforts. This can be achieved by synthesizing appropriate affinity probes capable of photo labeling of target protein(s) and performing respective pull-down, proteomics-based or imaging experiments.

The further optimization of the chemotype structure is recommended to address certain limitations. Eliminating the permanent positive charge associated with the imidazolium ring might be necessary to reduce the potential for the scaffold's indiscriminate protein binding, while also making the less flat analogues of the most promising **H1** derivatives can reduce their similarity to typical substrates of efflux pumps found Gram-negative bacteria.

Therefore, the aforementioned modifications have the potential to 1) rule out possible additional modes of action and mitigate the risks of chemotype's idiosyncratic toxicity; 2) enhance compounds' penetration and retention of DnaN inhibitors in Gram-negative bacteria, broadening the spectrum of their antibacterial activity; 3) improve *in vitro* ADME/T and *in vivo* pharmacokinetic profile of analogues.

Fragment-based ligand design is a promising approach of increasing popularity in modern drug discovery, which allows for more efficient exploration of chemical space in the course of hit identification due to smaller size of fragments compared to average members of high-throughput or virtual screening libraries. The ascent of highly sensitive biophysical techniques plays a considerable part in detecting fairly weak interactions of fragment hits with target pro-

tein. This allows to interrogate even difficult targets, which have till recently been deemed “undruggable” and optimize weak binders into leads possessing high ligand efficiency.

Our studies also employed fragment-based screening, which led to the identification of several hits that were optimized for improved DnaN binding and enhanced activity against *M. smegmatis*.

However, further optimization and growing efforts are needed to enhance the DnaN affinity of these molecules and improve their ability to permeate the bacterial cell wall. This comprehensive approach is expected to pave the way for the development of more efficient, more potent and broad-spectrum antibacterial agents targeting DnaN.